

# Nonperturbative aspects of scattering amplitudes

Présentée le 19 décembre 2023

Faculté des sciences de base  
Laboratoire de théorie des champs et des cordes  
Programme doctoral en physique

pour l'obtention du grade de Docteur ès Sciences

par

**Miguel Alexandre RIBEIRO CORREIA**

Acceptée sur proposition du jury

Prof. H. Brune, président du jury  
Prof. J. M. Augusto Penedones Fernandes, Dr A. Sever, directeurs de thèse  
Prof. P. Vieira, rapporteur  
Prof. P. Tourkine, rapporteur  
Prof. V. Gorbenko, rapporteur



# Acknowledgements

I start by expressing my upmost gratitude and respect to every colleague and friend that have crossed my academic path so far. I apologize in advance for whomever I have unfortunately missed.

I was very lucky to have three world class scientists overseeing my PhD trajectory.

Alexander Zhiboedov, one of two supervisors at CERN, the person I've interacted the most with throughout my PhD and who has mostly influenced my growth and how I think about physics. Sasha is an incredibly gifted, brave and thorough researcher, who has a unique 'four' dimensional view of the field - widespread, in-depth, and across modern and old literature - which I naturally aspire to achieve one day.

João Penedones, my supervisor at EPFL, an exceptional physicist with a remarkable capacity to come up with simple, precise and creative explanations<sup>1</sup>. Countless times have I come to João with a confused head and get a "maybe this is what you mean" which precisely nailed the problem. All while balancing heavy university duties and providing important life and professional advice. João is the gold standard for a PhD advisor.

Amit Sever, who also supervised me while at CERN and was my co-supervisor at EPFL, played an important role in easing me into CERN's senior postdoc environment. Amit was very open to discuss various topics and underdeveloped ideas. A skilled and passionate physicist with a distinctive ability of 'cutting to the chase', focusing on the core concepts and asking pertinent questions, which he often encouraged me to do.

At EPFL I found a vibrant academic environment. I am grateful to Riccardo Rattazzi for his mentorship and for having lifted the veil on quantum field theory, first as a master student during my exchange at EPFL and second as a teaching assistant during my PhD. Likewise to the whole Cubotron crew (in no particular order): Alfredo, Lorenzo, Gabriel, Gil, Marten, Siyu, Marco, Denis, Jan, Matthijs, Biswajit, Xiang, Jiabin, Dean, Marc, Angelo, Manuel, João Silva, José, Matt, Brian, Alessandro and Victor. I had the pleasure to help Marko Pesut and Antoine Vuignier on their master thesis, the latter leading to a paper and an ongoing further collaboration with Antoine, who is now a thriving PhD student of Joao. And, of course, Corinne, who never let me miss a deadline.

My office mates, Aditya Hebbbar and Kamran Salehi Vaziri, who quickly became my friends for life. If one day I eventually get married these two will be my best men.<sup>2</sup> We were sharing so

---

<sup>1</sup>and, unfortunately to his undergrad students, to also think of intricate exam problems.

<sup>2</sup>Depending of course on the nature of the material they will exhibit at the thesis defense in front of my family.

## Acknowledgements

---

many memes in that office that João would often walk in the office and see us laughing, likely wondering why he decided to hire us. We also discussed physics of course (e.g. at GigaTacos while watching Arsenal getting destroyed by my childhood team) and took active part in the many conferences we attended (we certainly did go to bed early and avoided watching Arrested Development until late). There are so many inside jokes and sensitive information that is hard to fit here, and should for the sake of *everyone* remain hidden.

At CERN, the lunch and coffee breaks (and sometimes dinners!) were incredible opportunities to learn about the forefront of research. I am grateful (in no particular order) to Gabor, Shouvik, Alex, Alba, Irene, Bernardo, Jose, Matthew (my table tennis partner), Matjin and Eyoab (my companions for dinners at CERN), Anders, Joao Caetano, Paolo, Kyriakos, Andrew and Lucía Córdova who I have had the pleasure to collaborate with.

I naturally became closer to the other students working with Sasha. João Silva would come very often to CERN from Lausanne. I thank João for giving me very solid life advice, especially on the intricacies of modern dating (nao é malandro?). Kelian Häring, thank you for always being a reliable and available friend and, especially, for showing me that it is possible to have a balanced work-life while still being very productive.

As the pandemic ended I had the opportunity to travel and meet many other talented people. I especially thank Sebastian, Hofie, Nima, Carolina, Matteo and Alfredo for welcoming me so warmly to the institute and introducing me to the fascinating creative sides of amplitudes. I am also grateful to Pedro, Jandira, Alexandre, Harish, Sabrina, Zahra, Frank, Beatrix, Matt, Enrico and Andrea for the vibrant discussions and dinners at Perimeter. Finally, I thank all the different people I've met in various conferences and have learned greatly from: António, Barak, Jan, Giulia, Suzanne, Piotr, Felipe, Bernardo, Alessandro, Balt, Joan, Martin, Yifei, Miguel, Julio, Stefano, Francisco, Sergio, Dalimil, Leonardo, Francesco, Kara, Carl and Sergio.

I am also grateful to my friends from Portugal. In particular the *wizards club*, a curious mix of childhood friends and undergrad colleagues: António, Martim, Luís, Joao, Pousada, Xico, and my long-time handball teammates from Bairro de Janeiro: Mendonça, Filipe, Gouveia, Fábio, Bento.

To Patrícia Vieira with whom I was very happy and shared my life with for almost nine years and also to her parents who were essential for my development as a young man and aspiring physicist.

To my family, I express my gratitude and respect for always encouraging me to enquire and wonder, and thank them for having given me the conditions to chase my dreams. Obrigado.

At last, to Giulia Isabella, thank you for putting a smile on my face everyday, for allowing myself to live and for allowing yourself to believe. We came a long way.

To Everyone, it has been a pleasure. Thank you.

Miguel Correia

# Abstract

In this thesis we study how physical principles imposed on the S-matrix, such as Lorentz invariance, unitarity, crossing symmetry and analyticity constrain quantum field theories at the nonperturbative level. We start with a pedagogical introduction to the S-matrix bootstrap and showcase some basic consequences, such as the Froissart bound on the total cross-section. We then more carefully revisit and extend old results from 1960s including an interesting relation between large spin, low energy data and Landau singularities. We revisit the Afsar theorem asserting the necessity of particle production in relativistic scattering in  $d > 2$ . We establish the nonperturbative support for the spectral density, which is needed for a double dispersive representation of the scattering amplitude (or Mandelstam representation). This is a result of an extensive Landau and graph-theoretical analysis in which the leading inelastic Landau curves are determined and in particular an infinite subclass of these curves are found to accumulate at finite energies. We also consider the scattering of heavier particles where so-called anomalous thresholds are present. We show that anomalous thresholds are a consequence of the aforementioned principles and a key extra assumption: analyticity in the mass. We find a nonperturbative formula for the imaginary part across the anomalous threshold which, in particular, is shown *not* to be positive definite. Finally, we add form factors and spectral densities of local operators to the bootstrap setup, such as the stress-energy tensor. This let us include information about the UV conformal field theory and allows to better target certain quantum field theories such as Ising field theory.

**Keywords:** Quantum field theory, S-matrix, bootstrap, nonperturbative, Landau singularity, anomalous threshold, form factor, spectral density.



# Résumé

Dans cette thèse, nous étudions comment les principes physiques imposés sur la matrice  $S$ , tels que l'invariance de Lorentz, l'unitarité, la symétrie de croisement et l'analyticité, contraignent les théories quantiques des champs de manière non perturbative. Nous commençons par une introduction pédagogique au bootstrap de la matrice  $S$  et mettons en évidence quelques conséquences de base, telles que la borne de Froissart sur la section efficace totale. Nous revisitons ensuite en détail et étendons d'anciens résultats des années 1960, y compris une relation intéressante entre le grand spin, les données à basse énergie et les singularités de Landau. Nous réexaminons le théorème d'Aks qui affirme la nécessité de la production de particules lors de la diffusion relativiste en  $d > 2$ . Nous établissons le support non perturbatif de la densité spectrale, qui est nécessaire pour une représentation doublement dispersive de l'amplitude de diffusion (ou représentation de Mandelstam). Ceci est le résultat d'une Landau-analysis approfondie et de la théorie des graphes dans laquelle les courbes de Landau inélastiques dominantes sont déterminées et où, en particulier, nous identifions une sous-classe comprenant une infinité de courbes s'accumulant à des énergies finies. Nous considérons également la diffusion de particules plus massives où des seuils anormaux sont présents. Nous montrons que les seuils anormaux sont une conséquence des principes mentionnés précédemment et d'une hypothèse clé supplémentaire : l'analyticité de la masse. Nous dérivons une formule non perturbative pour la partie imaginaire à travers le seuil anormal qui, en particulier, est montrée *ne pas* être définie positive. Enfin, nous ajoutons des facteurs de forme et des densités spectrales d'opérateurs locaux à la configuration du bootstrap, tels que le tenseur énergie-impulsion. Cela nous permet d'inclure des informations sur la théorie quantique des champs conforme dans les UV et permet de cibler plus précisément certaines théories quantiques des champs telles que la théorie des champs de Ising.

**Mots clés :** Théorie quantiques des champs, matrice  $S$ , bootstrap, nonperturbative, singularité de Landau, seuil anormal, facteur de forme, densité spectrale.





# Contents

<b>Acknowledgements</b>	<b>i</b>
<b>Abstract (English/Français)</b>	<b>iii</b>
<b>1 Introduction</b>	<b>1</b>
1.1 The scattering amplitude: unitarity, analyticity and crossing symmetry . . . . .	2
1.2 Bootstrapping Newton's law of universal gravitation . . . . .	6
1.3 Large spin bootstrap and the need for Landau singularities . . . . .	8
1.4 Unitarity meets the Mass gap: The Froissart bound on the total cross-section .	10
1.5 Outline and executive summary of this thesis . . . . .	12
<b>2 An analytical toolkit for the S-matrix bootstrap</b>	<b>15</b>
2.1 Introduction . . . . .	15
2.1.1 Assumptions . . . . .	16
2.2 Amplitude Basics . . . . .	19
2.2.1 Analyticity . . . . .	20
2.2.2 Unitarity and Elastic Unitarity . . . . .	22
2.2.3 Partial Wave Expansion . . . . .	24
2.2.4 Froissart-Gribov Formula . . . . .	27
2.2.5 Further Continuity Assumption . . . . .	30
2.3 Analytic Continuation of Elastic Unitarity . . . . .	31
2.3.1 Mandelstam Kernel . . . . .	31
2.3.2 The Double Spectral Density and Crossing . . . . .	32
2.3.3 Analytic Continuation in Spin . . . . .	35
2.3.4 Analytic Continuation in $s$ . . . . .	37
2.3.5 Elastic Landau Curves . . . . .	38
2.4 Positivity of $\rho$ and Multi-Particle Production . . . . .	41
2.4.1 Positivity of The Double Spectral Density . . . . .	41
2.4.2 The Aks Theorem and Necessity of Particle Production . . . . .	43
2.4.3 Bounding Inelasticity . . . . .	45
2.5 Threshold Expansion . . . . .	47
2.5.1 Threshold Expansion of $f_J(s)$ . . . . .	49
2.5.2 Threshold Expansion of Discontinuity . . . . .	51
2.5.3 Threshold Expansion for Double Spectral Density . . . . .	52

## Contents

---

2.5.4	Radius of Convergence . . . . .	53
2.6	Large $J$ Expansion . . . . .	54
2.6.1	Large Spin Expansion of $f_J(s)$ . . . . .	55
2.6.2	Large Spin Expansion of $\text{Im}f_J(s)$ . . . . .	56
2.6.3	Threshold Expansion in the $J$ -space . . . . .	59
2.7	Finite $J$ and Finite $s$ . . . . .	61
2.7.1	A Toy Model Example . . . . .	63
2.7.2	Elastic Unitarity and Coupling Maximization . . . . .	66
2.8	Analytical Methods and Numerical Bootstrap . . . . .	67
2.8.1	Review of the Numerical Framework of [1] . . . . .	67
2.8.2	Why and What Should be Improved . . . . .	68
2.8.3	How the Numerical Framework Can Be Improved . . . . .	69
2.8.4	Mahoux-Martin Positivity . . . . .	73
2.9	Comments on CFTs . . . . .	74
2.10	Discussion . . . . .	76
<b>3</b>	<b>Probing multi-particle unitarity with the Landau equations</b>	<b>79</b>
3.1	Analytically continued unitarity and the Landau equations . . . . .	81
3.2	Graph selection . . . . .	85
3.3	Discussion . . . . .	90
3.3.1	Highest particle maximal analyticity . . . . .	90
3.3.2	Analytic continuation of multi-particle unitarity . . . . .	91
3.3.3	Lightest particle $\alpha$ -positive Landau curves . . . . .	91
3.3.4	Extended elastic unitarity region . . . . .	92
3.3.5	Accumulation points of the Landau curves are generic . . . . .	93
3.3.6	Higher multi-particle Landau curves . . . . .	93
3.3.7	$S$ -matrix bootstrap applications . . . . .	94
3.3.8	Other future directions . . . . .	94
<b>4</b>	<b>Nonperturbative Anomalous Thresholds</b>	<b>97</b>
4.1	Setup . . . . .	100
4.2	Simple perturbative example: Triangle diagram in $d = 2$ . . . . .	103
4.3	Continuation in $M^2$ of the solution to extended unitarity . . . . .	105
4.4	Results: Nonperturbative discontinuity . . . . .	108
4.4.1	Anomalous threshold of $mm \rightarrow MM$ . . . . .	108
4.4.2	Anomalous threshold of $MM \rightarrow MM$ . . . . .	109
4.5	Anomalous thresholds in integrable models . . . . .	111
4.5.1	Cancellation of the “anomalous” pole in $MM \rightarrow mm$ . . . . .	112
4.5.2	The anomalous double pole of $MM \rightarrow MM$ : Four overlapping singularities	115
4.6	Discussion and outlook . . . . .	120
<b>5</b>	<b>Injecting the UV into the Bootstrap: Ising Field Theory</b>	<b>125</b>
5.1	Dual $S$ -matrix and form factor Bootstrap . . . . .	128

5.1.1 Example: Minimization of $c_{UV}$ for fixed quartic coupling $\Lambda$ . . . . .	132
5.2 Numerical bootstrap . . . . .	134
5.2.1 $\mathbb{Z}_2$ symmetric theories . . . . .	134
5.2.2 Ising Field Theory . . . . .	137
5.3 Analytical bootstrap . . . . .	145
5.3.1 $\mathbb{Z}_2$ symmetric theories . . . . .	149
5.3.2 Ising Field Theory . . . . .	154
5.4 Discussion . . . . .	160
<b>6 Conclusion: Past, Present and Future of the S-matrix Bootstrap</b>	<b>163</b>
6.1 Pre-Asymptotic freedom period . . . . .	163
6.2 Post-Asymptotic freedom period . . . . .	164
6.3 Modern day S-matrix Bootstrap . . . . .	166
6.4 Have we exhausted the $2 \rightarrow 2$ space of constraints? . . . . .	167
6.5 Some big open problems . . . . .	168
6.6 Epilogue: The on-shell promise . . . . .	168
<b>A Appendix to Chapter 2</b>	<b>171</b>
A.1 Derivation of the Mandelstam Kernel . . . . .	171
A.2 Useful Identities for Gegenbauer $P$ - and $Q$ -functions . . . . .	173
A.3 The $Q_f^{(d)}(z)$ Large $J$ Expansion . . . . .	176
A.4 Gribov's Theorem . . . . .	177
A.5 Elastic Landau curves from the Mandelstam Equation . . . . .	178
A.6 Threshold Expansion for Non-Integer $J$ . . . . .	181
A.7 Threshold expansion in $J$ -space: Technical Details . . . . .	183
A.7.1 Higher Order Corrections to $\rho(s, t)$ . . . . .	186
A.7.2 More General Integral . . . . .	189
A.8 Keyhole Integrals in Odd $d$ . . . . .	190
A.8.1 Partial Wave . . . . .	190
A.8.2 Double Spectral Density . . . . .	192
<b>B Appendix to Chapter 3</b>	<b>195</b>
B.1 Analytical multi-particle Landau curves . . . . .	195
B.2 Multi-particle Landau curves from 2-particle unitarity . . . . .	196
B.3 Landau equations and automorphisms . . . . .	199
B.4 Trivial subgraphs . . . . .	201
B.5 Graph-theoretic implementation . . . . .	206
<b>C Appendix to Chapter 4</b>	<b>213</b>
C.1 Simple nonperturbative dispersive argument . . . . .	213
C.2 Derivation of the general solution to extended unitarity . . . . .	215
C.3 Box and double triangle diagrams in $d = 4$ . . . . .	216

## Contents

---

C.4	Supporting appendix to the discussion on the global existence of anomalous thresholds . . . . .	219
C.5	Kinematics, unitarity and Legendre functions in the unequal mass case . . . . .	220
<b>D</b>	<b>Appendix to Chapter 5</b>	<b>225</b>
D.1	Dual Bootstrap of the Sine-Gordon model . . . . .	225
D.2	Dual optimization problems . . . . .	226
D.2.1	$\mathbb{Z}_2$ symmetric theories . . . . .	226
D.2.2	Ising Field Theory . . . . .	229
D.2.3	Two poles : minimization of the central charge . . . . .	235
D.3	Numerical implementation . . . . .	236
D.4	Form factor perturbation theory . . . . .	238
D.4.1	Perturbation theory for $\mathcal{F}_1^\Theta$ . . . . .	239
D.4.2	Perturbation theory for $S(s)$ . . . . .	246
D.5	Integral representation for $c_{UV}$ : c-sum rule . . . . .	248
D.6	Normalization of the stress energy tensor form factors . . . . .	249
	<b>Bibliography</b>	<b>268</b>
	<b>Curriculum Vitae</b>	<b>269</b>

# 1 Introduction

Smoothness has been a guiding principle for physics as we know it. Fermi used to say “when in doubt, expand in a power series” [2]. It is a general observation that ‘laws’ of physics can typically be written in the form of differential equations. However, since the past century we have been faced with a shift in this paradigm. From the magnetization of a ferromagnet across its critical temperature to the scattering cross-section of proton-proton collisions at the Large Hadron Collider (LHC), many physical observables are *not* smooth. Quantum field theory (QFT) is a universal framework that lives in the space of distributions and is applicable across this range of phenomena.

Remarkably, in QFT, smoothness still plays a crucial role - but in the complex momentum plane - in the form of *analyticity*. For instance, the total cross-section is related to the discontinuity of an analytic function: the scattering amplitude. A further consequence of QFT is that the same analytic function describes distinct scattering processes, a property known as *crossing symmetry*, where different physical scattering regions are connected by some analyticity domain. Furthermore, all the scattering outcomes must add up to one, according to basic quantum mechanics, which translates into a distribution-valued constraint, *unitarity* of the scattering amplitude.

The S-matrix bootstrap aims at finding the space of amplitudes carved out by the constraints of analyticity, crossing and unitarity. The S-matrix program arose in the 60s as a way to tackle the problem of the strong interactions. However, imposing all the constraints in a predictive way proved difficult until, eventually, Quantum Chromodynamics (QCD) rose to prominence with the observation of deep inelastic scattering and the discovery of asymptotic freedom, which allowed the use of Feynman perturbation theory at high energies.

Today, nonetheless, our understanding of QFT, especially non-perturbative QFTs like low energy QCD, is far from complete. Because it’s based on general physical principles, the S-matrix bootstrap remains a valid tool, worth revisiting with modern analytical and computational methods.

## Chapter 1. Introduction

---

The modern incarnation of the numerical S-matrix bootstrap focus on constraining *classes* of QFTs by placing bounds on several observables such as couplings or scattering lengths, which is particularly relevant in the study of effective field theories (EFTs). Namely, in understanding which EFTs, such as gravitational theories, admit a UV completion consistent with basic physical principles, or, conversely, in mapping out the set of EFTs consistent with a certain expected spectrum or global symmetries coming from an already known UV completion whose renormalization group flow to the IR is strongly coupled, as is the case of QCD. Considerable progress has been done in several of these directions - see the recent Snowmass paper [3] for a more in-depth overview.

We should not proceed without mentioning that in recent years we have witnessed an “on-shell” revolution where these bootstrap principles have also been put to use in perturbation theory and have lead to simplifications and considerable progress in our computational ability when compared to the usual QFT Feynman diagram approach (refer e.g. to [4, 5] for references). At tree-level or to build the integrand of Feynman integrals, a variety of techniques have been developed, from recursion relations such as BCFW, to “generalized unitarity” or the double copy method which makes use of the yet mysterious color-kinematics duality, which for example relates gravitational and Yang-Mills amplitudes. At loop level, direct integration can be done numerically and, to a lesser extent, analytically via differential equation methods with so-called integration by part identities. These techniques have a wide range of applicability ranging from integrable theories, such as  $\mathcal{N} = 4$  Super Yang-Mills, where they have had the most success, to state-of-the-art real world predictions, e.g. of classical black hole scattering relevant for gravitational wave astronomy.

In what follows we will introduce the three key bootstrap principles and then showcase some basic consequences of these principles. First, at the perturbative level we will show how Newton’s law of universal gravitation arises from bootstrap considerations and then nonperturbatively - as is the main topic of this thesis - we will show one consequence at small energies, the necessity of “weird” singularities, so-called Landau curves, and one at large energies, namely the Froissart bound on total scattering cross-section. We then briefly summarize and outline the thesis.

### 1.1 The scattering amplitude: unitarity, analyticity and crossing symmetry

Let  $|\text{in}\rangle$  be an in-going state in a scattering experiment and  $|\text{out}\rangle$  an out-going state. The S-matrix operator connects both states:

$$|\text{out}\rangle = \hat{S} |\text{in}\rangle \tag{1.1.1}$$

## 1.1 The scattering amplitude: unitarity, analyticity and crossing symmetry

---

These states are assumed free, momentum eigenstates, or  $n$ -particle states.<sup>1</sup> We are interested in studying the case in which the particles interact, i.e.  $|\text{out}\rangle \neq |\text{in}\rangle$ . So it is natural to separate

$$\hat{S} = \mathbb{1} + i\hat{T} \quad (1.1.2)$$

where  $\hat{T}$  is the interacting part.

Matrix elements of  $\hat{T}$  involving  $n$ -particle momentum states will take the form

$$\langle \vec{k}_1, \dots, \vec{k}_m | \hat{T} | \vec{p}_1, \dots, \vec{p}_n \rangle = (2\pi)^4 \delta^4 \left( \sum_i p_i - \sum_i k_i \right) T_{n \rightarrow m}(p_i \cdot p_j, p_i \cdot k_j, k_i \cdot k_j) \quad (1.1.3)$$

where energy-momentum conservation requires the presence of the delta function and where the *scattering amplitude*  $T_{n \rightarrow m}$ , due to Lorentz invariance, may only depend on dot products of momenta.

For example, for the scattering of two particles with momenta  $\vec{p}_1$  and  $\vec{p}_2$  going into  $\vec{k}_1$  and  $\vec{k}_2$  we typically write

$$T(s, t) \equiv T_{2 \rightarrow 2}(s, t) \quad (1.1.4)$$

where  $s$  and  $t$ , known as Mandelstam variables, are related to momenta dot products,

$$s = (p_1 + p_2)^2, \quad t = (p_1 - k_1)^2, \quad u = (p_1 - k_2)^2, \quad (1.1.5)$$

with  $s + t + u = \sum_i m_i^2$ , where  $m_i$  is the mass of particle  $i$ .

$s$  and  $t$  are related to the center of mass total energy  $E_{CM}$  and the scattering angle  $\theta$ . In the equal mass case  $m_i = m$  these read

$$E_{CM} = \sqrt{s}, \quad \cos\theta = 1 + \frac{2t}{s - 4m^2}. \quad (1.1.6)$$

Note that

$$E_{CM} \geq 2m, \quad -1 \leq \cos\theta \leq 1 \quad \implies \quad s \geq 4m^2, \quad 4m^2 - s \leq t \leq 0 \quad (1.1.7)$$

Scattering amplitudes satisfy the following properties

- **Unitarity.** Total probability conservation requires the S-matrix to be a *unitary* operator,

$$\hat{S}^\dagger \hat{S} = 1 \quad \iff \quad 2\text{Im} \hat{T} = \hat{T}^\dagger \hat{T} \quad (1.1.8)$$

---

<sup>1</sup>We will purposefully avoid rigour in favor of emphasizing the main ideas and tools used in this thesis. Please refer to the first chapter or standard texts [6] for further details.

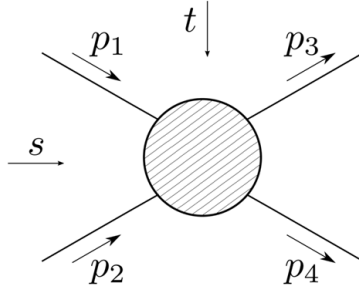


Figure 1.1: Graphical representation of the  $2 \rightarrow 2$  scattering amplitude  $T(s, t)$ .

Bra-ketting with  $n$ -particle states and making use of the identity operator

$$\mathbb{1} = \int_{n=1}^{\infty} |\vec{p}_1, \dots, \vec{p}_n\rangle \langle \vec{p}_1, \dots, \vec{p}_n| \quad (1.1.9)$$

leads to a relation between scattering amplitudes involving different number of particles. For example, bra-ketting with 2-particle states leads to a relation of the type

$$2 \operatorname{Im} T(s, t) = |T_{2 \rightarrow 1}|^2 \delta(s - M^2) + \int_{n=2}^{\infty} T_{2 \rightarrow n}^*(s, \dots) T_{2 \rightarrow n}(s, \dots) \Theta\left(\sqrt{s} - \sum_i^n m_i\right) \quad (1.1.10)$$

where the integration is over the ‘dotted’ variables which are omitted for visual clarity. The theta-function follows from energy conservation, ensuring support whenever there is enough center of mass energy  $\sqrt{s}$  to produce  $n$  particles. For  $n = 1$ , the delta-function comes from the trivial fact that a single particle is always at rest in its center of mass.

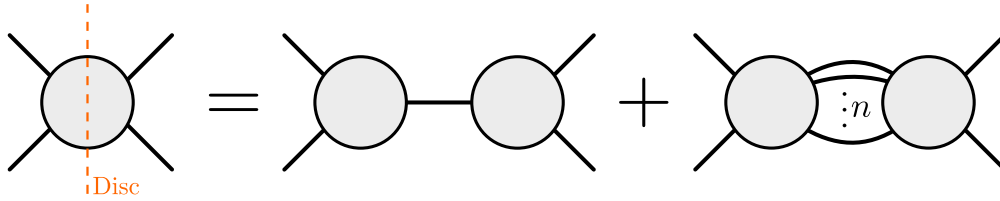


Figure 1.2: Graphical representation of unitarity, equation (1.1.10). On the left, the imaginary part of discontinuity of the amplitude. On the right the sum over intermediate processes.

- **Analyticity.** Scattering amplitudes still make sense when the momenta are taken complex. They are *analytic* functions of their variables, and this is related to *causality*. In fact, in the *physical region* for scattering where  $s \geq (m_1 + m_2)^2$ , where eq. (1.1.10) applies, we should actually evaluate the amplitude slightly above the real axis,

$$T_{\text{physical}}(s, t) = \lim_{\epsilon \rightarrow 0^+} T(s + i\epsilon, t). \quad (1.1.11)$$

This is known as Feynman  $i\epsilon$ -prescription, and the necessity for it will be obvious shortly. Amplitudes are still real functions, whenever  $s, t$  are real (one can think of them as



## 1.1 The scattering amplitude: unitarity, analyticity and crossing symmetry

*potentials*). This property is preserved in the complex plane as *real analyticity*, which for the  $2 \rightarrow 2$  amplitude amounts to

$$T^*(s, t) = T(s^*, t^*). \quad (1.1.12)$$

This implies that  $\text{Im } T(s, t) = 0$  for  $s, t$  real, which appears to contradict equation (1.1.10), unless (1.1.11) prescription is taken, in which case

$$\text{Im } T_{\text{physical}}(s, t) = \text{Disc}_s T(s, t) \equiv \lim_{\epsilon \rightarrow 0^+} \frac{T(s + i\epsilon, t) - T(s - i\epsilon, t)}{2i}. \quad (1.1.13)$$

Unitarity is then an equation for the *discontinuity* of the amplitude. It implies the presence of branch cuts, whose branch points are at production thresholds  $s = (\sum_i m_i)^2$ . We call these branch cuts *normal thresholds*. At first sight unitarity may seem like a weird constraint. However, noting that analytic functions are essentially determined by their analytic structure (via e.g. dispersion relations), then unitarity becomes very useful because it specifies some of the branch cuts, at least in the  $s$  plane. What about the analytic structure in  $t$ ?

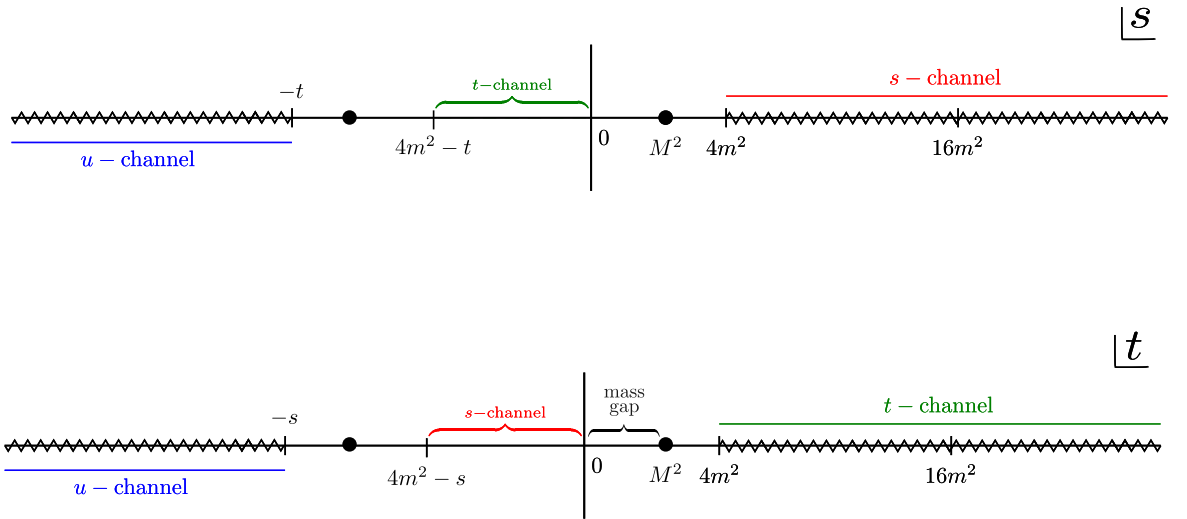


Figure 1.3: The amplitude is an analytic function of  $s$  and  $t$ . Here we represent the branch cuts and poles due to unitarity and their crossing symmetric images. In particular, in the  $s$ -channel, for  $s = M^2$  due to the exchange of a single particle of mass  $M$ ,  $n = 1$  in eq. (1.1.10) and the branch cuts for multi-particle production for  $s \geq 4m^2$ ,  $n \geq 2$  in (1.1.10). The regions for physical scattering are also represented in red ( $s$ -channel), green ( $t$ -channel) and blue ( $u$ -channel). In particular, region (1.1.7) for the  $s$ -channel,  $0 \leq t \leq 4m^2 - s$  and  $s \geq 4m^2$  slightly *above* the cut, according to (1.1.11). The partial wave decomposition (1.3.2) converges for  $t$  in this region but also in the *mass gap* where  $0 < t < M^2$ .

- **Crossing Symmetry.** This property is special to quantum field theory. It states that

## Chapter 1. Introduction

---

scattering amplitudes are permutation invariant in the momenta,

$$T(s, t, u) = T(t, s, u) = T(s, u, t). \quad (1.1.14)$$

This follows from the fact that the amplitude is the ‘‘Fourier transform’’ of the quantum field correlator, via the LSZ reduction formula [6],

$$T(s, t) = \int \prod_i d^4 x_i (\square + m_i^2) \langle \hat{\phi}(x_1) \hat{\phi}(x_2) \hat{\phi}(x_3) \hat{\phi}(x_4) \rangle e^{-i p_1 \cdot x_1 - i p_2 \cdot x_2 + i p_3 \cdot x_3 + i p_4 \cdot x_4} \quad (1.1.15)$$

where the correlator  $\langle \hat{\phi}(x_1) \hat{\phi}(x_2) \hat{\phi}(x_3) \hat{\phi}(x_4) \rangle$  is permutation invariant.

More than permutation invariance (1.1.14), crossing is also an analyticity statement: namely, that the above formula still makes sense in the different physical regions and, in particular, that there is an analyticity domain connecting them, e.g. from the  $s$ -channel physical region, where  $s \geq 4m^2$ , to the  $t$ -channel, where  $s < 0$  now corresponds to a scattering angle.

Crossing symmetry then leads to further branch cuts due to unitarity on the other physical scattering channels. Assuming that no other singularities are present (which is an unproven assumption known as *maximal analyticity*) we end up with the analyticity domain shown in fig. 1.3.

## 1.2 Bootstrapping Newton’s law of universal gravitation

We scatter two different particles of masses  $m$  and  $M$ , with initial momenta  $\vec{p}$  and  $\vec{P}$  and final momenta  $\vec{p}'$  and  $\vec{P}'$ , respectively, and let their interaction be mediated by a massless particle, a ‘graviton’  $g$ .

We want to compute the  $T_{mM \rightarrow mM}(s, t)$  scattering amplitude, and see how Newton’s law of gravitation is recovered in the non-relativistic limit.

We start by noting that since the graviton is not an external state, it can only appear as an ‘intermediate’ state in unitarity (1.1.10). For example as a single intermediate graviton involving a three point coupling  $T_{2 \rightarrow g}$ .

Now,

1. Gravity should not change particle type, so the only non-zero three-point amplitudes can be  $T_{mm \rightarrow g}$  and  $T_{MM \rightarrow g}$ .
2. Gravity is universal which requires  $T_{mm \rightarrow g}$  and  $T_{MM \rightarrow g}$  to be related via  $m \leftrightarrow M$ .
3. No non-trivial Lorentz invariant can be built out of the three momenta (due to momentum conservation), so the three-point amplitudes are *constant*.

## 1.2 Bootstrapping Newton's law of universal gravitation

---

4. The three-point amplitudes have dimensions of mass, while the gravitational constant  $G$  has dimensions of  $\text{mass}^{-2}$ .

These considerations lead to

$$T_{mm \rightarrow g} = mf(Gm^2), \quad T_{MM \rightarrow g} = Mf(GM^2), \quad (1.2.1)$$

for some real function  $f$ .

These 3-point amplitudes do not appear in the unitarity equation for  $mM \rightarrow mM$  but they do appear for the crossing-related process  $mm \rightarrow MM$ . In which case unitarity reads

$$\text{Disc}_s T_{mm \rightarrow MM}(s, t) = T_{mm \rightarrow g} T_{MM \rightarrow g} \delta(s) + \dots \quad (1.2.2)$$

Dropping the ‘...’ which we assume to contribute at higher orders in  $G$ , and making use of  $\text{Disc}(\frac{1}{s}) = -\delta(s)$ , implies

$$T_{mm \rightarrow MM}(s, t) = -\frac{mMf(Gm^2)f(GM^2)}{s} \quad (1.2.3)$$

Crossing then implies

$$T_{mM \rightarrow mM}(s, t) = T_{mm \rightarrow MM}(t, s) = -\frac{mMf(Gm^2)f(GM^2)}{t} \quad (1.2.4)$$

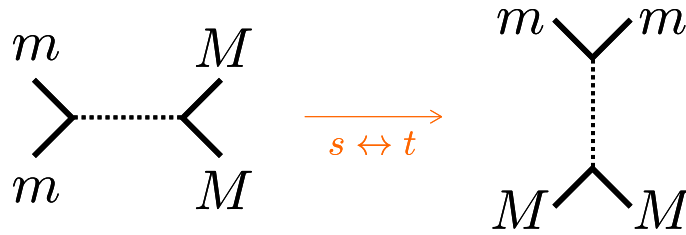


Figure 1.4: Diagrammatic representation of equation (1.2.4).

In the non-relativistic limit we have

$$t = (p - p')^2 \approx -|\vec{k}|^2, \quad (1.2.5)$$

where  $\vec{k} = \vec{p} - \vec{p}'$  is the exchanged momentum (or the graviton's momentum).

To find the potential we connect with quantum mechanics, where at leading order, i.e. in the Born approximation, the scattering amplitude is the Fourier transform of the potential. So we

## Chapter 1. Introduction

---

have

$$V(\vec{r}) = \frac{1}{mM} \int d^3\vec{k} e^{i\vec{k}\cdot\vec{r}} T_{mM \rightarrow mM}(\vec{k}), \quad (1.2.6)$$

up to some numerical factor.<sup>2</sup>

We find

$$V(\vec{r}) = -\frac{f(Gm^2)f(GM^2)}{|\vec{r}|} = -\hbar c \frac{f\left(\frac{Gm^2}{\hbar c}\right)f\left(\frac{GM^2}{\hbar c}\right)}{|\vec{r}|} \quad (1.2.7)$$

where in the last step we reinstated factors of  $\hbar$  and  $c$ . Requiring the final answer to be independent of either of them leads to  $f(x) = \sqrt{x}$  and we recover Newton's law

$$V(\vec{r}) = -\frac{GMm}{|\vec{r}|}. \quad (1.2.8)$$

To arrive here we have assumed the *equivalence principle*, encapsulated in assumptions 1. and 2. These in fact become a necessity if, instead of a scalar, the graviton is taken to have spin 2 [5]. In this case the amplitude (1.2.4) will be different, but the non-relativistic limit derived here will be the same.

We have also assumed that the extra terms in unitarity are subleading, which should only hold for sufficiently small coupling  $G$ . These corrections can however be systematically taken into account to iteratively build the amplitude in powers of  $G$  [5].

### 1.3 Large spin bootstrap and the need for Landau singularities

Let us now explore some simple nonperturbative consequences of unitarity, analyticity and crossing. The strategy will be as follows. Instead of assuming the interaction to be weak, we will simplify the bootstrap constraints by focusing on specific regions of  $s$  and  $t$ , which will allow us to conclude something about the nonperturbative amplitude in these regions.

One basic observation is that for small enough center of mass energy  $\sqrt{s}$  there should be no particle production i.e. unitarity should only involve  $2 \rightarrow 2$  scattering. In this case, only the  $n = 2$  eq. (1.1.10) term should have support and we have a closed equation for the amplitude itself, *elastic unitarity*:

$$\text{Disc}_s T(s, t) = \int dt_1 dt_2 K(t, t_1, t_2) T^*(s, t_1) T(s, t_2) \quad (1.3.1)$$

where  $K(t, t_1, t_2)$  represents the 2-body phase space kernel whose precise form does not

---

<sup>2</sup>The pre-factor of  $1/mM$  ensures the potential has the right mass dimension and it comes e.g. from matching the cross-section in QM and QFT:  $(\frac{d\sigma}{d\Omega})_{\text{QM}} \propto |\mu \tilde{V}(\vec{k})|^2$ , where  $\mu = \frac{mM}{m+M}$  is the reduced mass and  $\tilde{V}(\vec{k})$  is the Fourier transform of  $V(\vec{r})$ , whereas  $(\frac{d\sigma}{d\Omega})_{\text{QFT}} \propto |T_{2 \rightarrow 2}(s, t)|^2/s$  with  $s \approx (m+M)^2$  in the non-relativistic limit.

### 1.3 Large spin bootstrap and the need for Landau singularities

concern us for now.

Eq. (1.3.1) is still a complicated integral equation. We can simplify it by changing variables. In particular, we can project onto angular momentum eigenstates in which the S-matrix is expected to be diagonal (owing to rotational invariance). The spin  $J$  amplitude, or partial wave  $f_J(s)$ , is related to the scattering amplitude  $T(s, t)$  in the familiar way

$$T(s, t) = \sum_{J=0}^{\infty} (2J+1) f_J(s) P_J(z) \quad (1.3.2)$$

where  $z$  is the cosine of the scattering angle given by eq. (1.1.6) and  $P_J$  is the Legendre polynomial.

The partial wave decomposition (1.3.2) not only converges in the physical region  $-1 < z < 1$ , or  $4m^2 - s < t < 0$ , but also for  $z > 1$  or positive  $t > 0$  until the nearest singularity of  $T(s, t)$ , say a  $t$ -channel pole at  $t = M^2$ . We call this region the *mass gap* (see figure 1.3).

In this region the Legendre polynomial will grow exponentially with  $J$ ,

$$P_J(z) \rightarrow \lambda^J(z), \quad J \rightarrow \infty, \quad \text{with} \quad \lambda(z) = z + \sqrt{z^2 + 1} > 1. \quad (1.3.3)$$

Therefore, in order for the partial wave decomposition to converge (1.3.2) we must have exponential decay of the partial wave<sup>3</sup>

$$f_J(s) \sim [\lambda_M(s)]^{-J}, \quad J \rightarrow \infty, \quad \text{with} \quad \lambda_M(s) \equiv \lambda(z(s, M^2)) > 1 \quad (1.3.4)$$

We therefore see the first hints of the interesting connection

$$\text{Analytic structure in } t \leftrightarrow \text{Large spin } J \text{ behavior} \quad (1.3.5)$$

With this in mind we go back to unitarity. In terms of  $f_J(s)$ , elastic unitarity (1.3.1) simplifies greatly:

$$\text{Im } f_J(s) = |f_J(s)|^2 \quad (1.3.6)$$

Making use of (1.3.4) we see that the large spin decay of the imaginary part is much stronger compared to the real part,

$$\text{Im } f_J(s) \sim [\lambda_M(s)]^{-2J}, \quad J \rightarrow \infty. \quad (1.3.7)$$

Owing to (1.3.5), we may now wonder what this stronger spin decay implies for the analytic structure in  $t$ .

---

<sup>3</sup>Note that if we also send  $s \rightarrow \infty$  keeping the impact parameter  $b = \frac{J}{\sqrt{s/2}}$  fixed we find  $f_b \equiv \lim_{s \rightarrow \infty} f_{b\sqrt{s}}(s) \sim e^{-bM}$  which is the expected Yukawa-like decay.

## Chapter 1. Introduction

---

Namely, the object

$$\text{Disc}_s T(s, t) = \sum_{J=0}^{\infty} (2J+1) P_J(z) \text{Im} f_J(s) \quad (1.3.8)$$

should have a large domain of convergence in  $t$ . The sum will stop converging once

$$\lambda(z)^J \lambda_M^{-2J} \sim 1, \quad (1.3.9)$$

which occurs for

$$\lambda(z(s, t)) = \lambda_M^2(s) \implies t = t_{LC}(s) = 4M^2 \left( \frac{s - 4m^2 + M^2}{s - 4m^2} \right), \quad (1.3.10)$$

this is a Landau curve.

So, even though  $T(s, t)$  is singular at  $t = M^2$ , unitarity implies that the discontinuity  $\text{Disc}_s T(s, t)$  will be regular at this point and beyond, to only be singular at the Landau curve  $t = t_{LC}(s) > M^2$ .

This singularity appears in perturbation theory, for example in the box diagram (see fig. 1.5), but here we showed that it is a nonperturbative feature of the amplitude.

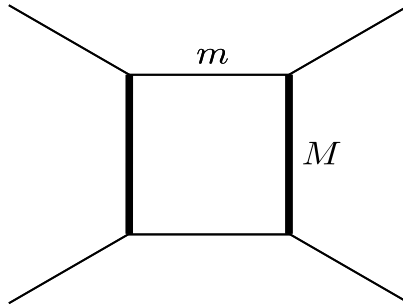


Figure 1.5: Feynman diagram singular at the Landau curve (1.3.10).

### 1.4 Unitarity meets the Mass gap: The Froissart bound on the total cross-section

We have explored a consequence of unitarity, crossing and analyticity at small energies  $s$  where particle production is absent. Let us now constrain the amplitude at large energies, in particular in the way it grows as  $s \rightarrow \infty$ . This will translate into a bound on the total cross-section, via unitarity (1.1.10)

$$\sigma(s) = \frac{1}{s} \sum_n \int |T_{2 \rightarrow n}(s, \dots)|^2 = \frac{\text{Im} T(s, 0)}{s}. \quad (1.4.1)$$

This relation is known as the *optical theorem*.

## 1.4 Unitarity meets the Mass gap: The Froissart bound on the total cross-section

Making use of the partial wave decomposition (1.3.2), we have

$$\text{Im } T(s, 0) = \sum_{J=0}^{\infty} (2J+1) \text{Im } f_J(s) \quad (1.4.2)$$

and unitarity in terms of  $f_J(s)$ , for any  $s$ , can be put into an inequality, as every term in the RHS of (1.1.10) will contribute positively when written in terms of partial waves,

$$\text{Im } f_J(s) \geq |f_J(s)|^2 \quad (1.4.3)$$

This implies that each partial wave cannot be arbitrarily large. Relevant for bounding the total cross-section from above is the upper bound

$$\text{Im } f_J(s) \leq 1. \quad (1.4.4)$$

Note however that this upper bound on  $\text{Im } f_J(s)$  by itself does not put an upper bound on  $\text{Im } T(s, 0)$  in eq. (1.4.2). We can however ally this with the fact that there is a mass gap which implies the large spin behavior (1.3.7). This in turn implies that the unitarity upper bound (1.4.4) *cannot* be saturated at large spins.

Let us now estimate the “critical” spin  $J = J^*$  beyond which the exponential decay dominates over the unitarity bound in  $s \rightarrow \infty$  limit.

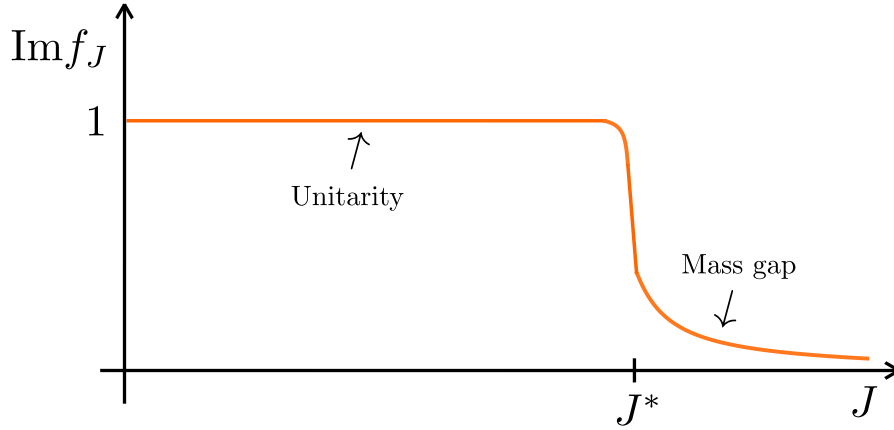


Figure 1.6: Profile in spin  $J$  of an amplitude with maximal cross-section. Unitarity (1.4.4) is saturated until a critical spin  $J^*$ , above which the large spin decay ensues (1.3.4). It is still an open problem whether such a physical amplitude exists.

This requires knowing the large  $s$ -dependence of the pre-factor of  $f_J(s) \sim [\lambda_M(s)]^{-J}$ . We will make the extra assumption of *polynomial boundedness*, namely that  $T(s, t) \lesssim s^N$ , as  $s \rightarrow \infty$ , which in turn puts a bound on the pre-factor<sup>4</sup>

$$f_J(s) \lesssim s^N [\lambda_M(s)]^{-J}, \quad J, s \rightarrow \infty \quad (1.4.5)$$

<sup>4</sup>This follows from  $s^N \gtrsim \text{Im } T(s, t) = \sum_{J=0}^{\infty} (2J+1) P_J(z) \text{Im } f_J(s) > \text{Im } f_{J \rightarrow \infty}(s)$ , for  $t > 0$  where  $P_J(z > 1) > 1$ .

## Chapter 1. Introduction

---

Now  $J^*$  is defined as

$$1 \sim s^N [\lambda_M(s)]^{-J^*} \quad (1.4.6)$$

or, qualitatively,

$$\text{Unitarity} \sim \text{Mass gap} \times \text{Polynomial boundedness} \quad (1.4.7)$$

which gives

$$J^*(s) \sim \sqrt{s} \log s, \quad s \rightarrow \infty \quad (1.4.8)$$

and, therefore,

$$\text{Im } T(s, 0) = \sum_{J=0}^{\infty} (2J+1) \text{Im } f_J(s) \lesssim \sum_{J=0}^{J^*(s)} (2J+1) \lesssim [J^*(s)]^2 = s \log^2(s) \quad (1.4.9)$$

so we find the Froissart bound on the total cross-section

$$\sigma(s \rightarrow \infty) \lesssim \log^2(s), \quad s \rightarrow \infty. \quad (1.4.10)$$

## 1.5 Outline and executive summary of this thesis

We now briefly outline and summarize the main results of this thesis. Please refer to the initial section of each chapter for a more in-depth outline.

### Chapter 2: An analytical toolkit for the S-matrix bootstrap

In chapter 2 we uncover important analytic results on the nonperturbative S-matrix bootstrap, and extend them in several directions of current interest. We go further in-depth into what was already briefly touched upon in the introduction.

Namely, elastic unitarity and its analytic continuation, as originally done by Mandelstam, the partial wave decomposition and the Froissart-Gribov projection for which the connection between analyticity in  $t$  and large spin  $J$  behavior becomes even more apparent.

These tools allow to further leverage unitarity, crossing symmetry and analyticity leading to many interesting results. For example, the existence of additional Landau curves deeper into the large  $t$  region, the Aks theorem asserting the necessity of particle production in space-time dimension larger than 2, the fact that the spectral density  $\rho$  (double discontinuity of the amplitude) enjoys some positivity region carved out by a set of Landau curves, and an interesting connection between large spin (or impact parameter) and low energy data, which can be directly extracted from experiment (viz. scattering lengths). We put this together in [7], a work which functions both as a modern review and a beacon for future explorations/im-



plementations on the numerical bootstrap, having also some relevance for the perturbative scattering amplitudes community.

### Chapter 3: Probing multi-particle unitarity with the Landau equations

As already briefly shown, a non-trivial consequence of the bootstrap constraint is the existence of additional singularities of the amplitude, Landau singularities. This is made precise in the elastic regime (see chapter 2) but, so far, not in the multi-particle (MP) regime, due to the complexity of MP unitarity.

The lowest-lying Landau curves carve out the support for the spectral density of the amplitude, which is necessary for the Mandelstam representation. In this chapter we uncover the support of the spectral density in the MP region, by determining the leading MP Landau curves.

Crucially, because Landau singularities are also present in Feynman diagrams, we find them by solving directly the Landau equations of Feynman diagrams. Solving the Landau equations is however a non-trivial task, except for the simplest graphs. We start by automating this procedure in a computationally efficient way.<sup>5</sup> Because there are infinitely many graphs, one still has to understand which graphs could give the leading MP Landau curves. Starting from all the graphs (for a given number of vertices and vertex degree) we impose several sharp graph-theoretic constraints based on physical principles, such as limiting the number of exchanged particles, to identify the leading MP graphs. To solve the problem we have to go to a considerably large number of vertices (12 vertices).<sup>6</sup> About 7 million graphs were analyzed, from which a few survived. The end result is a seemingly infinite family of Landau curves accumulating towards the curve

$$(s - 16m^2)(t - 16m^2) = 192m^4,$$

We argue that these accumulations should be even more frequent as one goes deeper into the MP region. They appear to be a generic feature of QFT.

### Chapter 4: Nonperturbative Anomalous Thresholds

Landau curves are singularities on the physical sheet, but in the equal-mass case they always seem to be hidden by the normal threshold branch cuts, so the analyticity domain remains as in fig. 1.3.

In the non-equal mass case, however, the situation changes. Feynman diagrams (notably the triangle diagram) involving heavy enough particles contain branch cuts on the physical

---

<sup>5</sup>Our algorithm is implemented on Mathematica. It takes as input a Feynman diagram and outputs the Landau curve (numerical value). The algorithm takes advantage of several graph-theory tools, such as the incidence matrix to automate momentum conservation and graph automorphism identification to reduce the system of equations.

<sup>6</sup>We made use of cutting edge non-isomorphic graph generation (*nauty and Traces*) and network analysis tools (*igraph*).

## Chapter 1. Introduction

---

sheet - anomalous thresholds - which, unlike normal thresholds and bound-state poles, do not correspond to any asymptotic  $n$ -particle state.

In this chapter we show that anomalous thresholds arise as a consequence of established S-matrix principles and two reasonable assumptions: unitarity below the physical region and analyticity in the mass. We find explicit nonperturbative formulas for the discontinuity across the anomalous threshold in  $d = 2$ , and in  $d = 4$ , ready to be used in dispersion relations for bootstrap and phenomenological applications.

## Chapter 5: Injecting the UV into the Bootstrap

So far we have been constraining the space of S-matrices consistent with bootstrap principles. One crucial question however is how to target specific QFTs and one interesting possibility is to use information about the UV.

A UV complete QFT can be defined non-perturbatively as a conformal field theory (CFT) in the UV deformed by relevant deformations that trigger a renormalization group (RG) flow to the IR. We can include information about the UV in the bootstrap by considering states given by the action of local operators such as the stress-energy tensor. In this way form factors and spectral densities join the S-matrix in a mixed bootstrap setup.<sup>7</sup> Concretely, in  $d = 2$ , UV information can be included via the  $c$ -sum rule which relates the spectral density of the trace of the stress-energy tensor to  $c_{UV}$ , the central charge of the UV CFT.

Contrarily to the usual *primal* bootstrap, which constructs an explicit ansatz for the S-matrix, we implement a *dual* approach which can be tackled with SDPB and produces rigorous bounds at finite numerical truncation (akin to the conformal bootstrap). In chapter 5, we: (1) find a rigorous lower bound on  $c_{UV}$  of a class of  $\mathbb{Z}_2$  symmetric theories, and (2) target Ising Field Theory (IFT), which can be thought of as the QFT describing the  $d = 2$  Ising model near the critical point, i.e. the Ising CFT deformed by both relevant deformations (thermal and magnetic). By fixing  $c_{UV} = 1/2$  we find the S-matrix and form factor parameter space where IFT lies inside, for different values of the magnetic field.

---

<sup>7</sup>The CFT in the IR is assumed to be empty, such that the QFT has a mass gap and the S-matrix is a well-defined object.

# 2 An analytical toolkit for the S-matrix bootstrap

## 2.1 Introduction

The idea of bootstrapping the S-matrix of a unitary, relativistic, gapped theory in  $d \geq 3$  was actively pursued in the 60's. While many interesting results have been derived [8, 9, 10, 11], no nonperturbative physical S-matrices have been computed. The main reason being that no solid, nonperturbative calculation scheme was ever put forward without relying on some unreliable approximations. In addition to that, analytic properties of the multi-point amplitudes were never fully understood. Moreover, even at the level of the two-to-two scattering amplitude, the region of analyticity that is usually assumed in the bootstrap analysis has not been rigorously established.

While the problem of analytic properties of multi-point scattering amplitudes is still widely open, the question of finding a good calculation scheme has recently acquired an interesting twist with the development of the conformal bootstrap [12, 13]. In this context, by exploring bounds on the OPE data in the space of solutions to the CFT bootstrap equations, it was found that sometimes the physical theories of interest saturate the bootstrap bounds [14, 15, 16] and are in this sense solvable.<sup>1</sup> Remarkably, a similar phenomenon was observed for 2d S-matrices [17, 18, 19, 20], where some previously known two-dimensional scattering amplitudes of physical theories were found to saturate the bootstrap bounds. We can loosely call such theories *bootstrap-solvable*. A fundamental, open question in the S-matrix theory program therefore is: *Are there bootstrap-solvable S-matrices in  $d \geq 3$ ?*

A distinguishing feature characteristic to scattering in  $d \geq 3$  dimensions is a remarkable connection between scattering and particle production. Here, by scattering we mean a non-trivial  $2 \rightarrow 2$  amplitude and by particle production, we mean a non-zero  $2 \rightarrow n$  amplitude with  $n > 2$ . While scattering without particle production is a commonplace in  $d = 2$  [21], in  $d \geq 3$  it is widely believed that scattering implies production [22].<sup>2</sup> The underlying reason is

---

<sup>1</sup>It is still an open question if the islands observed in the exclusion plots shrink to zero size or not.

<sup>2</sup>This result is sometimes called the Aks theorem. However, since it relies on some unproven assumptions that we discuss in detail below, its status is still not completely solid.

## Chapter 2. An analytical toolkit for the S-matrix bootstrap

---

an elegant interplay between analyticity, elastic unitarity and crossing symmetry.

The simplest non-trivial S-matrix element is a  $2 \rightarrow 2$  connected scattering amplitude  $T(s, t)$  as a function of Mandelstam invariants  $s$  and  $t$ . In a gapped theory, this amplitude is subject to an exact non-linear equation called *elastic unitarity*. This equation originates from the fact that when we scatter the lightest particles in the theory at energies below the first multi-particle threshold ( $s_0$ ), only two particles can be produced in the final state.<sup>3</sup> As a result, unitarity of the S-matrix becomes a non-linear equation satisfied by  $T(s, t)$  for  $4m^2 < s < s_0$ . It is the purpose of the present chapter to revisit the implications of elastic unitarity, when combined with crossing and analyticity, on the structure of the nonperturbative amplitude  $T(s, t)$ .

One motivation for our analysis is recent numerical investigations of higher-dimensional scattering in [1, 23]. In these works elastic unitarity was not imposed and it was observed that various bootstrap bounds tend to be saturated by purely elastic functions. It is therefore an interesting, open question how to efficiently implement elastic unitarity and particle production in the current S-matrix bootstrap program. An obvious way to tackle the problem is to include higher-point amplitudes in the bootstrap analysis explicitly. However, due to unknown and complicated analytic properties of higher-dimensional amplitudes it is not clear if it is feasible in  $d \geq 3$ . Another possible way to make progress, which we will follow in the present work, is to focus on how to implement structures of the amplitude that are dictated by elastic unitarity into the current numerical approach of [1, 23]. In this way we hope to be able to zoom in closer on the physical higher-dimensional S-matrices and, if we are lucky, maybe eventually solve them. We start by laying out our assumptions that serve as the basis for the further analytic study.

### 2.1.1 Assumptions

We assume that in the far past and in the far future states of the system are described by a set of free particles. The Hilbert space therefore is taken to be the Fock space of free particles.<sup>4</sup> For simplicity we assume that the spectrum contains a single scalar particle of mass  $m$  together with its multi-particle states. Under these conditions it has been rigorously proven that the amplitude satisfies:

1. **Crossing symmetry:** for scattering of identical particles we have

$$T(s, t) = T(t, s) = T(u, t), \quad s + t + u = 4m^2. \quad (2.1.1)$$

---

<sup>3</sup>As such elastic unitarity is absent in theories with massless particles. Similarly, there is no elastic unitarity in CFTs.

<sup>4</sup>To the best of our knowledge this assumption, known as *asymptotic completeness*, does not follow from the non-zero gap and Wightman axioms, see e.g. [24].

2. **Real analyticity:** for scattering of identical particles we have

$$T(s^*, t^*) = T^*(s, t) . \quad (2.1.2)$$

Our extra assumptions for the connected two-to-two scattering amplitude  $T(s, t)$ , which have not been rigorously established, are the following:

3. **Extended analyticity:**  $T(s, t)$  is an analytic function for complex  $s$  and  $t$  in some region  $\mathcal{D}$ , except for potential poles in  $0 < s < 4m^2$  and a cut starting at  $s = 4m^2$ , as well as images of these singularities under crossing. We will often assume that the region of analyticity  $\mathcal{D}$  extends to the full complex  $s$ -plane ( $t$ -plane) for some finite region in  $t$ -plane ( $s$ -plane), but many of our arguments can be adopted to the situation when  $\mathcal{D}$  is bounded in both variables simultaneously.<sup>5</sup> As usual,  $T(s, t)$  stands for the analytic continuation of the amplitude from the physical regime to the principle sheet – without going through the multi-particle cuts.

4. **Polynomial Boundedness:** for fixed  $t$

$$|T(s, t)| < |s|^{J_0(t)} , \quad |s| \rightarrow \infty , \quad (s, t) \in \mathcal{D} . \quad (2.1.3)$$

The formula above assumes that  $\mathcal{D}$  includes  $s = \infty$  for fixed  $t$ . More generally, we will assume that the amplitude is polynomially bounded on the principal sheet (away from the bound states poles and multi-particle thresholds).

We also have two extra technical assumptions:

5. **Continuity:** partial waves  $f_j(s)$  are real analytic functions in the elastic region  $4m^2 < s < s_0$ .<sup>6</sup>
6.  **$\mathbb{Z}_2$  symmetry and no bound states:** for simplicity we assume no bound states in the spectrum. We also assume that we have a single stable particle of mass  $m$  which is odd under  $\mathbb{Z}_2$  symmetry. Therefore only an even number of particles can be produced in the scattering of two particles.

In section 2.2 we review basics of the two-to-two scattering amplitude. We consider scattering of identical scalar particles and briefly review known analyticity results. We discuss unitarity and elastic unitarity in terms of  $T(s, t)$ . We introduce partial wave expansion and the Froissart-Gribov formula. We briefly discuss continuity properties of  $T(s, t)$ .

<sup>5</sup>If  $\mathcal{D} = \mathbb{C}^2$  one says that the function is maximally analytic. Maximal analyticity is not necessary for the present work.

<sup>6</sup>This is closely related to what is called absence of pathologies a-la A. Martin [25]. We discuss it in more detail in section 2.2.5.

## Chapter 2. An analytical toolkit for the S-matrix bootstrap

---

In section 2.3 we consider analytic continuation of elastic unitarity. We first review the derivation of the Mandelstam equation for the double spectral density  $\rho(s, t)$ , or equivalently double discontinuity of  $T(s, t)$ , based on analytic continuation of elastic unitarity in one of the Mandelstam variables ( $s$  or  $t$ ). We then discuss its relation to analytic continuation of partial waves in spin  $J$  via the Froissart-Gribov formula. We also consider analytic continuation of elastic unitarity in energy  $s$ . Finally, we exhibit the structure of the Landau-Karplus curves along which the double spectral density develops a nontrivial support in the elastic region.

We then analyze various implications of elastic unitarity:

- In section 2.4 we discuss positivity properties of double spectral density  $\rho(s, t)$ . We review the argument that scattering implies production in  $d \geq 3$ . This result follows from the combination of crossing symmetry and positivity of  $\rho(s, t)$ .
- In section 2.5 we introduce the notion of the threshold expansion for partial waves, as well as for the first and second discontinuities of the scattering amplitude. The threshold expansion of partial waves and the discontinuity of the scattering amplitude is a consequence of elastic unitarity and it describes low-energy or non-relativistic scattering. The Mandelstam equation then maps it to the expansion of double spectral density close to the boundary of its nontrivial support, the so-called Kaplus-Landau curve.
- In section 2.6 we map the threshold expansion in the  $t$ -channel to the large  $J$  expansion of partial wave coefficients in the  $s$ -channel. It comes from “inversion” of the threshold expansion via the Froissart-Gribov formula. Turning to the  $\frac{1}{J}$  corrections we find that remarkably the computations can be sometimes done exactly in  $\frac{1}{J}$ .
- In section 2.7 we turn the large  $J$  results into finite  $J$  predictions plus an error estimate. This error estimate is deduced from a local bound on the discontinuity of the amplitude in the region  $s, t > 4m^2$ . No such rigorous bound is known. We discuss natural error estimates and perform the finite spin, finite energy computations in a simple toy model.

In section 2.8 we consider the modern numerical approach to the S-matrix bootstrap following [1]. We discuss why and what should be improved in the existing approach. We suggest several ways in which this approach can be improved. In particular, we discuss various ways to implement elastic unitarity numerically. In section 2.9 we briefly comment on the relation between the present analysis and similar ideas in the conformal bootstrap. Finally, in section 2.10 we conclude and present some future directions. Several appendices contain technical details that should be helpful in understanding the details of our arguments and calculations.

## 2.2 Amplitude Basics

In this section we briefly review the basic kinematics of the two-to-two scattering of identical, scalar particles to set the conventions for the further analysis. We will repeat some definitions that were presented in chapter 1 with additional rigor.

As usual we write the  $S$ -matrix as

$$\hat{S} \equiv \hat{\mathbf{1}} + i \hat{T}, \quad (2.2.1)$$

where  $\hat{T}$  is zero in the theory of a free massive scalar. We are interested in the matrix elements that describe two-to-two scattering

$$S_{2,2}(p_3, p_4 | p_1, p_2) \equiv \langle p_3, p_4 | \hat{S} | p_2, p_1 \rangle, \quad (2.2.2)$$

where the initial and final states are characterized by the on-shell momenta

$$p^2 = \vec{p}^2 - (p^0)^2 = -m^2, \quad \vec{p}^2 = \sum_{i=1}^{d-1} (p^i)^2, \quad p^0 > 0. \quad (2.2.3)$$

As in (2.2.1) we can separate the contribution of the disconnected and connected parts of the  $S$ -matrix

$$S_{2,2}(p_3, p_4 | p_1, p_2) = S_{1,1}(p_3 | p_1) S_{1,1}(p_4 | p_2) + S_{1,1}(p_4 | p_1) S_{1,1}(p_3 | p_2) + S_{2,2}^c(p_3, p_4 | p_1, p_2). \quad (2.2.4)$$

The disconnected part is given by an overlap of the one particle states which is uniquely fixed by Lorentz symmetry

$$S_{1,1}(p | q) = \mathbf{1}_{1,1}(p | q) = 2(2\pi)^{d-1} \sqrt{\vec{p}^2 + m^2} \times \delta^{d-1}(\vec{p} - \vec{q}), \quad (2.2.5)$$

The connected part is the main object of our interest

$$S_{2,2}^c(p_3, p_4 | p_1, p_2) \equiv i \langle p_3, p_4 | \hat{T} | p_2, p_1 \rangle = i(2\pi)^d \delta^d(p_1 + p_2 - p_3 - p_4) T(s, t). \quad (2.2.6)$$

In the formula above we introduced Mandelstam invariants

$$\begin{aligned} s &= -(p_1 + p_2)^2 = 4(m^2 + \vec{p}^2), \\ t &= -(p_1 - p_3)^2 = -2\vec{p}^2(1 - \cos\theta), \\ u &= -(p_1 - p_4)^2 = -2\vec{p}^2(1 + \cos\theta), \end{aligned} \quad (2.2.7)$$

where in the last equality we wrote their form in the center-of-mass frame,  $p_1 = (m, \vec{p})$ ,  $p_2 = (m, -\vec{p})$ . Here,

$$\cos\theta = 1 + \frac{2t}{s - 4m^2}, \quad (2.2.8)$$

## Chapter 2. An analytical toolkit for the S-matrix bootstrap

---

is cosine of the scattering angle. Only two of the Mandelstam invariant are independent while the third is related to the other two through the relation

$$s + t + u = 4m^2 . \quad (2.2.9)$$

From above, the dimension of the amplitude is

$$[T(s, t)] = m^{4-d} . \quad (2.2.10)$$

### 2.2.1 Analyticity

In the discussion above scattering matrix elements were defined for physical momenta that correspond to actual scattering. The starting point of the S-matrix considerations is the statement that the physical matrix element  $T(s, t)$  is a boundary value of an analytic function of the relativistic invariants regarded as complex variables

$$T(s, t) = \lim_{\epsilon \rightarrow 0} T(s + i\epsilon, t) , \quad (2.2.11)$$

where we assumed  $s$  and  $t$  to be real and  $-(s - 4m^2) < t < 0$ ,  $4m^2 < s$ . This corresponds to scattering in the  $s$ -channel  $1, 2 \rightarrow 3, 4$ . Using the basic principles of QFT correlation functions, reduction formulas that relate them to the S-matrix elements, and techniques of analytic completion one can establish various analytic properties of the scattering amplitudes as functions of complex  $s$  and  $t$ , see e.g. [26, 27, 9] for a pedagogical exposition.

The first result of this type is subtracted dispersion relations in  $s$  for fixed  $-t_0 < t \leq 0$  in the physical  $s$ -channel region [27, 28]. In this case one has to understand analytic properties of  $T(s, t)$  as a function of complex  $s$ . For the case of  $\pi^0\pi^0 \rightarrow \pi^0\pi^0$  scattering, for which our treatment applies directly, one can show that  $T(s, t)$  is an analytic function of  $s$  with two cuts:  $s > 4m^2$  and  $u > 4m^2$ , with  $t_0 = 28m^2$ . See Table 1 of [27] for the processes for which a fixed- $t$  dispersion relation has been proven and the corresponding values of  $t_0$ .<sup>7</sup>

Another well-known property, originally due to Lehmann [30], concerns analytic properties of  $T(s, t)$  as a function of  $t$  for fixed physical  $s > 4m^2$ . Lehmann showed that  $T(s, \cos\theta)$  is analytic inside an ellipse, the so-called Lehmann ellipse, in the  $\cos\theta$  complex plane with foci at  $\cos\theta = \pm 1$  and semi-major axis  $\cos\theta_{sL} > 1$  which depends on the details of the theory, energy and masses of particles, as well as the scattering process. Lehmann also showed that the absorptive part or discontinuity of the amplitude  $\text{Disc}_s T(s, \cos\theta)$  is analytic in a larger ellipse, the so-called large Lehmann ellipse, with a semi-major axis  $\cos\theta_{LL} = 2\cos^2\theta_{sL} - 1$ .

The third class of results concerns analyticity of  $T(s, t)$  when both  $s$  and  $t$  are complex. Bros, Epstein and Glaser [31] showed that any point  $(s, \cos\theta)$  in the physical region is surrounded by

---

<sup>7</sup>The cases for which a dispersion relation has not been proven, baryon-baryon scattering for instance [27], still enjoy a domain of analyticity that connects the  $s$ - and  $u$ -channel cuts. Thus, the property of crossing (see below) can still be established for these cases [29].



an analyticity neighborhood whose precise form is not known in general, see e.g. [9] for details. An explicit domain of simultaneous analyticity in both variables was derived by Lehmann [32] for elastic processes that obey a fixed- $t$  dispersion relation by continuing the Lehmann ellipse to complex  $s$ . For cases with single variable dispersion relations in all three channels (as in  $\pi\pi \rightarrow \pi\pi$  scattering), Mandelstam [33] derived domains of the form  $|s t| < b$  for any complex  $s$  and  $t$  outside the single variable dispersion relation cuts. For pion scattering the largest domain occurs for  $b = 256m_\pi^4$ . These domains have the drawback that when  $s \rightarrow \infty$  the Lehmann domain shrinks to the line  $-t_0 < t < 0$  and the Mandelstam domain shrinks to the point  $t = 0$ .

Based on the results above, the analyticity domain was further enlarged using unitarity by A. Martin [34]. The final result is that the amplitude is analytic within  $|t| < R$  and  $s$  cut-plane. For scattering of identical particles that we consider in the present chapter  $R = 4m^2$ . From this result the standard bounds on high energy behavior of the amplitudes follow. It also follows that for  $|t| < 4m^2$  the scattering amplitude admits fixed  $t$  dispersion relations with at most two subtractions.

Finally, let us introduce the notion of maximal analyticity (or Mandelstam analyticity) which states that the scattering amplitude is analytic in the  $(s, t)$  complex planes with only singularities on the principal sheet being unitarity cuts  $s, t, u > 4m^2$  and bound state poles for  $0 < s, t, u < 4m^2$ . This property is consistent, at least for the scattering of lightest particles in the theory, with expectations from unitarity and analysis of perturbation theory. However it is important to keep in mind that it has not been proven. The original attempts to prove maximal analyticity in perturbation theory [35] were later found to have a loophole [36] which, to the best of our knowledge, has never been closed even for the scattering of lightest particles. In this chapter we freely assume analyticity beyond what has been rigorously proven but we do not assume maximal analyticity.

There are two other properties that we will use. One is crossing

$$T(s, t) = T(t, s) = T(u, t) , \tag{2.2.12}$$

which states that in particular that scattering in different channels is described by different boundary values of a single analytic function. For the two-to-two scattering it has been proven in [29]. Beyond the two-to-two scattering only a partial progress has been achieved [37]. Another property is real analyticity

$$T(s^*, t^*) = T^*(s, t) . \tag{2.2.13}$$

This was established within axiomatic quantum field theory in [38]. For the S-matrix argument see e.g. [8].

Finally, let us also mention in a related context the result by A. Martin [39] who showed that maximal analyticity in the form of the Mandelstam representation together with knowledge

## Chapter 2. An analytical toolkit for the S-matrix bootstrap

---

of the double spectral density in the elastic region fix the scattering amplitude completely. Similarly, knowledge of the amplitude at fixed energy in the elastic region as a function of the scattering angle is believed to fix it almost completely, see e.g. [40].

### 2.2.2 Unitarity and Elastic Unitarity

In terms of the  $T$ -matrix, the unitarity of the  $S$ -matrix  $\hat{S} \cdot \hat{S}^\dagger = \hat{\mathbf{1}}$  reads

$$\begin{aligned} \frac{1}{i} \langle p_3, p_4 | \hat{T} - \hat{T}^\dagger | p_2, p_1 \rangle &= \langle p_3, p_4 | \hat{T} \cdot \hat{T}^\dagger | p_2, p_1 \rangle \\ &= \sum_{n=1}^{\infty} \int d\mu(q_1, \dots, q_{2n}) \langle p_3, p_4 | \hat{T} | \{q_i\}_{i=1}^{2n} \rangle \langle \{q_i\}_{i=1}^{2n} | \hat{T}^\dagger | p_2, p_1 \rangle, \end{aligned} \quad (2.2.14)$$

where in the second line we have inserted a complete basis of asymptotic states and the Lorentz invariant measure is

$$d\mu(p_1, \dots, p_n) \equiv \frac{1}{n!} \prod_{i=1}^n d\mu(p_i), \quad d\mu(p) \equiv \frac{1}{(2\pi)^{d-1}} \theta(p^0) \delta(p^2 + m^2) d^d p. \quad (2.2.15)$$

Due to the momentum conservation, a  $2n$ -particle intermediate state can only contribute if  $s > (2nm)^2$ . Otherwise, there is not enough energy to create an on-shell state with  $2n$  particles. In particular, for  $4m^2 < s < 16m^2$ , only two particle states are possible. Hence, in that regime we can replace the sum in (2.2.14) by the first term and the equation closes on the  $2 \rightarrow 2$  transitions only. This is the elastic unitarity regime. Explicitly, we have

$$2T_s(s, t) = \frac{1}{2} \int \frac{d^{d-1} \vec{q}'}{(2\pi)^{d-1} (2E_{\vec{q}'})} \int \frac{d^{d-1} \vec{q}''}{(2\pi)^{d-1} (2E_{\vec{q}''})} (2\pi)^d \delta^d(p_1 + p_2 - q' - q'') T^{(+)}(s, t') T^{(-)}(s, t''), \quad (2.2.16)$$

where we have introduced the notations

$$T^{(\pm)} \equiv \lim_{\epsilon \rightarrow 0} T(s \pm i\epsilon, t), \quad T_s(s, t) = \text{Disc}_s T(s, t) \equiv \frac{1}{2i} (T^{(+)}(s, t) - T^{(-)}(s, t)), \quad (2.2.17)$$

and  $t' = -(\vec{p}_1 - \vec{q}')^2$ ,  $t'' = -(\vec{q}'' - \vec{p}_4)^2$ . In writing the above we used real analyticity of the amplitude (2.2.13). Finally, the overall factor of one half is a symmetry factor for identical bosons.

We will now reduce the integral to an integration over the two scattering angles by performing all the kinematical integrations explicitly. For that aim, we first go to the center of mass frame where  $\vec{q}' = -\vec{q}'' \equiv p \vec{n}$ , where  $\vec{n}$  is a unit  $d-1$  vector and  $p = \sqrt{s - 4m^2}/2$ . In these variables the elastic unitarity constraint (2.2.16) becomes

$$2T_s(s, t) = \frac{p^{d-2}}{(2\pi)^{d-2} (2E_p)^2} \frac{E_p}{4p} \int d^{d-2} \Omega_{\vec{n}} T^{(+)}(s, t') T^{(-)}(s, t''), \quad (2.2.18)$$

where  $\frac{E_p}{2p} = \frac{\sqrt{s}}{2\sqrt{s-4m^2}}$  is the Jacobian coming from the energy conservation delta-function. The integrand only depends on the two scattering angles

$$z' = \cos\theta' = \frac{\vec{p}_1 \cdot \vec{n}}{|\vec{p}_1|} \quad \text{and} \quad z'' = \cos\theta'' = \frac{\vec{p}_3 \cdot \vec{n}}{|\vec{p}_3|}, \quad (2.2.19)$$

in terms of which we can write the measure as

$$\int d^{d-2}\Omega_{\vec{n}} \equiv \int_{-1}^1 dz' \int_{-1}^1 dz'' \mathcal{P}_d(z, z', z'') \quad \text{where} \quad z = \cos\theta = \frac{\vec{p}_1 \cdot \vec{p}_3}{|\vec{p}_1||\vec{p}_3|} = 1 + \frac{2t}{s-4m^2}, \quad (2.2.20)$$

is the cosine of the external scattering angle. We find that (see appendix A.1 for more details)

$$\begin{aligned} \mathcal{P}_3(z, z', z'') &= 2\sqrt{1-z^2} \delta(1-z^2-z'^2-z''^2+2zz'z''), \quad (2.2.21) \\ \mathcal{P}_{d>3}(z, z', z'') &= \frac{2\pi^{\frac{d-3}{2}}}{\Gamma\left(\frac{d-3}{2}\right)} (1-z^2)^{\frac{4-d}{2}} \frac{\Theta(1-z^2-z'^2-z''^2+2zz'z'')}{(1-z^2-z'^2-z''^2+2zz'z'')^{\frac{5-d}{2}}}. \end{aligned}$$

Using that  $E_k = \sqrt{s}/2$ , we can write (2.2.18) covariantly as

$$T_s(s, t) = \frac{(s-4m^2)^{\frac{d-3}{2}}}{8(4\pi)^{d-2}\sqrt{s}} \int_{-1}^1 dz' \int_{-1}^1 dz'' \mathcal{P}_d(z, z', z'') T^{(+)}(s, t(z')) T^{(-)}(s, t(z'')), \quad 4m^2 \leq s \leq 16m^2, \quad (2.2.22)$$

where  $t(x) \equiv -(s-4m^2)(1-x)/2$ , not to be confused with the external momentum transfer  $t$ , which is held fixed. The step/delta function in the phase space integration kernel  $\mathcal{P}_d(z, z', z'')$  has a simple geometrical origin, see figure 2.1.

For  $s > 16m^2$  and general  $t$  the unitarity constraint involves scattering elements with more than two particles. To get a constraint on the two particle amplitude, we note that  $\hat{T} \cdot \hat{T}^\dagger$  on the right hand side of (2.2.14) is a positive semi-definite matrix. Hence, for any state  $\Psi$  we have that

$$\langle \Psi | \hat{T} | \{q_i\}_{i=1}^{2n} \rangle \langle \{q_i\}_{i=1}^{2n} | \hat{T}^\dagger | \Psi \rangle = |\langle \Psi | \hat{T} | \{q_i\}_{i=1}^{2n} \rangle|^2 \geq 0, \quad (2.2.23)$$

and hence, if we drop all the contributions with more than two particles in (2.2.14) we get an inequality for the  $2 \rightarrow 2$  scattering matrix

$$\begin{aligned} &\frac{1}{i} \int d\mu(p_1, p_1) d\mu(p_3, p_4) \psi(p_1, p_2) \psi^*(p_3, p_4) \times \langle p_3, p_4 | \hat{T} - \hat{T}^\dagger | p_2, p_1 \rangle \quad (2.2.24) \\ &\geq \int d\mu(p_1, p_1) d\mu(p_3, p_4) \psi(p_1, p_2) \psi^*(p_3, p_4) \times \int d\mu(q_1, q_2) \langle p_3, p_4 | \hat{T} | q_1, q_2 \rangle \langle q_1, q_2 | \hat{T}^\dagger | p_2, p_1 \rangle \geq 0. \end{aligned}$$

For example, if we pick a wave function that consists of two particles with a specific momenta then we have the the amplitude in the forward limit where  $p_3 = p_1$  and  $p_4 = p_2$ . For this choice

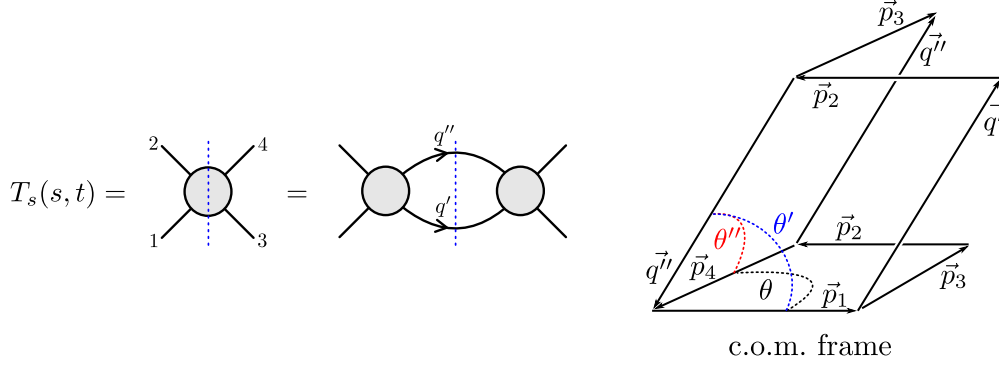


Figure 2.1: In the elastic strip  $4m^2 < s < 16m^2$  the discontinuity of the amplitude comes from two intermediate particle exchange only. This result in the exact elastic unitarity equation (2.2.22). The corresponding phase space integration kernel  $\mathcal{P}_d(\cos\theta, \cos\theta', \cos\theta'')$  in (2.2.21) is proportional to a step/delta function which has a simple geometrical origin. In the center of mass frame we have three  $(d-1)$ -dimensional vectors,  $\vec{p}_1 = -\vec{p}_2$ ,  $\vec{p}_3 = -\vec{p}_4$ , and  $\vec{q}' = -\vec{q}''$ . The geometrical angles between these three vectors,  $\{\theta, \theta', \theta''\}$  are therefore restricted to the range  $\theta_1 + \theta_2 \geq \theta_3$ , where  $\theta_{1,2,3}$  are any permutation of  $\{\theta, \theta', \theta''\}$ .

of wave function, the unitarity constraint (2.2.24) becomes<sup>8</sup>

$$\begin{aligned}
 T_s(s, 0) &\geq \frac{(s-4m^2)^{\frac{d-3}{2}}}{8(4\pi)^{d-2}\sqrt{s}} \int_{-1}^1 dz' \int_{-1}^1 dz'' \mathcal{P}_d(1, z', z'') T^{(+)}(s, t(z')) T^{(-)}(s, t(z'')) \\
 &\propto \int_{-1}^1 dz' (1-z'^2)^{\frac{d-4}{2}} |T^{(+)}(s, t(z'))|^2, \quad s \geq 16m^2, \quad (2.2.26)
 \end{aligned}$$

where we used that  $\mathcal{P}_d(1, z', z'') \propto \delta(z' - z'')$ , see (A.2.7) for the precise formula. We also used that  $T^{(-)}(s, t(z')) = (T^{(+)}(s, t(z')))^*$  for  $-1 \leq z' \leq 1$ .

### 2.2.3 Partial Wave Expansion

Unitarity of the S-matrix implies the non-linear integral relations that the  $2 \rightarrow 2$   $T$ -matrix has to satisfy, (2.2.22) and (2.2.24). To simplify these complicated constraints we choose a wave function  $\Psi$  that diagonalizes the  $T$ -matrix and therefore also the integral kernel in (2.2.22), (2.2.24). This can be done using the Lorentz symmetry of the problem. Namely, we decompose the amplitude  $T(s, t)$  in a complete basis of intermediate states which transform in irreducible representations of the  $SO(1, d-1)$  symmetry. These representations are characterised by their energy and the little group  $SO(d-1)$  angular momentum in the center of mass frame,  $E$  and  $J$ . For two particle states the  $SO(1, d-1)$  quantum numbers are enough to characterize the

<sup>8</sup>The unitarity relation in the forward limit is nothing but the optical theorem. In  $d$  dimensions it takes the form

$$T_s(s, 0) = \text{Im}[T(s, 0)] = \sqrt{s(s-4m^2)} \sigma_{tot}(s), \quad (2.2.25)$$

where  $\sigma_{tot}(s)$  is the total cross-section, of dimension  $[\sigma(s)] = L^{d-2}$ .

states and we have

$$\langle p_1, p_2 | p, J, \vec{m} \rangle \propto \delta^d(p - p_1 - p_2) Y_{J, \vec{m}}^{(d)}(\hat{p}_1), \quad (2.2.27)$$

where  $p^2 = E^2$ ,  $Y_{J, \vec{m}}^{(d)}$  are the  $d$ -dimensional spherical harmonics, and the energies dependant pre-factor will not be relevant for us.<sup>9</sup> We can now insert a complete basis to these states to decompose the S-matrix element  $\langle p_3, p_4 | \hat{T} | p_1, p_2 \rangle$  in all possible spins. Since the operator  $\hat{T}$  is both, translation and  $SO(1, d-1)$  invariant, due to the Wigner-Eckart theorem we have that

$$f_J(p^2) \propto \frac{\langle p, J, \vec{m} | \hat{T} | p, J, \vec{m} \rangle}{\langle p, J, \vec{m} | p, J, \vec{m} \rangle}, \quad (2.2.28)$$

where the convention-dependent proportionality factor is independent of the energy and and the angular momentum  $\vec{m}$ . These functions are the so-called partial wave coefficients, in terms of which the amplitude takes the form

$$T(s, t) = \sum_{J=0}^{\infty} n_J^{(d)} f_J(s) P_J^{(d)}(\cos\theta), \quad (2.2.29)$$

where the sum runs over all (even) spins and  $n_J^{(d)}$  are convention-dependent normalization factors. Here,  $P_J^{(d)}(\cos\theta)$  are the partial waves. They represents the angular dependence of the amplitude due to the exchange of all the states with spin  $J$ . A simple way of determining these functions is to go to the center of mass frame and act with the  $SO(d-1)$  quadratic Casimir on the two outgoing particle, while holding the momentum of the two incoming particles fixed. This equation takes the form

$$\left[ (1-z^2)^{\frac{4-d}{2}} \frac{d}{dz} (1-z^2)^{\frac{d-2}{2}} \frac{d}{dz} + J(J+d-3) \right] P_J^{(d)}(z) = 0, \quad (2.2.30)$$

where  $z = \cos\theta$  is cosine of the scattering angle (2.2.20). This second order differential equation has two independent solutions. Spin  $J$  unitary representations are composed of states with angular momentum in the plane of scattering ranging between  $-J$  and  $J$ . Hence, the corresponding solution of (2.2.30) is a degree  $J$  polynomial of  $\cos\theta$  that is given by

$$P_J^{(d)}(z) = {}_2F_1\left(-J, J+d-3, \frac{d-2}{2}, \frac{1-z}{2}\right). \quad (2.2.31)$$

The partial wave coefficients can be extracted from the amplitude using the orthogonality relation of these polynomials

$$\frac{1}{2} \int_{-1}^1 dz (1-z^2)^{\frac{d-4}{2}} P_J^{(d)}(z) P_{\bar{J}}^{(d)}(z) = \frac{\delta_{J\bar{J}}}{\mathcal{N}_d n_J^{(d)}}. \quad (2.2.32)$$

<sup>9</sup>For  $d = 4$  the factor is  $\sqrt{\frac{E_{\vec{p}}}{|\vec{p}_1| E_{\vec{p}_1} E_{\vec{p}_2}}}$ , see [6] for details.

## Chapter 2. An analytical toolkit for the S-matrix bootstrap

---

Here we have chosen the convention

$$\mathcal{N}_d = \frac{(16\pi)^{\frac{2-d}{2}}}{\Gamma\left(\frac{d-2}{2}\right)}, \quad n_J^{(d)} = \frac{(4\pi)^{\frac{d}{2}}(d+2J-3)\Gamma(d+J-3)}{\pi\Gamma\left(\frac{d-2}{2}\right)\Gamma(J+1)}, \quad (2.2.33)$$

for which the unitarity constraint presented below takes a simple form. In this convention we have

$$f_J(s) = \frac{\mathcal{N}_d}{2} \int_{-1}^1 dz (1-z^2)^{\frac{d-4}{2}} P_J^{(d)}(z) T(s, t(z)). \quad (2.2.34)$$

Because the S-matrix is diagonal in the spin basis, so does the unitarity constraint. We consider first the elastic regime  $4m^2 < s < 16m^2$  where this constraint takes the form (2.2.22). Using (2.2.34), we project both sides to a fixed spin  $J$ . On the left hand side we find the discontinuity of the partial wave coefficient. Real analyticity (2.2.13) of  $T(s, t)$  leads to real analyticity of  $f_J$

$$f_J(s^*) = f_J^*(s). \quad (2.2.35)$$

Hence, the discontinuity of the partial wave is equal to the imaginary part  $\frac{1}{2i}(f_J(s+i\epsilon) - f_J(s-i\epsilon)) = \text{Im}f_J(s)$ . On the right hand side, it is useful to first represent the kernel as a sum over partial waves of  $z_1, z_2$  and  $z$ . Because this kernel represents the angular integration in (2.2.18), its partial wave decomposition must also be diagonal in spin. It takes the form (see appendix A.2).

$$\mathcal{P}_d(z, z', z'') = (4\pi)^{d-2} \mathcal{N}_d^2 (1-z'^2)^{\frac{d-4}{2}} (1-z''^2)^{\frac{d-4}{2}} \sum_{J=0}^{\infty} n_J^{(d)} P_J^{(d)}(z) P_J^{(d)}(z') P_J^{(d)}(z''), \quad (2.2.36)$$

Using (2.2.34) for the three integrals and real analyticity (2.2.35), we arrive at the elastic unitarity constraint

$$\boxed{2\text{Im}f_J(s) = \frac{(s-4m^2)^{\frac{d-3}{2}}}{\sqrt{s}} |f_J(s)|^2}, \quad (2.2.37)$$

or equivalently

$$|S_J(s)| = 1, \quad \text{with} \quad S_J(s) \equiv 1 + i \frac{(s-4m^2)^{\frac{d-3}{2}}}{\sqrt{s}} f_J(s). \quad (2.2.38)$$

Here 1 can be traced back to  $\hat{\mathbf{1}}$  in (2.2.1). In this way the trivial unitary S-matrix  $\hat{S} = \hat{\mathbf{1}}$  becomes  $S_J = 1$  in the partial wave basis.

The solution to this is

$$f_J(s) = \frac{\sqrt{s}}{(s-4m^2)^{\frac{d-3}{2}}} i(1 - e^{2i\delta_J(s)}), \quad (2.2.39)$$

with  $\delta_J(s)$  being real for  $4m^2 < s < 16m^2$  and is called the scattering phase.

Similarly to the above, for  $s > 16m^2$  we chose  $\psi(p_1, p_2) = \langle p_1, p_2 | p, J, \vec{m} \rangle$  in (2.2.24). In that way we arrive at the same equation, but with an inequality instead of an equality

$$2\text{Im}f_J(s) \geq \frac{(s - 4m^2)^{\frac{d-3}{2}}}{\sqrt{s}} |f_J(s)|^2. \quad (2.2.40)$$

or equivalently,  $|S_J(s)| \leq 1$ ,  $\text{Im}[\delta_J(s)] \geq 0$ .

We close this section with a short discussion on the range of convergence of the partial wave sum (2.2.29) for fixed physical  $s$  as a function of  $\cos\theta$ .<sup>10</sup> It is a well-known fact that the amplitude  $T(s, \cos\theta)$  is analytic inside the small Lehmann-Martin ellipse and its absorptive part,  $T_s(s, \cos\theta)$  is analytic inside the large Lehmann-Martin ellipse. These ellipses have foci at  $\cos\theta = \pm 1$  and semi-major axis  $z_{\text{small}}$  and  $z_{\text{large}}$ . Correspondingly, inside these ellipses the sum (2.2.29) and its discontinuity converge.

In the case of scattering of identical lightest particles which is our main interest we have

$$z_{\text{small}} = 1 + \frac{8m^2}{s - 4m^2}, \quad z_{\text{large}} = 2z_{\text{small}}^2 - 1 = 1 + \frac{32m^4}{(s - 4m^2)^2}. \quad (2.2.42)$$

In section 2.4.1 we will see that extended analyticity, elastic unitarity and crossing imply that the partial wave expansion converges in a larger region.

## 2.2.4 Froissart-Gribov Formula

The Froissart-Gribov formula is a representation of the partial wave coefficients in terms of the discontinuity of the amplitude. It has multiple applications and, in particular, it allows us to analytically continue partial wave coefficients in spin. Correspondingly, in section 2.3.3 we will use the Froissart-Gribov formula to analytically continue elastic unitarity in spin. It will also allow us to better understand the analytic structure of the amplitude in the Mandelstam invariants and relate the threshold expansion, see section 2.5, to the large spin expansion, see section 2.6.

<sup>10</sup> The convergence of the partial wave expansion can be seen using Neumann's argument [41]. Consider a function  $f(z)$  analytic inside some region  $\mathcal{C}$  which includes the  $[-1, 1]$  interval. We can then write

$$f(z) = \oint_{\gamma} \frac{dt}{2\pi i} \frac{f(t)}{t-z} = \oint_{\gamma} \frac{dt}{2\pi i} \sum_{J=0}^{\infty} n_J^{(d)} P_J^{(d)}(z) \left( \mathcal{N}_d(t^2 - 1)^{\frac{d-4}{2}} Q_J^{(d)}(t) f(t) \right) = \sum_{J=0}^{\infty} n_J^{(d)} f_J P_J^{(d)}(z), \quad (2.2.41)$$

where  $\gamma \in \mathcal{C}$  is some contour that wraps the interval  $[-1, 1]$  counterclockwise and contains  $z$  inside the integration contour. To exchange the summation and integration, we also used that given  $z$ ,  $\frac{1}{t-z} = \mathcal{N}_d(t^2 - 1)^{\frac{d-4}{2}} \sum_{J=0}^{\infty} n_J^{(d)} P_J^{(d)}(z) Q_J^{(d)}(t)$  converges uniformly in  $t$  as long as  $t$  is outside the ellipse with foci at  $-1$  and  $1$  that passes through  $z$ . We also used the relation between  $Q_J^{(d)}(z)$  and  $P_J^{(d)}(z)$  which will be explained below, see (2.2.46). Therefore, the partial wave expansion (2.2.41) converges when  $z$  is inside the ellipse with foci at  $-1$  and  $1$  and  $\in \mathcal{C}$ . Note therefore that the size of the domain of convergence of the partial wave expansion can be less than the analyticity domain  $\mathcal{C}$ .

## Chapter 2. An analytical toolkit for the S-matrix bootstrap

---

Let us introduce the Gegenbauer  $Q$ -functions. These are given by the second linearly independent solution of the second order Casimir equation (2.2.30). They are uniquely fixed by their asymptotic behavior

$$\lim_{|z| \rightarrow \infty} Q_J^{(d)}(z) = \frac{c_J^{(d)}}{z^{J+d-3}} + \dots, \quad (2.2.43)$$

where  $c_J^{(d)}$  is a normalization constant. The corresponding  $Q$ -function is

$$Q_J^{(d)}(z) = \frac{c_J^{(d)}}{z^{J+d-3}} {}_2F_1\left(\frac{J+d-3}{2}, \frac{J+d-2}{2}, J + \frac{d-1}{2}, \frac{1}{z^2}\right). \quad (2.2.44)$$

Our convention is

$$c_J^{(d)} = \frac{\sqrt{\pi} \Gamma(J+1) \Gamma(\frac{d-2}{2})}{2^{J+1} \Gamma(J + \frac{d-1}{2})}. \quad (2.2.45)$$

The  $Q$ -function has a cut running between  $z = -1$  and  $z = 1$ . The fact that there are only two independent solutions to the Casimir equation means that the discontinuity of  $Q$  can be expressed in terms of  $Q$  and  $P$ . The precise relation takes the form

$$\text{Disc}_z(z^2 - 1)^{\frac{d-4}{2}} Q_J^{(d)}(z) = -\frac{\pi}{2} (1 - z^2)^{\frac{d-4}{2}} P_J^{(d)}(z), \quad z \in [-1, 1], \quad (2.2.46)$$

or equivalently (for integer  $J$ )

$$Q_J^{(d)}(z) = \frac{1}{2} \int_{-1}^1 dz' \left( \frac{1 - z'^2}{z^2 - 1} \right)^{\frac{d-4}{2}} \frac{P_J^{(d)}(z')}{z - z'}. \quad (2.2.47)$$

We can then plug (2.2.46) into the partial wave coefficient (2.2.34) as

$$f_J(s) = \mathcal{N}_d \oint_{[-1,1]} \frac{dz}{2\pi i} (z^2 - 1)^{\frac{d-4}{2}} Q_J^{(d)}(z) T(s, t(z)), \quad (2.2.48)$$

where the integral is counterclockwise around the interval  $z \in [-1, 1]$ . By blowing up the contour, we get two integrals along the  $t$ - and the  $u$ -channel cuts, see figure 2.2

$$f_J(s) = \frac{\mathcal{N}_d}{\pi} \left[ \int_{z_1}^{\infty} dz (z^2 - 1)^{\frac{d-4}{2}} Q_J^{(d)}(z) T_t(s, t(z)) + \int_{-\infty}^{-z_1} dz (z^2 - 1)^{\frac{d-4}{2}} Q_J^{(d)}(z) T_u(s, u(z)) \right], \quad (2.2.49)$$

where

$$z_1 \equiv z|_{t=4m^2} = 1 + \frac{8m^2}{s - 4m^2}, \quad (2.2.50)$$

and we have assumed that  $s > 4m^2$ , so that the  $t$  channel cut runs from  $z_1 = z_1 > 1$  to infinity. Here we have dropped the contributions of the arcs at infinity. This is justified for large enough



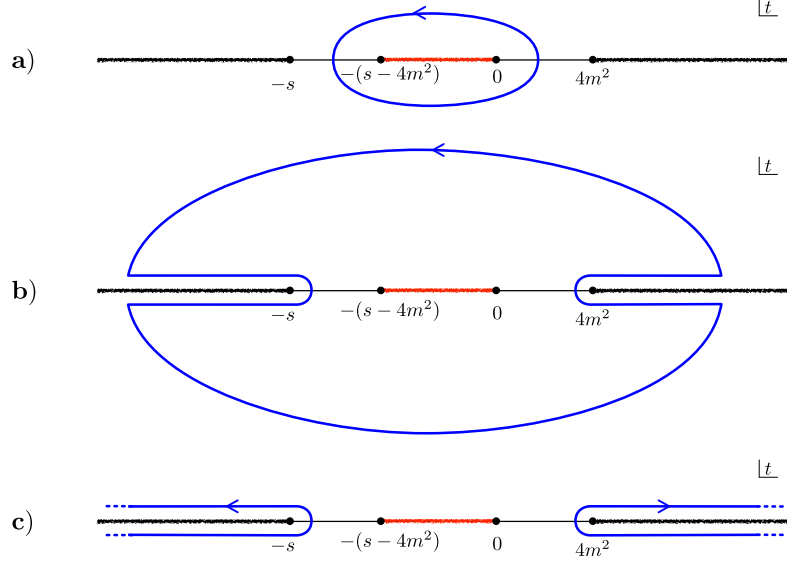


Figure 2.2: **a.** The partial wave projection integral (2.2.48) is a contour integral (in blue) that circles around the cut of the  $Q$ -function, between  $t = 0$  and  $t = -(s - 4m^2)$ , (in red). **b.** We partially open up the contour. Sometimes this representation for partial waves is called the truncated Froissart-Gribov formula. The advantage of this representation is that we only use a finite amount of extended analyticity that has not been rigorously proven. **c.** We open the contour all the way to infinity and arrive at the usual Froissart-Gribov formula (2.2.49) with two integrations of the discontinuity of the amplitude along the  $t$ -channel and  $u$ -channel cuts (in black).

spin  $J > J_0(s)$  using (2.2.43), where  $J_0(s)$  is the Regge intercept

$$\lim_{|t| \rightarrow \infty} |T(s, t)| < |t|^{J_0(s)}. \quad (2.2.51)$$

We can now use crossing to simplify (2.2.49). We change the integration variable for the  $u$ -channel integral from  $z$  to  $-z$ . Crossing symmetry implies that  $T_u(s, u(z)) = -T_t(s, t(-z))$ , where we have used that  $z(u) = -z$ . Under this change of variables

$$(z^2 - 1)^{\frac{d-4}{2}} \rightarrow (-1)^{d-4} (z^2 - 1)^{\frac{d-4}{2}}, \quad Q_J^{(d)}(z) \rightarrow Q_J^{(d)}(-z) = (-1)^{J+3-d} Q_J^{(d)}(z). \quad (2.2.52)$$

We get that  $f_J = 0$  for odd  $J$ . For even  $J$  we get

$$f_J(s) = \frac{2 \mathcal{N}_d}{\pi} \int_{z_1}^{\infty} dz (z^2 - 1)^{\frac{d-4}{2}} Q_J^{(d)}(z) T_t(s, t(z)), \quad \text{Re} J > J_0(s). \quad (2.2.53)$$

As opposed to (2.2.34), the Froissart-Gribov representation of the partial waves (2.2.53) is suitable for analytic continuation in  $J$ . It follows from the Carlson theorem that this analytic continuation is the unique continuation that does not grow too fast at large  $J$ . The Froissart-Gribov integral (2.2.53) converges as long as  $\text{Re} J > J_0(s)$  thanks to (2) and (2.2.43).

## Chapter 2. An analytical toolkit for the S-matrix bootstrap

---

This integral is written for  $s > 4m^2$ . As  $s$  approaches the threshold from above  $s - 4m^2 \rightarrow 0^+$ , the lower end of the integral is pushed to infinity,  $z_1 \rightarrow \infty$ . To analyze  $f_J(s)$  in this limit, it is useful to use (2.2.43) and to switch back to an integral over  $t$ . In that way one finds

$$f_J(s) = \frac{2\mathcal{N}_d}{\pi} c_J^{(d)} \left( \frac{s - 4m^2}{2} \right)^J \int_{4m^2}^{\infty} \frac{dt}{t^{J+1}} T_t(4m^2, t) (1 + O((s - 4m^2)/t)) . \quad (2.2.54)$$

This integral should be understood as follows. The large  $t$  contribution is finite because  $|\text{Im}_t T(4m^2, t)| < |T(4m^2, t)| < t^{J_0(4m^2)}$  and  $J > J_0(4m^2)$  by assumption. If the integrand diverges at some finite  $t$ , and in particular as  $t - 4m^2 \rightarrow 0^+$ , then we should step back and write it as a contour integral of  $T(4m^2, t)$  around the cut, which is manifestly finite.

### 2.2.5 Further Continuity Assumption

Based on the standard QFT axioms, scattering amplitudes, cross sections and partial waves are distributions rather than continuous functions. This leads to various subtleties, sometimes known as *pathologies a-la Martin* [25]. For example, we can imagine total cross-section having singularities which are local in energy variable  $s$ , that are not detectable by the finite resolution experiments. As such it is hard to exclude them based on physical grounds. One way to produce such a singularity is to consider an infinite number of resonances that accumulate on the real axis, see [25].

To the best of our knowledge there is no known, first principle argument that can exclude these possibilities. One way to eliminate them is to simply assume that various cross sections are continuous functions of energy  $s$ . We adopt this practical approach add this to the list of our assumptions. More precisely, we assume that boundary values of  $T(s, t)$  (this includes both single and double discontinuity) are continuous functions. It is common in the literature to impose the condition that boundary values of  $T(s, t)$  are uniformly continuous or Hölder continuous, see e.g. [42], but we will not use it in the present analysis.

Another related common assumption is regarding finiteness of scattering lengths which are commonly measured in the experiments or using the lattice. They are defined as follows, see (2.2.54),

$$a_J = \lim_{s \rightarrow 4m^2} \frac{m^{d-4} f_J(s)}{\left(\frac{s}{4m^2} - 1\right)^J} \geq 0, \quad J \geq 2 . \quad (2.2.55)$$

We will assume that the scattering lengths are finite for  $J \geq 2$ . Through the Froissart-Gribov formula these are related to the assumption of finiteness of the discontinuity  $T_t(4m^2, t)$  at  $s = 4m^2$  as well as convergence of the  $J = 2$  Froissart-Gribov integral (2.2.54).

There is an interesting connection between the continuity of the amplitude and macrocausality [43, 44]. Macrocausality is a set of statements about scattering amplitudes when particles grouped according to space and time of interactions and then moved away from each other by

large translation. The notion relevant for the continuity of scattering amplitudes is what is called *strong asymptotic causality* in [43] and it has not been proved within the field theory.

## 2.3 Analytic Continuation of Elastic Unitarity

The elastic unitarity relations (2.2.21) was derived for energies in the elastic region, above the two particle threshold  $4m^2 < s < 16m^2$ , and for physical kinematics  $4m^2 - s < t < 0$ . In this section we analytically continue this relation in  $t$ , outside of the regime of real scattering angles. We also consider the double discontinuity of the amplitude and the closely related analytic continuation of elastic unitarity in spin.

### 2.3.1 Mandelstam Kernel

The dependence on the scattering angle  $z = \cos\theta$  enters the right-hand side of the elastic unitarity relation (2.2.22) through the kernels (2.2.21). These kernels contain a delta or a step functions and are thus not suitable for analytic continuation. To overcome this difficulty, we use the analyticity of  $T^{(\pm)}(s, t(z))$  inside the small Lehmann-Martin ellipse to express them as a counterclockwise Cauchy integral around  $[-1, 1]$

$$\mathcal{T}^{(\pm)}(s, z') = \oint_{[-1,1]} \frac{d\eta'}{2\pi i} \frac{\mathcal{T}^{(\pm)}(s, \eta')}{\eta' - z'}, \quad -1 < z' < 1, \quad \mathcal{T}(s, z) \equiv T(s, t(z)). \quad (2.3.1)$$

We can now exchange the order on integrations in (2.2.22) and perform the  $z'$  and  $z''$  integrals explicitly. In this way we arrive at

$$\mathcal{T}_s(s, z) = \frac{(s - 4m^2)^{(d-3)/2}}{8(4\pi)^{d-2}\sqrt{s}} \oint_{[-1,1]} \frac{d\eta'}{2\pi i} \oint_{[-1,1]} \frac{d\eta''}{2\pi i} \mathcal{T}^{(+)}(s, \eta') \mathcal{T}^{(-)}(s, \eta'') \times K_d(z, \eta', \eta''), \quad (2.3.2)$$

where the new kernel is

$$K_d(z, \eta', \eta'') \equiv \int \frac{d^{d-2}\Omega_{\vec{n}}}{(\eta' - z')(\eta'' - z'')} = \int_{-1}^1 dz' \int_{-1}^1 dz'' \frac{\mathcal{P}_d(z, z', z'')}{(\eta' - z')(\eta'' - z'')}. \quad (2.3.3)$$

These integrals are evaluated in appendix A.1. For  $|\eta'|, |\eta''| > 1$  the result is

$$K_{d=3}(z, \eta', \eta'') = \frac{2\pi}{\eta_+ - z} \left( \frac{\eta'}{\sqrt{\eta'^2 - 1}} + \frac{\eta''}{\sqrt{\eta''^2 - 1}} \right), \quad (2.3.4)$$

$$K_{d \geq 4}(z, \eta', \eta'') = \frac{4\pi^{\frac{d-1}{2}}}{\Gamma(\frac{d-3}{2})} \int_{\eta_+}^{\infty} \frac{d\eta}{\eta - z} \frac{(\eta^2 - 1)^{\frac{4-d}{2}}}{(\eta - \eta_+)^{\frac{5-d}{2}} (\eta - \eta_-)^{\frac{5-d}{2}}}.$$

## Chapter 2. An analytical toolkit for the S-matrix bootstrap

where

$$\eta_{\pm}(\eta', \eta'') \equiv \eta' \eta'' \pm \sqrt{\eta'^2 - 1} \sqrt{\eta''^2 - 1}. \quad (2.3.5)$$

The Mandelstam kernel for  $|\eta'| < 1$  or  $|\eta''| < 1$  is obtained from (2.3.4) by analytic continuation. Note that in (2.3.3)  $\mathcal{P}_d(z, z', z'')$  is not analytic in  $z$ , see (2.2.21). On the other hand, the Mandelstam kernel  $K_d(z, \eta', \eta'')$  is analytic in  $z$  and therefore is suitable for analytic continuation.

Similarly, the representation of  $\mathcal{F}_s(s, z)$  in (2.3.2) is now suitable for analytic continuation in  $t$ . That is because  $t$  only enters through the Mandelstam kernel that is manifestly analytic in  $z$ .

As for the kernel  $\mathcal{P}_J^{(d)}$  (2.2.36), the Mandelstam kernel (2.3.3) is also diagonal in spin. To represent it in angular momentum basis, we start from the representation of  $\mathcal{P}_J^{(d)}$  in (2.2.36) and plug it into the definition (2.3.3). We then note that the  $z'$  and  $z''$  integration has the effect of converting the partial waves  $P_J^{(d)}(z')$  and  $P_J^{(d)}(z'')$  into  $Q_J^{(d)}(z')$  and  $Q_J^{(d)}(z'')$  correspondingly, (2.2.47). In that way we arrive at

$$K_d(z, \eta', \eta'') = 4(4\pi)^{d-2} \mathcal{N}_d^2 (\eta'^2 - 1)^{\frac{d-4}{2}} (\eta''^2 - 1)^{\frac{d-4}{2}} \sum_{J=0}^{\infty} n_J^{(d)} P_J^{(d)}(z) Q_J^{(d)}(\eta') Q_J^{(d)}(\eta''). \quad (2.3.6)$$

### 2.3.2 The Double Spectral Density and Crossing

The combination of elastic unitarity with crossing symmetry is very restrictive. In the next sections we will explore some of its consequences at length. With this aim in mind, we now represent elastic unitarity in a form that is more suitable for imposing crossing. By taking another discontinuity of (2.3.2) with respect to  $t$ , the left-hand side becomes the double discontinuity of the amplitude<sup>11</sup>

$$\begin{aligned} \rho(s, t) &\equiv -\frac{1}{4} \lim_{\epsilon \rightarrow 0} [T(s + i\epsilon, t + i\epsilon) - T(s - i\epsilon, t + i\epsilon) - T(s + i\epsilon, t - i\epsilon) + T(s - i\epsilon, t - i\epsilon)] \\ &= \text{Disc}_t \text{Disc}_s T(s, t) = \text{Disc}_s \text{Disc}_t T(s, t) = \rho(t, s). \end{aligned} \quad (2.3.7)$$

This crossing-symmetric function is known as *the double spectral density*.

By taking the  $t$  discontinuity of (2.3.2) we arrive at

$$\rho(s, t) = \frac{(s - 4m^2)^{\frac{d-3}{2}}}{8(4\pi)^{d-2} \sqrt{s}} \oint_{[-1,1]} \frac{d\eta'}{2\pi i} \oint_{[-1,1]} \frac{d\eta''}{2\pi i} \mathcal{F}^{(+)}(s, \eta') \mathcal{F}^{(-)}(s, \eta'') \times \text{Disc}_t K_d(z, \eta', \eta''), \quad (2.3.8)$$

where  $4m^2 < s < 16m^2$ . Outside of the elastic region there are additional non-elastic contributions to the double discontinuity that will be considered elsewhere. Next, we deform the  $\eta'$  and  $\eta''$  integration to wrap the  $t$  and  $u$  channel cuts of  $\mathcal{F}^{(\pm)}(s, \eta)$ . The discontinuity of the

<sup>11</sup>Stated in words, the double spectral density  $\rho(s, t)$  is defined as a certain combination of boundary values of the analytic function  $T(s, t)$  unambiguously specified by  $i\epsilon$  in the definition above.

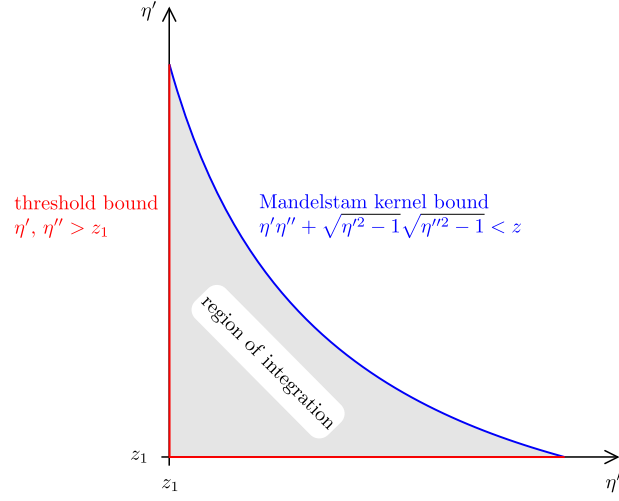


Figure 2.3: The region of integration in equation (2.3.9). As  $s$  or  $t$  approaches the Landau curve from above, the integration region shrinks to zero. As a result, the double spectral density vanishes below the Landau curve  $z = 2z_1^2 - 1$ .

Mandelstam kernel in (2.3.8) is analytic in  $\eta'$  and  $\eta''$  along the deformation. In that way, we end with real  $\eta'$  and  $\eta''$  that are positive on the  $t$  channel cut and are negative on the  $u$  channel cut. For  $\eta'\eta'' < -1$  the integral in the Mandelstam kernel (2.3.4) starts at  $\eta_+( \eta', \eta'') < -1$  and can be chosen to run along the negative real  $\eta$ -axis. This choice make it manifest that the discontinuity of the kernel for  $z > 1$  and  $\eta_+( \eta', \eta'') < -1$  is zero. We remain with<sup>12</sup>

$$\rho(s, t) = \frac{(s - 4m^2)^{\frac{d-3}{2}}}{4\pi^2 (4\pi)^{d-2} \sqrt{s}} \int_{z_1}^{\infty} d\eta' \int_{z_1}^{\infty} d\eta'' \mathcal{F}_t^{(+)}(s, \eta') \mathcal{F}_t^{(-)}(s, \eta'') \text{Disc}_z K_d(z, \eta', \eta''), \quad (2.3.9)$$

where we have mapped the  $u$ -channel cut to the  $t$ -channel cut using  $\mathcal{F}_u^{(\pm)}(s, \eta) = -\mathcal{F}_t^{(\pm)}(s, -\eta)$  and  $K(z, -\eta', -\eta'') = K(z, \eta', \eta'')$ . Here, the lower limit of integration is the point where the  $t$  channel cut starts (2.2.50). The discontinuity of the kernel, for  $\eta'\eta'' > 0$  and  $z > 1$  is given by

$$\begin{aligned} \text{Disc}_z K_3(z, \eta', \eta'') &= 4\pi^2 \delta(z - \eta_+) \frac{\sqrt{z^2 - 1}}{\eta_+ - \eta_-}, \\ \text{Disc}_z K_{d \geq 4}(z, \eta', \eta'') &= \frac{4\pi^{\frac{d+1}{2}}}{\Gamma(\frac{d-3}{2})} \Theta(z - \eta_+) \frac{(z^2 - 1)^{\frac{4-d}{2}}}{(z - \eta_-)^{\frac{5-d}{2}} (z - \eta_+)^{\frac{5-d}{2}}} \geq 0. \end{aligned} \quad (2.3.10)$$

This formula was first derived by Mandelstam in  $d = 4$  [45]. In appendix A.1 we present the derivation for any dimension  $d \geq 3$ .

We now discuss the region of support of the double discontinuity  $\rho(s, t)$ . Because the first discontinuity has only support for energies above the two particle threshold, so does the double discontinuity. Looking at (2.3.9), it is clear that the situation is more interesting. The

<sup>12</sup>The result for  $z < -1$  is obtained by analytic continuation and takes the same form as (2.3.9) with  $\text{Disc}_z K(-z, \eta', \eta'')$  instead of  $\text{Disc}_z K(z, \eta', \eta'')$ .

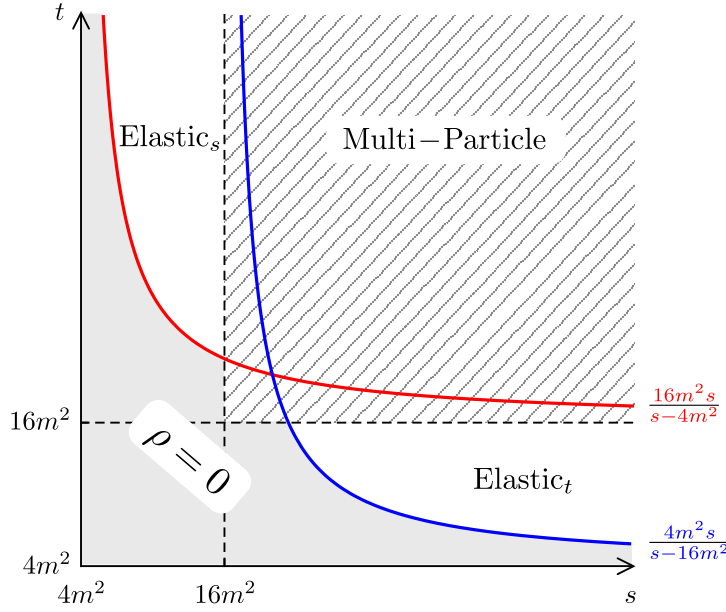


Figure 2.4: The double discontinuity of the amplitude  $\rho(s, t)$  in the real  $(s, t)$  plane. In gray is *the Steinmann shadow* region where  $\rho$  vanishes. This region extends inside the elastic bands,  $\{(4m^2 < s < 16m^2, t), (s, 4m^2 < t < 16m^2)\}$ , and is bounded by the Landau curve  $t_1(s) = \frac{16m^2 s}{s-4m^2}$  (in red) and its crossed curve  $t_1^{\text{cross}}(s) = \frac{4m^2 s}{s-16m^2}$  (in blue). These two curves extend out of the elastic bands, where there are additional multi-particle contributions. They cross at  $s = t = 20m^2$ .

discontinuities of the amplitude only start at  $\eta', \eta'' > z_1$ . At the same time, the Mandelstam kernel has a non-zero support only for  $z > \eta_+( \eta', \eta'' )$ . This constraint is an upper bound on the  $\eta', \eta''$  limits of integration, see figure 2.3. Hence, the double spectral density in the elastic region is non-zero only for

$$z = 1 + \frac{2t}{s-4m^2} > \eta_+(z_1, z_1) = 1 + \frac{32m^2 s}{(s-4m^2)^2}. \quad (2.3.11)$$

In terms of  $s$  and  $t$ , the boundary of this region is known as the Landau or Karplus curve and is given by (red in figure 2.4)

$$t = \frac{16m^2 s}{s-4m^2} \equiv t_1(s). \quad (2.3.12)$$

As  $t$  is increased above  $t_1(s)$ , the range of the  $\eta'$  and  $\eta''$  integration opens up. For example, for any value of  $t > t_1(s)$ , the integral over  $\eta'$  is bounded in the range

$$z_1 \leq \eta' \leq z\eta'' - \sqrt{(z^2-1)(\eta''^2-1)} \leq z z_1 - \sqrt{(z^2-1)(z_1^2-1)}. \quad (2.3.13)$$

Hence, as we increase  $t$  inside the elastic region  $4m^2 < s < 16m^2$  (where (2.3.9) is valid), more and more channels of  $\mathcal{T}_t^{(+)}(s, \eta')$  and  $\mathcal{T}_t^{(-)}(s, \eta'')$  kick in. Their corresponding contributions to  $\rho(s, t)$  start at other Landau curves in the  $(s, t)$  plane that are above the elastic one (2.3.12),

## 2.3 Analytic Continuation of Elastic Unitarity

---

see figure 2.4. In section 2.3.5 we present a minimal and complete set of Landau curves in the elastic region  $4m^2 < s < 16m^2$  that appears in the physical  $S$ -matrices.

In general, the positions of the Landau curves look somewhat technical. However, they are all kinematic and therefore have a geometrical origin. For example, the constraint (2.3.11) takes a simple form in terms of the integral scattering angles  $\eta' = \cosh \theta'$ ,  $\eta'' = \cosh \theta''$ , and is given by

$$\theta' + \theta'' \geq \theta. \quad (2.3.14)$$

In physical kinematics, this constraint follows from a simple geometrical consideration that is described in figure 2.1. The analytic continuation to the non-physical kinematical regime of positive  $s$  and  $t$  effect the range of the angles, but leaves this geometrical constraint unchanged. At the technical level, this is because the kinematical constraint only involves the cosines of the scattering angles.

We end this section with a comment regarding the region below the Landau curve, where the double discontinuity vanishes (the gray region in figure 2.4). For the two-to-two scattering, existence of this region is a direct consequence of elastic unitarity continued to  $s, t > 4m^2$ . The precise shape of the region depends on the details of the unitarity kernel  $K_d$ , as well as on the analytic structure of the amplitude that enters into the elastic unitarity relation. A similar phenomenon occurs in the higher-point amplitudes as well. In this case one considers double discontinuity in the so-called overlapping channels, see e.g. [46] for a detailed definition. This time it is possible to consider double discontinuity for physical kinematics directly, as opposed to the two-to-two case which requires continuation in one of the Mandelstam invariants. It then follows that for physical kinematics the double discontinuity vanishes for the overlapping channels. These are known as the *Steinmann relations* [47, 48], and it is again a direct consequence of the multi-particle unitarity. Steinmann relations are useful for constraining the analytic structure of amplitudes with six and more particles, see [49] for a recent discussion. Based on the two-to-two case one can try to analytically continue the relevant unitarity relations to the unphysical values of the relevant kinematical invariants, and find the extended region where the double discontinuity vanishes. It would be interesting to understand the precise shape of this region for the multi-particle case. This would require an analytic continuation of multiparticle unitarity kernels, as well as relevant scattering amplitudes, analogous to the one made above.

### 2.3.3 Analytic Continuation in Spin

We will now argue that the elastic unitarity relation (2.2.37) holds in the complex  $J$  plane, provided that the partial wave coefficients are analytically continued using the Froissart-Gribov representation (2.2.53). For that aim, we first rewrite the elastic unitarity condition

## Chapter 2. An analytical toolkit for the S-matrix bootstrap

---

(2.2.37) with the  $i\epsilon$  prescription explicitly

$$f_J(s+i\epsilon) - f_J(s-i\epsilon) = i \frac{(s-4m^2)^{\frac{d-3}{2}}}{\sqrt{s}} f_J(s+i\epsilon) f_J(s-i\epsilon), \quad 4m^2 < s < 16m^2. \quad (2.3.15)$$

In our previous discussions  $f_J(s) \equiv f_J(s+i\epsilon)$ . For integer  $J$  and real  $s$  in that range, real analyticity (2.2.35) leads to (2.2.37). The form (2.3.15) is however more suitable for analytic continuation.

Originally, (2.3.15) was derived for  $J$  being integer and even, however using the Froissart-Gribov representation we can continue partial waves in spin  $J$

$$f_J(s \pm i\epsilon) = \frac{2\mathcal{N}_d}{\pi} \int_{z_1}^{\infty} dz (z^2 - 1)^{\frac{d-4}{2}} Q_J^{(d)}(z) \mathcal{T}_t^{(\pm)}(s, z), \quad \text{Re}[J] > \text{Re}[J_0(s)]. \quad (2.3.16)$$

This representation can in principle be continued to the whole complex  $J$  plane, going beyond the  $\text{Re}[J] > \text{Re}[J_0(s)]$  region. However, the continued partial waves are not guaranteed to coincide with the physical ones for  $J < J_0$ . Moreover, it is clear from (2.2.13) and the reality properties of  $Q_J^{(d)}(z)$  (2.3.16), that real analyticity of partial waves (2.2.35) is only guaranteed to hold for real  $J > J_0$ .

We can then use (2.3.16) to separately analytically continue the left and right hand sides of (2.3.15). It follows from the Carlson theorem that these two analytic continuations have to agree in the whole complex  $J$  plane. Namely, the two analytic continuations agree for real integer  $J > J_0$  and do not grow too fast at large  $|J|$ , as can be seen from the large  $J$  exponential decay of  $f_J(s)$ , see section 2.6.1 for more details,

$$f_J(s) \sim \left( \frac{\sqrt{s} + 2m}{\sqrt{s} - 2m} \right)^{-J}. \quad (2.3.17)$$

Let us relate the analytic continuation in  $J$  of (2.3.15) to the Mandelstam equation (2.3.9). To get the former from the latter we integrate (2.3.9) with  $\int_{2z_1^2-1}^{\infty} dz (z^2 - 1)^{\frac{d-4}{2}} Q_J(z)$ , where  $Q_J(z)$  are given in (2.2.47). We then use the following identity (for derivation see appendix A.2)

$$\int_{\eta_+}^{\infty} dz (z^2 - 1)^{\frac{d-4}{2}} Q_J(z) \text{Disc}_z K_d(z, \eta', \eta'') = \frac{4\pi^{d/2}}{\Gamma(\frac{d-2}{2})} \left[ (\eta'^2 - 1)^{\frac{d-4}{2}} Q_J^{(d)}(\eta') \right] \left[ (\eta''^2 - 1)^{\frac{d-4}{2}} Q_J^{(d)}(\eta'') \right], \quad (2.3.18)$$

which is valid for  $\text{Re}[J] > -1$ ,  $d \geq 3$  and  $|\eta_1|, |\eta_2| > 1$ . In practice, we will use this identity in (2.3.9), where  $\eta'$  and  $\eta''$  are real and positive.



## 2.3 Analytic Continuation of Elastic Unitarity

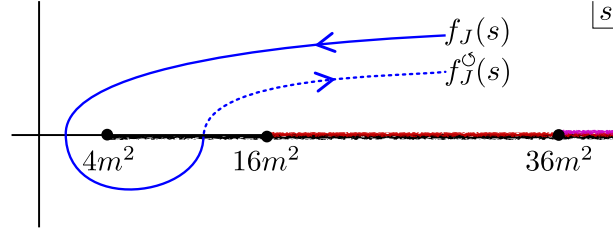


Figure 2.5: The analytic continuation of  $f_J(s)$  to the second sheet through the elastic cut  $4m^2 < s < 16m^2$  is denoted by  $f_J^\circ(s)$ .

Finally, we can write

$$f_J(s+i\epsilon) - f_J(s-i\epsilon) = 2i \frac{2\mathcal{N}_d}{\pi} \int_{z_1^2-1}^{\infty} dz (z^2-1)^{\frac{d-4}{2}} Q_J^{(d)}(z) \rho(s, t(z)), \quad \text{Re}[J] > \text{Re}[J_0(s)]. \quad (2.3.19)$$

By combining (2.3.18) with (2.3.19), it is easy to check that (2.3.9) becomes precisely (2.3.15).

Let us also mention that analytically continued elastic unitarity constrain the possible Regge limit behavior of the amplitude. In particular, the leading Regge singularity of the amplitude in the elastic region  $4m^2 < s < 16m^2$  cannot be a pole located at some real Regge spin  $\tilde{J}_0(s)$ . We review the derivation of this and a slightly more general result, known as Gribov's theorem, in appendix A.4.

### 2.3.4 Analytic Continuation in $s$

As  $s$  is increased above  $16m^2$  there are new multi-particle cuts contributions to  $\text{Im}f_J(s)$  that are not captured by (2.2.37). Still, if we denote by  $f_J^\circ(s)$  the partial wave that was analytically continued on the second sheet through the elastic cut  $4m^2 < s < 16m^2$ , see figure 2.5, then the equation

$$f_J(s) - f_J^\circ(s) = i \frac{(s-4m^2)^{\frac{d-3}{2}}}{\sqrt{s}} f_J(s) f_J^\circ(s) \quad (2.3.20)$$

holds true when analytically continued away from the elastic strip in the full multi-sheet complex  $s$  plane. In that sense, elastic unitarity can be analytically continued in  $s$ .

Note that there is a difference in the nature of the two-particle cut between odd and even dimensions. Due to the power of  $(s-4m^2)$  in (2.2.38) we get that

$$S_J^\circ(s) \equiv 1 + i \frac{(s-4m^2)^{\frac{d-3}{2}}}{\sqrt{s}} f_J^\circ(s) \times \begin{cases} -1 & d\text{-even} \\ +1 & d\text{-odd} \end{cases}. \quad (2.3.21)$$

Correspondingly, for even dimension the continued elastic unitarity condition (2.3.20) be-

## Chapter 2. An analytical toolkit for the S-matrix bootstrap

---

comes

$$S_J(s)S_J^\circ(s) = 1, \quad d\text{-even}. \quad (2.3.22)$$

This relation implies that the elastic cut  $4m^2 < s < 16m^2$  describes a two-sheeted Riemann surface in even  $d$ . Indeed, continuing (2.3.22) around the elastic cut again we conclude that  $S_J^{2 \times \circ}(s) = S_J(s)$ . In odd  $d$ , because of the sign difference in (2.3.21), we do not have (2.3.22) and the elastic cut is not two-sheeted. Similar conclusion holds for  $T(s, t)$ . As we will see below, the nature of the elastic unitarity cut is the one of a simple square-root for even  $d$  and is infinitely-sheeted for odd  $d$ . It immediately follows from (2.3.22) that a pole of  $S_J^\circ(s)$  (resonance) corresponds to a zero of  $S_J(s)$  in even  $d$ . Similarly, in odd  $d$ , a pole of  $S_J^\circ(s)$  corresponds to a zero of  $1 - i \frac{(s-4m^2)^{\frac{d-3}{2}}}{\sqrt{s}} f_J(s)$  on the principal sheet.

### 2.3.5 Elastic Landau Curves

In this section we further study the kinematical properties of the double spectral density in the elastic strip. In general, discontinuities of the amplitude result from the exchange of intermediate on-shell states. Correspondingly, the double discontinuity of the amplitude receives its support from intermediate on-shell particles exchanged in both channels. As we have seen in section 2.3.2, the first double discontinuity in the elastic strip starts at the leading Landau curve (2.3.12). It comes from the exchange of two particle in the  $s$ -channel and four particles in the  $t$ -channel. As we increase  $s$  or  $t$ , more and more processes become accessible. The curves in the  $s - t$  plane where they start to contribute are higher Landau curves. We now derive an infinite set of higher Landau curves in the elastic strip that are required by elastic unitarity.

To each of these Landau curves one can associate a Landau diagram. In the elastic strip, all these diagrams have a simple iterative structure that is plotted in figure 2.6. Correspondingly, the shape of the curve has a relatively simple geometrical origin, (for the case of the first Landau curve, see figure 2.1 and the discussion around (2.3.14)). Here instead, we follow a shortcut and derive their shape directly from the Froissart-Gribov representation and the elastic unitarity constraint.

The starting point is the kinematical structure of the discontinuity and the double discontinuity of the amplitude as function of one of the Mandelstam invariants

$$\text{Disc}_t T(s, t) = T_t(s, t) = \sum_{n=1}^{\infty} \Theta(t - (2nm)^2) T_t^{2 \rightarrow 2n}(s, t), \quad 4m^2 - t < s < 0, \quad (2.3.23)$$

$$\text{Disc}_s \text{Disc}_t T(s, t) = \rho(s, t) = \sum_i \Theta(t - t^{(i)}(s)) \rho^{(i)}(s, t), \quad 4m^2 < s, t, \quad (2.3.24)$$

where the functions  $t^{(i)}(s, t)$  are the Landau curves we are after. For that aim, we first have to analytically continue the discontinuities of the amplitudes,  $T_t^{2 \rightarrow 2n}(s, t)$ , to the regime of

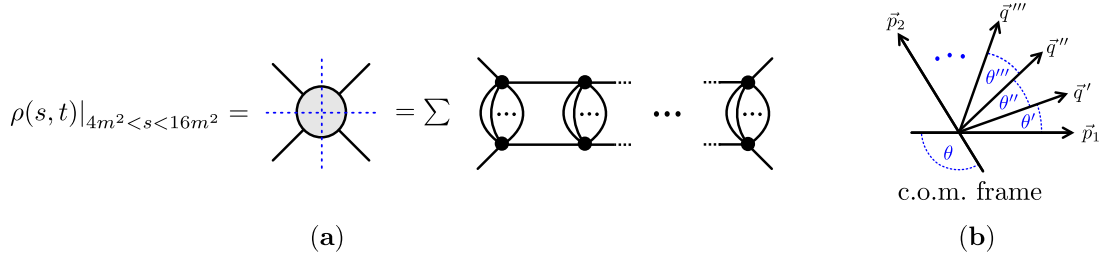


Figure 2.6: **a.** The Landau diagrams that contribute to the double spectral density in the elastic strip  $4m^2 < s < 16m^2$  and  $4m^2 < t$ . In this kinematical regime there can be only two particles in the  $s$ -channel. Hence, the corresponding Landau diagrams have a simple structure of iterative two-particle exchange in the  $s$ -channel and in between, any number of particles exchange in the  $t$ -channel. **b.** Analogously to figure 2.1, the corresponding Landau curves originate from a simple geometric constraint on physical kinematics, see discussion after (2.3.14).

positive  $s$  and  $t$ . As we do so, they develop new thresholds. Because  $T_t(s, t)$  is a real analytic function, these new thresholds must coincide with the Landau curves  $t^{(i)}(s)$ . What is important for us here is that the multi-particle thresholds that are manifest in (2.3.23) are also present in the non-physical kinematical regime.

To derive the functional shape of the Landau curves in the elastic strip we impose the consistency of (2.3.24) and (analytically continued) (2.3.23) with elastic unitarity. This can be done by either plugging them into the Mandelstam equation or by imposing elastic unitarity at the level of the partial waves. Here we follow the latter strategy and in appendix A.5 we present the former, both leading to the same result.

To impose consistency of (2.3.23) and (2.3.24) with the partial waves elastic unitarity, we plug them into the Froissart-Gribov projection (2.2.53), that we quote here for convenience

$$\operatorname{Re} f_J(s) + i \operatorname{Im} f_J(s) = \frac{2 \cdot \mathcal{N}_d}{\pi} \int_{z_1}^{\infty} dz (z^2 - 1)^{\frac{d-4}{2}} Q_J^{(d)}(z) [\operatorname{Re} T_t(s, t(z)) + i \rho(s, t(z))] . \quad (2.3.25)$$

Next, we take the large  $J$  limit of (2.3.25). Using the large  $J$  decay of the  $Q$  functions that can be schematically written as, see section 2.6.1,

$$Q_J^{(d)}(z) \sim \lambda^{-J}(z) , \quad \lambda(z) \equiv z + \sqrt{z^2 - 1} = e^\theta , \quad z > 1 , \quad (2.3.26)$$

as well as the two-particle step function in (2.3.23), we conclude that the leading large  $J$  behavior of  $\operatorname{Re} f_J(s)$  is

$$\operatorname{Re} f_J(s) \sim \lambda^{-J}(z_1) . \quad (2.3.27)$$

Similarly to (2.3.27), the  $n$ -particle threshold of  $T_t(s, t)$  and the  $i$ 'th Landau curve threshold of  $\rho(s, t)$  in (2.3.23) result in contributions to  $\operatorname{Re} f_J(s)$  and  $\operatorname{Im} f_J(s)$  that start at large  $J$  as

$$\operatorname{Re} f_J(s) \sim \lambda^{-J}(z_n) , \quad \operatorname{Im} f_J(s) \sim \lambda^{-J}(z) \Big|_{t=t^{(i)}(s)} , \quad (2.3.28)$$

## Chapter 2. An analytical toolkit for the S-matrix bootstrap

---

where  $z_n \equiv 1 + \frac{8n^2 m^2}{s-4m^2}$ . Importantly, (2.3.26) receives only  $1/J$ -power corrections and no non-perturbative exponential corrections, see appendix A.3. Hence,  $\text{Im } f_J(s)$  does not receive any exponential large  $J$  behavior other than the ones that result from Landau curves thresholds (2.3.28). Similarly, the exponential large  $J$  behavior of  $\text{Re } f_J(s)$  can only come from thresholds of  $T_t(s, t)$  in (2.3.25), but not from nonperturbative terms in the large  $J$  expansion of  $Q_J^{(d)}(z)$ .

We now plug these set of large  $J$  exponential behaviors into elastic unitarity and derive the minimal set of Landau curves,  $t^{(i)}(s)$ , that are required to close the equation, together with new thresholds of  $T_t(s, t)$  that are not present in physical kinematics.

Elastic unitarity (2.2.37) can be written in the following schematic form

$$\text{Im } f_J(s) \propto [\text{Re } f_J(s)]^2 + [\text{Im } f_J(s)]^2, \quad (2.3.29)$$

where we omitted the pre-factor because it is irrelevant for the present discussion. First, we see that the multi-particle threshold exponents of  $\text{Re } f_J(s)$  in (2.3.28) result in the following exponents in  $\text{Im } f_J(s)$

$$\text{Im } f_J(s) \sim [\lambda(z_n)\lambda(z_m)]^{-J}, \quad n, m \geq 1. \quad (2.3.30)$$

Using (2.3.28), these then lead to the Landau curves

$$\lambda(z)|_{t=t^{(n,m)}(s)} = \lambda(z_n)\lambda(z_m). \quad (2.3.31)$$

For example, the leading Landau curve (2.3.12) corresponds to the case where  $m = n = 1$ . This behavior must then also exist in  $\text{Re } f_J(s)$ . To see that, recall that  $T_t(s, t)$  is a real analytic function of  $t$  for fixed  $s > 4m^2$ . Hence, a threshold in the imaginary part of  $T_t(s, t)$ , namely in  $\rho(s, t)$ , must be accompanied by a corresponding threshold in  $\text{Re } T_t(s, t)$ .

Having established the presence of the quadratic in  $\lambda(z_n)$  terms in the large  $J$  expansion of  $\text{Re } f_J(s)$  and  $\text{Im } f_J(s)$ , we now come back to elastic unitarity (2.3.29). The presence of these terms together with the linear one (2.3.28), now induces higher powers of  $\lambda(z_n)$  in the large  $J$  expansion of  $\text{Im } f_J(s)$  and, via real analyticity, of  $\text{Re } f_J(s)$  as well. These take the general form

$$\text{Re } f_J(s) \sim [\lambda(z_{n_1}) \cdots \lambda(z_{n_L})]^{-J}, \quad n_i \geq 1, \quad L \geq 1, \quad (2.3.32)$$

$$\text{Im } f_J(s) \sim [\lambda(z_{n_1}) \cdots \lambda(z_{n_L})]^{-J}, \quad n_i \geq 1, \quad L \geq 2. \quad (2.3.33)$$

This large  $J$  structure implies existence of an infinite set of Landau curves labeled by a set of integers  $\{N_1, N_2, N_3, \dots\}$  and given by the following equation

$$\lambda(z(t_{\{N_1, N_2, N_3, \dots\}})) = \lambda^{N_1}(z_1) \lambda^{N_2}(z_2) \lambda^{N_3}(z_3) \cdots. \quad (2.3.34)$$

In terms of the scattering angle, for which  $z = \cosh \theta$  and  $\lambda = e^\theta$ , these Landau curves take the

## 2.4 Positivity of $\rho$ and Multi-Particle Production

form

$$\theta(z) = N_1\theta_1 + N_2\theta_2 + N_3\theta_3 + \dots, \quad (2.3.35)$$

with  $\theta_n = \text{arccosh}(z_n)$ . This form is the generalization of (2.3.14) for all the elastic Landau curves. In a direct analogy with figure 2.1, it also has a simple geometrical origin that is discussed in figure 2.6.b. Using that  $z = 1 + \frac{2t}{s-4m^2}$ , we can translate (2.3.34) into polynomial equations in  $s$  and  $t$  with real coefficients.<sup>13</sup> For example, we have

$$t_{\{2,0,\dots\}} = \frac{16m^2 s}{s-4m^2}, \quad t_{\{3,0,\dots\}} = \frac{36m^2(s + \frac{4m^2}{3})^2}{(s-4m^2)^2}, \quad t_{\{4,0,\dots\}} = \frac{64m^2 s(s+4m^2)^2}{(s-4m^2)^3}. \quad (2.3.36)$$

The Landau curves have the following asymptotic behavior

$$\lim_{s \rightarrow 4m^2} t_{\{N_1, N_2, \dots\}}(s) \sim (s-4m^2)^{1-\sum_{j=1}^{\infty} N_j}, \quad \lim_{s \rightarrow \infty} t_{\{N_1, N_2, \dots\}}(s) = \left(2m \sum_{j=1}^{\infty} j N_j\right)^2. \quad (2.3.37)$$

These asymptotes are precisely the  $t$ -channel normal thresholds (2.3.23). This is evident from the Landau diagram interpretation of figure 2.6 and it would be interesting to see if it can be established rigorously.<sup>14</sup>

## 2.4 Positivity of $\rho$ and Multi-Particle Production

Drawing an analogy with the conformal bootstrap, one can expect that combining crossing symmetry of  $\rho(s, t)$  with some sort of positivity property leads to nontrivial constraints on scattering amplitudes.

In this section we show that there is indeed a finite region in the elastic strips of the  $(s, t)$ -plane, where  $\rho(s, t)$  is positive, as noted in [53]. In subsection 2.4.2 we discuss a direct consequence of this positivity and crossing – the necessity of multi-particle production  $T_{2 \rightarrow 2n}$  for any  $n$ .

### 2.4.1 Positivity of The Double Spectral Density

To establish positivity, we assume that the integral in the Mandelstam equation for the double spectral density (2.3.9) converges and study under what conditions the integrand is positive.

Consider first the discontinuity of the Mandelstam kernel  $\text{Disc}_z K_d(z, \eta', \eta'')$  given in (2.3.10). This function is strictly positive for  $z > 1$ , which is the case for any  $s, t > 4m^2$ . Next we turn our attention to  $\mathcal{T}_t^{(\pm)}(s, \eta')$ . It is clear that  $\mathcal{T}_t(s, \eta')$  is non-negative in the region where the partial

<sup>13</sup>In this form they are familiar in the study of perturbative Feynman integrals, see e.g. [8] for more details.

<sup>14</sup>For the case of two particles in the final state it was done by Mandelstam and we reviewed it in section 2.3.1. For the multi-particle case some limited results have been obtained [50, 51, 52].

## Chapter 2. An analytical toolkit for the S-matrix bootstrap

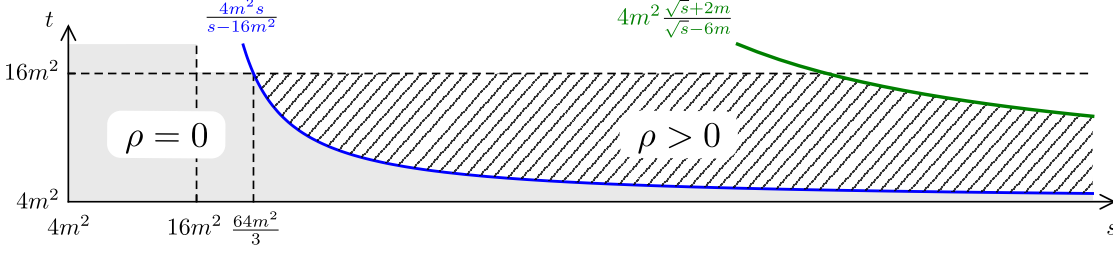


Figure 2.7: The regime of positivity of the double spectral density  $\rho(s, t)$  in the elastic strip  $4m^2 < t < 16m^2$ , (dashed region). This is the region above the first Karplus curve  $s_1(t)$  (in blue) and below the curve  $t = 4m^2 \frac{\sqrt{s+2m}}{\sqrt{s-6m}}$  (in green). There is an identical positive region in the crossed strip of  $4m^2 < s < 16m^2$ , see (2.4.4).

wave expansion converges<sup>15</sup>

$$\mathcal{F}_t(s, \eta') = T_t(s, t') = \sum_J n_J^{(d)} \text{Im} f_J(t') P_J^{(d)} \left( 1 + \frac{2s}{t' - 4m^2} \right), \quad t' = \frac{\eta' - 1}{2} (s - 4m^2), \quad (2.4.1)$$

where  $t'$  is not to be confused with the external  $t$  in (2.3.9). Indeed, unitarity implies that  $\text{Im} f_J(t') \geq 0$  and  $P_J^{(d)} \left( 1 + \frac{2s}{t' - 4m^2} \right)$  is positive for  $s, t' > 4m^2$ . Consider the function  $g \left( 1 + \frac{2s}{t' - 4m^2} \right) \equiv T_t(s, t')$  for fixed  $t'$ . Provided that  $g(z)$  is analytic inside an ellipse in the complex  $z$ -plane with foci at  $z = \pm 1$ , it then follows from Neumann's argument, see footnote 10, that the partial wave expansion (2.4.1) converges inside that ellipse. Under the assumption of extended analyticity and for fixed  $t'$ , the first singularity is where  $T_t(s, t')$  develops a discontinuity with respect to  $s$ . Namely, the partial wave expansion (2.4.1) converges below the first Landau curve, red in figure 2.4,<sup>16</sup>

$$t' < t_1(s) = \frac{16m^2 s}{s - 4m^2} \quad \text{or equivalently} \quad \eta' < 1 + \frac{36m^2}{(s - 4m^2)^2}, \quad 4m^2 < s < 16m^2. \quad (2.4.2)$$

This region of convergence is called the large  $s$ -channel Martin-Lehmann ellipse [34]. Note that the standard argument of [34] refers to the convergence of (2.3.19) in the crossed region of  $s < s_1(t')$ ,  $4m^2 < t' < 16m^2$  and does not require the extended analyticity assumption. Here, we are saying that under this assumption, the partial wave expansion (2.4.1) converges in the union of the  $t$ - and  $s$ -channel large Martin-Lehmann ellipses.

The maximal value of the  $\eta'$  integration is given in (2.3.13). Hence, we conclude that the double

<sup>15</sup>In this region we can drop the  $(\pm)$  subscript of  $\mathcal{F}_t^{(\pm)}(s, \eta')$  and  $\mathcal{F}_t^{(\pm)}(s, \eta'')$  in (2.3.9) because both functions are equal.

<sup>16</sup>As a consistency check, we can also study the convergence region of (2.4.1) using the large  $J$  asymptotics of the partial wave coefficients. Using (2.3.19) and the shape of the first Landau curve we have arrived at the same conclusion.

## 2.4 Positivity of $\rho$ and Multi-Particle Production

spectral density is non-negative for

$$zz_1 - \sqrt{(z^2 - 1)(z_1^2 - 1)} \leq 1 + \frac{36m^2}{(s - 4m^2)^2}. \quad (2.4.3)$$

By solving this condition for  $t$  we conclude that

$$\boxed{\rho(s, t) > 0, \quad 4m^2 < s < 16m^2, \quad \frac{16m^2 s}{s - 4m^2} < t \leq 4m^2 \frac{(3s + 4m^2)^2}{(s - 4m^2)^2}}. \quad (2.4.4)$$

where the lower bound comes from (2.3.12), and the upper bound from (2.4.3). This region of positivity was first derived in [53] and is plotted in figure 2.7.<sup>17</sup>

Note that at the upper bound of that region  $\rho(s, t)$  is strictly positive. Hence, the region of positivity can always be extended from above. A question to which we do not know the answer is whether the region of positivity of the double spectral density can be extended to arbitrary large  $s$  and  $t$ . Here we only list some known implications of such a scenario. In [54] A. Martin argued that positivity of the double spectral density for all  $s$  and  $t$  implies that the total cross-section at high energies satisfies the following bound

$$\sigma_{tot}(s) \leq \frac{C}{\log s}, \quad s \rightarrow \infty. \quad (2.4.5)$$

This immediately implies that for theories that saturate the Martin-Froissart bound  $\sigma_{tot}(s) \sim \log^2 s$  [55, 34], the double spectral density is not positive-definite.

Similarly, in [56] A. W. Martin explored implications of the positive-definite double spectral density for scattering at finite angles. He showed that amplitudes with positive double spectral density *do not* exhibit diffraction peak in the near-forward scattering, which is

$$T_t(s, t) \sim e^{sb(t)+\dots}, \quad (2.4.6)$$

where  $b(t)$  is a slowly-varying function. Such a diffraction peak is observed, for example, in the scattering of pions. Therefore, the double spectral density for pion scattering cannot be positive for arbitrary  $s$  and  $t$ .

It would be interesting to understand positivity properties of  $\rho(s, t)$  in physical theories more systematically.

### 2.4.2 The Aks Theorem and Necessity of Particle Production

We now review an elegant argument for scalar particles by Aks [22].<sup>18</sup> It states that scattering implies particle production. Namely, provided that  $T_{2 \rightarrow 2} \neq 0$ , also  $T_{2 \rightarrow n} \neq 0$  with  $n > 2$ . The

<sup>17</sup>Note that this is the regime between the curves  $t_{\{2,0,\dots\}}$  and  $t_{\{3,0,\dots\}}$  in (2.3.36).

<sup>18</sup>For the generalization to the case of spinning particles or particles in nontrivial representations of some global symmetry, see [57].

## Chapter 2. An analytical toolkit for the S-matrix bootstrap

---

theorem applies to any crossing symmetric scalar scattering amplitude in  $d \geq 3$  that satisfies extended analyticity in a finite region above the leading Landau curve.

To derive Aks's result, let us therefore assume that we have a nontrivial scattering amplitude  $T(s, t)$ , but  $T_{2 \rightarrow n}$  are identically zero for  $n > 2$ . This implies that elastic unitarity in the form of Mandelstam (2.3.9) holds for any  $s \geq 4m^2$ , whereas in the theories with particle production elastic unitarity only holds below the first threshold  $s_0 > s \geq 4m^2$ . It then follows that  $\rho(s, t) = 0$  below the first  $s$ -channel Landau curve  $4m^2 < t < t_1(s)$  (2.3.12) for any  $s$ , see red curve in figure 2.4. This region however includes the crossed Mahoux-Martin region of positive  $\rho(s, t) > 0$  (2.4.4),  $s < 4m^2 \frac{(3t+4m^2)^2}{(t-4m^2)^2}$ , see gray region in figure 2.7.<sup>19</sup> Therefore, we conclude that our assumptions of crossing symmetry and scattering without production are not consistent.

Note that in the case of an infinite  $J = 0$  scattering length, the derivation of the positivity of  $\rho(s, t)$  in the Mahoux-Martin region does not always apply. That is because in that case, the integral in (2.3.9) fails to converge for  $d \geq 5$ . However, when the  $J = 0$  scattering length is infinite,  $\rho(s, t)$  is already non-zero at the leading Landau curve and we reach the same conclusion that there must be particle production.

A way to relax the assumption of extended analyticity was explained in [58] by exploiting polynomial boundedness and continuity assumptions. The idea is to use elastic unitarity to extend the region of analyticity of the amplitude. One starts with fixed  $t < 4m^2$  dispersion relations and then use elastic unitarity to first extend the analyticity domain of  $T_s$  and then use dispersion relations to continue the scattering amplitude itself. The key point being that assuming no production we can use elastic unitarity to continue the discontinuity at arbitrary energy, which is necessary if we want to use this inside the dispersion relations.

Note that the argument above also implies that we must have four-particle production. That is because the crossed region of positivity starts at  $s_1(16m^2) = \frac{64}{3}m^2 < 36m^2$ , it is enough to assume that  $T_{2 \rightarrow 4} = 0$  to reach a contradiction. One can wonder if having  $T_{2 \rightarrow 4}$  is enough to fix the problem, or  $T_{2 \rightarrow 2n}$  with  $n > 2$  are also necessary? To address this question, we can then proceed via crossing.<sup>20</sup> By unitarity of the  $4 \rightarrow 4$  amplitude,  $\text{Im} T_{4 \rightarrow 4} \sim |T_{2 \rightarrow 4}|^2$ , non-vanishing  $T_{2 \rightarrow 4}$  implies that we have a non-vanishing  $T_{4 \rightarrow 4}$  amplitude. Applying crossing this becomes  $T_{2 \rightarrow 6}$ . Continuing this recursion we conclude that all  $T_{2 \rightarrow 2n}$  should be non-zero. Therefore, not only scattering implies production but it requires all possible production (here we assumed  $Z_2$  symmetry so that only an even number of particles is present in the final state).

An alternative argument that does not use crossing symmetry of higher-point amplitudes was put forward in [59]. This argument relies on an unproven assumption that Landau curves can only asymptote to normal thresholds for the scattering of lightest particles, see section 2.3.5. This assumption is consistent with the perturbative analysis of [35, 36] and it would be interesting to establish it rigorously.

<sup>19</sup>Recall that positivity of  $\rho(s, t) > 0$  is a direct consequence of our assumption about nontriviality of scattering.

<sup>20</sup>Note that crossing has been only rigorously proven within the standard QFT framework for  $2 \rightarrow 2$  amplitudes [29]. For some further progress in the multi-particle case  $2 \rightarrow n$  see [37].



## 2.4 Positivity of $\rho$ and Multi-Particle Production

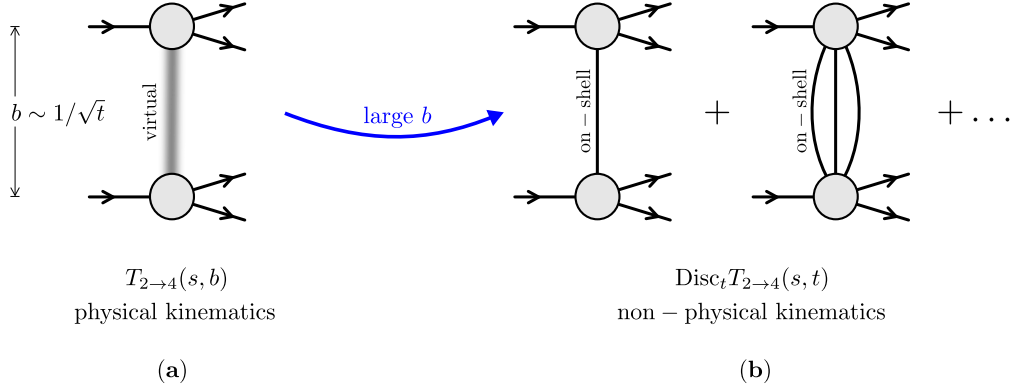


Figure 2.8: **a.** We consider a scattering experiment at fixed impact parameters  $b$ . This process is controlled by the exchanged momentum  $t \sim \frac{1}{b^2} > 0$ . **b.** At large impact parameters the amplitude can be organized as a sum over on-shell particles exchange. The dominant contribution comes from the exchanged of the lightest on-shell particle.

### 2.4.3 Bounding Inelasticity

There is another, more intuitive way to think about the result of Aks and necessity of particle production in higher dimensions. Ideally, one would like to take a discontinuity of the  $2 \rightarrow 4$  amplitude that is given by a product of two  $2 \rightarrow 2$  amplitudes. For physical kinematics however, such a discontinuity only exist for the  $3 \rightarrow 3$  setup. Instead, let us discuss impact parameter scattering, which is only possible in  $d \geq 3$ .

As reviewed for example in appendix E of [60], the effect of going to the impact parameter space is the same as continuing the conjugate momentum invariant to the unphysical kinematics. It follows that inelasticity in a gapped theory cannot be exactly zero at very large impact parameters. To see this, decompose the four particles in the final state into a pair of dipoles. Then consider a scattering in which the two dipoles in the final state, as well as the pair of incoming particles in the initial state, are separated by a finite distance  $b$  in the transverse space, see figure 2.8.a. Unitarity becomes, in the impact parameter space, the expansion in Yukawa potential suppressed terms  $T_{2 \rightarrow 4}(s, b) \sim T_{2 \rightarrow 2}^2 \times e^{-bm} + [\text{multi-particle} \sim e^{-nbm}]$ . At large separation, this expansion is dominated by the one-particle exchange  $e^{-bm}$ , while the multi-particle corrections are further exponentially suppressed.<sup>21</sup> In that way, a non-trivial (analytically continued) four-point amplitude imply a non-trivial  $2 \rightarrow 4$  amplitude. We would then like to bound the  $2 \rightarrow 4$  amplitude from below.

There is a convenient way of bounding the integrated discontinuity of  $T_{2 \rightarrow 4}$  in the kinematical regime of figure 2.8.b from below. It is based on the discussion in the previous sections, see in particular sections 2.3.2 and 2.4.1, 2.4.2. It also highlights how the crossing of  $\rho(s, t)$  discussed in the section above works microscopically. Let us start with the the square of  $T_{2 \rightarrow 4}$  that

<sup>21</sup>In terms of partial waves, large impact parameter scattering corresponds to the large spin limit and therefore we expect to have inelasticity at large spin which will be analyzed in detail in the sections below.

## Chapter 2. An analytical toolkit for the S-matrix bootstrap

appears in the discontinuity of the  $2 \rightarrow 2$  amplitude,  $T_s(s, t)$

$$T_s^{\text{inel}, 2 \rightarrow 4}(s, t) \equiv \frac{1}{2} \frac{1}{4!} \int \prod_{i=1}^4 \frac{d^{d-1} \vec{q}_i}{(2\pi)^{d-1} (2E_{\vec{q}_i})} (2\pi)^d \delta^d(p_1 + p_2 - \sum_{i=1}^4 q_i) T_{2 \rightarrow 4}^{(+)}(p_1, p_2 | q_i) T_{2 \rightarrow 4}^{(-)}(q_i | p_3, p_4) . \quad (2.4.7)$$

By construction, the unitarity integral in the right-hand side of (2.4.7) depends only on  $s$  and  $t$ . For physical scattering we consider  $s > 16m^2$  and  $t < 0$ .

We would like next to analytically continue (2.4.7) to the unphysical Martin-Mahoux region discussed above

$$4m^2 < t < 16m^2 , \quad \frac{16m^2 t}{t - 4m^2} < s < 4m^2 \frac{(3t + 4m^2)^2}{(t - 4m^2)^2} . \quad (2.4.8)$$

We also would like to consider  $16m^2 < s < 36m^2$  to focus on the  $T_{2 \rightarrow 4}$  amplitude. This condition together with (2.4.8) imply  $\frac{36m^2}{5} < t$ . For the  $2 \rightarrow 2$  case we reviewed the procedure in the sections above. For the multi-particle case it was discussed in [50, 51, 52].

After taking a discontinuity in  $t$  and using crossing symmetry of the double spectral density, we arrive at the following schematic form<sup>22</sup>

$$\begin{aligned} \rho(s, t) &= \frac{(t - 4m^2)^{\frac{d-3}{2}}}{4\pi^2 (4\pi)^{d-2} \sqrt{t}} \int_{\bar{z}_1}^{\infty} d\eta' \int_{\bar{z}_1}^{\infty} d\eta'' \text{Disc}_s \mathcal{F}_{2 \rightarrow 2}^{(+)}(t, \eta') \text{Disc}_s \mathcal{F}_{2 \rightarrow 2}^{(-)}(t, \eta'') \times \text{Disc}_{\bar{z}} K_d(\bar{z}, \eta', \eta'') \\ &= \int d\text{LIPS}_4 \times \text{Disc}_t T_{2 \rightarrow 4}^{(+)} \text{Disc}_t T_{2 \rightarrow 4}^{(-)} \times K_{\text{Mandelstam}}^{2 \rightarrow 4} , \end{aligned} \quad (2.4.9)$$

where in the formula above we switched to  $\bar{z} = 1 + \frac{2s}{t - 4m^2}$  and  $\bar{z}_1 = 1 + \frac{8m^2}{t - 4m^2}$ . Here in the right-hand side each  $\text{Disc}_{T_{2 \rightarrow 4}}$  contains a delta-function that puts the exchanged particle in figure 2.8 on-shell. The phase space integral  $d\text{LIPS}_4$  should be understood in terms of the analytic continuation a-la Mandelstam.

Note that since we are in the Mahoux-Martin region, the partial wave expansion of  $\text{Disc}_s \mathcal{F}_{2 \rightarrow 2}^{(\pm)}(t, \eta)$  converges and both the Mandelstam kernel and the Legendre polynomials that enter into partial waves are positive. Therefore we can write

$$T_s(t, s) = \sum_{J=0}^{\infty} n_J^{(d)} \text{Im} f_J(s) P_J\left(1 + \frac{2t}{s - 4m^2}\right) \geq \sum_{J=0}^{J_0} n_J^{(d)} \text{Im} f_J(s) P_J\left(1 + \frac{2t}{s - 4m^2}\right) . \quad (2.4.10)$$

By plugging (2.4.10) into (2.4.9) and using positivity of the Mandelstam kernel  $\text{Disc}_{\bar{z}} K_d(\bar{z}, \eta', \eta'')$  we arrive at the lower bound on the integrated discontinuity  $\text{Disc}_t T_{2 \rightarrow 4}$ .

While this argument bounds the discontinuity of  $T_{2 \rightarrow 4}$  in the unphysical kinematics of figure

<sup>22</sup>Note that  $T_{2 \rightarrow 2}$  is not present in the second line of (2.4.9) since the region  $4m^2 < t < 16m^2$ ,  $16m^2 < s < 36m^2$  lies below the leading  $t$ -channel Landau curve  $t = 16m^2 s / (s - 4m^2)$ . See Figure 2.4.

## 2.5 Threshold Expansion

2.8.b, for  $\frac{36m^2}{5} \leq t < 16m^2$  from below, it does not tell us anything about  $T_{2 \rightarrow 4}$  in the physical kinematics  $t < 0$ . Let us however comment why one expects to have  $T_{2 \rightarrow 4}$  of the same order also in the physical kinematics. Schematically, we can write the following representation of the  $2 \rightarrow 4$  impact parameter amplitude

$$T_{2 \rightarrow 4}(s, b) = (T_{2 \rightarrow 2})^2 e^{-bm} + \int_{3m}^{\infty} dM \rho(M) e^{-Mb}. \quad (2.4.11)$$

We can rewrite this as follows

$$|T_{2 \rightarrow 4}(s, b) - (T_{2 \rightarrow 2})^2 e^{-bm}| \leq c_{\text{MP}} e^{-3mb}, \quad c_{\text{MP}} = \int_{3m}^{\infty} dM |\rho(M)| e^{-(M-3m)b}, \quad (2.4.12)$$

where  $c_{\text{MP}}$  encodes the contribution of the multi-particle exchanges.

Without extra fine-tuning we expect that in a strongly coupled theory  $T_{2 \rightarrow 2}$ ,  $c_{\text{MP}} \sim \mathcal{O}(1)$  and therefore the one-particle exchange to dominate for  $b \gtrsim \frac{1}{m}$ . This would make  $T_{2 \rightarrow 4} \sim \mathcal{O}(1)$ . On the other hand, making  $T_{2 \rightarrow 4} \ll 1$  given  $T_{2 \rightarrow 2} \sim \mathcal{O}(1)$  would require a very fine-tuned cancellation between the exchange of one-particle state and the multi-particle state as well as  $c_{\text{MP}} \gg 1$ . It seems quite possible that such a scenario is not consistent with multi-particle unitarity, but it is very hard to show it explicitly due to the complexity of the latter.

One scenario in which the regime of single particle dominance can be delayed to arbitrary large impact parameters is if the theory contains extended objects, such as strings. In such case we can choose  $l_{\text{string}} \gg \frac{1}{m}$ , and the one-particle exchange is expected to dominate only for  $b \gtrsim l_{\text{string}}$ . In this case however, the spectrum is expected to contain particles of mass  $\frac{1}{l_{\text{string}}} \ll m$  which contradicts our assumption about  $m$  being the lightest particle.

In some numerical applications that we discuss in more detail below, see e.g. [1], it was observed that small  $J$  partial wave converge very well. Therefore we can set in the formula (2.4.10)  $J_0 = 2$  and then use it in (2.4.9). We can then evaluate the integral above to rigorously bound from below  $\text{Disc} T_{2 \rightarrow 4}$  in the Mahoux-Martin kinematical region. In the numerical analysis when maximizing some couplings, one usually finds  $\text{Im} f_0(s) \sim 1$  therefore the formulas (2.4.9), (2.4.10) will produce  $\text{Disc} T_{2 \rightarrow 4} \sim 1$ . It is however still an open problem to translate this fact into a rigorous statement about  $T_{2 \rightarrow 4}$  for physical kinematics.

Independently of the discussion above, in section 2.7 we bound inelasticity using an additional input about the discontinuity of the  $2 \rightarrow 2$  amplitude.

## 2.5 Threshold Expansion

To further analytically constrain a nonperturbative amplitude a small parameter is needed. In this section, as well as the next one, we will study the expansions of the amplitude in two

2.5 Threshold expansion

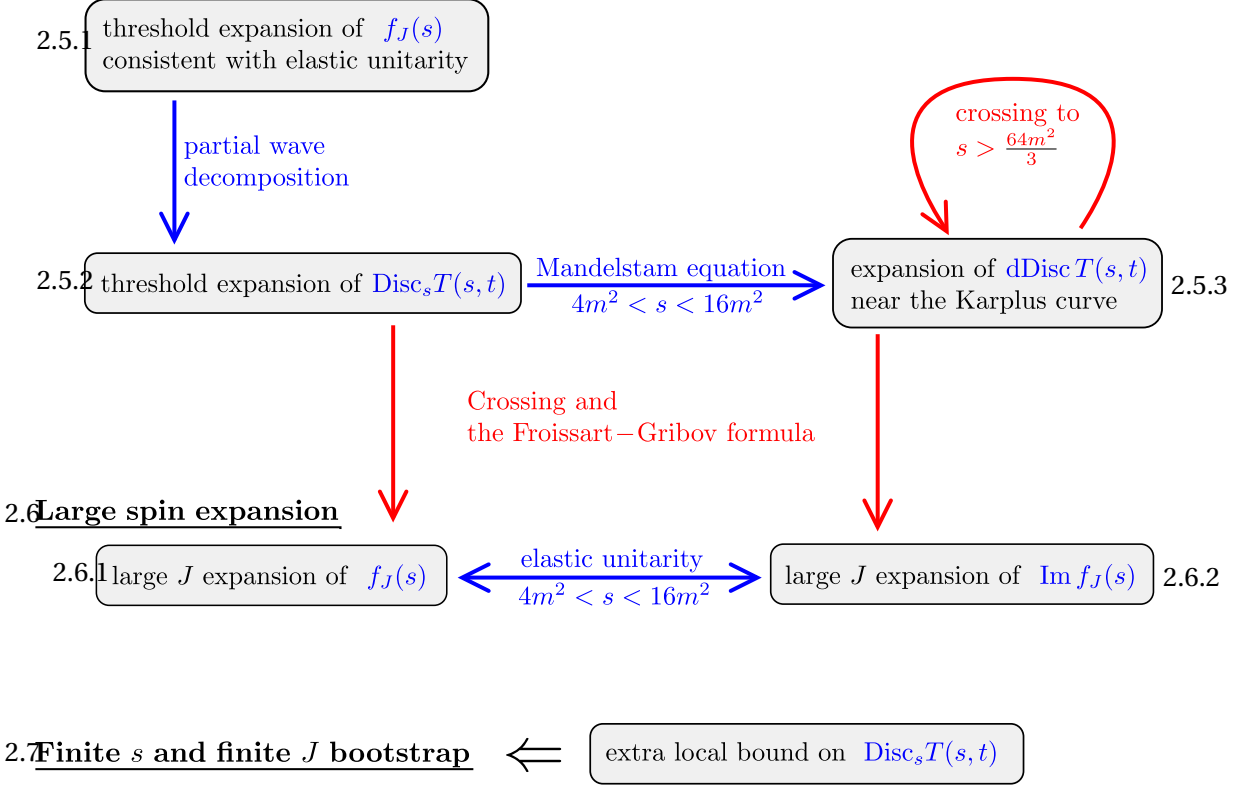


Figure 2.9: The logical structure of sections 2.5, 2.6 and 2.7. We start in section 2.5 by developing the idea of the threshold expansion. We solve elastic unitarity for  $f_J(s)$  close to  $s = 4m^2$ . This naturally leads to the threshold expansion both for the discontinuity of the amplitude  $T_s(s, t)$  and its double discontinuity  $\rho(s, t)$ . In section 2.6 we use the Froissart-Gribov formula and crossing symmetry of  $\rho(s, t)$  to translate the threshold expansion of discontinuity  $T_s(s, t)$  into the large  $J$  expansion of  $f_J(s)$  and the threshold expansion of  $\rho(s, t)$  into the large  $J$  expansion of  $\text{Im} f_J(s)$  correspondingly. In section 2.7 we give an error bound on these expansion in terms of an extra phenomenological bound on the discontinuity of the amplitude.

kinematical small parameters, as well as the relation between the two expansions.

One kinematical small parameter that always exists in a gapped theory is the energy distance from the two-particle threshold in units of the mass gap,

$$\sigma_s = \frac{s}{4m^2} - 1 = \frac{\vec{p}^2}{m^2}, \tag{2.5.1}$$

where in the last equality we evaluated  $\sigma_s$  in the center-of-mass frame (2.2.7).

The threshold expansion is, thus, an expansion in powers of  $\sigma_s$ . The small  $\sigma_s$  expansion is known in nuclear physics as *the effective range expansion* [61]. As we take  $\sigma_s \ll 1$  or, equivalently,  $|\vec{p}| \ll m$  scattering becomes non-relativistic and we can characterize it by some effective potential whose properties are captured by the threshold expansion parameters [62].

In this section we use elastic unitarity, extended analyticity and crossing to argue that both the discontinuity and the double discontinuity of the scattering amplitude admit a natural threshold expansion. Importantly, the parameters that enter the threshold expansion are controlled by the low energy physics which is well-known from the experiments or lattice simulations, see e.g. [63].

Whenever a theory has a conserved charge, there is a natural small parameter – one over the charge of states that are being exchanged. In the case at hand, the only symmetry we assume is Lorentz symmetry. Correspondingly, the only available conserved charge is the spin. Indeed, in the next section we will show that the partial wave coefficients admit a systematic large  $J$  expansion. Moreover, by combining the Froissart-Gribov formula with crossing we will relate the threshold expansion to the large spin expansion.

The logical structure and steps of this and following sections is summarized in figure 2.9. We start by constructing a threshold expansion of the partial wave coefficients that is consistent with elastic unitarity.

### 2.5.1 Threshold Expansion of $f_J(s)$

To expand the the partial wave coefficients close to the threshold in a way that is consistent with elastic unitarity, it is first convenient to solve the latter in a different fashion than (2.2.39). After dividing by  $|f_J(s)|^2$ , the elastic unitarity condition (2.2.37) takes the form

$$2\text{Im}\frac{1}{f_J(s)} = \frac{1}{i} \left( \frac{1}{f_J(s+i\epsilon)} - \frac{1}{f_J(s-i\epsilon)} \right) = -\frac{(s-4m^2)^{\frac{d-3}{2}}}{\sqrt{s}} \times \begin{cases} 1 & 4m^2 < s < 16m^2 \\ 0 & 0 < s < 4m^2 \end{cases} . \quad (2.5.2)$$

Hence,  $1/f_J$  has a branch cut at threshold for even  $d$  and a logarithmic cut for odd  $d$ . The general solution to (2.5.2) combined with real analaticity (2.2.35) takes the form

$$\frac{1}{f_J(s+i\epsilon)} = b_J(\sigma_s) - \frac{i}{2} \frac{(4m^2\sigma_s)^{\frac{d-3}{2}}}{\sqrt{s}} \times \begin{cases} 1 & d \text{ even} \\ \frac{i}{\pi} [\log \sigma_s - i\pi] & d \text{ odd} \end{cases} , \quad (2.5.3)$$

where  $b_J(\sigma_s)$  is a real analytic and single-valued function in some finite neighborhood around the origin, except for potentially isolated singularity at  $\sigma_s = 0$ . Note that in writing (2.5.3) we used the continuity assumption for  $f_J(s)$ , see assumption 5 at the introduction and section 2.2.5.

As we have learned from the Froissart-Gribov representation (see (2.2.54)), as  $\sigma_s \rightarrow 0^+$  from above,  $f_J(s) \rightarrow a_J \sigma_s^J$  (2.2.55). In terms of the function  $b_J(\sigma)$ , this behavior is

$$b_J(\sigma) = \frac{m^{d-4}}{a_J \sigma_s^J} + \mathcal{O}(\sigma_s^{1-J}), \quad J \geq 2, \quad (2.5.4)$$

where we have assumed that  $J_0(4m^2) < 2$ . For  $J = 0$  we do not expect the Froissart-Gribov

## Chapter 2. An analytical toolkit for the S-matrix bootstrap

representation to hold close to  $\sigma_s = 0$ . Therefore we do not have a similar prediction. After factoring out the leading threshold singularity of  $b_{J \geq 2}(\sigma)$ , it has a regular expansion

$$b_{J \geq 2}(\sigma_s) = \frac{m^{d-4}}{\sigma_s^J} \left( \frac{1}{a_J} + \sum_{i=1}^{\infty} b_{J,i} \sigma_s^i \right) \quad \text{and} \quad b_0(\sigma_s) = \frac{m^{d-4}}{\sigma_s^{\tilde{J}_0}} \sum_{i=0}^{\infty} b_{0,i} \sigma_s^i, \quad (2.5.5)$$

where  $\tilde{J}_0$  is an unconstrained integer at this point and  $a_J, b_{J,i}$  are real coefficients. Reality of scattering lengths  $a_J$  and effective ranges  $b_{i,J}$  follows from real analyticity property of the partial waves coefficients (2.2.35). For actual values of these parameters in various QCD processes see e.g. [64].

Similarly, using real analaticity of  $b_J(s)$ , we have the following equations for the imaginary part of the partial wave in the elastic unitarity region

$$\begin{aligned} \text{Im} f_J(s) &= \frac{(4m^2 \sigma_s)^{\frac{d-3}{2}}}{2\sqrt{s}} \left[ b_J^2(\sigma_s) + \frac{(4m^2 \sigma_s)^{d-3}}{4s} \right]^{-1} & d \text{ even}, \\ \text{Im} f_J(s) &= \frac{(4m^2 \sigma_s)^{\frac{d-3}{2}}}{2\sqrt{s}} \left[ \left( b_J(\sigma_s) + \frac{(4m^2 \sigma_s)^{\frac{d-3}{2}}}{2\pi\sqrt{s}} \log \sigma_s \right)^2 + \frac{(4m^2 \sigma_s)^{d-3}}{4s} \right]^{-1} & d \text{ odd}. \end{aligned} \quad (2.5.6)$$

To summarize, by plugging (2.5.5) into (2.5.3) and (2.5.6) we have constructed a threshold expansion of  $f_J(s)$  and  $\text{Im} f_J(s)$  that automatically solves elastic unitarity for any real coefficients.

Note that the most singular possible threshold behavior is completely fixed by elastic unitarity, with no free coefficient. It comes from  $J = 0$  and corresponds to setting  $b_0(\sigma_s) = 0$  in (2.5.3), so that the partial wave is dominated by the universal term

$$\text{Im} f_0(s) = \frac{2^{5-d} m^{4-d}}{\sigma_s^{\frac{d-3}{2}}} \times \begin{cases} 1 + \dots & d \text{ even} \\ \frac{\pi^2}{\log^2 \sigma_s + \pi^2} + \dots & d \text{ odd} \end{cases}. \quad (2.5.7)$$

In particular, this implies that the spin zero scattering length is infinite. In  $d = 3$  the threshold behavior (2.5.7) is realized in massive  $\phi^4$  theory [65]. In  $d = 4$  the asymptotic behavior (2.5.7) appeared in the study of coupling maximization in [1] and corresponds to having a bound state at  $s = 4m^2$ .<sup>23</sup> For  $J \geq 2 \geq J_0(s)$  the singular behavior (2.5.7) does not occur due to (2.2.54).

Below we will also be interested in the case of finite  $\text{Im} f_0(s)$ . In this case, the spin zero scattering length is finite, namely  $b_0(s) = \frac{m^{d-4}}{a_0}$ , and we get the following leading behavior of  $\text{Im} f_0(s)$

$$\text{Im} f_0(s) = 2^{d-5} m^{4-d} a_0^2 \sigma_s^{\frac{d-3}{2}} + \dots, \quad d > 3. \quad (2.5.8)$$

As a final remark, note that the analysis of this section can also be generalized to non-integer

<sup>23</sup>By tuning the parameters of the theory it could be possible to reach this situation in QCD as well. We thank Mattia Bruno and Maxwell Hansen for the discussion.

spin, see appendix A.6.

### 2.5.2 Threshold Expansion of Discontinuity

For our purposes we will be interested in a closely related expansion, that of the discontinuity of the amplitude  $T_s(s, t)$  for  $t > 4m^2$  and  $\sigma_s \rightarrow 0$ . As we will see, the Froissart-Gribov formula (2.2.53) relates this expansion to the large  $J$  behavior of the partial wave coefficients.

We proceed by considering the  $s$ -channel partial wave expansion for the discontinuity of the amplitude

$$T_s(s, t) = n_{J=0}^{(d)} \text{Im} f_0(s) + \sum_{J=2}^{\infty} n_J^{(d)} \text{Im} f_J(s) P_J^{(d)} \left( 1 + \frac{2t}{s-4m^2} \right). \quad (2.5.9)$$

For  $s$  close to  $4m^2$ , the sum over  $J$  above converges inside the large  $s$ -channel Lehmann ellipse which is for  $t < \frac{16m^2 s}{s-4m^2}$ . Given some fixed  $t$ , and considering the limit  $s \rightarrow 4m^2$  we stay within the convergence region.

We can now plug (2.5.6) into (2.5.9) and perform the threshold expansion under the sum. We get

$$T_s(s, t) = n_0^{(d)} \text{Im} f_0(s) + n_2^{(d)} a_2^2 m^{4-d} \left( \frac{t}{m^2} \right)^2 \frac{2^{d-7} (d-1)}{(d-2)} \sigma_s^{2+\frac{d-3}{2}} + \dots, \quad (2.5.10)$$

where we can systematically expand  $T_s(s, t)$  using the threshold expansion of partial waves (2.5.5) which is based on elastic unitarity. Note that the expansion parameter in even dimensions is simply  $\sigma_s$ , whereas in odd dimensions we have in addition powers of  $\log \sigma_s$ , as well as inverse powers  $\frac{1}{\log \sigma_s}$ , which we do not write here explicitly.

Let us emphasize that in the argument above it was absolutely crucial to consider the discontinuity of the amplitude  $T_s(s, t)$  and not the amplitude  $T(s, t)$  itself. Indeed, if we were to try repeating the argument above for  $T(s, t)$  itself, we would run into the following problem. In (2.5.9) we have partial waves  $f_J(s) \sim (s-4m^2)^J$  and Legendre polynomials behaving as  $P_J^{(d)} \left( 1 + \frac{2t}{s-4m^2} \right) \sim (s-4m^2)^{-J}$ . Therefore the expansion for  $s \rightarrow 4m^2$  requires re-summation of partial waves of all spins which is beyond our control.

The conclusion is that  $T_s(s, t)$  admits a systematic threshold expansion in terms of the solution to elastic unitarity in the  $s$ -channel. Moreover, the contribution of higher spin partial waves are suppressed by an additional factor of  $\sigma_s^J$ . We expect the threshold expansion converges as long as we stay below the leading Landau curve, namely for  $t < \frac{16m^2 s}{s-4m^2}$ . Luckily for us, it is the discontinuity of the amplitude and not the amplitude itself that enters the Froissart-Gribov inversion formula. Therefore the results of this section can be readily put to use.

### 2.5.3 Threshold Expansion for Double Spectral Density

We now turn to the study the double spectral density (2.3.7) close to the leading Landau curve. We consider the Mandelstam equation (2.3.9) that is repeated here for convenience

$$\rho(s, t) = \frac{(s - 4m^2)^{\frac{d-3}{2}}}{4\pi^2 (4\pi)^{d-2} \sqrt{s}} \int_{z_1}^{\infty} d\eta' \int_{z_1}^{\infty} d\eta'' \mathcal{T}_t^{(+)}(s, \eta') \mathcal{T}_t^{(-)}(s, \eta'') \text{Disc}_z K(z, \eta', \eta''), \quad (2.5.11)$$

where  $4m^2 < s < 16m^2$ . The crucial observation is that when we are very close to the leading Landau curve  $t = \frac{16m^2 s}{s - 4m^2}$ , the integral in (2.5.11) is again controlled by the threshold expansion of  $\mathcal{T}_t^{(+)}(s, \eta')$  and  $\mathcal{T}_t^{(-)}(s, \eta'')$ . The reason for this is that the region of integration starts at the threshold,  $\eta', \eta'' \geq z_1$ , and ends at the boundary of support of the kernel,  $\eta_+( \eta', \eta'') \leq z$ . As  $t$  approach the leading Landau curve, this region shrinks close to the threshold for both  $\eta'$  and  $\eta''$  integrals, see figure 2.3.

A convenient small parameter in the problem is the dimensionless distance from the Landau curve, see (2.3.11)

$$\delta z \equiv z - (2z_1^2 - 1) \propto t - \frac{16m^2 s}{s - 4m^2}. \quad (2.5.12)$$

We can now plug the threshold expansion of the discontinuity (2.5.5) into (2.5.11) and expand the result in powers of  $\delta z$ . At any given order in that expansion only finite number of terms in the threshold expansion of the discontinuity contribute. For even spacetime dimension, the relevant integrals that appears in the expansion are

$$\tilde{I}_{n_1, n_2}^{(d)}(z) \equiv \int_{z_1}^{\infty} d\eta' \int_{z_1}^{\infty} d\eta'' \sigma_{t(\eta')}^{n_1 - \frac{d-3}{2}} \sigma_{t(\eta'')}^{n_2 - \frac{d-3}{2}} \text{Disc}_z K(z, \eta', \eta''). \quad (2.5.13)$$

To leading order in  $\delta z$  this integral is given by<sup>24</sup>

$$\tilde{I}_{n_1, n_2}^{(d)}(z) = 2 \frac{\pi^{\frac{d+1}{2}} (z_1 - 1)^{d-3-n_1-n_2}}{z_1^{n_1+n_2+1} (z_1^2 - 1)^{1/2}} \left( \frac{\delta z}{2} \right)^{n_1+n_2+\frac{5-d}{2}} \frac{\Gamma(n_1 + \frac{5-d}{2}) \Gamma(n_2 + \frac{5-d}{2})}{\Gamma(n_1 + n_2 + \frac{7-d}{2})} (1 + \mathcal{O}(\delta z)). \quad (2.5.15)$$

For  $n_1, n_2 \leq \frac{d-5}{2}$  the integral (2.5.13) diverges, but this apparent divergence is not physical. Namely, the integral in (2.5.15) originates from the contour integral that wraps around  $\eta', \eta'' = z_1$ . Therefore, the integral can be safely deformed to a keyhole contour around the dangerous region, see figure 2.10. The result of the keyhole integration is equivalent to analytically continuing (2.5.15) in  $m, n$  (as long as the final result is finite).

<sup>24</sup>To derive (2.5.15) it is useful to do the following change of integration variables close to  $\delta z = 0$

$$\eta' = z_1 + \frac{\delta z}{2z_1} \alpha x, \quad \eta'' = z_1 + \frac{\delta z}{2z_1} \alpha (1 - x), \quad (2.5.14)$$

where the integration in (2.5.11) for  $\delta z \ll 1$  is restricted to  $0 \leq x$  and  $\alpha \leq 1$ .



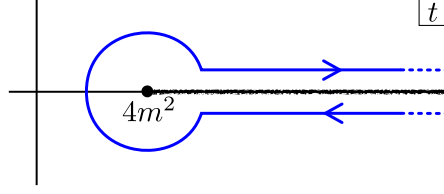


Figure 2.10: The discontinuity of the Mandelstam equation (2.3.9) has been obtained by deforming the contour of integration in the finite integral (2.3.8). Hence, the result cannot diverge. This means that an apparent divergence in (2.5.13) that comes from the region of integration close to the threshold should be understood as a finite keyhole contour integral plotted here.

We see that indeed, higher powers in the threshold expansion result in higher powers of  $\delta z$ . For odd spacetime dimension, due to the presence of  $\frac{1}{\log^2 \sigma_s + \pi^2}$  in (2.5.6), the relevant integral is more complicated, but the power suppression in  $\delta z$  is of course the same. We discuss it more in appendix A.8.2.

The most singular possible behavior close to the Landau curve comes from the corresponding universal threshold behavior of  $\text{Im } f_0(t)$  in (2.5.7) and corresponds to  $n_1 = n_2 = 0$  in (2.5.13). In that case we find

$$\rho(s, t) = (2^{5-d} n_0^{(d)})^2 \frac{(d-3)\pi^{\frac{3-d}{2}} m^{4-d} (z_1 - 1)^{\frac{d-3}{2}}}{32(5-d) \cos\left(\frac{\pi d}{2}\right) \Gamma\left(\frac{d-1}{2}\right) z_1 (z_1 + 1)} \delta z^{\frac{5-d}{2}} + \dots, \quad d \text{ even}. \quad (2.5.16)$$

On the other hand, for the case where the spin zero scattering length is finite (2.5.8), we have  $n_1 = n_2 = d - 3$  in (2.5.13) and correspondingly the approach to the Landau curve is much softer

$$\rho(s, t) = \frac{a_0^4 \pi^{\frac{1-d}{2}} m^{4-d} (z_1 - 1)^{\frac{9-3d}{2}} z_1^{5-2d} \Gamma\left(\frac{d-1}{2}\right)^2 (n_0^{(d)})^2}{512(z_1 + 1) \Gamma\left(\frac{3d-5}{2}\right)} \delta z^{\frac{3d-7}{2}} + \dots \quad (2.5.17)$$

#### 2.5.4 Radius of Convergence

Let us briefly discuss the radius of convergence of the threshold expansion introduced above. As usual the radius of convergence is controlled by the analytic properties of the function at hand.

Consider first  $f_J(s)$ . It has a normal threshold cut starting at  $s = 4m^2$  and multi-particle cuts at  $s \geq 16m^2$ , as well as the  $u$ -channel cut for  $s \leq 0$ . In addition to that we can have bound states and resonances (which correspond to poles on the second sheet). In a given theory, we expect the singularity that is the closest to  $s = 4m^2$  to control the convergence radius of the threshold expansion of  $f_J(s)$ . In this chapter we assume for simplicity that there are no bound states, however it should be easy to include them in the analysis.

Consider next  $T_s(s, t)$ . In this case, the partial wave expansion (2.5.9) converges below the first

## Chapter 2. An analytical toolkit for the S-matrix bootstrap

---

Landau curve. For  $4m^2 < s < 16m^2$  and  $t > 16m^2$ , that is the regime of  $\sigma_s < \frac{16m^2}{t-16m^2}$ . Moreover, if we are to first expand each  $\text{Im}f_J(s)$  close to the threshold under the sum, we will have to argue that the sum over  $J$  and the threshold expansion commute. It is not clear to us how to do it. Instead below we adopt a different approach. We separate a few low spin partial waves in (2.5.9) and apply the threshold expansion to them. We then bound the sum over spins without doing the threshold expansion under the sum over spins.

### 2.6 Large $J$ Expansion

In this section we map the threshold expansion developed in the previous section to the large  $J$  expansion of the partial waves coefficients  $f_J(s)$ .<sup>25</sup>

The basic idea is very simple. The Froissart-Gribov formula (2.2.53) directly maps the threshold expansion of the discontinuity of the amplitude (2.5.10) to the large  $J$  expansion of the partial wave coefficients in the crossed channel.<sup>26</sup> Interestingly, once combined with crossing, the Froissart-Gribov formula allows us to map the low energy threshold expansion, that is dominated by the low spins, to the large spin behavior of the partial wave coefficients for any energy and in the same channel. In particular, it automatically predicts the amount of inelasticity at large  $J$ .

In this section we will use the results for the threshold expansion of the double spectral density and the discontinuity of the amplitude in the crossed  $t$ -channel as opposed to the  $s$ -channel threshold expansion of the previous section. We hope this will not cause any confusion. In sections 2.6.1 and 2.6.2 we work out the leading large  $J$  expressions for  $f_J(s)$  and  $\text{Im}f_J(s)$  correspondingly. In section 2.6.3 we compute the exact contribution of a given term in the threshold expansion of the amplitude to the partial waves. This includes infinitely many  $\frac{1}{J}$  corrections to the results of 2.6.1 and 2.6.2.

Note that in this section we only concern ourselves with the threshold expansion of the amplitude close to the two-particle threshold. Of course, in addition there are contributions from multi-particle thresholds. These lead to further nonperturbative in  $\frac{1}{J}$  corrections to the results of this section and are potentially important if we would like to discuss partial waves at finite  $J$  which is the subject of the next section.

---

<sup>25</sup>In  $d = 4$  this was pioneered by Dragt [66], see also [67], and further developed by A. W. Martin in [68]. Here we consider a slightly more general form of the amplitude, as well as generalize the analysis to any spacetime dimension.

<sup>26</sup>This is analogous to the analytic bootstrap in CFTs [69, 70, 71].

### 2.6.1 Large Spin Expansion of $f_J(s)$

We start by analyzing the Froissart-Gribov integral (2.2.53) in the large spin limit  $J \gg 1$ . For convenience, we quote the integral here

$$f_J(s) = \frac{2\mathcal{N}_d}{\pi} \int_{z_1}^{\infty} dz (z^2 - 1)^{\frac{d-4}{2}} Q_J^{(d)}(z) T_t(s, t(z)), \quad \text{Re}[J] > J_0(s). \quad (2.6.1)$$

The large  $J$  behavior of  $Q_J^{(d)}(z)$  is given by<sup>27</sup>

$$Q_J^{(d)}(z) = 2^{d-4} \sqrt{\pi} \frac{\Gamma\left(\frac{d-2}{2}\right)}{J^{\frac{d-3}{2}}} \frac{\lambda(z)^{-J}}{(\lambda(z)^2 - 1)^{\frac{d-3}{2}}} (1 + \mathcal{O}(1/J)), \quad (2.6.3)$$

where

$$\lambda(z) \equiv z + \sqrt{z^2 - 1} = e^\theta \quad \text{for} \quad |z| > 1, \quad \text{Re}\theta > 0. \quad (2.6.4)$$

Crucially,  $Q_J^{(d)}(z)$  decays very fast for fixed  $z > 1$  at large  $J$ . The integral is therefore dominated by the region close to the threshold  $z_1$ . Explicitly, for  $J \gg 1$  we have

$$Q_J^{(d)}\left(z_* + \frac{\sqrt{z_*^2 - 1} \delta z}{J}\right) = 2^{d-4} \sqrt{\pi} \frac{\Gamma\left(\frac{d-2}{2}\right)}{J^{\frac{d-3}{2}}} \frac{\lambda(z_*)^{-J}}{(\lambda(z_*)^2 - 1)^{\frac{d-3}{2}}} e^{-\delta z} (1 + \mathcal{O}(1/J)), \quad (2.6.5)$$

and therefore the integral in (2.6.1) is controlled by the region of the size  $\sim \frac{1}{J}$  close to  $z_* = z_1$ . In that way, the large  $J$  behavior is controlled by the threshold expansion of  $T_t(s, t(z))$  established in the previous section in a manifest way.

Next, we explicitly plug the threshold expansion into (2.6.1) and compute the leading large  $J$  behavior of the partial wave coefficients. For that aim, it is convenient to express the integral

<sup>27</sup>An efficient way to systematically expand  $Q_J^{(d)}(z)$  to an arbitrary order in the large  $J$ , fixed  $z$  expansion is to start from its representation in terms of the hypergeometric function [72]

$$Q_J^{(d)}(z) = 2^{d-4} \sqrt{\pi} \frac{\Gamma\left(\frac{d-2}{2}\right) \Gamma(J+1)}{\Gamma\left(J + \frac{d-1}{2}\right)} \frac{\lambda(z)^{-J}}{(\lambda(z)^2 - 1)^{\frac{d-3}{2}}} {}_2F_1\left(1 - \frac{d-3}{2}, \frac{d-3}{2}; J + \frac{d-1}{2}; \frac{1}{1-\lambda(z)^2}\right), \quad (2.6.2)$$

and then use the series representation for the hypergeometric function as  ${}_2F_1(a, b; c; x) = \sum_{k=0}^{\infty} \frac{(a)_k (b)_k}{k! (c)_k} x^k$ . The spin,  $J$ , only enters in the Pochhammer  $(c)_k = (J + \frac{d-1}{2})_k$  and therefore the  $k$ 'th term only contributes at order  $1/J^k$  and higher. Note that for  $d = 3$  there are no  $\frac{1}{J}$  corrections to (2.6.3). More generally, in odd  $d$  the large  $J$  properties of  $Q_J^{(d)}(z)$  can be made manifest, see appendix A.3.

## Chapter 2. An analytical toolkit for the S-matrix bootstrap

---

as follows

$$f_J(s) \equiv \frac{\mathcal{N}_d}{\sqrt{\pi}} \frac{\Gamma\left(\frac{d-2}{2}\right)}{J^{\frac{d-1}{2}}} \frac{(\lambda(z_1)^2 - 1)^{\frac{d-3}{2}}}{\lambda(z_1)^{J+d-3}} \hat{f}_J(s), \quad \hat{f}_J(s) = \int_0^\infty d\delta z T_t(s, t(\delta z, J)) e^{-\delta z} (1 + \mathcal{O}(1/J)), \quad (2.6.6)$$

where we have<sup>28</sup>

$$\sigma_t = \frac{1}{J} \left( \frac{z_1 + 1}{z_1 - 1} \right)^{1/2} \delta z. \quad (2.6.7)$$

Note that in deriving (2.6.6) we took into account the integration measure  $(z^2 - 1)^{\frac{d-4}{2}}$  and the Jacobian from switching the integration variable to  $\delta z$ .

After performing the crossing transformation  $s \leftrightarrow t$ , we can now plug the leading threshold expansion expressions from the previous section (2.5.10) to get the  $J \gg 1$  limit of  $f_J(s)$ . Let us start with the universal and most singular case (2.5.7). For this case we get

$$\hat{f}_J(s) = 2^{5-d} n_0^{(d)} m^{4-d} J^{\frac{d-3}{2}} \left( \frac{z_1 - 1}{z_1 + 1} \right)^{\frac{d-3}{4}} (1 + \mathcal{O}(1/J)) \times \begin{cases} \pi^2 g_{\frac{d-3}{2}} \left( \log J \sqrt{\frac{z_1 - 1}{z_1 + 1}} \right) & d \text{ odd} \\ \Gamma\left(\frac{5-d}{2}\right) & d \text{ even} \end{cases}, \quad (2.6.8)$$

where the explicit form of the slowly-varying function  $g_{\frac{d-3}{2}}(\log x)$  is computed in appendix A.8.

If, on the other hand, we consider the situation with a finite spin zero scattering length (2.5.8), we get

$$\hat{f}_J(s) = 2^{d-5} n_0^{(d)} a_0^2 \Gamma\left(\frac{d-1}{2}\right) m^{4-d} \frac{1}{J^{\frac{d-3}{2}}} \left( \frac{z_1 + 1}{z_1 - 1} \right)^{\frac{d-3}{4}} (1 + \mathcal{O}(1/J)). \quad (2.6.9)$$

It is clear that we can systematically include  $\frac{1}{J}$  correction in this expansion. Note that in all cases, the leading large  $J$  result for  $f_J(s)$  is exponentially small and purely real. In the next section we compute the leading  $J$  contribution to  $\text{Im} f_J(s)$ .

### 2.6.2 Large Spin Expansion of $\text{Im} f_J(s)$

We now repeat the analogues large  $J$  expansion for  $\text{Im} f_J(s)$  in terms of the threshold expansion of the double spectral density. In this case, the Froissart-Gribov formula can be written as

$$\text{Im} f_J(s) = \frac{2\mathcal{N}_d}{\pi} \int_{z_1}^\infty dz (z^2 - 1)^{\frac{d-4}{2}} Q_J^{(d)}(z) \rho(s, t(z)), \quad \text{Re}[J] > J_0(s). \quad (2.6.10)$$

---

<sup>28</sup>Note that  $\delta z$  in (2.6.7) is different from the one used in the previous section.

It is instructive to separate  $s$  into three regions,  $4m^2 < s < 16m^2$ ,  $\frac{64}{3}m^2 > s > 16m^2$  and  $s > \frac{64}{3}m^2$ .

### The Elastic Region $4m^2 < s < 16m^2$

In this elastic strip the double spectral density is zero for  $t < \frac{16m^2 s}{s-4m^2}$  or, equivalently, for  $z < 2z_1^2 - 1$ , see figure 2.4. The large  $J$  limit of  $\text{Im} f_J(s)$  is thus dominated by the expansion of double spectral density close to the leading Landau curve which we worked out in section 2.5.3. Hence, we can simply use (2.6.5) with  $z_* = 2z_1^2 - 1$ , otherwise the consideration is identical to the one in the previous subsection. Explicitly, we have

$$\begin{aligned} \text{Im} f_J(s) &= \frac{\mathcal{N}_d}{\sqrt{\pi}} \frac{\Gamma\left(\frac{d-2}{2}\right)}{J^{\frac{d-1}{2}}} \frac{([\lambda(2z_1^2 - 1)]^2 - 1)^{\frac{d-3}{2}}}{[\lambda(2z_1^2 - 1)]^{J+d-3}} \text{Im} \hat{f}_J(s), \quad 4m^2 < s < 16m^2, \\ \text{Im} \hat{f}_J(s) &= \int_0^\infty d\delta z e^{-\delta z} \rho(s, t(\delta z, J)) (1 + \mathcal{O}(1/J)), \end{aligned} \quad (2.6.11)$$

where

$$z = (2z_1^2 - 1) + \frac{2z_1 \sqrt{z_1^2 - 1}}{J} \delta z, \quad t(\delta z, J) = 8m^2 \left( z_1 + 1 + \frac{z_1}{J} \left( \frac{z_1 + 1}{z_1 - 1} \right)^{1/2} \delta z \right). \quad (2.6.12)$$

Therefore, upon making a substitute  $\delta z \rightarrow \frac{2z_1 \sqrt{z_1^2 - 1}}{J} \delta z$  in the formulas of section 2.5.3, we can directly plug them into (2.6.11). The resulting large  $J$  behavior with the universal threshold expansion (2.5.7) takes the following form

$$\text{Im} \hat{f}_J(s) = 2^{-5\frac{(d-3)}{2}} \left( n_0^{(d)} \Gamma\left(\frac{5-d}{2}\right) \right)^2 m^{4-d} \pi^{\frac{1-d}{2}} J^{\frac{d-5}{2}} z_1^{\frac{3-d}{2}} \left( \frac{z_1 - 1}{z_1 + 1} \right)^{\frac{d-1}{4}} (1 + \mathcal{O}(1/J)), \quad d \text{ even}, \quad (2.6.13)$$

where again the case of  $d$  odd should be considered separately using the results of appendix A.8.

Turning to the case with a finite spin zero scattering length (2.5.8), we get

$$\text{Im} \hat{f}_J(s) = \frac{2^{\frac{3d-25}{2}} \left( n_0^{(d)} a_0^2 \Gamma\left(\frac{d-1}{2}\right) \right)^2}{\pi^{\frac{d-1}{2}} m^{d-4} J^{\frac{3d-7}{2}}} \frac{1}{z_1^{\frac{d-3}{2}}} \left( \frac{z_1 + 1}{z_1 - 1} \right)^{\frac{3d-11}{4}} (1 + \mathcal{O}(1/J)). \quad (2.6.14)$$

An alternative way to arrive at (2.6.13) and (2.6.14) is to start from the large  $J$  expansion of  $f_J(s)$  discussed in the previous section (2.6.8) and use elastic unitarity. Indeed, one can check

## Chapter 2. An analytical toolkit for the S-matrix bootstrap

---

that (2.6.8) and (2.6.13), (2.6.14) are consistent with elastic unitarity

$$\log \frac{2\text{Im}f_J(s)}{\frac{(s-4m^2)^{\frac{d-3}{2}}}{\sqrt{s}} |f_J(s)|^2} = 0, \quad 4m^2 < s < 16m^2. \quad (2.6.15)$$

### The Inelastic Region $16m^2 < s < \frac{64}{3}m^2$

This regime is in the multi-particle part of figure 2.4. To analyze it one should first identify the leading Landau curve in that segment, which is beyond the scope of this work.

### The Inelastic Region $s > \frac{64}{3}m^2$

As  $s$  increases passed  $\frac{64m^2}{3}$ , we know from crossing that the leading Landau curve is the one of the dual channel (the blue curve in figure 2.4). A remarkable consequence of this fact is that crossing allows us to measure the non-zero inelasticity at large spin  $J$ .

As before the leading large  $J$  behavior of  $\text{Im}f_J(s)$  is controlled by the leading Landau curve in the relevant kinematics. For  $s > \frac{64}{3}m^2$  the leading Landau curve is at  $t = t_1(s) = \frac{4m^2s}{s-16m^2}$ , or equivalently at

$$z = \tilde{z}_1 \equiv \frac{4 - 3z_1 + z_1^2}{5 - 3z_1}. \quad (2.6.16)$$

See blue curve on figure 2.4.

In this case we get that the Froissart-Gribov integral takes the same form as in (2.6.10) with

$$z_1 \rightarrow \tilde{z}_1, \quad t(\delta z, J) = 4m^2 \left( \frac{\tilde{z}_1 - 1}{z_1 - 1} + \frac{1}{J} \frac{\sqrt{\tilde{z}_1^2 - 1}}{z_1 + 1} \delta z \right) \quad \text{and} \quad s > \frac{64}{3}m^2, \quad (2.6.17)$$

where  $t(\delta z, J)$  is a definition of  $\delta z$  that we will use below.

The double spectral density close to  $\tilde{z}_1$  is given by the results of section 2.5.3 upon application of crossing  $s \leftrightarrow t$ .<sup>29</sup> Considering the amplitudes with the universal threshold expansion (2.5.7) we get

$$\text{Im}\hat{f}_J(s) = \frac{J^{\frac{d-5}{2}} \left( n_0^{(d)} \Gamma\left(\frac{5-d}{2}\right) \right)^2}{8(2m)^{d-4} (\tilde{z}_1^2 - 1)^{\frac{d-5}{4}} \pi^{\frac{d-1}{2}}} \frac{(z_1 - 1)^{\frac{3d-13}{2}}}{(1+z_1)(3-z_1)(5-3z_1)^{d-6}} (1 + \mathcal{O}(1/J)), \quad d \text{ even}. \quad (2.6.18)$$

---

<sup>29</sup>By taking  $s \rightarrow \infty$  with  $x = \frac{m^3}{s^{3/2}} J$  kept fixed in (2.6.11), (2.6.17) one gets the  $d$ -dimensional version of the Haan-Mütter scaling law [73, 74].

In odd  $d$  the situation is more complicated due to the logarithmic nature of the threshold singularity. While the leading power dependence on  $J$  can be easily computed, we do not give an explicit form for the dependence on  $\log J$  that multiplies the leading power.<sup>30</sup>

For the case of finite spin zero scattering length (2.5.8), we get in any  $d$

$$\text{Im} \hat{f}_J(s) = \frac{\left(n_0^{(d)} a_0^2 \Gamma\left(\frac{d-1}{2}\right)\right)^2}{2^{d+7} m^{d-4} \pi^{\frac{d-1}{2}}} \frac{(\bar{z}_1^2 - 1)^{\frac{3d-7}{4}} (5 - 3z_1)^{3(d-2)} (z_1 - 1)^{\frac{11-5d}{2}}}{J^{\frac{3d-7}{2}} (1+z_1)(3-z_1)^{2d-5}} (1 + \mathcal{O}(1/J)). \quad (2.6.19)$$

We can use the results above for the leading large  $J$  behavior of  $\text{Im} \hat{f}_J(s)$  for  $s > \frac{64}{3} m^2$  to estimate the amount of inelasticity that exists at given  $s$  and  $J$ . Recall that if the scattering were purely elastic partial waves would satisfy  $2\text{Im} f_J(s) = \frac{(s-4m^2)^{\frac{d-3}{2}}}{\sqrt{s}} |f_J(s)|^2$ , see (2.6.15).

Using the explicit results of this section we conclude that elastic unitarity together with crossing lead to the universal inelasticity ratio at large  $J$

$$r_J(s) \equiv \log \frac{2\text{Im} f_J(s)}{\frac{(s-4m^2)^{\frac{d-3}{2}}}{\sqrt{s}} |f_J(s)|^2} = J \log \frac{\lambda(z_1)^2}{\lambda(\bar{z}_1)} + O(1), \quad s > \frac{64m^2}{3}. \quad (2.6.20)$$

In figure 2.11 we plotted  $r_J(s)$  as a function of  $s/m^2$  for fixed  $J$ . We see that  $r_J(s)$  approaches 0 for  $s = 20m^2$  and  $s = \infty$ . It acquires its maximal value of about  $0.47J$  at  $s = 40m^2$ .

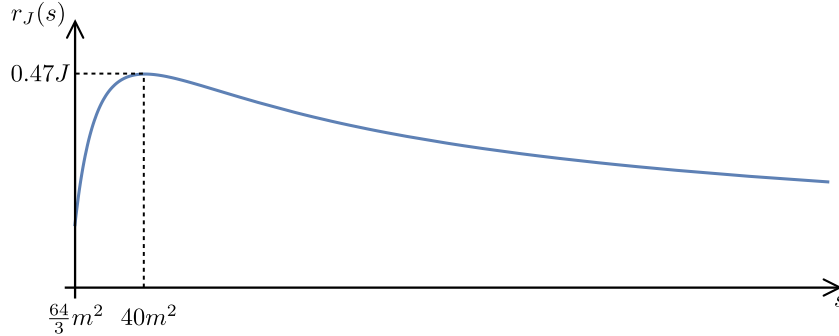


Figure 2.11: The large spin inelasticity ratio  $r_J(s)$  in (2.6.20) plotted for  $s > \frac{64}{3} m^2$ . The maximum value of the ratio is achieved at  $s = 40m^2$  for which we get  $r_J(40m^2) \simeq 0.473J(1 + \mathcal{O}(1/J))$ .

### 2.6.3 Threshold Expansion in the $J$ -space

In this section we evaluate exactly the contribution of a given term in the threshold expansion to the partial waves. This generalizes the results above which correspond to the large  $J$  limit of the exact formulas that we present in the current section. For simplicity let us first focus on  $d$  even, when the threshold behavior is of the square-root type.

<sup>30</sup>It should be possible to use the integral form for  $\rho(s, t)$  given in appendix A.8.2 to efficiently evaluate the integral numerically for given  $J$  but we do not pursue it here.

## Chapter 2. An analytical toolkit for the S-matrix bootstrap

---

Consider the threshold expansion of the discontinuity of the amplitude. In the regime where it converges close to the threshold we can write

$$T_t(s, t(z)) = \sum_{n=0}^{\infty} c_n(s) \left( \frac{z-z_1}{z_1-1} \right)^{n+\frac{3-d}{2}} = \sum_{n=0}^{\infty} c_n(s) \sigma_t^{n+\frac{3-d}{2}}. \quad (2.6.21)$$

In practice we truncate this expansion at any desired order and plug it into the Froissart-Gribov formula. Note that the Froissart-Gribov integral goes all the way to infinite  $z$  where the expansion (2.6.21) is no longer valid. However, that regime of integration is exponentially suppressed in  $J$  and therefore only affects the nonperturbative corrections at large  $J$ . It turns out that the relevant integral can be done exactly. It is given by

$$I_{n,J}^{(d)}(z_1) \equiv \frac{2\mathcal{N}_d}{\pi} \int_{z_1}^{\infty} dz (z^2-1)^{\frac{d-4}{2}} \sigma_{t(z)}^{n+\frac{3-d}{2}} Q_J^{(d)}(z) = \frac{2^{\frac{5}{2}} \Gamma(n+\frac{5-d}{2})}{2^n (8\pi)^{\frac{d}{2}} \Gamma(\frac{3}{2}+n)} \frac{(z_1+1)^{n+\frac{1}{2}}}{(z_1-1)^{\frac{2-d}{2}}} Q_{J-n+\frac{d-5}{2}}^{(2n+5)}(z_1). \quad (2.6.22)$$

This formula is derived in appendix A.7 and holds for arbitrary  $J$ ,  $d$  and  $n$ , not necessarily integer. If we expand both sides at large  $J$ , we reproduce the formulas of the previous section. In this way, we arrive at the explicit expression for the large  $J$  expansion of  $f_J(s)$  in terms of the coefficients of the threshold expansion in the crossed channel

$$f_J(s) = \sum_{n=0}^{\infty} c_n I_{n,J}^{(d)}(z_1) + [\text{nonperturbative}]. \quad (2.6.23)$$

Using this expression and the large  $J$  expansion of  $I_{n,J}^{(d)}(z_1)$

$$I_{n,J}^{(d)}(z_1) = \frac{1}{J^{n+1}} \times \frac{2\Gamma(n+\frac{5-d}{2})}{(8\pi)^{\frac{d-1}{2}} \lambda(z_1)^{J+\frac{d-3}{2}}} \frac{(z_1+1)^{n+\frac{1}{2}}}{(z_1-1)^{\frac{2-d}{2}}} \left( \frac{2\lambda(z_1)}{\lambda^2(z_1)-1} \right)^{n+1} (1 + \mathcal{O}(1/J)), \quad (2.6.24)$$

we see that higher orders in the sum are more suppressed in  $J$ . Hence, one can use this representation to explicitly and systematically obtain all the coefficients in the large  $J$  expansion of  $f_J(s)$ , the leading  $1/J$  result of course coincides with the previous analysis.

Similarly, we can write down the threshold expansion formula for  $\rho(s, t)$ . Based on the previous discussion we have

$$\rho(s, t(z)) = \frac{1}{(z-(2z_1^2-1))^{\frac{d-5}{2}}} \sum_{m=0}^{\infty} d_m(s) (z-(2z_1^2-1))^m. \quad (2.6.25)$$

The problem of finding  $d_m(s)$  becomes completely algebraic after we note that (2.6.25) implies

$$\text{Im} f_J(s) = \sum_{m=0}^{\infty} d_m(s) I_{m+1,J}^{(d)}(2z_1^2-1) + [\text{nonperturbative}], \quad (2.6.26)$$

where we again performed the Froissart-Gribov integral exactly.



Elastic unitarity (2.6.15) relates the two expansions, (2.6.23) and (2.6.26). It then allows one to express the  $d_m(s)$ 's in terms of the  $c_n(s)$ 's. This is possible because the  $d_m(s)$ 's do not depend on  $J$ . Equivalently, we can use (2.5.11) to directly map the threshold expansion of  $T_t(s, t)$  to that of  $\rho(s, t)$  near the Landau curve. The details of this expansion are presented in appendix A.7.

## 2.7 Finite $J$ and Finite $s$

In practice, one is interested in making statements about partial waves at some finite (but potentially large) spin  $J$  and finite energy  $s$ . Our ability to make such statements crucially depends on our ability to estimate an error in the Froissart-Gribov integral produced by the approximation to the amplitude. To that extent we can think of the discontinuity of the amplitude as follows

$$T_t(s, t) = T_t^{\text{approx}}(s, t) + T_t^{\text{error}}(s, t), \quad (2.7.1)$$

where  $T_t^{\text{approx}}(s, t)$  is an approximation to  $T_t(s, t)$  based on our knowledge about it. It can involve expansion coefficients close to various normal thresholds, information about resonances, or about the Regge limit. The more information is available to us, the less we can make  $T_t^{\text{error}}(s, t)$  and therefore the better is our knowledge of  $f_J(s)$ .

Assuming continuity of the amplitude we can try to bound the amplitude as follows. Consider a given  $s$  and let us assume that  $T_t(s, t) \sim t^{J_0(s)}$  at large  $t$ . Let us consider an integer  $N > J_0(s) + \frac{d-3}{2}$  and write

$$T_t^{\text{approx}}(s, t) = \sum_{n=0}^{N-1} c_n(s) \left( \frac{z - z_1}{z_1 - 1} \right)^{n + \frac{3-d}{2}}. \quad (2.7.2)$$

Continuity of the amplitude then implies that there exists  $c_N(s)$  such that

$$|T_t^{\text{error}}(s, t)| < c_N(s) \left( \frac{z - z_1}{z_1 - 1} \right)^{N + \frac{3-d}{2}}. \quad (2.7.3)$$

Indeed, this bound matches the neglected term close to the threshold and is also consistent with the Regge behavior since  $N > J_0(s) + \frac{d-3}{2}$ . The minimal value of  $c_N(s)$  depends on the behavior of the amplitude at intermediate  $s$ . In particular if at some fixed  $t = t_0$  the discontinuity develops a ‘‘bump’’, see figure 2.12, then  $c_N(s)$  should be made large enough for (2.7.3) to hold. A familiar example of such a bump is a resonance and it is due to a singularity on the second sheet. More generally, we can call such a bump an outlier. Correspondingly, we call the problem of bounding  $c_N(s)$  ‘‘the problem of outliers.’’<sup>31</sup>

Note that for the integral on (2.7.3) to converge at large  $z$ , we need to take  $J > N + 1$ . Hence, a

<sup>31</sup>For a similar discussion in the context of the CFT bootstrap see [75].

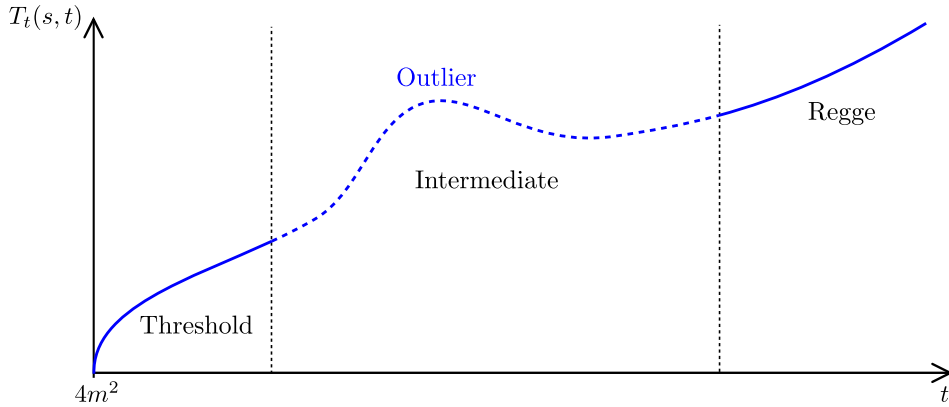


Figure 2.12: The error in our approximation for the inelasticity depends on our knowledge about the discontinuity of the amplitude  $T_t(s, t)$ . Here, the discontinuity is plotted for different energy scales ( $t$ ) at fixed  $s$ . Its structure in the large energy (Regge) and the low energy (threshold) regions are under relatively good control (solid blue line). At intermediate energy scales the amplitude may develop a bump. The problem of outliers is the problem of bounding the discontinuity in this regime, and hence bounding our error for the inelasticity.

better choice of variables to encode our knowledge about the threshold behavior of  $T_t(s, t)$  are ones that do not grow at large  $z$ . For example, we can replace  $(z_1 - 1) \rightarrow (z - 1)$  in (2.7.2). Doing so is necessary if one wants to go to higher orders in the threshold expansion, but we will not pursue this in the present work. The advantage of using just  $(z - z_1)/(z_1 - 1)$  is that the Froissart-Gribov integral is known explicitly, see (2.6.22).

In a related manner, when deriving the Froissart-Gribov formula we do not have to close the contour all the way to infinity. We can instead keep arcs in the complex plane at some finite energy, see figure 2.2.b. This is sometimes called the truncated Froissart-Gribov formula, see e.g. [74, 76]. The problem of deriving finite  $s$  and  $J$  formulae then requires bounding the contribution of the arcs. The advantage of this approach is that we do not have to assume extended analyticity all the way to  $t = \infty$ .

Let us proceed with  $c_N(s)$  in (2.7.3) being our phenomenological parameter and see how various quantities depend on it. First of all, we can immediately bound the error in  $f_J(s)$ . We have

$$\left| f_J(s) - \sum_{n=0}^{N-1} c_n I_{n,J}^{(d)}(z_1) \right| < c_N(s) I_{N,J}^{(d)}(z_1). \quad (2.7.4)$$

where  $I_{n,J}^{(d)}(z)$  is the integral (2.6.22).

Next, we consider  $\text{Im} f_J(s)$ . The relevant regime to study is  $s > \frac{64m^2}{3}$ , where we can estimate inelasticity using our knowledge about the threshold expansion in the crossed channel. In this

case we can start from

$$\text{Im} f_J(s) = \frac{2\mathcal{N}_d}{\pi} \int_{\bar{z}_1}^{\infty} dz (z^2 - 1)^{\frac{d-4}{2}} Q_J^{(d)}(z) \rho(s, t(z)), \quad (2.7.5)$$

and split the  $z$ -integral in two regions,  $4m^2 < t < 16m^2$  and  $t \geq 16m^2$ .

In the region  $4m^2 < t < 16m^2$  we can use the Mandelstam equation to compute  $\rho(s, t)$ . It will involve the terms in the threshold expansion that we worked out above together with an error term that is controlled by (2.7.2) and (2.7.3). For  $t \geq 16m^2$ , since  $\text{Disc}_s T_t^{\text{approx}}(s, t) = 0$ , we have

$$|\rho(s, t)| = |\text{Disc}_s T_t^{\text{error}}(s, t)| < |T_t^{\text{error}}(s, t)|. \quad (2.7.6)$$

Together with (2.7.2) and (2.7.3), this can be used to estimate the bound on  $\text{Im} f_J(s)$ .

If one is not willing to make an assumption of the form (2.7.3) about  $T_t^{\text{error}}(s, t)$  then one can still derive a bound on inelasticity [76], albeit very weak and only asymptotic when  $s \rightarrow \infty$ .

### 2.7.1 A Toy Model Example

We now study a toy model example that is motivated by the numerical analysis of [1]. We consider four-dimensional spacetime ( $d = 4$ ) and take  $T_t^{\text{approx}}(s, t)$  to be given by the first universal term in the threshold expansion (2.5.7)

$$T_t^{\text{approx}}(s, t) = 32\pi \sqrt{\frac{z_1 - 1}{z - z_1}}. \quad (2.7.7)$$

We assume that the Regge limit is bounded by  $J_0(s) \leq \frac{1}{2}$  for real  $s$  in some region. Hence, for this case we can take  $N = 1$  in (2.7.3) and bound the error as

$$|T_t^{\text{error}}(s, t)| < \delta c(s) \times 32\pi \sqrt{\frac{z - z_1}{z_1 - 1}}. \quad (2.7.8)$$

where for convenience we have introduced the notation  $\delta c(s) = c_1(s)/(32\pi)$ , (2.7.3).

We will now go through the steps in figure 2.9 and apply them to the toy model (2.7.7). We will use the bound on the error (2.7.8) to have a finite  $J$  and finite  $s$  bound on the error at each step.

We start with the error on the partial waves coefficients. Using the Froissart-Gribov formula, it is given by (2.7.4)

$$\left| f_J(s) - f_J^{\text{approx}}(s) \right| = \left| f_J(s) - 32\pi I_{0,J}^{(d=4)}(z_1) \right| < 32\pi \delta c(s) I_{1,J}^{(d=4)}(z_1), \quad (2.7.9)$$

Note that due to our assumption on the Regge trajectory, the Froissart-Gribov formula is applicable all the way down to  $J \geq 2$  for any  $s \geq 4m^2$ .

## Chapter 2. An analytical toolkit for the S-matrix bootstrap

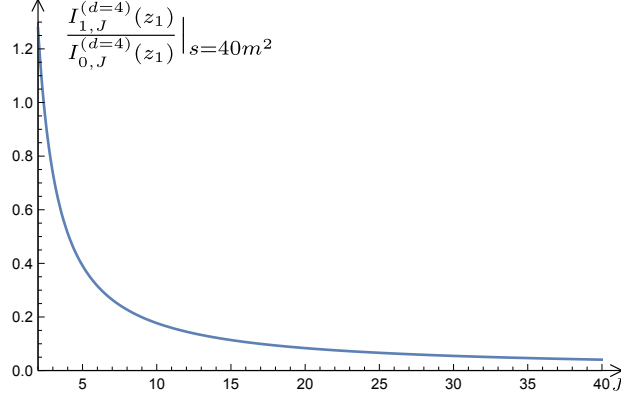


Figure 2.13: We plot the ratio of the leading and subleading threshold integrals in (2.7.10) as a function of spin  $J$  for  $s = 40m^2$ . In particular, we get  $\frac{I_{1,J}^{(d=4)}(z_1)}{I_{0,J}^{(d=4)}(z_1)}|_{s=40m^2, J=4} \simeq 0.51$ , and  $\frac{I_{1,J}^{(d=4)}(z_1)}{I_{0,J}^{(d=4)}(z_1)}|_{s=40m^2, J=20} \simeq 0.08$ .

To quantify the error in (2.7.9) we take the ratio between the error integral  $I_{1,J}^{(d=4)}(z_1)$  to the approximation one  $I_{0,J}^{(d=4)}(z_1)$

$$err_J(s) \equiv \delta c(s) \times \frac{I_{1,J}^{(d=4)}(z_1)}{I_{0,J}^{(d=4)}(z_1)} = \frac{\delta c(s)}{2J} \sqrt{\frac{z_1 + 1}{z_1 - 1}} (1 + \mathcal{O}(1/J)). \quad (2.7.10)$$

The approximation for the partial waves is good when this ratio is small. For example, we can focus on the point  $s = 40m^2$ , where the large  $J$  inelasticity ratio (2.6.20) is maximal. In figure 2.13 we have plotted this ratio for  $s = 40m^2$  as a function of spin. For example, we have

$$err_{J=4}(40m^2) \simeq 0.51 \delta c(40m^2), \quad err_{J=20}(40m^2) \simeq 0.08 \delta c(40m^2). \quad (2.7.11)$$

Next, we use the Mandelstam equation (2.3.9) to evaluate the double spectral density in the elastic strip and bound the error there. We get (see appendix A.7.1 for more details)

$$\rho(s, t) = \frac{16}{\pi^2} \sqrt{\frac{s - 4m^2}{s}} \tilde{I}_{0,0}^{(4)} + \rho^{\text{error}}(s, t), \quad s_1^{\text{cross}}(t) < s < 16m^2, \quad (2.7.12)$$

where  $\tilde{I}_{n_1, n_2}^{(d)}$  was defined in (2.5.13), and recall that  $s_1^{\text{cross}}(t) = \frac{4m^2 t}{t - 16m^2}$ .

$$|\rho^{\text{error}}(s, t)| < \frac{16}{\pi^2} \sqrt{\frac{s - 4m^2}{s}} \left( 2\delta c(s) \tilde{I}_{1,0}^{(4)} + \delta c^2(s) \tilde{I}_{1,1}^{(4)} \right). \quad (2.7.13)$$

In estimating the error we used the fact that both the Mandelstam kernel  $\text{Disc}_z K(z, \eta_1, \eta_2)$ , and  $T_t^{\text{approx}}$  are non-negative.

Next, we perform crossing transformation to the formulas above to estimate  $\rho(s, t)$  at  $s > \frac{64m^2}{3}$ . We plug (2.7.12) into the Froissart-Gribov formula and use it to evaluate  $\text{Im} f_J(s)$ . As before,

we focus on the point of maximal large  $J$  inelasticity,  $s = 40m^2$ . At this point,  $\rho(40m^2, t)$  has only support for  $t \geq t_1^{\text{cross}}(40m^2) = \frac{20m^2}{3}$ . We then consider the regions  $\frac{20m^2}{3} \leq t < 16m^2$  and  $t > 16m^2$  separately

$$\text{Im}f_J(s) = \frac{2\mathcal{N}_d}{\pi} \int_{\tilde{z}_1}^{z_2} dz Q_J^{(d)}(z) \rho(s, t(z)) + \frac{2\mathcal{N}_d}{\pi} \int_{z_2}^{\infty} dz Q_J^{(d)}(z) \rho(s, t(z)), \quad (2.7.14)$$

where  $\tilde{z}_1$  was defined in (2.6.16) and  $z_2 = 1 + \frac{32m^2}{s-4m^2}$ .

In the elastic  $t$ -strip the double spectral density is given by the crossing of (2.7.13).<sup>32</sup> To get a bound on the integral (2.7.14) in that region, we replace  $\delta c(t)$  by its maximal value there

$$\delta c_{el} = \max_{\frac{20m^2}{3} < t < 16m^2} \delta c(t). \quad (2.7.15)$$

Above the elastic strip we use (2.7.6) ( $|\rho(s, t(z))| \leq |T_t^{\text{error}}(s, t)|$ ) and the positivity of  $Q_J^{(d)}(z)$ . We do not have an explicit formula for the integral over this region but we can trivially compute it numerically for various values of  $J$ .

In total, we find that for  $J = 20$  and  $s = 40m^2$

$$\lambda_1^{2J}(s) 2\text{Im}f_J(s) \Big|_{J=20, s=40m^2} = 88.53 \pm [16.6\delta c_{el} + 0.67\delta c_{el}^2 + 0.14\delta c(40m^2)]. \quad (2.7.16)$$

For these values we also get from (2.7.9) that

$$\lambda_1^{2J}(s) \sqrt{\frac{s-4m^2}{s}} |f_J(s)|^2 \Big|_{J=20, s=40m^2} = 0.002 \pm 3.5 \times 10^{-4} \delta c(40m^2) + 1.46 \times 10^{-5} (\delta c(40m^2))^2. \quad (2.7.17)$$

Note that in this case the term  $\sim (\delta c(40m^2))^2$  is sign-definite — the consequence of using (2.7.9) to bound  $|f_J(s)|^2$ .

Similarly, for  $J = 2$  and  $s = 40m^2$  the result takes the form

$$\begin{aligned} \lambda_1^{2J}(s) 2\text{Im}f_J(s) \Big|_{J=2, s=40m^2} &= 0.389 \pm [0.19\delta c_{el} + 0.015\delta c_{el}^2 + 2.18\delta c(40m^2)] \\ \lambda_1^{2J}(s) \sqrt{\frac{s-4m^2}{s}} |f_J(s)|^2 \Big|_{J=2, s=40m^2} &= 0.14 \pm 0.358\delta c(40m^2) + 0.228(\delta c(40m^2))^2. \end{aligned} \quad (2.7.18)$$

Let us comment on the origin of the various terms. The error in  $f_J(s)$  is given by (2.7.9). In the expression for  $\lambda_1^{2J} 2\text{Im}f_{J=20}(s = 40m^2)$  the term linear in  $\delta c_{el}$  comes from the error in the elastic region, and similarly the term linear in  $\delta c(40m^2)$  comes from the integral over  $t > 16m^2$ . The  $\delta c_{el}^2$  term comes from the error in  $\rho(s, t)$  in the elastic region.

<sup>32</sup>Note that for  $s = 40m^2$  this region is inside the Mahoux-Martin positivity region (2.4.4).

## Chapter 2. An analytical toolkit for the S-matrix bootstrap

---

To summarize, given a bound on our ignorance about  $T_t(s, t)$ , specified by  $\delta c(s)$  for the case at hand, we can explicitly derive a lower bound on the amount of inelasticity that is present in the toy model. This is of course assuming that the underlying amplitude satisfies elastic unitarity. It would be also interesting if the analysis above can be improved using more refined error estimates. For example, a better approach would be to bound the error distributionally, see section 2.8.3 below.

### 2.7.2 Elastic Unitarity and Coupling Maximization

In [1] the numerical procedure outlined below in section 2.8.1 has been put forward and carried out for the problem of maximizing  $T(\frac{4m^2}{3}, \frac{4m^2}{3})$ . It was observed that the low spin partial waves  $f_J(s)$ , with  $J = 0$  and  $J = 2$ , converge very well as a function of  $N_{\max}$  which characterizes the number of terms used to approximate the amplitude, see section 2.8.1 for details. Moreover, it was found that that  $f_{J=0,2}(s)$  tend to saturate elastic unitarity above  $s \geq 4m^2$ .

It is interesting to apply the finite  $J$  and  $s$  analysis described above to this case. We find that the function produced by the numerics fits the toy model approximation we considered above in section 2.7.1. In particular, the relevant bounds on the the discontinuity of the amplitude  $T_t(s, t)$  come from the threshold behavior of the amplitude

$$\delta c(s) = \frac{T_t(s, t) - 32\pi \sqrt{\frac{z_1-1}{z-z_1}}}{32\pi \sqrt{\frac{z-z_1}{z_1-1}}} \Big|_{t=4m^2}, \quad \delta c_{el} = \delta c(16m^2). \quad (2.7.19)$$

The convergence properties of  $\delta c(s)$  at general  $s > 4m^2$  are less clear as they probe the unphysical region. An interesting possibility to avoid the question of their convergence is to add the bounds on (2.7.19) as extra conditions to the bootstrap algorithm. Note, that in theories that satisfy elastic unitarity  $\delta c(s)$  does not depend on  $s$  since in this case only  $f_0(t)$  contributes. Therefore dependence of  $\delta c(s)$  can itself be used as a probe of elastic unitarity.

Nevertheless, we proceed and consider numerics for  $N_{\max} = 11$  and  $J_{\max} = 36$  with the leading threshold behavior fixed to the universal behavior dictated by elastic unitarity. In this case we find

$$\delta c_{el} = 0.67, \quad \delta c(40m^2) = 1.17. \quad (2.7.20)$$

In figure 2.14 we plot the results for the inelasticity ratio  $r_J(40m^2)$  (2.6.20) obtained in the toy model of the previous section with the parameters taken from the numerics (2.7.20).

As we discuss below, there are several ways to improve the numerical procedure so that the plots would agree at finite  $N_{\max}$ .

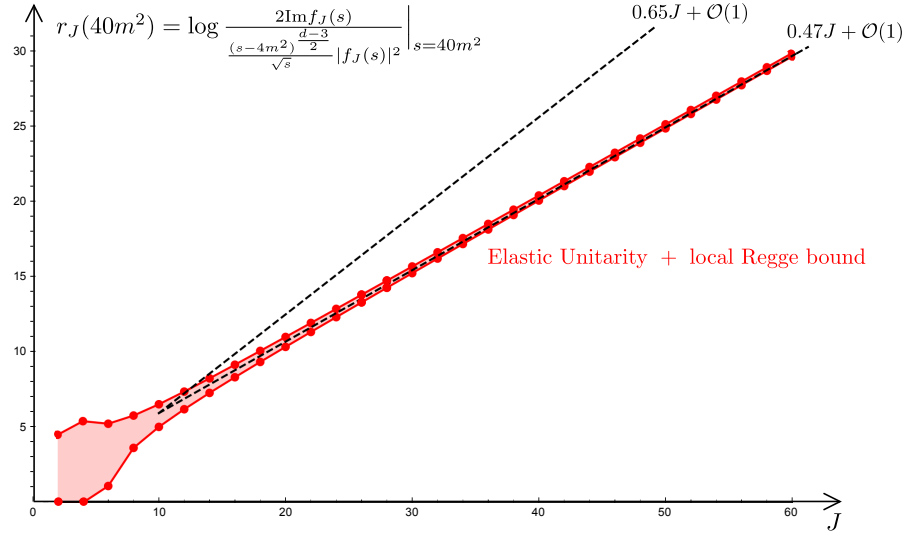


Figure 2.14: Inelasticity ratio  $r_J(s = 40m^2)$ , (2.6.20), as a function of spin  $J$ . The region between the red curves is the analytic prediction for a function that satisfies elastic unitarity and the local error bound (2.7.8) with parameters (2.7.20) as taken from the numerics. For a function that satisfies elastic unitarity, the presence of the Steinmann shadow region where  $\rho(s, t) = 0$ , see figure 2.11, gives  $r_J(40m^2) \sim 0.47J$  at large  $J$ . This is the asymptotic behavior of the red curves. On the other hand, a function that has  $\rho(s, t) \neq 0$  in the Steinmann shadow region is expected to behave as  $r_J(40m^2) \sim \log \lambda(z_1)|_{s=40m^2} \sim 0.65J$  this is what numerics produces for any finite  $N_{\max}$ .

## 2.8 Analytical Methods and Numerical Bootstrap

In this section<sup>33</sup> we discuss how some of the analytical methods described before can be implemented in the numerical approach to the S-matrix bootstrap that has been put forward in [1].

### 2.8.1 Review of the Numerical Framework of [1]

Let us briefly review the setup of [1]. The basic idea is to write an ansatz for the expansion of the scattering amplitude which is linear in unknown real parameters  $\alpha_{abc}$

$$T(s, t) = \sum_{a,b,c=0} \alpha_{abc} \rho_s^a \rho_t^b \rho_u^c + \text{extra} \Big|_{u=4m^2-s-t}, \quad (2.8.1)$$

where, the function  $\rho_s \equiv \frac{\sqrt{4m^2-s_0}-\sqrt{4m^2+s}}{\sqrt{4m^2-s_0}+\sqrt{4m^2+s}}$  maps the complex  $s$ -plane minus the  $s$ -channel cut to the unit circle and the point  $s_0$  to the origin. Here, the extra terms may be added to make some particular properties of the amplitude manifest. Their presence or absence depends on the particular problem at hand. Crossing symmetry is imposed by demanding that the coefficients  $\alpha_{abc}$  are permutation-invariant. Finally, the relation  $s + t + u = 4m^2$  leads to a redundancy in the basis of coefficients that can be addressed systematically.

<sup>33</sup>We thank Madalena Lemos for collaboration on this section.

## Chapter 2. An analytical toolkit for the S-matrix bootstrap

---

To approximate an amplitude using the ansatz (2.8.1), the sum is truncated such that

$$a + b + c \leq N_{\max}. \quad (2.8.2)$$

Given a finite  $N_{\max}$ , unitarity in the form

$$|S_J(s)| \leq 1, \quad s \geq 4m^2, \quad J \in 2\mathbb{Z}_+, \quad (2.8.3)$$

is imposed over a finite grid of points and for spins that are truncated by some maximal value  $J \leq J_{\max}(N_{\max})$ . As shown in [1], remarkably unitarity in the form of (2.8.3) can be restated as a semidefiniteness condition as follows. We write for physical  $J$  and  $s$

$$S_J(s) = 1 + i\vec{\alpha} \cdot \vec{f}_J(s), \quad (2.8.4)$$

where  $\hat{f}_J(s)$  are kinematical objects and all the dynamical information is in the coefficients  $\vec{\alpha}$ . The condition (2.8.3) can be then rewritten as a semi-definiteness condition for the matrix

$$M \equiv \begin{pmatrix} 1 + \vec{\alpha} \cdot \text{Re} \vec{f}_J(s) & 1 - \vec{\alpha} \cdot \text{Im} \vec{f}_J(s) \\ 1 - \vec{\alpha} \cdot \text{Im} \vec{f}_J(s) & 1 + \vec{\alpha} \cdot \text{Re} \vec{f}_J(s) \end{pmatrix} \succcurlyeq 0. \quad (2.8.5)$$

At this point one can maximize numerically some quantity linear in the  $\alpha$ -parameters by imposing unitarity in the form (2.8.5) over the chosen grip in  $s$  and for  $J \leq J_{\max}(N_{\max})$ . For example, in [1] the ‘‘coupling’’,  $T(\frac{4m^2}{3}, \frac{4m^2}{3})$ , is maximized. If a certain maximization task reliably saturates as a function of  $N_{\max}$  we stop the process and trivially extrapolate to  $N_{\max} = \infty$  to get the actual bound on the space of physical S-matrices.

### 2.8.2 Why and What Should be Improved

The setup of [1] has several very important and desirable properties:

- It is simple and practical. It is not too hard to implement, manipulate and obtain bounds.
- The space of functions (2.8.1) is complete inside the  $\rho$  unit circle. Hence, any function analytic inside the circle (except, maybe a finite number of isolated poles which can be added explicitly) can be expanded in that way.
- Crossing is trivialized and is satisfied exactly.
- At any finite  $N_{\max}$ , (2.8.1) satisfies maximal analaticity.

At the same time, there is some tension and potential issues in applying the procedure above for exploring physical amplitudes that we list below and comment on how one may improve on them:



- Physical amplitudes exhibit a set of normal multi-particle thresholds at  $s > 4m^2$ . Hence, the  $\rho$ -expansion of such a function is not expected to converge point by point for real  $s > 4m^2$  ( $|\rho_s| = 1$ ). On the other hand, in the procedure above unitarity is imposed point-wise in exactly that regime. Thus, it is unclear if the space of functions that are probed in this procedure includes among them physical amplitudes, with multi-particle thresholds. Below we discuss two possible ways of addressing this point. One is to improve the ansatz and the other is to change the way in which unitarity is imposed.
- The ansatz (2.8.1) has restrictive behavior at  $s = \infty$ . In particular, the partial waves satisfy  $\lim_{s \rightarrow \infty} S_J(s) = 1$ . There is no reason to expect this to be a correct property of physical amplitudes. Hence, similar to multi-particle thresholds, the  $\rho$ -expansion is expected to be a poor approximation in this kinematical regime. One way to fix it is to explicitly add extra terms to the ansatz. Another way, which we discuss in more detail below, is to change the way in which unitarity is imposed.
- Elastic unitarity is not satisfied. This is manifest for any finite  $N_{\max}$  – elastic unitarity implies that  $\rho(s, t) = 0$  in the elastic strips, below the first Landau curve. If one tries to impose it exactly on the truncated ansatz (2.8.1) then clearly the only solution is  $\alpha_{abc} = 0$ . One may still hope that elastic unitarity will emerge at large  $N_{\max}$ . However, without extra constraints, we see no reason for that to happen. In practice, there is no conclusive evidence that the functions that emerge at the boundary of the allowed space satisfy elastic unitarity within the numerical error.

Imposing elastic unitarity is hard for the simple reason that this condition

$$|S_J(s)|^2 = 1, \quad 4m^2 < s < 16m^2, \quad J \in 2\mathbb{Z}_+, \quad (2.8.6)$$

is nonlinear in the unknown parameters  $\alpha_{abc}$ . Therefore, within the approach of [1], we can only hope to impose elastic unitarity-type constraints. Namely, constraints that go beyond (2.8.3), but still include physical amplitudes in the space of functions that satisfy them. This is important if eventually we want to explore the space of physical amplitude that in particular do satisfy (2.8.6).

Below, we elaborate on several ways in which elastic unitarity can be pursued within the numerical approach of [1]. Importantly, each of them is still linear in  $\alpha_{abc}$  and therefore possible to implement using the standard solvers.

### 2.8.3 How the Numerical Framework Can Be Improved

We now suggest a few ways of addressing the issues identified above within the framework of [1].

## Chapter 2. An analytical toolkit for the S-matrix bootstrap

---

### Distributional Unitarity

Here we address some of the issues identified above, namely the lack of point-wise convergence for real  $s$ , or  $|\rho_s| = 1$ , and too restrictive behavior at  $s = \infty$  by suggesting a different way in which unitarity can be imposed numerically.

The basic idea is that even though the truncated expansion of a function with multi-particle thresholds does not converge at  $|\rho| = 1$ , it can still converge to it as a distribution. Indeed, this is what is expected for the functions that are polynomially bounded as we approach  $|\rho| = 1$  or real Mandelstam variables  $s$  and  $t$ . A relevant mathematical result that addresses this question is known as Vladimirov's theorem [77]. It was recently discussed in detail in the context of the conformal bootstrap in [78] to which we refer the reader for technical details.

Let us consider negative  $t$  needed to compute  $S_J(s)$  starting from the amplitude. For such  $t$ , it is known that the amplitude is polynomially bounded as  $|s| \rightarrow \infty$ . It is also polynomially bounded for real  $s$ , namely as  $\text{Im}s \rightarrow 0$ , see e.g. [79]. These facts imply that we can apply Vladimirov's theorem to partial waves  $S_J(s)$  and we expect that partial waves of physical amplitudes computed using the ansatz (2.8.1) will converge for real  $s$  distributionally, namely after integrating  $S_J(s)$  against some smooth test function  $g(s)$ . Note that this includes also amplitudes that grow with  $s$  or  $t$ , which can be modeled by  $\frac{(1+\rho_t)^n}{(1+\rho_s)^n}$  type terms. Expanding such terms around  $\rho_t = \rho_s = 0$  leads to a series that converges distributionally for  $|\rho_s| = 1$  as explained in [78].

Therefore, if we treat the amplitude (and the partial wave coefficients) as a distribution, we can still approximate it by the ansatz (2.8.1). Given  $N_{\max}$ , however, this approximation is expected to be good only for test functions that do not resolve the local in  $s$  features of the amplitude/partial waves, or have support for very large  $s$ . In other words, given  $N_{\max}$  we can only hope to have a reliable approximation on average over big enough intervals of  $s$ , with the intervals becoming smaller as we increase  $N_{\max}$ .

Similarly, considering test functions localized at larger  $s$  requires taking larger  $N_{\max}$ . This is a consequence of the accumulation of the multi-particle thresholds at large  $s$ , as well as due to the potential growth of the amplitude as  $s$  or  $t$  become large. Both effects lead to poor distributional convergence of the ansatz (2.8.1) at large  $s$ , or, equivalently, close to  $\rho_s = -1$ . By restricting the support of the test functions away from that region we can use the ansatz (2.8.1) to probe functions that have multi-particle thresholds and grow in the Regge limit.

Given a real, non-negative function  $g(s)$ , unitarity on average takes the form

$$\left| \int_{4m^2}^{\infty} ds g(s) S_J(s) \right| \leq 1, \quad \int_{4m^2}^{\infty} ds g(s) = 1. \quad (2.8.7)$$

This can be still restated as a semi-definiteness condition and therefore can be implemented numerically using the same methods. In practice, given  $N_{\max}$  and expected properties of the

physical amplitude there is a set of test functions  $g(s, N_{\max})$  that we can use.

To understand what are the reasonable functions to be used let us note that on the boundary of the circle, truncation of the maximal power in  $\rho^n$  is the same as truncating the Fourier harmonics of  $\rho = e^{i\phi}$ . Therefore if we truncate  $n \leq N_{\max}$  we cannot hope to resolve the amplitudes on scale  $\delta\phi < \frac{2\pi}{N_{\max}}$ . Through the map  $\rho(s)$ , this translates into a statement about the  $s$ -plane. We leave the detailed discussion of the test functions  $g(s, N_{\max})$  for the future.

Distributional convergence puts the numerical S-matrix bootstrap algorithm of [1] on a much more solid mathematical ground. It justifies imposing distributional unitarity (2.8.7) for the truncated ansatz (2.8.1).

In practice, for certain types of problems it can happen that a more naive point-wise analysis of unitarity still leads to correct results. Based on the reasons explained above this is expected to work if the underlying amplitude does not exhibit multi-particle thresholds and does not grow in the Regge limit. This expectation agrees with the numerical results observed in [1].

### Extended Basis

Another way of addressing the issue of multi-particle thresholds is to extend the ansatz (2.8.1). This ansatz makes the structure of the two-particle normal threshold manifest. An obvious extension of the basis which makes the structure of the multi-particle cuts manifest is to add to it any power of the functions

$$\rho_s^{(n)} \equiv \frac{\sqrt{(2n)^2 m^2 - s_0} - \sqrt{(2n)^2 m^2 + s}}{\sqrt{(2n)^2 m^2 - s_0} + \sqrt{(2n)^2 m^2 + s}}. \quad (2.8.8)$$

Such an extension while making the structure of the multi-particle normal thresholds manifest still has the property that the double spectral density misses the regions where  $\rho(s, t) = 0$  carved out in the  $(s, t)$ -plane by the Landau curves.

Ideally, one would like to write down an ansatz which does not only make maximal analyticity manifest but also has a correct structure of the Landau curves. Such functions are naturally generated in perturbation theory. We can use them to write down functions that have expected behavior in the elastic strip. Let us take  $\phi^4$  in  $d = 3$  and consider the following diagram

$$\text{Box}(s, t, u) = \text{Box}(s, t) + \text{Box}(s, u) + \text{Box}(t, u), \quad (2.8.9)$$

$$\text{Box}(s, t) = \text{Diagram 1} + \text{Diagram 2}. \quad (2.8.10)$$


This function has the property that it is crossing symmetric and has the zero double discontinuity in the expected region.

## Chapter 2. An analytical toolkit for the S-matrix bootstrap

---

We can consider for example the following ansatz

$$T(s, t) = \text{Box}(s, t, u) \times \sum_{a,b,c=0} \alpha_{abc} (\rho_s^{(n)})^a (\rho_t^{(n)})^b (\rho_u^{(n)})^c |_{u=4m^2-s-t} + \text{extra}, \quad n > 2. \quad (2.8.11)$$

By choosing  $n > 2$  we make sure that the normal threshold coming from  $\rho_{s,t,u}^{(n)}$  starts after  $16m^2$  and the correct analytic structure inside the elastic strip comes from the sum of the  $\phi^4$  diagrams. Hence, this ansatz has an advantage of having the built-in analytic structure consistent with elastic unitarity.

Similarly, other Landau curves can be manifestly incorporated by choosing different perturbative diagrams and dressing them by an appropriate  $\rho$ -ansatz. In this way we can hope to have an ansatz which has more structure of the actual scattering built in. At the same time, linearity in  $\alpha_{abc}$  as well as crossing are still manifest.

That said, without imposing extra constraints that result from elastic unitarity, there is no a priori reason for the numerics to turn on the  $\alpha_{abc}$ 's that are associated to sub-leading Landau curves. We turn to such conditions next.

### Elastic-type Unitarity at Non-integer $J$

Another way of injecting constraints from elastic unitarity into the numerical bootstrap is by imposing unitarity for non-integer spins. As we explained in section 2.3.3, the elastic unitarity condition (2.8.6) can be analytically continued to complex  $J$  as long as  $\text{Re} J > J_0(s)$ , where  $J_0(s)$  is the leading Regge trajectory.

Let us consider real  $J > J_0(s)$ . Numerically, we can then impose the following elastic unitarity-type condition

$$\left| \int_{4m^2}^{16m^2} ds g(s) S_J(s) \right| \leq 1, \quad \int_{4m^2}^{16m^2} ds g(s) = 1, \quad J > J_0(s). \quad (2.8.12)$$

Imposing this unitarity-type condition numerically for non-integer spin goes beyond (2.8.3), while keeping the problem linear in the  $\alpha$ -coefficients. In this case, the partial waves  $S_J(s) = 1 + i \frac{(s-4m^2)^{\frac{d-3}{2}}}{\sqrt{s}} f_J(s)$  for non-integer  $J$  are computed via the Froissart-Gribov integral (2.2.53).

While physical amplitudes will saturate this bound the condition above still includes them as a part of the solution however goes beyond the integer spin unitarity conditions. Importantly, it is still linear in  $\alpha_{abc}$  and therefore can be easily implemented numerically.

When imposed in that way, the elastic unitarity-type conditions (2.8.12) are very similar to the original conditions (2.8.3). Note that the Froissart-Gribov projection probes the regime of arbitrary large  $t$  where the numerics convergence is slower. On the other hand, for integer spin one normally uses the partial wave projection (2.2.34) that only probes physical  $t$ 's.

### Lower Bound on Inelasticity

As we discussed in section 2.7 an additional knowledge of the behavior of the discontinuity of the amplitude  $T_t(s, t)$  leads to a more refined prediction about the amount of inelasticity at finite  $J$  and finite  $s$ . For example, we can put in some expectation about the Regge behavior and low energy data on the scattering length, as well as structure of bumps or resonances to get a relatively accurate estimate of  $T_t(s, t)$ . Similarly, it can happen that while running the numerical algorithm one observes that the gross features of  $T_t(s, t)$  saturate quickly as one increases  $N_{max}$ . In this way one can get an accurate estimate of  $c_N(s)$  in (2.7.3). This in turn allows us to put a lower bound on the amount of inelasticity  $r_J(s)$  (2.6.20) for finite  $J$  and finite  $s$ .

The minimal amount of inelasticity can be easily implemented numerically. We can replace (2.8.5) by a set of modified matrices

$$M_a^{\text{lower}} \equiv \begin{pmatrix} 1 + a_J(s) \vec{\alpha} \cdot \text{Re} \vec{f}_J(s) & 1 - a_J(s) \vec{\alpha} \cdot \text{Im} \vec{f}_J(s) \\ 1 - a_J(s) \vec{\alpha} \cdot \text{Im} \vec{f}_J(s) & 1 - a_J(s) \vec{\alpha} \cdot \text{Re} \vec{f}_J(s) \end{pmatrix} \succcurlyeq 0, \quad a_J(s) \geq 1. \quad (2.8.13)$$

The corresponding modified positive semi-definiteness condition (2.8.13) is equivalent to the inequality

$$\frac{2\vec{\alpha} \cdot \text{Im} \vec{f}_J(s)}{|\vec{\alpha} \cdot \text{Re} \vec{f}_J(s)|^2} \geq a_J(s) \geq 1, \quad (2.8.14)$$

where in the original problem  $a_J(s) = 1$  and more generally  $a_J(s)$  specifies the minimal amount of inelasticity at given  $J$  and  $s$ .

From our discussion in section (2.7) and the large  $J$  analysis we know that  $a_J(s) \gg 1$  for large enough  $J$  and  $s > \frac{64m^2}{3}$ , see (2.6.20). Moreover, given a local bound on the discontinuity of the scattering amplitude of the type (2.7.3), we can derive a set of improved elastic unitarity-type bounds (2.8.13) at finite  $J$  and finite  $s$ , see section 2.7. Luckily, a bound of the type (2.7.3) is again linear in  $\alpha_{abc}$ . Hence, the improved bound can be implemented numerically.

CITE [80]

#### 2.8.4 Mahoux-Martin Positivity

As we reviewed in section 2.4 elastic unitarity leads to the positivity property of the double spectral density in the so-called Mahoux-Martin region, see 2.4.4.

Positivity or more generally non-negativity of the double spectral density is obviously linear in  $\alpha_{abc}$  and therefore is straightforward to implement numerically. We can think of this either using the improved basis described in section 2.8.3 which directly implements the Steinmann shadow region where  $\rho(s, t) = 0$ . Alternatively, we can consider the original ansatz (2.8.1) and

## Chapter 2. An analytical toolkit for the S-matrix bootstrap

---

impose the Mahoux-Martin type positivity constraints

$$\rho(s, t) \geq 0, \quad 4m^2 < s < 16m^2, \quad 4m^2 \leq t \leq 4m^2 \frac{(3s + 4m^2)^2}{(s - 4m^2)^2}. \quad (2.8.15)$$

The condition (2.8.15) still includes physical amplitudes, which in the elastic strip  $4m^2 < s < 16m^2$  satisfy the more restrictive conditions  $\rho(s, 4m^2 \leq t < \frac{16m^2 s}{s - 4m^2}) = 0$  and  $\rho(s, \frac{16m^2 s}{s - 4m^2} < t \leq 4m^2 \frac{(3s + 4m^2)^2}{(s - 4m^2)^2}) > 0$ .

### 2.9 Comments on CFTs

In this work we assumed extended analyticity and we studied the structure of the amplitude for  $s, t > 0$ , where the amplitude develops crossing-symmetric double spectral density  $\rho(s, t)$ . It is interesting to understand what are the analogous statements in CFTs.

Let us list a map between the S-matrix and CFT quantities:

S-matrix elements	CFT correlators
$T(s, t)$	$\mathcal{G}(u, v)$
Disc $T(s, t)$	dDisc $\mathcal{G}(u, v)$
$\rho(s, t)$	qDisc $\mathcal{G}(u, v)$
$f_J(s)$	$c_J(\Delta)$
Froissart-Gribov formula (2.2.53)	Lorentzian inversion formula [71, 81]
Dispersion relations (2.9.1)	CFT Dispersion relations [82]
Elastic unitarity	?

The double discontinuity dDisc  $\mathcal{G}$  and the quadruple discontinuity qDisc  $\mathcal{G}$  were introduced in [71]. It was shown in [71] that crossing symmetry of qDisc  $\mathcal{G}$ , see also [83, 84], readily implies the presence of multi-twist operators in the OPE. This is the CFT analog of the Aks theorem reviewed above.

Elastic unitarity is a consistency condition of the two-particle sector of the S-matrix. In generic CFTs, the analog of two-particle states in the dual AdS space are double-twist operators [69, 70] that are defined at large spin  $J$ . In large  $N$  CFTs the two-particle states in AdS correspond to double trace operators. Similarly, in AdS QFTs, see e.g. [85], we expect a natural set of operators corresponding to two-particle states to be present in the spectrum. However unitarity, as formulated in the CFT language through the OPE, does not admit a truncation analogous to elastic unitarity that emerges as we take the flat space limit of the theory.

Imposing that the twist spectrum structure of a CFT is the one coming from the light-cone bootstrap leads to the so-called Polyakov conditions, see e.g. [86] for a recent discussion in the nonperturbative context. It is interesting to understand to what extent the consequences

of imposing the Polyakov conditions in AdS are analogous to elastic unitarity in flat space.<sup>34</sup> Using this analogy, the exploration of the present chapter suggests that an interplay between the Polyakov conditions and crossing symmetry of the quadruple discontinuity can lead to interesting results. It will be interesting to investigate it further.

Let us next comment on extended analyticity. In the context of amplitudes it implies in particular that the analytic structure of the discontinuity  $T_s(s, t)$  is similar to the one of the scattering amplitudes, modulo interchanging normal thresholds to Landau curves. In the context of CFTs it would require understanding analytic properties of  $d\text{Disc}\mathcal{G}$ . In general this is a complicated problem since it requires going to the region of the  $(u, v)$  space in which no OPE channel converges, see e.g. [87] for a detailed, recent discussion. It is however possible to make progress in 2d CFTs. Indeed, in this case thanks to the Virasoro symmetry [88], the OPE converges on an arbitrary sheet [89]. One finds that a statement analogous to Mandelstam analyticity indeed holds, namely the only singularities on an arbitrary sheet of  $\mathcal{G}(u, v)$  are branch points at  $u, v = 0, \infty$ . One does not expect an analogous statement in higher dimensional CFTs due to a more complicated structure of Lorentzian singularities of the correlator. However, it would be very interesting to investigate this analytic structure in more detail.

Finally, let us comment on the validity of the Mandelstam representation in CFTs. Recall, that to obtain Mandelstam representation in flat space we start with the usual dispersion relation (we ignore subtractions for simplicity)

$$T(s, t) = \int_{4m^2}^{\infty} \frac{ds'}{\pi} \frac{T_s(s', t)}{s' - s} + \int_{4m^2}^{\infty} \frac{du'}{\pi} \frac{T_u(u', t)}{u' - u}. \quad (2.9.1)$$

We then write the dispersion relation for the discontinuity of  $T_s(s', t)$

$$T_s(s, t) = \int \frac{dt'}{\pi} \frac{\rho(s, t')}{t' - t} + \int \frac{du'}{\pi} \frac{\rho(s, u')}{u' - u}, \quad (2.9.2)$$

and plug in the formula above to get

$$T(s, t) = \frac{1}{\pi^2} \int_{4m^2}^{\infty} \frac{ds' dt' \rho(s', t')}{(s' - s)(t' - t)} + \frac{1}{\pi^2} \int_{4m^2}^{\infty} \frac{du' dt' \rho(u', t')}{(u' - u)(t' - t)} + \frac{1}{\pi^2} \int_{4m^2}^{\infty} \frac{ds' du' \rho(s', u')}{(s' - s)(u' - u)}. \quad (2.9.3)$$

An important ingredient in this argument, apart from maximal analyticity, is polynomial boundedness of  $T_s(s, t)$  for arbitrary  $s$ .<sup>35</sup>

Let us now see what is the analogous situation in CFTs. Let us first consider 2d CFTs where maximal analyticity follows from the Virasoro symmetry as described above. Let us recall what were the main ingredients in the derivation of CFT dispersion relations in [82]. There it was

<sup>34</sup>We thank S. Caron-Huot and J. Penedones for discussion on this point.

<sup>35</sup>This is not expected to be a true property of nonperturbative amplitudes [90].

## Chapter 2. An analytical toolkit for the S-matrix bootstrap

---

shown that given a single-valued  $\mathcal{G}(u, v)$  analytic in the cut-plane and bounded in the Regge (and Euclidean OPE) limit one can write a dispersion relation. What happens if as above we try to write dispersion relations for  $d\text{Disc}\mathcal{G}(u, v)$ ? Using the OPE, as described in [89], one can clearly bound any limit of the correlator or  $d\text{Disc}\mathcal{G}(u, v)$  on any sheet.

Single-valuedness of  $d\text{Disc}\mathcal{G}(u, v)$  is however not obvious using the Virasoro block OPE [88] and in general we do not expect it to hold. It is easy to check explicitly what happens in the case of minimal models. For the critical Ising model it is easy to see that  $d\text{Disc}\mathcal{G}(u, v)$  is single-valued. It therefore satisfies all the necessary properties to write dispersion relations [82]. In this sense 2d Ising model correlators (somewhat trivially) admit Mandelstam representation. On the other hand, already in the tricritical Ising case single-valuedness does not hold, so we cannot apply the dispersion relations of [82].

In higher dimensions the situation is much more complicated due to absence of Virasoro symmetry. Here again there is no reason to expect single-valuedness of  $d\text{Disc}\mathcal{G}(u, v)$ . On the other hand, single-valuedness is a true property of the double discontinuity in free field theories, which therefore also admit the CFT analog of Mandelstam representation. One can wonder if this property continues to hold for the theories with slightly broken higher spin symmetry, e.g. Chern-Simons vector models in  $d = 3$ .

It would be also interesting to understand if there exists some other, more sophisticated way to think about writing an analog of Mandelstam representation in CFTs. As a different direction, thinking about some other versions of dispersion relations, see e.g. [91], that do not rely on single-valuedness of the underlying correlator might very well be useful in certain applications.

### 2.10 Discussion

One of the challenges of the modern conformal bootstrap is to efficiently combine analytical insights with the numerical methods to corner and solve physical theories [83]. Analogously, in this chapter we revisited analytical techniques for the nonperturbative S-matrix bootstrap. A natural next step for the S-matrix bootstrap program is to combine them with the existing [1] or future numerical methods to compute physical amplitudes.

Concretely, in this chapter we studied the implications of elastic unitarity and extended analyticity for the relativistic, unitary, gapped S-matrix in  $d \geq 3$ . Our goal was to develop the analytical methods to constrain the nonperturbative scattering amplitude, which can be further used in the numerical bootstrap approaches.<sup>36</sup> The analytic bootstrap was the subject of active investigation in the 60's. Most of our ideas and results, when restricted to  $d = 4$ ,

---

<sup>36</sup>Many remarkable structures were recently unraveled in the study of perturbative scattering amplitudes of both massless [92] and massive [93] particles. In this chapter we have focused on nonperturbative aspects of the two-to-two massive particle scattering. It would be interesting to see if any of these new insights can be put to use in the nonperturbative setting.



are contained in some form in the old works of Dragt [66] and A. W. Martin [68], as well as more recent chapter of Roy and A. Martin [76]. We believe however that there is some value in “re-discovering” these methods from the modern perspective and in pushing forward the current incarnation of the  $S$ -matrix bootstrap.

As usual, if one wants to do analytic computations in a nonperturbative setting, a small parameter is needed. For a nonperturbative  $S$ -matrix, there are two expansions in two small kinematical parameters – the threshold expansion in  $\frac{s-4m^2}{4m^2}$ , and the large spin expansion in  $1/J$ . These two are related via the Froissart-Gribov formula (2.2.53). Ones combined with elastic unitarity and crossing symmetry, these two expansions lead to the bootstrap scheme outline in figure 2.9. The upshot of this analysis is that one can start with the low energy, low spin data (the threshold expansion), and use it to bootstrap the amplitude away from this regime. We, however, do not restrict the low energy data. In this sense, the scheme is analogous to the analytic CFT bootstrap [69, 70, 71].

While the analytic bootstrap methods reveal important structural properties of the amplitude, by themselves, they are not strong enough to “solve” the problem. Correspondingly, the low energy data that enters the threshold expansion and the bound on Regge are taken here as an unconstrained input for the analytic bootstrap scheme. Currently, the only known way of constraining these parameters systematically is using the numerical bootstrap techniques [1] or experiment [63]. As we discussed in the present work, the numerical methods should be improved by implementing the structure that originates from elastic unitarity and extended analyticity. Indeed, it was observed in the numerical studies that the putative amplitude functions that saturate bounds tend to saturate unitarity. That seems in tension with the Aks theorem of section 2.4. The problem with the latter is that it does not provide us with a finite energy lower bound on particle production that can be implemented numerically. Provided a local bound on the discontinuity of the amplitude however, one does get a finite lower bound on particle production. Moreover, it can be implemented numerically as an extra constraint. Hence, it is instructive to consider the  $S$ -matrix bootstrap in a given class of discontinuity bounded amplitudes. We discussed this in more detail in section 2.7, where an explicit example is also given. In section 2.8 we suggest various ways in which inelasticity and other constraints that emerge from elastic unitarity can be implemented.

A related important question is to what extent physics in the elastic regions  $4m^2 < (s \text{ or } t) < 16m^2$  studied in the present chapter dominates the dynamics of the amplitude? In other words, under which conditions our ignorance of the multi-particle kinematics at  $s, t > 16m^2$  leads to a small controllable error? As we have seen in section 2.7, when considering the toy model, in the case where the low energy interaction is strong (infinite scattering length) and the Regge behavior is relatively soft, the elastic region strongly constrains the behavior of partial waves at finite  $s$  and  $J$ . We can easily imagine a different situation, e.g. relevant for pion scattering, when the low energy interaction is weak. Based on our analysis in this case we do not have a reason to expect the physics of the partial waves to be dominated by the elastic region (unless the spin is very large). Correspondingly, in this case the dynamics in the multi-particle region

## Chapter 2. An analytical toolkit for the S-matrix bootstrap

---

is expected to be important. Bootstrapping such an  $S$ -matrix would then potentially require a more detailed understanding of the analytic constraints that result from the physics in the multi-particle region.

It would be very interesting to extend the current numerical approaches to the  $S$ -matrix bootstrap by implementing structures that originate from elastic unitarity in one of the ways suggested in this work, and a first big step in this direction has been recently achieved [80] wherein the elastic support of the double discontinuity was built-in in an iterative scheme that solves elastic unitarity asymptotically. Moreover, most of the explorations in this chapter were bounded to the elastic strips, where one of the Mandelstam invariants is between the two- and the four-particle threshold energies, see figure 2.4. This region is particularly manageable because in one of the channels it is controlled by two-to-two amplitude only. It is an interesting and important task to explore the multi-particle region, where the energy is above the four-particle threshold in two of the channels. Finally, it would be interesting to explore the landscape  $S$ -matrices, other than  $d = 4$  QCD. Ideally, one would like to find an  $S$ -matrix in  $d \geq 3$  that may play the analogous role to the one played by the Ising model in the conformal bootstrap. Whether such “bootstrap-solvable”  $S$ -matrices in  $d \geq 3$  exist or not is yet to be shown. If it exists, we expect its solution to teach us a lot about nonperturbative QFT in general. Implementing efficiently the structure of the amplitude that we discuss in the present chapter would be an important step towards constructing an example. A natural candidate theory to explore is  $\phi^4$  theory in  $d = 3$ .

There are also a few technical avenues along which our work can be extended. One is relaxing the  $\mathbb{Z}_2$  symmetry we assumed, which restricted the spin and the number of particles to be even. Another related extension is to include single-particle poles. Doing so will affect many of the details, but will not change the global picture. A more interesting generalization is to consider particles with spin, see e.g. [94]. Similarly, it is an open problem to implement the known structure of the UV of the theory, say asymptotic freedom or the CFT data of the UV fixed point, into the  $S$ -matrix bootstrap.

Finally, one can wonder if there is anything to be learned from this analysis for the conformal bootstrap. In the latter case, the theory is gapless so naively there is no elastic unitarity. However, CFTs in  $d > 2$  have a twist gap, and multi-twist operators are mapped to the multi-particle states in the AdS dual theory. Therefore, it would be interesting to understand the AdS analog of the various aspects of the present chapter more directly.

### 3 Probing multi-particle unitarity with the Landau equations

Implementation of multi-particle unitarity is among the biggest challenges in the nonperturbative  $S$ -matrix bootstrap. This chapter explores the “shadow” that multi-particle unitarity casts on the  $2 \rightarrow 2$  amplitude.

It is a well-known fact that scattering amplitudes develop a nontrivial discontinuity along the normal thresholds. This fact is a direct consequence of unitarity. Once combined with analyticity, unitarity also predicts the existence of infinitely many curves in the  $s - t$  plane along which the amplitude develops double discontinuity. These so-called *Landau curves* are more detailed characteristics of the amplitude’s analytic structure. This chapter explores the  $2 \rightarrow 2$  scattering of identical scalar particles of mass  $m$ . The Landau curves found here should be present in any massive quantum field theory. Relatedly, the support of the double discontinuity found in the present chapter enters the Mandelstam representation of the nonperturbative amplitude.

We assume that  $m$  is the lightest particle in a theory. For simplicity we also assume that the theory has  $\mathbb{Z}_2$ -symmetry, such that the scattered particles are  $\mathbb{Z}_2$ -odd.<sup>1</sup>

We only concern ourselves with the behavior of the amplitude on *the physical sheet*. This is the region in the complex  $s, t$  planes that is continuously connected to  $0 < s, t, u < 4m^2$ , without going through the multi-particle normal thresholds.

Let us quickly summarize the state-of-the-art results in this context, see figure 3.1. When one of the Mandelstam variables is in the elastic region, say  $4m^2 \leq s \leq 16m^2$ , unitarity relates the  $2 \rightarrow 2$  amplitude to itself. Correspondingly, the Landau curves in this regime are known explicitly [95, 7], see appendix B.2. In figure 3.1 we plot the leading elastic Landau curves and below, in gray, the region where the double discontinuity is known to be zero.

On the other hand, in the multi-particle regime where both  $s, t > 16m^2$ , the full non-perturbative support of the double discontinuity is not known.<sup>2</sup> This is directly related to the fact that in

---

<sup>1</sup>For example, this applies to the pion scattering in QCD.

<sup>2</sup>For example, in figure 3.1 one can imagine that there exists a multi-particle Landau curve bulging below both

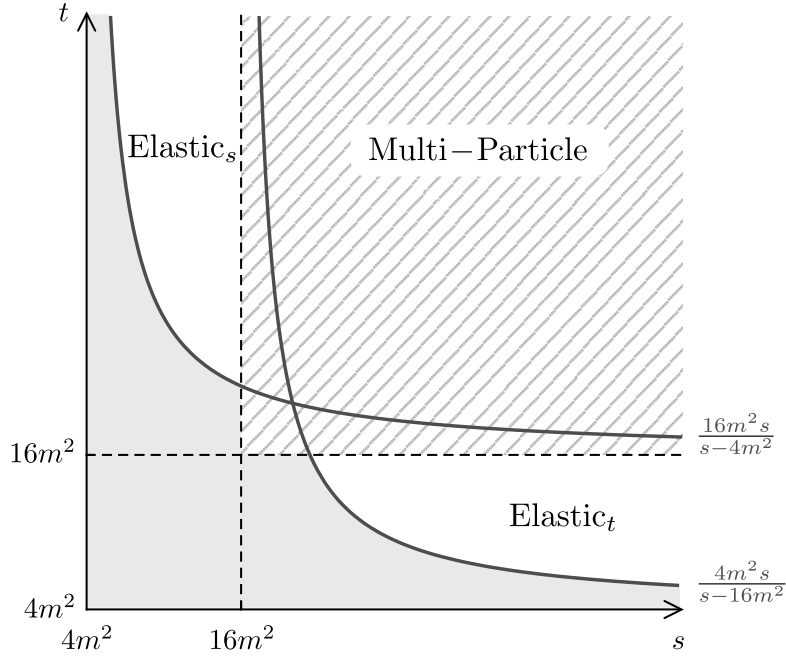


Figure 3.1: The Landau curves in the elastic region  $4m^2 \leq s, t < 16m^2$  are known thanks to elastic unitarity. The first of these are plotted in this figure. In the gray region, the double discontinuity is equal to zero. The main purpose of the present chapter is to explore the structure of the Landau curves in the multi-particle region  $s, t \geq 16m^2$ .

this regime unitary relates the discontinuities of the  $2 \rightarrow 2$  amplitude to amplitudes with four external particles or more. These are very hard to analyze and only a few results are available in the literature. In [96], five Landau curves in this region were identified, out of which some were found explicitly in [96, 97].

Using graph-theoretic tools implemented through a systematic computer search, we find all the Landau curves that asymptote to both,  $t = 16m^2$  at large  $s$  and to  $s = 16m^2$  at large  $t$ .<sup>3</sup> Our results are summarized on figure 3.5 and figure 3.4. In particular, we find infinitely many Landau curves that accumulate towards the curve

$$(s - 16m^2)(t - 16m^2) - 192m^4 = 0. \quad (3.0.1)$$

We expect such accumulation points to be a generic characteristic of multi-particle unitarity and that there are infinitely many of them at higher  $s, t$ , on the physical sheet.<sup>4</sup>

elastic curves. In this chapter we will argue that this does not happen for the scattering of lightest particles.

<sup>3</sup>When claiming that the set of Landau singularities we find is complete, we will also assume that there are no bound states. By bound states we mean poles on the physical sheet in the region  $0 < s, t, u < 4m^2$ .

<sup>4</sup>This is in sharp contrast to the situation in the physical region where in every bounded portion of kinematic space only a finite number of singularities exists [98]. By *the physical region* we mean kinematics that can be directly probed in a scattering experiment.

### 3.1 Analytically continued unitarity and the Landau equations

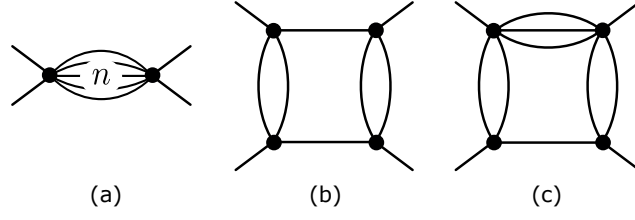


Figure 3.2: A few simplest examples of graphs that represent various singularities of the  $2 \rightarrow 2$  scattering amplitude. a) The bubble diagram represents multi-particle normal thresholds. b) The two-particle box diagram. It represents a Landau curve along which the scattering amplitude develops double discontinuity. c) The four-particle box diagram. This diagram corresponds to four-particle scattering both in the  $s$ - and in the  $t$ -channel. In this chapter we systematically study the graphs of this type and the corresponding Landau curves.

The plan of the chapter is as follows. In section 3.1 we review the relation between analytically continued unitarity and the Landau equations. We also formulate the problem of finding the leading multi-particle Landau curves addressed in the present chapter. In section 3.2 we present the solution to the problem. In section 3.3 we collect implications of our results, future directions, and relation to other works. Many technical details are collected in the appendices.

### 3.1 Analytically continued unitarity and the Landau equations

The  $2 \rightarrow 2$  scattering process is characterized by an analytic function  $T(s, t)$  that depends on two independent (complex) Mandelstam variables  $s = -(p_1 + p_2)^2$  and  $t = -(p_1 + p_4)^2$ , where  $p_i^\mu$  are the on-shell momenta,  $p_i^2 = -m^2$ , of the scattered scalar particles.<sup>5</sup>

We would like to understand the minimal set of singularities possessed by  $T(s, t)$  as a consequence of unitarity and crossing. While the general answer to this question is beyond the scope of this chapter, here we aim at revealing an infinite subset of singularities associated with multi-particle unitarity. The simplest singularities of this kind are normal thresholds. These are branch-point singularities at  $s, t, u = (nm)^2$ , with  $n \geq 2$ . Their presence follows directly from unitarity

$$\text{Disc}_s T(s, t) = \sum_n T_{2 \rightarrow n} T_{2 \rightarrow n}^\dagger, \quad \text{with } s \geq 4m^2, \quad 4m^2 - s < t < 0, \quad (3.1.1)$$

and the fact that  $T_{2 \rightarrow n} = 0$  for  $s < (nm)^2$ , where Disc is the discontinuity defined in eq. (2.2.17). Here, the integral is over the  $n$ -particle phase space. To each term in the sum in (3.1.1) we can assign the graph in figure 3.2.a.

The vertices in this graph represent the amplitudes  $T_{2 \rightarrow n}$ ,  $T_{n \rightarrow 2}^\dagger$  and the lines between them represent the  $n$ -particle state.

As we analytically continue (3.1.1) to  $t > 0$ , we may encounter discontinuities of  $\text{Disc}_s T(s, t)$  in

<sup>5</sup>The results derived in this chapter should equally apply to spinning particles.

### Chapter 3. Probing multi-particle unitarity with the Landau equations

---

$t$ . For example, consider the term in (3.1.1) with  $n = 2$ . Both  $T_{2 \rightarrow 2}(s, t')$  and  $T_{2 \rightarrow 2}^\dagger(s, t'')$  have a normal 2-particle threshold in the  $t$ -channel. These start to contribute to the corresponding phase space integral in (3.1.1) at a new branch-point that is located at

$$(s - 4m^2)(t - 16m^2) - 64m^4 = 0, \quad (3.1.2)$$

along which the scattering amplitude develops double discontinuity, see [7] for details.

We can assign to this double discontinuity the graph in figure 3.2.b, where again, the lines represent (on-shell) particles and the vertices represent four-point amplitudes that have been analytically continued outside the regime of real scattering angles.

As we take  $s > 16m^2$  more  $n$ 's contribute to (3.1.1) and more singularities are produced by the corresponding phase space integration. For example, the integration over the four-particle phase space ( $n = 4$ ) can produce a cut of  $\text{Disc}_s T(s, t)$  in  $t$  that results from the analytically continued two-particle normal threshold of  $T_{2 \rightarrow 4}$  and  $T_{2 \rightarrow 4}^\dagger$ . A graph that represents such a contribution to the double discontinuity  $\text{Disc}_t \text{Disc}_s T(s, t)$  is plotted in figure 3.2.c.

Similarly, for any singularity that follows from multiple iteration of (analytically continued) unitarity we can associate a corresponding graph. By iteration of unitarity we mean the double discontinuity of the amplitude that is generated from a singularity of  $T_{2 \rightarrow n}$  and another singularity of  $T_{2 \rightarrow n}^\dagger$ , through the analytic continuation of the phase space integration in (3.1.1) to  $t > 0$ . The singularities of  $T_{2 \rightarrow n}$  and  $T_{2 \rightarrow n}^\dagger$  themselves follows from analytically continued unitarity in a similar fashion. The graph that we associate to such a contribution to  $\text{Disc}_t \text{Disc}_s T(s, t)$  is defined recursively, by gluing together a graph that represents a singularity of  $T_{2 \rightarrow n}$  with a one that represents a singularity  $T_{2 \rightarrow n}^\dagger$  with  $n$ -lines.

To enumerate all singularities that emerge in this way, we can go in the opposite direction and first enumerate all graphs that may result in a singularity of the amplitude. Whether a given graph leads to a singularity of the amplitude in a certain region in the complex  $s, t$  planes is a kinematical question that does not depend on the details of the sub-amplitudes, represented by the vertices in the graph.<sup>6</sup> Hence, to answer this question we can equivalently take them to be constants. After doing so, it becomes evident that the same singularity, if it exists, is also generated by the Feynman diagram that coincides with the graph obtained from unitarity. The relevant singularity of the diagram comes from the region of loop integration where all propagators go on-shell [99, 100]. Other singularities of Feynman diagrams may result from a region of the loop integration where only a subset of propagators is on-shell. Those propagators that remain off-shell at the locus of a given singularity can thus be regarded as part of an higher point vertex that is not constant. For example, the Feynman diagrams that correspond to the graph in figure 3.2.a with two lines and the graph in figure 3.2.b, both

---

<sup>6</sup>The described way of generating new singularities from old ones involves analytic continuation of the amplitudes. It might happen that due to some special properties of the amplitude, the expected singularity is not there. Here we assume that this does not happens and expect the singularities which follow from unitarity to be generically present.

### 3.1 Analytically continued unitarity and the Landau equations

have normal threshold at  $s = 4m^2$ . Hence, the set of all singularities of a Feynmann diagram includes the singularities of the corresponding graph and graphs obtained from it by collapsing some subset of lines into vertices with more legs. This operation is called a contraction.

If a generic diagram has an  $n$ -particle cut then it has a normal threshold starting at  $n^2 m^2$  in  $s$ ,  $t$  or  $u$  (depending on which external legs are considered incoming/outgoing). This can be seen by contracting the rest of the lines into a bubble diagram as in figure 3.2.a, with  $n$  legs.<sup>7</sup>

In this way we immediately conclude that figure 3.2.b has normal thresholds at  $s = 4m^2$ ,  $t = 16m^2$ , and figure 3.2.c at  $s = 16m^2$ ,  $t = 16m^2$ .

To summarize, in spite of their perturbative nature, Feynman integrals have kinematic singularities (normal thresholds and Landau curves) that can be traced back to (analytically-continued) unitarity, a principle which the non-perturbative amplitude is expected to satisfy. Therefore, to enumerate the singularities that follow from non-perturbative unitarity we can equally enumerate the singularities of individual Feynman diagrams.<sup>8</sup>

In this classification, the Feynman diagrams are only used as a device to study the location of kinematic singularities of the non-perturbative amplitude.<sup>9</sup> For more than two intermediate particles, we find this tool more practical than directly analyzing the analytic continuation of the unitarity relation (3.1.1).

The locations of singularities of Feynmann diagrams can be found using the Landau equations. These are summarized in appendix B.3 and we refer the reader, for example, to [8, 102] for a detailed review.

The so-called *leading singularity* of a Feynmann diagram occurs when every internal momentum goes to the mass-shell. This is precisely the singularity that is described by the corresponding graph, as defined above through unitarity, where each line represents an on-shell particle.

Therefore we may restrict our dissection to singularities of this type only. The Landau equations then read

1. All propagators are on-shell,  $k_i^2 = m^2$ , where the index  $i = 1, \dots, P$  labels all the propagators and  $k_i$ 's are complex-valued oriented momenta that flow through them.
2. At each vertex  $v$ , the momentum is conserved,  $\sum_{j \in v} \pm k_j^\mu = 0$ , with  $+$  ( $-$ ) for ingoing (outgoing) momenta.

<sup>7</sup>In fact, the set of contractions only leads to a pair of single vertices if each side remains *connected* after the cut. In graph-theoretic terms this requires the cut to be *minimal* [101]. Physically, this is consistent with the fact that on the RHS of unitarity (3.1.1) only *connected* S-matrix elements participate.

<sup>8</sup>Related to that, let us emphasize particles that propagate in these auxiliary Feynman graphs are true asymptotic states. For example, in QCD these are pions and not quarks.

<sup>9</sup>In particular, note that  $m$  is the mass of a particle in the spectrum, which need not be associated with a fundamental field.

### Chapter 3. Probing multi-particle unitarity with the Landau equations

---

3. For any loop  $l$ , the momenta satisfy

$$\sum_{j \in l} \pm \alpha_j k_j^\mu = 0, \text{ with } + (-) \text{ sign for momenta along (opposite) the orientation of the loop, and non-zero coefficients, } \alpha_i \neq 0.$$

Two solutions that are related by an overall rescaling of the coefficients corresponds to the same singularity. We may therefore normalize them such that  $\sum \alpha_i = 1$ .

For any solution to these equations we can associate a story in complexified spacetime. In this story the Feynman parameters,  $\alpha_i$ , are the proper times of on-shell particles,  $k_i^2 = m_i^2$ , that propagate along the spacetime interval  $\Delta x_i^\mu = \alpha_i k_i^\mu$ . Every vertex represents a scattering of these particles that takes place at a point. The spacetime interval between two vertices should not depend on the path between the vertices. This means that for a closed path (i.e. a loop) we have  $\sum_{i \in l} \Delta x_i^\mu = 0$ .

No general answer is known to the question of which parts of the Landau curve lead to singularities on the physical sheet (which is our main interest here).

With present understanding, answering it requires a careful case-by-case analysis. There is however a special class of solutions to the Landau equations, called  $\alpha$ -positive, for which the singularity on the physical sheet is sometimes easier to establish.<sup>10</sup> These are solutions for which  $\alpha_i > 0$ .<sup>11</sup> Below we concern ourselves with  $\alpha$ -positive solutions only.

The double discontinuity  $\text{Disc}_t \text{Disc}_s T(s, t)$  does not depend on the order in which the two discontinuities are taken. For example, the graph in figure 3.2.b can equally be interpreted as a contribution to the double discontinuity that comes about by first considering the four particle contribution to  $t$ -channel unitarity and then plugging in the single-particle pole of the analytically continuation of  $T_{2 \rightarrow 4}$  and  $T_{2 \rightarrow 4}^\dagger$  in the  $s$ -channel. We can therefore group the Landau curves into families that are characterized by two integers  $(n_s, n_t)$ , which are the maximal number of particles in the  $s$ -channel and  $t$ -channel unitarity they can be obtained from.

In this chapter we focus on the  $(4_s, 4_t)$  family of double discontinuities. These are the ones that originate from the analytic continuation of unitarity (3.1.1) up until  $n = 4$  in both channels. Physically, this corresponds to restricting energies to  $s, t < 36m^2$ .

We expect that all Landau curves in families with  $(n_s \geq 4, n_t > 4)$  and  $(n_s > 4, n_t \geq 4)$ , which are not already included in the  $(4_s, 4_t)$  family, to lay above the  $(4_s, 4_t)$  family in the  $s - t$  plane of figure 3.1.

---

<sup>10</sup>More precisely, this has only been shown for planar Feynman diagrams [103]. We believe that all  $\alpha$ -positive solutions found in this chapter correspond to singularities on the physical sheet. However, we do not prove this for the non-planar graphs.

<sup>11</sup>Let us emphasize an important subtlety. In the literature the notion of  $\alpha$ -positive graphs typically involves an extra assumption: all  $k_i^\mu$  are real, and  $k_i^0 > 0$ . These are the solutions of the Landau equations that capture singularities of the amplitude in *the physical region* [104]. On the other hand, the  $\alpha$ -positive graphs considered here are relevant for singularities of the  $2 \rightarrow 2$  amplitude on *the physical sheet*.



### 3.2 Graph selection

We now describe our systematic method of finding the  $\alpha$ -positive Landau curves in the  $(4_s, 4_t)$ . A characteristic feature of a graph associated with such a curve is that any of its internal lines can be taken to be one of the four (or less) particles in the unitarity relation in either the  $s$ -channel or the  $t$ -channel. In other words, any leg of the graph should have a 2- or 4-particle cut in at least one of the channels.

The number of potentially contributing graphs is infinite. We study finitely many graphs with a fixed number of vertices,  $V$ , of fixed maximum vertex-degree  $D$ ,<sup>12</sup> and increase  $V$  and  $D$  gradually. As we do so, the number of graphs to be analyzed grows factorially and the problem rather quickly becomes intractable.<sup>13</sup> To overcome this difficulty, we rule out graphs that a priori cannot possibly have  $\alpha$ -positive Landau curve or involve more than four particles in the  $s$ - or  $t$ - channel. Importantly, this selection process has a precise graph-theoretic implementation, so that it can be imposed before solving the Landau equations. Eventually we find that the number of the relevant graphs stabilizes at a handful number of graphs.

Throughout our analysis we assume  $\mathbb{Z}_2$  symmetry of the amplitude that restricts the vertex degree  $D$  to be even.

The set of criteria that we use to select the relevant graphs are as follows:

- We look for Landau curves in the  $(4_s, 4_t)$  family. Correspondingly, we demand that any leg of a graph should have a four-particle or two-particle cut in at least one of the channels. Even though this criteria sounds very intuitive, we have not proved it. Instead, we will see that all the curves that result from graphs that satisfy it pass through the region  $16m^2 < s, t < 36m^2$  and asymptote to  $16m^2$ .<sup>14</sup>
- A graph only admits an  $\alpha$ -positive solution to the Landau equations if each of its sub-graphs admits an  $\alpha$ -positive solution to the Landau equations.  
According to this criterion, we can discard a graph by identifying that one of its sub-graphs cannot have an  $\alpha$ -positive solution.
- We can discard a graph if a subgraph of it can be contracted without affecting the solution. That is because the corresponding Landau curve if it exists, is already accounted for by the contracted graph.

We denote *trivial sub-graph* a graph that falls into one of the last two categories. We have

<sup>12</sup>Because of the aforementioned contractions, graphs with higher vertex degree  $D$  can arise in theories with a smaller vertex degree. For example, the graph (c) in Fig. 3.2, which has two degree-6 vertices, gives a Landau curve in  $\phi^4$  theory.

<sup>13</sup>For  $D = 4$  we analyzed all the graphs with  $V \leq 12$  and for  $D = 6, 8$  up to  $V \leq 8$ .

<sup>14</sup>Conversely, no graph that was left out by this criterion was found to have a curve in this region. This check was made until  $V = 8$  for  $D = 4$  and until  $V = 6$  for  $D = 6$ .

### Chapter 3. Probing multi-particle unitarity with the Landau equations

---

identified a few families of trivial graphs that involve bubbles, triangles, and boxes.<sup>15</sup> They are discussed in appendix B.4.

Computationally, we found it most efficient to proceed as follows

1. We start by generating all graphs without trivial bubbles, with fixed number of vertices  $V$  that contain at least one vertex of degree  $D$ , but no vertices of higher degree.
2. We discarded graphs with trivial sub-triangles.
3. We discarded graphs without 2-particle or 4-particle cuts in at least two channels.
4. We selected the graphs for which all legs can be cut by 2-particle or 4-particle cuts.
5. We discard graphs with trivial sub-boxes.
6. Finally, we select graphs for which an  $\alpha$ -positive solution to the Landau equations is found.

Step 1 was implemented using *nauty and Traces* [105]. Steps 2-5 were implemented using the open source network analysis package *igraph* [106], adapted to *mathematica* by the *igraph/M* package [107]. Step 6 was implemented in *mathematica*. The details of the implementations of each step can be found in appendix B.5.

As we increase  $D$ , it is harder to satisfy the four-particle constraint and the absence of trivial sub-graphs. In particular, we did not find any graphs satisfying our criteria with  $D \geq 8$ . In table 3.1, we list the number of graphs at each step for  $D = 4$  and  $D = 6$ .

As can be seen from table 3.1, considerable reduction in the number of graphs occurs at step 4 as the number of vertices increases. At this order it becomes an incredibly tight criterion, but also very computationally expensive. For comparison, given the same set of graphs, we observe step 3 to be roughly a hundred times faster and step 2 around a thousand times faster.

Step 3 is logically included in step 4. Even though it is not necessary, it reduces total computing time.

Interestingly, step 2, the elimination of trivial sub-triangles, is essential to observe the quench in the growth of diagrams. We observe that the number of diagrams with trivial triangles that survives the criterion imposed by step 4 grows at least exponentially with the number of vertices.

Let us now summarize our findings. Figures 3.4 and 3.5 depict all the graphs that satisfy  $\alpha$ -positive Landau equations with at most four particles in the  $s$ - and  $t$ -channels, and figure 3.5 the corresponding Landau curves. The graphs in figure 3.4 and figure 3.5, as well as the

---

<sup>15</sup>These are subgraphs with 2, 3, and 4 vertices correspondingly.

### 3.2 Graph selection

Quartic graphs ( $D = 4$ )									
# of vertices ( $V$ )	4	5	6	7	8	9	10	11	12
All graphs (no trivial bubbles)	2	3	23	111	788	5639	46603	410114	3587793
No trivial triangles	2	1	10	33	232	1522	12696	113034	1023415
2- or 4-particle cuts (exist)	2	1	7	25	157	955	7070	54835	429093
2- or 4-particle cuts (all legs)	2	1	4	5	12	7	10	7	9
No trivial boxes	2	1	3	4	9	4	4	3	3
$\alpha$ -positive Landau curves	2	1	2	1	3	1	1	1	1

Quartic & sextic graphs ( $D = 6$ ) w/ sextic vertex					
# of vertices ( $V$ )	4	5	6	7	8
All graphs (no trivial bubbles)	9	109	2678	73918	2477395
No trivial triangles	6	22	553	14714	538309
2- or 4-particle cuts (exist)	1	3	27	476	10356
2- or 4-particle cuts (all legs)	1	0	2	1	3
No trivial boxes	1	0	1	0	0
$\alpha$ -positive Landau curves	1	0	1	0	0

Table 3.1: The number of graphs with vertex degree 4 (top) and vertex degree  $\leq 6$  with at least one sextic vertex (bottom). Each column specifies the number of vertices and each row specifies a reduction step. We show the total number of  $2 \rightarrow 2$  graphs without trivial bubbles in the second row. In the third row, graphs with trivial triangle subgraphs have been discarded. Next, we require that all legs can be put on-shell with at most 4-particle cuts since we are looking for Landau curves in the  $(4_s, 4_t)$  family. We first demand that there exists at least one such cut of the diagram in each channel (fourth row). Next we demand that every line can be cut with a 2-particle or a 4-particle cut (fifth row). As a next step we discard the graphs containing a trivial box subgraph (sixth row). The last row has the number of graphs for which an  $\alpha$ -positive solution has been found by numerically solving the Landau equations. For quartic graphs, this number does not go to zero as the number of vertices is increased. This is due to an infinite family of diagrams generated by consecutive insertion of triangles (see figure 3.4). The corresponding Landau curves accumulate at finite  $s, t$ , see figure 3.5. Current computational limitation prevents us from increasing the number of vertices any further, but we believe that all the relevant diagrams have been identified.

### Chapter 3. Probing multi-particle unitarity with the Landau equations

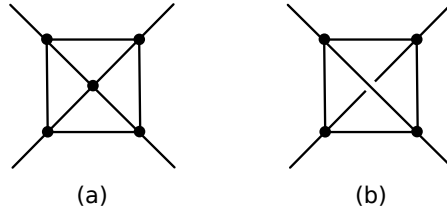


Figure 3.3: The planar cross and the non-planar cross (open envelope) graphs. Each of the diagrams is the first one in an infinite chain of diagrams, see figure 3.4, that generates the Landau curves on the physical sheet, in the region  $16m^2 \leq s, t < 36m^2$ .

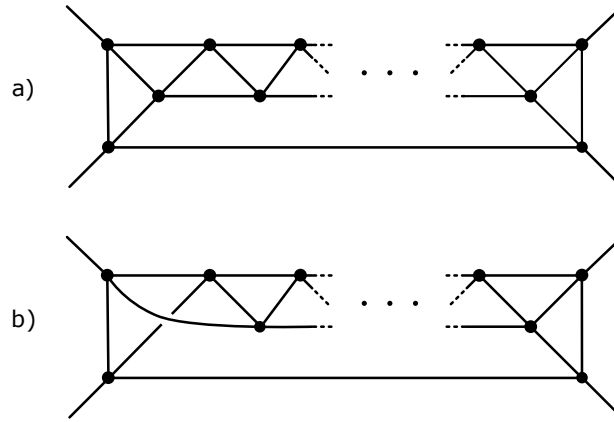


Figure 3.4: The planar, a), and non-planar, b), triangle chain graphs. Remarkably, each of the graphs involves four-particle scattering both in the  $s$ - and in the  $t$ - channel. As the number of triangles grows, the corresponding Landau curves quickly accumulate around the locus (3.0.1) on the physical sheet. Notice that adding a single triangle to each chain increases the number of vertices  $V$  by 2. Closely related diagrams appeared before in [108, 103, 109].

Landau curves in figure 3.5 are the main results of the chapter.<sup>16</sup> In appendix B.1 we exhibit the equations for some of the multi-particle Landau curves depicted in figure 3.5.

Interestingly, we find Landau curves crossing  $16m^2 \leq s, t < 36m^2$  which originate from graphs with arbitrarily large  $V$ . These are depicted in figure 3.4 and their Landau curves (shown in black on figure 3.5) accumulate to the red curve on figure 3.5. This is a new feature compared to the elastic region  $4m^2 \leq s, t < 16m^2$ , where every bounded region of the kinematic space contains a finite number of Landau curves. We believe that this feature is characteristic for the multi-particle region and there are infinitely many accumulation points of the Landau curves there. We discuss this further below.

<sup>16</sup> All the curves that we found cross the region  $16m^2 < s, t < 36m^2$ . We believe that the presented here list of curves in this region is complete. Showing this requires proving some further properties of the  $\alpha$ -positive Landau curves which we discuss in the conclusions. It also requires making sure that non  $\alpha$ -positive solutions to the Landau equations do not lead to the singularities on the physical sheet.

### 3.2 Graph selection

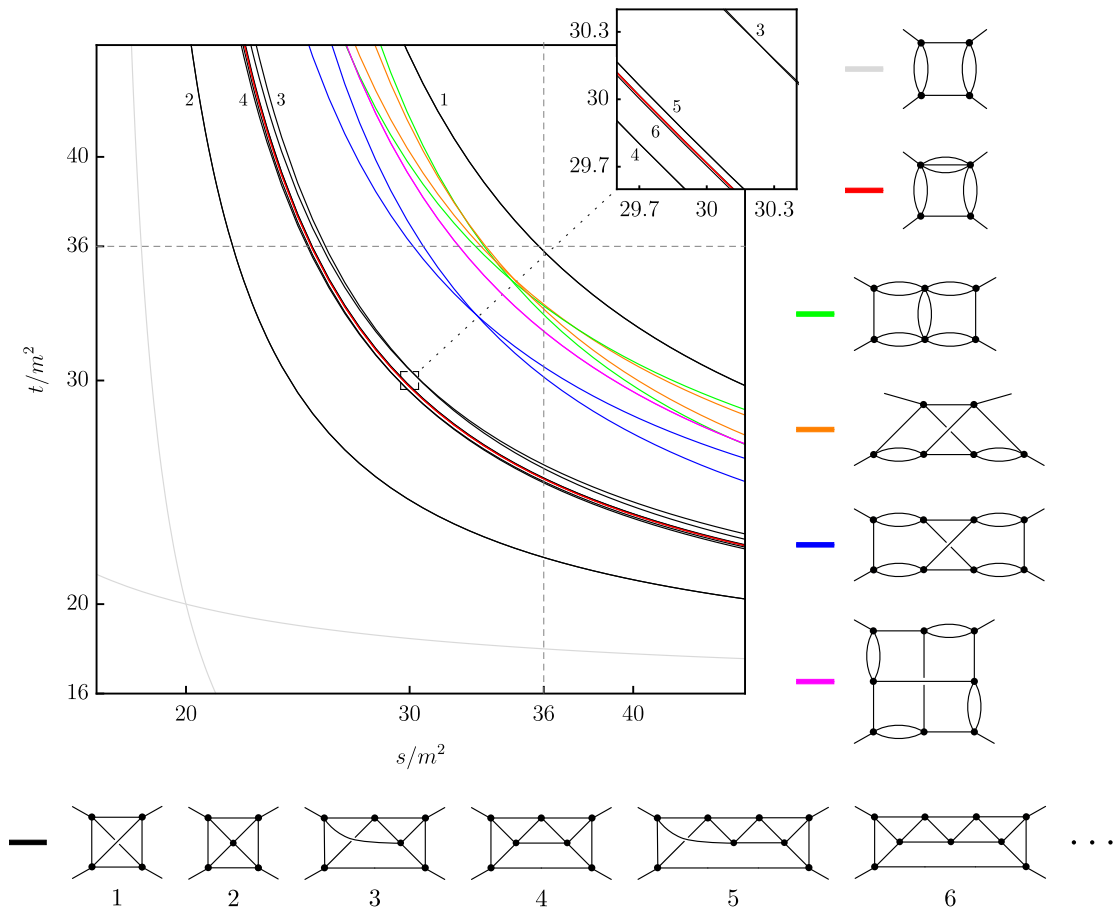


Figure 3.5: The Landau curves in the  $2 \rightarrow 4$  multi-particle region. To each diagram corresponds a pair of crossing symmetry-related curves. For crossing symmetric diagrams, there is only one curve. The red curve, given by equation (3.0.1), is an accumulation point of infinitely many Landau curves. The uppermost curve (black #1) is given by the non-planar cross diagram, figure 3.3 (b), while the planar cross, figure 3.3 (a), gives the lowermost curve (black #2). The planar triangle chain graphs (#2, #4, #6,...), figure 3.4 (a), approach the red curve from below while non-planar triangle chain graphs (#1, #3, #5,...), figure 3.4 (b), approach it from above. As shown in the inset panel, the approach is fast (see table 3.2). We expect that the Landau curves presented here are all the curves that cross the square  $16m^2 < s, t < 36m^2$  on the physical sheet. We collect explicit equations for some of the Landau curves in appendix B.1.

Triangle chain curves at symmetric point: $s = t = x_n$ .										
$n$	1	2	3	4	5	6	7	8	...	$\infty$
$x_n$	35.8885	27	30.2385	29.7511	29.8799	29.8504	29.8579	29.8560	...	29.8564
$\frac{x_n - x_\infty}{x_{n-1} - x_\infty}$	-	0.4735	0.1338	0.2756	0.2235	0.2533	0.2482	0.2547	...	?

Table 3.2: Accumulation of Landau curves at finite  $s$  and  $t$ . The table lists the symmetric point ( $s = t$ ) of the first few Landau curves produced by the infinite set of triangle chain diagrams (depicted in black in figure 3.5). The curves accumulate towards the red curve in figure 3.5. The last row of the table indicates that the approach towards the limiting curve is very quick (approximately geometric).

### 3.3 Discussion

In this chapter we have analyzed analytic properties of the  $2 \rightarrow 2$  scattering amplitude on the physical sheet. In particular, we have focused on the leading Landau curves in the multi-particle region which originate from the analytic continuation of four-particle unitarity both in the  $s$ - and  $t$ - channels (in our notations  $(4_s, 4_t)$  curves). Here we discuss various implications of our results as well as some interesting directions to explore.

#### 3.3.1 Highest particle maximal analyticity

Eventually we would like to fully understand the analytic properties of the scattering amplitude on the physical sheet. In the context of perturbation theory a rich structure of singularities has been discovered already in a  $2 \rightarrow 2$  scattering amplitude. These include anomalous thresholds (see next chapter) [110, 111, 112]<sup>17</sup>, crunodes, acnodes and cusps [115]. No systematic understanding of these latter singularities exists up to this day.

Nevertheless in the course of these explorations a remarkable hypothesis has emerged. It concerns the  $2 \rightarrow 2$  scattering of the lightest particles in a gapped theory (which is the subject of the present chapter) and can be stated as follows.

**Highest Particle Maximal Analyticity:** The  $2 \rightarrow 2$  scattering amplitude of the lightest particles in the theory,  $T(s, t)$ , is analytic on the physical sheet for arbitrary complex  $s$  and  $t$ , except for potential bound-state poles, a cut along the real axis starting at  $s = 4m^2$  with branch points associated with production normal thresholds and Landau curves, as well as images of these singularities under the crossing symmetry transformations.

Establishing this hypothesis even within the framework of perturbation theory is an important, open problem in  $S$ -matrix theory. Assuming highest particle maximal analyticity (LPMA), the analytic structure of the  $2 \rightarrow 2$  amplitude is concisely encapsulated by the Mandelstam representation.<sup>18</sup> From the point of view of our analysis, the nontrivial fact about LPMA is that scattering of lightest particles contains infinitely many subgraphs that by themselves do not respect maximal analyticity. For example, some of the trivial boxes subgraphs depicted in figure B.13 do not admit the Mandelstam representation [116]. For LPMA to hold, embedding these subgraphs inside a larger graph that describes scattering of the lightest particles in the theory should render the complicated singularities of the subgraph harmless on the physical sheet.<sup>19</sup>

---

<sup>17</sup>Anomalous thresholds do not arise in the  $2 \rightarrow 2$  scattering of the lightest particles, see e.g. [103] for a perturbative argument. However they are present in the  $3 \rightarrow 3$  (or  $2 \rightarrow 3$ ) scattering, see [113, 114].

<sup>18</sup>The Mandelstam representation involves an extra assumption that the discontinuity of the amplitude is polynomially bounded on the physical sheet.

<sup>19</sup>As an example, the top center box in figure B.13 has an  $\alpha$ -positive section of the Landau curve for  $s < 4m^2$ , which is associated with a complex singularity and for which the Mandelstam representation does not hold [116]. For the case of scattering of lightest particles, this anomalous box is embedded in the graph in fig. B.5, where LPMA applies. For this graph we have verified numerically that no  $\alpha$ -positive solution exists for  $s < 4m^2$ . While at present we cannot rule out the presence of complex singularities in this graph, we see that, at least, there is no

We have not studied the mechanism of how this happens, and we leave this important question for future work.

LPMA is a working assumption in some of the recent explorations of the S-matrix bootstrap, see e.g. [1, 23, 117, 7]. It is also one of the main reasons we have restricted our study to the physical sheet.

It would be very interesting to revisit the problem of establishing LPMA in perturbation theory. For example, showing that all the graphs considered in the present chapter admit Mandelstam representation might provide a clue as to why it is valid more generally.

### 3.3.2 Analytic continuation of multi-particle unitarity

As we discussed at the beginning of the chapter, a direct way to see the emergence of double discontinuity of the amplitude is to analytically continue the unitarity relations (3.1.1) which involves  $T_{2 \rightarrow n}$  scattering amplitude. While for  $n = 2$  this has been done already by Mandelstam [95], very little work has been done for  $n > 2$ . Let us mention that some progress has been made for  $n = 3$  in the works [118, 119] but the connection between analytically continued multi-particle unitarity and the multi-particle Landau curves has not been explored systematically. It could be useful, for example, to better understand the lower bound on particle production along the lines of [7].

### 3.3.3 Lightest particle $\alpha$ -positive Landau curves

All the elastic Landau curves [7] and the multi-particle curves discussed in the present chapter satisfy the following properties:

1. Asymptotic to normal thresholds. As  $t$  (or  $s$ ) goes to infinity,  $s$  (or  $t$ ) approaches normal thresholds.
2. Monotonic. For  $s > 4m^2$  we have  $\frac{dt}{ds} < 0$ .

It is tempting to conjecture that in the context of *the lightest particle scattering* the properties above fully capture the nonperturbative analytic structure of the  $2 \rightarrow 2$  amplitude on the physical sheet. Assuming it is true, the Landau curves form a simple hierarchical structure, where the  $\alpha$ -positive curve (if it exists) of a graph with a minimum cut across  $n_s$  legs in the  $s$ -channel, and a minimum cut across  $n_t$  legs in the  $t$ -channel has support in the region  $s > (n_s m)^2$ ,  $t > (n_t m)^2$ . It then follows that the curves found in the present chapter are complete in the region  $16m^2 \leq s, t < 36m^2$ . This is an extra assumption to which we referred in the footnote 16.

Even if heavier particles flow in the internal lines, as long as the external states are the lightest anomalous  $\alpha$ -positive real section.

### Chapter 3. Probing multi-particle unitarity with the Landau equations

---

particles, we expect that the above properties should hold. Clearly, in fig. 3.5 we see diagrams with 2-particle and 3-particle internal bubbles which are equivalent (i.e. would give the same Landau curve) to diagrams where these bubbles are replaced by single particles with mass  $2m$  and  $3m$ , respectively.

However, due to the presence of anomalous thresholds [116], monotonicity of the Landau curves does not necessarily hold outside lightest particle scattering. See section 3.3.8 for a discussion on the general external mass case.

#### 3.3.4 Extended elastic unitarity region

The results of this chapter strengthen the picture in which the double discontinuity vanishes below the first elastic Landau curves

$$\rho(s, t) \equiv \text{Disc}_t \text{Disc}_s T(s, t) = 0 \quad (3.3.1)$$

$$\text{for } s, t \geq 4m^2 \text{ and } \begin{cases} (s - 4m^2)(t - 16m^2) < 64m^4 \\ (t - 4m^2)(s - 16m^2) < 64m^4 \end{cases} .$$

We see that the multi-particle Landau curves do not spoil this relation and, therefore, we expect it to hold non-perturbatively.

Another outcome of our analysis is an extended region of validity of the analytically continued elastic unitarity. Let us consider the first multi-particle Landau curve that we encounter as we enter the region  $s, t > 16m^2$ . It is the planar cross curve given by the equation [96] (black curve #2 in figure 3.5)

$$s^3(t - 16) + t^3(s - 16) + 24st(s + t - 18) - 2s^2t^2 = 0. \quad (3.3.2)$$

Let us call  $\{4m^2 < s, t < \text{planar cross}\}$  *the extended elastic unitarity region*. In this region the double discontinuity  $\rho(s, t)$  satisfies the following relation

$$\begin{aligned} &\text{Extended elastic unitarity :} \\ &\rho(s, t) = \rho^{\text{el}}(s, t) + \rho^{\text{el}}(t, s), \quad 4m^2 < s, t < \text{planar cross}, \end{aligned} \quad (3.3.3)$$

where  $\rho^{\text{el}}(s, t)$  is the double discontinuity given by the Mandelstam equation in the  $s$ -channel, which expresses analytically continued elastic unitarity.

Notice that the equation (3.3.3), on one hand, involves only the  $2 \rightarrow 2$  scattering amplitude. On the other hand, its origin lies in the details of multi-particle unitarity.



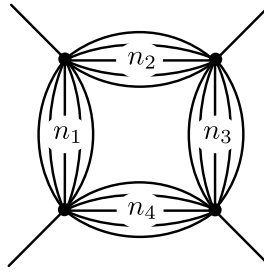


Figure 3.6: A box graph with bridges of size  $(n_1, n_2, n_3, n_4)$ . The Landau curve that is associated to this graph is expected to be an accumulation curve of infinitely many Landau curves. They correspond to graphs that are obtained from this one by replacing an  $n_i$ -bridge with an  $n_i$ -chain.

### 3.3.5 Accumulation points of the Landau curves are generic

We believe that the basic mechanism found in the present chapter for the accumulation of the Landau curves on the physical sheet is generic. For example, we expect that the Landau curves that originate from the graphs depicted in figure 3.6 are accumulation points of infinitely many Landau curves on the physical sheet.

The basic mechanism is the one we observed for the triangle chains depicted in figure 3.4. By exchanging an  $n_i$ -particle bridge with a chain of  $n_i$ -particle sub-graphs, an infinite family of Landau curves is generated. As the length of the chain is increased, it is natural to expect that the solution of the Landau equations, if it exists, converges to the one of the  $n_i$ -particle bridge. In particular, we have already established existence of the  $\alpha$ -positive solution to the Landau equations for a chain of triangles. The triangle chain can now be exchanged with any  $n_i = 3$  bridge of a diagram with an  $\alpha$ -positive solution to produce an accumulation sequence.<sup>20</sup>

This scenario leads to a very complicated structure of the Landau curves on the physical sheet. We will have an infinite number of accumulation points, accumulation points of accumulation points, etc.

Let us also emphasize that this feature should be present in any interacting gapped theory with at least one massive particle in the spectrum, with any spin. We also see no reason why such accumulations would not occur in the general mass case, i.e. with different species being exchanged. It would be interesting to check this explicitly.

### 3.3.6 Higher multi-particle Landau curves

Our method is systematic and, given enough computational ability, can be used to find Landau curves above  $s, t > 36m^2$ . Graph selection should now involve 6-particle (or heavier) cuts.

<sup>20</sup>Note that the triangle chain diagrams correspond to embedding  $3 \rightarrow 3$  elastic scattering amplitude inside a  $2 \rightarrow 2$  process. Similarly, the mechanism for accumulation of the Landau curves described above seems to be related to the behavior of the  $n \rightarrow n$  multi-particle amplitudes close to the normal multi-particle thresholds. It would be interesting to study this behavior in more detail (for a related discussion see [109]).

### Chapter 3. Probing multi-particle unitarity with the Landau equations

---

It is likely, however, that the elimination of trivial bubbles and triangles will no longer be sufficient to quench the growth of the number of graphs. Unfortunately, the condition for larger subgraphs to be trivial is not so simple (see appendix B.4 where we identify some trivial boxes). The problem becomes more complicated the deeper one delves into the multi-particle region. One may need to discard multiple-loop subgraphs, for example.

Direct use of unitarity may be a viable alternative, as shown in the elastic region. However, as mentioned earlier, analytic continuation of multi-particle kernels is a difficult task. The accumulation mechanism discussed here, which should follow from 4-particle unitarity, indeed does not indicate otherwise.

#### 3.3.7 *S*-matrix bootstrap applications

Our results have implications for the *S*-matrix bootstrap program. Indeed, the stumbling block of the current incarnation of the *S*-matrix bootstrap in  $d > 2$  is that it was not possible so far to include the multi-particle amplitudes in the analysis.

Here we took an alternative route, where we tried to understand how the presence of multi-particle unitarity is reflected on the structure of the  $2 \rightarrow 2$  amplitude. In some sense, we can think of the Landau curves found in the present chapter as seeing multi-particle shadows on the elastic scattering wall.

Implementing the structure of the few leading Landau curves in the analytic structure of the amplitude will already be a step forward compared to some of the current explorations of the *S*-matrix bootstrap [1, 23, 120, 117]. Indeed, even (3.3.1) has not been realized in this context.<sup>21</sup>

Another interesting question is to what extent the detailed analytic structure is relevant for the low-energy observables, e.g. a few low-energy Wilson coefficients. We do not know the answer to this question, but recent works [1, 23] suggest that the low-energy observables are not very sensitive to that. It would be very interesting to better understand the origin of this phenomenon.

#### 3.3.8 Other future directions

A few other future directions are

- An interesting generalization of our analysis is to relax  $\mathbb{Z}_2$  symmetry. Effectively it allows vertices of odd degree  $D$  and will lead to new graphs and the corresponding Landau curves. It would be interesting to understand them in detail. While the Landau curves found in fig. 3.5 should still be present, these will not be all the curves crossing the

---

<sup>21</sup>The fixed point unitarity methods [121] do realize this structure but these have not been implemented in  $d > 2$  yet [122].

region  $16m^2 < s, t < 36m^2$ . There will be new curves that asymptote to  $9m^2$  and that cross this region, similarly to what happens with the elastic curves, which asymptote to  $4m^2$  and also cross  $16m^2 < s, t < 36m^2$ .

A presumably simpler problem to what we have studied here would be to map out all the curves in the region  $9m^2 < s, t < 16m^2$ . Are there accumulations of Landau curves inside this region? We believe that this is not case since no analog of the triangle chain depicted in figure 3.4 exists in this case.

- Another possibility is to consider the presence of bound-states, or particles with different mass. We can think of a couple of difficulties here. One is that the graph selection procedure is more involved. The simple graph-theoretic rules derived in appendix B.4 for discarding trivial sub-graphs become much more complex in the general mass case, and a systematic selection as done here might be unfeasible. The other problem, a more fundamental one, is that the different mass case leads to several new features on the Landau curves. First, there are anomalous thresholds and Landau curves are in general non-convex, namely they can bulge below the asymptotic normal threshold. This could invalidate our cut criteria which discard Landau curves that asymptote to normal thresholds outside the kinematic region of interest. Surely the curves found in fig. 3.5 should be present in any theory (with at least one massive particle). However, in the general mass case these won't very likely be *all* the curves that cross a given kinematic region on the physical sheet. Secondly, cusps, acnodes and more generally complex singularities [116, 8] could appear on the physical sheet. These are not necessarily associated with  $\alpha$ -positive solutions to the Landau equations.
- It would be interesting to apply techniques developed in [123] to better understand the approach of the Landau curves to the accumulation point, as well as the analysis of [124] to better understand the nature of multi-sheeted analytic structure of the corresponding Feynman graphs.
- It would be important to prove that all the curves we have found are indeed present on the physical sheet. For the planar graphs it is guaranteed, see [103, 125, 102]. For the non-planar cross in figure 3.3.b, the question was addressed in [126]. For the other non-planar graphs an extra analysis is required, either by following the analytic continuation of the corresponding Feynman integral or by directly analyzing the 4-particle unitarity kernel. It is also important to prove that non  $\alpha$ -positive solutions to the Landau equations do not lead to singularities on the physical sheet. Finally, one would like to show that there is a unique  $\alpha$ -positive solution associated with each nontrivial graph (which we assumed to be the case in appendix B.3).
- Our results should emerge from the flat space limit of the theory in AdS [127, 85, 128, 129, 130]. In the latter case, one computes the conformal correlators on the boundary of AdS. The double spectral density of the amplitude corresponds to the quadruple discontinuity of the corresponding correlator [71]. Complexity of the multi-particle

### Chapter 3. Probing multi-particle unitarity with the Landau equations

---

scattering in this case translates into the complexity of the  $n$ -twist operators with  $n > 2$ , [69, 70].

- For large  $N$  confining gauge theories, a new classical description emerges at large  $s, t \gg m^2$  [131]. Can there also be a universal classical description in this regime for the non-perturbative amplitude? A crucial step in answering this question seems to be a better understanding of the analytic structure in this regime. Understanding this regime is necessary for establishing the Mandelstam representation of the scattering amplitude non-perturbatively. It is also important for developing possible truncation schemes in which the complicated multi-particle unitarity structure can be simplified.

## 4 Nonperturbative Anomalous Thresholds

Despite the intricate analytic structure of scattering amplitudes most singularities have a clear on-shell explanation. As mentioned in the previous chapters, a basic consequence of unitarity is the presence of normal thresholds: branch cuts on the physical sheet starting at energies where particle production occurs, i.e. where intermediate states can be made on-shell (see Fig. 1). While rigorous unitarity only holds in the physical scattering region, perturbation theory indicates that the exchange of states lighter than the physical threshold should still correspond to singularities, such as the usual simple poles (single particles going on-shell). These can be accounted for by *extended* unitarity [132, 133, 134, 113, 8, 135, 136, 137, 138], which assumes that unitarity remains valid *below* the physical region (see Fig. 1).

Yet, when going beyond the  $2 \rightarrow 2$  scattering of the lightest particle (i.e.  $2 \rightarrow 2$  scattering of heavier particles or generic multi-particle scattering) one typically encounters singularities in perturbation theory which are not captured by extended unitarity (as defined above). The prototypical example is the triangle diagram in Fig. 1. When the mass  $M$  of the heavier particle exceeds  $\sqrt{2}$  of the mass  $m$  of the lightest particle (and remains stable),

$$2m > M > \sqrt{2}m, \quad (4.0.1)$$

the triangle singularity occurs on the physical sheet below the normal thresholds, at  $s = a$ , where

$$a = 4M^2 - M^4/m^2 < 4m^2. \quad (4.0.2)$$

This is known as an *anomalous threshold* [110, 111, 112, 114].

Anomalous thresholds have a physical interpretation for certain composite objects.<sup>1</sup> They are nonetheless present regardless of compositeness, and they have physical consequences. In the absence of poles, the anomalous threshold is the closest singularity to the crossed channel

---

<sup>1</sup>Namely, for loose bound states, such as the deuteron, whose mass  $M = 2m - \epsilon$ , with binding energy  $\epsilon \ll m$ , satisfies the relation (4.0.1). It follows from non-relativistic quantum mechanics that the anomalous threshold is related to the spatial extension of the bound state's wavefunction [139, 140] (see also [141] for a recent treatment).

## Chapter 4. Nonperturbative Anomalous Thresholds

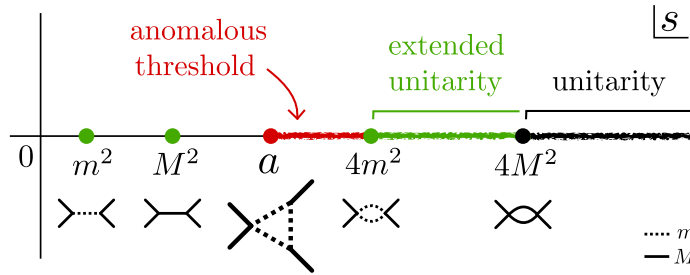


Figure 4.1: Complex  $s$ -plane for  $MM \rightarrow MM$ . Physical scattering occurs for  $s \geq 4M^2$  where unitarity applies. Typically, unitarity is extended below to find further normal thresholds and simple poles, but not anomalous thresholds [113].

physical region (where  $s \leq 0$  is a scattering angle, see Fig. 1), and therefore controls the decay at large impact parameters of the amplitude and the corresponding Froissart bound on the asymptotic cross-section [141].<sup>2</sup>

Perturbation theory indicates that anomalous thresholds are not only present in  $2 \rightarrow 2$  scattering of heavy enough particles, but also in generic multi-particle scattering (even of the lightest particle, say  $mm \rightarrow mmm$ ) [113, 114]. The absence of anomalous thresholds (or other exotic singularities [151, 152, 8]) in Feynman diagrams of  $2 \rightarrow 2$  scattering of the lightest particle (here  $mm \rightarrow mm$ ) is quite special and motivates the hypothesis of lightest particle maximal analyticity (LPMA) [153] which states that the nonperturbative  $mm \rightarrow mm$  amplitude  $A(s, t)$  is analytic in the double complex plane of  $s$  and  $t$  apart from normal thresholds and bound-state poles.<sup>3</sup>

LPMA has important practical implications: Bounds on physical observables (e.g a cubic coupling defined as the residue of a pole) can be determined since *all* branch cuts of the amplitude are normal thresholds and are directly constrained by unitarity. On the other hand, the presence of an unconstrained branch cut, such as an anomalous threshold, would make it impossible to find bounds in general, as the amplitude can oscillate wildly across this cut (where it is a distribution). Given the renewed interest on the numerical S-matrix bootstrap understanding whether anomalous thresholds can be constrained, and how, is paramount.

What is then the state of the art on anomalous thresholds beyond perturbation theory? It is useful to split the discussion in the following way.

- *Where* is the anomalous threshold? Can we rigorously determine its presence on the physical sheet?
- *How* does the amplitude behave at the anomalous branch point? What is the nature of

<sup>2</sup>The triangle singularity can also affect the direct channel (even in the non-anomalous regime where it is on the second sheet). It appears to be in the origin of threshold enhancements or resonance-like effects in some processes involving exotic hadrons [142, 143, 144, 145, 146, 147]. See [148] for a list of processes where the triangle singularity is suspected to play a role (of note the  $a_1(1420)$  ‘peak’ [149, 150]).

<sup>3</sup>LPMA remains unproven in axiomatic quantum field theory [27].

---

the singularity?

- *What* is the discontinuity of the amplitude across the anomalous threshold? Is there an explicit nonperturbative formula?

The location of the anomalous threshold and, in general, the singularities of a given Feynman graph can be found via the Landau equations [154], where the so-called  $\alpha$ -positive criterion determines whether they are on the physical sheet or not. Current understanding is that Landau singularities are a consequence of unitarity [151, 8, 7, 153] (even if this connection has only been made explicit so far with elastic unitarity [151, 7]), and that they are in fact singularities of the nonperturbative amplitude. So we expect the anomalous threshold (4.0.2) derived for the triangle graph to indeed be there nonperturbatively.

Regarding the nature of the anomalous threshold, the triangle singularity is logarithmic in  $d = 4$  and a simple pole in  $d = 2$ , by explicit computation. Less is known beyond perturbation theory. In  $d = 2$ , exactly solvable integrable models provide some hints. A remarkable consequence of the integrable bootstrap [155, 156, 157, 21] is the existence of poles of higher degree in the integrable  $S$ -matrices, known as Coleman-Thun poles [158] which are the incarnation of anomalous thresholds in  $d = 2$ . Depending on the mass of the scattered particles these Coleman-Thun poles can achieve a very high order. For example, in the  $E_8$  Toda field theory [159, 160, 161] the  $S$ -matrix of the second lightest particle has a Coleman-Thun pole of order 2, while the  $S$ -matrix of the heaviest particle has two Coleman-Thun poles of order 12 [162]! These integrable models however involve a very special set of masses and couplings, and it is hard to say what are the lessons for general theories with particle production. For example, the  $mm \rightarrow MM$  process, which vanishes identically in integrable models, is expected to have an anomalous threshold in general.

Finally, on the discontinuity across the anomalous threshold the main reference is in  $d = 4$  due to Mandelstam [132] in which he showed how anomalous thresholds arise in dispersion relations. The key point is that analytic continuation in the mass  $M$  leads to a pinch of the dispersive integral as  $M \rightarrow \sqrt{2}m$ , and consequent contour dragging as  $M > \sqrt{2}m$ . The end result is an extension of the integration contour below the normal threshold, which is the anomalous threshold contribution. Several generalizations of this idea ensued [163, 164, 165, 166, 167, 168, 169, 170, 171, 172], many of which were implemented and are being further developed today in various contexts in hadron physics [173, 174, 175, 176, 177, 178, 179, 177, 180, 181].<sup>4</sup> These dispersive approaches, however, rely on weak coupling or other approximations [114] so it is unclear what can rigorously be learned about the discontinuity across the anomalous threshold. Notable exceptions are the works [184, 185] where the nonperturbative discontinuity across the anomalous threshold was found via *local* analytic continuation of extended unitarity in the mass  $M$ . These approaches exploit the simplicity of

---

<sup>4</sup>In particular, anomalous thresholds need to be taken into account for the computation of the hadronic light-by-light contribution to the anomalous magnetic moment of the muon [182, 183] (which is a major source to the present theoretical uncertainty) since photons can be off-shell [173, 174, 175, 176, 177].

## Chapter 4. Nonperturbative Anomalous Thresholds

---

extended unitarity for the  $mm \rightarrow MM$  process and do not appear to generalize easily beyond this case. We are not aware of any nonperturbative treatment for  $MM \rightarrow MM$  in the literature.

Two essential ingredients in the aforementioned studies are extended unitarity and analyticity in the mass. While extended unitarity seems very reasonable to assume (and, in fact, appears to have been recently established from the flat space limit of AdS/CFT [186]), analyticity in the mass is harder to justify. Why would the S-matrices of particles of different mass be related? This can be motivated within quantum field theory, where the S-matrix is defined via the LSZ formula in terms of a Green's function that is expected to enjoy some analyticity in the 'virtuality'  $P^2$  (which is then taken on-shell  $P^2 \rightarrow M^2$ ) [187]. While we are not aware of a rigorous nonperturbative proof, analyticity in the mass is verified in perturbation theory, as  $m^2$  and  $M^2$  appear on equal footing with Mandelstam invariants  $s$  and  $t$  in Feynman integrals.<sup>5</sup>

In this chapter, we assume extended unitarity and analyticity in  $M^2$  to find exact nonperturbative formulas for the discontinuity across the anomalous thresholds (4.0.2) of the  $mm \rightarrow MM$  and  $MM \rightarrow MM$  processes in  $d = 2$  and  $d = 4$ . We describe our setup in section 4.1 and list our results in section 4.4. We conclude, in section 4.6, where we mention applications and possible extensions of our results, and end with a discussion on maximal analyticity beyond lightest particle scattering.

We first show how the anomalous threshold arises in the triangle diagram in  $d = 2$  in section 4.2. The main derivation is in section 4.3, where we find the general nonperturbative solution to extended unitarity and show how anomalous thresholds arise via continuation in the mass  $M$ . In appendix C.1, we use a simple dispersive argument that generalizes the previous result nonperturbatively. In appendix C.3 we perform some non-trivial perturbative checks of our formulas in  $d = 4$  where we reproduce the discontinuity across the anomalous threshold of the box and double triangle diagrams. In appendix C.5 we collect some details regarding kinematics, and appendix C.4 provides technical backup to the discussion in section 4.6.

### 4.1 Setup

We assume a gapped spectrum where  $m$  and  $M$  are the masses of the lightest particles, with  $m < M$ . We let  $s$ ,  $t$  and  $u$  be the usual Mandelstam invariants. We use the following notation for the amplitudes  $A(s, t)$ ,  $B(s, t)$  and  $C(s, t)$ :

$$A: mm \rightarrow mm, \quad B: mm \rightarrow MM, \quad C: MM \rightarrow MM.$$

We define the partial wave  $A_J(s)$  in the usual way [7],

$$A_J(s) = \frac{1}{16\pi} \int_{-1}^1 P_J(z) A(s, t(z)) dz, \quad (4.1.1)$$

---

<sup>5</sup>For multi-particle scattering of the lightest particle, say  $mm \rightarrow mmm$ , anomalous thresholds should instead follow from analytic continuation in the 'sub-energies', which should be easier to justify on the basis of causality.



and likewise for  $B_J(s)$  and  $C_J(s)$ , where  $P_J(z)$  is the Legendre polynomial and  $z$  is the cosine of the scattering angle (see appendix C.5 for the precise relation between  $z$  and  $t$ ). In  $d = 4$ , due to  $t - u$  symmetry the odd  $J$  partial waves vanish (note that  $u(z) = t(-z)$ ). In  $d = 2$ ,  $t$  is not independent of  $s$  given that only forward/backward scattering is allowed,  $z = \pm 1$ . We define the  $d = 2$  amplitude  $B(s) \equiv B(s, t(s))$ , with  $t(s)$  given by eq. (C.5.3), and likewise for  $A(s)$  and  $C(s)$ .

We assume the presence of a cubic coupling  $g$  between  $mmM$ , which we define nonperturbatively via the residues of the poles of  $B(s, t)$ ,

$$B(s, t) \supset -\frac{g^2}{t - m^2} - \frac{g^2}{u - m^2}, \quad (4.1.2)$$

represented diagrammatically in Fig. 4.2.

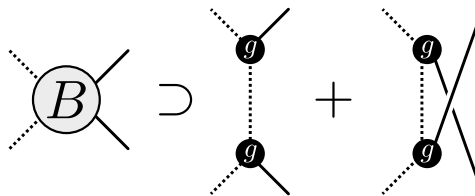


Figure 4.2: Graphical representation of eq. (4.1.2).

In terms of the partial waves, extended unitarity (see fig. 4.3) takes the simple form [188, 135, 7]

$$\text{Disc } B_J(s) = \rho(s) A_J(s) B_J^*(s), \quad (4.1.3)$$

$$\text{Disc } C_J(s) = \rho(s) |B_J(s)|^2, \quad (4.1.4)$$

across the cut  $s \geq 4m^2$  (and below the next threshold assumed to be at  $s = 4M^2$ )<sup>6</sup>. The phase space volume reads

$$\rho(s) = \frac{(s - 4m^2)^{\frac{d-3}{2}}}{2\sqrt{s}}. \quad (4.1.5)$$

Note that (4.1.3) and (4.1.4) also applies in  $d = 2$  directly for the amplitudes  $A(s)$ ,  $B(s)$  and  $C(s)$  (where they are technically the  $J = 0$  partial waves).

Assuming:

1. Analyticity in the mass  $M$ ,
2. Extended unitarity, eqs. (4.1.3) and (4.1.4),

<sup>6</sup>Our results do not depend on the exact location of the next threshold.

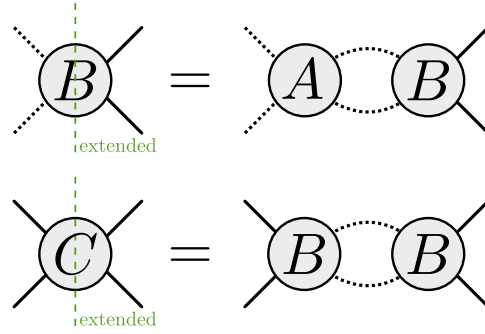


Figure 4.3: Graphical representation of eqs. (4.1.3) and (4.1.4).

3. The presence of the poles in eq. (4.1.2),

we show that, for  $M < \sqrt{2}m$  there is a singularity on the second sheet of  $B_J(s)$  and  $C_J(s)$  at  $s = a$ , given by eq. (4.0.2). As  $M$  is increased past  $M > \sqrt{2}m$ , the  $s = a$  singularity comes onto the first sheet by going around the  $s = 4m^2$  extended branch point (see Fig. 4.4).<sup>7</sup> This is shown explicitly via a simple dispersive argument in  $d = 2$  for  $B(s)$  (see appendix C.1) and, more generally, via an exact solution to equations (4.1.3) and (4.1.4) (see appendix 4.3, in particular eqs. (4.3.4), (4.3.5) and (4.3.6) and fig. 4.7).

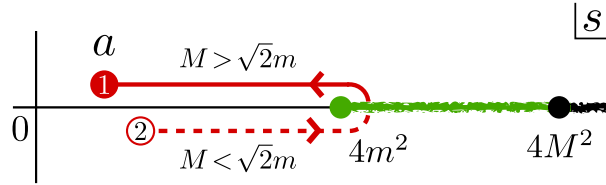


Figure 4.4: Motion of the  $s = a$  singularity from the second sheet where  $M < \sqrt{2}m$  across the extended unitarity cut  $s = 4m^2$  to the physical sheet for  $M > \sqrt{2}m$ . A small imaginary part can be given to  $M^2$  to see the encircling.

Before we proceed it is useful to introduce  $\rho(s)$  such that  $\rho(s + i0) = i\rho(s)$ , for  $s \geq 4m^2$ . We have

$$\rho(s) = \pm \frac{(4m^2 - s)^{\frac{d-3}{2}}}{2\sqrt{s}}, \quad (4.1.6)$$

with (+) sign for  $d = 2$  and (-) sign for  $d = 4$ .

We also make use of the  $mm \rightarrow mm$  S-matrix  $S(s)$ , in  $d = 2$ , which is related to the amplitude  $A(s)$  via

$$S(s + i0) = 1 + 2i\rho(s)A(s + i0). \quad (4.1.7)$$

<sup>7</sup>We also assume that no other singularity prevents the motion of 'a', namely that no other branch cut is crossed during the continuation (besides the extended unitarity cut).

## 4.2 Simple perturbative example: Triangle diagram in $d = 2$

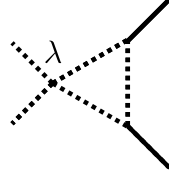


Figure 4.5: Triangle diagram for the process  $mm \rightarrow MM$ . A quartic coupling  $\lambda$  is assumed (together with the cubic couplings  $g$ ).

Here we find the anomalous threshold (Coleman-Thun pole) of the triangle diagram in fig. 4.5. The Feynman parameter representation of the triangle diagram in  $d = 2$  reads [8]

$$T(s) = \frac{\lambda g^2}{2\pi} \int_0^1 \int_0^{1-x} \frac{dx dy}{(szy + M^2 xy + M^2 xz - m^2)^2} \quad (4.2.1)$$

with  $z = 1 - x - y$ . The answer reads

$$T(s) = -\frac{\lambda g^2}{m^2} \frac{W(s) - W(a)}{s - a} \quad (4.2.2)$$

with

$$W(s) \equiv \frac{2M^2 - s}{\pi \sqrt{s(4m^2 - s)}} \arctan \sqrt{\frac{s}{4m^2 - s}} \quad (4.2.3)$$

and  $a$  given by eq. (4.0.2).<sup>8</sup>

Let us look at the analyticity structure of  $T(s)$ . First, the function  $W(s)$  only has a cut for  $s \geq 4m^2$ , as required by unitarity, The role of the ‘arctan’ is to cancel the square-root branch cut for  $s \leq 0$  on the physical sheet.

Now,  $T(s)$  inherits this singularity structure from  $W(s)$  via eq. (4.2.2). Note that  $T(s)$  is regular at  $s \rightarrow a$  because the numerator cancels the pole. In other words, no anomalous threshold exists for  $M < \sqrt{2}m$ .

The situation changes when going to  $M > \sqrt{2}m$ . In this case,  $a$  will go around the branch cut of the function  $W(a)$  (precisely as depicted in Fig. 4.4). So to write  $T(s)$  explicitly in this regime we continue  $W(a)$  to the second sheet, i.e. find its monodromy (to the unfamiliar reader, see dispersive argument below), which is given by

$$W(a) \rightarrow W(a) - \frac{2M^2 - a}{\sqrt{a(4m^2 - a)}}. \quad (4.2.4)$$

<sup>8</sup>Note that  $W(s)/(2M^2 - s)$  is the bubble diagram in  $d = 2$ .

## Chapter 4. Nonperturbative Anomalous Thresholds

Making use of (4.1.6), i.e.  $\rho(a) = 1/\sqrt{a(4m^2 - a)}$  we have

$$T(s) \rightarrow T(s) - 2\rho(a) \frac{\lambda g^2}{m^2} \frac{2M^2 - a}{s - a} \quad (4.2.5)$$

And we see the appearance of a pole at  $s \rightarrow a$  on the physical sheet, i.e. an anomalous threshold.

Following Mandelstam [132] we can reproduce the same result directly from a dispersive representation. Taking a discontinuity of (4.2.2), or using unitarity directly (see next appendix C.1), we get

$$\text{Disc } T(s) = \frac{\lambda g^2}{m^2} \frac{s - 2M^2}{s - a} \frac{\Theta(s - 4m^2)}{2\sqrt{s(s - 4m^2)}} \quad (4.2.6)$$

Identifying the last factor as the phase space volume  $\rho(s)$  given by eq. (4.1.5), a dispersion relation for  $T(s)$  reads

$$T(s) = \frac{\lambda g^2}{\pi m^2} \int_{4m^2}^{\infty} \frac{\rho(s')}{s' - s} \frac{s' - 2M^2}{s' - a} ds' \quad (4.2.7)$$

It can be checked that performing the integral gives back eq. (4.2.2). Now, from this representation it is clear that  $T(s \rightarrow a)$  is regular, the pole  $s' \rightarrow a$  in the integrand is outside the integration domain  $s' \geq 4m^2$ . However, if we increase  $M$  we see that  $a$  approaches the integration contour and forces its deformation for  $M > \sqrt{2}m$  (see Fig. 4.4). So the integral will pick up an extra term that wraps around  $a$ ,

$$T(s) \rightarrow T(s) + \frac{\lambda g^2}{m^2} \frac{1}{\pi} \oint_a \frac{\rho(s' - i\epsilon)}{s' - s} \frac{s' - 2M^2}{s' - a} ds' \quad (4.2.8)$$

If  $a$  is chosen to approach the contour from above, i.e.  $M^2$  is given a small positive imaginary part, the contour in (4.2.8) is counter-clockwise (see fig. 4.6). Note, however that  $\rho(s') \propto 1/\sqrt{s' - 4m^2}$  has a cut for  $s' \leq 4m^2$ , and from fig. 4.6 it is clear that  $a$  will be below this cut after the continuation. So we have  $\rho(s - i\epsilon) = i\rho(s)$  and we recover eq. (4.2.5).<sup>9</sup>

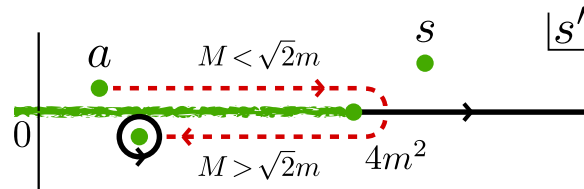


Figure 4.6:  $s'$  complex plane. In black: integration contour. In green: singularities of the integrand. Note in particular the presence of a branch cut of  $\rho(s')$  for  $s' \leq 4m^2$ . In red: trajectory of  $a$  as  $M$  is increased. At  $M = \sqrt{2}$ ,  $a = 4m^2$  pinches the integration contour and forces a deformation.

<sup>9</sup>Note that the direction in which  $a$  wraps around the contour does not matter. Say it comes from below, then the contour would be clockwise but  $a$  would end up on top of the branch cut of  $\rho(s')$  instead and the sign difference would cancel out.

### 4.3 Continuation in $M^2$ of the solution to extended unitarity

In this section we derive the formulas presented in section 4.4. According to the setup laid out in section 4.1 we take the following procedure:

1. We find the general solution across the extended unitarity cut.
2. We impose the presence of the poles (4.1.2) on the solution.
3. We continue the solution in  $M$ , and confirm that anomalous thresholds develop for  $M > \sqrt{2}m$ .
4. We take the discontinuity of the continued solution across the anomalous threshold to find the answer.

Omitting the spin label  $J$ , unitarity across the  $s = 4m^2$  cut reads [171, 135]

$$\text{Disc } A(s) = \rho(s) |A(s)|^2 \quad (4.3.1)$$

$$\text{Disc } B(s) = \rho(s) B(s) A^*(s) \quad (4.3.2)$$

$$\text{Disc } C(s) = \rho(s) |B(s)|^2 \quad (4.3.3)$$

for  $4m^2 \leq s < 4M^2$ , where  $\rho(s)$  is the phase space factor (4.1.5). The general solution to this system of equations is (see graphical interpretation in Fig. 4.7)

$$A(s) = \frac{\alpha(s)}{1 - \rho(s)\alpha(s)}, \quad (4.3.4)$$

$$B(s) = \frac{\beta(s)}{1 - \rho(s)\alpha(s)}, \quad (4.3.5)$$

$$C(s) = \sigma(s) + \frac{\rho(s)\beta^2(s)}{1 - \rho(s)\alpha(s)}, \quad (4.3.6)$$

with

$$\text{Disc } \alpha(s) = \text{Disc } \beta(s) = \text{Disc } \sigma(s) = 0, \quad (4.3.7)$$

$$\text{Disc } \rho(s) = \rho(s), \text{ for } 4m^2 \leq s < 4M^2 \quad (4.3.8)$$

In other words,  $\alpha(s)$ ,  $\beta(s)$  and  $\sigma(s)$  are real across the extended unitarity cut, and  $\rho(s)$  is the analytic continuation of the phase space factor  $\rho(s)$  onto the complex plane. It can be checked that this solution solves extended unitarity.<sup>10</sup> A proper derivation is included at the end of the appendix.

Now, in  $d = 2$ ,  $t$  and  $u$  are functions of  $s$  (see appendix C.5). The  $t$ - and  $u$ -channel poles (4.1.2)

<sup>10</sup>This solution had already been found by Gribov [188] (and partially by Oehme [165]). It also follows from the 'K-matrix' solution with the second cut set to zero [189].

## Chapter 4. Nonperturbative Anomalous Thresholds

$$\begin{aligned}
 A &= \alpha + \alpha \underset{\rho}{\alpha} + \alpha \underset{\rho}{\alpha} \underset{\rho}{\alpha} + \dots = \frac{\alpha}{1 - \rho \alpha} \\
 B &= \beta + \alpha \underset{\rho}{\beta} + \alpha \underset{\rho}{\alpha} \underset{\rho}{\beta} + \dots = \frac{\beta}{1 - \rho \alpha} \\
 C &= \sigma + \beta \underset{\rho}{\beta} + \beta \underset{\rho}{\alpha} \underset{\rho}{\beta} + \dots = \sigma + \frac{\beta \underset{\rho}{\beta}}{1 - \rho \alpha}
 \end{aligned}$$

Figure 4.7: Graphical representation of solution to unitarity across the  $2m$  cut, eqs. (4.3.1), (4.3.2), (4.3.3). The sub-graphs  $\alpha$ ,  $\beta$  and  $\sigma$  are  $2m$ -irreducible, i.e. do not contain any internal exchange of  $2m$  (in the  $s$ -channel), which is what eq. (4.3.7) means graphically.

lead in fact to a pole at  $s = a$  already in the non-anomalous regime,

$$B(s \rightarrow a) = -\frac{\mathcal{N} g^2}{s-a}, \quad \text{for } M < \sqrt{2}m, \quad (4.3.9)$$

with  $\mathcal{N} \equiv \frac{2M^2 - a}{m^2}$ .

Imposing this pole on the solution (4.3.5) requires  $\beta(s)$  to have a pole itself,

$$\beta(s) = -\frac{\mathcal{N} g^2}{s-a} [1 - \alpha(a)\rho(a)] + \beta^{\text{reg}}(s) \quad (4.3.10)$$

where  $\beta^{\text{reg}}(s)$  is regular as  $s \rightarrow a$ .

Upon continuation of  $M$  from  $M < \sqrt{2}m$  to  $M > \sqrt{2}m$ ,  $a$  will cross through the cut of the function  $\rho(a)$  (see fig. 4.4). Since it is a square root cut, we simply get  $\rho(a) \rightarrow -\rho(a)$  after continuation. So we find

$$\beta(s) \rightarrow \beta_a(s) = -\frac{\mathcal{N} g^2}{s-a} [1 + \alpha(a)\rho(a)] + \beta^{\text{reg}}(s), \quad (4.3.11)$$

where we assumed that no other cut was crossed in the procedure, so that  $\beta^{\text{reg}}(s)$  is unaffected

### 4.3 Continuation in $M^2$ of the solution to extended unitarity

by the continuation.<sup>11</sup> Therefore, after continuation,

$$\begin{aligned} B(s \rightarrow a) &= -\frac{\mathcal{N} g^2}{s-a} \frac{1 + \alpha(a)\rho(a)}{1 - \alpha(a)\rho(a)} \\ &= -\frac{\mathcal{N} g^2}{s-a} [1 + 2\rho(s)A(s)], \end{aligned} \quad (4.3.12)$$

where we made use of (4.3.4) to relate  $\alpha(s)$  with  $A(s)$ . This is eq. (4.4.1).

Let us now consider  $C(s)$ . The point here is that plugging  $\beta(s)$  given by (4.3.10) into the solution for  $C(s)$  (4.3.6) will lead to a double pole, which needs to be canceled by  $\sigma(s)$ , because  $C(s)$  by assumption should be regular there for  $M < \sqrt{2}m$ . This fixes  $\sigma(s)$  to take the form

$$\begin{aligned} \sigma(s) &= -\frac{\mathcal{N}^2 g^4 \rho(a)[1 - \alpha(a)\rho(a)]}{(s-a)^2} + \frac{2\mathcal{N} g^2 \beta^{\text{reg}}(a)\rho(a)}{s-a} \\ &\quad - \frac{\mathcal{N}^2 g^4 [1 - \alpha(a)\rho(a)]^2}{s-a} \frac{d}{da} \left[ \frac{\rho(a)}{1 - \alpha(a)\rho(a)} \right] + \sigma^{\text{reg}}(s), \end{aligned} \quad (4.3.13)$$

where  $\sigma^{\text{reg}}(s)$  is regular as  $s \rightarrow a$ .

As before, analytic continuation onto the anomalous regime  $\rho(a) \rightarrow -\rho(a)$  in eqs. (4.3.13) and (4.3.10) no longer leads to cancellation of the poles in  $C(s)$ . We find that  $C(s)$  develops a double and simple pole given by eq. (4.4.5), where  $\bar{B} = \frac{\beta^{\text{reg}}}{1-\alpha\rho}$  is the regular piece of  $B$  (without the pole (4.3.9)).

Moving onto  $d = 4$  the main difference here is that now the poles (4.1.2) in  $B(s, t)$  will lead to a left-hand cut for  $B_J(s)$ . The partial wave integral over the poles can be easily done using the Froissart-Gribov representation (see eq. (C.5.16)). We get (4.1.2)

$$B_J^{\text{poles}}(s) = \frac{g^2 Q_J(z_a(s))}{4\pi w(s)}, \quad \text{for even } J, \quad (4.3.14)$$

with  $w(s) \equiv \sqrt{(4m^2 - s)(4M^2 - s)}$ ,  $z_a(s)$  given by (4.4.3) and where  $Q_J(z_a(s))$  is the Legendre function of the second kind which has a cut for  $z_a(s) \in [-1, 1]$ , or  $s \in (-\infty, a]$ . We now want to impose the presence of this left cut on the solution to extended unitarity (4.3.5). For this we make use of the relation (C.5.14), to fix  $\beta_J(s)$ ,

$$\beta_J(s) = -\frac{g^2}{8\pi} \int_{-\infty}^a \frac{P_J(z_a(s')) [1 - \alpha_J(s')\rho(s')]}{w(s')(s' - s)} ds' + \beta_J^{\text{reg}}(s) \quad (4.3.15)$$

where  $\beta_J^{\text{reg}}(s)$  is regular across this particular cut.<sup>12</sup> It is easy to see that inserting (4.3.15) into

<sup>11</sup>For example,  $\beta^{\text{reg}}(s) = \frac{\bar{\rho}(s) - \bar{\rho}(a)}{s-a}$  is regular at  $s \rightarrow a$ . If  $\bar{\rho}(a)$  is some function with a cut across the path of  $a$  (square-root, say) then  $\bar{\rho}(a) \rightarrow -\bar{\rho}(a)$  upon continuation and  $\beta^{\text{reg}}(s)$  would now be singular and contribute to the anomalous threshold. Note that the cut of  $\bar{\rho}(s)$  cannot be the extended unitarity cut  $s \in [4m^2, 4M^2]$ , i.e.  $\bar{\rho}(s) \neq \rho(s)$ , otherwise  $\beta(s)$  would violate (4.3.7).

<sup>12</sup>Note that  $\beta_J^{\text{reg}}(s)$  can have other left-hand cuts. In writing (4.3.15) we are isolating the contribution coming from the poles (4.1.2).

## Chapter 4. Nonperturbative Anomalous Thresholds

---

the solution (4.3.5) gives the correct result:  $\text{Disc } B_J(s) = \text{Disc } B_J^{\text{poles}}(s)$ , across the cut  $s \leq a$ .

Now the continuation in the mass  $M$  is more interesting. We find that as  $M$  increases,  $a$  encircles the  $4m^2$  branch point and the integration contour (4.3.15) will go onto the second sheet of  $\varrho(s')$ . Therefore, as  $a$  recedes (see fig. 4.4) the difference between the contours from  $a \rightarrow 4m^2$  and back from  $4m^2 \rightarrow a$  is nonzero, where on the return trip  $\varrho(s') \rightarrow -\varrho(s')$  in (4.3.15). We find that (4.3.15) gets corrected by<sup>13</sup>

$$\beta_J(s) \rightarrow \beta_J(s) + \frac{g^2}{4\pi} \int_a^{4m^2} \frac{P_J(z_a(s')) \alpha_J(s') \varrho(s')}{w(s')(s' - s)} \quad (4.3.16)$$

We see that this extra piece now gives a cut for  $s \geq a$ , i.e. an anomalous threshold. Plugging for  $B_J(s)$  into (4.3.5) and taking the Disc we get eq. (4.4.2).

Finally, let us outline the derivation of the anomalous threshold in  $C_J(s)$ . Analogously to the  $d = 2$  case, insertion of (4.3.15) onto  $C_J(s)$  in (4.3.6) will lead to a cut for  $s \leq a$  which needs to be cancelled by  $\sigma_J(s)$  such that  $\text{Disc } C_J(s) = 0$  across this cut. This will fix  $\sigma_J(s)$  akin to (4.3.13) in  $d = 2$ . Then, continuation in  $M$  is similar to the previous case - the contour enters the second sheet of  $\varrho(s')$  - and one (patiently) arrives at eq. (4.4.6).

While the results derived here assume no coinciding singularities with the anomalous threshold (e.g. in (4.4.1),  $S(a)$  is assumed regular), it is easy to account for these possibilities. One just has to include those singularities explicitly into  $\beta(s)$  and  $\sigma(s)$  in the solution to extended unitarity (4.3.5) and (4.3.6). In most cases the answer will be simply corrected by taking the "principal part". For example, in (4.4.4),  $A_J(s) \rightarrow \text{Re } A_J(s)$ , in case  $A_J(s)$  has a cut overlapping with the anomalous threshold (coming e.g. from a pole in the  $t$ -channel of  $A(s, t)$ ).

## 4.4 Results: Nonperturbative discontinuity

### 4.4.1 Anomalous threshold of $mm \rightarrow MM$

Fig. 4.8 represents the nonperturbative cut across the anomalous threshold for the  $MM \rightarrow MM$  process.

In  $d = 2$ , we find that  $mm \rightarrow MM$  develops a simple Coleman-Thun pole whose residue gets enhanced by the  $mm \rightarrow mm$  process,

$$B(s \rightarrow a) = -\mathcal{N} \frac{g^2 S(a)}{s - a}, \quad \mathcal{N} \equiv \frac{2M^2 - a}{m^2}. \quad (4.4.1)$$

---

<sup>13</sup>There is an important subtlety here. Naively,  $w(s') \propto \sqrt{4m^2 - s'}$  would also be encircled. However, what is being integrated over in (4.3.15) is the discontinuity of (4.3.14) which *only* has a left cut,  $B_J(s) \propto Q_J\left(\frac{s-2M^2}{w(s)}\right) / w(s)$  is regular across the cut of  $w(s)$ , as it should. Therefore, in the continuation of (4.3.15) we should keep in mind that  $1/w(s')$  is in fact  $\text{Re}[1/w(s')]$ , even if this detail only plays a role when  $a$  is going around  $4m^2$ .



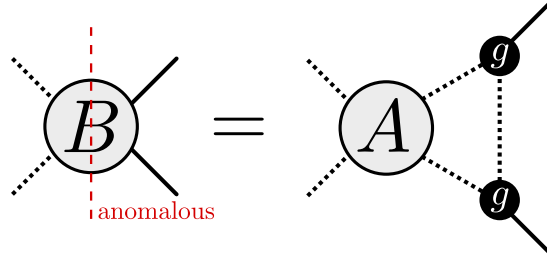


Figure 4.8: Graphical representation of eqs. (4.4.1), (4.4.2) and (4.4.4).

This result is derived in two different ways in appendices C.1 and 4.3.<sup>14</sup>

In  $d = 4$ , we find that the partial wave for the  $mm \rightarrow MM$  process develops an anomalous threshold of logarithmic nature (note that the monodromy is regular as  $s \rightarrow a$ ),

$$\text{Disc } B_J(s) = -\frac{P_J(z_a(s))}{8\sqrt{s(4M^2 - s)}} g^2 A_J(s), \quad (4.4.2)$$

for  $s \in [a, 4m^2)$ , and where  $P_J$  is the usual Legendre polynomial and

$$z_a(s) \equiv \frac{s - 2M^2}{\sqrt{(4m^2 - s)(4M^2 - s)}}, \quad (4.4.3)$$

is such that  $z_a(a) = +1$  if  $M < \sqrt{2}m$ , or  $z_a(a) = -1$  if  $M > \sqrt{2}m$ . Mandelstam's result [132] is reproduced by taking  $J = 0$  in (4.4.2).

We can invert (4.4.2) back for the amplitude,

$$\text{Disc}_s B(s, t(z)) = -\frac{g^2 \int_{-1}^1 \mathcal{P}(z, z', z_a(s)) A(s, t(z')) dz'}{8\pi \sqrt{s(4M^2 - s)}}, \quad (4.4.4)$$

for  $s \in [a, 4m^2)$ , and where  $z$  is the cosine of the scattering angle and  $\mathcal{P}$  is the 2-particle unitarity kernel (see appendix C.5). Eq. (4.4.4) matches the results from [184, 185].

#### 4.4.2 Anomalous threshold of $MM \rightarrow MM$

Fig. 4.9 represents the nonperturbative cut across the anomalous threshold for the  $MM \rightarrow MM$  process.

In  $d = 2$ , the  $MM \rightarrow MM$  amplitude develops a double ‘Coleman-Thun’ pole which takes contributions from  $S(a)$  but also  $\bar{B}(a)$ , the pole-subtracted amplitude, i.e.  $\bar{B}(s) \equiv B(s) - B(s \rightarrow$

<sup>14</sup>Note that even when  $A(s) \rightarrow 0$ , i.e.  $S(s) \rightarrow 1$ , the pole (4.4.1) survives. This is precisely the contribution from the poles (4.1.2) (in  $d = 2$ ,  $t$  and  $u$  depend on  $s$ , see eq. (C.5.3)).

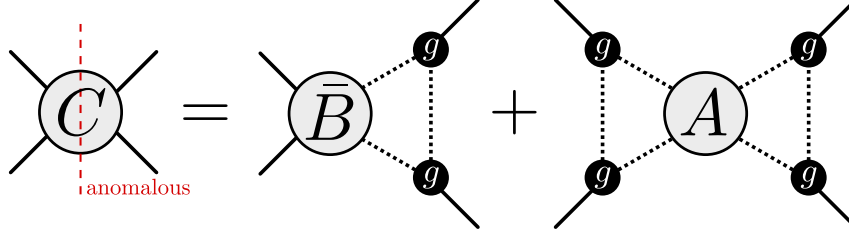


Figure 4.9: Graphical representation of eqs. (4.4.5) and (4.4.6).

a). We find

$$\begin{aligned}
 C(s \rightarrow a) &= -4\mathcal{N}\rho(a) \frac{g^2 \bar{B}(a)}{s-a} + 2\mathcal{N}^2 \rho(a) \frac{g^4 S(a)}{(s-a)^2} \\
 &+ 2\mathcal{N}^2 \frac{g^4}{s-a} \left[ \frac{d\rho(a)}{ds} S(a) - \rho(a) \frac{dS(a)}{ds} \frac{1-S(a)}{1+S(a)} \right], \quad (4.4.5)
 \end{aligned}$$

Moving onto  $d = 4$  we find

$$\begin{aligned}
 \text{Disc } C_J(s) &= -\frac{P_J(z_a(s))}{4\sqrt{s(4M^2-s)}} \left[ g^2 \bar{B}_J(s) \right. \\
 &+ \frac{g^4}{8\pi} \int_{-\infty}^a \frac{\tilde{P}_J(s')}{s'-s} \frac{1+\rho(s)A_J(s)}{1+\rho(s')A_J(s')} ds' \\
 &\left. - \frac{g^4}{4\pi} \int_a^{4m^2} \frac{\tilde{P}_J(s')\rho(s')A_J(s')}{s'-s} \frac{1+\rho(s)A_J(s)}{1+\rho(s')A_J(s')} ds' \right], \quad (4.4.6)
 \end{aligned}$$

a logarithmic branch cut with support on  $s \in [a, 4m^2)$  and where

$$\tilde{P}_J(s) \equiv \frac{\text{sgn} z'_a(s)}{\sqrt{(4m^2-s)(4M^2-s)}} P_J(z_a(s)). \quad (4.4.7)$$

Moreover, in eq. (4.4.6),  $\bar{B}(s, t) \equiv B(s, t) - (4.1.2)$  and  $\int$  is the principal value integral.

The non-linear dependence on  $A_J(s)$  makes it hard to express eq. (4.4.6) back in terms of the amplitudes (the piece dependent on  $\bar{B}_J(s)$  can nonetheless be put in the form of (4.4.4)). This was already expected given that, contrarily to the partial wave  $C_J(s)$ , the anomalous branch point of the amplitude  $C(s, t)$  may in general depend on  $t$ , i.e. be a Landau curve  $s(t)$  [151], which will in general vary diagram by diagram.<sup>15</sup> In appendix C.3 we check (4.4.6) in perturbation theory where we recover the discontinuity across the anomalous threshold of the box and double triangle diagrams.

<sup>15</sup>Interestingly, for  $mm \rightarrow MM$  there is a universal branch point at  $s = a$  not only for  $B_J(s)$  but also for the amplitude  $B(s, t)$ . This can be traced back to the fact that the anomalous threshold is always of the 'triangle' type (see Fig. 4.8).

## 4.5 Anomalous thresholds in integrable models

The only explicit known nonperturbative S-matrices which we can test our formulas are integrable models in  $d = 2$ . These theories are famously known to have no particle production. So immediately we see that formula (4.3.9) for the anomalous threshold of the  $MM \rightarrow mm$  amplitude cannot apply.

What is going on? The advantage of our analysis here is that it is *local* meaning that we can be agnostic to the analytic structure away from the anomalous threshold. However, it is entirely possible that another singularity, say a pole due to a different bound-state than  $m$  or  $M$ , can come arbitrarily close and even sit on top of the anomalous threshold for a given value of  $M$ . This sort of singularity cancellation is precisely what happens in the integrable models and leads to the absence of multi-particle processes.

Let us look explicitly at the  $E_8$  integrable model. In units where  $m = 1$ , the six lightest particles (out of eight) in the  $E_8$  model are [190]

$$\begin{aligned} m = m_1 = 1, \quad M = m_2 = 2 \cos \frac{\pi}{5} = \frac{1 + \sqrt{5}}{2} \approx 1.618, \\ m_3 = 2 \cos \frac{\pi}{30} \approx 1.989, \quad m_4 = 2m_2 \cos \frac{7\pi}{30} \approx 2.405, \\ m_5 = 2m_2 \cos \frac{2\pi}{15} \approx 2.956, \quad m_6 = 2m_2 \cos \frac{\pi}{30} \approx 3.218. \end{aligned} \quad (4.5.1)$$

To describe the S-matrices in integrable models it useful to use the basic CDD building block which solves elastic unitarity and crossing symmetry in  $d = 2$ . Let us define it in an abbreviated way as

$$[\mu^2] \equiv \frac{\varrho(\mu^2) + \varrho(s)}{\varrho(\mu^2) - \varrho(s)} \quad (4.5.2)$$

where  $\varrho(s)$  is the phase space factor in eq. (4.1.6) for  $mm \rightarrow mm$ .<sup>16</sup> In the sector of the two

<sup>16</sup>For the scattering of particles of different mass we have

$$mm \rightarrow mm: \quad \varrho(s) = \frac{1}{2\sqrt{4m^2 - s\sqrt{s}}}, \quad (4.5.3)$$

$$mm \rightarrow MM: \quad \varrho(s) = \frac{1}{2\sqrt{(m+M)^2 - s\sqrt{s - (m-M)^2}}}, \quad (4.5.4)$$

$$MM \rightarrow MM: \quad \varrho(s) = \frac{1}{2\sqrt{4M^2 - s\sqrt{s}}} \quad (4.5.5)$$

$$(4.5.6)$$

## Chapter 4. Nonperturbative Anomalous Thresholds

---

lightest particles  $m$  and  $M$  we have [190]

$$\begin{aligned}
 S_{mm \rightarrow mm}(s) &= [m^2] [M^2] [m_3^2], \\
 S_{mM \rightarrow mM}(s) &= [m^2] [M^2] [m_3^2] [m_4^2], \\
 S_{MM \rightarrow mm}(s) &= 1, \\
 S_{MM \rightarrow MM}(s) &= [m^2] [M^2] [m_4^2] [m_5^2] [m_6^2] [a]^2.
 \end{aligned} \tag{4.5.7}$$

This means in particular that  $mm \rightarrow mm$  has three simple poles at  $m^2$ ,  $M^2$  and  $m_3^2$  (and their crossing symmetric images  $s \leftrightarrow 4m^2 - s$ ), and likewise that  $MM \rightarrow MM$  has simple poles at  $m^2$ ,  $M^2$ ,  $m_4^2$ ,  $m_5^2$ ,  $m_6^2$  and a double pole at

$$a = 4M^2 - M^4/m^2, \tag{4.5.8}$$

which is the anomalous threshold (also known as Coleman-Thun pole). Plugging the numbers we get  $\sqrt{a} \approx 1.902$  so the anomalous threshold sits between the second and third particles  $M < \sqrt{a} < m_3$ .

### 4.5.1 Cancellation of the “anomalous” pole in $MM \rightarrow mm$

How is it possible that  $T_{MM \rightarrow mm}(s) = 0$  if  $T_{mM \rightarrow mM}(s) \neq 0$ ? These two objects are related by crossing symmetry in  $d > 2$  but in  $d = 2$  since  $t = t(s)$  and  $u = u(s)$  this is not necessarily the case. Let us see explicitly how  $T_{MM \rightarrow mm}(s) = 0$  at “tree level”. By “tree level” we mean just looking at how the simple poles cancel each other.

The  $MM \rightarrow mm$  process should be able to exchange the same particles as the “crossing symmetric” process  $mM \rightarrow mM$ , namely  $m$ ,  $M$ ,  $m_3$  and  $m_4$ . Since  $t = t(s)$  and  $u = u(s)$  according to eq. (C.5.3) all these exchanges will give rise to poles in  $s$ . From eq. (C.5.3) we have that a pole in  $t$ -channel or  $u$ -channels at  $\mu^2$  gives rise to the following pole in  $s$ ,

$$t(s) = \mu^2 \text{ or } u(s) = \mu^2 \quad \Longrightarrow \quad s(\mu^2) = -\frac{(m^2 - M^2)^2}{\mu^2} + 2(m^2 + M^2) - \mu^2 \tag{4.5.9}$$

For the particular values where  $t(s) = \mu = m, M$  we find

$$\begin{aligned}
 \mu = m &\Longrightarrow s = a = 4M^2 - \frac{M^4}{m^2}, \\
 \mu = M &\Longrightarrow s = b = 4m^2 - \frac{m^4}{M^2},
 \end{aligned} \tag{4.5.10}$$

The first value is the already studied  $t$ -channel and  $u$ -channel pole in eq. (4.1.2). As we can see in figure 4.10, it wraps around the  $s = 4m^2$  branch cut as  $M$  increases and its residue changes as a result, i.e. becomes “anomalous” for  $M > \sqrt{2}m$  as argued in the main text. The second value, on the other hand, does not wrap around  $s = 4m^2$  as  $M$  increases.

## 4.5 Anomalous thresholds in integrable models

Both poles will coincide if  $a = b$ ,

$$4M^2 - \frac{M^4}{m^2} = 4m^2 - \frac{m^4}{M^2} \implies M = \left( \frac{1 + \sqrt{5}}{2} \right) m, \quad (4.5.11)$$

which is precisely the mass of the second bound state in the  $E_8$  model.<sup>17</sup>

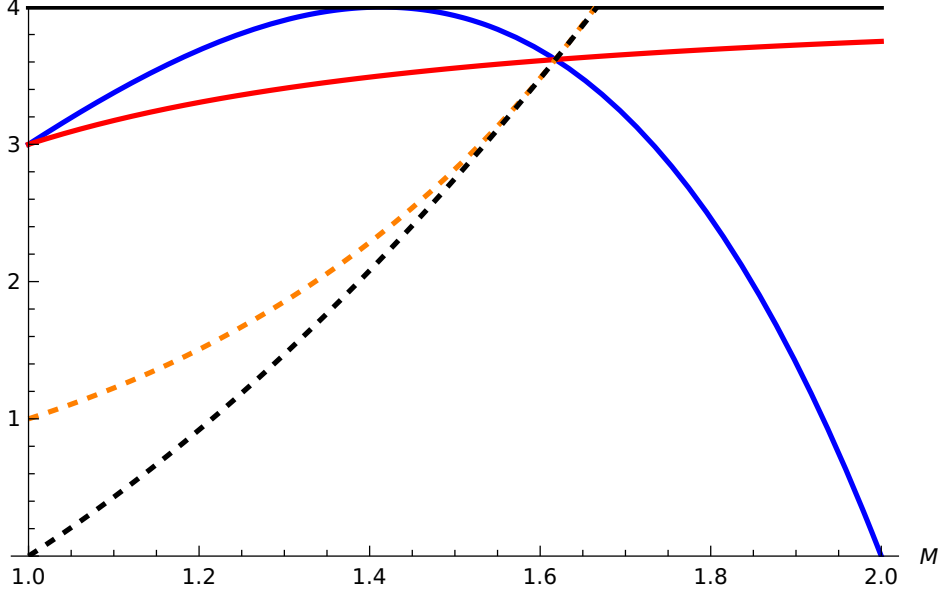


Figure 4.10: In black: the normal thresholds at  $s = 4m^2$  and  $t = 4M^2 - s = (m + M)^2$ . In thick line:  $s$ -channel singularities in the  $mm \rightarrow MM$  process. In dashed line:  $t$ -channel singularities in the  $MM \rightarrow MM$  process. Red and blue are given by  $s = a$  and  $s = b$  in eq. (4.5.10). Orange is given by  $4M^2 - t_-$  with  $t_-$  in eq. (4.5.42). As  $M$  increases  $a = 4M^2 - M^4$  touches the  $s = 4$  branch point at  $M = \sqrt{2} \approx 1.41$  and comes back. When  $M = \frac{1+\sqrt{5}}{2} \approx 1.62$ ,  $b$  overlaps with  $a$  and cancels production of  $MM \rightarrow mm$ . For the  $MM \rightarrow MM$  the other singularities from the  $t$ -channel (in dashed) and contribute to the anomalous threshold at  $s \rightarrow a$ . In total the 4 singularities contribute to the double pole in the  $E_8$  model.

So, in order to have  $T_{mm \rightarrow MM} = 0$ , the residues coming from these two poles must cancel out. A proposal for the “anomalous” residue was computed in eq. (4.4.1) where, in the notation of this section, the amplitude was found to behave as

$$T_{mm \rightarrow MM}(s \sim a) = -\mathcal{N}_m \frac{g_{mmM}^2 S_{mm \rightarrow mm}(a)}{s - a} \quad (4.5.12)$$

with the relation between the amplitude and the S-matrix being, as usual,  $S(s) = 1 + 2\rho(s)T(s)$ , and

$$\mathcal{N}_m = \frac{2M^2 - a}{m^2} = \left( \frac{M}{m} \right)^4 - 2 \left( \frac{M}{m} \right)^2. \quad (4.5.13)$$

<sup>17</sup>There are other solutions to eq. (4.5.11). However, the solution in eq. (4.5.11) is the only one for which  $M > m$ .

## Chapter 4. Nonperturbative Anomalous Thresholds

---

We now want to compare this with the residue coming from the other pole,

$$-\frac{g_{mMM}^2}{t(s) - M^2} - \frac{g_{mMM}^2}{u(s) - M^2} = -\frac{g_{mMM}^2(s - 2m^2)}{M^2(s - b)} \quad (4.5.14)$$

so when  $s \sim b$  we have

$$T_{mm \rightarrow MM}(s \sim b) = -\mathcal{N}_M \frac{g_{mMM}^2}{s - b}, \quad (4.5.15)$$

with

$$\mathcal{N}_M = \left(\frac{m}{M}\right)^4 - 2\left(\frac{m}{M}\right)^2 \quad (4.5.16)$$

For these two to cancel we must have

$$\mathcal{N}_m g_{mmM}^2 S_{mm \rightarrow mm}(a) + \mathcal{N}_M g_{mMM}^2 = 0. \quad (4.5.17)$$

We can now verify that this is indeed the case in the  $E_8$  model. We can extract  $g_{mmM}$  by looking at the  $s$ -channel exchange of  $M$  of the  $mm \rightarrow mm$  process, i.e.

$$T_{mm \rightarrow mm}(s \sim M^2) = -\frac{g_{mmM}^2}{s - M^2} \quad (4.5.18)$$

which, making use of the S-matrices in eq. (4.5.7), gives

$$g_{mmM}^2 = \sqrt{30} \sqrt{4605 + 2047\sqrt{5} + 10\sqrt{30} \sqrt{14045 + 6281\sqrt{5}}} \approx 742.201 \quad (4.5.19)$$

taking the values in (4.5.1).

To extract  $g_{mMM}$  we look at

$$T_{MM \rightarrow MM}(s \sim m^2) = -\frac{g_{mMM}^2}{s - m^2} \quad (4.5.20)$$

and find

$$g_{mMM}^2 = 2\sqrt{15} \sqrt{33814455 + 15122284\sqrt{5} + 10\sqrt{15} \sqrt{1524538572625 + 681794376542\sqrt{5}}} \approx 90085.8. \quad (4.5.21)$$

Likewise, we find

$$S_{mm \rightarrow mm}(a) = 13 + 3\sqrt{5} + 5\sqrt{15 + 6\sqrt{5}} \approx 46.3617 \quad (4.5.22)$$

and, finally,

$$\mathcal{N}_m = \frac{1 + \sqrt{5}}{2} \approx 1.61803, \quad \mathcal{N}_M = \frac{1 - \sqrt{5}}{2} \approx -0.618034. \quad (4.5.23)$$

We then verify that eq. (4.5.17) is exactly satisfied.

We can also verify cancellation of the other singularities. No other anomalous threshold should exist, as also argued in appendix C.4: Any singularity coming from  $t(s) = \mu^2$  or  $u(s) = \mu^2$  only wraps around the  $s = 4m^2$  branch cut if  $M^2 > \mu^2 + m^2$  and none of the other masses  $M$ ,  $m_3$  and  $m_4$  satisfy this except  $m$  which gives the only anomalous threshold at  $s = a$ .<sup>18</sup>

The presence of  $m_3$  and  $m_4$  is nonetheless necessary to cancel out the remaining singularities. In particular, we find

$$t(s) = m_3^2 \implies s = M^2, \quad t(s) = m_4^2 \implies s = m^2. \quad (4.5.24)$$

It is a straightforward exercise to see that the residues also cancel each other.

Finally, the singularities at  $s = m_3^2$  and  $s = m_4^2$  whose residues are respectively  $g_{MMm_3}g_{mmm_3}$  and  $g_{MMm_4}g_{mmm_4}$  are not present since  $g_{MMm_3} = g_{mmm_4} = 0$ . Notice in eq. (4.5.7) how  $mm \rightarrow mm$  does not exchange  $m_4$  and how  $MM \rightarrow MM$  does not exchange  $m_3$ .

In summary:

- The  $t$ - and  $u$ -channel exchanges of  $m_3$  cancel the  $s$ -channel exchange of  $M$ .
- The  $t$ - and  $u$ -channel exchanges of  $m_4$  cancel the  $s$ -channel exchange of  $m$ .
- There are no  $s$ -channel exchanges of  $m_3$  and  $m_4$ , since  $g_{MMm_3} = g_{mmm_4} = 0$ .
- The  $t$ - and  $u$ -channel exchanges of  $M$  cancel the  $t$ - and  $u$ -channel exchanges of  $m$  whose residue is "anomalous" according to eq. (4.4.1).

#### 4.5.2 The anomalous double pole of $MM \rightarrow MM$ : Four overlapping singularities

As seen in eq. (4.5.7) the  $MM \rightarrow MM$  S-matrix of the  $E_8$  contains a double pole at  $s = 4M^2 - M^4/m^2$ . In units of  $m = 1$  its numerical value reads (the exact expressions in terms of radicals are too extensive to print here)

$$T_{MM \rightarrow MM}^{E_8}(s \rightarrow a) = -\frac{2.40930 \times 10^8}{(s-a)^2} - \frac{2.78375 \times 10^8}{s-a} \quad (4.5.25)$$

Can the formula in eq. (4.4.5) reproduce this? Immediately we see that this cannot be the

<sup>18</sup>In perturbation theory, the condition  $M^2 > \mu^2 + m^2$  for the existence of the anomalous threshold follows from requiring that the solution to the Landau equations of the triangle diagram is ' $\alpha$ -positive'.

## Chapter 4. Nonperturbative Anomalous Thresholds

---

case due to the term  $\bar{B}(a) = \bar{T}_{mm \rightarrow MM}(a)$  which is defined as the “subtracted”  $mm \rightarrow MM$  amplitude

$$\bar{T}_{mm \rightarrow MM}(s) = T_{mm \rightarrow MM}(s) - \mathcal{N}_m g_{mmM} S_{mm \rightarrow mm}(a)/(s-a) \sim 1/(s-b) \quad (4.5.26)$$

which diverges at the integrable point since  $b \rightarrow a$ , as seen in the previous section.

Indeed, in the derivation of eq. (4.4.5) no overlapping singularities were assumed which could explain its failure. One can nonetheless account for this extra overlapping singularity at  $s \sim b \rightarrow a$ .

In eq. (4.3.6) we have the solution to unitarity across the  $2m$  branch cut (see also Fig. 4.7). In the notation of this chapter unitarity reads

$$\text{Disc } T_{mm \rightarrow mm}(s) = \rho_{mm}(s) |T_{mm \rightarrow mm}(s)|^2 \quad (4.5.27)$$

$$\text{Disc } T_{mm \rightarrow MM}(s) = \rho_{mm}(s) T_{mm \rightarrow MM}(s) T_{mm \rightarrow mm}^*(s) \quad (4.5.28)$$

$$\text{Disc } T_{MM \rightarrow MM}(s) = \rho_{mm}(s) |T_{mm \rightarrow MM}(s)|^2 \quad (4.5.29)$$

where  $\rho_{mm}(s)$  is the phase space factor (4.1.5) with solution

$$T_{mm \rightarrow mm}(s) = \frac{\alpha(s)}{1 - \varrho_{mm}(s)\alpha(s)}, \quad (4.5.30)$$

$$T_{mm \rightarrow MM}(s) = \frac{\beta(s)}{1 - \varrho_{mm}(s)\alpha(s)}, \quad (4.5.31)$$

$$T_{MM \rightarrow MM}(s) = \sigma(s) + \frac{\varrho_{mm}(s)\beta^2(s)}{1 - \varrho_{mm}(s)\alpha(s)}, \quad (4.5.32)$$

where  $\text{Disc}\alpha(s) = \text{Disc}\beta(s) = \text{Disc}\sigma(s) = 0$  across the  $2m$  cut. The advantage of this representation is that it isolates the analytic structure around the  $2m$  branch cut (where the anomalous threshold comes from).

Now, we are interested in the behavior of  $T_{mm \rightarrow MM}(s)$  around the two singularities  $s \sim a$  and  $s \sim b$  which will cancel each other at the integrable point. These are the two t-channel poles at  $t = m^2$  and  $t = M^2$  in eq. (4.5.15) and (4.1.2),

$$T_{mm \rightarrow MM}(s) = -\mathcal{N}_m \frac{g_{mmM}^2}{s-a} - \mathcal{N}_M \frac{g_{mMM}^2}{s-b} + \dots, \quad (4.5.33)$$

where the ‘...’ are regular as  $s \rightarrow a, b$  and can be ignored for our purposes since they will also go to zero at the integrable point (and regardless will not contribute to the anomalous threshold).

Looking at eq. (4.5.31) this fixes

$$\beta(s) = -\mathcal{N}_m \frac{g_{mmM}^2}{s-a} [1 - \varrho_{mm}(a)\alpha(a)] - \mathcal{N}_M \frac{g_{mMM}^2}{s-b} [1 - \varrho_{mm}(b)\alpha(b)] \quad (4.5.34)$$



## 4.5 Anomalous thresholds in integrable models

This now must be inserted in eq. (4.5.32) for  $T_{MM \rightarrow MM}(s)$ , which in turn fixes

$$\sigma(s) = - \left[ \frac{\varrho_{mm}(s) \beta^2(s)}{1 - \varrho_{mm}(s) \alpha(s)} \right]_{s \rightarrow a} - \left[ \frac{\varrho_{mm}(s) \beta^2(s)}{1 - \varrho_{mm}(s) \alpha(s)} \right]_{s \rightarrow b} \quad (4.5.35)$$

However, upon continuation from  $M < \sqrt{2}$  to  $M > \sqrt{2}$  the  $s = a$  singularity goes around the  $2m$  branch cut and  $\rho_{mm}(a) \rightarrow -\rho_{mm}(a)$ , and  $\sigma(s)$  no longer cancels the singularity at  $s \rightarrow a$ , giving rise to a double pole on  $T_{MM \rightarrow MM}(s)$ : the anomalous threshold.

Letting

$$M = \frac{1 + \sqrt{5}}{2} + \epsilon \quad (4.5.36)$$

carefully expanding in  $\epsilon$  we find again a formal divergence, as if we had naively used the original formula (4.4.5),

$$\begin{aligned} T_{MM \rightarrow MM}(s \rightarrow a) &= \frac{1}{\epsilon} \frac{1}{s-a} \frac{2}{\sqrt{5}} g_{mmM}^2 g_{mMM}^2 \rho_{mm}(a) \\ &+ \frac{1}{(s-a)^2} g_{mmM}^2 \rho_{mm}(a) \left[ (3 + \sqrt{5}) g_{mmM}^2 S_{mm}(a) - \frac{8}{\sqrt{5}} g_{mMM}^2 \right] \\ &+ \frac{1}{s-a} g_{mMM}^2 \left[ \rho'_{mm}(a) \left( (3 + \sqrt{5}) g_{mmM}^2 S_{mm}(a) - \frac{8}{\sqrt{5}} g_{mMM}^2 \right) \right. \\ &+ \rho_{mm}(a) \left( g_{mMM}^2 \left( \frac{5\sqrt{5}-9}{10} - \frac{4S'_{mm}(a)}{1+S_{mm}(a)} \right) \right. \\ &\left. \left. - g_{mmM}^2 \left( 2(1 + \sqrt{5}) S_{mm}(a) + (3 + \sqrt{5}) S'_{mm}(a) \frac{1-S_{mm}(a)}{1+S_{mm}(a)} \right) \right) \right] \end{aligned} \quad (4.5.37)$$

plugging the values for the  $E_8$  model we find numerically

$$T_{MM \rightarrow MM}(s \rightarrow a) = \frac{g_{mmM}^2 g_{mMM}^2}{\epsilon} \frac{0.380423}{s-a} - \frac{4.48669 \times 10^7}{(s-a)^2} + \frac{1.30302 \times 10^8}{s-a} \quad (4.5.38)$$

where on the last two terms we replaced the values taken from the  $E_8$  model in eq. (4.5.7) around  $s \rightarrow a$ , namely  $\alpha(s \sim a)$  was related to  $T_{mm \rightarrow mm}(s \sim a)$  via eq. (4.3.4), and  $g_{mMM}$  and  $g_{mMM}$  were replaced from eqs. (4.5.19) and (4.5.21).

The first term is formally infinite as  $\epsilon \rightarrow 0$ . We have not replaced the  $E_8$  values to try to isolate where it comes from. Notice that it does not depend on  $T_{mm \rightarrow mm}$  and just depends on the product  $g_{mMM} g_{mMM}$  which suggests that this divergent term only comes from the box diagram with all external legs  $M$ , three internal legs with  $m$  and one with  $M$ .

Is this box diagram infinite when  $M \rightarrow \frac{1+\sqrt{5}}{2}$ ? By explicit computation (which we have not included here) we verify that this is not the case. This suggests that there may be another overlapping singularity as  $M \rightarrow \frac{1+\sqrt{5}}{2}$ , possibly coming from the crossed channel.

## Chapter 4. Nonperturbative Anomalous Thresholds

---

This is indeed the case. The  $t = (m + M)^2$  threshold, in terms of  $s$ , reads

$$\begin{aligned} t\text{-channel } mM \text{ threshold: } \quad t(s) = (m + M)^2 &\implies \\ &\implies s = 4M^2 - (m + M)^2 \rightarrow a, \text{ if } M \rightarrow \frac{1 + \sqrt{5}}{2}m. \end{aligned} \quad (4.5.39)$$

And this is not the only singularity from the  $t$ -channel that overlaps with  $s \rightarrow a$ ! There is one more. Cutting this box through the  $mM$  cut leads to the square of the following tree level exchange on the  $t$ -channel

$$T_{MM \rightarrow mM}(t) = -\frac{\mathcal{G}_{mmM}\mathcal{G}_{mMM}}{\bar{s}(t) - m^2} - \frac{\mathcal{G}_{mmM}\mathcal{G}_{mMM}}{\bar{u}(t) - m^2} \quad (4.5.40)$$

$$= -\frac{\mathcal{G}_{mmM}\mathcal{G}_{mMM}P(t)}{(t - t_-)(t - t_+)} \quad (4.5.41)$$

with  $P(t) = (m^2 - 3M^2 + t)t/m^2$  and

$$t = t_{\pm} = \frac{3M^2}{2} \pm \frac{\sqrt{-4m^6M^2 + 17m^4M^4 - 4m^2M^6}}{2m^2} \quad (4.5.42)$$

where we made use  $d = 2$  kinematics for  $MM \rightarrow mM$  scattering to find  $\bar{s}(t)$  and  $\bar{u}(t)$ .<sup>19</sup> The motion of the singularity  $4M^2 - t_+$  is plotted in Fig. 4.10. As  $M \rightarrow \frac{1+\sqrt{5}}{2}m$  it comes in contact with the  $mM$  threshold and becomes an anomalous threshold for  $M > \frac{1+\sqrt{5}}{2}m$ .<sup>20</sup> So in total we expect to have 4 singularities contributing at  $s = a$  to the  $E_8$  model anomalous threshold (see summary at the end).

Let us now try to account for the latter two nonperturbatively. We write down the unitarity equations across the  $mM$  threshold in the  $t$ -channel [191]:

$$\text{Disc } T_{mM \rightarrow mM}(t) = \rho_{mM}(t) |T_{mM \rightarrow mM}(t)|^2 \quad (4.5.45)$$

$$\text{Disc } T_{MM \rightarrow mM}(t) = \rho_{mM}(t) T_{MM \rightarrow mM}(t) T_{mM \rightarrow mM}^*(s) \quad (4.5.46)$$

$$\text{Disc } T_{MM \rightarrow MM}(t) = 2\rho_{mM}(t) |T_{MM \rightarrow mM}(t)|^2 \quad (4.5.47)$$

where the factor of 2 in eq. (4.5.47) comes from the fact that  $m$  and  $M$  are not identical. In eqs. (4.5.45) and (4.5.46),  $T_{mM \rightarrow mM}$  is the forward amplitude and the backwards amplitude

---

<sup>19</sup>

$$\bar{s}(t) = \frac{1}{2} \left( m^2 + 3M^2 - t + \frac{\sqrt{t(t-4M^2)}\sqrt{m^4 + (M^2 - t)^2 - 2m^2(M^2 + t)}}{t} \right) \quad (4.5.43)$$

$$\bar{u}(t) = \frac{1}{2} \left( m^2 + 3M^2 - t - \frac{\sqrt{t(t-4M^2)}\sqrt{m^4 + (M^2 - t)^2 - 2m^2(M^2 + t)}}{t} \right) \quad (4.5.44)$$

<sup>20</sup>In fact, as  $M \rightarrow \frac{1+\sqrt{5}}{2}m$  we also have  $t_- \rightarrow m^2$  which gets canceled in the  $E_8$  model by an  $s$ -channel exchange of  $m^2$  of the process  $MM \rightarrow mM$ .

$mM \rightarrow mM$  is assumed to vanish (which it does in the  $E_8$  model) and should not contribute to the anomalous threshold at  $s \rightarrow a$ .

The solution is

$$T_{mM \rightarrow mM}(t) = \frac{\bar{\alpha}(t)}{1 - \varrho_{mM}(t)\bar{\alpha}(t)}, \quad (4.5.48)$$

$$T_{MM \rightarrow mM}(t) = \frac{\bar{\beta}(s)}{1 - \varrho_{mM}(t)\bar{\alpha}(t)}, \quad (4.5.49)$$

$$T_{MM \rightarrow MM}(t) = \bar{\sigma}(s) + \frac{2\varrho_{mM}(t)\bar{\beta}^2(t)}{1 - \varrho_{mM}(t)\bar{\alpha}(t)}, \quad (4.5.50)$$

where  $\text{Disc}\bar{\alpha}(t) = \text{Disc}\bar{\beta}(t) = \text{Disc}\bar{\sigma}(t) = 0$  across the  $mM$  cut.

Noting eq. (4.5.40) in order to include the singularity at  $t \rightarrow t_+$  in this solution for  $T_{MM \rightarrow mM}$  we must have

$$\bar{\beta}(t) = -\frac{\mathfrak{g}_{mmM}\mathfrak{g}_{mMM}P(t)}{(t-t_-)(t-t_+)}[1 - \varrho_{mM}(t_-)\bar{\alpha}(t_-)] + \dots \quad (4.5.51)$$

In turn, to prevent  $T_{MM \rightarrow MM}(t)$  from having this singularity we must have

$$\bar{\sigma}(t) = -\left[ \frac{2\varrho_{mM}(t)\bar{\beta}^2(t)}{1 - \varrho_{mM}(t)\bar{\alpha}(t)} \right]_{t \rightarrow t_+} \quad (4.5.52)$$

We now plug this back into (4.5.50), make use of  $t = 4M^2 - s$ , let  $M = \frac{1+\sqrt{5}}{2} + \epsilon$  and expand in  $\epsilon$ . Since in this limit  $M \rightarrow \frac{1+\sqrt{5}}{2}$  the normal threshold at  $t(s) = (m+M)^2$  will overlap with the anomalous threshold  $s \rightarrow a$  from the  $s$ -channel we must especially be careful because  $T_{mM \rightarrow mM}(s)$  will have a branch point and will not be analytic. Therefore it is better to expand in the variable  $\bar{\alpha}(s)$  which should be analytic across the normal threshold. The Taylor coefficients of  $\bar{\alpha}(s)$  should be seen as “scattering lengths” and “effective ranges” of the amplitude  $T_{mM \rightarrow mM}(s)$  as defined in [7]. Another important technical point is that in expanding in the mass  $\alpha_{mM}$  generically can lead to two contributions.

$$\frac{d\alpha(a)}{dM} = \frac{da}{dM} \frac{\partial \alpha}{\partial s}(a) + \frac{\partial \alpha}{\partial M}(a) \quad (4.5.53)$$

The second contribution depends on how the integrable  $E_8$  point is achieved. Such a contribution dropped out from the  $s$ -channel computation in eq. (4.5.37) but in the  $t$ -channel this is not the case.

## Chapter 4. Nonperturbative Anomalous Thresholds

In the end we find the following contribution from the  $t$ -channel to the singularity at  $s \rightarrow a$ :

$$T_{MM \rightarrow MM}^t(s \rightarrow a) = -\frac{1}{\epsilon} \frac{1}{s-a} \frac{4\sqrt{2}\sqrt{5+\sqrt{5}}}{5} \frac{g_{mmM}^2 g_{mMM}^2}{1+S_{mM}(a)} - \frac{g_{mmM}^2 g_{mMM}^2}{(s-a)^2} \frac{\sqrt{130+38\sqrt{5}}}{5} + \frac{g_{mmM}^2 g_{mMM}^2}{s-a} \left( \sqrt{\frac{373}{200} - \frac{229}{200\sqrt{5}}} - \frac{5+\sqrt{5}}{20} \frac{\partial \bar{\alpha}}{\partial s}(a) + \frac{1+\sqrt{5}}{20} \frac{\partial \bar{\alpha}}{\partial M}(a) \right). \quad (4.5.54)$$

Inverting relation (4.5.48) for  $\bar{\alpha}(s)$ ,

$$\bar{\alpha}(s) = \frac{1}{\varrho_{mM}(t(s))} \frac{S_{mM \rightarrow mM}(t(s)) - 1}{S_{mM \rightarrow mM}(t(s)) + 1}, \quad \text{with} \quad t(s) = 4M^2 - s, \quad (4.5.55)$$

and plugging the  $E_8$  S-matrix in eq. (4.5.7) we find

$$\frac{\partial \bar{\alpha}}{\partial s}(a) = 12 \sqrt{2 + \frac{2}{\sqrt{5}}} \quad (4.5.56)$$

using the values for the couplings  $g_{mmM}$  and  $g_{mMM}$  in eqs. (4.5.19) and (4.5.21) we find

$$T_{MM \rightarrow MM}^t(s \rightarrow a) = -\frac{g_{mmM}^2 g_{mMM}^2}{\epsilon} \frac{0.380423}{s-a} - \frac{1.96064 \times 10^8}{(s-a)^2} - \frac{(4.16099 - 0.10819 \partial_M \bar{\alpha}) \times 10^8}{s-a}. \quad (4.5.57)$$

Unfortunately we still have an unknown term  $\partial_M \bar{\alpha}$  which would require perturbing the  $E_8$  model away from the integrable point.  $\partial_M \bar{\alpha}$  represents the first order correction to the "scattering length" of the  $mM \rightarrow mM$  forward scattering process.

Nonetheless, adding eq. (4.5.57) to the s-channel contribution in eq. (4.5.38) we see that the divergent  $1/\epsilon$  terms cancel each other and the double pole contribution add up to exactly match the double pole residue of the  $E_8$  value in eq. (4.5.25).

For the simple poles to match we should have

$$\frac{\partial \bar{\alpha}}{\partial M}(a) = 4 \sqrt{85 - 38\sqrt{5}} \approx 0.68860537006 \quad \text{in Ising Field Theory very close to } E_8. \quad (4.5.58)$$

## 4.6 Discussion and outlook

In this work we propose nonperturbative formulas for the discontinuity across anomalous thresholds. Eqs. (4.4.4) and (4.4.2), for the anomalous threshold of the  $mm \rightarrow MM$  process in  $d = 4$ , which match previous results in the literature [132, 184, 185], and eq. (4.4.1) for  $mm \rightarrow MM$  in  $d = 2$ , and eqs. (4.4.5) and (4.4.6) for  $MM \rightarrow MM$  in  $d = 2$  and the partial wave in  $d = 4$ , respectively, which we believe are novel results.

One natural testing ground for these formulas are integrable models which also possess

anomalous thresholds, typically known as Coleman-Thun poles. However, integrable models are quite particular in that they have fine-tuned spectrum and couplings as to cancel out particle production and satisfy the Yang-Baxter equations. In particular, the  $mm \rightarrow MM$  process is zero and therefore the formula (4.4.1), as it is does not apply. In deriving these formulas we have assumed non-degenerate singularity structure, i.e. that other singularities (e.g a bound-state pole) do not overlap with the anomalous threshold. Indeed, as shown in section 4.5 for the  $E_8$  model such a cancellation happens which relates the coupling  $g_{mMM}^2 \sim g_{mmM}^2 S_{mm \rightarrow mm}(a)$ . This sort of cancellation has already been advertised before [192] however here we believe we provide an argument for the first time for the  $O(1)$  factor in the relation  $g_{mMM}^2 \sim g_{mmM}^2 S_{mm \rightarrow mm}(a)$ .

For the  $MM \rightarrow MM$  anomalous threshold in eq. (4.4.5), the situation is far more intricate when trying to apply it to integrable models. As seen in section 4.5 for the  $E_8$  model there are four overlapping singularities at  $s = a$ : two anomalous thresholds (one from  $s$ -channel and other from  $t$ -channel), a  $t$ -channel exchange of  $M^2$  and a normal threshold in the  $t$ -channel of production  $t = (m + M)^2$ . These all overlap at the integrable point when  $M = \frac{1+\sqrt{5}}{2}$ . The individual contributions to the residues from each channel is singular as  $M \rightarrow \frac{1+\sqrt{5}}{2}$ . However, the sum is finite and we find exact agreement with the double pole residue of the  $E_8$  model. The simple pole residue however depends on how the integrable point is reached, in particular on the first order correction to the scattering length of the  $Mm \rightarrow Mm$  forward scattering length away from the integrable  $E_8$  point. To have agreement this correction should be an  $O(1)$  number, see eq. (4.5.58). It would be interesting to check if this number is verified in Ising Field Theory.

We believe that the formulas derived here should directly apply away from the integrable point, when there are no overlapping and cancellation of singularities and the spectrum is “generic”.

It would be great if these formulas could be checked with other nonperturbative methods. For example, via the LSZ reduction formula (viz. the very concrete numerical implementation of [193] that makes use of Hamiltonian truncation data), or via the flat space limit of AdS/CFT, as done e.g. in [129, 194] which so far have only considered the Witten triangle diagram.

We focused on  $d = 2$  and  $d = 4$  but our method should apply to any  $d$ . One difference is that in odd  $d$  the 2-particle cut is a logarithm [7] (so the kernel has monodromy  $\rho(s) \rightarrow \rho(s) + 2\pi i$ ). We expect the anomalous threshold to be of square-root nature in odd dimensions.

We have shown that the presence of the  $t$ - and  $u$ -channel poles (4.1.2) leads to an anomalous branch point at  $s = a$  for  $M > \sqrt{2}m$ . It is natural to ask:

- Besides the poles (4.1.2), can other singularities contribute to the same anomalous threshold at  $s = a$  and change its discontinuity?
- Is  $s = a$  the only anomalous branch point in the  $mm \rightarrow MM$  and  $MM \rightarrow MM$  partial waves, or can there be more?

## Chapter 4. Nonperturbative Anomalous Thresholds

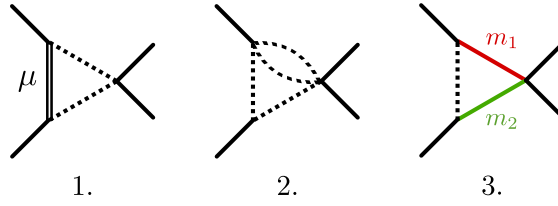


Figure 4.11: Triangle graphs: 1. Has an anomalous threshold coming from the  $s = 4m^2$  extended cut when (4.6.1) is satisfied; 2. Has an anomalous threshold coming from the  $s = 9m^2$  extended unitarity cut, if  $M > \sqrt{3}m > 3m/2$ ; 3. Does *not* have an anomalous threshold for  $m_1 + m_2 \geq 2M$ , which would come from a unitarity cut on the physical region  $s \geq 4M^2$ .

Let us address these questions *by* branch cut, i.e. by the branch cut from which the anomalous threshold may cross onto the physical sheet. We will separately consider:

1. The extended unitarity cut at  $s = 4m^2$ . Are there other singularities crossing this cut onto the physical sheet, besides the one already analyzed?
2. Other potential extended unitarity cuts. Can there be other branch points between  $4m^2 < s < 4M^2$ , from which new anomalous thresholds can appear?
3. Usual physical unitarity cuts, i.e. at  $s \geq 4M^2$ . Can anomalous thresholds come onto the physical sheet via normal thresholds on the physical region?

We start with point 1 (refer to appendix C.4 for supporting technical details). Before anomalous thresholds arise, we assume LPMA so that there are only the usual simple poles and normal thresholds. In the  $s$ -channel these are ‘static’, e.g.  $s = m^2$  or  $s = M^2$ , and would not encircle any branch point as  $M$  is increased. Looking at the  $t$ - and  $u$ -channels, a singularity at  $t, u = \mu^2$  leads to a left-hand cut in the partial wave  $B_J(s)$  (and also in  $C_J(s)$  in the second sheet, see appendix 4.3). Now, if

$$M^2 > \mu^2 + m^2 \quad (4.6.1)$$

the rightmost branch point of this left-hand cut, given by eq. (C.4.2), will move to the right as  $M$  increases and will encircle the extended unitarity branch point at  $s = 4m^2$  and come back to generate an anomalous threshold (qualitatively as in Fig. 4.4). Note that this is the usual  $\alpha$ -positive condition for the Landau singularity of triangle 1 in Fig. 4.11 to be on the physical sheet [8], which arises here nonperturbatively from a partial wave analysis.<sup>21</sup> From (4.6.1) we see that, since  $M < 2m$  is stable, *only*  $\mu = m$  satisfies condition (4.6.1), which corresponds to the  $s = a$  singularity analyzed here coming from the poles (4.1.2) which require a cubic coupling  $g$  between  $Mmm$ .<sup>22</sup> There should be no other anomalous threshold coming from

<sup>21</sup>This is not surprising because Landau singularities are intimately connected with unitarity [151, 8, 7, 153], which is diagonalized by the partial wave decomposition.

<sup>22</sup>If there were a lighter particle in the spectrum  $\bar{m}$  then  $\mu = 2\bar{m}$  could satisfy (4.6.1) via a quartic coupling  $Mm\bar{m}\bar{m}$ . I thank A. Zhiboedov for raising this point.

the  $s = 4m^2$  cut.<sup>23</sup>

Let us now address point 2. Indeed, other extended unitarity cuts can be present. Namely, the branch points  $s = (m + M)^2$  and  $s = 9m^2$  can be between  $s \in [4m^2, 4M^2)$ , which we chose not to represent in Fig. 4.1. Note that  $s = 9m^2$  is only extended if  $M > 3m/2$ . Further extended cuts cannot exist since  $M < 2m$  is stable. From these two additional cuts, new anomalous thresholds can in fact arise. E.g. the triangle 2 in Fig. 4.11.<sup>24</sup> Note however that these are not present if  $m$  is  $\mathbb{Z}_2$  odd as the intermediate processes are disallowed.

Finally, we come to point 3. Can anomalous thresholds arise from physical unitarity cuts? Landau analysis indicates that this is *not* the case. For example, for triangle 3 in Fig. 7 we see that if the mass of the particles exchanged in the  $s$ -channel is larger than the physical threshold, i.e.  $m_1 + m_2 > 2M$ , then there is no anomalous threshold (no  $\alpha$ -positive solution). Naturally, this question can also be asked for lightest particle scattering  $mm \rightarrow mm$ , where there are no extended cuts and no anomalous thresholds are seen (as ascertained by LPMA). This suggests that:

**Anomalous thresholds can only arise from extended branch cuts.**

We define an extended branch cut as a branch cut with a branch point below the physical scattering region. This includes extended unitarity cuts, i.e. normal thresholds below the physical region and, possibly, other already present anomalous thresholds.<sup>25</sup>

It would be interesting to test this hypothesis beyond the examples in perturbation theory considered here. Note that this hypothesis implies that, given a fixed particle spectrum there is only a *finite* number of extended unitarity cuts which need to be analyzed. Naturally, the higher the number of extended cuts the harder it is, in general, to find an exact solution to extended unitarity, which our method relies on (see appendix 4.3).

In summary, we just argued here (see also appendix C.4) that for a theory with two particles  $m$  and  $M$ , where  $m$  is  $\mathbb{Z}_2$  odd, there is one extended cut at  $s = 4m^2$  from which *only* the anomalous threshold at  $s = a$  studied here should arise for  $M > \sqrt{2}m$ . In particular, expressions (4.4.1) and (4.4.5) should suffice to go beyond  $M > \sqrt{2}m$  in the  $d = 2$  numerical S-matrix bootstrap of [135].<sup>26</sup> Let us then close with a challenge for the reader: Is there a  $2 \rightarrow 2$  graph in this theory

<sup>23</sup>We still have to consider crossing symmetry. Namely, the process  $mM \rightarrow mM$ , which is related to  $mm \rightarrow MM$ . If  $m$  is  $\mathbb{Z}_2$  odd, then  $mM \rightarrow mM$  cannot exchange  $mm$ , hence no branch point at  $s = 4m^2$  is present. A similar analysis holds for  $MM \rightarrow MM$ . Here, however, there is the possibility that  $\mu^2$  is itself an anomalous threshold, i.e. coming from the crossed channel. In appendix C.4 we argue that this does not lead to further anomalous thresholds in the direct channel in  $d = 2$  if  $m$  is  $\mathbb{Z}_2$  odd.

<sup>24</sup>I thank H. Hannesdottir and S. Mizera for pointing out this diagram.

<sup>25</sup>I thank A. Hebbbar for raising this possibility.

<sup>26</sup>One still has to adapt the non-linear dependence of the residues for semi-definite optimization. It is also unclear how these poles would affect the bounds as they would overlap with cuts (coming from the crossed channel) and could get “screened” (see appendix E of [135]). I thank A. Homrich and P. Vieira for discussions on this.

## Chapter 4. Nonperturbative Anomalous Thresholds

---

which cannot be drawn in the form of Figs. 4.8 and 4.9 and that has an anomalous threshold? We dare to say *no*, but would happily be wrong.



## 5 Injecting the UV into the Bootstrap: Ising Field Theory

Besides the S-matrix bootstrap, which has seen a revival in recent years, other modern techniques include Monte-Carlo simulations of lattice discretizations, Hamiltonian truncation and tensor networks. The latter techniques typically involve an UV cutoff whose extrapolation to infinity is a non-trivial computational problem, whereas the S-matrix bootstrap is directly set up in the continuum, as required by Poincaré invariance.

The primal approach to the S-matrix bootstrap constructs an explicitly analytic and crossing-symmetric ansatz for the amplitude and then constrains its parameters by imposing unitarity on the physical scattering region [17, 195, 1, 18, 19, 23, 135, 196, 197, 198, 199, 200, 201, 202, 203, 204, 205]. In practice, the infinite-dimensional space of amplitudes is truncated to finite dimension  $N$  (the number of parameters in the ansatz). By maximizing a given observable (e.g. the residue of a pole) one directly explores the space of amplitudes from the “inside” with the true boundary of the allowed space for the observable (presumably) reached asymptotically, i.e. as  $N$  is taken to infinity. This means that the primal approach is incapable of producing rigorous bounds at finite  $N$ .

Conversely, the dual approach, as the name suggests, approaches the boundary of the allowed space from the “outside” by excluding disallowed regions of parameter-space using a finite number  $N$  of parameters. Therefore, for each  $N$ , there is a rigorous bound on the observable. As  $N$  is increased the excluded region becomes larger, and the bound becomes tighter. Dual formulations of the S-matrix bootstrap were first developed in 70s [206, 207, 208, 209, 210] and recently revived in  $d = 2$  [20, 211, 212, 213] and in  $d = 4$  [117, 120]. Reference [120], in particular, showed that the dual approach can be formulated as a linear optimization problem amenable to implementation in SDPB [214, 215].

The S-matrix, which dictates how asymptotic one-particle states scatter, is an IR observable. Nonetheless, if the S-matrix originates from a UV complete QFT,<sup>1</sup> knowledge of the UV conformal

---

<sup>1</sup>A UV complete QFT can be defined non-perturbatively as a CFT in the UV deformed by relevant deformations that trigger a renormalization group (RG) flow to the IR. The CFT in the IR is assumed to be empty, such that the QFT has a mass gap and the S-matrix is a well-defined object.

## Chapter 5. Injecting the UV into the Bootstrap: Ising Field Theory

---

mal field theory (CFT) from which the QFT flows from should further constrain the S-matrix. This was the idea behind [216] which, besides scattering states, considered states given by the action of local operators, such as the stress-energy tensor, on the vacuum. Concretely, in  $d = 2$ , UV information can be included via the  $c$ -sum rule [217] which relates the spectral density of the trace of the stress-energy tensor to  $c_{UV}$ , the central charge of the UV CFT,

$$c_{UV} = 12\pi \int_{m^2 > 0}^{\infty} \frac{\rho(s)}{s^2} ds. \quad (5.0.1)$$

Here, we make the next logical step in this story. We merge these ideas together to develop a dual bootstrap approach in  $d = 2$  that encompasses S-matrix elements, form factors and spectral densities. Our method, which is described in section 5.1, produces a linear optimization problem that can be tackled with SDPB and which, moreover, converges appreciably faster than the primal approach of [216].

With our method we can address the following question: *Given a gapped unitary QFT with no bound states how small can the central charge  $c_{UV}$  of the UV CFT be?* Our method outputs  $c_{UV}^{(min)} = 1/2$ , the central charge of the Ising CFT, which is the smallest among the unitary conformal minimal models [218]. Indeed, our optimal S-matrix is given by  $S(s) = -1$  corresponding to a free massive Majorana fermion in the IR, which can originate from the pure thermal deformation of the Ising CFT.

We can refine the previous question by fixing a parameter  $\Lambda$  in the IR. For example: the amplitude at the crossing-symmetric point,  $T(s = 2m^2) = -\Lambda$ , which plays the role of a ‘quartic coupling’. In this case we find a minimal  $c_{UV}$  for a given  $\Lambda$ . The result is plotted below in fig. 5.1.

In section 5.2.1, we further refine the previous studies. Following [219], we parameterize the theory space by  $(\Lambda, \Lambda^{(2)})$ , where  $\Lambda^{(2)}$  is the second derivative of the amplitude at the crossing symmetric point. As in the case above, we assume no cubic coupling, i.e. no poles on the physical sheet for the amplitude nor for the form factor. In this way, we target a class of  $\mathbb{Z}_2$  symmetric theories, in which  $\phi^4$  theory is included. Using the numerical dual approach, we rigorously bound  $c_{UV}$  across the allowed range of couplings  $(\Lambda, \Lambda^{(2)})$  generating the 3-dimensional plots in fig. 5.4. Remarkably, we also found analytical expressions (described in appendix 5.3) that match the extremal solutions (see e.g. figs. 5.9 to 5.11 for a comparison).

In section 5.2.2 we consider the Ising Field Theory (IFT) which can be thought of as the QFT describing the  $d = 2$  Ising model near the critical point. Above the critical temperature  $T > T_c$  and for zero magnetic field  $h = 0$  IFT reduces to the theory of a free massive Majorana fermion. For  $h > 0$  the theory becomes fully interacting making it an appropriate playground for non-perturbative methods.<sup>2</sup>

---

<sup>2</sup>The parameter space of IFT is very rich (see e.g. [162] for a short review). For  $T > T_c$  and as  $h$  increases the number of stable particles goes from 1 to 3 [159, 220, 221], and then jumps to 8 (5 resonances become stable) at the  $h \rightarrow \infty$  integrable point where IFT becomes equivalent to the  $E_8$  affine Toda theory [159, 160, 161]. For  $T < T_c$

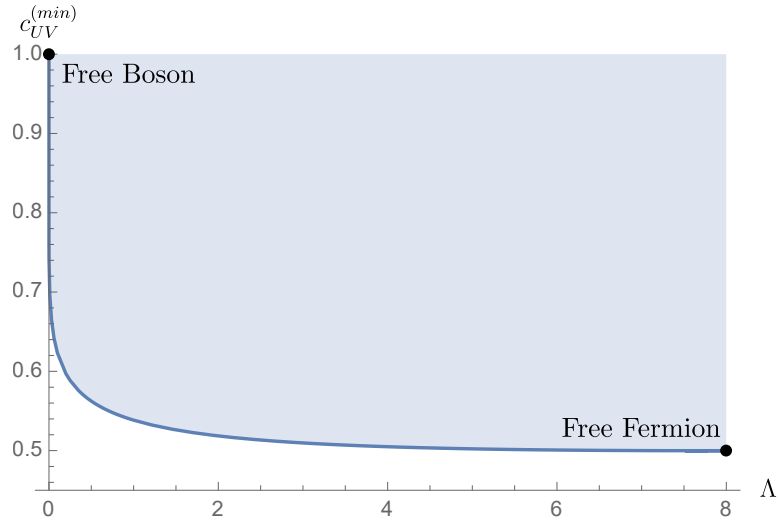


Figure 5.1: Rigorous lower bound on the UV central charge in  $\mathbb{Z}_2$  symmetric QFTs with a single stable particle, which is  $\mathbb{Z}_2$  odd. The parameter  $\Lambda$  is defined as (minus) the value of the amplitude at the crossing-symmetric point  $s = 2m^2$ . The lower bound on  $c_{UV}$  goes from  $c_{UV}^{(min)} = 1$  at  $\Lambda = 0$ , where the S-matrix, form factor and spectral density become that of a free massive boson, to  $c_{UV}^{(min)} = 1/2$  at the other end  $\Lambda = 8$ , where the matrix elements are that of a free massive fermion.

We have at our disposal several pieces of information that we can use to target IFT:

1. The UV central charge of IFT has the value  $c_{UV} = 1/2$  given that IFT is, by definition, a deformation of the Ising CFT. Specifically, both relevant deformations are turned on, namely the operators conjugate to the temperature ( $T - T_c$ ) and the magnetic field  $h$ .
2. At sufficiently low  $h$  (but still outside the perturbative regime) there is only one stable particle in the spectrum [220]. This particle self-interacts via a cubic interaction, meaning that both S-matrix and the two-particle form factor contain a pole at the location of the particle's own mass.
3. As shown in [220, 221], the S-matrix has a real zero which slides towards the two-particle threshold as  $h$  is increased.<sup>3</sup> The position of the zero provides a non-perturbative IR handle on the value of the magnetic field  $h$ .

We first implement points 2. and 3. and minimize the central charge  $c_{UV}$  over a range of magnetic fields  $h$  (parameterized by the position of the zero). We find that the lower bound on  $c_{UV}$  drops below  $c_{UV} = 1/2$  for non-zero  $h$  (see fig. 5.12). We then fix  $c_{UV} = 1/2$  and find the allowed range of cubic coupling and one-particle form factors for a range of values of the magnetic field. We carve a 3-dimensional ‘pyramid’ in these parameters inside which IFT

the spectrum of IFT consists of a tower of “mesons” [222]. Further interesting phenomena occur when  $h$  is taken to be complex, namely the existence of Lee-Yang edge singularities [223].

<sup>3</sup>If  $h$  is increased past a certain value the zero makes its way across the two-particle branch cut and the associated pole pops up on the physical sheet, as the second lightest particle becomes stable. See e.g. [221].

## Chapter 5. Injecting the UV into the Bootstrap: Ising Field Theory

---

must lie (see fig. 5.17). We conclude with section 5.4 where we discuss our results in further detail and point out some potential future directions.

Let us now briefly outline the remaining appendices. In appendix D.1 we present a further application of our dual method targeting the Sine-Gordon model where we noticeably improve on the primal result of [216]. Technical and numerical details regarding the dual optimization problems are collected in appendices D.2 and D.3. Appendix D.4 contains the perturbative computations of the one particle form factor and cubic coupling used to place IFT within the dual bounds (fig. 5.17). Finally, appendices D.5 and D.6 respectively review the c-sum rule and the normalization of the 2 particle form factor of the stress energy tensor.

### 5.1 Dual S-matrix and form factor Bootstrap

In this section we develop our setup by recalling some definitions and results from standard massive QFT. We will be complete but concise, more details can be found in [216, 224].

The first ingredient in our setup is the 2 to 2 scattering amplitude defined by

$${}_{out}\langle p_1 p_2 | k_1 k_2 \rangle_{in} \equiv (2\pi)^2 \delta^{(2)}(k_1 + k_2 - p_1 - p_2) \mathcal{N}_2 S(s), \quad \mathcal{N}_2 \equiv 2\sqrt{s}\sqrt{s-4m^2}, \quad (5.1.1)$$

with  $s = -(p_1 + p_2)^2$ . We also define  $\mathcal{F}(s)$ , the interacting part of the scattering amplitude, by

$$S(s) \equiv 1 + i\mathcal{N}_2^{-1}\mathcal{F}(s). \quad (5.1.2)$$

We are also interested in some scalar local operator  $\mathcal{O}(x)$ , which leads us to consider its  $n$  particles form factors

$$\mathcal{F}_n^{\mathcal{O}}(p_1, p_2, \dots, p_n) \equiv {}_{out}\langle p_1 p_2 \dots p_n | \mathcal{O}(0) | 0 \rangle, \quad (5.1.3)$$

and its spectral density

$$2\pi\rho_{\mathcal{O}}(s) \equiv \int d^2x e^{-ipx} \langle 0 | \mathcal{O}^\dagger(x) \mathcal{O}(0) | 0 \rangle, \quad (5.1.4)$$

where we used Lorentz invariance to write  $\rho_{\mathcal{O}} = \rho_{\mathcal{O}}(s = -p^2)$ .

We focus on massive QFTs whose Hilbert space  $\mathcal{H}$  is spanned by asymptotic multi particle states  $|p_1, \dots, p_n\rangle$  with completeness relation

$$\mathbb{1}_{\mathcal{H}} = \sum_{n=0}^{\infty} \frac{1}{n!} \int \frac{d\mathbf{p}_1}{(2\pi)2E_{\mathbf{p}_1}} \dots \frac{d\mathbf{p}_n}{(2\pi)2E_{\mathbf{p}_n}} |p_1 \dots p_n\rangle_{in} {}_{in}\langle p_1 \dots p_n| \equiv \int [p_1 \dots p_n]_{in} {}_{in}\langle p_1 \dots p_n|, \quad (5.1.5)$$

where  $E_{\mathbf{p}} \equiv \sqrt{\mathbf{p}^2 + m^2}$  and  $\mathbf{p}$  is the spatial part of the 2-momentum  $p$ . The complete set of states can be inserted in the two point function (5.1.4) to get the relation between the spectral

## 5.1 Dual S-matrix and form factor Bootstrap

density and the form factors

$$2\pi\rho_{\Theta}(s) = \sum_{\mathcal{F}} (2\pi)^2 \delta^{(2)}(p - p_n) |\mathcal{F}_n^{\Theta}|^2, \quad (5.1.6)$$

where  $p_n \equiv p_1 + \dots + p_n$  is the total momentum of the form factor. Note that the first contribution is a delta function at  $s = m^2$  and the second contribution starts at  $s = 4m^2$ . Explicitly

$$\rho_{\Theta}(s) = |\mathcal{F}_1^{\Theta}|^2 \delta(s - m^2) + \frac{|\mathcal{F}_2^{\Theta}(s)|^2}{2\pi\mathcal{N}_2} \theta(s - 4m^2) + \dots \quad (5.1.7)$$

In this work we are interested in the trace of the stress energy tensor, so we introduce the simplified notation

$$\mathcal{F}(s) \equiv \mathcal{F}_2^{\Theta}(s), \quad \rho(s) \equiv \rho_{\Theta}(s), \quad (5.1.8)$$

where the  $s$  dependence of the 2 particle form factor comes from Lorentz invariance. The normalization of the stress energy tensor acting on one particle states implies the following normalization of the 2 particle form factor (see appendix D.6)

$$\mathcal{F}(s = 0) = -2m^2. \quad (5.1.9)$$

The value of the UV central charge can be computed from the spectral density of  $\Theta$  as [216] (in alternative, see appendix D.5)

$$c_{UV} = 12\pi \left( m^{-4} |\mathcal{F}_1^{\Theta}|^2 + \int_{4m^2}^{\infty} ds \frac{\rho(s)}{s^2} \right). \quad (5.1.10)$$

Let us now turn to the analytic structure of these functions depicted on Figure 5.2. Assuming the existence of only one massive particle of mass  $m$ , the scattering amplitude is analytic except for a pole at  $s = m^2$  and a cut starting from the two particles production threshold  $s = 4m^2$ , and also crossing symmetric. This can be written through the dispersion relation<sup>4</sup>

$$\begin{aligned} \mathcal{F}(s) - \mathcal{F}(2m^2) &= -g^2 \left( \frac{1}{s - m^2} + \frac{1}{3m^2 - s} - \frac{2}{m^2} \right) \\ &+ \int_{4m^2}^{\infty} \frac{dz}{\pi} \text{Im}\mathcal{F}(z) \left( \frac{1}{z - s} + \frac{1}{z + s - 4m^2} - \frac{2}{z - 2m^2} \right). \end{aligned} \quad (5.1.11)$$

The 2-particle form factor  $\mathcal{F}(s)$  has a similar analytic structure except that it does not satisfy

---

<sup>4</sup>In writing this dispersion relation, we assumed that  $\lim_{|s| \rightarrow \infty} \frac{\mathcal{F}(s)}{s} = 0$ . Our dual optimization problem will however not depend on this assumption, i.e. the behavior of the amplitude at infinity is unconstrained. See equation (5.1.30) and footnote 9.

## Chapter 5. Injecting the UV into the Bootstrap: Ising Field Theory

crossing. The dispersion relation reads<sup>5</sup>

$$\mathcal{F}(s) - \mathcal{F}(0) = -g_F \left( \frac{1}{s-m^2} + \frac{1}{m^2} \right) + \int_{4m^2}^{\infty} \frac{dz}{\pi} \text{Im} \mathcal{F}(z) \left( \frac{1}{z-s} - \frac{1}{z} \right). \quad (5.1.12)$$

As shown in [216], the form factor residue  $g_F$  is given by

$$g_F = g \mathcal{F}_1^{\Theta}, \quad (5.1.13)$$

where  $g$  is the (square root of the) residue of the scattering amplitude.

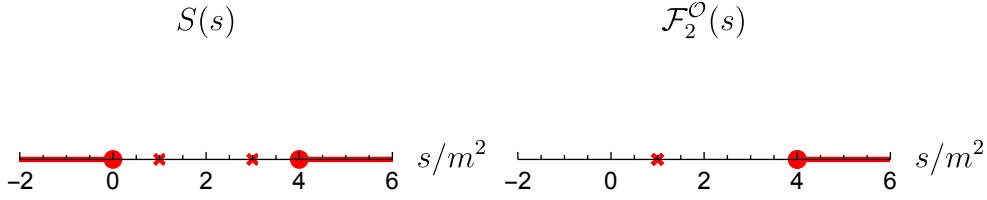


Figure 5.2: Complex planes of the two particles form factor  $\mathcal{F}_2^{\Theta}(s)$  (right) and the scattering amplitude  $S(s)$  (left) in the presence of an asymptotic particle of mass  $m = 1$ . The red crosses symbolize the presence of a pole and the red lines represent the branch cuts.

For future convenience, we define the analyticity and crossing constraints for the S-Matrix and form factor, denoted respectively by  $\mathcal{A}_S(s) = 0$  and  $\mathcal{A}_{\mathcal{F}}(s) = 0$ , with

$$\begin{aligned} \mathcal{A}_S(s) &\equiv \mathcal{F}(s) - \mathcal{F}(2m^2) + g^2 \left( \frac{1}{s-m^2} + \frac{1}{3m^2-s} - \frac{2}{m^2} \right) \\ &\quad - \int_{4m^2}^{\infty} \frac{dz}{\pi} \text{Im} \mathcal{F}(z) \left( \frac{1}{z-s} + \frac{1}{z+s-4m^2} - \frac{2}{z-2m^2} \right), \\ \mathcal{A}_{\mathcal{F}}(s) &\equiv \mathcal{F}(s) - \mathcal{F}(0) + g_F \left( \frac{1}{s-m^2} + \frac{1}{m^2} \right) - \int_{4m^2}^{\infty} \frac{dz}{\pi} \text{Im} \mathcal{F}(z) \left( \frac{1}{z-s} - \frac{1}{z} \right). \end{aligned} \quad (5.1.14)$$

Following [216], the unitarity constraints in presence of local operators such as  $\Theta(x)$  can be implemented by defining 3 states

$$\begin{aligned} |\Psi_1\rangle &\equiv |p_1, p_2\rangle_{in}, \\ |\Psi_2\rangle &\equiv |p_1, p_2\rangle_{out}, \\ |\Psi_3\rangle &\equiv m^{-1} \int d^2x e^{i(p_1+p_2)x} \Theta(x) |0\rangle. \end{aligned} \quad (5.1.15)$$

We now define a  $3 \times 3$  matrix by taking inner products between those states and extracting an

<sup>5</sup>We have used the fact that both functions are real analytic functions, i.e.  $\mathcal{F}^*(s) = \mathcal{F}(s^*)$  and  $\mathcal{F}^*(s) = \mathcal{F}(s^*)$ , which can be traced back to LSZ and CPT invariance [225].

## 5.1 Dual S-matrix and form factor Bootstrap

overall delta function, which reads

$$B_{ij} \times (2\pi)^2 \delta^{(2)}(p_1 + p_2 - p'_1 - p'_2) \equiv \langle \Psi'_i | \Psi_j \rangle. \quad (5.1.16)$$

Using equations (5.1.1), (5.1.3), (5.1.4) and the definition of  $B$  as inner products between states, the unitarity of the theory imposes the semi positive definite constraint<sup>6</sup>

$$B(s) \equiv \begin{pmatrix} 1 & S^* & m^{-1}\omega\mathcal{F}^* \\ S & 1 & m^{-1}\omega\mathcal{F} \\ m^{-1}\omega\mathcal{F} & m^{-1}\omega\mathcal{F}^* & 2\pi m^{-2}\rho \end{pmatrix} \succcurlyeq 0, \quad \omega \equiv \mathcal{N}_2^{-1/2}. \quad (5.1.17)$$

The problem we want to solve is the minimization of some parameter, say the central charge  $c_{UV}$ , under the bootstrap constraints which can be implemented via Lagrange multipliers. More precisely, we write

$$c_{UV} \geq \inf_{\mathcal{F}, \mathcal{F}^*, \rho} \sup_{w, \Lambda \succcurlyeq 0} \mathcal{L} \geq \sup_{w, \Lambda \succcurlyeq 0} \inf_{\mathcal{F}, \mathcal{F}^*, \rho} \mathcal{L} \quad (5.1.18)$$

$$\mathcal{L} = c_{UV}(\mathcal{F}_1^\Theta, \rho) + \int_{4m^2}^{\infty} ds [w_{\mathcal{F}}(s)\mathcal{A}_{\mathcal{F}}(s) + w_{\mathcal{F}^*}(s)\mathcal{A}_{\mathcal{F}^*}(s) - \text{Tr} \Lambda(s)B(s)] + \dots \quad (5.1.19)$$

where  $\mathcal{A}_{\mathcal{F}}(s)$  and  $\mathcal{A}_{\mathcal{F}^*}(s)$  are the analyticity and crossing constraints,  $w_{\mathcal{F}}$  and  $w_{\mathcal{F}^*}$  are Lagrange multipliers,  $\Lambda$  is a hermitian and positive semidefinite  $3 \times 3$  matrix of Lagrange multipliers and "..." stands for any other constraint we would like to implement (e.g. fixing some parameter).

The positive semidefiniteness of  $\Lambda$  is the direct generalisation of positiveness in the pure S-Matrix (non-linear) dual problem from [211]. Here we are searching for the lower bound instead of the upper bound, which accounts for the sign difference in the trace term.

We parametrize  $\Lambda$  as

$$\Lambda \equiv \begin{pmatrix} \lambda_1 & \lambda_4 & \lambda_6 \\ \lambda_4^* & \lambda_2 & \lambda_5 \\ \lambda_6^* & \lambda_5^* & \lambda_3 \end{pmatrix}. \quad (5.1.20)$$

With the dual approach, we will first extremize (5.1.19) over the primal variables  $\mathcal{F}$ ,  $\mathcal{F}^*$  and  $\rho$  analytically to get the dual Lagrangian, and then over the dual variables  $w_{\mathcal{F}}$ ,  $w_{\mathcal{F}^*}$  and  $\lambda_i$ ,  $i = 1, \dots, 8$ , numerically. The problem being linear in the dual variables can be tackled down with SDPB [214, 215].

Having the solution for the optimal dual variables we can get optimal primal variables if the duality gap closes, which is guaranteed because the primal problem is convex.<sup>7</sup> Therefore, at

<sup>6</sup>Here we used the relation  ${}_{in}\langle p_1, p_2 | \Theta(0) | 0 \rangle = \langle 0 | \Theta^\dagger(0) | p_1, p_2 \rangle_{out} = \mathcal{F}^*(s)$  that comes from CPT invariance [216].

<sup>7</sup>Since the primal problem can be implemented in SDPB [214, 215] both the objective and the constraints must be convex. To ensure strong duality, i.e. that the duality gap closes, we must further require that there exists an interior point, i.e. a non-optimal primal solution. This is known as Slater's condition [226] (see appendix A of [211] for a proof in the S-matrix language). Slater's condition can be shown to be satisfied by explicitly constructing a

## Chapter 5. Injecting the UV into the Bootstrap: Ising Field Theory

the optimum we have  $\text{Tr } \Lambda(s)B(s) = 0$  and, since  $\Lambda$  and  $B$  are both semipositive definite, the product must vanish by itself<sup>8</sup>

$$\Lambda(s)B(s) = 0. \quad (5.1.22)$$

Solving this equation we get constraints between dual variables

$$\lambda_5 = \lambda_6^*, \quad \lambda_1 = \lambda_2, \quad 2\lambda_1|\lambda_6|^2 - \lambda_3\lambda_1^2 - 2\text{Re}(\lambda_4^*\lambda_6^2) + \lambda_3|\lambda_4|^2 = 0. \quad (5.1.23)$$

We would like to stay with entries that are linear in the dual variables in the matrix  $\Lambda$ , and therefore we do not use the last constraint to eliminate one of the variables.

Since the duality gap closes we can find the optimal primal solution:

$$S = \frac{\lambda_6^*\lambda_1 - \lambda_6\lambda_4^*}{\lambda_6\lambda_1 - \lambda_6^*\lambda_4}, \quad \omega_{\mathcal{F}} = \frac{|\lambda_4|^2 - \lambda_1^2}{\lambda_6\lambda_1 - \lambda_6^*\lambda_4}, \quad 2\pi\rho = \frac{(|\lambda_4|^2 - \lambda_1^2)^2}{|\lambda_6\lambda_1 - \lambda_6^*\lambda_4|^2}. \quad (5.1.24)$$

Note that we automatically saturate the unitarity bounds

$$|S|^2 - 1 = 0, \quad 2\pi\rho - |\omega_{\mathcal{F}}|^2 = 0, \quad 2\pi\rho(1 - |S|^2) - 2|\omega_{\mathcal{F}}|^2 + 2\text{Re}(\omega^2 \mathcal{F}^2 S^*) = 0. \quad (5.1.25)$$

Watson's equation  $\mathcal{F}/\mathcal{F}^* = S$  follows from using the first equation on the last equation.

### 5.1.1 Example: Minimization of $c_{UV}$ for fixed quartic coupling $\Lambda$

We will now present an explicit and detailed example of a dual linear bootstrap formulation. We want to find the lower bound on the central charge  $c_{UV}$  when there is only one particle that is  $\mathbb{Z}_2$  odd and the scattering amplitude obeys  $\mathcal{T}(2) = -\Lambda$ . For simplicity we work in units where  $m = 1$ . The Lagrangian reads

$$\begin{aligned} \mathcal{L} = & 12\pi \int_4^\infty ds \frac{\rho(s)}{s^2} + \int_4^\infty ds w_{\mathcal{T}}(s) \left[ \mathcal{T}(s) - \mathcal{T}(2) - \int_4^\infty \frac{dz}{\pi} \text{Im} \mathcal{T}(z) \left( \frac{1}{z-s} + \frac{1}{z+s-4} - \frac{2}{z-2} \right) \right] \\ & + \int_4^\infty ds w_{\mathcal{F}}(s) \left[ \mathcal{F}(s) - \mathcal{F}(0) - \int_4^\infty \frac{dz}{\pi} \text{Im} \mathcal{F} \left( \frac{1}{z-s} - \frac{1}{z} \right) \right] \\ & - \int_4^\infty ds \text{Tr } \Lambda(s) \cdot B(s). \end{aligned} \quad (5.1.26)$$

non-optimal primal solution, as it usually happens in the primal bootstrap at finite  $N$  [216]. Physically, moreover, the existence of such an interior point is guaranteed since we can always have inelastic S-matrices and form factors which do not saturate unitarity.

<sup>8</sup>Indeed we have

$$\text{Tr } \Lambda \cdot B = \text{Tr } \sqrt{\Lambda}^\dagger \sqrt{\Lambda} \cdot \sqrt{B} \sqrt{B}^\dagger = \text{Tr}(\sqrt{\Lambda} \sqrt{B})^\dagger (\sqrt{\Lambda} \sqrt{B}) \equiv \|\sqrt{\Lambda} \sqrt{B}\|_F, \quad (5.1.21)$$

where  $\|\cdot\|_F$  is the Frobenius norm. It follows that  $\text{Tr } \Lambda \cdot B = 0 \Rightarrow \Lambda B = 0$ .



## 5.1 Dual S-matrix and form factor Bootstrap

The subtractions are chosen so that we can easily implement the constraint  $\mathcal{F}(2) = -\Lambda$  and the normalization  $\mathcal{F}(0) = -2$ .

Following [211] we define the dual scattering function

$$\begin{aligned} W_{\mathcal{F}}(s) &\equiv \int_4^\infty \frac{dz}{\pi} w_{\mathcal{F}}(z) \left( \frac{1}{z-s} - \frac{1}{z+s-4} + \frac{2}{s-2} \right), \\ \text{Im } W_{\mathcal{F}}(s) &= w_{\mathcal{F}}(s), \quad \text{Re } W_{\mathcal{F}}(s) = -P \int_4^\infty \frac{dz}{\pi} w_{\mathcal{F}}(z) \left( \frac{1}{s-z} + \frac{1}{s-(4-z)} - \frac{2}{s-2} \right), \end{aligned} \quad (5.1.27)$$

and the dual form factor function

$$W_{\mathcal{F}}(s) \equiv \int_4^\infty \frac{dz}{\pi} w_{\mathcal{F}}(z) \left( \frac{1}{z-s} + \frac{1}{s} \right). \quad (5.1.28)$$

The analyticity constraints can then be considerably simplified. We get<sup>9</sup>

$$\mathcal{L} = 12\pi \int_4^\infty ds \frac{\rho(s)}{s^2} + \int_4^\infty ds [\text{Im}(\mathcal{T} W_{\mathcal{F}}) + \text{Im}(\mathcal{F} W_{\mathcal{F}}) + 2 \text{Im } W_{\mathcal{F}} + \Lambda \text{Im } W_{\mathcal{F}} - \text{Tr } \Lambda \cdot B] \quad (5.1.30)$$

We are now ready to eliminate the primal variables. Varying with respect to  $\mathcal{F}$ ,  $\mathcal{T}$  and  $\rho$  we get

$$\lambda_4 = -\frac{\mathcal{N}_2}{2} W_{\mathcal{F}}, \quad \lambda_6 = -i \frac{\sqrt{\mathcal{N}_2}}{4} W_{\mathcal{F}}, \quad \lambda_3 = \frac{6}{s^2}. \quad (5.1.31)$$

The dual Lagrangian then reads

$$\mathcal{L} = \int_4^\infty ds (-2\lambda_1 + 2 \text{Im } W_{\mathcal{F}} - \mathcal{N}_2 \text{Re } W_{\mathcal{F}} + \Lambda \text{Im } W_{\mathcal{F}}). \quad (5.1.32)$$

All the primal variables are eliminated and we are ready to extremize over dual variables. We can finally formulate the dual problem that can be implemented in SDPB:

---

<sup>9</sup>Eq. (5.1.30) can be derived directly without introducing  $w_{\mathcal{F}}$  or  $w_{\mathcal{T}}$ . The analyticity constraint for  $\mathcal{T}(s)$ , say, can be written as  $\oint W_{\mathcal{F}}(s) \mathcal{T}(s) ds = 0$  where  $W_{\mathcal{F}}(s)$  is an analytic function, for an arbitrary closed cycle enclosing no singularity. Now, we blow up this contour and, seeing  $W_{\mathcal{F}}(s)$  as infinitely many Lagrange multipliers (one for each  $s$ ), we are free to choose  $W_{\mathcal{F}}(s)$  so that the contour only picks up the contributions of  $\mathcal{T}(s)$  we wish to constrain, which is the unitarity cut  $s \geq 4$  and the value at  $\mathcal{T}(2) = -\Lambda$ . Therefore, we let  $W_{\mathcal{F}}$  have a cut for  $s \geq 4$ , a pole at  $s = 2$ , and sufficiently fast decay at infinity (faster than  $\mathcal{T}(s)$ ). Blowing up the contour will then lead to

$$0 = \oint \mathcal{T} W_{\mathcal{F}} ds = 4i \int_4^\infty \text{Im}(\mathcal{T} W_{\mathcal{F}}) ds - 2\pi i [\text{Res}_{s=2} W_{\mathcal{F}}] \mathcal{T}(2). \quad (5.1.29)$$

Note that the residue on the pole is fixed by blowing up  $0 = \oint W_{\mathcal{F}} ds = -2\pi i \text{Res}_{s=2} W_{\mathcal{F}} + 4i \int_4^\infty \text{Im } W_{\mathcal{F}} ds$ . Including crossing symmetry, repeating the argument for the form factor will lead us to eq. (5.1.30).

Dual Problem ( $c_{UV}$  minimization)

$$\text{Maximize}_{\{\lambda_1, W_{\mathcal{F}}, W_{\mathcal{F}}^*\}} \left[ \int_4^\infty ds (-2\lambda_1 + 2 \text{Im } W_{\mathcal{F}} - \mathcal{N}_2 \text{Re } W_{\mathcal{F}} + \Lambda \text{Im } W_{\mathcal{F}}) \right] \quad (5.1.33)$$

Subject to

$$\begin{pmatrix} \lambda_1 & \frac{\mathcal{N}_2}{2} W_{\mathcal{F}} & i \frac{\sqrt{\mathcal{N}_2}}{4} W_{\mathcal{F}} \\ \frac{\mathcal{N}_2}{2} W_{\mathcal{F}}^* & \lambda_1 & -i \frac{\sqrt{\mathcal{N}_2}}{4} W_{\mathcal{F}}^* \\ -i \frac{\sqrt{\mathcal{N}_2}}{4} W_{\mathcal{F}}^* & i \frac{\sqrt{\mathcal{N}_2}}{4} W_{\mathcal{F}} & \frac{6}{s^2} \end{pmatrix} \succcurlyeq 0, \quad \forall s \in [4, \infty). \quad (5.1.34)$$

The result is given in figure 5.1.

## 5.2 Numerical bootstrap

### 5.2.1 $\mathbb{Z}_2$ symmetric theories

A first application of our dual formalism is to explore the allowed region in the subspace spanned by  $(\Lambda, \Lambda^{(2)}, c_{UV})$  where  $c_{UV}$  is the UV central charge and

$$\Lambda \equiv -\mathcal{F}(2), \quad \Lambda^{(2)} \equiv \lim_{s \rightarrow 2} \frac{\partial^2}{\partial s^2} \mathcal{F}(s). \quad (5.2.1)$$

Before considering the central charge we look at the space spanned by  $\Lambda$  and  $\Lambda^{(2)}$ , which is commonly called the "leaf", that was already explored using a primal approach in [219] and also analytically in [227]. Exploring the same region with the dual formalism we get Figure 5.3 on which we also plotted the analytical bounds derived in the appendix 5.3 and given by (5.3.24) that we repeat here for convenience

$$\Lambda_-^{(2)}(\Lambda) = \frac{1}{32} \Lambda^2, \quad \Lambda_+^{(2)}(\Lambda) = \frac{1}{32} (16\Lambda - \Lambda^2), \quad \Lambda \in [0, 8], \quad (5.2.2)$$

where  $\Lambda_+^{(2)}$  and  $\Lambda_-^{(2)}$  denote respectively the analytical upper and lower bounds for  $\Lambda^{(2)}$  for a given  $\Lambda$ . We reproduce these bounds numerically with our dual approach purely applied to the S-matrix sector (see figure 5.3 below).

We now minimize the UV central charge  $c_{UV}$  for a given value of  $(\Lambda, \Lambda^{(2)})$ , which we do over the allowed region. The minimal  $c_{UV}$  is represented in color in fig. 5.3 over the allowed parameter space for  $(\Lambda, \Lambda^{(2)})$  and also in 3D in fig. 5.4 below.

On the edge corresponding to the lower bound  $\Lambda_-^{(2)}$ , the numerical bounds on the central

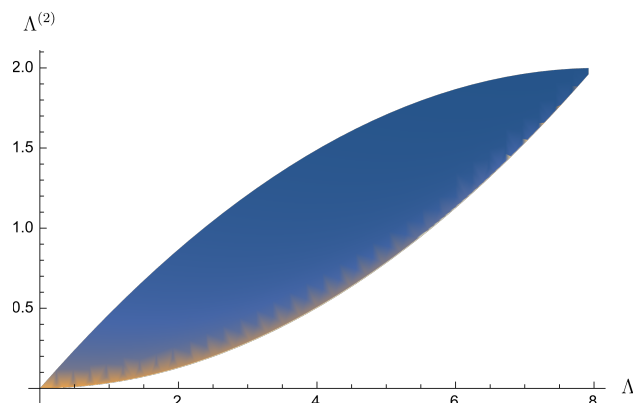


Figure 5.3: Allowed region in the  $(\Lambda, \Lambda^{(2)})$  plane. The boundary is obtained from the dual bootstrap problem and matches perfectly the analytical bounds, with the color gradient corresponding to the value of the minimal central charge discussed below. Using the non linear dual approach given by eq.(D.2.11) to (D.2.15), the numerics for the points on the boundary were simple enough to be done on Mathematica with only  $N = 2$  parameters in the Ansatz.

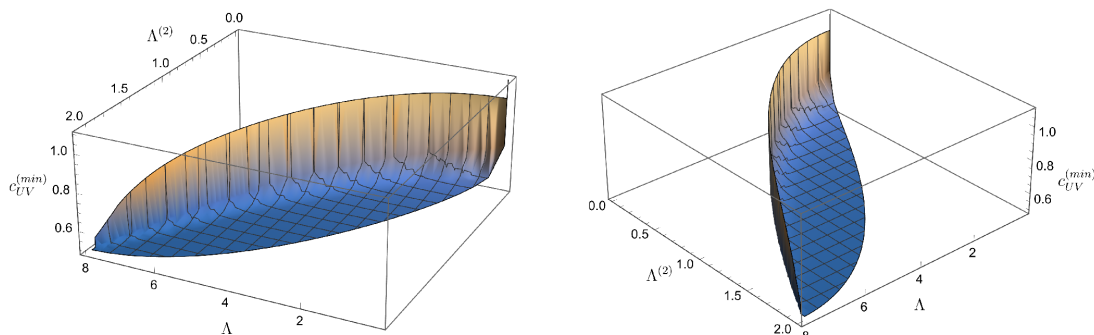


Figure 5.4: Allowed region in the  $(\Lambda, \Lambda^{(2)}, c_{UV}^{(min)})$  space from different angles. We used  $N = 50$ . We find perfect agreement with the analytical bootstrap result which assumes that the optimal S-matrix minimizes  $\Lambda^{(4)} = \lim_{s \rightarrow 2} \frac{\partial^4}{\partial s^4} \mathcal{F}(s)$  (see appendix 5.3).

charge  $c_{UV}^{(min)}(\Lambda, \Lambda^{(2)})$  at the tips are

$$c_{UV}^{(min)}(0, 0) = 0.99999\dots, \quad c_{UV}^{(min)}(8, 2) = 0.49985\dots, \quad (5.2.3)$$

corresponding to the central charges of the free boson and free fermion that are respectively 1 and 1/2. We now check that we also recover the scattering amplitudes, form factors and spectral densities of these theories. The analytical results for the free Majorana fermion can be found in [228] and those for the free boson can be found in [216]. We repeat them here for

## Chapter 5. Injecting the UV into the Bootstrap: Ising Field Theory

convenience, they are

$$\begin{aligned}
 S(s) = 1, \quad \mathcal{F}(s) = -2, \quad \rho(s) &= \frac{1}{\pi\sqrt{s}\sqrt{s-4}}, & \text{(free boson),} \\
 S(s) = -1, \quad \mathcal{F}(s) = -\sqrt{4-s}, \quad \rho(s) &= \frac{\sqrt{s-4}}{4\pi\sqrt{s}}, & \text{(free fermion).}
 \end{aligned}
 \tag{5.2.4}$$

The numerical results for these quantities at the tips of the leaf are plotted on Figure 5.5 (at  $\Lambda = 0$ ) and Figure 5.6 (at  $\Lambda = 8$ ). We observe a nice convergence of our numerics toward the analytical results.

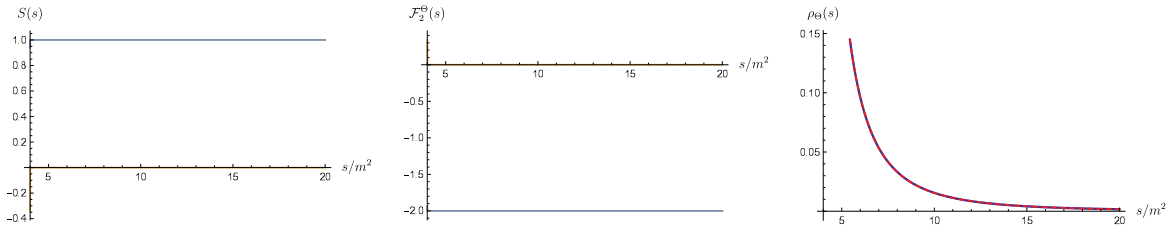


Figure 5.5: Scattering amplitude  $S(s)$  (on the left), form factor  $\mathcal{F}(s)$  (in the middle) and spectral density  $\rho(s)$  (on the right) at the free boson point ( $\Lambda = 0, \Lambda^{(2)} = 0$ ). The blue lines are the real parts, the orange lines are the imaginary parts, and the dashed red line is the analytical solution for the free boson. We used  $N = 50$ .

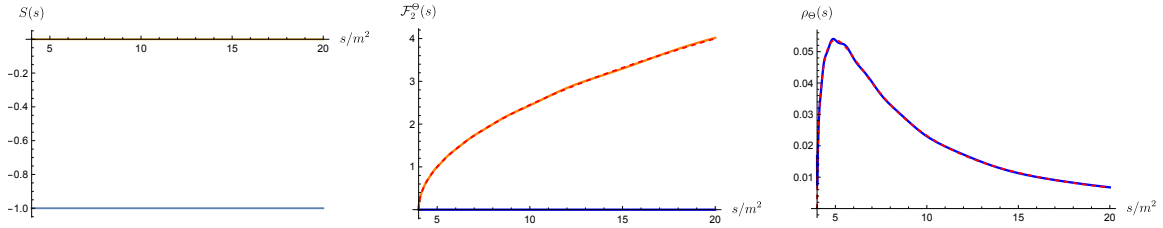


Figure 5.6: Scattering amplitude  $S(s)$  (on the left), form factor  $\mathcal{F}(s)$  (in the middle) and spectral density  $\rho(s)$  (on the right) at the free fermion point ( $\Lambda = 8, \Lambda^{(2)} = 2$ ). The blue lines are the real parts, the orange lines are the imaginary parts, and the dashed red line is the analytical solution for the free fermion. We used  $N = 25$ .

It is interesting to compute the allowed region with a primal approach and to compare with the dual bounds. We do it<sup>10</sup> in Fig. 5.7, and various sections of this 3D plot are shown on Figs. 5.8. It is reassuring to see that the primal lower bound is always greater than the dual, and that the two shapes seem to converge toward each other. We believe that the reason for the gap is the slow convergence of the primal formalism, which we also observe on Figure 5.12, where the dual reaches the analytical bound.

We now compare our numerical results with the analytical results from the appendix 5.3 where we assume that  $c_{UV}$  minimization for fixed  $(\Lambda, \Lambda^{(2)})$  minimizes  $\Lambda^{(4)} = \lim_{s \rightarrow 2} \frac{\partial^4}{\partial s^4} \mathcal{F}(s)$ . For the

<sup>10</sup>We use the numerical primal setup from [216] and the ansatz for the scattering amplitude given by eq. (4.4) and (4.5) in [219].

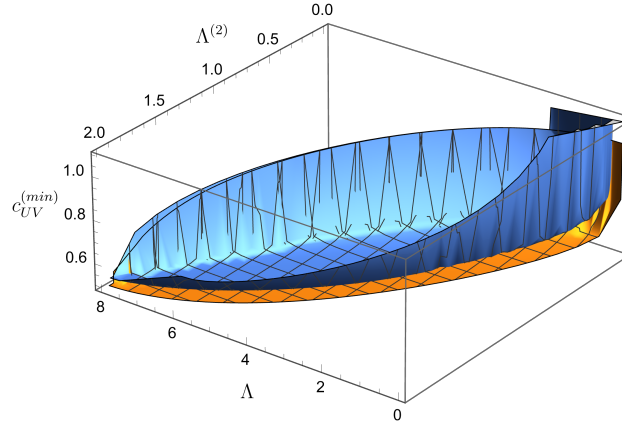


Figure 5.7: Minimal central charge in the  $(\Lambda, \Lambda^{(2)}, c_{UV})$  space computed with the dual approach (in orange) and the primal (in blue). We used  $N = 50$ .

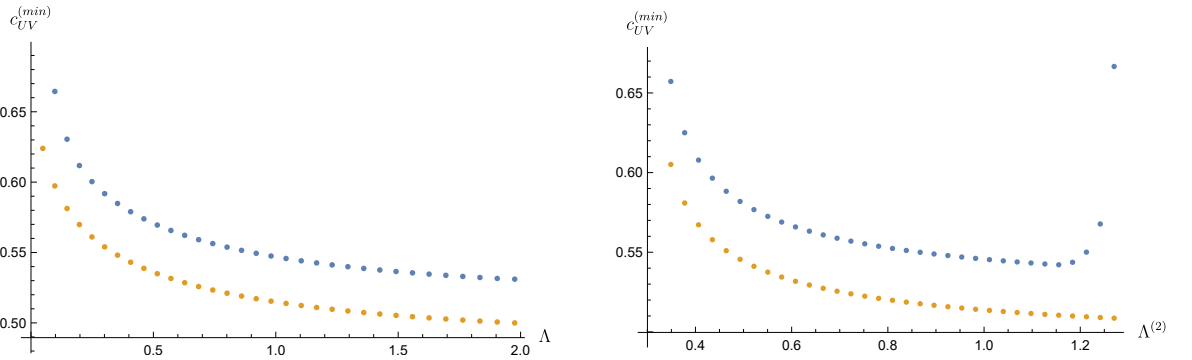


Figure 5.8: Minimal central charge in the  $(\Lambda, c_{UV})$  space (left) and in the  $(\Lambda^{(2)}, c_{UV})$  space (right) computed with the dual approach (in orange) and the primal (in blue). The value of  $\Lambda^{(2)}$  is defined by  $\Lambda^{(2)} = \frac{1}{5} \frac{\Lambda^2}{32} + \frac{1}{5} \Lambda$  (left) and on the one of  $\Lambda$  by  $\Lambda = 3.2$  (right). We used  $N = 50$ .

scattering amplitude on the edges the analytical result is given by (5.3.6) and (5.3.22). The form factor on the upper edge is given by (5.3.34) and (5.3.35), and on the lower edge by (5.3.27). Figure 5.9 shows a point on the upper edge of the leaf, Figure 5.10 shows one on the lower edge and Figure 5.11 shows a point in the middle. The agreement is perfect.

### 5.2.2 Ising Field Theory

Our second application is to target the Ising Field Theory. We use the fact that the S-Matrix has a zero whose position varies with the magnetic field

$$S(m^2(1-x)) = 0, \quad x = x(\eta), \quad \eta = \frac{m}{h^{8/15}}. \quad (5.2.5)$$

The limit  $x \rightarrow 0$  corresponds to  $h \rightarrow 0$  and then should give back the free massive Majorana

## Chapter 5. Injecting the UV into the Bootstrap: Ising Field Theory

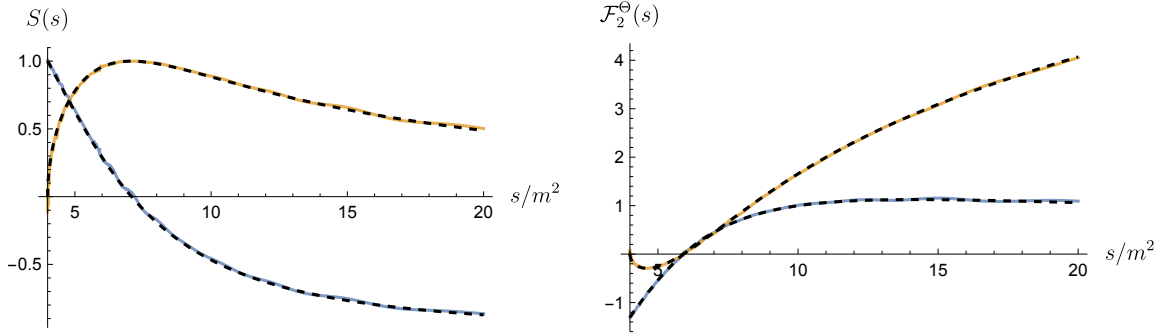


Figure 5.9: Comparison of the real part (in blue) and imaginary part (in orange) of the S-Matrix (left) and the form factor (right) between the numerical (plain line) and analytical (black dashed line) results, on the upper edge of the leaf with  $\Lambda = 2.4$ . We used  $N = 50$ . The numerical and analytical central charges are  $c_{UV}^{(num,min)} = 0.514419\dots$ ,  $c_{UV}^{(an,min)} = 0.514451\dots$

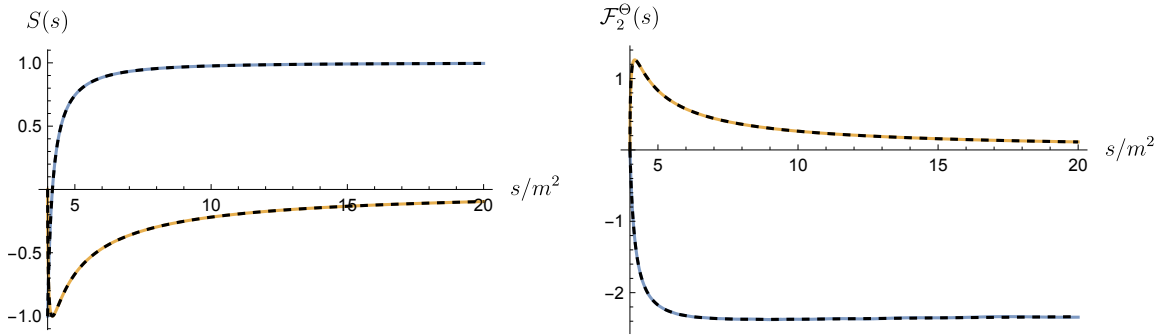


Figure 5.10: Comparison of the real part (in blue) and imaginary part (in orange) of the S-Matrix (left) and the form factor (right) between the numerical (plain line) and analytical (black dashed line) results, on the lower edge of the leaf with  $\Lambda = 2.4$ . We used  $N = 50$ . The numerical and analytical central charges are  $c_{UV}^{(num,min)} = 0.993662\dots$ ,  $c_{UV}^{(an,min)} = 0.993812\dots$

fermion. When  $x \rightarrow 1$  we are in the region just before the second lightest particle emerges from the two particle cut.

### Minimization of $c_{UV}$ for fixed magnetic field

The first exercise is to minimize the UV central charge for different values of  $x$  and the result is shown on Figure 5.12. We performed this analysis with both primal<sup>11</sup> and dual formulations and for different  $N$  to compare them. We also plotted the analytical central charge given by (5.3.53) which assumes that optimal S-matrix maximizes the cubic coupling  $g$  (and has the zero (5.2.5)).

As a simple check, when  $x \rightarrow 0$  the zero cancels the pole, so we are back to asking for the

<sup>11</sup>We use the primal numerical implementation described in [216]

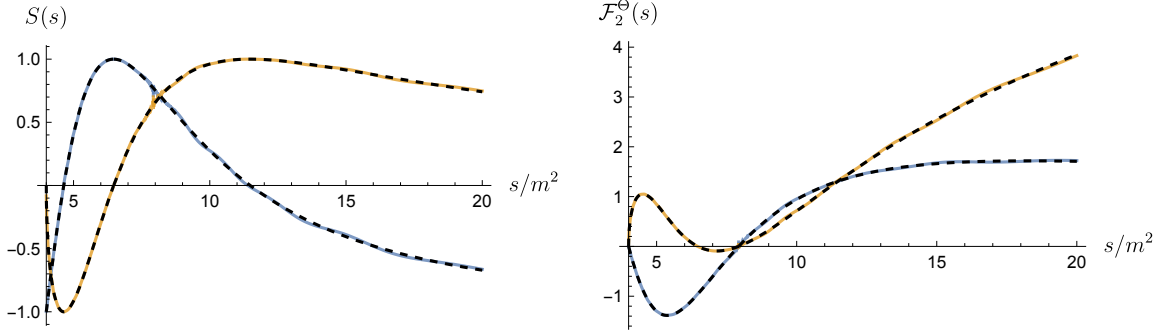


Figure 5.11: Comparison of the real part (in blue) and imaginary part (in orange) of the S-Matrix (left) and the form factor (right) between the numerical (plain line) and analytical (dashed line) results, in the interior of the leaf with  $\Lambda = 4.56$  and  $\Lambda^{(2)} = 0.85$ . We used  $N = 50$ . The numerical and analytical central charges are  $c_{UV}^{(num,min)} = 0.526354\dots$ ,  $c_{UV}^{(an,min)} = 0.526591\dots$

minimal  $c_{UV}$  for an S-matrix with no poles. With the dual for  $N = 30$  we get

$$x = 0.01, \quad \min c_{UV} = 0.498814\dots, \quad (5.2.6)$$

which numerically approaches the result for the free Majorana fermion where  $c_{UV} = 1/2$ .

We now compare primal and dual methods in more detail. First, it is clear that the duality gap closes as  $N \rightarrow \infty$ . We also note the difference in the rate of convergence between the two formalisms. For the primal we parametrize the three functions  $\mathcal{T}$ ,  $\mathcal{F}$  and  $\rho$  while for the dual we parametrize  $\lambda_1$ ,  $W_{\mathcal{T}}$  and  $W_{\mathcal{F}}$ . Therefore the number of numerical parameters scales like  $3N$  for both problems and it makes sense to compare them for a given  $N$ . Hence we claim that the rate of convergence for the dual formalism is much better than the one for the primal.

We can now look at the observables. The scattering amplitude, the two particles form factor and the spectral density are plotted respectively on Figures 5.13, 5.14, and 5.15.

We also observe perfect agreement between the dual numerical results and the analytical results derived in appendix 5.3. They are given by (5.3.40), (5.3.50) and (5.3.53).

There is an interesting observation for the spectral density when  $x \rightarrow 1$ . We know that  $x = 1$  is exactly the point where the pole associated to the second lightest particle enters the first sheet and exchanges place with the zero. We also know that the spectral density has delta functions at the positions of the masses of the stable asymptotic particle states. On the figure we see a peak forming  $s = 4m^2$ , which is exactly where the zero and the pole exchange their places. This is illustrated more precisely in Figure 5.16, where we see the position of the peak moving toward  $4m^2$ .

Note however that the central charge of this theory is  $c_{UV} \approx 0.34$  and therefore it can not be the IFT. Nevertheless it is still interesting to see that those two theories share the presence

## Chapter 5. Injecting the UV into the Bootstrap: Ising Field Theory

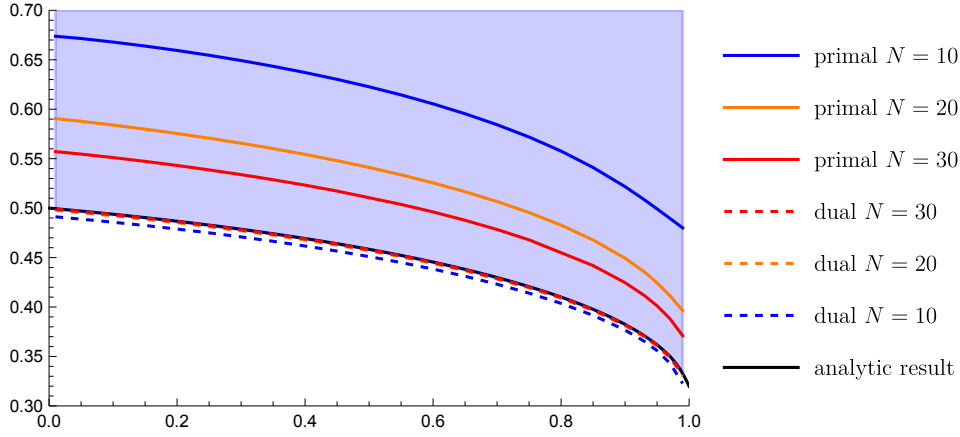


Figure 5.12: Lower bound on the UV central charge as function of  $x$ , the position of the zero of the scattering amplitude  $S(m^2(1-x)) = 0$ . The blue region is allowed. For  $x = 0.01$  and  $N = 30$  with the dual we obtained  $c_{UV}^{(min)} = 0.498814\dots$ . The black line corresponds to the analytical result (5.3.53) assuming that the S-matrix has maximal cubic coupling.

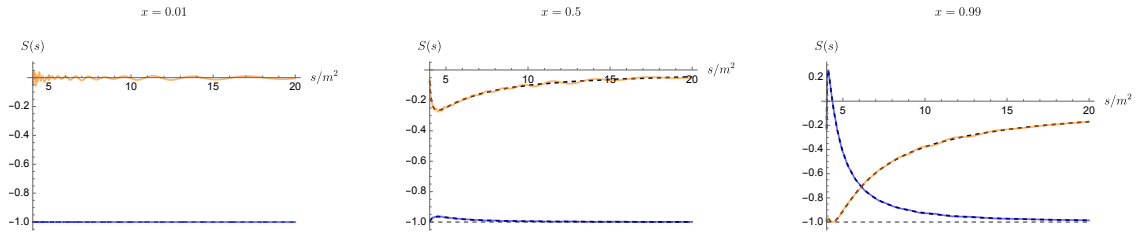


Figure 5.13: Scattering amplitude  $S(s)$  for different values of  $x$  when there is a zero at  $S(m^2(1-x))$ . The imaginary part (in orange) and the real part (in blue) tend toward the free fermion (in dashed gray) when  $x \rightarrow 0$ . The dashed black line is the analytical result given by (5.3.40). We used  $N=50$ .

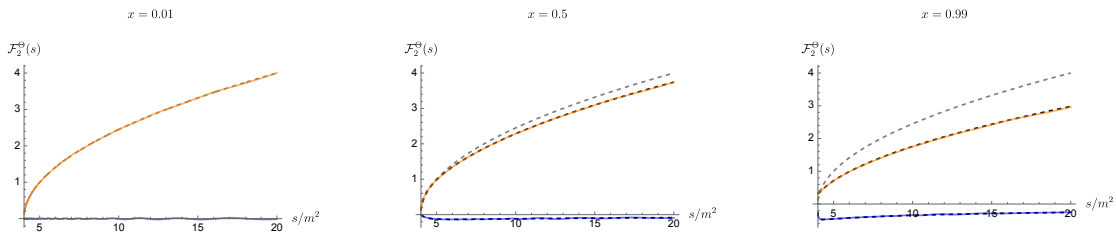


Figure 5.14: Two particles form factor  $\mathcal{F}_2^\theta(s)$  for different values of  $x$  when there is a zero at  $S(m^2(1-x))$ . The imaginary part (in orange) and the real part (in blue) tend toward the free fermion (in dashed gray) when  $x \rightarrow 0$ . The dashed black line is the analytical result given by (5.3.50) and (5.3.53). We used  $N=50$ .

of the zero in the S-Matrix and also seem to share the resonance associated to an unstable particle when  $x \rightarrow 1$ .



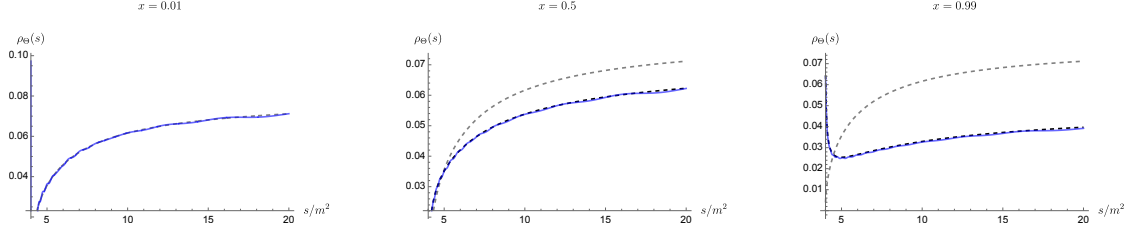


Figure 5.15: Spectral density  $\rho_\Theta(s)$  for different values of  $x$  when there is a zero at  $S(m^2(1-x))$ . The bootstrap result (in blue) tends toward the free fermion (in dashed gray) when  $x \rightarrow 0$ . We also observe the delta function appearing at  $s = 4m^2$  when  $x \rightarrow 1$  which corresponds to the second lightest particle that will become stable. The dashed black line is the analytical result given by (5.3.50) and (5.3.53) and the elasticity relation (5.3.1). We used  $N=50$ .

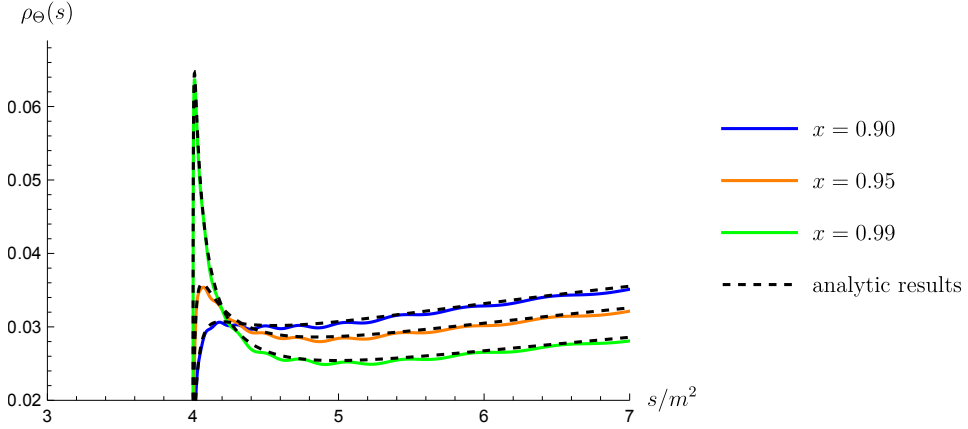


Figure 5.16: Spectral density  $\rho_\Theta(s)$  for different values of  $x$  when there is a zero at  $S(m^2(1-x))$ . We used  $N=50$ .

### Carving out IFT parameter space: $c_{UV} = 1/2$

We now target the IFT by fixing the central charge to  $c_{UV} = 1/2$  and explore the allowed region in the  $(g\mathcal{F}_1^\Theta, g^2, x)$  3-dimensional space, where we recall

$$\mathcal{T}(s) = -\frac{g^2}{s-m^2} + \dots, \quad \mathcal{F}(s) = -\frac{\mathcal{F}_1^\Theta g}{s-m^2} + \dots \quad (5.2.7)$$

We compute the bounds for  $g^2$  and  $g\mathcal{F}_1^\Theta$  for  $x \in (0, 1)$ , which corresponds to the range in magnetic field with only one stable particle. The result is the pyramid shown in Figure 5.17 inside which IFT must lie.

We noticed that the lower edge of the pyramid, corresponding to the lowest bounds on  $g^2$  for different  $x$ , is slightly in-curved toward the negative  $g\mathcal{F}_1^\Theta$ . The effect is tiny and shown on Figure 5.18.

The slice at  $x = 1/10$  of the pyramid is shown in Figure 5.19, where we also place IFT using

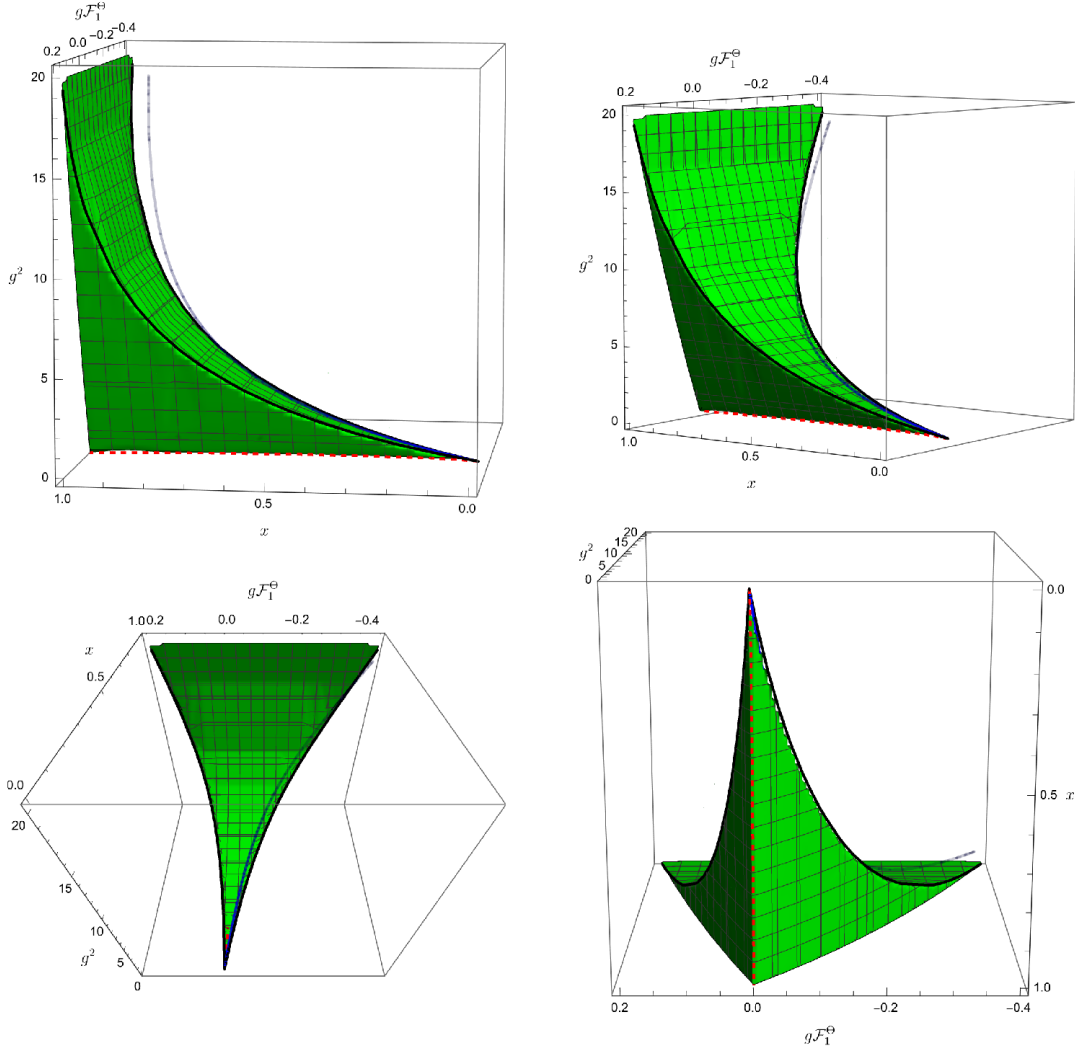


Figure 5.17: Allowed region (in green) in the  $(g\mathcal{F}_1^\theta, x, g^2)$  space. The blue line is the perturbative trajectory for  $g^2(x)$  and  $g(x)\mathcal{F}_1^\theta(x)$  in IFT (computed in appendix D.4), the black lines are the analytical result (5.3.54) and the dashed red line is the minimal cubic coupling discussed in Figure 5.18.

form factor perturbation theory: the cubic coupling  $g$  was computed in [229] and  $\mathcal{F}_1^\theta$  is an original computation (both calculations are in appendix D.4).

The figure is generated by first computing the bounds on  $g\mathcal{F}_1^\theta$  for which we got

$$g\mathcal{F}_1^{\theta,(min)} = -0.0110843..., \quad g\mathcal{F}_1^{\theta,(max)} = 0.0047159..., \quad (5.2.8)$$

and then computing the bounds on  $g^2$  with fixed values of  $g\mathcal{F}_1^\theta$ .

Note that the perturbative result for  $g^2$  saturates the higher bound for the cubic coupling allowed by the bootstrap. The perturbative result for  $\mathcal{F}_1^\theta$  however does not saturate the bounds but still is inside the allowed region. At the points where the red and orange lines meet we

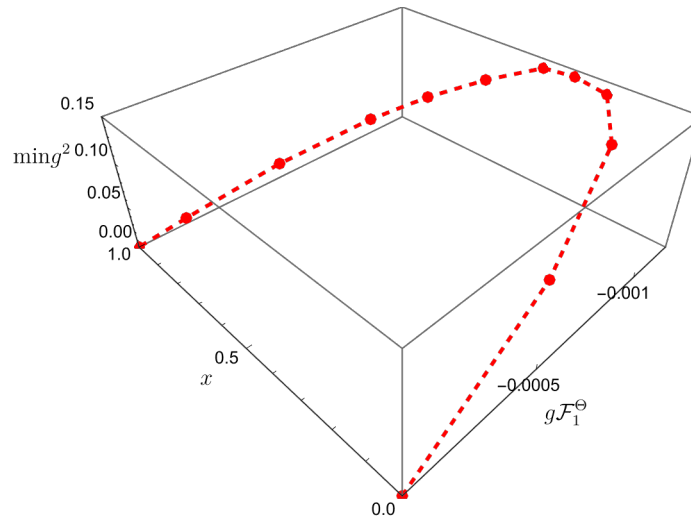


Figure 5.18: Lower edge of the pyramid corresponding to the lowest bounds on  $g^2$ . This is computed with  $N = 70$ .

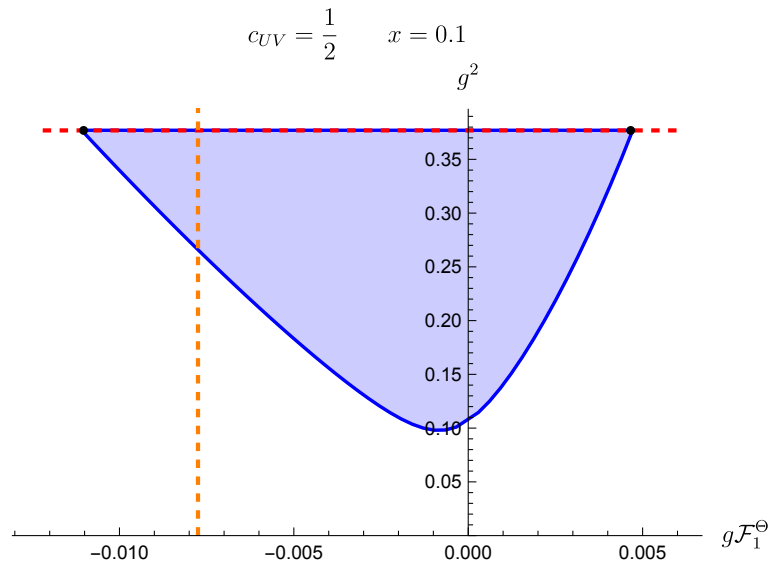
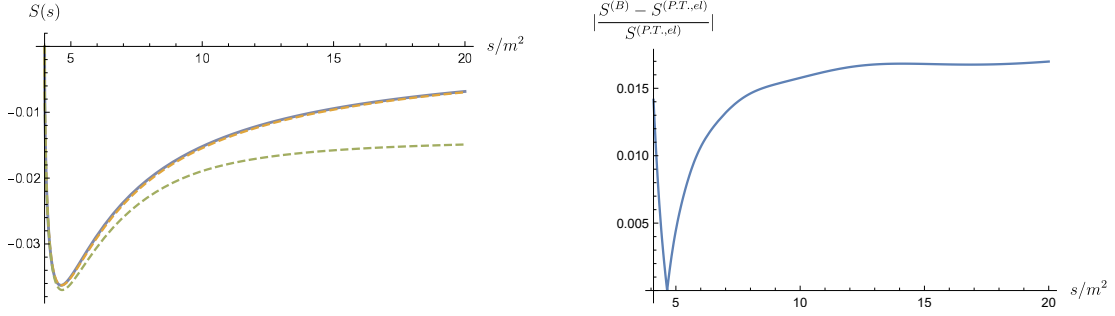


Figure 5.19: Allowed region in the  $(g\mathcal{F}_1^\ominus, g^2)$  plane when the central charge is  $c_{UV} = 1/2$  and there is a zero in the S-Matrix at  $x = 1/10$ . The red and orange dashed line are the values of  $\mathcal{F}_1^\ominus$  and  $g^2$  computed with perturbation theory. This is computed with  $N = 70$ . The black dots are the analytical solutions (5.3.54).

can compare the optimal scattering amplitude to the one known in perturbation theory from [229]. This is shown in the figure below. We observe that we match perfectly with the elastic contribution of the perturbative S-Matrix. This is expected since our bootstrap setup saturates unitarity at all energies and does not account for theories with particle production. Therefore we are not surprised that inelastic contributions are not obtained.

In Figure 5.20 we perform a convergence study for the upper corners of the triangle with

## Chapter 5. Injecting the UV into the Bootstrap: Ising Field Theory



respect to the analytical roots given by (5.3.54). The corners of the allowed region coming from the dual bootstrap approach the analytical roots

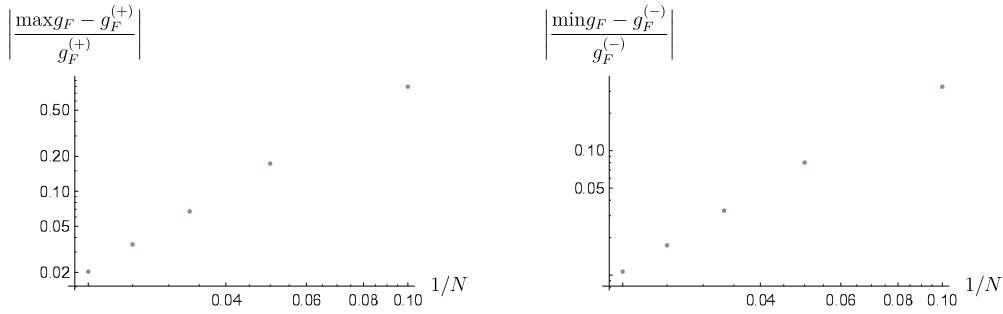


Figure 5.20: Convergence study (on a logarithmic scale) for the upper corners of the triangle approaching the analytical roots  $g_F^{(\pm)}$ .

Since the perturbative result for  $\mathcal{F}_1^\Theta$  does not saturate the bootstrap bounds we can investigate what happens when the position of the zero (or equivalently the magnetic field) is changed. We plot the perturbative result and the bootstrap bounds for different magnetic fields in Figure 5.22. We observe that both perturbation theory and bootstrap bounds scale with  $x$  or, equivalently, with  $h^2$ , but at a different rate,

$$g_F^{(\pm)} = \left( \frac{1}{2\sqrt{3}} - \frac{1}{\pi} \pm \frac{1}{\sqrt{3}\pi} \mp \frac{1}{9} \right) x \approx (-0.1023, +0.0430) x \approx (-11.7601, +4.9466) h^2. \quad (5.2.9)$$

whereas

$$g_F^{(P.T)} = -\frac{1}{3\sqrt{2}} \left( \frac{15}{8} + \frac{1}{2\pi} - \sqrt{3} \right) x \approx -0.0712x \approx -8.1857h^2. \quad (5.2.10)$$

These numbers were computed in appendices 5.3 and D.4, respectively.

In Figure 5.23 we show the bounds on  $g^2$  and  $g_{\mathcal{F}_1^\Theta}$  in the strongly interacting regime  $x = 0.7$ . The upper boundary is again saturated by the analytical results (5.3.54) and (5.3.43). In particular the roots of eq.(5.3.54) correspond to the corners.

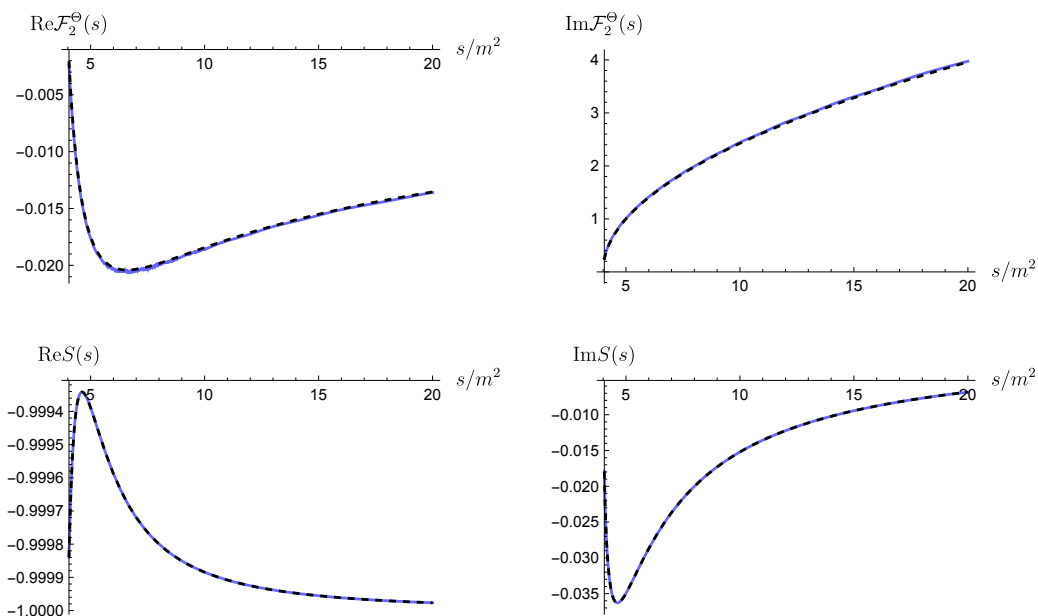


Figure 5.21: Numerical scattering amplitude and form factor on the upper edge of the triangle (in blue) compared to the analytical result (in dashed). We took the point  $g\mathcal{F}_1^\Theta = 0$  for reference but the data looks identical on the whole upper edge. We used  $N = 50$ .

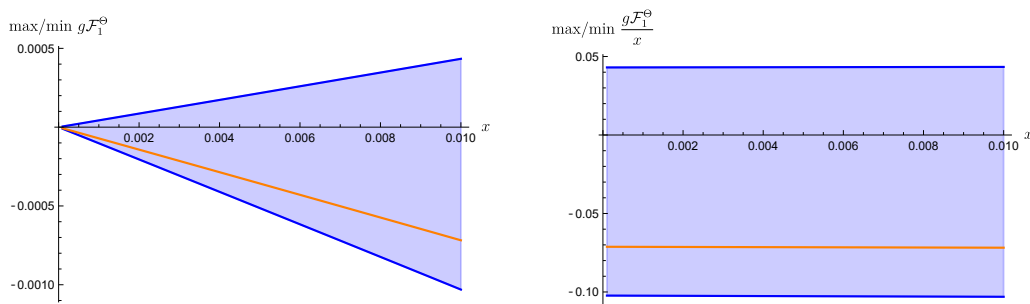


Figure 5.22: Evolution of the upper boundary of the allowed region (in blue) via the numerical bootstrap compared to the evolution of the perturbative result (in orange) in the perturbative regime for small values of  $x$ . We observe that the bootstrap bounds and perturbation theory both scale linearly with  $x$ , or quadratically with  $h$ . We used  $N = 70$ .

### 5.3 Analytical bootstrap

There are three objects we want to constrain. The  $2 \rightarrow 2$  scattering matrix  $S(s)$  or amplitude  $\mathcal{F}(s)$ , the 2-particle form factor  $\mathcal{F}(s)$  and the spectral density  $\rho(s)$ . The first two are real analytic functions,<sup>12</sup> and the S-matrix further satisfies crossing symmetry,  $S(s) = S(4m^2 - s)$ . There is still the constraint of unitarity which relates all of them. We observe from the

<sup>12</sup>A real analytic function  $f(s)$  satisfies  $f^*(s) = f(s^*)$ .

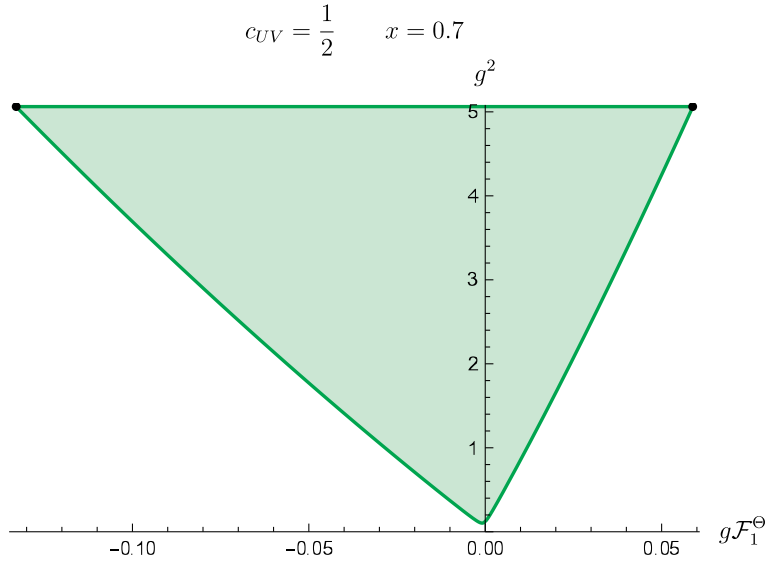


Figure 5.23: Allowed region in the  $(g\mathcal{F}_1, g^2)$  plane when the central charge is  $c_{UV} = 1/2$  and there is a zero in the S-Matrix at  $x = 7/10$ . This is computed with  $N = 70$ . The black dots are the analytical roots (5.3.54).

optimization problem that unitarity is “saturated”, eq. (5.1.25), meaning

$$|S(s)|^2 = 1, \quad \frac{\mathcal{F}(s)}{\mathcal{F}^*(s)} = S(s), \quad \rho(s) = \frac{|\mathcal{F}(s)|^2}{4\pi\sqrt{s(s-4m^2)}}, \quad (5.3.1)$$

for  $s \geq 4m^2$  slightly above the real axis.

Counting separately for real and imaginary parts we have five variables and three equations, which implies that there is two-fold freedom left over from eqs. (5.3.1). The general solution for (5.3.1) should possess this freedom.

We start by solving the first equation of eq. (5.3.1). It will be particularly useful to us here to exploit a well-known trick used for solving elastic unitarity in  $d > 2$  (see e.g. [7]). We write  $S(s)$  in terms of the amplitude  $\mathcal{F}(s)$ ,

$$S(s) = 1 + \frac{\mathcal{F}(s)}{2\sqrt{s(4m^2-s)}}. \quad (5.3.2)$$

Then, elastic unitarity  $|S(s)|^2 = 1$  reads

$$\text{Im}\mathcal{F}(s) = \frac{|\mathcal{F}(s)|^2}{4\sqrt{s(s-4m^2)}}. \quad (5.3.3)$$

Noting that  $\text{Im}[1/\mathcal{F}(s)] = -\text{Im}\mathcal{F}(s)/|\mathcal{F}(s)|^2$  we can write the above as

$$\text{Im}\left(\frac{1}{\mathcal{F}(s)}\right) = -\frac{1}{4\sqrt{s(s-4m^2)}} \quad (5.3.4)$$

The general solution to the above is then

$$\frac{1}{\mathcal{F}(s)} = -\frac{1}{4\sqrt{s(4m^2-s)}} + \frac{A(s)}{4} \quad (5.3.5)$$

where  $A(s)$  is some crossing symmetric real function on the real line.

We then have

$$\mathcal{F}(s) = \frac{4}{A(s) - 1/\sqrt{(4m^2-s)s}}, \quad \text{or} \quad S(s) = \frac{A(s)\sqrt{(4m^2-s)s+1}}{A(s)\sqrt{(4m^2-s)s-1}}. \quad (5.3.6)$$

Now, since  $\mathcal{F}(s)$  is analytic,  $A(s)$  must be meromorphic in the physical sheet.

Poles of  $A(s)$  translate into zeros of  $\mathcal{F}(s)$ . Note that if  $A(s) = \text{const}$  the solution for  $S(s)$  is precisely the so-called Castillejo-Dalitz-Dyson (CDD) factor. In fact, any solution to elastic unitarity, crossing and analyticity can be written as a product of CDD factors. It is straightforward to show that this amounts to (5.3.6) with rational  $A(s)$ .

The function  $A(s)$  encodes the large freedom that the first equation of (5.3.1) allows for. We may further fix  $A(s)$  at certain values if further constraints are involved, e.g. bound-state poles or zeros.

With solution (5.3.6) in hand we can now try to solve for the form factor using the second equation in (5.3.1). If we write

$$\mathcal{F}(s) = -2m^2 B(s) e^{\alpha(s) - \alpha(0)}, \quad (5.3.7)$$

where  $B(s)$  is real, Watson's equation will only fix  $\alpha(s)$ ,

$$\frac{\mathcal{F}(s)}{\mathcal{F}^*(s)} = S(s) \implies \text{Im}\alpha(s) = -\frac{i}{2} \log S(s + i\epsilon), \quad \text{for } s \geq 4m^2 \quad (5.3.8)$$

Making use of the solution for the S-matrix (5.3.6) we have

$$\text{Im}\alpha(s) = \text{arccot}\left(A(s)\sqrt{(s-4m^2)s}\right) \Theta(s-4m^2) \quad (5.3.9)$$

It is difficult to explicitly find a function which gives such imaginary part for a generic  $A(s)$ . We may still find numerically  $\alpha(s)$  through a dispersion relation,

$$\alpha(s) - \alpha(0) = \frac{s}{\pi} \int_{4m^2}^{\infty} \frac{\text{arccot}\left(A(s')\sqrt{(s'-4m^2)s'}\right)}{s'(s'-s)} ds'. \quad (5.3.10)$$

## Chapter 5. Injecting the UV into the Bootstrap: Ising Field Theory

---

Note that any analytic function could be added to the right hand side of the above. Such analytic function would drop out upon taking the imaginary part meaning that eq. (5.3.9) would still be satisfied. The presence of a non-trivial analytic function,<sup>13</sup> i.e. a polynomial, will lead to an essential singularity for  $\mathcal{F}(s)$  so we discard this possibility.

The real function  $B(s)$  is not fixed by Watson's equation. It plays a similar role to  $A(s)$  in eq. (5.1.2), i.e.  $B(s)$  is analytic in a neighbourhood of the physical region. These properties are of course fixed by whatever analyticity assumption we may have on  $\mathcal{F}(s)$ . Causality requirements indicate that  $B(s)$  should at most be meromorphic, with poles signalling potential bound-states.

We now impose the normalization

$$\mathcal{F}(0) = -2m^2 \implies B(0) = 1. \quad (5.3.11)$$

With  $\mathcal{F}(s)$  in hand, via eqs. (5.3.7) and (5.3.10), we can now simply solve for the spectral density from eq. (5.3.1). The two-fold freedom left over from eq. (5.3.1) is encoded into the meromorphic functions  $A(s)$  and  $B(s)$ .  $A(s)$  can be determined if some coupling is being extremized over in the S-matrix space, which appears to occur when  $c_{UV}$  is minimized.  $B(s)$  is determined by minimizing over  $c_{UV}$  explicitly,

$$c_{UV} = 12\pi \int_{4m^2}^{\infty} \frac{\rho(s)}{s^2} ds = 12m^4 \int_{4m^2}^{\infty} \frac{B^2(s) e^{2\bar{\alpha}(s)}}{s^2 \sqrt{s(s-4m^2)}} ds, \quad (5.3.12)$$

where we made use of the relation between  $\rho(s)$  and  $\mathcal{F}(s)$ , eq. (5.3.1), and eq. (5.3.7) for  $\mathcal{F}(s)$ , and where  $\bar{\alpha}(s)$  is the real part of  $\alpha(s) - \alpha(0)$ , i.e. the principal value of (5.3.10),

$$\bar{\alpha}(s) = \text{Re}[\alpha(s) - \alpha(0)] = \frac{s}{\pi} \int_{4m^2}^{\infty} \frac{\text{arccot}\left(\frac{A(s') \sqrt{(s'-4m^2)s'}}{s'(s'-s)}\right)}{s'(s'-s)} ds'. \quad (5.3.13)$$

As we will see in more detail, the polynomial degree of  $B(s)$  must be bounded from above so that the integral (5.3.12) for  $c_{UV}$  is convergent. In fact, we will see that for every case considered here  $B(s)$  is at most linear in  $s$  (apart from a very special case described in 5.3.2 where it can be quadratic). The constant coefficient in  $B(s)$  is fixed by the normalization  $\mathcal{F}(0) = -2m^2$ , so we only need to minimize  $c_{UV}$  over the free linear coefficient, which can be done analytically.

---

<sup>13</sup>By trivial we mean a constant piece which can be simply absorbed into  $B(s)$ .



### 5.3.1 $\mathbb{Z}_2$ symmetric theories

#### Finding the leaf

We are interested in finding the allowed space of the following parameters

$$\Lambda \equiv -\mathcal{T}(2), \quad \Lambda^{(2)} \equiv \lim_{s \rightarrow 2} \frac{\partial^2}{\partial s^2} \mathcal{T}(s). \quad (5.3.14)$$

where  $S$  and  $\mathcal{T}$  are related by eq. (5.1.2),

$$S(s) = 1 + \frac{\mathcal{T}(s)}{2\sqrt{s(4m^2 - s)}}. \quad (5.3.15)$$

Elastic unitarity for the S-matrix reads

$$|S(s)|^2 = 1, \quad \text{for } s \geq 4m^2 \vee s \leq 0. \quad (5.3.16)$$

Crossing symmetry further implies

$$S(s) = S(4m^2 - s). \quad (5.3.17)$$

Now, we start by assuming that the S-matrix that extremizes the bounds is elastic and has the minimal number of CDD zeros. We have two parameters that we need to fix,  $\Lambda$  and  $\Lambda^{(2)}$ , so we need at least two CDD factors,

$$S = S_{a_-} S_{a_+}, \quad (5.3.18)$$

with

$$S_a = \frac{a - \sqrt{s(4m^2 - s)}}{a + \sqrt{s(4m^2 - s)}}. \quad (5.3.19)$$

Let us now set  $m = 1$  as choice of units. From eqs. (5.3.15) and (5.3.18) we then solve for the amplitude (5.3.6) to find

$$A(s) = -\frac{1 + \frac{a_+ a_-}{s(4-s)}}{a_+ + a_-}, \quad (5.3.20)$$

We now fix  $a_-$  and  $a_+$  in terms of (5.3.14) (or (5.2.1) in the main text):

$$a_{\pm} = -\frac{2\Lambda^2 \pm 8\sqrt{\Lambda^3 - 32\Lambda\Lambda^{(2)} + 64(\Lambda^{(2)})^2}}{(\Lambda - 16)\Lambda + 32\Lambda^{(2)}}, \quad (5.3.21)$$

so that

$$A(s) = \left( \frac{1}{4} - \frac{4}{\Lambda} + \frac{8(\Lambda^{(2)})}{\Lambda^2} \right) + \frac{1 - 32\Lambda^{(2)}/\Lambda^2}{s(4-s)}. \quad (5.3.22)$$

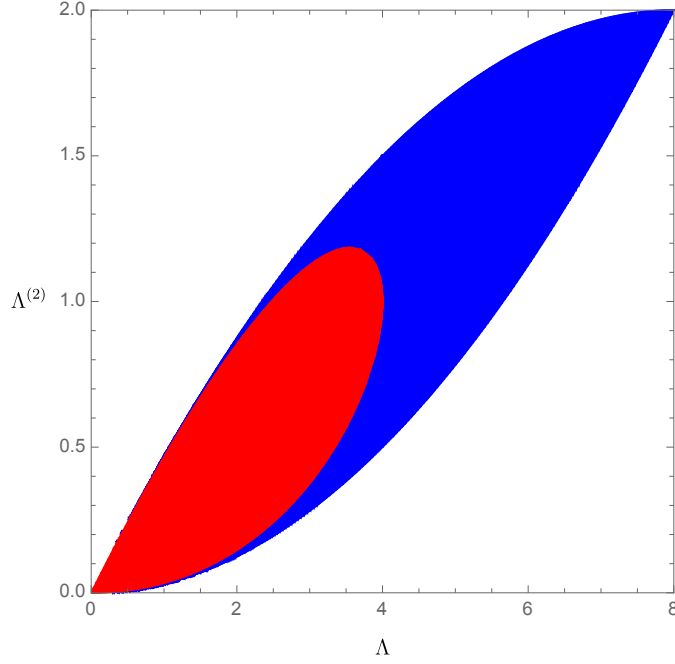


Figure 5.24: Allowed space for  $(\Lambda, \Lambda^{(2)})$  such that the amplitude (5.3.20) has no poles on the physical sheet. The blue region corresponds to the case where both CDD zeros are real, and is given by  $\left( 0 < \Lambda < 4 \wedge \left( \frac{\Lambda^2}{32} < \Lambda^{(2)} \leq \frac{\Lambda}{4} - \frac{1}{8}\sqrt{4\Lambda^2 - \Lambda^3} \vee \frac{1}{8}\sqrt{4\Lambda^2 - \Lambda^3} + \frac{\Lambda}{4} \leq \Lambda^{(2)} < \frac{1}{32}(16\Lambda - \Lambda^2) \right) \right) \vee \left( 4 \leq \Lambda < 8 \wedge \frac{\Lambda^2}{32} < \Lambda^{(2)} < \frac{1}{32}(16\Lambda - \Lambda^2) \right)$ . The red region corresponds to the case where the CDD zeros are complex, and is given by  $0 < \Lambda < 4 \wedge \frac{\Lambda}{4} - \frac{1}{8}\sqrt{4\Lambda^2 - \Lambda^3} < \Lambda^{(2)} < \frac{1}{8}\sqrt{4\Lambda^2 - \Lambda^3} + \frac{\Lambda}{4}$ . Their union is given by eq. (5.3.24).

What remains to impose is the analyticity constraint. Concretely, for what values of  $\Lambda$  and  $\Lambda^{(2)}$  does  $\mathcal{F}(s)$  or  $S(s)$  not develop any other singularities on the physical sheet besides the physical cuts for  $s \geq 4m^2$  and  $s \leq 0$ ? We want  $a_-$  and  $a_+$  to be such that the denominator in eq. (5.1.2) is never zero on the physical sheet, i.e. that no pole develops and that the CDD factors remain CDD zeros.

Note that the square root function only covers half of the complex plane. On the principal sheet it covers the right half plane, i.e. the real part of the square root function is always positive. This means that if

$$\operatorname{Re} a_- > 0 \quad \text{and} \quad \operatorname{Re} a_+ > 0 \quad (5.3.23)$$

we are sure that the denominator of (5.3.6) is never zero. Therefore, imposing (5.3.23) on (5.3.21) we find the allowed range for  $\Lambda$  and  $\Lambda^{(2)}$ .

So here we can split the problem in two. If the discriminant of (5.3.21) is positive then  $a_{\pm}$  is real, meaning that if  $a_{\pm} > 0$  the S-matrix will have two real zeros on the physical sheet. This region is represented in blue in fig. 5.24.

If the discriminant of (5.3.21) is negative then  $a_{\pm}$  will be complex. However, if  $\text{Re } a_{\pm} > 0$ , i.e.  $(\Lambda - 16)\Lambda + 32\Lambda^{(2)} < 0$ , then the denominator of (5.3.6) will never be zero on the physical sheet. Instead, the numerator will have (complex) zeros. This region is represented in red in fig. 5.24.

The union of these regions is the leaf in the main text, fig. 5.3. Explicitly, in agreement with eqs. (A.8) and (A.10) of [204],

$$0 < \Lambda < 8 \quad \wedge \quad \frac{\Lambda^2}{32} < \Lambda^{(2)} < \frac{16\Lambda - \Lambda^2}{32} \quad (5.3.24)$$

The optimal amplitude on the lower bound, i.e. when  $\Lambda^{(2)} = \frac{\Lambda^2}{32}$ , and on the upper bound, i.e. when  $\Lambda^{(2)} = \frac{16\Lambda - \Lambda^2}{32}$  is given by eq. (5.3.20) with, respectively,

$$\text{Lower bound: } A(s) = \frac{1}{2} \left( 1 - \frac{8}{\Lambda} \right), \quad \text{Upper bound: } A(s) = \frac{2}{s(4-s)} \left( 1 - \frac{8}{\Lambda} \right) \quad (5.3.25)$$

It is straightforward to see that multiplying the 2-CDD ansatz (5.3.18) by any further CDD zero will lead to values of  $\Lambda$  and  $\Lambda^{(2)}$  inside the leaf, and the same holds true if inelasticity is considered. So we conclude that the bounds are optimal.

#### $c_{UV}$ at the edges of the leaf

We can now find the two-particle stress tensor form factor  $\mathcal{F}(s)$  on the edges of the leaf. We plug eqs. (5.3.25) for  $A(s)$  at the edges of the leaf into eqs. (5.3.7) and (5.3.10).

We want minimize  $c_{UV}$  over  $B(s)$ . First note that  $B(s)$  must not have any poles outside the real cut, as it would be inconsistent with the analyticity assumptions for the form factor  $\mathcal{F}(s)$ . In principle it may have poles, e.g. at  $s \rightarrow 4m^2$  or somewhere along the real axis, as long as as the integral (5.3.12) converges, which can only be the case if  $e^{2\bar{\alpha}(s)}$  cancels such poles. While we could not find an explicit form for  $\bar{\alpha}(s)$  for either of the lower or upper bounds (5.3.25) we do observe numerically that  $e^{2\bar{\alpha}(s)}$  is never zero, indicating that  $B(s)$  cannot have poles and therefore be holomorphic, i.e. a polynomial.<sup>14</sup> Finally, we can constrain the polynomial degree of  $B(s)$  according to the convergence of the integral (5.3.12).

**Lower edge.** On the lower edge, we find that, according to eq. (5.3.9),  $\text{Im } \alpha(\infty) = \text{arccot}(-\infty) = 0$ , meaning that  $\alpha(s \rightarrow \infty) \rightarrow \text{const}$  and  $e^{2\bar{\alpha}(s)} \rightarrow 1$ . We conclude that the integrand of (5.3.12) will go as  $\sim B^2(s)s^{-3}$  and, therefore,  $B(s)$  must be a constant. Otherwise, the integral will not

<sup>14</sup>The only way we could make  $e^{2\bar{\alpha}(s)}$  have a zero was to have  $A(s)$  be zero at some point, making the arccot function jump by  $\pi$ . However,  $A(s)$  is sign definite at the edges of the leaf (5.3.25).

## Chapter 5. Injecting the UV into the Bootstrap: Ising Field Theory

---

converge. Since  $B(0) = 1$  we are led to the following unique choice on the lower edge,

$$\text{Lower edge: } B(s) = 1. \quad (5.3.26)$$

So the form factor is entirely specified by  $A(s)$ ,

$$\mathcal{F}(s) = -2me^{\alpha(s)-\alpha(0)}. \quad (5.3.27)$$

As a simple check we may explicitly compute  $\mathcal{F}(s)$  and  $c_{UV}$  at the tips of the leaf,  $\Lambda = 0$  and  $\Lambda = 8$ . In the former case we have  $A(s) = \frac{1}{2}\left(1 - \frac{8}{\Lambda}\right) \rightarrow -\infty$ , for which  $\text{arccot}(-\infty) = 0$  and  $\text{Im } \alpha(s) = 0$ . In this case eq. (5.3.10) gives  $\alpha(s) - \alpha(0) = 0$  and we have  $\mathcal{F}(s) = -2m^2$  and  $c_{UV} = 1$ .

For  $\Lambda = 8$  instead we have  $A(s) = 0^-$ , meaning  $\text{arccot}(0^-) = -\frac{\pi}{2}$ . From eq. (5.3.10) it follows that

$$\alpha(s) - \alpha(0) = \frac{1}{2} \log\left(1 - \frac{s}{4m^2}\right) \quad (5.3.28)$$

and

$$\mathcal{F}(s) = -m\sqrt{4m^2 - s}, \quad c_{UV} = 12m^4 \int_{4m^2}^{\infty} \sqrt{\frac{s-4m^2}{s}} \frac{ds}{s^2} = \frac{1}{2}. \quad (5.3.29)$$

For  $0 < \Lambda < 8$  we perform both integrals (5.3.13) and (5.3.10) numerically. In fig. 5.10 we show the optimal  $S(s)$  and  $\mathcal{F}(s)$  at  $\Lambda = 2.4$ .

**Upper edge.** Let us now consider the upper edge of the leaf. In this case we have  $A(s) = \frac{2}{s(4-s)}\left(1 - \frac{8}{\Lambda}\right) > 0$  across the integration region  $s > 4m^2$  in (5.3.10). Now we find that  $e^{2\tilde{\alpha}(s)} \sim s^{-1}$  when  $s \rightarrow \infty$  so that the integrand of (5.3.10) goes as  $\sim B^2(s)s^{-4}$ . We see that  $B(s)$  can at most be linear in  $s$  to ensure convergence of the integral. Therefore,

$$\text{Upper edge: } B(s) = 1 - bs, \quad (5.3.30)$$

where  $b$  is a free real parameter.

Plugging into (5.3.12) we have

$$c_{UV}(b) = I_0 - 2bI_1 + b^2I_2, \quad \text{with} \quad I_n \equiv 12m^4 \int_{4m^2}^{\infty} \frac{s^n e^{2\tilde{\alpha}(s)}}{s^2 \sqrt{s(s-4m^2)}} ds, \quad (5.3.31)$$

We now minimize the central charge with respect to  $b$ ,

$$\frac{dc_{UV}}{db} = 0 \quad \implies \quad b_{min} = \frac{I_1}{I_2}, \quad c_{UV}(b_{min}) = I_0 - \frac{I_1^2}{I_2}. \quad (5.3.32)$$

We may again test these expressions for the trivial cases  $\Lambda = 0, 8$ . For the former we have  $A(s) \rightarrow \infty$ , for which again  $\text{Im } \alpha(s) = 0$  and  $\alpha(s) - \alpha(0) = 0$ . In this case  $I_2 \rightarrow \infty$  and we'll trivially

get  $b_{min} \rightarrow 0$  and  $c_{UV}(b_{min}) = I_0 = 1$ . For  $\Lambda \rightarrow 8$  we have  $A(s) \rightarrow 0^+$ , for which  $\text{arccot}(0^+) = +\frac{\pi}{2}$ . From eq. (5.3.10) it follows that

$$\alpha(s) - \alpha(0) = -\frac{1}{2} \log\left(1 - \frac{s}{4m^2}\right) \quad (5.3.33)$$

and

$$e^{2\bar{\alpha}(s)} = \left(1 - \frac{s}{4m^2}\right)^{-1}, \quad \mathcal{F}(s) = -4m^2 \frac{1 - bs}{\sqrt{4m^2 - s}} \quad (5.3.34)$$

Plugging into (5.3.32) we find<sup>15</sup>

$$b_{min} = \frac{1}{4m^2}, \quad (5.3.35)$$

i.e. that the polynomial  $B(s)$  softens the singularity of integrand at  $s \rightarrow 4m^2$ , and we recover eqs. (5.3.29).

For  $0 < \Lambda < 8$  we find  $\bar{\alpha}(s)$  numerically eq. (5.3.13). Then, we plug the result into eq. (5.3.32) and compute the  $I_n$ 's numerically. In fig. 5.9 we show the optimal  $S(s)$  and  $\mathcal{F}(s)$  for  $\Lambda = 2.4$ .

#### $c_{UV}$ in the interior of the leaf

To find  $c_{UV}$  in the interior of the leaf we have to first find the optimal S-matrix. At the edges of the leaf the S-matrix is uniquely fixed because  $\Lambda^{(2)}$  is either maximal (upper edge) or minimal (lower edge). In the interior of the leaf we consider extremizing over  $\Lambda^{(4)}$ , with

$$\Lambda \equiv -\mathcal{F}(2), \quad \Lambda^{(2)} \equiv \lim_{s \rightarrow 2} \frac{\partial^2}{\partial s^2} \mathcal{F}(s), \quad \Lambda^{(4)} \equiv \lim_{s \rightarrow 2} \frac{\partial^4}{\partial s^4} \mathcal{F}(s), \quad (5.3.36)$$

under the hypothesis that  $c_{UV}$  minimization for fixed  $(\Lambda, \Lambda^{(2)})$  extremizes  $\Lambda^{(4)}$ .

We can proceed as in section 5.3.1 and consider three CDD zeros which can be fixed in terms of the three parameters  $(\Lambda, \Lambda^{(2)}, \Lambda^{(4)})$ . Then explore the parameter-space for which these zeros remain zeros and do not turn into poles. Avoiding further technical details we find that

$$\frac{3(-\Lambda^3 + 24\Lambda^2 - 128\Lambda\Lambda^{(2)} + 256(\Lambda^{(2)})^2)}{128(8 - \Lambda)} \leq \Lambda^{(4)} \leq \frac{3(-\Lambda^3 + 128\Lambda\Lambda^{(2)} - 256(\Lambda^{(2)})^2)}{128\Lambda}, \quad (5.3.37)$$

in agreement with eq. (A.12) of [204] which determined these bounds using the Schwarz-Pick theorem.

We observe that the optimal amplitude coming from  $c_{UV}$  minimization is the one for which  $\Lambda^{(4)}$  is minimal, where  $\Lambda^{(4)}$  assumes the lower bound of (5.3.37). The optimal amplitude at the

<sup>15</sup>Technically, in this limiting case,  $I_n$  does not converge due to the end-point singularity at  $s \rightarrow 4m^2$ . However, upon regulating, the ratio  $I_1/I_2$  is finite and is given by  $1/4m^2$ .

## Chapter 5. Injecting the UV into the Bootstrap: Ising Field Theory

---

lower bound is specified by

$$A(s) = -\frac{4(8-\Lambda)^2}{64\Lambda + \Lambda^2(s^2 - 4s - 4) - 32\Lambda^{(2)}(s-2)^2}, \quad (5.3.38)$$

for which the S-matrix  $S(s)$  follows via (5.3.6). For  $A(s)$  given by eq. (5.3.38) we have the same asymptotics of the upper edge of the leaf,  $e^{2\tilde{\alpha}(s)} \sim s^{-1}$ , so  $B(s)$  is at most linear:  $B(s) = 1 - bs$ . As in the previous section, the form factor  $\mathcal{F}(s)$  and the minimal  $c_{UV}$  follow from eqs. (5.3.7), (5.3.10), (5.3.31) and (5.3.32). In fig. 5.11 we compare the analytical result with the output of dual optimization for  $\Lambda = 4.56$  and  $\Lambda^{(2)} = 0.85$ .

### 5.3.2 Ising Field Theory

Here the analyticity assumptions consist of a zero for the S-matrix  $S(s)$  at  $s = m^2(1-x)$ , where  $x$  is related to the magnetic field, and a pole at  $s = m^2$ , and their crossing-symmetric counterparts. Similarly, the form factor  $\mathcal{F}(s)$ , has a pole at  $s = m^2$ .

#### Minimization of the central charge $c_{UV}$

The first problem consists of minimizing the central charge  $c_{UV}$ ,

$$c_{UV} = 12\pi \left( m^{-4} |\mathcal{F}_1^\Theta|^2 + \int_{4m^2}^{\infty} ds \frac{\rho(s)}{s^2} \right) \quad (5.3.39)$$

where  $\mathcal{F}_1^\Theta$  is the 1-particle form-factor, which is a constant. The residue of the 2-particle form factor  $F(s)$  at  $s \rightarrow m^2$  is given by  $g\mathcal{F}_1^\Theta$ , where  $g$  is the cubic coupling, i.e.  $-g^2$  is the residue of the S-matrix pole at  $s \rightarrow m^2$ .

The minimal choice for an S-matrix with the above properties, and which is also purely elastic, is the product of one CDD pole at  $s = m^2$  and one CDD zero at  $s = m^2(1-x)$ ,

$$S_\pm(s) = \pm \frac{m^2 \sqrt{(1-x)(3+x)} - \sqrt{s(4m^2-s)}}{m^2 \sqrt{(1-x)(3+x)} + \sqrt{s(4m^2-s)}} \cdot \frac{\sqrt{3}m^2 + \sqrt{s(4m^2-s)}}{\sqrt{3}m^2 - \sqrt{s(4m^2-s)}}. \quad (5.3.40)$$

Now, near the pole we must have  $S(s) \sim -\frac{g^2}{s-m^2}$ , i.e.  $S(s)$  must have a negative residue. Only  $S_-(s)$  satisfies this requirement. We again observe that  $S_-(s)$  matches with the optimal S-matrix in fig. 5.13 coming from minimizing the central charge.

By writing  $S_-(s)$  in the form (5.3.6) we find (in units where  $m = 1$ )

$$A(s) = -\frac{\sqrt{3} - \sqrt{(1-x)(x+3)}}{(s-4)s + \sqrt{3}(1-x)(x+3)}, \quad (5.3.41)$$

From eq. (5.3.6) we see that, near the pole, we have

$$T(s \rightarrow m^2) \sim -\frac{g^2}{s - m^2}, \quad (5.3.42)$$

with

$$g^2 = \frac{4\sqrt{3} \left(3 - \sqrt{3(1-x)(x+3)}\right)^2}{x(x+2)} > 0 \quad (5.3.43)$$

Now, given  $A(s)$ , the form factor  $F(s)$  follows from eqs. (5.3.9) and (5.3.7). The function  $B(s)$  must contain the simple pole of  $F(s)$  when  $s \rightarrow m^2 = 1$  but no other singularity. We must therefore have

$$B(s) = \frac{P(s)}{1-s}, \quad (5.3.44)$$

where  $P(s)$  is a polynomial, for which  $B(0) = 1$  implies  $P(0) = 1$ . If, furthermore,

$$F(s \rightarrow 1) \sim -\frac{g_F}{s-1}, \quad (5.3.45)$$

where  $g_F \equiv g_{\mathcal{F}_1^\Theta}$ , we must have, from (5.3.7),

$$P(1) = -\frac{g_F e^{\alpha(0)-\alpha(1)}}{2}. \quad (5.3.46)$$

To constrain further  $P(s)$  we consider the central charge,

$$c_{UV} = 12\pi \frac{g_F^2}{g^2} + 12 \int_4^\infty \frac{P^2(s) e^{2\bar{\alpha}(s)}}{(1-s)^2 s^2 \sqrt{s(s-4)}} ds. \quad (5.3.47)$$

Similarly to the previous section, we see that convergence of the above integral bounds the degree of  $P(s)$ . According to eq. (5.3.9), we see that  $\text{Im } \alpha(s \rightarrow \infty) = \text{arccot}(0^-) = -\frac{\pi}{2}$  meaning that  $e^{2\bar{\alpha}(s)} \sim s$ , when  $s \rightarrow \infty$ . The integrand in (5.3.47) will then go like  $\sim P^2(s)s^{-4}$ . In order for the integral to converge, we see that  $P(s)$  must be at most linear,

$$P(s) = 1 - bs \quad (5.3.48)$$

where  $b$  is some real constant parameter, which can be fixed in terms of  $g_F$  via equation (5.3.46),

$$b = 1 + \frac{g_F e^{\alpha(0)-\alpha(1)}}{2}, \quad (5.3.49)$$

for which the form factor reads,

$$\mathcal{F}(s) = -2e^{\alpha(s)-\alpha(0)} + \frac{g_F s}{1-s} e^{\alpha(s)-\alpha(1)} \quad (5.3.50)$$

## Chapter 5. Injecting the UV into the Bootstrap: Ising Field Theory

---

and the central charge (5.3.47) can be expressed as

$$c_{UV} = I_0 + g_F (e^{-\bar{\alpha}(1)} I_1) + g_F^2 \left( \frac{12\pi}{g^2} + \frac{e^{-2\bar{\alpha}(1)}}{4} I_2 \right), \quad (5.3.51)$$

with

$$I_n \equiv 12 \int_4^\infty \frac{e^{2\bar{\alpha}(s)}}{(s-1)^n s^{2-n} \sqrt{s(s-4)}} ds. \quad (5.3.52)$$

We now minimize the central charge  $c_{UV}$  with respect to  $g_F$ ,

$$\frac{dc_{UV}}{dg_F} = 0 \quad \Rightarrow \quad g_{F,min} = -\frac{2I_1}{I_2 e^{-\bar{\alpha}(1)} + 48\pi g^{-2} e^{\bar{\alpha}(1)}}, \quad c_{UV,min} = I_0 - \frac{I_1^2}{I_2 + 48\pi g^{-2} e^{2\bar{\alpha}(1)}}, \quad (5.3.53)$$

with  $g^2$  given by eq. (5.3.43), and  $\bar{\alpha}(s)$  given by eqs. (5.3.13) and (5.3.41).

### Bounds on $g_F$ for fixed central charge $c_{UV} = 1/2$ and maximal $g$

For a fixed central charge  $c_{UV} = 1/2$  we find two possible roots for  $g_F$  from eq. (5.3.51),

$$g_F^{(\pm)} = \frac{-e^{-\bar{\alpha}(1)} I_1 \pm \sqrt{e^{-2\bar{\alpha}(1)} I_1^2 - (48\pi g^{-2} + e^{-2\bar{\alpha}(1)} I_2)(I_0 - \frac{1}{2})}}{2I_0 - 1}, \quad (5.3.54)$$

where  $g^2$  is maximal and given by (5.3.43) in terms of the zero  $x$ . For  $x = 1/10$  we find

$$g_F^{(-)} = -0.011028\dots, \quad g_F^{(+)} = 0.004658\dots \quad (5.3.55)$$

These correspond to the leftmost and rightmost corners in fig. 5.19.

Note that fig. 5.19 seems to indicate that there exists a line of solutions with the maximal coupling connecting the two extrema (5.3.54), whereas our previous analysis only provides two isolated points for an S-matrix with maximal coupling. The solution to this apparent paradox lies in the possibility of having an S-matrix with cubic coupling arbitrarily close to the maximal one, but with different asymptotics, such that  $P(s)$  in (5.3.47) can now be quadratic with a free parameter, instead of just linear as in (5.3.48).

Take for example

$$S(s) = S_-(s) \frac{a_1 + a_2 s(4-s) - \sqrt{s(4-s)}}{a_1 + a_2 s(4-s) + \sqrt{s(4-s)}}, \quad (5.3.56)$$

where  $S_-(s)$  is the maximal S-matrix given by eq. (5.3.40). Now, for  $a_1 \rightarrow \infty$  we have  $S(s) \rightarrow S_-(s)$ . On the other hand, it is not hard to see that solving for  $A(s)$  using eq. (5.3.6) leads to the



following asymptotics

$$A(s \rightarrow \infty) \rightarrow -\frac{\sqrt{3} - 3\sqrt{31}/10 - 1/a_2}{s^2} + O\left(\frac{1}{s^3}\right) \quad (5.3.57)$$

which only depends on  $a_2$ . In particular, if we take  $a_2$  large enough we get back the previous case, for which  $A(s \rightarrow \infty) \rightarrow 0^-$ . Now, however,  $a_2$  can be tuned such that  $A(s \rightarrow \infty) \rightarrow 0^+$  while also keeping  $S(s)$  free of further poles, i.e. for  $0 < a_2 < (\sqrt{3} - 3\sqrt{31}/10)^{-1} \approx 16.2$ . In this case we have  $\text{Im } \alpha(s \rightarrow \infty) = \text{arccot}(0^+) = +\frac{\pi}{2}$  so that  $e^{2\bar{\alpha}(s)} \sim s^{-1}$ . The integrand in (5.3.47) will then go like  $\sim P^2(s)s^{-6}$ , which allows for a quadratic degree polynomial  $P(s)$ . Two of the coefficients of  $P(s)$  are fixed by the normalization  $P(0) = 1$  and by the residue of the form factor  $g_F$ , the remaining coefficient is free, i.e. it allows for a line of solutions with near-maximal cubic coupling (by letting  $a_1$  be arbitrarily large) as observed in fig. 5.19.

### Small magnetic field limit $h \rightarrow 0$ : Bounds on $g_F$ and extra zeros

We first find how the analytical  $g_F$  scales in the small magnetic field limit,

$$g_F(x \rightarrow 0) = x \tilde{g}_F. \quad (5.3.58)$$

We assume this behavior for now, but will then confirm it by explicit computation. We start by noting that in the limit  $x \rightarrow 0$ , the cubic coupling  $g^2$  (5.3.43) goes as

$$g^2(x \rightarrow 0) = 2\sqrt{3}x \quad (5.3.59)$$

Then, the central charge (5.3.47) reads

$$c_{UV} = \frac{6\pi}{\sqrt{3}} \tilde{g}_F^2 x + 12 \int_4^\infty \frac{P^2(s) e^{2\bar{\alpha}(s)}}{(1-s)^2 s^2 \sqrt{s(s-4)}} ds + O(x^2). \quad (5.3.60)$$

We still have to determine the  $x \rightarrow 0$  limit of  $P(s)$  and  $\bar{\alpha}(s)$ . Let us first consider  $\bar{\alpha}(s)$ . From (5.3.41) we have

$$A(s) = -\frac{x/\sqrt{3}}{3+s(s-4)} + O(x^2) \quad (5.3.61)$$

Plugging into (5.3.9) and expanding at small  $x$

$$\text{Im } \alpha(s) = \left[ -\frac{\pi}{2} + x \frac{\sqrt{s(s-4)}/3}{3+s(s-4)} + O(x^2) \right] \Theta(s-4) \quad (5.3.62)$$

We find

$$\alpha(s) - \alpha(0) = \frac{1}{2} \log\left(1 - \frac{s}{4}\right) + x [\alpha_1(s) - \alpha_1(0)] + O(x^2) \quad (5.3.63)$$

## Chapter 5. Injecting the UV into the Bootstrap: Ising Field Theory

---

with

$$\alpha_1(s) = \frac{\beta(s)}{(s-3)(s-1)} - \frac{\beta(3)}{2(s-3)} + \frac{\beta(1)}{2(s-1)}, \quad \beta(s) = -\frac{2}{\pi} \sqrt{\frac{s(4-s)}{3}} \arctan \sqrt{\frac{s}{4-s}}. \quad (5.3.64)$$

Let us now take the limit  $x \rightarrow 0$  of the polynomial  $P(s) = 1 - bs$  in (5.3.60), where  $b$  is given by (5.3.49). We have

$$b = 1 + x \frac{\tilde{g}_F e^{\alpha(0) - \alpha(1)}}{2} + O(x^2) = 1 + x \frac{\tilde{g}_F}{\sqrt{3}} + O(x^2) \quad (5.3.65)$$

where we made use of (5.3.63).

We then have

$$\frac{P^2(s) e^{2\tilde{\alpha}(s)}}{(1-s)^2} = \frac{s-4}{4} + x(s-4) \left[ \frac{\sqrt{3}\tilde{g}_F s}{6(s-1)} + \frac{\text{Re}[\alpha_1(s) - \alpha_1(0)]}{2} \right] + O(x^2). \quad (5.3.66)$$

Now, replacing the above formulas into (5.3.60) and performing the simple integrals, we find

$$c_{UV} - \frac{1}{2} = x \left[ 2\sqrt{3}\pi \tilde{g}_F^2 + (4\sqrt{3} - 2\pi) \tilde{g}_F - \frac{126 - 23\sqrt{3}\pi}{81} - \frac{2}{\sqrt{3}\pi} I_t \right] + O(x^2). \quad (5.3.67)$$

where

$$I_t = \int_4^\infty \frac{s-4}{s^2(s^2-4s+3)} \log \left( \frac{\sqrt{s-4} + \sqrt{s}}{2} \right) ds = \frac{23}{648} \pi^2 - \frac{1}{3}. \quad (5.3.68)$$

Notice that setting  $x = 0$  in (5.3.67) leads necessarily to  $c_{UV} = 1/2$ , the central charge of the free fermion. Since we are studying IFT we set  $c_{UV} = 1/2$  regardless, which leads to a quadratic equation for the rate  $\tilde{g}_F$  with the following roots

$$\tilde{g}_F^{(\pm)} = \frac{1}{2\sqrt{3}} - \frac{1}{\pi} \pm \frac{1}{\sqrt{3}\pi} \mp \frac{1}{9} = (-0.1023000, +0.0430304) \quad (5.3.69)$$

To express this in terms of the magnetic field  $h$  we make use of the relation  $x = 36\sqrt{3}(\mathcal{F}_1^\sigma)^2 h^2$ , where  $\mathcal{F}_1^\sigma = 1.3578$ , to find the rates,

$$g_F^{(\pm)} = x \tilde{g}_F^{(\pm)} = (-11.7601, +4.9466) h^2. \quad (5.3.70)$$

**Extra zeros.** Let us now see what we can say about potential extra zeros of the IFT S-matrix in the small magnetic field limit  $h \rightarrow 0$ .

For the case of IFT at lowest order in  $h^2$  we have [229] (see also eqs. (D.4.51) and (D.4.52))

$$S_{\text{IFT}}(s) = -1 - ih^2 \sqrt{(s-4)s} \left( \frac{72(\mathcal{F}_1^\sigma)^2}{s^2 - 4s + 3} + \int_4^\infty \frac{(s'-2)\sigma_{2\rightarrow 3}(s') ds'}{\pi \sqrt{(s'-4)s'(s'-s)(s+s'-4)}} \right) + O(h^4) \quad (5.3.71)$$

with  $\sigma_{2\rightarrow 3}(s)$  given by eq. (D.4.54).

Let us now match eq. (5.3.71) with the general nonperturbative solution to unitarity and crossing symmetry. In  $d = 2$  unitarity reads

$$|S(s)|^2 = 1 - \sigma_{inel}(s) \quad (5.3.72)$$

where  $\sigma_{inel}(s) > 0$  is the particle production cross-section. The general solution to this equation and crossing symmetry  $S(s) = S(4m^2 - s)$  reads [230, 231, 232]

$$S(s) = S_{CDD}(s) \exp \left[ \int_{4m^2}^\infty \frac{ds'}{2\pi i} \log(1 - \sigma_{inel}(s')) \sqrt{\frac{s(s-4m^2)}{s'(s'-4m^2)}} \left( \frac{1}{s'-s} + \frac{1}{s'-(4m^2-s)} \right) \right] \quad (5.3.73)$$

where  $|S_{CDD}(s)|^2 = 1$ . Now,  $S_{CDD}(s)$  can be any product of CDD factors. In particular for IFT, it should include the CDD pole at  $s = m^2 = 1$  and the CDD zero (5.2.5). So we take

$$S_{CDD}(s) = S_-(s) \frac{\sqrt{a(4-a)} - \sqrt{s(4-s)}}{\sqrt{a(4-a)} + \sqrt{s(4-s)}} \frac{\sqrt{b(4-b)} - \sqrt{s(4-s)}}{\sqrt{b(4-b)} + \sqrt{s(4-s)}} \dots \quad (5.3.74)$$

with  $S_-(s)$  given by eq. (5.3.40) and the remaining zeros  $a, b, \dots$  we wish to constrain as  $h \rightarrow 0$ .

Letting  $\sigma_{inel} = h^2 \sigma_{2\rightarrow 3} + O(h^4)$  and expanding (5.3.73) at small  $h$ , assuming  $a = a_0 h^{-2} + O(h^{-4})$ , and likewise for  $b$  and etc, we find

$$S(s) - S_{\text{IFT}}(s) = 2h^2 \sqrt{s(s-4)} (|a_0| + |b_0| + \dots) + O(h^4) \quad (5.3.75)$$

Since  $S(s)$  and  $S_{\text{IFT}}(s)$  must match at order  $h^2$  we see that  $a_0 = b_0 = \dots = 0$ .

In case the zeros are complex we must have  $a = b^*$  so that  $S_{CDD}$  is real. Letting  $a_0 = \alpha + i\beta$ , and  $b_0 = \alpha - i\beta$  we have

$$|a_0| + |b_0| = \sqrt{\alpha^2 + \beta^2} + \sqrt{\alpha^2 + \beta^2} = \sqrt{\alpha^2 - \beta^2 + 2i\alpha\beta} + \sqrt{\alpha^2 - \beta^2 - 2i\alpha\beta} = 2|\alpha| \quad (5.3.76)$$

Meaning that  $\alpha = 0$ , but the imaginary part  $\beta$  of the zeros is unconstrained.

Therefore, the (real part of the) extra zeros must go to infinity at least as  $\sim h^{-4}$  when  $h \rightarrow 0$ .

## 5.4 Discussion

In this work we have merged the primal S-Matrix and form factor bootstrap proposed in [216] with the dual S-Matrix bootstrap developed in [211]. With our method we can relate UV data, namely the central charge  $c_{UV}$  of the UV CFT, with couplings of the gapped QFT in the IR, and place rigorous bounds on any of these parameters. We observe a vastly improved numerical convergence compared to the primal bootstrap of [216].

We established a lower bound on  $c_{UV}$  in a class of  $\mathbb{Z}_2$  symmetric QFTs (fig. 5.4) and also for QFTs for which the particle self-interacts with a cubic coupling and where the S-matrix has a real zero (a dial for the magnetic field in IFT) - see fig. 5.12. In all these cases we find that the optimal S-matrix extremizes some coupling. This allows us to find the optimal S-matrix via pure analytical S-matrix bootstrap (viz. CDD bootstrap [233]). Then, in appendix 5.3, we showed how the form factor and the minimal  $c_{UV}$  can be obtained analytically if the S-matrix is known. We find perfect agreement between the dual optimization and the analytical bootstrap.

To specifically target Ising Field Theory we fix  $c_{UV} = 1/2$  and find the allowed space in cubic couplings and magnetic field, see fig 5.17. We insert IFT inside this ‘pyramid’ for small magnetic field - close to the tip of the pyramid - using form factor perturbation theory (see appendix D.4). For larger magnetic fields we enter the non-perturbative regime of IFT and this is where our results can be useful: IFT *must* lie somewhere inside the pyramid.

We know however that IFT cannot lie on the boundary of the pyramid because the boundary is elastic: the optimal S-matrix does not have inelasticity, and we know that IFT has particle production [229]. But even for small enough magnetic field  $h$  (where particle production is negligible) IFT is still somewhat away from the boundary, as the bounds on the one particle form factor go to zero as  $h^2$  with a different numerical coefficient than the perturbative form factor (see fig. 5.22).

We can think of several ways to improve our setup and ‘shrink’ the pyramid wherein IFT must lie. One way is to include more UV information. So far we are only fixing the value of the central charge, but we are not ‘telling’ the bootstrap that the RG flow is being triggered by the thermal and magnetic deformations,  $\epsilon$  and  $\sigma$ , respectively. The central charge is straightforward to include in  $d = 2$  due to the  $c$ -sum rule which gives an *integrated* relation over the spectral density of the trace of the stress energy tensor  $\Theta$ , and not just via some asymptotic constraint at  $s \rightarrow \infty$ , which is difficult to implement numerically.<sup>16</sup> So, can we find similar integral relations that involve somehow  $\epsilon$  or  $\sigma$  (besides the combination  $\Theta$ )? One possibility is the sum rule derived in Eq. (29) of [192] to fix the scaling dimension of an operator. However, this sum rule requires knowing the vacuum expectation value of that operator. For the case of  $\sigma$ , its expectation value should be related to the magnetic field and therefore to the zero of the S-matrix, but the precise relation is unknown to us. It should be possible to measure it using

---

<sup>16</sup>Moreover, the normalization of the two particle form factor of  $\Theta$  is fixed (see appendix D.6), which is one less parameter to vary over in the bootstrap.

other methods like the lattice or Hamiltonian truncation.

Another possibility is to use the twist property of the order field  $\sigma$ . Twist fields are reviewed in [234, 235] and references therein. The fact that  $\sigma$  acts as a twist field is derived in [236]. This could be coupled to the input from lattice measurements, for example using tensor networks. In order to measure the two point function  $\langle \sigma \Theta \rangle$  on the lattice, one needs to map the continuum stress tensor to the lattice stress tensor. This might be done by generalizing some ideas developed in [237] and [238]. We plan to explore this direction in the near future.

In addition, we can include more IR information. IFT is known to interpolate between the free massive Majorana fermion and the  $E_8$  Toda theory, which has 8 particles. While we are studying the region close to the free fermion, where there is only one particle, it is natural to expect, due to analyticity, that the other particles exist in other ‘sheets’, i.e. as resonances (corresponding to zeros on the physical sheet). We already impose one zero, which eventually becomes the second lightest particle as the magnetic field is increased. It is possible that the other particles imply the presence of further zeros on the physical sheet [221].

If we are feeling brave, we can dial the magnetic field a bit higher and go to the regime where more particles are stable. If we want to go beyond lightest particle scattering we would have to import the multiple amplitude bootstrap of [135] and extend it in several directions. Namely, to dualize it, to include form factors and, on a more fundamental level, to understand the singularity structure of the scattering amplitude of heavier particles, where anomalous thresholds are expected (see previous chapter) [158, 239].

In a similar vein, we can also consider multi-particle scattering, i.e. to not only consider 2-particle states but also states of 3- or more particles. In this way we could try target the inelasticity of IFT. However, a systematic understanding of the analyticity structure of multi-particle amplitudes remains a big open problem dating back to the 60s.

The latter directions we have mentioned are of course relevant to many other QFTs besides IFT. We have put a lower bound on the  $c_{UV}$  of a class of  $\mathbb{Z}_2$  symmetric theories but we could have chosen to be more specific. For example, it would be interesting to target  $\phi^4$  which has been the focus of many recent nonperturbative studies [240, 241, 242, 243, 244, 245, 202, 246]. This theory is a deformation of the free massless boson, so we could fix  $c_{UV} = 1$  in our  $\mathbb{Z}_2$  symmetric setup to target it. Moreover, we could place  $\phi^4$  inside our bounds, not only using perturbation theory but also with Hamiltonian truncation data [202].

Finally, it would be interesting to generalize our setup to higher dimensions. A primal approach incorporating UV input via the  $a$ -anomaly was developed in [203]. Can we reproduce these bounds more rigorously and more efficiently with a dual method?



# 6 Conclusion: Past, Present and Future of the S-matrix Bootstrap

## 6.1 Pre-Asymptotic freedom period

The original idea of directly constraining the S-matrix can be traced back to Heisenberg's paper of 1943 *The "Observable Quantities" in the Theory of Elementary Particles* [247]. In view of "the known divergence difficulties in the theory of elementary particles" Heisenberg calls for an effort to "isolate from the conceptual nature of quantum theory of wave fields those concepts which will probably not be affected by future modification". Heisenberg focus on what special relativity and quantum mechanics imply for the general structure of the S-matrix, emphasizing crucial differences with respect to the non-relativistic case, in particular the possibility of "emission of particles" and how unitarity becomes a non-trivial constraint. Heisenberg asserts that "finding the other conditions [on the S-matrix] seems to me to be the central, as yet completely unresolved problem of the theory of elementary particles".<sup>1</sup>

The S-matrix program however needed at least another decade to start being considered as a serious alternative to quantum field theory. With the experimental discoveries of hadrons in the late 1950s, S-matrix proponents advocated for "nuclear democracy" [2] in that an understanding of the origin of the strong force may not be required in order to describe the observed hadronic physics.

I think it is fair to say that the S-matrix theory developed over four main fronts:

1. The approach notably pursued by French researchers of rigorously deriving S-matrix principles from axiomatic quantum field theory. In particular, how field-theoretic properties such as micro-causality and CPT invariance lead to the analyticity properties of the S-matrix (see overview on Chapter 2). The two biggest achievements are arguably the proof of the Froissart-Martin bound on the total 2-body scattering cross-section [34] and the proof of crossing symmetry by Bros, Epstein and Glaser [29, 31].
2. The understanding of the analyticity of scattering amplitudes from perturbation theory.

---

<sup>1</sup>Translated from German.

## Conclusion

---

This approach was popularized by the Cambridge group that included Eden, Landshoff, Olive and Polkinghorne, whose efforts are summarized in their book [8] and have arguably led to limited results.<sup>2</sup> But also on the other side of the Iron Curtain, by the likes of Landau, Gribov, Kolkunov, Okun, Rudik, and many others (see chapter 3 for some of these works), who focused more on the actual computation of Landau singularities.

3. The more constructive approach that makes use of stronger analyticity assumptions, such as maximal analyticity, typically together with elastic unitarity and further input from experiment such as scattering lengths. Spearheaded by Chew and Mandelstam on the American side, this approach conventionally involves the use of dispersion relations such as the Mandelstam representation (see [2] for a nice overview). The biggest early achievement was likely Frazer and Fulco's prediction of the  $\rho$  meson [249].
4. Regge theory and the exploration of the angular momentum complex plane. This approach gained popularity first with Chew and Frautschi's realization that mesons lie on linear Regge trajectories [250, 251] and then with Gribov's identification of the pomeron trajectory which could explain the rise of the total scattering cross-section and the shrinkage of the diffractive cone of the differential cross-section [11].

Naturally this distinction is only true to some extent as many authors worked on and combined several of these ideas/approaches, as illustrated in chapter 2. One such example, which has to be mentioned, is of course Veneziano's construction of a crossing-symmetric and unitary meromorphic amplitude whose poles lie on linear Regge trajectories [252]. Many of the original results of this thesis also came from this fruitful interplay.

## 6.2 Post-Asymptotic freedom period

Despite the initial promise, imposing all the constraints in a predictive way proved increasingly difficult and eventually the observation of deep inelastic scattering led to strong support in favor of the parton model. The 'killing blow' came shortly after with the discovery of asymptotic freedom in '72 essentially confirming QCD as the underlying field theory and allowing the use of Feynman perturbation theory at high energies.

A couple of amusing quotes illustrate well the situation at the time.

"Unfortunately to use these assumptions it was necessary to make uncontrolled approximations, such as the strip approximation, whose mention will bring tears to the eyes of those of us who are old enough to remember it. By the mid-1960's it was clear that S-matrix theory had failed in dealing with the one problem it had tried hardest to solve, that of  $\pi\pi$  scattering." - Weinberg [253].

---

<sup>2</sup>Regge's review [8] illustrates this point: "I am personally unsatisfied by the status of the theory expressed in chapter 2. My feeling is that chapter 2 will have to be replaced in the future by more advanced techniques borrowed from algebraic homology [...]. Until that day the best we have is a sort of heuristic theory that becomes rapidly inadequate for higher-order graphs." [248]



“Ironically, [the  $\rho$ -meson] was one of the very few quantitative predictions the theory ever produced. Some years later, Sidney Coleman introduced me to give a seminar at Harvard as *Bill Frazer, whose work set back the progress of physics by ten years.*” - Frazer [254].

Nonetheless, QCD is not applicable at low energies, and the S-matrix bootstrap methods kept being applied to the description of hadron scattering. The direction outlined in point 3. is still an active and useful topic of research today (see brief overview in chapter 4) namely in the development of partial wave dispersion relations [255] which are able to capture - given enough low energy data - further resonances beyond the  $\rho$ , including the elusive  $\sigma$  meson [189].

The approach outlined in point 4. naturally evolved in the direction of trying to explain some aspects of Regge phenomenology with perturbative QCD (see [256] for a review). The most well-known attempt consists of the BFKL pomeron which resums ladder diagrams but whose exact relation to the original “soft” pomeron is still unclear.

Another direction (a very famous one!) which stemmed from Regge theory and, in particular, Veneziano’s seminal work [252] is of course String theory, from the observation that rotating strings realize linear Regge trajectories (see [257] for an historical perspective on the early days of String theory).

From points 1. and 2. on the analyticity properties of scattering amplitudes from either axiomatic QFT or perturbation theory, respectively, very little was achieved afterwards. Sommer’s 1970 review on the “Present State of Rigorous Analytic Properties of Scattering Amplitudes” [27] is still very much “Present”. Limited progress can be said to have been achieved on the perturbation theory side and Regge’s comment still applies to some extent (see footnote 2). Of worth mentioning is Pham’s work (see [258] for a recent review).

On the other hand, the idea of imposing constraints on the S-matrix at the perturbative level, unitarity in particular, turned out to be very useful in the 90s and has since led to a revolution in Feynman diagram computation and simplification (see brief overview in section 1).

Moreover, with the understanding of effective field theories, the use of dispersion relations regained popularity as the Wilson coefficients could be directly related to the UV amplitude [259]. This in turns constrains the possible space of EFTs compatible with a physically healthy UV completion, the so-called positivity bounds.

At the nonperturbative level, the bootstrap idea was shown to be vastly more practical once applied to physical systems enjoying a higher degree of symmetry: Integrable models in  $d = 2$ , which do not have particle production and satisfy an additional set of constraints known as Yang-Baxter equations (see [21] for a review); and conformal field theories, starting with the seminal works of Polyakov [260] and the BPZ paper [261] which paved the way for conformal bootstrap in  $d = 2$ . The conformal bootstrap in  $d > 2$  only came to fruition more than three decades later where 3D Ising the CFT was unexpectedly found to lie at a ‘kink’ of the allowed

## Conclusion

---

space giving the best estimate to date of the critical exponents of the 3D Ising model (see [13] for a recent review).

The success of the conformal bootstrap inspired a return of the more formally oriented high-energy theory community to the S-matrix bootstrap in the hopes of replicating the success of the conformal bootstrap for gapped theories and find a QFT at some corner of the allowed space. Taking the risk of annoying my own community I have to say that this has not turned out quite right (yet).

### 6.3 Modern day S-matrix Bootstrap

The present numerical S-matrix bootstrap is essentially based on an explicit decomposition of the amplitude over a complete set of basis functions on top of which the  $2 \rightarrow 2$  bootstrap constraints are imposed. Then, couplings - values of the amplitude in the Euclidean region - are extremized. What is found is that optimal amplitudes at the boundary of the allowed space look purely elastic (up to numerical precision).

In  $d = 2$  these extremal elastic amplitudes can be perfectly healthy as they may correspond to integrable QFTs. Indeed, had we not known beforehand of the existence of integrable theories, we could have found them for the first time in this way (and bump into Yang-Baxter!) [17, 137]. In  $d > 2$ , however, purely elastic S-matrices are not allowed (see chapter 2) so it is unclear as to whether these extremal solutions correspond to any physical theory. It seems very plausible that the extremal boundary is unphysical and would get entirely excluded by adding multi-particle constraints.

It is hard to analytically quantify how much inelasticity would be required (as the lower bound is only at infinite angular momentum). Likewise the numerical amplitudes are hard to analyze on the physical region as the sum over basis functions is not guaranteed to converge there. However, this question was recently tackled in the work [80] which showed indeed the presence of a small bump of inelasticity at finite energies at least in some portion of the extremal boundary, by explicitly constructing an amplitude satisfying elastic unitarity.

Regardless of the ‘unphysical’ nature of the extremal boundary, the obtained bounds can be said to be ‘rigorous’ (more on this below) and, in many cases, appear to sit close to physical theories. For example, it comes to mind the recent work [262] which minimizes the leading Wilson coefficient that controls the first correction to maximal supergravity which deviates by  $\sim 1\%$  from the unique value coming from M-theory (the difference possibly coming from inelasticity due to black hole production).

Since the revival papers of 2016 [1, 17] a variety of QFTs have been targeted and compared with the numerical bootstrap bounds (please refer to [3] for an extensive list) and, it is fair to say, the general feeling among the S-matrix bootstrap community is that it is getting increasingly harder to find interesting problems that could be targeted by a bootstrap approach that only

constrains the  $2 \rightarrow 2$  scattering amplitude.

### 6.4 Have we exhausted the $2 \rightarrow 2$ space of constraints?

I now want to argue that is not the case (yet) and that, in my view, there is still a lot to explore.

Can we put a bound on the cross-section? The most famous result from the bootstrap of the 60s is arguably the Froissart-Martin bound on the total cross-section, which only makes partial use of the  $2 \rightarrow 2$  constraints, namely unitarity and axiomatic analyticity. It is unknown to this day whether maximal analyticity and crossing-symmetry could improve the Froissart bound. More generally, can we bound the amplitude on the physical region?

This class of problems seems hard to attack with the current *primal* formulation of the S-matrix bootstrap. This is due to two limitations. One is the fact that the truncated ansatz cannot grow at large energies, and therefore would have trouble in replicating a Froissart-like growth, and the second is the already mentioned possible lack of convergence of the ansatz on the physical region which can lead to computational difficulties.

In principle, these two issues could be solved either with a better ansatz or alternatively with a dual bootstrap formulation as employed in chapter 5. Indeed the central charge is sort of a ‘cross-section’ as in it takes values over an interval *on* the physical region, and in this case the dual formulation really made a difference compared to the previously attempted primal approach [136]. A dual formulation in  $d > 2$  that implements maximal analyticity however still remains at large.

Having a dual formulation would be extremely useful as the coupling space could be *carved out* similarly to the conformal bootstrap instead of *filled in* as with a primal approach. A natural concern is that the current primal ansatz can only explore a subspace of the full allowed space, owing to its lack of growth when truncated.

Another avenue continues to be the bootstrap of low energy QCD and making contact with experiment. Just last year, from the JPAC collaboration: “We highlight the need for the development of comprehensive amplitude analysis methods to further our understanding of hadron spectroscopy. Reaction amplitudes constrained by first principles of S-matrix theory and by QCD phenomenology are needed to extract robust interpretations of the data from experiments and from lattice calculations.” [263]

A recent good step in this direction was made in [264] in which the authors made use of the S-matrix/form factor bootstrap outlined in chapter 5 and included UV information via QCD sum rules.

### 6.5 Some big open problems

Let me now briefly enumerate some of the biggest open problems in S-matrix theory whose solution should involve some new conceptual insight (no effort will be made in giving a complete list of references at this point).

- *The multi-particle frontier.* As already mentioned, being able to bootstrap the multi-particle amplitude would allow to further constrain the  $2 \rightarrow 2$  amplitude, but also put bounds on other observables such as higher point Wilson coefficients. Here the challenges are multiple (pun intended), from the analyticity and crossing properties of multi-point amplitudes to the computational hassle of dealing with unitarity constraints involving multivariable integrals. Some references on previous attempts can be found in chapter 3 (see also the recent work [265]).
- *Analyticity VS Causality.* The relationship between causality and analyticity continues to be mostly unclear as little to no progress has been made since the original axiomatic attempts. One recent avenue seems to be the approach of starting from CFT axioms and take the flat-space limit of AdS [3], but it is still too early to tell what will be rigorously learned. Alternatively, in the spirit of the modern on-shell perspective we should perhaps rethink of causality not as some statement on the field correlator but on the scattered ‘wavepacket’ [266].
- *IR finite S-matrices.* Unfortunately, in the four space-time dimensions that we live in, there is no concept of a scattering amplitude involving (non-derivatively coupled) massless particles. Current understanding is that inclusive quantities, such as cross-sections, are IR finite (at least in QED). Using coherent or ‘dressed’ states we can also correct for the IR divergence, but it is still unclear what are the physical constraints obeyed by these objects, and how they can be used in practice for bootstrap purposes.

### 6.6 Epilogue: The on-shell promise

It is often heard the complaint that the 60s and 70s were a much better period to be a theoretical physicist given the abundance of experimental discoveries at the time compared to today. Indeed, LHC only discovered the Higgs boson which had already been predicted five decades before - with so far no sign of supersymmetry or extra dimensions - and more recently LIGO with the observation of gravitational waves that is giving even more support to general relativity while ruling out some of its alternatives.

I find it amazing on the other hand that we were able to make so many predictions out of such a convoluted and mathematically deficient formalism. The fact that the question "What are the equations of motion of QFT?" does not have an immediate answer is a symptom of this. At EPFL, and I imagine the situation is not so different in most places, the vast majority of the two QFT courses is spent on the free theory and only at the end of the year do students get to

do some tree-level Compton scattering. Of course quantum field theory is very hard to teach, not because it is inherently hard but as a result of being phrased in the wrong language.

This is evident once after all the pain of going through archaic canonical quantization, gauge fixing of the Maxwell field and all the Wick contractions, the final answer for the probability amplitude of Coulomb scattering is a simple pole in the Lorentz invariant “momentum transfer”  $t$ . Could it have been something more complicated, e.g. a double pole? No, otherwise unitarity (or “factorization”) would have been violated.

If Heisenberg and Chew’s original idea of directly constraining the S-matrix to circumvent the lack of our understanding of the elementary theory of particles did not exactly pan out as they perhaps envisioned, ironically today the paradigm is somewhat inverted. Our understanding of QFTs, especially effective field theories, has been greatly improved by the use of the S-matrix principles.

There is a rising feeling, particularly among the Amplitudes community, that there might be an on-shell formulation of QFT just around the corner. A framework that makes no mention to the Lagrangian and is purely based on the S-matrix. In fact, already in the 60s Landau believed that “the Lagrangian is dead and should be buried with all due honors” [267].<sup>3</sup> After almost three centuries of being a staple in theoretical physics, the Lagrangian appears to start breaking through the seams. Coincidentally in a period where we lack new experimental stimuli and can fully focus on finding an appropriate replacement. This seems too big of an opportunity to miss.

The Lagrangian keeps on limping, but for how long?

---

<sup>3</sup>although at that time he was probably referring to the Landau pole of QED.



# A Appendix to Chapter 2

## A.1 Derivation of the Mandelstam Kernel

In this appendix we compute the kernels  $\mathcal{P}_d(z, z', z'')$  and  $K_d(z, \eta', \eta'')$  defined in (2.2.20) and (2.3.3) correspondingly.

**The kernel  $\mathcal{P}_d(z, z', z'')$**  Recall that  $z'$  and  $z''$  are cosine of the angles between  $\vec{n}$  in (2.2.20) and the vectors  $\vec{p}_1$  and  $\vec{p}_3$ , (2.2.19). They are related to the coordinates in the Sudakov decomposition of the unit vector  $\vec{n}$

$$\vec{n} = \alpha \frac{\vec{p}_1}{|\vec{p}_1|} + \beta \frac{\vec{p}_3}{|\vec{p}_3|} + \vec{n}_\perp, \quad \vec{n}_\perp \cdot \vec{p}_1 = \vec{n}_\perp \cdot \vec{p}_3 = 0 \quad (\text{A.1.1})$$

as

$$z' = \alpha + \beta z, \quad z'' = \beta + \alpha z, \quad \alpha = \frac{z' - z z''}{1 - z^2}, \quad \beta = \frac{z'' - z z'}{1 - z^2}. \quad (\text{A.1.2})$$

In term of these coordinates, the angular integration in (2.2.20) reads

$$\begin{aligned} \int d^{d-2} \Omega_{\vec{n}} &= 2 \int d^{d-1} \vec{n} \delta(\vec{n}^2 - 1) \\ &= 2 \sqrt{1 - z^2} \int d\alpha d\beta d^{d-3} \vec{n}_\perp \delta(\vec{n}_\perp^2 + \alpha^2 + \beta^2 + 2\alpha\beta z - 1) \\ &= 2 \sqrt{1 - z^2} \int d\alpha d\beta \frac{\Theta(1 - \alpha^2 - \beta^2 - 2\alpha\beta z)}{(1 - \alpha^2 - \beta^2 - 2\alpha\beta z)^{\frac{5-d}{2}}} \int d^{d-3} \vec{n}_\perp \delta(\vec{n}_\perp^2 - 1), \\ &= \sqrt{1 - z^2} \text{Vol}_{S^{d-4}} \int d\alpha d\beta \frac{\Theta(1 - \alpha^2 - \beta^2 - 2\alpha\beta z)}{(1 - \alpha^2 - \beta^2 - 2\alpha\beta z)^{\frac{5-d}{2}}}, \end{aligned} \quad (\text{A.1.3})$$

where  $\text{Vol}_{S^{d-4}} = \frac{2\pi^{(d-3)/2}}{\Gamma(\frac{d-3}{2})}$ . The above formula is only true in  $d \geq 4$ . In  $d = 3$  we have

$$\int d\Omega_{\vec{n}} = 2 \int d^2 \vec{n} \delta(\vec{n}^2 - 1) = 2 \sqrt{1 - z^2} \int d\alpha d\beta \delta(\alpha^2 + \beta^2 + 2\alpha\beta z - 1), \quad (\text{A.1.4})$$

## Appendix A. Appendix to Chapter 2

---

which can be also obtained as a distributional limit from (A.1.3) when  $d \rightarrow 3$ . By plugging the relation (A.1.2) into (A.1.3) and (A.1.4), we arrive at (2.2.21).

**The Mandelstam kernel**  $K_d(z, \eta', \eta'')$  Instead of plugging the explicit form of  $\mathcal{P}_d(z, z', z'')$  into the definition (2.3.3), we have find it simpler to compute the Mandelstam kernel directly using the Sudakov decomposition (A.1.1). For  $|\eta'|, |\eta''| > 1$  we have

$$\begin{aligned} K_d(z, \eta', \eta'') &= \int \frac{d^{d-2} \Omega_{\vec{n}}}{(\eta' - z')(\eta'' - z'')} = \int \frac{d^{d-2} \Omega_{\vec{n}}}{(\eta' - \alpha - z\beta)(\eta'' - \beta - z\alpha)} \\ &= \sqrt{1 - z^2} \text{Vol}_{S^{d-4}} \int \frac{\Theta(1 - \alpha^2 - \beta^2 - 2\alpha\beta z)}{(1 - \alpha^2 - \beta^2 - 2\alpha\beta z)^{\frac{5-d}{2}}} \frac{d\alpha d\beta}{(\eta' - \alpha - z\beta)(\eta'' - \beta - z\alpha)}, \end{aligned} \quad (\text{A.1.5})$$

where in the second step we have used (A.1.2) with  $d \geq 4$  and in the third we have used (A.1.3).

Next, we shift  $\alpha \rightarrow \alpha - z\beta$  and after it we rescale  $\beta \rightarrow \frac{\beta}{\sqrt{1-z^2}}$ . In this way we get in  $d > 3$

$$\begin{aligned} K_d(z, \eta', \eta'') &= \text{Vol}_{S^{d-4}} \int d\alpha d\beta \frac{\Theta(1 - \alpha^2 - \beta^2)}{(1 - \alpha^2 - \beta^2)^{\frac{5-d}{2}}} \frac{1}{(\eta' - \alpha)(\eta'' - \sqrt{1 - z^2}\beta - z\alpha)} \\ &= \text{Vol}_{S^{d-4}} \int_0^1 dr \int_0^{2\pi} d\phi \frac{r}{(1 - r^2)^{\frac{5-d}{2}}} \frac{1}{(\eta' - r \cos \phi)(\eta'' - r \cos(\phi + \theta))}, \end{aligned} \quad (\text{A.1.6})$$

where  $re^{i\phi} = \alpha - i\beta$ . The integral over  $\phi$  gives

$$\int_0^{2\pi} \frac{d\phi}{(\eta' - r \cos \phi)(\eta'' - r \cos(\phi + \theta))} = \frac{2\pi}{\eta' \eta'' + \sqrt{(\eta'^2 - r^2)(\eta''^2 - r^2)} - zr^2} \left[ \frac{\eta'}{\sqrt{\eta'^2 - r^2}} + \frac{\eta''}{\sqrt{\eta''^2 - r^2}} \right]. \quad (\text{A.1.7})$$

for  $|\eta'|, |\eta''| > 1$ . Otherwise, we analytically continue (A.1.7). Next, we change the  $r$  integration variable to

$$\eta \equiv \frac{1}{r^2} \left( \eta' \eta'' + \sqrt{(\eta'^2 - r^2)(\eta''^2 - r^2)} \right). \quad (\text{A.1.8})$$

In that way we arrive at

$$K_{d \geq 4}(z, \eta', \eta'') = 2\pi \text{Vol}_{S^{d-4}} \int_{\eta_+}^{\infty} \frac{d\eta}{\eta - z} \frac{(\eta^2 - 1)^{\frac{4-d}{2}}}{(\eta - \eta_+)^{\frac{5-d}{2}} (\eta - \eta_-)^{\frac{5-d}{2}}}, \quad |\eta'|, |\eta''| > 1, \quad (\text{A.1.9})$$

where  $\eta_{\pm}$  are defined in (2.3.5).



## A.2 Useful Identities for Gegenbauer $P$ - and $Q$ -functions

Similarly, for  $d = 3$  we have

$$\begin{aligned}
 K_3(z, \eta', \eta'') &= 2\sqrt{1-z^2} \int d\alpha d\beta \frac{\delta(\alpha^2 + \beta^2 + 2\alpha\beta z - 1)}{(\eta' - \alpha - z\beta)(\eta'' - 2\beta - z\alpha)} \quad (\text{A.1.10}) \\
 &= 2 \int d\alpha d\beta \frac{\delta(\alpha^2 + \beta^2 - 1)}{(\eta' - \alpha)(\eta'' - \sqrt{1-z^2}\beta - z\alpha)} = \int_0^{2\pi} \frac{d\phi}{(\eta' - r \cos \phi)(\eta'' - r \cos(\phi + \theta))} \\
 &= \frac{2\pi}{\eta_+ - z} \left( \frac{\eta'}{\sqrt{\eta'^2 - 1}} + \frac{\eta''}{\sqrt{\eta''^2 - 1}} \right), \quad |\eta'|, |\eta''| > 1.
 \end{aligned}$$

Finally, the Mandelstam kernel with  $|\eta'| < 1$  or  $|\eta''| < 1$  is obtained from (A.1.9) and (A.1.10) by analytical continuation.

## A.2 Useful Identities for Gegenbauer $P$ - and $Q$ -functions

As discussed in the main text, due to the  $SO(1, d-1)$  symmetry, the elastic unitarity kernel and the Mandelstam kernel are diagonal in spin. They take the form (2.2.36) and (2.3.6) correspondingly. In this appendix we derive these forms together with the related integrated expression (2.3.18).

The literature on the properties and identities of the Gegenbauer functions is extensive [268], starting with the Gegenbauer addition formula. Better suited for us is the integrated form of this identity [268] which in our conventions reads

$$2^{4-d} \frac{\Gamma(d-3)}{\Gamma^2(\frac{d-3}{2})} \int_{-1}^1 dz P_J^{(d)} \left( z_1 z_2 + z \sqrt{1-z_1^2} \sqrt{1-z_2^2} \right) (1-z^2)^{\frac{d-5}{2}} = P_J^{(d)}(z_1) P_J^{(d)}(z_2). \quad (\text{A.2.1})$$

Perhaps the cleanest way to derive the above formula is to use group theoretic techniques. If  $z_1$  and  $z_2$  are the cosines of the polar angles of unit vectors  $\mathbf{n}_1$  and  $\mathbf{n}_2$  and  $z$  is the cosine of the azimuthal angle difference between  $\mathbf{n}_1$  and  $\mathbf{n}_2$ , then  $z_1 z_2 + z \sqrt{1-z_1^2} \sqrt{1-z_2^2} = \mathbf{n}_1 \cdot \mathbf{n}_2$ . One can then apply a rotation to make  $\mathbf{n}_2$  aligned along the  $z$ -axis, as the vector product is invariant under this transformation. The relation between  $P_J^{(d)} \left( z_1 z_2 + x \sqrt{1-z_1^2} \sqrt{1-z_2^2} \right)$  and  $P_J^{(d)}(z_2)$  will then involve the  $SO(d-1)$  matrix representation of this rotation, the Wigner  $D$ -matrix, which for a specific entry is given up to a factor by  $P_J^{(d)}(z_1)$ . The integration in  $z$  will select this entry and project out the others, so we end up with a closed equation between Gegenbauer polynomials.

Let us change variable to

$$y = z_1 z_2 + z \sqrt{1-z_1^2} \sqrt{1-z_2^2} \quad (\text{A.2.2})$$

## Appendix A. Appendix to Chapter 2

---

with integration limits

$$z_1 z_2 - \sqrt{1 - z_1^2} \sqrt{1 - z_2^2} < y < z_1 z_2 + \sqrt{1 - z_1^2} \sqrt{1 - z_2^2}, \quad (\text{A.2.3})$$

or equivalently,

$$1 - z_1^2 - z_2^2 - y^2 + 2y z_1 z_2 > 0. \quad (\text{A.2.4})$$

The Gegenbauer addition formula then becomes

$$\frac{1}{2} \pi^{\frac{2-d}{2}} \Gamma\left(\frac{d-2}{2}\right) \int_{-1}^1 dy \mathcal{P}_d(y, z_1, z_2) (1 - y^2)^{\frac{d-4}{2}} P_J^{(d)}(y) = (1 - z_1^2)^{\frac{d-4}{2}} P_J^{(d)}(z_1) (1 - z_2^2)^{\frac{d-4}{2}} P_J^{(d)}(z_2), \quad (\text{A.2.5})$$

with  $\mathcal{P}_d$  given in (2.2.21).

Multiplying the above by  $n_J^{(d)} P_J^{(d)}(z)$  and summing over  $J$  allows usage of the Gegenbauer completeness relation

$$\sum_{J=0}^{\infty} n_J^{(d)} P_J^{(d)}(y) P_J^{(d)}(z) = \frac{2}{\mathcal{N}_d} (1 - z^2)^{\frac{4-d}{2}} \delta(y - z), \quad (\text{A.2.6})$$

with  $n_J^{(d)}$  given by (2.2.29). We then arrive at

$$\mathcal{P}_d(z, z', z'') = (4\pi)^{d-2} \mathcal{N}_d^2 (1 - z'^2)^{\frac{d-4}{2}} (1 - z''^2)^{\frac{d-4}{2}} \sum_{J=0}^{\infty} n_J^{(d)} P_J^{(d)}(z) P_J^{(d)}(z') P_J^{(d)}(z''). \quad (\text{2.2.36})$$

When  $z \rightarrow 1$ , we can use (A.2.6) and the kernel localizes to

$$\mathcal{P}_d(1, z_1, z_2) = 2(4\pi)^{d-2} \mathcal{N}_d (1 - z_1^2)^{\frac{d-4}{2}} \delta(z_1 - z_2). \quad (\text{A.2.7})$$

We can get a similar identity to (2.2.36) for the Mandelstam kernel,

$$K_d(z, \eta_1, \eta_2) \equiv \int_{-1}^1 dz_1 \int_{-1}^1 dz_2 \frac{\mathcal{P}_d(z, z_1, z_2)}{(\eta_1 - z_1)(\eta_2 - z_2)}, \quad (\text{A.2.8})$$

by using the definition of the Gegenbauer function of the second kind, eq. (2.2.47), to get (2.3.6).

We can get a hint at the analytic structure of the Mandelstam kernel from (2.3.6). In terms of  $\eta'$  and  $\eta''$  the kernel shares the  $[-1, 1]$  branch cut of  $Q_J^{(d)}$ . The situation is more interesting in the  $z$  plane. Given that  $P_J^{(d)}(z)$  is a polynomial in  $z$ , analytic everywhere,  $K_d(z, \eta', \eta'')$  can only be singular whenever  $z$  is such that the sum in  $J$  no longer converges. Indeed, when  $J \rightarrow \infty$  we

## A.2 Useful Identities for Gegenbauer $P$ - and $Q$ -functions

have  $P_J^{(d)}(z) \sim \lambda(z)^J$  and  $Q_J^{(d)}(z) \sim \lambda(z)^{-J}$  (see appendix A.3), and the series diverges when

$$\lambda(z) = \lambda(\eta')\lambda(\eta''), \text{ or } z = \eta_+, \quad (\text{A.2.9})$$

which signals the singularity of the kernel as deduced in appendix A.

Representation (2.3.6) makes the symmetries of the kernel manifest. In particular,  $K_d(z, \eta', \eta'')$  is symmetric in its last two arguments, and further obeys

$$K_d(-z, \eta', \eta'') = -K_d(z, -\eta', \eta'') = -K_d(z, \eta', -\eta''), \quad (\text{A.2.10})$$

where we used  $Q_J^{(d)}(-z) = (-1)^{J+d-3}Q_J^{(d)}(z)$  and  $P_J^{(d)}(-z) = (-1)^J P_J^{(d)}(z)$ . This symmetry of the kernel is responsible for the  $t - u$  symmetry of the double spectral density (2.3.9).

Finally, let us derive (2.3.18). We start with integer  $J$  and  $|\eta_1|, |\eta_2| > 1$ . We take (A.2.5) and apply to it  $\iint_{-1}^1 \frac{dz_1 dz_2}{(\eta_1 - z_1)(\eta_2 - z_2)}$ . In this way we get

$$\frac{1}{8} \pi^{\frac{2-d}{2}} \Gamma\left(\frac{d-2}{2}\right) \int_{-1}^1 dy K_d(y, \eta_1, \eta_2) (1-y^2)^{\frac{d-4}{2}} P_J^{(d)}(y) = (\eta_1^2 - 1)^{\frac{d-4}{2}} Q_J^{(d)}(\eta_1) (\eta_2^2 - 1)^{\frac{d-4}{2}} Q_J^{(d)}(\eta_2), \quad (\text{A.2.11})$$

where we used the definition of  $K_d$  in terms of  $\mathcal{P}_d$  (A.2.8) and definition of  $Q_J^{(d)}$  in terms of  $P_J^{(d)}$  (2.2.47). Noting that  $P_J^{(d)}$  is related to the discontinuity of  $Q_J^{(d)}$ , see (2.2.46), we write the integral as an anticlockwise contour around  $[-1, 1]$

$$\int_{-1}^1 dy K_d(y, \eta_1, \eta_2) (1-y^2)^{\frac{d-4}{2}} P_J^{(d)}(y) = \frac{1}{\pi i} \oint_{[-1,1]} d\eta K_d(\eta, \eta_1, \eta_2) (\eta^2 - 1)^{\frac{d-4}{2}} Q_J^{(d)}(\eta), \quad (\text{A.2.12})$$

where we used the fact that for  $|\eta_1|, |\eta_2| > 1$  the kernel is analytic in a finite region around  $[-1, 1]$ . We now want to blow up this contour to infinity to pick up the branch cut of the Mandelstam kernel (A.1.9). At infinity we have  $K_d(\eta \rightarrow \infty, \eta_1, \eta_2) \sim \frac{\log \eta}{\eta}$  for  $d > 3$  and  $\sim \frac{1}{\eta}$  for  $d = 3$ . Given that  $Q_J(\eta \rightarrow \infty) \sim \eta^{3-d-J}$  we get that the integrand goes like  $\sim \eta^{-J-2}$ , which gives a null contribution to the arc at infinity for  $\text{Re} J > -1$ . In this way we arrive at

$$\frac{1}{\pi i} \oint_{(-1,1)} d\eta K_d(\eta, \eta_1, \eta_2) (\eta^2 - 1)^{\frac{d-4}{2}} Q_J^{(d)}(\eta) = \frac{2}{\pi} \int_{\eta_+}^{\infty} d\eta \text{Disc}_{\eta} K_d(\eta, \eta_1, \eta_2) (\eta^2 - 1)^{\frac{d-4}{2}} Q_J^{(d)}(\eta). \quad (\text{A.2.13})$$

Note that in the main text we included  $\theta(\eta - \eta_+)$  in the discontinuity of the kernel, see (2.3.10). In the formula above, which is valid for complex  $(\eta_1, \eta_2)$ , the variable  $\eta$  is integrated from  $\eta_+$

## Appendix A. Appendix to Chapter 2

---

to  $\infty$  and we can simply use

$$\text{Disc}_\eta K_d(\eta, \eta_1, \eta_2) = \frac{4\pi^{\frac{d+1}{2}}}{\Gamma(\frac{d-3}{2})} \frac{(\eta^2 - 1)^{\frac{4-d}{2}}}{(\eta - \eta_-)^{\frac{5-d}{2}} (\eta - \eta_+)^{\frac{5-d}{2}}}. \quad (\text{A.2.14})$$

Plugging (A.2.13) and (A.2.12) back into (A.2.11) yields (2.3.18).

$$\int_{\eta_+}^{\infty} d\eta (\eta^2 - 1)^{\frac{d-4}{2}} Q_J^{(d)}(\eta) \text{Disc}_\eta K_d(\eta, \eta_1, \eta_2) = \frac{4\pi^{d/2}}{\Gamma(\frac{d-2}{2})} (\eta_1^2 - 1)^{\frac{d-4}{2}} Q_J^{(d)}(\eta_1) (\eta_2^2 - 1)^{\frac{d-4}{2}} Q_J^{(d)}(\eta_2). \quad (\text{2.3.18})$$

This is valid for complex  $\eta_1, \eta_2$  satisfying  $|\eta_1|, |\eta_2| > 1$  and integer  $J$ . The integral is taken along the path that does not cross any cuts of the integrand, e.g.  $\arg[\eta] = \arg[\eta_+]$ .

The above equation can be continued in spin. Indeed, note that both sides of (2.3.18) are manifestly analytic in spin  $J$  for  $\text{Re}[J] > -1$  and coincide for positive integer  $J$ . To argue that they coincide for any  $J$  we also need to check the growth at infinity. One can check that both sides of (2.3.18) have a large  $J$  asymptotic  $\lambda(\eta_+)^{-J}$  and therefore the conditions of Carlson's theorem are satisfied.

### A.3 The $Q_J^{(d)}(z)$ Large $J$ Expansion

The large  $J$  expansion of the  $Q$ -function is given in (2.6.3) and (2.6.2). The aim of this appendix is to argue that there are no nonperturbative corrections to this expansion of the form  $\lambda(z)^{-\alpha J}$ , with  $\alpha > 1$ . This fact is used in section 2.3.5 to derive the Landau curves in the elastic region. We consider separately the cases when the spacetime dimension is even and when it is odd.

**Odd dimensions** In odd spacetime dimensions the  $Q$ -function (2.2.47) takes a simple form

$$Q_J^{(d \text{ odd})}(z) = \frac{2^{d-4} \sqrt{\pi} \Gamma(\frac{d-2}{2})}{\lambda(z)^J (\lambda(z)^2 - 1)^{d-4}} \frac{\Gamma(J+1)}{\Gamma(J+d-3)} \mathbb{P}_{\frac{d-5}{2}}(J, \lambda(z)^2 - 1) \quad (\text{A.3.1})$$

Where  $\mathbb{P}_n(J, x)$  is a polynomial of degree  $n$  in  $x$  and  $J$ . For example, we have

$$\mathbb{P}_{-1} = \frac{1}{Jx}, \quad \mathbb{P}_0 = 1, \quad \mathbb{P}_1 = x(J+3) + 2, \quad \mathbb{P}_2 = x^2(J+5)(J+4) + 6x(J+5) + 12. \quad (\text{A.3.2})$$

This form makes the large  $J$  expansion trivial.

**Even dimensions** For even spacetime dimensions, in analogues to (A.3.1), the  $Q$ -function takes the form

$$Q_J^{(d \text{ even})}(z) = \frac{(-1)^{\frac{d}{2}}}{2} P_J^{(d)}(z) \log \frac{z+1}{z-1} + \left( \frac{z^2}{z^2-1} \right)^{\frac{d-4}{2}} \mathbb{K}_{J-1}^{(d)}(z), \quad (\text{A.3.3})$$

where  $\mathbb{K}_n^{(d)}(x)$  is a polynom of degree  $n$ .<sup>1</sup> Because the degree of the polynom depends on  $J$ , this form is not so useful for understanding the large  $J$  expansion.

Instead, we consider the exact integral (2.6.22) for any integer  $n$ . We observe that on the right hand side of that equation we have again a  $Q$ -function, but now in odd spacetime dimension instead of an even one. By expanding both sides of that equation at large  $J$  (and fixed  $n$ ) one can map between the coefficients of the large  $J$  expansion of the  $Q$ -functions in even and odd spacetime dimensions. Now supposed  $Q^{(d \text{ even})}$  had an  $\lambda(z)^{-\alpha J}$ -type correction. Assuming no cancellations, such a correction would result in an analogous correction in the expansion of  $Q^{(d \text{ odd})}(z_1)$  in the right hand side of (2.6.22). From the above however it is clear that corrections of this type are absent.

## A.4 Gribov's Theorem

It is possible to use elastic unitarity condition continued in spin  $J$  (2.3.15) to constrain the high-energy asymptotic of the discontinuity of the amplitude [269, 270].

Consider the following ansatz for the discontinuity of the amplitude

$$\lim_{t \rightarrow \infty} T_t(s, t) = B(s, \log t) t^{\alpha(s)}, \quad \alpha(s) \in \mathbb{R}, \quad 4m^2 < s < 16m^2. \quad (\text{A.4.1})$$

where  $B(s, \log t)$  is a slowly varying function of  $t$  that grows slower than a power, e.g.  $B(s, \log t) \sim (\log t)^{q(s)}$ .

**Gribov's Theorem:** Let us assume the high energy behavior of the discontinuity (A.4.1) in the elastic region  $4m^2 < s < 16m^2$ . Elastic unitarity then implies that

$$\int_0^\infty d \log t B(s, \log t) < \infty. \quad (\text{A.4.2})$$

Historically, Gribov's theorem excluded the classical picture of diffraction from a black body  $T_t^{(+)}(s, t) = B(s) t$  in QFT.

The easiest way to prove Gribov's theorem is to note that if the integral (A.4.2) diverges  $f_J(s)$  develops a singularity on the real axis at  $J = \alpha(s)$ . Taking  $J = \alpha(s) + \epsilon$  where  $0 < \epsilon \ll 1$  and real, we get from the Froissart-Gribov formula

$$f_{\alpha(s)+\epsilon}(s) \sim \int_0^\infty dx B(s, x) e^{-\epsilon x}. \quad (\text{A.4.3})$$

<sup>1</sup>This form can be derived by expanding  $(1 - z'^2)^{\frac{d-4}{2}} P_J^{(d)}(z')$  in (2.2.47) in powers of  $(z' - z)$ . An explicit way of fixing  $\mathbb{K}_{J-1}^{(d)}$  from  $P_J^{(d)}$  is by demanding that  $Q_J^{(d)}$  decays as in (2.2.43). From (A.3.3) we see that the branch-cut discontinuity in odd  $d$  is replaced by a logarithmic one for even  $d$ .

## Appendix A. Appendix to Chapter 2

---

Elastic unitarity close to the leading Regge singularity  $J = \alpha(s)$  then takes the schematic form

$$\begin{aligned} \int^{\infty} dx \operatorname{Im} B(s, x) e^{-\epsilon x} &\propto \left| \int^{\infty} dx B(s, x) e^{-\epsilon x} \right|^2 \\ &= \left( \int^{\infty} dx \operatorname{Re} B(s, x) e^{-\epsilon x} \right)^2 + \left( \int^{\infty} dx \operatorname{Im} B(s, x) e^{-\epsilon x} \right)^2, \end{aligned} \quad (\text{A.4.4})$$

which can be only consistent if (A.4.2) holds. Indeed, otherwise we get that the singularity in the RHS of (A.4.4) does not match the singularity in the LHS of (A.4.4).

A simple, and physically natural, way out of the contradiction is to assume that  $\alpha(s) \in \mathbb{C}$ . Indeed, consider a model, where the leading Regge trajectory is given by a single Regge pole

$$f_J(s) = \frac{\beta(s)}{J - \alpha(s)} + \dots, \quad \operatorname{Im}[\alpha(s)] \neq 0, \quad 4m^2 < s < 16m^2. \quad (\text{A.4.5})$$

This corresponds to the discontinuity of the amplitude that takes the form  $T_t(s, t) = \beta(s) t^{\alpha(s)}$ .

Let us now impose elastic unitarity (2.3.15) at  $J = \alpha^*(s)$ . We get that the solution is

$$\beta(s) = \frac{2\sqrt{s}}{(s - 4m^2)^{\frac{d-3}{2}}} \operatorname{Im} \alpha(s). \quad (\text{A.4.6})$$

In  $d > 3$  the consideration above tacitly assumed that  $\operatorname{Re} \alpha(s) > -1$ . This is related to the fact that in  $d > 3$ , as can be seen explicitly from (2.2.47),  $Q_J^{(d)}(z)$  develop a pole at  $J = -1$  and we run into the same problem as above where the singularities do not match in the elastic unitarity equation.

It would be interesting to understand better properties of the full nonperturbative leading Regge trajectory in the complex  $s$  plane, see e.g. discussion in [42] for some common assumptions. The properties of the leading Regge trajectory in the planar theory are relatively well-understood, see e.g. [271, 131].

## A.5 Elastic Landau curves from the Mandelstam Equation

The functional shape of the Landau curves in the elastic strip can be derived by impose the consistency between the positions of the thresholds of  $T_t(s, t)$  (2.3.23) and those of  $\rho(s, t)$  (2.3.24) with elastic unitarity. In section 2.3.5 we have done so by imposing elastic unitarity at the level of the partial waves. In this appendix we use the Mandelstam equation instead to generate the same curves.

The Mandelstam equation (2.3.9) can be written as

$$\rho(s, t) = \mathbb{K}[\mathcal{F}_t^{(+)}, \mathcal{F}_t^{(-)}](s, z_s(t)), \quad (\text{A.5.1})$$

## A.5 Elastic Landau curves from the Mandelstam Equation

where we have introduced the functional

$$K[A, B](s, z) \equiv \frac{(s - 4m^2)^{\frac{d-3}{2}}}{4\pi^2(4\pi)^{d-2}\sqrt{s}} \int_{z_1}^{\infty} d\eta' \int_{z_1}^{\infty} d\eta'' A(s, \eta') B(s, \eta'') \text{Disc}_z K(z, \eta', \eta''). \quad (\text{A.5.2})$$

Permutation symmetry of the Mandelstam kernel,  $K_z(z, \eta', \eta'') = K_z(z, \eta'', \eta')$ , implies symmetry of the functional  $K[A, B] = K[B, A]$ . Due to real analyticity  $\left[\mathcal{F}_t^{(+)}\right]^* = \mathcal{F}_t^{(-)}$ , it then follows from (A.5.1) that  $\rho(s, t)$  is real when  $s, t$  are real and positive.

The structure of  $T_t(s, t)$  in physical ( $t$ -channel) kinematics is given in (2.3.23). As we continue  $s$  out of that region,  $T_t^{2-2n}(s, t)$  may develop a discontinuity at the Karplus curves. Given that  $\rho(s, t) \equiv \text{Disc}_s T_t(s, t) = \text{Im}_s T_t(s, t)$ , we can separate  $T_t(s, t)$  into real and imaginary parts as

$$T_t^{(\pm)}(s, t) = R(s, t) \pm i\rho(s, t), \quad (\text{A.5.3})$$

where for physical  $s$ ,  $\rho(s, t)$  vanishes and  $R(s, t)$  is simply given by the normal thresholds of (2.3.23). It can be written schematically as

$$R(s, t) \sim \sum_{n=1}^{\infty} \Theta(z - z|_{t=2nm^2}), \quad 4 - t < s < 0. \quad (\text{A.5.4})$$

By plugging (A.5.3) into (A.5.1) we get that

$$\rho = K[R, R] + K[\rho, \rho]. \quad (\text{A.5.5})$$

We now take  $R$  to just be given by (A.5.4) as a seed to (A.5.5) and iterate this equation to find the minimal consistent set of Landau curves in (2.3.24) that is consistent with this equation.

Note that for  $s > 4m^2$ ,  $R$  can have additional discontinuities in addition to normal thresholds. Hence, at each step we correct  $R$  with the additional thresholds of  $\rho$  that are generated through the iteration of (A.5.5). In the end we check the iteration procedure converges to a closed set of Landau curves.

The first contribution to  $\rho$  comes from inserting (A.5.4) into (A.5.5)

$$\begin{aligned} K[R, R](s, z) &\sim \sum_{n,m=1}^{\infty} \int_1^{\infty} d\eta' d\eta'' \Theta(\eta' - z_n) \Theta(\eta'' - z_m) \Theta(z - \eta^+(\eta', \eta'')) \\ &\sim \sum_{n,m=1}^{\infty} \Theta(z - \eta^+(z_n, z_m)) = \sum_{n,m}^{\infty} \Theta(\lambda(z) - \lambda(z_n)\lambda(z_m)). \end{aligned} \quad (\text{A.5.6})$$

We see that normal thresholds generate a first set of Landau curves for  $\rho(s, t)$  given by (2.3.31) via the  $K[R, R]$  term. Including the (A.5.6) Karplus curves into  $R$  requires, from consistency

## Appendix A. Appendix to Chapter 2

---

with (A.5.5), an additional set of “cubic” curves,

$$\begin{aligned} K[R, K[R, R]](s, z) &\sim \sum_{n,m,l=1}^{\infty} \int_1^{\infty} d\lambda' d\lambda'' \Theta(\lambda' - \lambda(z_n)) \Theta(\lambda'' - \lambda(z_m) \lambda(z_l)) \\ &\sim \sum_{n,m,l=1}^{\infty} \Theta(\lambda(z) - \lambda(z_n) \lambda(z_m) \lambda(z_l)), \end{aligned} \quad (\text{A.5.7})$$

and also “quartic” curves,

$$\begin{aligned} K[K[R, R], K[R, R]](s, z) &\sim \sum_{n,m,l,k=1}^{\infty} \int_1^{\infty} d\lambda' d\lambda'' \Theta(\lambda' - \lambda(z_n) \lambda(z_m)) \Theta(\lambda'' - \lambda(z_k) \lambda(z_l)) \Theta(\lambda(z) - \lambda' \lambda'') \\ &\sim \sum_{n,m,l,k=1}^{\infty} \Theta(\lambda(z) - \lambda(z_n) \lambda(z_m) \lambda(z_k) \lambda(z_l)). \end{aligned} \quad (\text{A.5.8})$$

Iterating further, we find that a natural set of Landau curves consistent with (A.5.5) and the existence of normal thresholds is

$$R(s, t(z)) \sim \sum_{L=1}^{\infty} \sum_{\{n_1, \dots, n_L\}} \Theta(\lambda(z) - \lambda(z_{n_1}) \cdots \lambda(z_{n_L})), \quad (\text{A.5.9})$$

and

$$\rho(s, t(z)) \sim \sum_{L=2}^{\infty} \sum_{\{n_1, \dots, n_L\}} \Theta(\lambda(z) - \lambda(z_{n_1}) \cdots \lambda(z_{n_L})), \quad (\text{A.5.10})$$

where importantly  $4m^2 < s < 16m^2$ . Note that the difference between the supports of (A.5.9) and (A.5.10) is precisely (A.5.4).

Below we present the curves that asymptote to  $t = 16m^2, 36m^2, 64m^2$ .

$$t_{\{2,0,\dots\}} = \frac{16m^2 s}{s - 4m^2}, \quad t_{\{3,0,\dots\}} = \frac{36m^2 (s + \frac{4m^2}{3})^2}{(s - 4m^2)^2}, \quad t_{\{4,0,\dots\}} = \frac{64m^2 s (s + 4m^2)^2}{(s - 4m^2)^3}, \quad (\text{A.5.11})$$

$$t_{\{1,1,0,\dots\}} = \frac{20m^2 s + 16m^2 \sqrt{s(s + 12m^2)} + 48m^4}{s - 4m^2}, \quad t_{\{0,2,0,\dots\}} = \frac{64m^2 (s + 12m^2)}{s - 4m^2}, \quad (\text{A.5.12})$$

$$\begin{aligned} t_{\{1,0,1,0,\dots\}} &= \frac{128m^4 + 40m^2 s + 24m^2 \sqrt{s(s + 32m^2)}}{s - 4m^2}, \\ t_{\{2,1,0,\dots\}} &= \frac{16m^2 \left( s + 2m\sqrt{s} + 2m\sqrt{s + 12m^2} + \sqrt{s(s + 12m^2)} + 8m^2 \right)^2}{(\sqrt{s} - 2m)^2 (s + 8m\sqrt{s + 12m^2} + 28m^2)}. \end{aligned} \quad (\text{A.5.13})$$

The curves are plotted below.



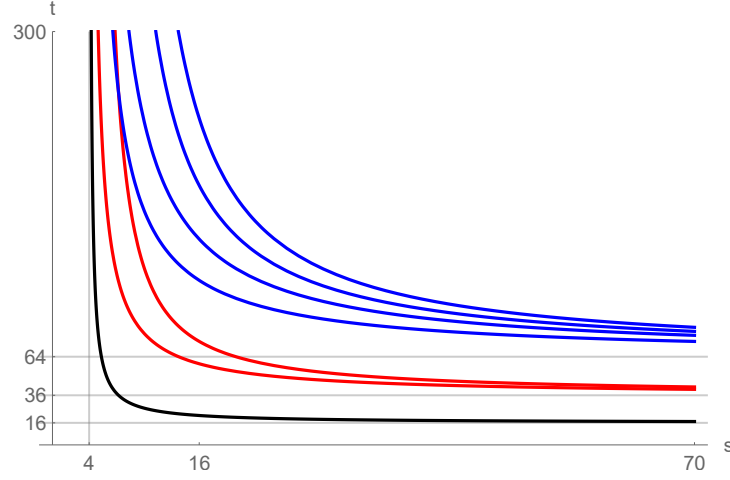


Figure A.1: Plot of the Landau curves given by equations (A.5.11) to (A.5.13) for  $m = 1$ . The curves are organized by color according to the asymptote at  $t \rightarrow \infty$ . Black is the leading curve  $t_{\{2,0,0,\dots\}}$ . Red curves obey  $t_{\{1,1,0,\dots\}} < t_{\{3,0,\dots\}}$ . Blue curves obey  $t_{\{1,0,1,0,\dots\}} < t_{\{0,2,0,\dots\}} < t_{\{2,1,0,\dots\}} < t_{\{4,0,\dots\}}$ .

## A.6 Threshold Expansion for Non-Integer $J$

It is interesting to ask about the continuation of the formula (2.5.3) for the solution to elastic unitarity to non-integer  $J$ . For a related discussion, see e.g. [272].

The starting point is the observation that the Froissart-Gribov formula can be written in the following form

$$\frac{f_J(s)}{(s-4m^2)^J} = 2 \frac{(16\pi)^{\frac{2-d}{2}}}{\Gamma\left(\frac{d-2}{2}\right)} \int_{z_1}^{\infty} \frac{dz}{\pi} (z^2-1)^{\frac{d-4}{2}} \frac{Q_J^{(d)}(z)}{(s-4m^2)^J} T_t(s, t(z)) \quad (\text{A.6.1})$$

admits a simple analytic continuation to  $s < 4m^2$  for real  $J$ .

Indeed,  $Q_J^{(d)}(z)$  for non-integer  $J$  have a branch point at  $s = 4m^2$  or, equivalently,  $z = \infty$ . On the other hand,  $\frac{Q_J^{(d)}(z)}{(s-4m^2)^J}$  has only branch cut for  $z \in [-1, 1]$  and satisfies

$$(z^2-1)^{\frac{d-4}{2}} \frac{Q_J^{(d)}(z)}{(s-4m^2)^J} = -((-z)^2-1)^{\frac{d-4}{2}} \frac{Q_J^{(d)}(-z)}{(4m^2-s)^J}, \quad (\text{A.6.2})$$

for  $|z| > 1$  as can be easily seen from (2.2.47).

Switching in the RHS of (A.6.1) to the integral  $\int_{4m^2}^{\infty} dt$  we can continue  $f_J(s)$  to  $s < 4m^2$ . Together with the fact that  $T_t(s, t(z))$  is positive and real for  $0 < s < 4m^2$  we conclude that  $\frac{f_J(s)}{(s-4m^2)^J}$  is real analytic function of  $s$  with a branch cut starting at  $s = 4m^2$ . Moreover,  $\frac{f_J(s)}{(s-4m^2)^J}$  is positive and real for  $0 < s < 4m^2$ .

## Appendix A. Appendix to Chapter 2

---

Let us now impose continued in spin elastic unitarity (2.3.15). It is convenient to rewrite it as follows

$$\frac{1}{i} \left( \frac{(s-4m^2)^J}{f_J(s+i\epsilon)} - \frac{(s-4m^2)^J}{f_J(s-i\epsilon)} \right) = -\frac{(s-4m^2)^{J+\frac{d-3}{2}}}{\sqrt{s}}. \quad (\text{A.6.3})$$

The general solution to it takes the form

$$f_J(s) = \frac{(s-4m^2)^J}{\tilde{b}_J(s) + \frac{e^{-i\pi(J+\frac{d-3}{2})}}{\sin\pi(J+\frac{d-3}{2})} \frac{(s-4m^2)^{J+\frac{d-3}{2}}}{2\sqrt{s}}}, \quad s > 4m^2, \quad (\text{A.6.4})$$

where  $\tilde{b}_J(s)$  are analytic around  $s = 4m^2$  and  $b_J(4) \sim a_J > 0$  for  $J \geq 2$ .

Few comments are in order. Let us first discuss how the formula above reduces to (2.5.3) when  $J$  is even integer. In even  $d$  it is trivial upon identifying  $\tilde{b}_{J=2k}(s) = (s-4m^2)^{2k} b_{2k}(s)$ . In odd  $d$  the situation is more subtle because in this case  $\frac{e^{-i\pi(J+\frac{d-3}{2})}}{\sin\pi(J+\frac{d-3}{2})} = \frac{e^{-i\pi J}}{\sin\pi J}$  which develops a pole for even  $J$ . The residue of this pole  $\frac{(s-4m^2)^{J+\frac{d-3}{2}}}{2\sqrt{s}}$  however is analytic around  $s = 4m^2$  and therefore it can be canceled by  $\tilde{b}_J(s)$  if we impose that

$$\lim_{J \rightarrow 2k} \tilde{b}_J(s) = -\frac{1}{J-2k} \frac{(s-4m^2)^{2k+\frac{d-3}{2}}}{2\pi} + (s-4m^2)^{2k} b_{2k}(s) + O(J-2k), \quad J > \text{Re}\alpha(s), \quad d \text{ odd}, \quad (\text{A.6.5})$$

the  $J^0$  term then correctly reproduces (2.5.3).

Secondly, note that when  $|J| \rightarrow \infty$  the ratio  $\frac{e^{-i\pi(J+\frac{d-3}{2})}}{\sin\pi(J+\frac{d-3}{2})}$  is polynomially bounded which is consistent with the expected behavior of  $f_J(s)$  at infinity. This poses a potential problem in even  $d$  for half-integer  $J$  and in odd  $J$  integer  $J$ .

Let us consider even  $d$  first. In this case  $\frac{e^{-i\pi(J+\frac{d-3}{2})}}{\sin\pi(J+\frac{d-3}{2})} = -i \frac{e^{-i\pi J}}{\cos\pi J}$  develops a pole at odd  $J$  which corresponds to zero of  $f_J(s)$ . Therefore unless there is a cancellation between the two terms in the denominator of (2.5.3) we have that  $f_{\frac{1}{2}+\mathbb{Z}} = 0$ . If this is the case via Carlson theorem we then conclude that  $f_J(s) = 0$  identically. Therefore, an infinite number of poles should cancel with the corresponding poles in  $\tilde{b}_J(s)$ . In this way we get

$$\lim_{J \rightarrow k-\frac{1}{2}} \tilde{b}_J(s) = -\frac{1}{J-(k-\frac{1}{2})} \frac{(s-4m^2)^{k+\frac{d-4}{2}}}{2\pi} + \dots, \quad J > \text{Re}\alpha(s), \quad d \text{ even}. \quad (\text{A.6.6})$$

Note again that in even  $d$   $(s-4m^2)^{k+\frac{d-4}{2}}$  is analytic at  $s = 4m^2$  which is consistent with the predicted property of  $\tilde{b}_J(s)$ .

Finally, in odd  $d$  for odd integer  $J$  we get the following cancellation condition

$$\lim_{J \rightarrow 2k-1} \tilde{b}_J(s) = -\frac{1}{J - (2k-1)} \frac{(s-4m^2)^{2k+\frac{d-5}{2}}}{2\pi} + \dots, \quad J > \text{Re} \alpha(s) \quad d \text{ odd.} \quad (\text{A.6.7})$$

## A.7 Threshold expansion in $J$ -space: Technical Details

In this appendix we collect various results and technical details that are relevant to the inversion of the threshold expansion using the Froissart-Gribov formula performed in section 2.6.3.

We start with the derivation of (2.6.22). Consider first  $d$  to be even. We would like to evaluate the following integral

$$I_{n,J}^{(d)}(z_1) \equiv \frac{2\mathcal{N}_d}{\pi} \int_{z_1}^{\infty} dz (z^2 - 1)^{\frac{d-4}{2}} Q_J^{(d)}(z) \frac{(z_1 - 1)^{\frac{d-3}{2}-n}}{(z - z_1)^{\frac{d-3}{2}-n}} = \frac{2\mathcal{N}_d}{\pi} (z_1 - 1)^{\frac{d-3}{2}-n} I(d, n, z_1),$$

$$I(d, n, z_1) \equiv \int_{z_1}^{\infty} dz (z^2 - 1)^{\frac{d-4}{2}} Q_J^{(d)}(z) \frac{1}{(z - z_1)^{\frac{d-3}{2}-n}}, \quad n \in \mathbb{Z}, \quad n \geq 0. \quad (\text{A.7.1})$$

We would like to do the integral for general  $J$ . The strategy is to do the integral first for integer  $J$  exactly and then analytically continue it to arbitrary  $J$ .

As a first step we note that the integrand can be interpreted as a discontinuity of some simple function

$$\text{Disc}_t \frac{1}{\sin \pi \left(\frac{d-3}{2} - n\right)} \frac{1}{(z_1 - z)^{\frac{d-3}{2}-n}} = \frac{1}{(z - z_1)^{\frac{d-3}{2}-n}}. \quad (\text{A.7.2})$$

For integer  $n$  and  $d$  this only holds for even  $d$ , where the power is half-integer and therefore we have a square-root type discontinuity.

Therefore if we interpret the integrand as a discontinuity  $T_t(s, t) = \frac{1}{(z - z_1)^{\frac{d-3}{2}-n}}$  of the amplitude  $T(s, t) = \frac{1}{\sin \pi \left(\frac{d-3}{2} - n\right)} \frac{1}{(z_1 - z)^{\frac{d-3}{2}-n}}$  then (A.7.1) is nothing but the Froissart-Gribov integral for this amplitude! In this way we can immediately rewrite it as follows

$$I(d, n, z_1) = \frac{\pi}{2} \frac{(-1)^n}{\sin \pi \frac{d-3}{2}} \int_{-1}^1 dz (z^2 - 1)^{\frac{d-4}{2}} P_J^{(d)}(z) \frac{1}{(z_1 - z)^{\frac{d-3}{2}-n}}. \quad (\text{A.7.3})$$

Here we used that  $J$  is integer and dropped the contour at infinity which requires  $J > n - \frac{d-3}{2}$ .

## Appendix A. Appendix to Chapter 2

---

We note that the integral (A.7.1) satisfies a very simple recursion relation based on the identity

$$\partial_{z_1} I(d, n, z_1) = -\left(n - \frac{d-3}{2}\right) I(d, n-1, z_1). \quad (\text{A.7.4})$$

Therefore we can first compute the integral for  $n = 0$  and then use this differential equation to compute the integral for  $n > 0$ .

Let us now find explicitly  $I(d, 0, z_1)$ . To do this let us do the following change of variable

$$\frac{1}{t} = \lambda(z_1) \equiv z_1 + \sqrt{z_1^2 - 1}. \quad (\text{A.7.5})$$

We can then write

$$\begin{aligned} \frac{1}{(z_1 - z)^{\frac{d-3}{2}}} &= \frac{1}{(2t)^{\frac{3-d}{2}}} \frac{1}{(1 - 2tz + t^2)^{\frac{d-3}{2}}} = \frac{1}{(2t)^{\frac{d-3}{2}}} \sum_{J=0}^{\infty} C_J^{(\frac{d-3}{2})}(z) t^J \\ &= \frac{1}{(2t)^{\frac{3-d}{2}}} \sum_{J=0}^{\infty} \frac{\Gamma(d-3)\Gamma(J+1)}{\Gamma(d+J-3)} P_J^{(d)}(z) t^J, \end{aligned} \quad (\text{A.7.6})$$

where we used the relation between  $P_J^{(d)}(z)$  and the Gegenbauer polynomials  $C_J^{(\frac{d-3}{2})}(z)$

$$P_J^{(d)}(z) = \frac{\Gamma(d+J-3)}{\Gamma(d-3)\Gamma(J+1)} C_J^{(\frac{d-3}{2})}(z). \quad (\text{A.7.7})$$

Using the orthogonality property of  $P_J^{(d)}(z)$  we immediately get

$$\begin{aligned} I(d, 0, z_1) &= \frac{\pi}{2} \frac{1}{\sin \pi \frac{d-3}{2}} \frac{1}{(2t)^{\frac{3-d}{2}}} \frac{2}{\mathcal{N}_d n_J^{(d)}} \frac{\Gamma(d+J-3)}{\Gamma(d-3)\Gamma(J+1)} t^J = \\ &= \frac{\pi}{\sin \frac{\pi d}{2}} \frac{2^{\frac{3d-11}{2}} \Gamma(\frac{d-2}{2})^2}{(2J+d-3)\Gamma(d-3)} \lambda(z_1)^{-(J+\frac{d-3}{2})}. \end{aligned} \quad (\text{A.7.8})$$

The rest we can get trivially using (A.7.4). Note that the final result holds in any  $d$  and for any  $J$ .

The basic integral is the following

$$\int dz_1 \lambda(z_1)^{-c} = \frac{1}{2} \left( \frac{\lambda^{-1-c}}{c+1} - \frac{\lambda^{1-c}}{c-1} \right). \quad (\text{A.7.9})$$

Therefore, it is clear that we get the following result for the integral

$$I(d, n, z_1) = \frac{\pi}{\sin \frac{\pi d}{2}} \frac{2^{\frac{3d-11}{2}} \Gamma(\frac{d-2}{2})^2}{(2J+d-3)\Gamma(d-3)} \lambda(z_1)^{n-(J+\frac{d-3}{2})} \sum_{k=0}^n c_{k,n} \lambda(z_1)^{-2k}, \quad (\text{A.7.10})$$

where  $c_{k,n}$  can be explicitly found.

## A.7 Threshold expansion in $J$ -space: Technical Details

We have  $c_{0,0} = 1$ . It is then easy to check that we have the following result

$$I(d, n, z_1) = \frac{2^{\frac{3d-13}{2}} \Gamma(\frac{d-2}{2})^2 \Gamma(\frac{d-3}{2}) \Gamma(n + \frac{5-d}{2})}{\Gamma(d-3)} \lambda(z_1)^{n-(J+\frac{d-3}{2})} \\ \times 2^{-n} \sum_{k=0}^n \binom{n}{k} \frac{(-1)^k}{\prod_{j=0}^n (J+k-j+\frac{d-3}{2})} \lambda(z_1)^{-2k}. \quad (\text{A.7.11})$$

Also note that when  $J \rightarrow \infty$ , the denominator  $\sim J^{n+1}$  factors out and the sum becomes Newton's binomial. We get

$$\lim_{J \rightarrow \infty} I(d, n, z_1) = \frac{2^{\frac{3d-13}{2}} \Gamma(\frac{d-2}{2})^2 \Gamma(\frac{d-3}{2}) \Gamma(n + \frac{5-d}{2})}{J^{n+1} \Gamma(d-3)} (z_1^2 - 1)^{\frac{n}{2}} \lambda(z_1)^{-(J+\frac{d-3}{2})} \quad (\text{A.7.12})$$

where we used  $\lambda(z_1) - \lambda^{-1}(z_1) = 2z_1^2 - 2$ .

From the above we conclude

$$\lim_{J \rightarrow \infty} \frac{I(d, n+1, z_1)}{I(d, n, z_1)} = \sqrt{z_1^2 - 1} \left( n + \frac{5-d}{2} \right) \frac{1}{J}. \quad (\text{A.7.13})$$

This is the essence of why a threshold expansion maps to a systematic large  $J$  expansion through the Froissart-Gribov integral: Consecutive terms in the threshold expansion are roughly suppressed by  $\sim \frac{1}{J}$  with respect to one another.

Note that the original integral  $I(d, 0, z_1)$  looks divergent in even  $d \geq 6$ , whereas the final result (A.7.8) is finite. The resolution to this apparent contradiction is that when we changed the contour and wrote the integral as (A.7.3) we implicitly used that the original integral was defined via the keyhole prescription. Therefore, the result (A.7.11) is correct.

Formula (A.7.11) can be rewritten as follows

$$I(d, n, z_1) = -\frac{1}{\pi} \frac{2^{\frac{3d-12}{2}} \Gamma(\frac{d-2}{2})^2 \Gamma(\frac{d-3}{2}) \Gamma(n + \frac{5-d}{2})}{\Gamma(d-3)} \lambda(z_1)^{n-(J+\frac{d-3}{2})} 2^{-n} \cos \frac{\pi(d+2J)}{2} \tilde{I} \\ \tilde{I} \equiv \sum_{k=0}^n \binom{n}{k} (-1)^k \Gamma\left(\frac{3-d}{2} - J - k\right) \Gamma\left(\frac{d-3}{2} + J + k - n\right) \lambda(z_1)^{-2k}. \quad (\text{A.7.14})$$

We now note that we can write

$$\tilde{I} = \Gamma\left(\frac{3-d-2J}{2}\right) \Gamma\left(\frac{2J-2n+d-3}{2}\right) {}_2F_1\left(\frac{d-3}{2} + J - n, -n, J + \frac{d-1}{2}, \frac{1}{\lambda_1(z)^2}\right), \quad (\text{A.7.15})$$

which we can now analytically continue away from integer  $n$ . Using the formula (2.6.3) for  $Q_J^{(d)}(z)$  we finally get (2.6.22) which can be now checked to hold for arbitrary  $J, d$  and  $n$ .

### Odd $d$

In odd dimensions we are also interested in the following integral

$$I_{\log}(d, n, z_1, c_i) = \int_{z_1}^{\infty} dz (z^2 - 1)^{\frac{d-4}{2}} Q_J^{(d)}(z) \frac{(z - z_1)^{n - \frac{d-3}{2}}}{\log^2(z - z_1) + c_1 \log(z - z_1) + c_2}. \quad (\text{A.7.16})$$

This comes from plugging the threshold expansion into the Froissart-Gribov integral. In this case we note that

$$(\partial_n^2 + c_1 \partial_n + c_2) I_{\log}(d, n, z_1, c_i) = I(d, n, z_1), \quad (\text{A.7.17})$$

where  $I(d, n, z_1)$  was computed in the subsection above. It is easy to write a general solution to this differential equation, which should suffice for doing the integrals numerically for given  $J$ . We have not pursued this further in the present paper.

#### A.7.1 Higher Order Corrections to $\rho(s, t)$

Here we present some details for computing the double spectral density that comes from plugging  $c_{n_1} c_{n_2} \frac{(\eta' - z_1)^{n_1 - \frac{d-3}{2}} (\eta'' - z_1)^{n_2 - \frac{d-3}{2}}}{(z_1 - 1)^{n_1 - \frac{d-3}{2}} (z_1 - 1)^{n_2 - \frac{d-3}{2}}}$  for the square of discontinuity of the amplitude in the Mandelstam equation (2.3.9). We denote the result of this integration by  $\rho_{n_1, n_2}(s, t(z))$ .

It admits the following expansion close to the leading Landau curve

$$\rho(s, t(z)) = \sum_{n_1, n_2} c_{n_1} c_{n_2} \rho_{n_1, n_2}(s, t(z)), \quad \rho_{n_1, n_2}(s, t(z)) \equiv \frac{(s - 4m^2)^{\frac{d-3}{2}}}{4\pi^2 (4\pi)^{d-2} \sqrt{s}} \tilde{I}_{n_1, n_2}^{(d)}(z), \quad (\text{A.7.18})$$

where  $\tilde{I}_{n_1, n_2}^{(d)}(z)$  was defined in (2.5.13). This can be expanded close to the leading Landau curve

$$\rho_{n_1, n_2}(s, t(z)) = \frac{1}{(z_1 - 1)^{n_1 + n_2 - (d-3)}} \frac{(z - (2z_1^2 - 1))^{n_1 + n_2}}{(z - (2z_1^2 - 1))^{\frac{d-5}{2}}} \sum_{m=0}^{\infty} d_{n_1, n_2; m}(s) (z - (2z_1^2 - 1))^m, \quad (\text{A.7.19})$$

where  $d_{n_1, n_2; m}(s)$  are the coefficients that we would like to compute.

Instead of computing the integral (2.3.9) we can use (A.7.1) to get  $\text{Im} f_J(s)$  and then extract  $d_{n_1, n_2; m}(s)$  by imposing elastic unitarity order by order in  $\frac{1}{j}$ . The result takes the following form

$$d_{n_1, n_2; 0}(s) = 2^{\frac{d-3}{2}} \frac{\mathcal{N}_d}{\sqrt{\pi}} \frac{(s - 4m^2)^{\frac{d-3}{2}}}{\sqrt{s}} \frac{\lambda_1^{2+n_1+n_2} (\lambda_1^2 - 1)^{n_1+n_2}}{(\lambda_1^4 - 1)^{n_1+n_2+1}} \frac{\Gamma(\frac{d-2}{2}) \Gamma(n_1 + \frac{5-d}{2}) \Gamma(n_2 + \frac{5-d}{2})}{\Gamma(n_1 + n_2 + \frac{7-d}{2})}, \quad (\text{A.7.20})$$

where  $\lambda_1 \equiv \lambda(z_1)$ .

Proceeding to higher orders we get

$$\frac{d_{n_1, n_2; m}(s)}{d_{n_1, n_2; 0}(s)} = \frac{\Gamma(n_1 + 1 + m)}{\Gamma(n_1 + 1)} \frac{\Gamma(n_2 + 1 + m)}{\Gamma(n_2 + 1)} \frac{\lambda_1^{2m}}{(\lambda_1^4 - 1)^{2m}} \frac{\Gamma(n_1 + n_2 + \frac{7-d}{2})}{\Gamma(n_1 + n_2 + \frac{7-d}{2} + m)} \frac{(-1)^m 2^m}{\Gamma(m + 1)} \text{poly}_m, \quad (\text{A.7.21})$$

where  $\text{poly}_m$  does not depend on  $d$  and takes the form

$$\text{poly}_m = \sum_{i=0}^{2m} \lambda_1^{2i} c_{i,m}. \quad (\text{A.7.22})$$

We quote here some results on the properties of the polynomial  $\text{poly}_m$

$$\begin{aligned} c_{0,m} &= c_{2m,m} = 1, & c_{i,m} &= c_{2m-i,m}, \\ c_{1,m} &= -m \left( \frac{n_2}{n_1 + 1} + \frac{n_1}{n_2 + 1} \right), \\ c_{2,m} &= m^2 + \frac{m(m-1)}{2} \left( \frac{n_2(n_2-1)}{(n_1+1)(n_1+2)} + \frac{n_1(n_1-1)}{(n_2+1)(n_2+2)} \right) \end{aligned} \quad (\text{A.7.23})$$

We can also write down an explicit result for  $n_1 = n_2 = 0$

$$c_{i,m} = \frac{1 + (-1)^i}{2} \binom{m}{\frac{i}{2}}^2, \quad (\text{A.7.24})$$

so that

$$\text{poly}_m = {}_2F_1(-m, -m, 1, \lambda_1^4), \quad n_1 = n_2 = 0. \quad (\text{A.7.25})$$

For  $n_1 = n_2 = 1$  and  $n_1 = 0, n_2 = 1$  we get

$$\begin{aligned} c_{i,m} &= (-1)^i \binom{m}{[\frac{i}{2}]} \binom{m}{[\frac{i+1}{2}]} \\ &= (-1)^i \left( \frac{1 + (-1)^i}{2} \binom{m}{\frac{i}{2}}^2 + \frac{1 - (-1)^i}{2} \binom{m}{\frac{i-1}{2}} \binom{m}{\frac{i+1}{2}} \right), \end{aligned} \quad (\text{A.7.26})$$

where  $[x]$  stands for the integer part of  $x$ . Similarly one can write an explicit result for  $\text{poly}_m$  in terms of hypergeometric functions.

Note that the threshold expansion of the double spectral density (A.7.19) does not reflect the behavior of  $\rho_{n_1, n_2}(s, t(z))$  at large  $z \gg 1$ . Indeed, one can check that it takes the form  $\rho_{n_1, n_2}(s, t(z)) \sim z^{\max[n_1, n_2] - \frac{d-3}{2}} (1 + \delta_{n_1, n_2} \log z)$ .<sup>2</sup>

---

<sup>2</sup>The fact that  $n_1 = n_2$  term acquires an extra  $\log z$  is closely related to Gribov's theorem which constrains the

## Appendix A. Appendix to Chapter 2

---

A. W. Martin [68] found an elegant closed expression for  $\rho_{n_1, n_2}(s, t(z))$  in  $d = 4$ . It takes the following form

$$\begin{aligned} \rho_{n_1, n_2}^{(d=4)}(s, t) &= \frac{d_{n_1, n_2; 0}}{(z_1 - 1)^{n_1 + n_2 - 1}} \frac{(\delta z)^{n_1 + n_2 + \frac{1}{2}}}{\left(1 + \frac{2\delta z \lambda_1^2}{(\lambda_1^2 - 1)^2}\right)^{\frac{1}{2}}} \\ &\times \sum_{p, q, r=0}^{\infty} \frac{\Gamma(n_1 + n_2 + \frac{3}{2})\Gamma(n_2 + 2p + r + \frac{1}{2})\Gamma(n_1 + 2q + r + \frac{1}{2})}{p!q!r!\Gamma(n_1 + \frac{1}{2})\Gamma(n_2 + \frac{1}{2})\Gamma(n_1 + n_2 + p + q + r + \frac{3}{2})} \\ &\times \left(\frac{\delta z}{4(z-1)z_1^2}\right)^{p+q} \left(\frac{-z\delta z}{2(z-1)z_1^2}\right)^r, \end{aligned} \quad (\text{A.7.27})$$

where  $\delta z \equiv z - (2z_1^2 - 1)$ . The advantage of the formula above is that by performing the sum over  $r$  it makes the large  $z$  limit of  $\rho(s, t)$  manifest.

Similarly, in  $d = 3$  the correction to the double spectral density takes the following form

$$\rho_{n_1, n_2}^{(d=3)} = \frac{1}{8\pi\sqrt{s}} \int_{\text{arccosh } z_1}^{\text{arccosh } z - \text{arccosh } z_1} d\theta_1 \frac{(\cosh \theta_1 - z_1)^{n_1}}{(z_1 - 1)^{n_1}} \frac{(\cosh(\text{arccosh } z - \theta_1) - z_1)^{n_2}}{(z_1 - 1)^{n_2}}, \quad (\text{A.7.28})$$

which can be explicitly evaluated for given  $n_1, n_2$ .

The representations above are particularly useful if one would like to perform computations at finite  $J$  and finite  $s$ , see section 2.7. Indeed, plugging the threshold expansion formula in the Froissart-Gribov integral becomes dangerous at high enough order because the integral goes all the way to  $z \rightarrow \infty$ . Martin's formula (A.7.27) does not have this problem after performing the  $r$  resummation. The same holds true for the  $d = 3$  result (A.7.28). These formulae make both the threshold and the large  $\delta z$  behavior of  $\rho(s, t)$  manifest. We discuss the generalization of the formulae above to other dimensions below.

### Mandelstam Integral for $\rho(s, t)$

In solving elastic unitarity (2.5.11) within the threshold expansion we sometimes want to compute the following integral

$$J_{n_1, n_2}^{(d)}(s, t) \equiv (z^2 - 1)^{\frac{d-4}{2}} \int_{z_1}^{\infty} \frac{d\eta'}{\pi} \int_{z_1}^{\infty} \frac{d\eta''}{\pi} (\eta' - z_1)^{n_1 - \frac{d-3}{2}} (\eta'' - z_1)^{n_2 - \frac{d-3}{2}} \text{Disc}_z K(z, \eta', \eta''). \quad (\text{A.7.29})$$

Above we discussed the results in case of  $d = 3$  and  $d = 4$  as well as the threshold expansion in general  $d$ . Here we would like to note that in other dimensions the integral can be evaluated

---

possible leading Regge behavior of the scattering amplitude in the elastic region, see appendix A.4.



recursively by noting that

$$\partial_{\delta z} J_{n_1, n_2}^{(d)}(\delta z) = -(d-5) \left( (1-z_1^2 - \delta z) J_{n_1-1, n_2-1}^{(d-2)} + J_{n_1, n_2}^{(d-2)} + z_1 (J_{n_1, n_2-1}^{(d-2)} + J_{n_1-1, n_2}^{(d-2)}) \right). \quad (\text{A.7.30})$$

This recursion can be used in even  $d$  and in odd  $d \geq 7$ . The case of  $d = 5$  can be treated explicitly similarly to the case of  $d = 3$  in the previous section.

### A.7.2 More General Integral

Above we obtained the following result

$$I(d, n, z_1) = \int_{z_1}^{\infty} dz (z^2 - 1)^{\frac{d-4}{2}} \frac{Q_J^{(d)}(z)}{(z-z_1)^{\frac{d-3}{2}-n}} = \frac{\Gamma(\frac{d}{2}-1)\Gamma(n+\frac{5-d}{2})}{2^{n-\frac{d-5}{2}}\Gamma(\frac{3}{2}+n)} (z_1^2-1)^{n+\frac{1}{2}} Q_{J-n+\frac{d-5}{2}}^{(2n+5)}(z_1). \quad (\text{A.7.31})$$

Let us consider a slightly more general integral

$$I(d, n, m, z_1) \equiv \int_{z_1}^{\infty} dz (z^2 - 1)^{\frac{d-4}{2}} Q_J^{(d)}(z) \frac{1}{(z-z_1)^{\frac{d-3}{2}}} \frac{(z-z_1)^n}{(z-1)^m}, \quad n, m \geq 0. \quad (\text{A.7.32})$$

The advantage of this integral is that for  $m = n$  this is a natural threshold expansion in terms of  $\frac{z-z_1}{z-1}$  which does not grow for  $z \rightarrow \infty$ . For  $m = 0$  we get (A.7.31).

We can rewrite this integral as follows

$$\begin{aligned} \frac{1}{(z-1)^m} &= \frac{1}{(z-z_1 + [z_1-1])^m} \\ &= \frac{1}{\Gamma(m)} \int_{-i\infty}^{i\infty} \frac{d\alpha}{2\pi i} \Gamma(m+\alpha)\Gamma(-\alpha) \frac{(z_1-1)^\alpha}{(z-z_1)^{m+\alpha}}, \quad -m < \text{Re } \alpha < 0. \end{aligned} \quad (\text{A.7.33})$$

In this way we immediately get

$$I(d, n, m, z_1) = \frac{1}{\Gamma(m)} \int_{-i\infty}^{i\infty} \frac{d\alpha}{2\pi i} \Gamma(m+\alpha)\Gamma(-\alpha) \frac{I(d, n-m-\alpha, z_1)}{(z_1-1)^{m+\alpha}}, \quad (\text{A.7.34})$$

where the large  $z$  convergence requires  $\text{Re } J > n - m - \text{Re } \alpha - \frac{d-3}{2}$ . Next we can use the Mellin representation for the hypergeometric function

$${}_2F_1(a, b, c, z) = \frac{\Gamma(c)}{\Gamma(a)\Gamma(b)} \int \frac{ds}{2\pi i} \frac{\Gamma(a+s)\Gamma(b+s)\Gamma(-s)}{\Gamma(c+s)} (-z)^s. \quad (\text{A.7.35})$$

## Appendix A. Appendix to Chapter 2

---

To use straight contour we would like to have  $\text{Re}[a, b, c] > 0$ . For the case above this becomes

$$n - m < \alpha < 1 - m + n. \quad (\text{A.7.36})$$

Therefore to apply the formula for  $n = m$  we need to deform the contour across  $\alpha = 0$  pole and pick the residue. We then perform the  $\alpha$  integration.

Let us for simplicity present the result for  $d = 4$  and  $m = n$

$$\begin{aligned} \frac{I(4, n, n, z_1)}{\sqrt{2\pi} \lambda_1^{-J-\frac{1}{2}}} &= \frac{1}{2J+1} - \sqrt{\frac{\lambda_1-1}{\lambda_1+1}} \sum_{k=0}^{\infty} \frac{1}{(\lambda_1^2-1)^k} \frac{\Gamma(1+J)\Gamma(n+\frac{1}{2})\Gamma(k+\frac{1}{2})}{\Gamma(\frac{1}{2}-k)\Gamma(k+1)\Gamma(J+k+\frac{3}{2})\Gamma(n)} \\ &\quad \times {}_3F_2\left(1+J, k+\frac{1}{2}, n+\frac{1}{2}; \frac{3}{2}, \frac{1}{2}-k, \frac{\lambda_1-1}{\lambda_1+1}\right) \\ &\quad + \frac{2}{\sqrt{\pi}} \frac{\lambda_1-1}{\lambda_1+1} \sum_{k=0}^{\infty} \left(\frac{4}{(1+\lambda_1)^2}\right)^{2k} \frac{\Gamma(k+n+1)\Gamma(k+\frac{1}{2})}{\Gamma(n)\Gamma(2k+3)} \\ &\quad \times {}_3F_2\left(\frac{3}{2}+J+k, 2k+1, n+k+1; k+\frac{3}{2}, k+2, \frac{\lambda_1-1}{\lambda_1+1}\right). \end{aligned} \quad (\text{A.7.37})$$

For given  $n$  this can be quite easily expanded at large  $J$ . Important property of this expansion is that higher terms in  $k$  have an extra suppression in  $\frac{1}{J}$ . Using this formula one can in principle repeat the analysis of section 2.6 up to an arbitrary high order in  $\frac{z-z_1}{z-1}$  without spoiling the Regge behavior of the amplitude.

## A.8 Keyhole Integrals in Odd $d$

In this appendix we collect some of the useful integrals in odd  $d$ . They appear both in the large  $J$  expansion of partial waves, and in the threshold expansion of the double spectral density. A key difference compared to even  $d$  is appearance of powers of both logarithm and inverse logarithm of the threshold expansion parameter  $\sigma_t$ .

### A.8.1 Partial Wave

In the discussion of the large  $J$  expansion we encountered the integral (2.6.6), and in odd  $d$  we introduced a function  $g_n(J)$  in (2.6.8) that controls the large  $J$  asymptotic behavior of partial waves. Let us compute it explicitly.

For the universal threshold asymptotic in odd  $d$ , see (2.5.7), the relevant integral takes the following form

$$g_n(\log J) = \frac{1}{2i} \oint_{\text{keyhole}} \frac{dz}{z^n} \frac{1}{\log \frac{z}{J} - i\pi} e^{-z}, \quad n = 0, 1, 2, \dots \quad (\text{A.8.1})$$

In our problem  $n = \frac{d-3}{2}$ . The keyhole contour is depicted in figure 2.10 and it naturally appears

when deriving the Froissart-Gribov formula.

For  $n = 0, 1$  ( $d = 3$  and  $d = 5$ ) it is not necessary to keep the keyhole since the integral (A.8.1) converges and we can simply write

$$g_{n=0,1}(\log J) = \int_0^\infty \frac{dz}{z^n} \frac{1}{\log^2 \frac{z}{J} + \pi^2} e^{-z}. \quad (\text{A.8.2})$$

To compute  $n \geq 2$  it is convenient to slightly modify the integral and use the following recursion relation

$$g_n(\log J, \alpha) = \frac{1}{2i} \oint_{\text{keyhole}} \frac{dz}{z^n} \frac{1}{\log \frac{z}{J} - i\pi} e^{-\alpha z},$$

$$\partial_\alpha g_n(\log J, \alpha) = -g_{n-1}(J, \alpha), \quad (\text{A.8.3})$$

with the starting point given by  $g_0(\log J, \alpha)$  which does not require regularization and can be efficiently computed numerically, see (A.8.2). We also note that

$$\lim_{J \rightarrow \infty} g_n(\log J, \alpha) = 0, \quad (\text{A.8.4})$$

which allows us to fix the integration constant in the differential equation (A.8.3). The original integral (A.8.2) is recovered by setting  $\alpha = 1$ .

Let us start with  $n = 0$ . It is convenient to rewrite the  $n = 0$  integral as follows

$$g_0(J) = \Gamma(1 - \partial_{\log J}) \frac{1}{(\log J)^2 + \pi^2} = \frac{1}{\log^2 J} + \dots \quad (\text{A.8.5})$$

A slight advantage of writing  $\Gamma(1 - \partial_{\log J})$  is that to generate the large  $J$  expansion we can treat  $\partial_{\log J}$  in the argument of gamma-function as a small parameter.

To derive (A.8.5) we can write more generally

$$\Gamma(1 - \partial_{\log J}) g(\log J) \equiv \int_0^\infty dt e^{-t} t^{-\partial_{\log J}} g(\log J) = \int_0^\infty dt e^{-t} g(\log \frac{J}{t}) = J \mathcal{L}[g(-\log t)](J), \quad (\text{A.8.6})$$

where we used that  $e^{-a\partial_x} g(x) = g(x - a)$ .

By solving the recursion we then then get

$$g_1(J) = \Gamma(1 - \partial_{\log J}) \frac{i}{2\pi} \log \frac{1 - \frac{i\pi}{\log J}}{1 + \frac{i\pi}{\log J}} = \frac{1}{\log J} + \dots,$$

$$g_n(J) = \frac{(-1)^{n-1}}{\Gamma(n) \log J} + \dots \quad (\text{A.8.7})$$

## Appendix A. Appendix to Chapter 2

---

More generally, we can write

$$g_n(\log J) = \Gamma(1 - \partial_{\log J}) \hat{g}_n(\log J) = J \mathcal{L}[\hat{g}_n(-\log t)](J), \quad (\text{A.8.8})$$

where a few of the  $\hat{g}_n$ 's were listed above in (A.8.7). Note that (A.8.7) can be easily computed numerically for finite  $J$  using (A.8.6). This is an advantage compared to the original integral (A.8.1) which requires a keyhole regularization.

The leading large  $J$  asymptotic of partial waves in odd  $d$  therefore takes the form

$$\begin{aligned} \hat{f}_J(s) &= 2^{5-d} n_0^{(d)} m^{4-d} J^{\frac{d-3}{2}} \left( \frac{z_1 - 1}{z_1 + 1} \right)^{\frac{d-3}{4}} \pi^2 g_{\frac{d-3}{2}} \left( \log J \sqrt{\frac{z_1 - 1}{z_1 + 1}} \right) \\ &= 2^{5-d} n_0^{(d)} m^{4-d} J^{\frac{d-3}{2}} \left( \frac{z_1 - 1}{z_1 + 1} \right)^{\frac{d-3}{4}} \pi^2 J \mathcal{L}[\hat{g}_{\frac{d-3}{2}}(-\log \sqrt{\frac{z_1 + 1}{z_1 - 1}} \delta z)](J). \end{aligned} \quad (\text{A.8.9})$$

### A.8.2 Double Spectral Density

We next consider the problem of computing of  $\rho(s, t)$  close to the threshold in odd  $d$  for the universal threshold asymptotic (2.5.7). The idea is to use the result of the previous subsection together with elastic unitarity.

Recall that due to elastic unitarity for  $4m^2 < s < 16m^2$  we have, see (2.6.11) and (2.6.12),

$$\text{Im} \hat{f}_J(s) = 2^{-\frac{d+5}{2}} J^{\frac{1-d}{2}} m^{d-4} \pi^{\frac{1-d}{2}} z_1^{\frac{3-d}{2}} \left( \frac{z_1 - 1}{z_1 + 1} \right)^{\frac{5-d}{4}} |\hat{f}_J(s)|^2. \quad (\text{A.8.10})$$

Using the results of the previous subsection we can immediately read off the large  $J$  expansion of  $\text{Im} \hat{f}_J(s)$ . The latter is related to  $\rho(s, t)$  as follows, see (2.6.11),

$$\begin{aligned} \text{Im} \hat{f}_J(s) &= J \mathcal{L}[\rho(s, t(\delta z))](J) = J \int_0^\infty d\delta z e^{-J\delta z} \rho(s, t(\delta z)), \\ t(\delta z, J) &= 8m^2 \left( z_1 + 1 + z_1 \left( \frac{z_1 + 1}{z_1 - 1} \right)^{1/2} \delta z \right), \end{aligned} \quad (\text{A.8.11})$$

where the integral in the first line should be defined via the keyhole contour whenever it is divergent. For the universal threshold behavior in odd  $d$  this happens for  $d \geq 9$ .

Let us limit ourselves to the situations when the integral (A.8.11) does not require the keyhole regularization, namely  $d < 9$ . In this case the elastic unitarity takes the form

$$\mathcal{L}[\rho(s, t(\delta z))](J) = 2^{-\frac{5}{2}(d-3)} m^{d-4} (n_0^{(d)})^2 \pi^{\frac{9-d}{2}} z_1^{\frac{3-d}{2}} \left( \frac{z_1 - 1}{z_1 + 1} \right)^{\frac{d-1}{4}} J^{\frac{d-3}{2}} \left( \mathcal{L}[\hat{g}_{\frac{d-3}{2}}(-\log \sqrt{\frac{z_1 + 1}{z_1 - 1}} \delta z)](J) \right)^2. \quad (\text{A.8.12})$$

Using the basic properties of the Laplace transform we can rewrite this as follows

$$\begin{aligned} \rho(s, t(\delta z)) &= 2^{-\frac{5}{2}(d-3)} m^{d-4} (n_0^{(d)})^2 \pi^{\frac{9-d}{2}} z_1^{\frac{3-d}{2}} \left( \frac{z_1-1}{z_1+1} \right)^{\frac{d-1}{4}} \\ & \quad (-1)^{\frac{d-3}{2}} \partial_{\delta z}^{\frac{d-3}{2}} \int_0^{\delta z} d\delta z' \hat{g}_{\frac{d-3}{2}}(-\log \sqrt{\frac{z_1+1}{z_1-1}} \delta z') \hat{g}_{\frac{d-3}{2}}(-\log \sqrt{\frac{z_1+1}{z_1-1}} [\delta z - \delta z']) . \end{aligned} \quad (\text{A.8.13})$$

Together with the result of the previous subsection it allows us to compute the leading threshold contribution to the double spectral density.

Let us analyze in a little bit more detail the case of  $d = 3$ . In this case we get

$$\begin{aligned} \rho(s, t(\delta z)) &= (n_0^{(d)})^2 m \pi^3 \left( \frac{z_1-1}{z_1+1} \right)^{\frac{1}{2}} \int_0^{\delta z} d\delta z' \frac{1}{[\log \left( \frac{z_1+1}{z_1-1} \right)^{\frac{1}{2}} \delta z']^2 + \pi^2} \frac{1}{[\log \left( \frac{z_1+1}{z_1-1} \right)^{\frac{1}{2}} (\delta z - \delta z')]^2 + \pi^2} \\ &= (n_0^{(d)})^2 m \pi^3 \left( \frac{z_1-1}{z_1+1} \right)^{\frac{1}{2}} \delta z \int_0^1 dx \frac{1}{[\log \left( \frac{z_1+1}{z_1-1} \right)^{\frac{1}{2}} \delta z x]^2 + \pi^2} \frac{1}{[\log \left( \frac{z_1+1}{z_1-1} \right)^{\frac{1}{2}} \delta z (1-x)]^2 + \pi^2} \\ &= (n_0^{(d)})^2 m \pi^3 \left( \frac{z_1-1}{z_1+1} \right)^{\frac{1}{2}} \frac{\delta z}{\left( \log \left( \frac{z_1+1}{z_1-1} \right)^{\frac{1}{2}} \delta z \right)^4} \left( 1 + \frac{4}{\log \left( \frac{z_1+1}{z_1-1} \right)^{\frac{1}{2}} \delta z} + \frac{20 - \frac{8}{3} \pi^2}{\log^2 \left( \frac{z_1+1}{z_1-1} \right)^{\frac{1}{2}} \delta z} + \dots \right) . \end{aligned} \quad (\text{A.8.14})$$

One can easily check that the leading order result agrees with the formulas in the main body.



# B Appendix to Chapter 3

## B.1 Analytical multi-particle Landau curves

Here we collect explicit equations for some of the multi-particle Landau curves discussed in the paper. For convenience we set the mass  $m = 1$ . We refer to the various diagrams by their colors as depicted on figure 3.5.

**Red curve** (the accumulation curve)

$$(s - 16)(t - 16) - 192 = 0. \quad (\text{B.1.1})$$

**Planar cross** (see figure 3.3.a, and [96])

$$s^3(t - 16) + t^3(s - 16) + 24st(s + t - 18) - 2s^2t^2 = 0. \quad (\text{B.1.2})$$

**Non-planar cross** (see figure 3.3.b, and [96])

$$\begin{aligned} & \frac{1}{3}s^3t^3u^3 - 48s^3t^3u^2 + 768s^3t^3u - 4096s^3t^3 + 4096s^3 \\ & + 8512s^2t^2u^2 - 503808s^2t^2 - 36864(s^2t + st^2) \\ & + 138240(s^3t^2 + s^2t^3) - 790528stu + (\text{cyclic}) = 0, \end{aligned} \quad (\text{B.1.3})$$

where  $s + t + u = 4$ . Curiously in the region  $0 < s, t, u < 4$  this curve can be written as [273]

$$\left(\frac{s}{16}\right)^{\frac{1}{3}} + \left(\frac{t}{16}\right)^{\frac{1}{3}} + \left(\frac{u}{16}\right)^{\frac{1}{3}} = 1. \quad (\text{B.1.4})$$

**Green curve**

$$s^2t^2 - 16s^2t - 32st^2 + 224st + 256(t - 1)^2 = 0. \quad (\text{B.1.5})$$

**Blue curve**

$$(s - 16)^3 t^2 + (s - 4)(s - 16)^3 t - 16((s - 10)s + 32)^2 = 0. \quad (\text{B.1.6})$$

Curves (B.1.1), (B.1.5) and (B.1.6) were found using the 2-particle kernel. See appendix B.2.

**B.2 Multi-particle Landau curves from 2-particle unitarity**

As explained in section 3.1, we can assign graphs to singularities that follow from continuation of unitarity. They represent how unitarity integrals relate singularities of sub-graphs to singularities of the bigger graph. In this appendix we demonstrate such explicit relation directly at the level of the Landau curves, without using the Landau equations. It follows from a detailed analysis of the two-particle unitarity integral – the so-called Mandelstam kernel, see [7] for details.

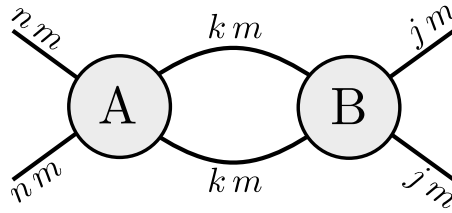


Figure B.1: The Landau curve of a graph **AB** that has a 2-particle cut is related to the singularities of sub-graphs **A** and **B**. The numbers indicate the mass of “on-shell” particles as integer multiples of  $m$ .

Consider a graph **AB** that can be split into two sub-graphs, **A** and **B**, by a 2-particle cut as illustrated in figure B.1. In this case, the Landau curve of **AB** ( $t_{\mathbf{AB}}(s)$ ) can be determined in terms of the curves of **A** ( $t_{\mathbf{A}}(s)$ ) and **B** ( $t_{\mathbf{B}}(s)$ ) from the following equation

$$\lambda_{n,j}(s, t_{\mathbf{AB}}(s)) = \lambda_{n,k}(s, t_{\mathbf{A}}(s)) \times \lambda_{k,j}(s, t_{\mathbf{B}}(s)), \quad (\text{B.2.1})$$

where

$$\lambda_{n,j}(s, t) = z_{n,j}(s, t) + \sqrt{z_{n,j}(s, t)^2 - 1}, \quad (\text{B.2.2})$$

and

$$z_{n,j}(s, t) = \frac{s - 2(nm)^2 - 2(jm)^2 + 2t}{\sqrt{s - 4(nm)^2} \sqrt{s - 4(jm)^2}}, \quad (\text{B.2.3})$$

is the cosine of the scattering angle between incoming particles of mass  $nm$  and outgoing particles of mass  $jm$ .

To illustrate (B.2.1) consider the leading elastic Landau curve that is plotted in gray in figure 3.5. It is represented by the graph on figure B.2 and has a single 2-particle cut along the  $s$ -channel. Since either sub-diagram has a normal threshold at  $t = 4m^2$  and all legs have the same mass



## B.2 Multi-particle Landau curves from 2-particle unitarity

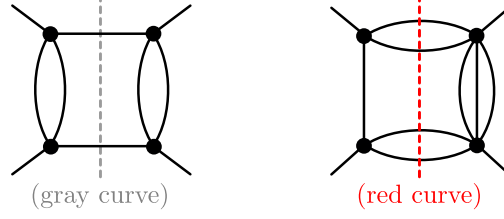


Figure B.2: Diagrams with a single  $s$ -channel cut which splits each diagram into a pair of  $t$ -channel bubbles. The Landau curves of these diagrams follows from the singularities of the bubbles, which are simple normal thresholds. The Landau curve of the diagram on the left (gray curve in figure 3.5) is given by equation (B.2.4) while the diagram on the right (red curve in figure 3.5) has Landau curve given by equation (B.2.7).

$m$ , the corresponding Landau curve is given by

$$\lambda_{1,1}(s, t_{\text{gray}}(s)) = \left( \lambda_{1,1}(s, 4m^2) \right)^2, \quad (\text{B.2.4})$$

which in polynomial form reads

$$(s - 4m^2)(t - 16m^2) - 64m^4 = 0. \quad (\text{B.2.5})$$

Swapping  $s \leftrightarrow t$  leads to the leading elastic curve that follows from  $t$ -channel unitarity. Both are represented in gray in figure 3.5.

Note that equation (B.2.1) can be iterated. By gluing **AB** to a new diagram **C** one can express the Landau curve of **ABC** as

$$\lambda_{n,j}(s, t_{\text{ABC}}(s)) = \lambda_{n,k}(s, t_{\text{A}}(s)) \times \lambda_{k,l}(s, t_{\text{B}}(s)) \times \lambda_{l,j}(s, t_{\text{C}}(s)). \quad (\text{B.2.6})$$

One may further iterate (B.2.6) by gluing more sub-diagrams. If all sub-diagrams **A**, **B**, **C**, ... are taken to be  $t$ -channel bubbles then the full graph **ABC**... becomes a ladder diagram. Every Landau curve belonging to the elastic region  $4m^2 < s < 16m^2$  is represented by a ladder diagram, and every elastic curve can be computed accordingly (see section 3.5 of [7]).

Interestingly, the 2-particle kernel may also be used to determine some of the Landau curves in the multi-particle regime  $s, t > 16m^2$ . This is because a bubble diagram with  $n$  legs of mass  $m$  is indistinguishable from a graph where this bubble is replaced by a single on-shell particle of mass  $nm$  (see appendix B.4). We may therefore use equation (B.2.1) to determine the red Landau curve in figure 3.5 whose diagram and cut is represented in figure B.2

$$\lambda_{1,1}(s, t_{\text{red}}(s)) = \lambda_{1,2}(s, m^2) \lambda_{2,1}(s, 9m^2). \quad (\text{B.2.7})$$

Similarly, we may use equation (B.2.6) to compute the blue and green Landau curves in figure

## Appendix B. Appendix to Chapter 3

3.5, according to the slicing in figure B.3.

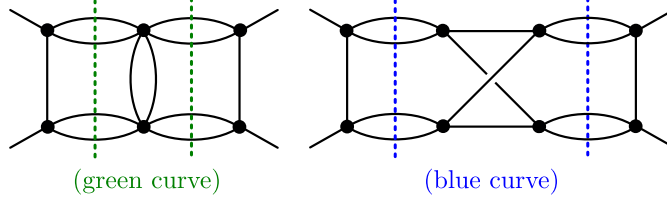


Figure B.3: Slicing of multi-particle graphs with 2-particle cuts where each cut bubble corresponds to a particle of mass  $2m$ . equation (B.2.6) may be used to find the Landau curves represented by these diagrams. Green is given by equation (B.2.8) and blue follows from eqs. (B.2.9) and (B.2.10).

The green Landau curve reads

$$\lambda(s, t_{\text{green}}(s)) = \lambda_{1,2}(s, m^2) \lambda_{2,2}(s, 4m^2) \lambda_{2,1}(s, m^2), \quad (\text{B.2.8})$$

which, in polynomial form, is given by equation (B.1.5).

The blue Landau curve can be expressed in terms of the Landau curve  $t_*(s)$  of the sub-diagram in the middle (see figure B.4),

$$\lambda(s, t_{\text{blue}}(s)) = \lambda_{1,2}(s, m^2) \lambda_{2,2}(s, t_*(s)) \lambda_{2,1}(s, m^2). \quad (\text{B.2.9})$$

We can now relate  $t_*(s)$  to the Landau curve of a simple box diagram by crossing  $s$ - and  $u$ -channels.

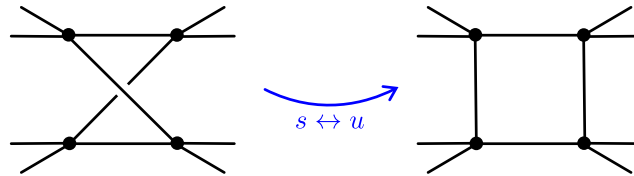


Figure B.4: Crossing  $s \leftrightarrow u$  channels relates the Landau curve of the middle sub-graph of (Blue) in figure B.3 with the curve of a simple box diagram. To each external vertex a bubble is connected, which is equivalent to considering  $2 \rightarrow 2$  scattering of particles with mass  $2m$ .

Using (B.2.1) we can find the Landau curve of the box diagram and  $t_*(s)$  is the solution of

$$\lambda_{2,2}(u, t_*(s)) = \lambda_{2,1}(u, m^2) \lambda_{1,2}(u, m^2), \quad (\text{B.2.10})$$

where in the formula above we set  $u = 16m^2 - s - t_*(s)$ . Plugging  $t_*(s)$  back into (B.2.9) leads to the blue curve in figure 3.5, which is expressed in polynomial form in (B.1.6).

For the graphs in this section, we have explicitly checked that the obtained Landau curves correspond to the  $\alpha$ -positive solutions of the Landau equations. However, this is not always the case. For example, the graph in figure B.5 does not admit an  $\alpha$ -positive solution. Applying to it the procedure described in this section produces a Landau curve which we believe is on

the second sheet.

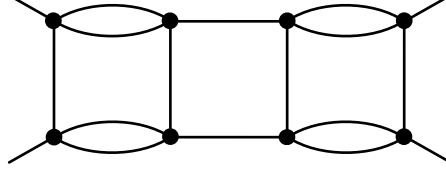


Figure B.5: A graph whose Landau curve (more precisely, its leading singularity) can be found using the method described in this section. The Landau curve sits between the blue and red curves in figure 3.5. Given that it is not  $\alpha$ -positive, we do not expect it to be on the physical sheet. In the graph selection procedure, this graph was discarded by identification of a trivial box (see figure B.13).

### B.3 Landau equations and automorphisms

Here we briefly review the standard derivation of the Landau equations for the Feynman diagrams, see for example [8] and [102] for a recent review. A generic Feynman integral with trivial numerators takes the form

$$F = \int \prod_{j=1}^L d^d k_j \int_0^1 \prod_{i=1}^P d\alpha_i \frac{\delta(1 - \sum_i \alpha_i)}{\psi^P}, \quad (\text{B.3.1})$$

where  $L$  are the number of loops,  $P$  the number of internal lines and the denominator reads

$$\psi = \sum_{j=1}^P \alpha_j (k_j^2 - m_j^2), \quad (\text{B.3.2})$$

where the  $k_{j>L}$  momenta depend linearly on the loop momenta  $k_{j\leq L}$ , due to momentum conservation at each vertex.

The integration over the loop momentum can then be readily done and yields

$$F = \int_0^1 \prod_{j=1}^P d\alpha_j \frac{\delta(1 - \sum_{j=1}^P \alpha_j) C^{P-2L-2}}{D^{P-2L}}, \quad (\text{B.3.3})$$

with

$$C = \det a_{ij}, \quad D = \det \begin{pmatrix} a_{ij} & -b_j \\ -b_j & c \end{pmatrix}, \quad (\text{B.3.4})$$

where  $i, j = 1, \dots, L$  and

$$a_{ij} = \frac{1}{2} \frac{\partial^2 \psi}{\partial k_i \partial k_j} \Big|_{k=0}, \quad b_j = \frac{1}{2} \frac{\partial \psi}{\partial k_j} \Big|_{k=0}, \quad c = \psi \Big|_{k=0}. \quad (\text{B.3.5})$$

As the integral is analytically continued in the Mandelstam variables, the contour of integration

## Appendix B. Appendix to Chapter 3

---

may be smoothly deformed to avoid the singularities. The integral becomes singular when the contour is pinched by singularities of the integrand.

The so-called *leading singularities* occur whenever two (or more) zeros of the denominator coincide.<sup>1</sup>

These can be found by solving

$$\frac{\partial \psi}{\partial \alpha_i} = 0, \quad \frac{\partial \psi}{\partial k_j} = 0. \quad (\text{B.3.6})$$

The first condition puts all internal legs on-shell,  $k_i^2 = m_i^2$ , while the third condition relates momenta belonging to the same loop,  $l$ , as

$$\sum_{i \in l} \alpha_i k_i = 0. \quad (\text{B.3.7})$$

An equivalent form of the Landau equations is obtained for representation (B.3.3),

$$D = 0, \quad \frac{\partial D}{\partial \alpha_i} = 0. \quad (\text{B.3.8})$$

Note that since  $D \propto \alpha_i \frac{\partial D}{\partial \alpha_i}$  is homogeneous,  $D = 0$  is automatically satisfied.

There are  $P + 2$  variables,  $s$ ,  $t$  and the  $\alpha$  parameters, and  $P + 1$  Landau equations, which are the  $P$  pinch conditions (B.3.8) supplemented by the normalization

$$\sum_{i=1}^P \alpha_i = 1. \quad (\text{B.3.9})$$

These equations may be solved for  $\alpha_i(s)$  and  $t(s)$ , the Landau curve.

In this work we made use of the form (B.3.6) to discard trivial subgraphs (see appendix B.4), while (B.3.8) is used for numerical computation of the Landau curves (see appendix B.5) since  $D$  is an explicit function of  $s$  and  $t$ .

As discussed in section 3.1, we restricted ourselves to the  $\alpha$ -positive solutions because these occur on the undistorted contour of integration of (B.3.1) and (B.3.3), and are therefore likely to be on the physical sheet.<sup>10</sup>

We observe that non-trivial graphs (see section 3.2) have a unique  $\alpha$ -positive solution, corresponding to the Landau curve represented by that graph. We assume that it is always the case.

Under this assumption, one can derive an important result which allows for dramatic simplifi-

---

<sup>1</sup>There are also end-point singularities, corresponding to pinches at end-points of the integration contour. However, in the context of Feynman integrals, these are also leading singularities of contractions of the original graph [8].

cation of the Landau equations in the search for  $\alpha$ -positive solutions.

Symmetries of a graph translate into symmetries of the corresponding Landau equations. Concretely, if a transformation mapping edge  $i \rightarrow i'$  is an *automorphism* [101] (which also leaves  $(s, t)$  invariant) then the change  $\alpha_i \rightarrow \alpha_{i'}$  is a symmetry of the Landau equations (B.3.8). Therefore, if  $\alpha_i$  is a solution, then  $\alpha_{i'}$  is a solution to (B.3.8) as well.

Now, under the assumption that the  $\alpha$ -positive solution is unique we see that the automorphism  $i \rightarrow i'$  has to map the  $\alpha$ -positive solution to itself. Hence,

$$\alpha_i = \alpha_{i'}. \quad (\text{B.3.10})$$

This property can be used to reduce the system of Landau equations, if one identifies the automorphisms that leave the Mandelstam invariants unchanged. Note that  $(s, t)$  are left invariant if the external legs are swapped in pairs or, trivially, if they remain still.<sup>2</sup> If there are also automorphisms that map  $s \leftrightarrow t$ , the Landau curve is crossing-symmetric and further reduction is possible at the point  $s = t$ .

Given a graph, the exact expression for  $D$  and the graph automorphisms can be found automatically using graph-theoretic tools. See appendix B.5 for the precise implementation.

## B.4 Trivial subgraphs

As discussed in the main text, a trivial sub-graph is a sub-graph that either do not have an  $\alpha$ -positive solution or can be contracted without affecting the solution to the Landau equations. In this appendix we identify a few families of trivial sub-graphs that are composed from bubbles, triangles and boxes.

### Bubbles

A bubble sub-graph is a set of  $n > 1$  legs connecting the same two vertices, see figure B.6. When solving the associated Landau equations, we attach to them parameters  $\alpha_i$  and momenta  $k_i$ , that are all taken to point towards the same vertex.

Each pair of these legs,  $(i, j)$ , form a loop and the associated Landau equation reads

$$\alpha_i k_i = \alpha_j k_j. \quad (\text{B.4.1})$$

Using the on-shell condition  $k_i^2 = m^2$  and requiring the  $\alpha$ 's to be positive leads to  $\alpha_i = \alpha_j$ .

<sup>2</sup>The latter case includes permutations between legs belonging to the same bubble. This implies that the corresponding parameters  $\alpha_i$  have the same value, as derived in appendix B.4.

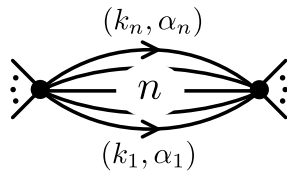


Figure B.6: A bubble sub-graph with  $n$  internal lines. Each line is associated with an on-shell momentum  $k_i^2 = m^2$  and a Feynman parameter  $\alpha_i$ . The Landau equation forces them all to be the same, making the bubble equivalent to a single line of mass  $n \times m$ .

Plugging this back into (B.4.1) leads to  $k_i = k_j$ .

Since all momenta are equal, the bubble diagram is indistinguishable from a single leg with mass  $n \times m$ .



Figure B.7: A sub-graph made of a chain of two bubbles with  $n$  and  $\tilde{n}$  lines correspondingly. The Landau equation forces  $n = \tilde{n}$ , making the chain equivalent to a single bubble and hence, a trivial sub-graph.

Consider now a chain of two bubbles, one with  $n$  lines and the other with  $\tilde{n}$  lines, connected through a single vertex, see figure B.7. Using momentum conservation at that vertex we conclude that in order to have a solution,  $\tilde{n}$  must be equal to  $n$ . In this case however, having two bubbles instead of one impose no further constraints on the external momenta. Hence, the Landau equations for the pair of bubbles are equivalent to the ones of a single bubble.

We conclude that a bubble is trivial if to one of its vertices another bubble is connected.

### Triangles

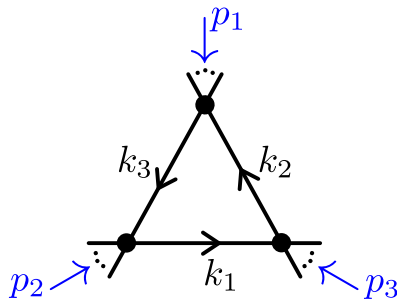


Figure B.8: A triangle sub-graph with three independent masses  $m_i^2$ . For  $p_1^2 = (m_2 \pm m_3)^2$  the triangle is trivial.

A triangle sub-graph consists of three vertices connected by three lines, (see figure B.8). To each line  $i = 1, 2, 3$  we associate an independent mass  $m_i$ , Feynman parameter  $\alpha_i$ , and momentum  $k_i$  that is oriented anti-clockwise around the loop. To each vertex we associate an incoming momentum  $p_i$ , with  $p_3 = k_1 - k_2$ , etc. The associated Landau equation reads

$$\alpha_1 k_1 + \alpha_2 k_2 + \alpha_3 k_3 = 0. \quad (\text{B.4.2})$$

By dotting this equation with  $k_{i=1,2,3}$ , we may express it as a condition on the Gram matrix

$$\begin{pmatrix} m_1^2 & k_1 \cdot k_2 & k_1 \cdot k_3 \\ k_1 \cdot k_2 & m_2^2 & k_2 \cdot k_3 \\ k_1 \cdot k_3 & k_2 \cdot k_3 & m_3^2 \end{pmatrix} \begin{pmatrix} \alpha_1 \\ \alpha_2 \\ \alpha_3 \end{pmatrix} = 0. \quad (\text{B.4.3})$$

Using momentum conservation, we express the Lorentz invariants in terms of the external momenta as

$$k_1 \cdot k_2 = \frac{m_1^2 + m_2^2 - p_3^2}{2}, \quad (\text{B.4.4})$$

and similarly for  $k_1 \cdot k_3$  and  $k_2 \cdot k_3$ .

The solutions to the Landau equations (B.4.3) can be classified into three types.

1. If one of the external momenta, say  $p_1$ , satisfies

$$p_1^2 = (m_2 \pm m_3)^2, \quad (\text{B.4.5})$$

but  $p_2$  and  $p_3$  do not satisfy an analogous relation then the only possible solution is with  $\alpha_1 = 0$ . This is not an  $\alpha$ -positive solution.

2. Suppose two of the external momenta satisfy conditions equivalent to (B.4.5). To have a solution with  $\alpha_i \neq 0$  also the third momenta has to obey a condition equivalent to (B.4.5) such that the product of signs in (B.4.5) is equal to  $-1$ . In that case, there is a line of solutions given by the relation

$$\pm \alpha_1 m_1 \pm \alpha_2 m_2 \pm \alpha_3 m_3 = 0, \quad (\text{B.4.6})$$

where the signs in (B.4.6) are dictated by the corresponding signs in (B.4.5). Requiring that  $\alpha_i > 0$  selects a line of solutions with one minus and two pluses in (B.4.6).

3. Finally, there are other solutions which are not of type (a), or (b) above, in which the triangle may be non-trivial.

While in principle a sub-triangle of type (b) may be non-trivial, we observed that until  $V = 8$  for quartic graphs and  $V = 5$  for sextic graphs, all such cases do not lead to a new curve. Two examples of this are given in figures B.9 and B.10. We assumed that this is general. Namely, that any type (b) sub-triangle belonging to a graph in the  $(4_s, 4_t)$  family does not lead to a new Landau curve. Under this assumption, if at least one of the external momenta satisfies (B.4.5) then the triangle is trivial.

Let us now translate this condition into a graph-theoretic criterion. A generic triangle will

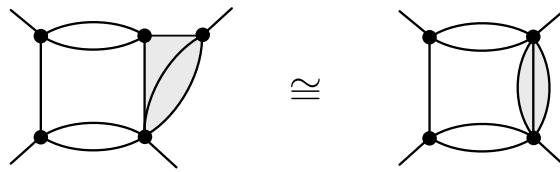


Figure B.9: An example of a sub-triangle (left) that is equivalent to a 3-particle bubble (right). The top right vertex of the triangle obeys condition (B.4.5) with a  $(-)$  sign while the top left vertex obeys this condition with a  $(+)$  sign. Therefore, in order for an  $\alpha$ -positive solution to be possible, the momenta  $p$  entering the bottom vertex must satisfy (B.4.5) with a  $(+)$  sign, i.e.  $p^2 = (m + 2m)^2 = 9m^2$ , which makes the triangle equivalent to the bubble with three legs on the right.



Figure B.10: The trivial “acnode” graph (left) and the accumulation graph (right) have the same Landau curve. Note that the acnode graph has two trivial triangles (top right and bottom left vertices satisfy (B.4.5), or equivalently (B.4.7)). No obvious graph-theoretic operation relates the graphs. It is also not clear to us how the Landau equations of the two are related, except by looking at the  $\alpha$ -positive solutions.

have bubbles as internal edges, (see figure B.11). As shown previously, a bubble is equivalent to single leg of mass  $n_i m$ , where  $n_i$  is the number of bubble legs.

Suppose that we further attach an external bubble to one of the vertices of the triangle, say the vertex where  $p_3$  in figure B.8 enters. Condition (B.4.5) for a triangle to be trivial then reads

$$N_3 = |n_1 \pm n_2|, \tag{B.4.7}$$

where  $N_3$  is the number of legs in the external bubble and  $n_1$  and  $n_2$  are the number of legs in internal bubbles that are attached to the vertex.

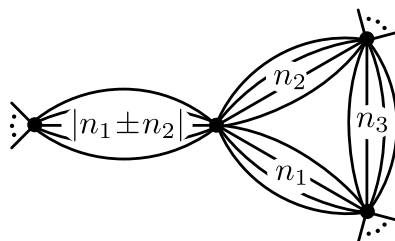


Figure B.11: A triangle is trivial if two of its internal bubbles, with  $n_1$  and  $n_2$  legs, are connected to an external bubble with  $|n_1 \pm n_2|$  legs.



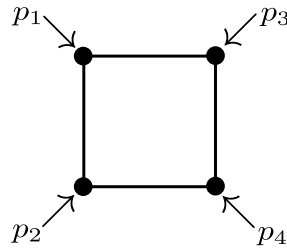


Figure B.12: Box graph. Besides the “masses”  $p_i^2$  there are also Mandelstam invariants  $s = (p_1 + p_2)^2$  and  $t = (p_1 + p_3)^2$  that participate in the Landau equations. This makes it hard to find a generic graph-theoretic condition for the box graph to be trivial.

### Boxes

A box sub-graph consists of four vertices, such that each vertex is connected to two other vertices, see figure B.12. For the box graph there are 4 external momenta  $p_i$  that flow into each vertex. Now, the kinematical invariants are not only the ‘masses’  $p_i^2$  but also the Mandelstam invariants  $s = -(p_1 + p_2)^2$  and  $t = -(p_1 + p_3)^2$ .

Because the Landau equations now involve  $s$  and  $t$ , a generic graph-theoretic condition for the box graph to be trivial is harder to find. However, for our purposes we do not need to discard trivial sub-boxes to quench the growth of graphs (identification of trivial triangles and bubbles allied with requiring all legs to be cut by 4-particle cuts is enough, see table 3.1.). Rather, after step 4 of the graph selection procedure described in section 3.2 there are still trivial graphs remaining. We were able to roughly discard half of them by identifying a trivial sub-box (see table 3.1). The remainder was eliminated by numerical search for an  $\alpha$ -positive solution (see appendix B.5).

In figure B.13 we present the boxes that were found to be trivial by explicitly solving the Landau equations (see [8]). Let us emphasize once again, that we call them trivial because the corresponding Landau equations do not admit an  $\alpha$ -positive solution. It does not mean that these boxes do not have a nontrivial double discontinuity.

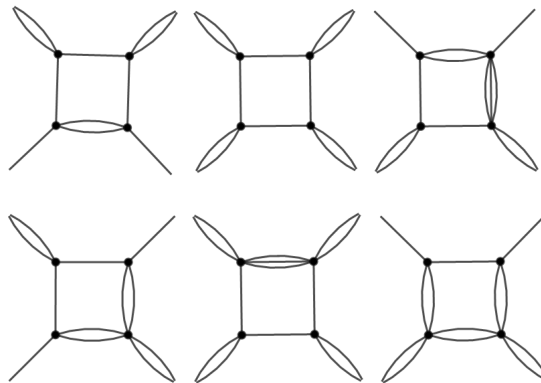


Figure B.13: A few examples of trivial boxes. We have explicitly checked that the presented graphs do not admit an  $\alpha$ -positive solution to the Landau equations.

## B.5 Graph-theoretic implementation

In this appendix we describe how the graph selection procedure outlined in section 3.2 is implemented in detail.

### Graph generation (step 1)

To obtain all graphs with  $V$  vertices and a certain maximal vertex degree, we start by generating all vacuum bubbles with  $V + 1$  vertices and the same maximal degree. We then remove a quartic vertex. The four legs that were connected to it become the external legs of the scattering graph (see figure B.14).

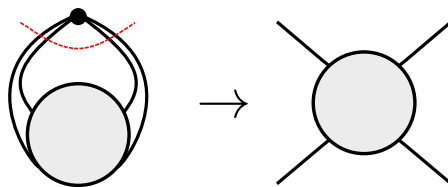


Figure B.14: Excision of a quartic vertex from a vacuum bubble (left) leads to a graph with 4 external legs (right).

To generate vacuum bubbles we make use of *nauty and Traces* [105], in particular the *geng* and *multig* commands. The *nauty/geng* command generates all simple non-isomorphic graphs with a given number of vertices  $V$  and minimum and maximum vertex degrees  $d_s$  and  $D_s$ .<sup>3</sup> The *nauty/multig* command takes a simple graph and turns each edge into a bubble (or multi-edge), according to maximum vertex degrees  $D_m$  and maximum edge multiplicity  $M$ . It outputs all possible graphs with bubbles out of that simple graph. See the documentation [105] for more information.

Finally, the output of *nauty/multig* (the *adjacency matrix* [101] of each graph) is inserted into *mathematica*. Using the package *igraph/M* [106, 107] and default tools we remove a quartic vertex from the vacuum bubble to obtain a graph with 4 external legs. This procedure is exemplified for the accumulation graph in figure B.15.

We now describe how the physical graph selection criteria described in 3.2 constrains the parameters  $D_s$ ,  $d$  and  $D_m$  and  $M$  that enter into *geng* and *multig*, respectively.

- $D_s = D_m = D$ . It is clear that if we are looking for graphs with 4 external legs with maximum vertex degree  $D$  then we can choose  $D_s = D_m = D$  as long as  $D \geq 4$  (so that there is a quartic vertex that can be removed from the vacuum bubble to generate the graph with 4 external legs). This condition is guaranteed because we are interested in  $D = 4, 6, 8, \dots$

---

<sup>3</sup>A simple graph is a graph without bubbles, only single edges [101], (see figure B.15).

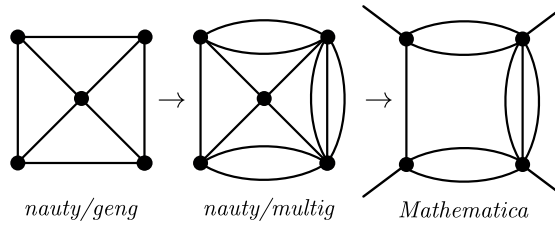


Figure B.15: Simple vacuum bubbles are generated using *nauty/geng* (left). Single lines are then replaced by bubbles in all possible ways using *nauty/multig* (center). Removal of quartic vertices (using *Mathematica*) leads to graphs with 4 external legs (right).

- $d_s = 3$ . Since we are only interested in vacuum bubbles it is clear that  $d_s > 1$ . Taking  $d_s = 2$  will generate quadratic simple vertices which, when run through *multig*, will give rise to bubble chains (see figure B.16) which are trivial sub-graphs (see appendix B.4). Thus, we should take  $d_s = 3$ . Indeed, in figure B.15 we see that the accumulation graph comes from a simple graph with cubic and quartic vertices (left).

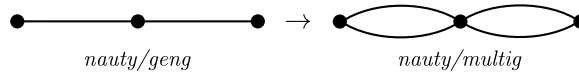


Figure B.16: Simple quadratic vertices (left) give rise to bubble chains (right).

- $M = 3$ .  $M$  is the maximum number of internal lines that a bubble can have. Since we are only interested in graphs with 4-particle cuts it is clear that  $M \leq 4$  suffices. Taking  $M = 4$  will generate 4-legged bubbles, which can be cut by a 4-particle cut, however for such graphs there will be no cut on any other channel (see figure B.17).

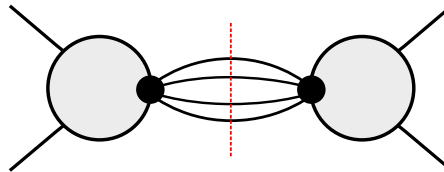


Figure B.17: A graph with a 4-legged bubble has a 4-particle cut on one channel. However, there is no space left for a cut on the other channel.

We import the vacuum bubbles generated by *multig* into *mathematica* and keep the ones with even degree vertices.

Finally, we discard graphs which only have a cut in one of the channels. This can be done at this stage without explicitly performing the cuts in the following way.

First, we require all graphs to be *bi-connected* [101]. A bi-connected graph can only be disconnected by removing two vertices. A non-bi-connected graph can be disconnected by removing a single vertex. Contracting the bubble in figure B.17 leads to a generic non-bi-connected

## Appendix B. Appendix to Chapter 3

---

graph with arbitrary ‘gray blobs’ connected by a single vertex. Similarly to the original graph, it only has a cut in one of the channels.

Second, we require that the quartic vertex that is excised from the vacuum bubble does not have any bubble incident to it. This avoids the scenario represented in figure B.18 where two external legs, which were originally part of a bubble, become incident to the same vertex. Such graphs also only have a cut in one of the channels. In practice, we can avoid generating such graphs by only excising vertices which were also quartic vertices in the original simple vacuum bubble.<sup>4</sup>

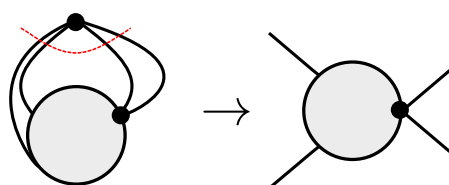


Figure B.18: Excising quartic vertices which are incident to bubbles (left) leads to graphs with cuts on only one single channel (right). Note that a quartic vertex which is incident to a bubble is a cubic simple vertex.

### Graph selection (steps 2-5)

Here we describe how steps 2-5 of the graph selection procedure described in section 3.2 are implemented in detail. We make use of *mathematica* and the package *igraph/M* [106, 107].

#### Trivial subgraphs

The function *IGTriangles* finds all triangles contained within any graph. Once the triangles are identified we select the cubic simple vertices (the vertices which can have an external bubble attached to it). Then, the *incidence list* [101] lists all incident edges to a given vertex. From this we can explicitly check condition (B.4.7). If any of the vertices satisfies (B.4.7) we have identified a trivial triangle and the graph is discarded.

A similar approach is taken to find boxes, except that there is no dedicated command to find boxes. We make use of *FindCycle* to find 4-cycles (i.e. boxes). We then compare the boxes with any of the trivial boxes in figure B.13 using *IGIsomorphic*. In fact, given the handful amount of graphs after step 4 (see table 3.1) one can just identify the trivial boxes by visual inspection.

---

<sup>4</sup>For example, in figure B.15 we have 3 quartic vertices on the vacuum bubble in the center. However, only the central vertex leads to a graph with cuts on both channels. It is also the only quartic vertex in the simple vacuum bubble (left).

**Cuts**

We are interested in minimal<sup>7</sup> cuts that separate external legs in pairs. There are three possible arrangements between pairs of external legs, corresponding to  $s$ -,  $t$ - and  $u$ -channels. To explicitly find these cuts for a given graph we apply the following procedure (depicted in figure B.19).

1. Identify the 4 vertices to which the external legs are incident. We call these *external* vertices.
2. Connect the external vertices in pairs, in all three possible ways ( $s$ ,  $t$  and  $u$ -channels).
3. Find the source-to-sink [101, 274] minimal cuts which separate a connected pair of external vertices (source) from the other pair of external vertices (sink). Here we use *IGMinimumCutValue* or *IGFindMinimalCuts* (see below).
4. The cuts of the original graph can then be obtained by matching the cut legs found in the previous step.

In step 3 of the graph selection procedure we only ask if there is a 2 or 4-particle cut in at least two channels. For this we make use of the fast *IGMinimumCutValue* which gives the size of the smallest cut.

In step 4 we ask if all legs can be cut by a 2 or 4-particle cut. Here, we make use of *IGFindMinimalCuts* and select the cuts of size up to 4. If every internal leg is contained in (the union of) these cuts we select that graph.

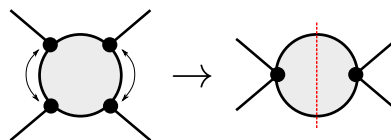


Figure B.19: A cut can be found by connecting external vertices (represented in black) in pairs. Each pair turns into two vertices, *source* and *sink*, and the cut separating external legs becomes a *source-to-sink cut* [101] which can be found using graph-theoretic algorithms [274].

**Numerical search for  $\alpha$ -positive solutions (step 6)**

Here, we describe how the final step of the graph selection procedure is implemented in practice. At this stage no more than a handful number of graphs exists (see table 3.1). Explicit numerical search for a solution to the Landau equations is therefore feasible.

We implement this step in `mathematica` (with the package *igraph/M* [106, 107]). We are given as input a graph, and the output is an  $\alpha$ -positive solution (if found) of the Landau equations at some fixed value of  $s$ . We in particular searched along the  $s = t$  line point due to the existence

## Appendix B. Appendix to Chapter 3

---

of enhanced symmetry and consequent reduction of the Landau equations for some graphs (see appendix B.3). We also set  $m = 1$  without loss of generality.

The algorithm is as follows.

1. Each bubble of  $n$  internal legs is replaced by a single line with mass  $n$ . The graph becomes a simple graph.
2. A random direction is assigned to the internal edges of the graph, the corresponding *incidence matrix* [101] is found and momentum conservation at each vertex follows (see below for more details).
3. The momentum conservation equations are solved in terms of a set of independent momenta (the loop momenta). Then, the on-shell action  $\psi$  as defined in eq. (B.3.2) is computed and from there the discriminant  $D$  is found from eqs. (B.3.4) and (B.3.5).
4. The Landau equations follow from (B.3.8). Since we are searching for the  $\alpha$ -positive solution under the assumption that it is unique. We can relate different  $\alpha_i = \alpha_{i'}$  if the graph is automorphic under the map  $i \rightarrow i'$  (see appendix B.3). The automorphisms are found using *GraphAutomorphismGroup*.
5. To solve the Landau equations numerically, we square the LHS of (B.3.8) and sum over  $i$  (after the reduction described in the previous step is performed). The solutions to the Landau equations will be the minima of  $\sum_i \left(\frac{\partial D}{\partial \alpha_i}\right)^2 = 0$ . We perform a random search using *FindMinimum* with random starting points  $\alpha_i \in (0, 1)$  and  $s \in (-1000, 1000)$ . The search stops when an  $\alpha$ -positive solution is found. A maximum of 1000 attempts was set.

Naturally, as the number of vertices increases, the system of equations becomes bigger, and the search for solutions becomes slower. Fortunately, at step 6 of the graph selection (see table 3.1), the majority of graphs for which this procedure was implemented enjoy some degree of symmetry, which drastically reduces the computing time. For example,  $\mathbb{Z}_2$  symmetry roughly halves the number of independent  $\alpha_i$ 's in the Landau equations of a generic large graph.

For  $V > 8$  all quartic graphs after elimination of trivial boxes (step 5) consist of triangle chains depicted in figure 3.4 and slight variations. For one particular variation (see figure B.20) there is no automorphism relating different  $\alpha_i$ . For graphs with  $V \geq 8$  belonging to this family we were not able to perform 1000 attempts. However, we believe that any graph belonging to this family is trivial given that for  $V = 4, 5, 6$  this can be proven analytically (identification of trivial triangle or box) and for  $V = 7$  no solution was found in 1000 attempts.

### Incidence matrix and momentum conservation

The incidence matrix  $a_{ij}$  is defined as  $a_{ij} = \pm 1$  if edge  $j$  is incident and directed into (+) or out of (-) vertex  $i$ , and  $a_{ij} = 0$  if edge  $j$  and vertex  $i$  are not incident (see figure B.21).

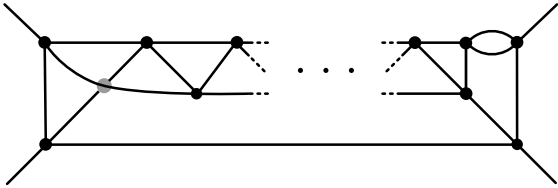


Figure B.20: Asymmetric variation of the triangle chain represented in figure 3.4. It is obtained by expanding into a bubble one of the vertices connecting to an external leg. This variation exists for both planar and non-planar iterations (represented by the gray vertex). For the first three iterations one can prove analytically that such graphs are trivial. For the fourth iteration, no solution was found in 1000 attempts. For the succeeding iterations we do not have a numerical argument for the absence of  $\alpha$ -positive solution.

$$a_{ij} = \begin{cases} +1 & \text{if } i \bullet \longleftarrow j \\ -1 & \text{if } i \bullet \longrightarrow j \\ 0 & \text{if } i \bullet \text{ --- } j \end{cases}$$

Figure B.21: A graph can be represented in terms of the incidence matrix defined above.

It is instructive to consider a particular example. Consider the generic box graph in figure B.22. Its incidence matrix is written in table B.1.

A few comments are in order. Note that for internal legs, the entries in the corresponding column add up to 0, while for an external legs we get +1 or -1 if the leg is incoming or outgoing, respectively.

The degree of a vertex is given by summing over the absolute value of the entry of the corresponding row. For the box graph we confirm that all vertices are cubic.

Importantly, the incidence matrix directly encodes momentum conservation at each vertex. If we multiply each column of the incidence matrix by the momentum that flows on the corresponding edge and sum over each line we obtain momentum conservation on that vertex.

$$\text{Momentum conservation at } i: \sum_j a_{ij} q_j = 0, \tag{B.5.1}$$

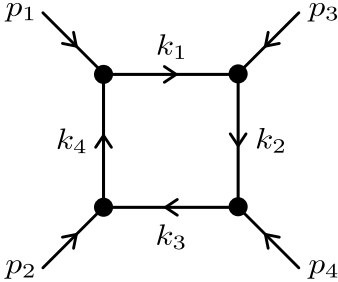


Figure B.22: Directed box graph.

## Appendix B. Appendix to Chapter 3

---

$a_{ij}$	$p_1$	$p_2$	$p_3$	$p_4$	$k_1$	$k_2$	$k_3$	$k_4$
1	+1	0	0	0	-1	0	0	+1
2	0	+1	0	0	0	0	+1	-1
3	0	0	+1	0	+1	-1	0	0
4	0	0	0	+1	0	+1	-1	0

Table B.1: The incidence matrix  $a_{ij}$  of the box graph in figure B.22. The columns are labelled according to momentum flowing on the corresponding edge, while the vertex  $i$  is labelled according to the incoming external momentum  $p_i$ .

where  $q_j$  is the momentum flowing on edge  $j$ .

Applying equation (B.5.1) to the incidence matrix (given in table B.1) we find the expected relations

$$\begin{aligned}
 p_1 - k_1 + k_4 &= 0, & p_2 + k_3 - k_4 &= 0, \\
 p_3 + k_1 - k_2 &= 0, & p_4 + k_2 - k_3 &= 0.
 \end{aligned}$$



# C Appendix to Chapter 4

## C.1 Simple nonperturbative dispersive argument

Here we will implement the setup described in section 4.1 via an explicit dispersion relation for  $B(s)$ . A first point to note is that in  $d = 2$  the  $t$ - and  $u$ - channel poles (4.1.2) will actually lead to a pole at  $s \rightarrow a$  *already* in the non-anomalous regime  $M < \sqrt{2}m$ . This is due to  $d = 2$  kinematics (see appendix C.5). Concretely,

$$-\frac{g^2}{t(s) - m^2} - \frac{g^2}{u(s) - m^2} = \frac{s - 2M^2}{m^2} \frac{g^2}{s - a} \quad (\text{C.1.1})$$

with  $t(s)$  and  $u(s)$  given by eqs. (C.5.3) and (C.5.4). Let us emphasize that (C.1.1) is *not* an anomalous threshold.

A dispersion relation for  $B(s)$  will then take the form

$$B(s) = -\frac{\mathcal{N}g^2}{s - a} + \frac{1}{\pi} \int_{4m^2}^{4M^2} \frac{\text{Disc}B(s')}{s' - s} ds' + \dots \quad (\text{C.1.2})$$

with  $\mathcal{N}$  given by eq. (4.4.1), and where the ‘...’ include the remaining contributions to the dispersion relation (arcs, poles, etc...), which are assumed not to be affected by the motion of the pole  $a$  as  $M^2$  is increased.

Plugging extended unitarity (4.1.3) into (C.1.2) we find

$$B(s) = -\frac{\mathcal{N}g^2}{s - a} + \frac{1}{\pi} \int_{4m^2}^{4M^2} \frac{\rho(s')A(s')B^*(s')}{s' - s} ds' \quad (\text{C.1.3})$$

where the extra contributions ‘...’ were omitted.

Figure C.1: Graphical representation of solution to unitarity across the  $2m$  cut, eqs. (4.3.1), (4.3.2), (4.3.3). The sub-graphs  $\alpha$ ,  $\beta$  and  $\sigma$  are  $2m$ -irreducible, i.e. do not contain any internal exchange of  $2m$  (in the  $s$ -channel), this is what eq. (4.3.7) means graphically.

Now this is a coupled integral equation for  $B(s)$ . Iterating it once gives

$$\begin{aligned}
 B(s) = & -\frac{\mathcal{N}g^2}{s-a} - \frac{\mathcal{N}g^2}{\pi} \int_{4m^2}^{4M^2} \frac{\rho(s')A(s')}{(s'-s)(s'-a)} ds' \\
 & + \frac{1}{\pi^2} \int_{4m^2}^{4M^2} ds' \int_{4m^2}^{4M^2} ds'' \frac{\rho(s')A(s')\rho(s'')A(s'')B^*(s'')}{(s'-s)(s''-s')}
 \end{aligned} \tag{C.1.4}$$

Now, as  $M$  is increased, the pole at  $s' = a$  in the first integral will come into contact with the integration contour and force its deformation. After  $M > \sqrt{2}m$ ,  $a$  will recede and carry along a piece of the integration contour.<sup>1</sup> So we find that  $B(s)$  will shift by

$$\begin{aligned}
 B(s) \rightarrow & B(s) - \mathcal{N}g^2 \frac{2i}{2\pi i} \oint_a ds' \frac{\rho(s')A(s')}{(s'-s)(s'-a)} \\
 = & B(s) - \mathcal{N}g^2 \frac{2\rho(a)A(a)}{s-a}
 \end{aligned} \tag{C.1.5}$$

and we reproduce eq. (4.4.1).

Note that for the triangle diagram  $A(s) = \lambda$  we recover eq. (4.2.5).

<sup>1</sup>Similar dragging will happen in the second integral but only in the  $s''$  contour so no anomalous contribution comes from the second integral.

## C.2 Derivation of the general solution to extended unitarity

We will solve extended unitarity in sequence. First for  $A(s)$ , then for  $B(s)$ , and finally for  $C(s)$ . Starting with  $A(s)$ :

$$\text{Disc}A = \rho|A|^2 \Leftrightarrow \text{Disc}\left(\frac{1}{A} + \varrho\right) = 0 \quad (\text{C.2.1})$$

meaning

$$\frac{1}{A} + \varrho = \frac{1}{\alpha}, \text{ with } \text{Disc}\alpha = 0 \quad (\text{C.2.2})$$

except for possible poles of  $\alpha$ . This is the usual ‘inverse amplitude’ trick [165, 7, 275].

Now, moving onto  $B(s)$ , we use the notation  $B_{\pm} = B(s \pm i\epsilon)$ ,

$$\text{Disc}B = \rho B A^* \Leftrightarrow \frac{B_+ - B_-}{2i} = \frac{\rho B_+ \alpha}{1 - \alpha \varrho_-} \Leftrightarrow \quad (\text{C.2.3})$$

$$B_+ [1 - \alpha(\varrho_- + 2i\rho)] - B_- [1 - \alpha\varrho_-] = 0 \Leftrightarrow \quad (\text{C.2.4})$$

$$B_+ [1 - \alpha\varrho_+] - B_- [1 - \alpha\varrho_-] = 0 \Leftrightarrow \quad (\text{C.2.5})$$

$$\text{Disc}[B(1 - \alpha\rho)] = 0 \Leftrightarrow B(1 - \alpha\rho) = \beta \quad (\text{C.2.6})$$

with  $\text{Disc}\beta = 0$ .

Finally, we go to  $C(s)$ :

$$\text{Disc}C = \rho|B|^2 \Leftrightarrow \text{Disc}C = \frac{\rho\beta^2}{|1 - \alpha\rho|^2} \quad (\text{C.2.7})$$

$$\Leftrightarrow \text{Disc}C = \text{Disc}\left[\frac{\varrho\beta^2}{1 - \alpha\rho}\right] \quad (\text{C.2.8})$$

$$\Leftrightarrow C = \sigma + \left[\frac{\varrho\beta^2}{1 - \alpha\rho}\right], \text{ with } \text{Disc}\sigma = 0, \quad (\text{C.2.9})$$

where we made use of

$$\text{Disc}\left[\frac{\varrho}{1 - \alpha\rho}\right] = \frac{1}{2i} \left[ \frac{\varrho_+}{1 - \alpha\rho_+} - \frac{\varrho_-}{1 - \alpha\rho_-} \right] = \quad (\text{C.2.10})$$

$$= \frac{\varrho_+(1 - \alpha\rho_-) - \varrho_-(1 - \alpha\rho_+)}{2i(1 - \alpha\rho_+)(1 - \alpha\rho_-)} \quad (\text{C.2.11})$$

$$= \frac{(\varrho_+ - \varrho_-)/2i}{(1 - \alpha\rho_+)(1 - \alpha\rho_-)} = \frac{\rho}{|1 - \alpha\rho|^2}. \quad (\text{C.2.12})$$

### C.3 Box and double triangle diagrams in $d = 4$

In this appendix we test expression (4.4.6) in perturbation theory. We will find the anomalous thresholds of the box and double triangle diagrams (fig. C.2).

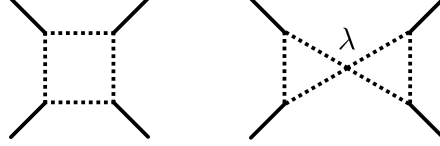


Figure C.2: Box and double triangle diagrams.

At lowest order in perturbation theory we have

$$A(s, t) = \bar{B}(s, t) = 0, \quad (\text{C.3.1})$$

meaning that  $A_J(s) = \bar{B}_J(s) = 0$ . Eq. (4.4.6) then reads

$$\text{Disc } C_J(s) = -\frac{g^4 P_J(z_a(s))}{32\pi \sqrt{s(4M^2 - s)}} \int_{-\infty}^a \frac{\tilde{P}_J(s')}{s' - s} ds' \quad (\text{C.3.2})$$

First, we note the identity

$$\begin{aligned} \text{Disc}_s Q_J(z_a(s)) &= \\ &= \frac{Q_J(z_a(s) + i\epsilon z'_a(s)) - Q_J(z_a(s) - i\epsilon z'_a(s))}{2i} \\ &= \text{sgn } z'_a(s) \text{Disc}_{z_a} Q_J(z_a(s)) \end{aligned} \quad (\text{C.3.3})$$

Now,

$$\begin{aligned} \frac{P_J(z_a(s))}{2\sqrt{s(4M^2 - s)}} &= -\frac{\varrho(s)P_J(z_a(s))}{w(s)} = \\ &= -\frac{2\varrho(s)}{\pi} \text{Disc}_s \left( \frac{Q_J(z_a(s))}{w(s)} \right) \end{aligned} \quad (\text{C.3.4})$$

with  $w(s) \equiv \sqrt{4m^2 - s}\sqrt{4M^2 - s}$  and phase space volume  $\varrho(s)$  given by eq. (4.1.6), where we also made use of  $z'_a(s) < 0$  for  $a < s < 4m^2$  in the anomalous regime  $M > \sqrt{2}m$  and eq. (C.5.14).<sup>2</sup>

Making use of the definition of  $\tilde{P}_J(s')$ , eq. (4.4.7), the relation between  $P_J(z)$  and  $Q_J(z)$ , eq.

---

<sup>2</sup>We are also abusing the notation in going from the first to the second line of eq. (C.3.4). The discontinuity should be seen as the monodromy (which is a function, not a distribution).

(C.5.14), and the identity (C.3.3) we have

$$\begin{aligned} \int_{-\infty}^a \frac{\tilde{P}_J(s')}{s' - s} ds' &= -\frac{2}{\pi} \int_{-\infty}^a \frac{\text{Disc}_s \left( \frac{Q_J(z_a(s'))}{w(s')} \right)}{s' - s} ds' \\ &= -2 \text{Re} \left[ \frac{Q_J(z_a(s))}{w(s)} \right]. \end{aligned} \quad (\text{C.3.5})$$

Plugging (C.3.4) and (C.3.5) into (C.3.2) we find

$$\begin{aligned} \text{Disc } C_J(s) &= -\frac{g^4 \varrho(s)}{4\pi^2} \text{Disc} \left[ \frac{Q_J(z_a(s))}{w(s)} \right] \text{Re} \left[ \frac{Q_J(z_a(s))}{w(s)} \right] \\ &= -\frac{g^4 \varrho(s)}{8\pi^2} \text{Disc} \left[ \frac{Q_J(z_a(s))}{w(s)} \right]^2, \quad s \in [a, 4m^2]. \end{aligned} \quad (\text{C.3.6})$$

We can see that this is already the discontinuity across the anomalous threshold of the partial wave of the box. Concretely, consider partial wave unitarity eq. (4.1.4) and for  $B_J(s)$  plug the partial wave of the  $t$ - and  $u$ -channel poles (4.1.2), which is given by eq. (4.3.14). We find

$$\text{Disc } C_J(s) = \frac{g^4 \rho(s)}{16\pi^2} \left[ \frac{Q_J(z_a(s))}{w(s)} \right]^2, \quad s \in [4m^2, \infty) \quad (\text{C.3.7})$$

with  $\rho(s)$  given by eq. (4.1.5).

We now plug this expression into a dispersion relation, and continue in the mass  $M$  (see appendices 4.2 and C.1). Akin to Fig. 4.6 the cut of  $Q_J(z_a(s))$ , which is for  $s \leq a$  will wrap around the branch point at  $s = 4m^2$  for  $M > \sqrt{2}m$ . This will force a deformation of the contour below the normal threshold, i.e. will lead to an anomalous threshold whose discontinuity is given by (C.3.6). Notice how the discontinuity ‘switches’ from  $\rho(s) = \text{Disc}\varrho(s)$  in the normal threshold (C.3.7) to the Legendre function in the anomalous threshold (C.3.6). The factor of  $(-2)$  difference is related to the wrapping of the contour.

Fortunately, expression (C.3.6) is simple enough to be inverted back for the amplitude  $C(s, t)$ . Summing over  $(2J + 1)P_J(z)$  on both sides of eq. (C.3.6), and using the  $PQQ$  identity (C.5.17) gives

$$\text{Disc}_s C(s, t) = -\frac{g^4}{4\pi^2} \frac{\text{Disc}_s K(z(t), z_a(s), z_a(s))}{\sqrt{s(4m^2 - s)} (4M^2 - s)} \quad (\text{C.3.8})$$

where  $K(z, z', z'')$  is the Mandelstam kernel given by eq. (C.5.12)

As seen from eq. (C.5.12), the Mandelstam kernel is singular for  $z = z_+(z_a(s), z_a(s)) = 2z_a^2(s) - 1$ . In terms of  $s$  and  $t$  this is

$$s(t) = \frac{4[M^4 + m^2(t - 4M^2)]}{t - 4m^2}, \quad (\text{C.3.9})$$

which is the Landau curve of the box diagram.

## Appendix C. Appendix to Chapter 4

---

Similarly to the previous analysis for the partial waves, starting with unitarity for  $s \geq 4m^2$ , eq. (C.5.9), inserting the poles (4.1.2), plugging the answer into a dispersion relation and continuing in  $M$  will lead to a discontinuity across an anomalous threshold (C.3.8) for  $M > \sqrt{2}m$ . Note, however, that the branch point will be different for each  $t$ , i.e. it will be determined by the Landau curve (C.3.9) that now appears below the normal threshold on the physical sheet (as a simple Landau analysis of the box diagram yields).

Let us now move to the case where<sup>3</sup>

$$\bar{B}(s, t) = 0, \quad A(s, t) = \lambda \ll 1. \quad (\text{C.3.10})$$

Note that  $A(s, t) = \lambda \implies A_J(s) = \lambda \delta_{J,0}$ . Plugging into (4.4.6) we find that only  $J = 0$  survives, and at linear order in  $\lambda$  we have

$$\begin{aligned} \text{Disc}C_0(s) = & -\frac{\lambda g^4}{16\pi\sqrt{s(4M^2-s)}} \times \\ & \left[ \frac{1}{2} \int_{-\infty}^a \frac{\tilde{P}_0(s')}{s'-s} [\rho(s) - \rho(s')] ds' - \int_a^{4m^2} \frac{\tilde{P}_0(s')}{s'-s} \rho(s') ds' \right]. \end{aligned} \quad (\text{C.3.11})$$

Let us now match this result from the double triangle diagram. The double triangle diagram is given by the square of the triangle diagram. The single triangle diagram  $B_T(s)$  (see Fig. 4.5) can be computed by unitarity

$$\text{Disc}B_T(s) = \lambda \delta_{J,0} \rho(s) B_J^{\text{poles}}(s+i0) \Theta(s-4m^2) \quad (\text{C.3.12})$$

with  $B_J^{\text{poles}}(s+i0)$  given by eq. (4.3.14). And we have

$$B_T(s) = \frac{\lambda g^2}{4\pi^2} \int_{4m^2}^{\infty} \frac{\rho(s') Q_0(z_a(s'))}{w(s')(s'-s)} ds' \quad (\text{C.3.13})$$

The double triangle will be given by  $B_T^2(s)$  (where we also divided by the extra factor of  $\lambda$ )

$$C_T(s) = \frac{\lambda g^4}{16\pi^4} \left[ \int_{4m^2}^{\infty} \frac{\rho(s') Q_0(z_a(s'))}{(s'-s)w(s')} ds' \right]^2. \quad (\text{C.3.14})$$

Let us now continue this expression in  $M$  to find the anomalous threshold. It is useful to first rewrap the contour around the cut of  $Q_0(z_a(s'))$  and the pole  $\frac{1}{s'-s}$ . We have

$$C_T(s) = \frac{\lambda g^4}{16\pi^2} \left[ \frac{1}{2} \int_{-\infty}^a \frac{\tilde{P}_0(s')}{s'-s} [\rho(s') - \rho(s)] ds' \right]^2 \quad (\text{C.3.15})$$

---

<sup>3</sup>Note that taking  $\bar{B}(s, t) \neq 0$  would lead to a ‘triangle’ type singularity no different than for the  $mm \rightarrow MM$  process as already inverted for the amplitude by eq. (4.4.4), so we will not analyze this case.

#### C.4 Supporting appendix to the discussion on the global existence of anomalous thresholds

with  $\tilde{P}_0(s)$  given by eq. (4.4.7). We now continue past  $M > \sqrt{2}m$  to find

$$C_T(s) = \frac{\lambda g^4}{16\pi^2} \left[ \frac{1}{2} \int_{-\infty}^a \frac{\tilde{P}_0(s')}{s' - s} [\varrho(s') - \varrho(s)] ds' + \int_a^{4m^2} \frac{\tilde{P}_0(s')}{s' - s} \varrho(s') ds' \right]^2 \quad (\text{C.3.16})$$

Taking the discontinuity of this expression, making use of the relation  $\text{Disc} f^2 = 2 \text{Re} f \text{Disc} f$ , and eqs. (4.1.5) and (4.4.7) we recover eq. (C.3.11).

#### C.4 Supporting appendix to the discussion on the global existence of anomalous thresholds

Let us first analyze what the presence of  $t$ - and  $u$ - channel singularities in  $B(s, t)$  imply for  $B_J(s)$ . A branch cut for  $t, u \geq \mu^2$  implies the following contribution to  $B_J(s)$  (making use of the Froissart-Gribov formula (C.5.16))

$$B_J(s) \supset \frac{1}{8\pi^2} \int_{z(\mu^2)}^{\infty} Q_J(z) \text{Disc}_z B(s, t(z)) dz = \frac{1}{8\pi^2 \sqrt{s - 4m^2} \sqrt{s - 4M^2}} \int_{\mu^2}^{\infty} Q_J(z(t)) \text{Disc}_t B(s, t) dt \quad (\text{C.4.1})$$

where we made use of  $t - u$  symmetry, i.e.  $B(s, t(z)) = B(s, t(-z))$ , and where  $z(t)$  is given by eq. (C.5.5).

Now, the Legendre function  $Q_J(z(t))$  has a branch cut for  $z(t) \in [-1, 1]$ , and, given that  $t$  is being integrated over  $t \geq \mu^2$ , we see that this implies a branch cut on  $B_J(s)$  via the relation (C.5.5). It is easy to see that the endpoint of the integral in  $t$  is what defines the rightmost branch point in  $s$ , which is given by plugging  $z = \pm 1$  and  $t = \mu^2$  in (C.5.5),

$$s_\mu = \frac{[(m - \mu)^2 - M^2][(m + \mu)^2 - M^2]}{\mu^2} \quad (\text{C.4.2})$$

and we conclude that  $B_J(s)$  has a left hand cut for  $s \leq s_\mu$ . A nice property of this function is that  $s_\mu \leq 4m^2$ , so this left-handed branch cut will never overlap with the right-handed extended cut. It can nonetheless wrap around it for certain values of  $(\mu, M)$ . This relation can be determined by imposing

$$s_\mu = 4m^2 \implies M^2 = \mu^2 + m^2 \quad (\text{C.4.3})$$

so we see  $\mu \neq M$ , i.e. exchange of  $M$  will not lead to an anomalous threshold. Moreover, since  $M < 2m$  is stable we find that  $s_\mu$  will only wrap around  $4m^2$  for

$$\mu \leq \sqrt{3}m < 2m \quad (\text{C.4.4})$$

## Appendix C. Appendix to Chapter 4

---

So only the single particle exchange  $\mu = m$  satisfies this condition (assuming of course that  $m$  and  $M$  are the lightest particles). This case corresponds to the already analyzed poles (4.1.2). As a simple check, plugging  $\mu = m$  into (C.4.3) leads to  $M = \sqrt{2}m$  and into (C.4.3) leads to eq. (4.0.2).

Repeating the same analysis for the  $MM \rightarrow MM$  partial wave  $C_J(s)$  amounts to taking  $m \rightarrow M$  in eq. (C.4.2), which implies  $s_\mu = 4M^2 - \mu^2$ . We see that for  $\mu$  independent of  $M$ ,  $s_\mu$  is monotonic in  $M^2$  and will not wrap around  $4m^2$ , and likewise for any normal threshold  $\mu = n_1 m + n_2 M$ , with  $n_1$  and  $n_2$  integers.<sup>4</sup>

What remains to consider is the possibility that  $\mu^2$  itself is an anomalous threshold. Let us first consider  $mm \rightarrow MM$ . Can an anomalous threshold appear in the crossed channel, i.e. in the  $mM \rightarrow mM$  process? If we assume  $m$  to be  $\mathbb{Z}_2$  odd,  $mM \rightarrow mM$  cannot exchange  $mm$  and therefore does not have an extended unitarity cut, so we discard the possibility of it having anomalous thresholds. Conversely, the  $MM \rightarrow MM$  process relates to itself by crossing symmetry. From the previous analysis we see that there is only the anomalous threshold at  $s = a$ . In  $d > 2$  we still have to relate this anomalous threshold in  $C_J(s)$  to the amplitude  $C(s, t)$ , which can in general depend on  $t$  itself (see appendix C.3). So, for simplicity, let us assume  $d = 2$ , where both objects coincide. In this case  $t = 4M^2 - s$ , so  $t(a) = M^4/m^2$ . Plugging this value for  $\mu^2$  in eq. (C.4.2) leads to

$$s_{t(a)} = m^2 + 2M^2 + \frac{2m^4}{M^2} - \frac{M^4}{m^2} - \frac{m^6}{M^4}. \quad (\text{C.4.5})$$

Now we have to analyze its trajectory for  $\sqrt{2}m < M < 2m$  (note that we have to start at  $M = \sqrt{2}m$  because that is when  $t = a$  comes on the physical sheet). It is easy to see that (C.4.5) for this range of  $M$  will not go around  $4m^2$ , and therefore will not give rise to any further anomalous threshold.

### C.5 Kinematics, unitarity and Legendre functions in the unequal mass case

Here we collect several technical details regarding kinematics, unitarity and Legendre functions.

---

<sup>4</sup>We see that  $\frac{ds_\mu}{dM} = 0$  has solution  $M = \frac{n_1 n_2}{4 - n_2^2} m^2$ , which for  $m < M < 2m$  requires  $n_2 = 1$  and  $n_1 = 4, 5$ . For these cases  $s_\mu$  will have minimum at  $s_\mu = -64m^2/3, -100m^2/3$  way below  $4m^2$ . It is however possible that these singularities come onto the physical sheet by crossing an already present left-hand cut. It is hard to say without further analysis if these would correspond to anomalous thresholds on the amplitude.



### Scattering angle

Let us relate  $t$  and  $u$  with the cosine of the scattering angle in the center of mass frame. We let  $\vec{p}$  and  $E_p$  be the momentum and energy of a particle of mass  $M$  and  $\vec{k}$  and  $E_k$  be the momentum and energy of a particle of mass  $m$ . Then, the cosine of the scattering angle is

$$z \equiv \frac{\vec{p} \cdot \vec{k}}{|\vec{p}||\vec{k}|}. \quad (\text{C.5.1})$$

For the scattering  $mm \rightarrow MM$ , in the center of mass we have  $E_p = E_k = \sqrt{s}/2$ . Further using  $|\vec{p}| = \sqrt{E_p^2 - M^2}$  and  $|\vec{k}| = \sqrt{E_k^2 - m^2}$  we get

$$\begin{aligned} t(z) &= (p - k)^2 = M^2 + m^2 - 2E_p E_k + 2|\vec{p}||\vec{k}|z \\ &= m^2 + M^2 + \frac{-s + z\sqrt{s-4m^2}\sqrt{s-4M^2}}{2}, \end{aligned} \quad (\text{C.5.2})$$

where, also,  $u(z) = t(-z)$ .

Now, in  $d = 2$  there is only forward or backward scattering, i.e.  $z = \pm 1$ , so  $t = t(s)$  and  $u = u(s)$  are fixed in terms of  $s$ ,

$$t(s) = m^2 + M^2 + \frac{-s + \sqrt{s-4m^2}\sqrt{s-4M^2}}{2}, \quad (\text{C.5.3})$$

$$u(s) = m^2 + M^2 + \frac{-s - \sqrt{s-4m^2}\sqrt{s-4M^2}}{2}. \quad (\text{C.5.4})$$

Relation (C.5.2) inverts to

$$z(t) = \frac{s - 2m^2 - 2M^2 + 2t}{\sqrt{s-4m^2}\sqrt{s-4M^2}}. \quad (\text{C.5.5})$$

### Extended unitarity for the amplitudes

In terms of the amplitudes, unitarity across the  $2m$  cut reads [7], for the  $mm \rightarrow MM$  process,

$$\begin{aligned} \text{Disc}_s B(s, t) &= \frac{1}{8(4\pi)^2} \sqrt{\frac{s-4m^2}{s}} \\ &\times \iint_{-1}^1 dz' dz'' \mathcal{P}(z, z', z'') A(s, t(z')) B^*(s, t(z'')) \end{aligned} \quad (\text{C.5.6})$$

where  $z$  and  $z''$ , scattering angles of  $mm \rightarrow MM$ , are related to  $t(z)$  and  $t(z'')$  via (C.5.5) and  $z' = 1 + \frac{2t(z')}{s-4m^2}$  is the usual relation for the scattering angle of  $mm \rightarrow mm$ .

## Appendix C. Appendix to Chapter 4

---

Likewise, for the  $MM \rightarrow MM$  process,

$$\begin{aligned} \text{Disc}_s C(s, t) &= \frac{1}{8(4\pi)^2} \sqrt{\frac{s-4m^2}{s}} \\ &\times \iint_{-1}^1 dz' dz'' \mathcal{P}(z, z', z'') B(s, t(z')) B^*(s, t(z'')), \end{aligned} \quad (\text{C.5.7})$$

where  $z = 1 + \frac{2t(z)}{s-4M^2}$  is the usual relation for the scattering angle of  $MM \rightarrow MM$  and  $z'$  and  $z''$ , scattering angles of  $mm \rightarrow MM$  are related to  $t(z')$  and  $t(z'')$  via eq. (C.5.5).

The 2-particle kernel reads (following conventions of [7])

$$\mathcal{P}(z, z', z'') = \frac{2\Theta(1-z^2-z'^2-z''^2+2zz'z'')}{\sqrt{1-z^2-z'^2-z''^2+2zz'z''}} \quad (\text{C.5.8})$$

Eqs. (C.5.6) and (C.5.7), because of the theta function in (C.5.8) only hold for real  $t$  in the scattering angle region  $-1 < z < 1$ . These equations can however be continued in  $t$  [151, 7] and be expressed in manifestly analytic form. Say for  $MM \rightarrow MM$ ,

$$\begin{aligned} \text{Disc}_s C(s, t) &= \frac{1}{8(4\pi)^2} \sqrt{\frac{s-4m^2}{s}} \left(\frac{1}{2\pi i}\right)^2 \\ &\times \oint_{-1}^1 dz' \oint_{-1}^1 dz'' K(z, z', z'') B(s, t(z')) B^*(s, t(z'')), \end{aligned} \quad (\text{C.5.9})$$

with Mandelstam kernel  $K(z, z', z'')$  which has discontinuity [7]

$$\text{Disc}_z K(z, z', z'') = 4\pi^2 \frac{\Theta(z-z_+(z', z''))}{\sqrt{(z-z_+(z', z''))(z-z_-(z', z''))}} \quad (\text{C.5.10})$$

with

$$z_{\pm}(z', z'') = z' z'' \pm \sqrt{(z'^2-1)(z''^2-1)}. \quad (\text{C.5.11})$$

Equation (C.5.10) can be integrated to give

$$K(z, z', z'') = \frac{8\pi}{\sqrt{(z_+-z)(z-z_-)}} \arctan \sqrt{\frac{z-z_-}{z_+-z}}. \quad (\text{C.5.12})$$

Note that  $K(z, z', z'')$ , as a function of  $z$ , has the same analyticity structure as the ‘bubble’ diagram  $W(s)$ , in eq. (4.2.3), as a function of  $s$ .

### Partial waves and Legendre functions

The partial wave decomposition of the amplitude  $B(s, t)$  reads [7]

$$B(s, t) = 16\pi \sum_{J=0}^{\infty} (1 + 2J) P_J(z(t)) B_J(s) \quad (\text{C.5.13})$$

where  $P_J(z)$  is the Legendre polynomial and  $z(t)$  the cosine of the scattering angle given by (C.5.5). Analogous expressions hold for  $A(s, t)$  and  $C(s, t)$ .

Now, eq. (C.5.13) can be inverted for the partial wave in the usual way via eq. (4.1.1). Alternatively, we can exploit analyticity in  $t$  by considering the Legendre function of the second kind  $Q_J(z)$ . These two functions are related by

$$\text{Disc } Q_J(z) = -\frac{\pi}{2} P_J(z) \Theta(1 - z^2) \quad (\text{C.5.14})$$

This turns eq. (4.1.1) into the so-called Froissart-Gribov representation [7]:

$$B_J(s) = \frac{1}{16\pi} \oint_{[-1,1]} \frac{dz}{2\pi i} Q_J(z) B(s, t(z)) \quad (\text{C.5.15})$$

where the contour is counter-clockwise. Using eq. (C.5.5) we have instead

$$B_J(s) = \frac{1}{8\pi \sqrt{s - 4m^2} \sqrt{s - 4M^2}} \times \oint \frac{dt}{2\pi i} Q_J(z(t)) B(s, t) \quad (\text{C.5.16})$$

Now, the partial wave decomposition diagonalizes unitarity, as can be seen from eqs. (4.1.3) and (4.1.4). This is made explicit by an interesting identity between the 2-particle kernels  $\mathcal{S}$  and  $K$  and the Legendre functions. In particular, for the latter [7]:

$$K(z, z', z'') = 4\pi \sum_{J=0}^{\infty} (2J + 1) P_J(z) Q_J(z') Q_J(z'') \quad (\text{C.5.17})$$

Plugging (C.5.17) into (C.5.9) leads to (4.1.4) and likewise for  $A(s, t)$  and  $B(s, t)$ .



# D Appendix to Chapter 5

## D.1 Dual Bootstrap of the Sine-Gordon model

In this appendix we reproduce one of the results of [216], namely the one presented on their Figure 3, but with the dual setup. The assumed spectrum consists of 2 particles of mass  $m_1 = 1$  and  $m_2 = \sqrt{3}$  to target the Sine-Gordon theory. Only one pole in the scattering amplitude is assumed, the one corresponding to an exchange of the particle  $m_2$ . This residue  $g$  is fixed and the central charge is minimized, which leads to Figure D.1.

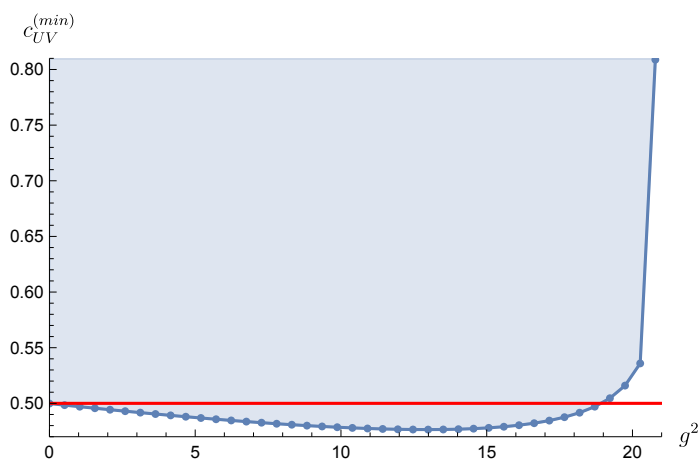


Figure D.1: Lower bound on the central charge of the UV CFT for different values of the cubic coupling  $g$  between two particles of mass  $m_1 = 1$  and one particle of mass  $m_2 = \sqrt{3}$ . We used  $N = 50$  and the bound extends until  $g^2 = 12\sqrt{3}$  after which the problem is unfeasible. The red line at  $c_{UV} = 1/2$  is added for convenience.

The maximal value of  $g^2$  for which the problem is feasible and the corresponding minimal central charge are

$$g^2 = 12\sqrt{3}, \quad c_{UV} = 0.808823... \quad (\text{D.1.1})$$

and they correspond to the cubic coupling and the contribution to the central charge of the Sine-Gordon model from the particle  $m_2$  and states with two particles  $m_1$ .

## Appendix D. Appendix to Chapter 5

The advantage of our dual setup is that the bound on  $c_{UV}$  is more accurate than what was presented in [216]. Indeed at  $g = 0$  we have for sure the free Majorana fermion that is allowed and the corresponding central charge of  $1/2$  should not be excluded. This is in agreement with our bound.

The optimal scattering amplitude and form factor are presented on Figure D.2, and correspond also to the analytical solutions in the Sine-Gordon model.

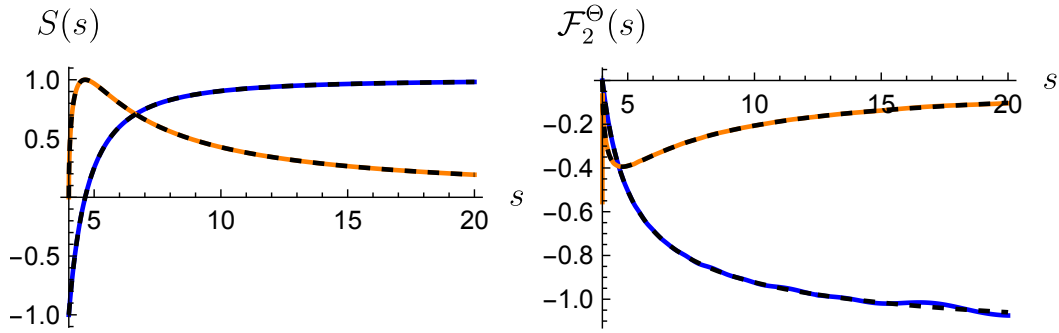


Figure D.2: Scattering amplitude (on the left) and form factor (on the right) for the optimal  $c_{UV}$  when  $g^2 = 12\sqrt{3}$ . The blue lines are the real parts and the orange lines are the imaginary parts. They correspond to the analytical solutions of the Sine-Gordon model with  $m_1 = 1$  and  $m_2 = \sqrt{3}$ , that are plotted in dashed lines and given by eq. (4.18) and (4.19) in [216]. We used  $N = 50$ .

## D.2 Dual optimization problems

In this appendix we derive various generalizations of the example in section 5.1 and present the dual optimization problems.

### D.2.1 $\mathbb{Z}_2$ symmetric theories

Here the goal is to minimize the central charge on top of the leaf parametrized by (5.2.2). We do not assume any pole in the S-matrix and form factor. We have

$$\begin{aligned}
 \mathcal{L} = & 12\pi \int_4^\infty ds \frac{\rho(s)}{s^2} + \int_4^\infty ds w_{\mathcal{T}}(s) \left[ \mathcal{T}(s) + \Lambda - \int_4^\infty \frac{dz}{\pi} \text{Im} \mathcal{T}(z) \left( \frac{1}{z-s} + \frac{1}{z+s-4} - \frac{2}{z-2} \right) \right] \\
 & + \int_4^\infty ds w_{\mathcal{F}}(s) \left[ \mathcal{F}(s) - \mathcal{F}(0) - \int_4^\infty \frac{dz}{\pi} \text{Im} \mathcal{F} \left( \frac{1}{z-s} - \frac{1}{z} \right) \right] \\
 & + \int_4^\infty ds \text{Tr} \Lambda(s) \cdot B(s) + b \left( \int_4^\infty \frac{dz}{\pi} \text{Im} \mathcal{T}(z) \frac{4}{(z-2)^3} - \Lambda^{(2)} \right)
 \end{aligned} \tag{D.2.1}$$

The dual scattering function is defined

$$W_{\mathcal{F}}(s) \equiv \int_4^\infty \frac{dz}{\pi} w_{\mathcal{F}}(z) \left( \frac{1}{z-s} - \frac{1}{z+s-4} + \frac{2}{s-2} \right),$$

$$\text{Im } W_{\mathcal{F}}(s) = w_{\mathcal{F}}(s), \quad \text{Re } W_{\mathcal{F}}(s) = -P \int_4^\infty \frac{dz}{\pi} w_{\mathcal{F}}(z) \left( \frac{1}{s-z} + \frac{1}{s-(4-z)} - \frac{2}{s-2} \right),$$
(D.2.2)

where the last term is not eliminated as in the example in section 5.1 since we do not extremize over the primal variable  $\mathcal{F}(2)$  which is fixed to be  $-\Lambda$ .

The elimination of the primal variable  $\mathcal{F}$  constrains the dual variables to obey

$$\lambda_4 = \frac{\mathcal{N}_2}{2} \left( W_{\mathcal{F}} + \frac{4b}{\pi(s-2)^3} \right). \quad (D.2.3)$$

We therefore get

Dual Problem (Minimization of the central charge on top of the leaf)

$$\text{Maximize}_{\{\lambda_1, W_{\mathcal{F}}, W_{\mathcal{F}}^*, b\}} \left[ \int_4^\infty ds (2\lambda_1 + 2 \text{Im } W_{\mathcal{F}} + \mathcal{N}_2 \text{Re } W_{\mathcal{F}} + \Lambda \text{Im } W_{\mathcal{F}}) + (1 - \Lambda^{(2)})b \right] \quad (D.2.4)$$

Constrained by

$$\begin{pmatrix} \lambda_1 & \frac{\mathcal{N}_2}{2} W_{\mathcal{F}} + \frac{2\mathcal{N}_2 b}{\pi(s-2)^3} & i \frac{\sqrt{\mathcal{N}_2}}{4} W_{\mathcal{F}} \\ \frac{\mathcal{N}_2}{2} W_{\mathcal{F}}^* + \frac{2\mathcal{N}_2 b}{\pi(s-2)^3} & \lambda_1 & -i \frac{\sqrt{\mathcal{N}_2}}{4} W_{\mathcal{F}}^* \\ -i \frac{\sqrt{\mathcal{N}_2}}{4} W_{\mathcal{F}} & i \frac{\sqrt{\mathcal{N}_2}}{4} W_{\mathcal{F}} & -\frac{6}{s^2} \end{pmatrix} \preceq 0, \quad \forall s \in [4, \infty), \quad (D.2.5)$$

where  $\Lambda \preceq 0$  means  $-\Lambda \succeq 0$ .

### Non-Linear dual for $\mathbb{Z}_2$ symmetric theories

In the pure S-Matrix context the dual problem is simpler and in particular we can get the leaf by computing the extreme values for  $\Lambda^{(2)} \equiv \mathcal{F}''(2)$  and then the extreme values for  $\Lambda \equiv \mathcal{F}(2)$  with fixed  $\Lambda^{(2)}$  within the allowed range.

For the first problem the lagrangian is

$$\mathcal{L} = \int_4^\infty \frac{dz}{\pi} \text{Im } \mathcal{F}(z) \frac{4}{(z-2)^3} + \int_4^\infty ds (\lambda(s)U(s) + w(s)\mathcal{A}(s)), \quad (D.2.6)$$

where  $w$  and  $\lambda \geq 0$  are Lagrange multipliers and  $\mathcal{A}$  is the usual analyticity and crossing constraint for the scattering amplitude and

$$U(s) \equiv 2 \text{Im } \mathcal{F}(s) - \frac{|\mathcal{F}(s)|^2}{\mathcal{N}_2(s)} \quad (D.2.7)$$

## Appendix D. Appendix to Chapter 5

---

is the unitarity constraint in the pure S-Matrix setup. Using the equations of motion for  $\mathcal{F}$  to eliminate it, we get the dual problem

$$\mathcal{L} = \int_4^\infty ds \mathcal{N}_2(s) \left[ \sqrt{(\text{Im } W(s))^2 + \left( \text{Re } W(s) + \frac{4}{\pi(s-2)^3} \right)^2} + \text{Re } W(s) + \frac{4}{\pi(s-2)^3} \right]. \quad (\text{D.2.8})$$

For the second problem we start with the lagrangian

$$\mathcal{L} = \mathcal{F}(2) + b \left( \Lambda^{(2)} - \int_4^\infty \frac{dz}{\pi} \text{Im } \mathcal{F}(z) \frac{4}{(z-2)^3} \right) + \int_4^\infty ds (\lambda(s) U(s) + w(s) \mathcal{A}(s)). \quad (\text{D.2.9})$$

Eliminating the primal variable  $\mathcal{F}$  we get

$$\begin{aligned} \mathcal{L} = & \mathcal{F}(2) \left( 1 - \int_4^\infty ds \text{Im } W(s) \right) + b \Lambda^{(2)} \\ & + \int_4^\infty ds \mathcal{N}_2(s) \left[ \sqrt{(\text{Im } W(s))^2 + \left( \text{Re } W(s) - \frac{4b}{\pi(s-2)^3} \right)^2} + \text{Re } W(s) - \frac{4b}{\pi(s-2)^3} \right] \end{aligned} \quad (\text{D.2.10})$$

To summarize we have

Dual Problem ( $\Lambda^{(2)}$  maximization)

$$\begin{aligned} \text{Minimize}_{\{W(s)\}} \left( \int_4^\infty ds \mathcal{N}_2(s) \left[ \sqrt{(\text{Im } W(s))^2 + \left( \text{Re } W(s) - \frac{4}{\pi(s-2)^3} \right)^2} \right. \right. \\ \left. \left. + \text{Re } W(s) - \frac{4}{\pi(s-2)^3} \right] \right) \end{aligned} \quad (\text{D.2.11})$$

Dual Problem ( $\Lambda^{(2)}$  minimization)

$$\begin{aligned} \text{Minimize}_{\{W(s)\}} \left( \int_4^\infty ds \mathcal{N}_2(s) \left[ -\sqrt{(\text{Im } W(s))^2 + \left( \text{Re } W(s) - \frac{4}{\pi(s-2)^3} \right)^2} \right. \right. \\ \left. \left. + \text{Re } W(s) - \frac{4}{\pi(s-2)^3} \right] \right) \end{aligned} \quad (\text{D.2.12})$$

Dual Problem ( $\Lambda$  maximization with fixed  $\Lambda^{(2)}$ )

$$\begin{aligned} \text{Minimize}_{\{b, W(s)\}} \left( b \Lambda^{(2)} + \int_4^\infty ds \mathcal{N}_2(s) \left[ \sqrt{(\text{Im } W(s))^2 + \left( \text{Re } W(s) - \frac{4b}{\pi(s-2)^3} \right)^2} \right. \right. \\ \left. \left. + \text{Re } W(s) - \frac{4b}{\pi(s-2)^3} \right] \right) \end{aligned} \quad (\text{D.2.13})$$



## D.2 Dual optimization problems

Constrained by

$$\int_4^\infty ds \operatorname{Im} W(s) = 1 \quad (\text{D.2.14})$$

Dual Problem ( $\Lambda$  minimization with fixed  $\Lambda^{(2)}$ )

$$\begin{aligned} \text{Minimize}_{\{b, W(s)\}} \left( b\Lambda^{(2)} + \int_4^\infty ds \mathcal{N}_2(s) \left[ -\sqrt{(\operatorname{Im} W(s))^2 + \left( \operatorname{Re} W(s) - \frac{4b}{\pi(s-2)^3} \right)^2} \right. \right. \\ \left. \left. + \operatorname{Re} W(s) - \frac{4b}{\pi(s-2)^3} \right] \right) \end{aligned} \quad (\text{D.2.15})$$

Constrained by

$$\int_4^\infty ds \operatorname{Im} W(s) = 1 \quad (\text{D.2.16})$$

Following [211], for the  $\Lambda^{(2)}$  maximization we use the ansatz

$$W(s) = \frac{1}{s(4-s)} \sum_{n=0}^N a_n (\rho^n(s, 2) - \rho^n(4-s, 2)), \quad (\text{D.2.17})$$

and for the  $\Lambda$  maximization we use

$$W(s) = \frac{1}{s(4-s)} \left( \frac{8}{\pi(s-2)} + \sum_{n=0}^N a_n (\rho^n(s, 2) - \rho^n(4-s, 2)) \right), \quad (\text{D.2.18})$$

with  $\rho(s, s_0)$  defined by (D.3.1).

### D.2.2 Ising Field Theory

**Zero in the S-Matrix at  $s = 1 - x$**

To implement the zero in the S-matrix we can use the subtraction

$$\begin{aligned} \mathcal{F}(s) - \mathcal{F}(1-x) = -g^2 \left( \frac{1}{s-1} + \frac{1}{3-s} - \frac{1}{1-x-1} - \frac{1}{3-(1-x)} \right) \\ - \int_4^\infty \frac{dz}{\pi} \operatorname{Im} T(z) \left( \frac{1}{z-s} + \frac{1}{z+s-4} - \frac{1}{z-1+x} - \frac{1}{z+1-x-4} \right), \end{aligned} \quad (\text{D.2.19})$$

and we will fix  $\mathcal{F}(1-x) = i\mathcal{N}_2(1-x)$  so that  $S(1-x) = 0$ . The dual scattering function is now defined as

$$W_{\mathcal{F}}(s) = \int_4^\infty \frac{dz}{\pi} w_{\mathcal{F}}(z) \left( \frac{1}{z-s} - \frac{1}{z+s-4} + \frac{1}{s+x-1} + \frac{1}{s-x-3} \right). \quad (\text{D.2.20})$$

Its ansatz therefore needs to have poles at  $s = 1 - x$  and  $s = 3 + x$  with residues  $\int \operatorname{Im} W_{\mathcal{F}} / \pi$  and to be odd under crossing. To moreover satisfy the fact that the objective must be integrable we

## Appendix D. Appendix to Chapter 5

---

can make the ansatz<sup>1</sup>

$$W_{\mathcal{F}}(s) = \frac{a}{s(4-s)} \left( \frac{1}{s+x-1} + \frac{1}{s-x-3} \right) + \frac{1}{s(4-s)} \sum_{n=1}^N f_n(\rho(s,2)^n - \rho(4-s,2)^n), \quad (\text{D.2.23})$$

where the second term is the ansatz that we make when we don't impose the zero, defined by (D.3.2).

The only modification to the lagrangian induced from the addition of the zero comes from the subtraction of  $\mathcal{F}(1-x)$  which gives the new term

$$\mathcal{L} \supset \int_4^\infty ds w_{\mathcal{F}}(s) (-\mathcal{F}(1-x)) = -i \mathcal{N}_2(1-x) \int_4^\infty \text{Im } W_{\mathcal{F}}. \quad (\text{D.2.24})$$

In summary to implement the zero in the S-Matrix, it suffices to derive the problem without the zero and at the end we modify the lagrangian as

$$\mathcal{L} \rightarrow \mathcal{L} - i \mathcal{N}_2(1-x) \int_4^\infty \text{Im } W_{\mathcal{F}}, \quad (\text{D.2.25})$$

and use (D.2.23) for  $W_{\mathcal{F}}$ .

### Minimization of the central charge

An interesting problem is the minimization of the UV central charge when there is the zero in the S-Matrix. We start with the lagrangian

$$\mathcal{L} = 12\pi \left( \frac{g_F^2}{g^2} + \int_4^\infty \frac{\rho}{s^2} \right) + \int_4^\infty (\mathcal{A}_{\mathcal{F}} w_{\mathcal{F}} + \mathcal{A}_{\mathcal{F}} w_{\mathcal{F}} + \text{Tr } \Lambda B), \quad (\text{D.2.26})$$

and primal variables  $\mathcal{T}$ ,  $\mathcal{F}$  and  $\rho$  are eliminated as before. It remains to eliminate  $g_F$  and  $g^2$ . For the former, a functional variation with respect to  $g_F$  yields

$$g_F = -\frac{W_{\mathcal{F}}(1)}{24} g^2. \quad (\text{D.2.27})$$

Then, variation of  $g^2$  yields the constraint

$$48W_{\mathcal{F}}(1) = W_{\mathcal{F}}(1)^2. \quad (\text{D.2.28})$$

---

<sup>1</sup>In principle the coefficient  $a$  should be fixed by the constraint on the residues. A direct computation gives

$$\frac{1}{\pi} \int_4^\infty \text{Im } W_{\mathcal{F}} = a \frac{1}{4} \left( \frac{1}{3+x} + \frac{1}{1-x} \right) = \frac{a}{(3+x)(1-x)}. \quad (\text{D.2.21})$$

On the other hand the residue is given by

$$\text{Res}_{s=1-x} W_{\mathcal{F}}(s) = \frac{a}{(1-x)(4-1+x)}, \quad (\text{D.2.22})$$

and the constraint is therefore satisfied for all  $a$  that can be a free parameter.

## D.2 Dual optimization problems

It was appearing in the lagrangian as  $g^2(W_{\mathcal{F}}(1) - W_{\mathcal{F}}(1)^2/48)$ , with positive  $g^2$ , and we are minimizing over the primal variables  $g^2$ , so it can be implemented linearly with the positive semidefinite constraint

$$\begin{pmatrix} W_{\mathcal{F}}(1) & W_{\mathcal{F}}(1) \\ W_{\mathcal{F}}(1) & 48 \end{pmatrix} \succcurlyeq 0. \quad (\text{D.2.29})$$

Therefore

Dual Problem (Minimization of the central charge  $c_{UV}$  with a zero  $S(1-x)=0$ )

$$\text{Maximize}_{\{\lambda_1, W_{\mathcal{F}}, W_{\mathcal{F}}^*\}} \left[ \int_4^\infty ds (2\lambda_1 + 2 \text{Im} W_{\mathcal{F}} + \mathcal{N}_2 \text{Re} W_{\mathcal{F}} - i\mathcal{N}_2(1-x) \text{Im} W_{\mathcal{F}}) \right] \quad (\text{D.2.30})$$

Constrained by

$$\begin{pmatrix} \lambda_1 & \frac{\mathcal{N}_2}{2} W_{\mathcal{F}} & i \frac{\sqrt{\mathcal{N}_2}}{4} W_{\mathcal{F}} \\ \frac{\mathcal{N}_2}{2} W_{\mathcal{F}}^* & \lambda_1 & -i \frac{\sqrt{\mathcal{N}_2}}{4} W_{\mathcal{F}}^* \\ -i \frac{\sqrt{\mathcal{N}_2}}{4} W_{\mathcal{F}}^* & i \frac{\sqrt{\mathcal{N}_2}}{4} W_{\mathcal{F}} & -\frac{6}{s^2} \end{pmatrix} \preccurlyeq 0, \quad \forall s \in [4, \infty), \quad \begin{pmatrix} W_{\mathcal{F}}(1) & W_{\mathcal{F}}(1) \\ W_{\mathcal{F}}(1) & 48 \end{pmatrix} \succcurlyeq 0. \quad (\text{D.2.31})$$

### Bounds in the $(g^2, g_{\mathcal{F}_1^\Theta})$ plane

We will now derive the problem to get bounds on  $g_F \equiv g_{\mathcal{F}_1^\Theta}$  and  $g^2$ . We start by getting absolute bounds on  $g_F$  and then we optimize  $g^2$  for fixed values of  $g_F$ . We will impose the zero in the S-Matrix at the end.

The lagrangian can be written

$$\begin{aligned} \mathcal{L} = & g_F + \int_4^\infty ds w_{\mathcal{F}}(s) \left[ \mathcal{F}(s) - \mathcal{F}(2) + g^2 \left( \frac{1}{s-1} + \frac{1}{3-s} - 2 \right) \right. \\ & \left. - \int_4^\infty \frac{dz}{\pi} \text{Im} \mathcal{F}(z) \left( \frac{1}{z-s} + \frac{1}{z+s-4} - \frac{2}{z-2} \right) \right] \\ & + \int_4^\infty ds w_{\mathcal{F}}(s) \left[ \mathcal{F}(s) - \mathcal{F}(0) + g_F \left( \frac{1}{s-1} + 1 \right) - \int_4^\infty \frac{dz}{\pi} \text{Im} \mathcal{F} \left( \frac{1}{z-s} - \frac{1}{z} \right) \right] \\ & + \int_4^\infty ds \text{Tr} \Lambda(s) \cdot B(s) \\ & + c_\rho \left[ 12\pi \left( \frac{g_F^2}{g^2} + \int_4^\infty ds \frac{\rho(s)}{s^2} \right) - c_{UV} \right], \end{aligned} \quad (\text{D.2.32})$$

where the last term constrains the UV central charge to be  $c_{UV}$ . The extremization over the primal variable  $\mathcal{F}(2)$  already gives

$$\int_4^\infty ds w_{\mathcal{F}}(s) = 0. \quad (\text{D.2.33})$$

## Appendix D. Appendix to Chapter 5

---

We can now define the dual scattering function

$$W_{\mathcal{T}}(s) \equiv \int_4^\infty \frac{dz}{\pi} w_{\mathcal{T}}(z) \left( \frac{1}{z-s} - \frac{1}{z+s-4} \right), \quad (\text{D.2.34})$$

and the dual form factor function

$$W_{\mathcal{F}}(s) \equiv \int_4^\infty \frac{dz}{\pi} w_{\mathcal{F}}(z) \left( \frac{1}{z-s} + \frac{1}{s} \right). \quad (\text{D.2.35})$$

The analyticity constraints can then considerably be simplified. We get

$$\begin{aligned} \mathcal{L} = g_F + \int_4^\infty ds (\text{Im}(\mathcal{T} W_{\mathcal{T}}) + \text{Im}(\mathcal{F} W_{\mathcal{F}}) + 2 \text{Im} W_{\mathcal{F}} + \text{Tr} \Lambda(s) \cdot B(s)) \\ + c_\rho \left[ 12\pi \left( \frac{g_F^2}{g^2} + \int_4^\infty ds \frac{\rho(s)}{s^2} \right) - c_{UV} \right] + \pi g^2 W_{\mathcal{T}}(1) + \pi g_F W_{\mathcal{F}}(1) \end{aligned} \quad (\text{D.2.36})$$

We are now ready to eliminate the primal variables. Varying with respect to  $\mathcal{F}$ ,  $\mathcal{T}$  and  $\rho$  we get

$$\lambda_4 = \frac{\mathcal{N}_2}{2} W_{\mathcal{T}}, \quad \lambda_6 = i \frac{\sqrt{\mathcal{N}_2}}{4} W_{\mathcal{F}}, \quad \lambda_3 = -\frac{6C_\rho}{s^2}. \quad (\text{D.2.37})$$

The lagrangian is reduced to

$$\mathcal{L} = g_F + \int_4^\infty ds (2\lambda_1 + 2 \text{Im} W_{\mathcal{F}} + \mathcal{N}_2 \text{Re} W_{\mathcal{T}}) + c_\rho \left( 12\pi \frac{g_F^2}{g^2} - c_{UV} \right) + \pi g^2 W_{\mathcal{T}}(1) + \pi g_F W_{\mathcal{F}}(1). \quad (\text{D.2.38})$$

To finalize the elimination of primal variables we need to do variations over  $g_F$  and  $g^2$ . The former gives the equation

$$g_F = -\frac{g^2}{24\pi C_\rho} (1 + \pi W_{\mathcal{F}}(1)), \quad (\text{D.2.39})$$

that yields the lagrangian

$$\mathcal{L} = -\frac{g^2}{48\pi C_\rho} (1 + \pi W_{\mathcal{F}}(1))^2 + \int_4^\infty ds (2\lambda_1 + 2 \text{Im} W_{\mathcal{F}} + \mathcal{N}_2 \text{Re} W_{\mathcal{T}}) - c_{UV} C_\rho + \pi g^2 W_{\mathcal{T}}(1). \quad (\text{D.2.40})$$

Now extremizing over  $g^2$  we get the constraint

$$C_\rho = \frac{(1 + \pi W_{\mathcal{F}}(1))^2}{48\pi^2 W_{\mathcal{T}}(1)}. \quad (\text{D.2.41})$$

Therefore the lagrangian becomes

$$\mathcal{L} = \int_4^\infty ds (2\lambda_1 + 2 \text{Im} W_{\mathcal{F}} + \mathcal{N}_2 \text{Re} W_{\mathcal{T}}) - c_{UV} \frac{(1 + \pi W_{\mathcal{F}}(1))^2}{48\pi^2 W_{\mathcal{T}}(1)}. \quad (\text{D.2.42})$$

## D.2 Dual optimization problems

All the primal variables are eliminated and we're ready to extremize over dual variables. The last term is not linear in those variables, and it's convenient to introduce a new variable  $u$  such that

$$\begin{pmatrix} -u & 1 + \pi W_{\mathcal{F}}(1) \\ 1 + \pi W_{\mathcal{F}}(1) & -48\pi^2 W_{\mathcal{F}}(1) \end{pmatrix} \succcurlyeq 0. \quad (\text{D.2.43})$$

We can finally add the zero in the scattering amplitude as described above and formulate the dual problem that can be implemented in SDPB :

Dual Problem ( $g_F$  maximization and  $S(m^2(1-x)) = 0$ )

$$\text{Minimize}_{\{\lambda_1, W_{\mathcal{F}}, W_{\mathcal{F}}^*, u\}} \left[ \int_4^\infty ds (2\lambda_1 + 2 \text{Im} W_{\mathcal{F}} + \mathcal{N}_2 \text{Re} W_{\mathcal{F}} - i \mathcal{N}_2 (1-x) \text{Im} W_{\mathcal{F}}) - c_{UV} u \right] \quad (\text{D.2.44})$$

Constrained by

$$\begin{pmatrix} \lambda_1 & \frac{\mathcal{N}_2}{2} W_{\mathcal{F}} & i \frac{\sqrt{\mathcal{N}_2}}{4} W_{\mathcal{F}} \\ \frac{\mathcal{N}_2}{2} W_{\mathcal{F}}^* & \lambda_1 & -i \frac{\sqrt{\mathcal{N}_2}}{4} W_{\mathcal{F}}^* \\ -i \frac{\sqrt{\mathcal{N}_2}}{4} W_{\mathcal{F}}^* & i \frac{\sqrt{\mathcal{N}_2}}{4} W_{\mathcal{F}} & -\frac{6u}{s^2} \end{pmatrix} \succcurlyeq 0, \quad \forall s \in [4, \infty), \quad \begin{pmatrix} -u & 1 + \pi W_{\mathcal{F}}(1) \\ 1 + \pi W_{\mathcal{F}}(1) & -48\pi^2 W_{\mathcal{F}}(1) \end{pmatrix} \succcurlyeq 0, \quad (\text{D.2.45})$$

and

$$\int_4^\infty ds W_{\mathcal{F}}(s) = 0. \quad (\text{D.2.46})$$

The minimization is similar, we just have to maximize the dual objective instead of minimizing and adjust the constraint on  $u$  so that it becomes the correct form when the dual objective is maximized. The dual matrix  $\Lambda(s)$  needs also to be negative instead of positive, or equivalently  $-\Lambda$  is positive. We get

Dual Problem ( $g_F$  minimization and  $S(m^2(1-x)) = 0$ )

$$\text{Maximize}_{\{\lambda_1, W_{\mathcal{F}}, W_{\mathcal{F}}^*, u\}} \left[ \int_4^\infty ds (2\lambda_1 + 2 \text{Im} W_{\mathcal{F}} + \mathcal{N}_2 \text{Re} W_{\mathcal{F}} - i \mathcal{N}_2 (1-x) \text{Im} W_{\mathcal{F}}) - c_{UV} u \right] \quad (\text{D.2.47})$$

Constrained by

$$\begin{pmatrix} \lambda_1 & \frac{\mathcal{N}_2}{2} W_{\mathcal{F}} & i \frac{\sqrt{\mathcal{N}_2}}{4} W_{\mathcal{F}} \\ \frac{\mathcal{N}_2}{2} W_{\mathcal{F}}^* & \lambda_1 & -i \frac{\sqrt{\mathcal{N}_2}}{4} W_{\mathcal{F}}^* \\ -i \frac{\sqrt{\mathcal{N}_2}}{4} W_{\mathcal{F}}^* & i \frac{\sqrt{\mathcal{N}_2}}{4} W_{\mathcal{F}} & -\frac{6u}{s^2} \end{pmatrix} \preceq 0, \quad \forall s \in [4, \infty), \quad \begin{pmatrix} u & 1 + \pi W_{\mathcal{F}}(1) \\ 1 + \pi W_{\mathcal{F}}(1) & 48\pi^2 W_{\mathcal{F}}(1) \end{pmatrix} \succcurlyeq 0, \quad (\text{D.2.48})$$

and

$$\int_4^\infty ds W_{\mathcal{F}}(s) = 0. \quad (\text{D.2.49})$$

## Appendix D. Appendix to Chapter 5

Now we have to maximize the cubic coupling  $g^2$  with fixed  $g_F$  and we start with the lagrangian

$$\begin{aligned}
\mathcal{L} = & g^2 + \int_4^\infty ds w_{\mathcal{F}}(s) \left[ \mathcal{F}(s) - \mathcal{F}(2) + g^2 \left( \frac{1}{s-1} + \frac{1}{3-s} - 2 \right) \right. \\
& \left. - \int_4^\infty \frac{dz}{\pi} \text{Im} \mathcal{F}(z) \left( \frac{1}{z-s} + \frac{1}{z+s-4} - \frac{2}{z-2} \right) \right] \\
& + \int_4^\infty ds w_{\mathcal{F}}(s) \left[ \mathcal{F}(s) - \mathcal{F}(0) + g_F \left( \frac{1}{s-1} + 1 \right) - \int_4^\infty \frac{dz}{\pi} \text{Im} \mathcal{F} \left( \frac{1}{z-s} - \frac{1}{z} \right) \right] \\
& + \int_4^\infty ds \text{Tr} \Lambda(s) \cdot B(s) \\
& + c_\rho \left[ 12\pi \left( \frac{g_F^2}{g^2} + \int_4^\infty ds \frac{\rho(s)}{s^2} \right) - c_{UV} \right] + C_g (g_F - g_F^*).
\end{aligned} \tag{D.2.50}$$

The primal variables are eliminated as before, and we arrive at

$$\begin{aligned}
\mathcal{L} = & g^2 + \int_4^\infty ds (2\lambda_1 + 2 \text{Im} W_{\mathcal{F}} + \mathcal{N}_2 \text{Re} W_{\mathcal{F}}) + c_\rho \left( 12\pi \frac{g_F^2}{g^2} - c_{UV} \right) \\
& + \pi g^2 W_{\mathcal{F}}(1) + \pi g_F W_{\mathcal{F}}(1) + C_g (g_F - g_F^*).
\end{aligned} \tag{D.2.51}$$

The variations with respect to  $g_F$  and then  $g^2$  give

$$g_F = -\frac{g^2}{24\pi C_\rho} (\pi W_{\mathcal{F}}(1) + C_g), \quad C_\rho = \frac{(\pi W_{\mathcal{F}}(1) + C_g)^2}{48\pi + 48\pi^2 W_{\mathcal{F}}(1)}. \tag{D.2.52}$$

Introducing a new variable  $u$  to linearize the objective as before, we get

Dual Problem ( $g^2$  maximization with fixed  $g_F = g_F^*$  and  $S(m^2(1-x)) = 0$ )

$$\text{Minimize}_{\{\lambda_1, W_{\mathcal{F}}, W_{\mathcal{F}}^*, C_g, u\}} \left[ \int_4^\infty ds (2\lambda_1 + 2 \text{Im} W_{\mathcal{F}} + \mathcal{N}_2 \text{Re} W_{\mathcal{F}} - i \mathcal{N}_2 (1-x) \text{Im} W_{\mathcal{F}}) - c_{UV} u - C_g g_F^* \right] \tag{D.2.53}$$

Constrained by

$$\begin{pmatrix} \lambda_1 & \frac{\mathcal{N}_2}{2} W_{\mathcal{F}} & i \frac{\sqrt{\mathcal{N}_2}}{4} W_{\mathcal{F}} \\ \frac{\mathcal{N}_2}{2} W_{\mathcal{F}}^* & \lambda_1 & -i \frac{\sqrt{\mathcal{N}_2}}{4} W_{\mathcal{F}}^* \\ -i \frac{\sqrt{\mathcal{N}_2}}{4} W_{\mathcal{F}}^* & i \frac{\sqrt{\mathcal{N}_2}}{4} W_{\mathcal{F}} & -\frac{6u}{s^2} \end{pmatrix} \succcurlyeq 0, \quad \forall s \in [4, \infty), \tag{D.2.54}$$

$$\begin{pmatrix} -u & \pi W_{\mathcal{F}}(1) + C_g \\ \pi W_{\mathcal{F}}(1) + C_g & -48\pi - 48\pi^2 W_{\mathcal{F}}(1) \end{pmatrix} \succcurlyeq 0, \tag{D.2.55}$$

and

$$\int_4^\infty ds W_{\mathcal{F}}(s) = 0. \quad (\text{D.2.56})$$

Again the minimization is similar and we get

Dual Problem ( $g_T^2$  minimization with fixed  $g_F = g_F^*$  and  $S(m^2(1-x)) = 0$ )

$$\text{Maximize}_{\{\lambda_1, W_{\mathcal{F}}, W_{\mathcal{F}}^*, C_g, u\}} \left[ \int_4^\infty ds (2\lambda_1 + 2 \text{Im} W_{\mathcal{F}} + \mathcal{N}_2 \text{Re} W_{\mathcal{F}} - i \mathcal{N}_2 (1-x) \text{Im} W_{\mathcal{F}}) - c_{UV} u - C_g g_F^* \right] \quad (\text{D.2.57})$$

Constrained by

$$\begin{pmatrix} -\lambda_1 & -\frac{\mathcal{N}_2}{2} W_{\mathcal{F}} & -i \frac{\sqrt{\mathcal{N}_2}}{4} W_{\mathcal{F}} \\ -\frac{\mathcal{N}_2}{2} W_{\mathcal{F}}^* & -\lambda_1 & i \frac{\sqrt{\mathcal{N}_2}}{4} W_{\mathcal{F}}^* \\ i \frac{\sqrt{\mathcal{N}_2}}{4} W_{\mathcal{F}}^* & -i \frac{\sqrt{\mathcal{N}_2}}{4} W_{\mathcal{F}} & \frac{6u}{s^2} \end{pmatrix} \succcurlyeq 0, \quad \forall s \in [4, \infty), \quad (\text{D.2.58})$$

$$\begin{pmatrix} u & \pi W_{\mathcal{F}}(1) + C_g \\ \pi W_{\mathcal{F}}(1) + C_g & 48\pi + 48\pi^2 W_{\mathcal{F}}(1) \end{pmatrix} \succcurlyeq 0, \quad (\text{D.2.59})$$

and

$$\int_4^\infty ds W_{\mathcal{F}}(s) = 0. \quad (\text{D.2.60})$$

### D.2.3 Two poles : minimization of the central charge

We now consider the case with two particles having masses  $m_1 = 1$  and  $m_2 = \sqrt{3}$ . There is only one pole in the scattering amplitude and in the form factor corresponding to an exchange of the second particle between two of the lightest particles. The pole terms in the dispersion relations are slightly modified and read

$$\mathcal{F}(s) - \mathcal{F}(2) = -g_{112}^2 \left( \frac{1}{s-3} + \frac{1}{1-s} + 2 \right) + \int_4^\infty \frac{dz}{\pi} \text{Im} \mathcal{F}(z) \left( \frac{1}{z-s} + \frac{1}{z+s-4} - \frac{2}{z-2} \right), \quad (\text{D.2.61})$$

$$\mathcal{F}(s) - \mathcal{F}(0) = -g_F \left( \frac{1}{s-3} + \frac{1}{3} \right) + \int_4^\infty \frac{dz}{\pi} \text{Im} \mathcal{F} \left( \frac{1}{z-s} - \frac{1}{z} \right).$$

## Appendix D. Appendix to Chapter 5

We therefore have the lagrangian

$$\begin{aligned}
\mathcal{L} = & 12\pi \left( \frac{g_F^2}{9g_{112}^2} + \int_4^\infty ds \frac{\rho(s)}{s^2} \right) \\
& + \int_4^\infty ds w_{\mathcal{F}}(s) \left[ \mathcal{F}(s) - \mathcal{F}(2) + g_{112}^2 \left( \frac{1}{s-1} + \frac{1}{3-s} - 2 \right) \right. \\
& \left. - \int_4^\infty \frac{dz}{\pi} \text{Im} \mathcal{F}(z) \left( \frac{1}{z-s} + \frac{1}{z+s-4} - \frac{2}{z-2} \right) \right] \\
& + \int_4^\infty ds w_{\mathcal{F}}(s) \left[ \mathcal{F}(s) - \mathcal{F}(0) + g_F \left( \frac{1}{s-1} + 1 \right) - \int_4^\infty \frac{dz}{\pi} \text{Im} \mathcal{F} \left( \frac{1}{z-s} - \frac{1}{z} \right) \right] \\
& + \int_4^\infty ds \text{Tr} \Lambda(s) \cdot B(s).
\end{aligned} \tag{D.2.62}$$

Again the steps are similar and we obtain the dual problem

Dual Problem ( $c_{UV}$  minimization with  $m_1 = 1, m_2 = \sqrt{3}$  and  $g_{112}$  fixed)

$$\text{Maximize}_{\{\lambda_1, W_{\mathcal{F}}, W_{\mathcal{F}}^*, u\}} \left[ \int_4^\infty ds (2\lambda_1 + 2 \text{Im} W_{\mathcal{F}} + \mathcal{N}_2 \text{Re} W_{\mathcal{F}}) - 3 \frac{g_{112}^2}{16\pi} u + \pi g_T^2 W_{\mathcal{F}}(3) \right] \tag{D.2.63}$$

Constrained by

$$\begin{pmatrix} \lambda_1 & \frac{\mathcal{N}_2}{2} W_{\mathcal{F}} & i \frac{\sqrt{\mathcal{N}_2}}{4} W_{\mathcal{F}} \\ \frac{\mathcal{N}_2}{2} W_{\mathcal{F}}^* & \lambda_1 & -i \frac{\sqrt{\mathcal{N}_2}}{4} W_{\mathcal{F}}^* \\ -i \frac{\sqrt{\mathcal{N}_2}}{4} W_{\mathcal{F}}^* & i \frac{\sqrt{\mathcal{N}_2}}{4} W_{\mathcal{F}} & -\frac{6u}{s^2} \end{pmatrix} \preceq 0, \quad \forall s \in [4, \infty), \tag{D.2.64}$$

$$\begin{pmatrix} 1 & \pi W_{\mathcal{F}}(3) \\ \pi W_{\mathcal{F}}(3) & u \end{pmatrix} \succeq 0, \tag{D.2.65}$$

and

$$\int_4^\infty ds W_{\mathcal{F}}(s) = 0. \tag{D.2.66}$$

### D.3 Numerical implementation

We are now almost ready to use our linear dual formulation to get non perturbative bounds on different quantities. The last step is to implement the dual problem numerically. The dual functions  $W_{\mathcal{F}}$  and  $W_{\mathcal{F}}^*$  have branch cuts on the segment  $[4, \infty)$  and it is therefore useful to use the new variable

$$\rho(s, s_0) \equiv \frac{\sqrt{4-s_0} + \sqrt{4-s}}{\sqrt{4-s_0} - \sqrt{4-s}} \tag{D.3.1}$$



that maps the  $s$  complex plane in the unit disk with the cut mapped on the boundary and that we depict on Figure D.3 for  $s_0 = 2$ . Then any function that is analytic apart for some poles and cuts starting at  $s = 4$  can be expressed as the sum of the pole terms to which we add a Taylor series in the variable  $\rho$ .

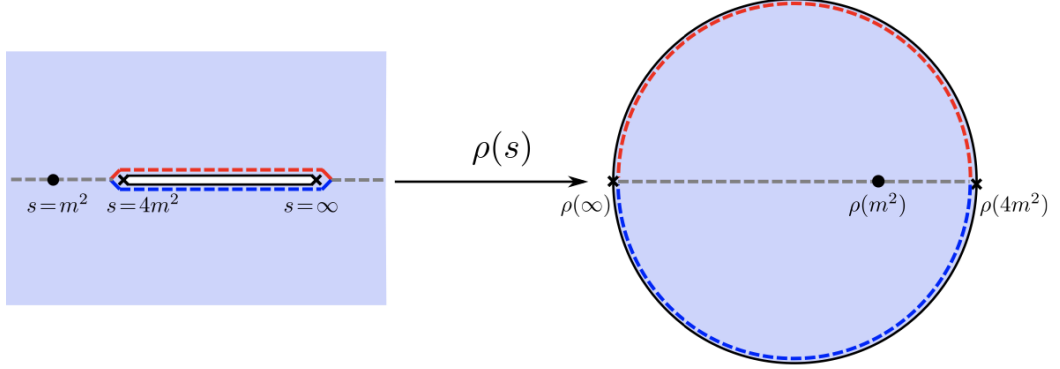


Figure D.3: Map  $\rho(s)$  from the  $s$  complex plane to the unit disk given in eq.(D.3.1). Figure taken from [1].

Accounting for the fact that  $W_{\mathcal{F}}$  is odd under crossing and  $\mathcal{N}_2 \text{Re } W_{\mathcal{F}}$  must be integrable, we make the ansatz

$$W_{\mathcal{F}}(s) = \frac{1}{s(4-s)} \sum_{n=1}^N f_n(\rho(s,2)^n - \rho(4-s,2)^n). \quad (\text{D.3.2})$$

In the case of  $\mathbb{Z}_2$  odd theories,  $W_{\mathcal{F}}$  also has a pole as can be seen from eq.(5.1.27). To account for this singularity and match the residue, the ansatz is modified as

$$W_{\mathcal{F}}(s) = -\frac{8}{\pi s(s-2)(s-4)} + \frac{1}{s(4-s)} \sum_{n=1}^N f_n(\rho(s,2)^n - \rho(4-s,2)^n). \quad (\text{D.3.3})$$

As derived in (D.2.2) when there is a zero in the scattering amplitude at  $s = 1 - x$  the ansatz becomes

$$W_{\mathcal{F}}(s) = \frac{f_0}{s(4-s)} \left( \frac{1}{s+x-1} + \frac{1}{s-x-3} \right) + \frac{1}{s(4-s)} \sum_{n=1}^N f_n(\rho(s,2)^n - \rho(4-s,2)^n). \quad (\text{D.3.4})$$

The second dual function  $W_{\mathcal{F}}$  must have an integrable imaginary part, and the definition ((5.1.28) implies the existence of a pole at  $s = 0$  with residue  $\int \text{Im } W_{\mathcal{F}} / \pi$ . We therefore propose the ansatz

$$\begin{aligned} W_{\mathcal{F}}(s) &= \frac{1}{s-4} \sum_{n=0}^N g_n \rho(s,0)^n + h_0 + \frac{1}{\pi s} \int_4^{\infty} ds \text{Im } W_{\mathcal{F}}(s) \\ &= \sum_{n=0}^N g_n \left( \frac{\rho(s,0)^n}{s-4} - \frac{(-1)^n}{s} \right) + h_0, \end{aligned} \quad (\text{D.3.5})$$

## Appendix D. Appendix to Chapter 5

---

where we were careful to include the contribution of the pole term in the imaginary part

$$\frac{1}{4-s} = \frac{1}{4-\bar{s}-i\epsilon} = \text{PV} \frac{1}{4-\bar{s}} + i\pi\delta(\bar{s}-4), \quad (\text{D.3.6})$$

where we wrote explicitly  $s = \bar{s} + i\epsilon$ ,  $\bar{s} \in \mathbb{R}$ . Finally the remaining dual variable  $\lambda_1$  is a real function that needs to be integrable. We use the ansatz

$$\lambda_1(s) = \frac{1}{s\sqrt{s-4}} \left( \sum_{n=0}^1 a_n \frac{\rho(s,0)^n + \rho(s,0)^{n,*}}{2} + \sum_{n=1}^N b_n \frac{\rho(s,0)^n - \rho(s,0)^{n,*}}{2i} \right). \quad (\text{D.3.7})$$

In some cases we observed the numerical convergence is improved if the ansatz for  $\lambda_1$  is modified as

$$\tilde{\lambda}_1(s) = \lambda_1(s) + \frac{1}{s^2} \sum_{n=1}^{10} c_n \frac{\rho(s,0)^n - \rho(s,0)^{n,*}}{2i}. \quad (\text{D.3.8})$$

In this work we use (D.3.4) and (D.3.8) in section 5.2.1, and (D.3.2) and (D.3.7) in section 5.2.2.

To implement the semipositive definite constraint on the interval  $[4m^2, \infty)$ , we discretize it on a Chebyshev grid with 200 points. We also checked, without rigorous analysis, that increasing this number does not change the results. Then we optimize numerically over the free parameters  $a_n, b_n, f_n, g_n, h_0$  and eventually  $c_n$  using SDPB to solve the dual optimization problem.

### D.4 Form factor perturbation theory

In this appendix we present our perturbative calculation for the one particle form factor  $\mathcal{F}_1^\Theta$  and then we review Zamolodchikov's result for the perturbative scattering amplitude [229].<sup>2</sup>

The Ising Field Theory has been extensively studied e.g. in [220, 222, 229] for non integrable directions. The starting point for perturbation theory will be the action

$$S_{IFT} = S_{CFT}^{(c=1/2)} + \frac{m}{2\pi} \int d^2x \epsilon(x) + h \int d^2x \sigma(x), \quad (\text{D.4.1})$$

where the scaling dimensions of the operators  $\epsilon$  and  $\sigma$  are respectively

$$\Delta_\epsilon = 1, \quad \Delta_\sigma = \frac{1}{8}. \quad (\text{D.4.2})$$

---

<sup>2</sup>Form factor perturbation theory was first proposed in [276] and was applied in different contexts (see e.g. [277, 278]).

### D.4.1 Perturbation theory for $\mathcal{F}_1^\Theta$

In the interacting theory the trace of the stress energy tensor can be deduced from (D.4.1) and (D.4.2) and takes the form<sup>3</sup>

$$\Theta(x) = \frac{m}{2\pi}\epsilon(x) + \frac{15h}{8}\sigma(x). \quad (\text{D.4.5})$$

We can split the IFT action in the thermal deformation part  $S_0$  and treat the magnetic deformation as a perturbation, which reads

$$S = S_0 + h \int d^2x \sigma(x). \quad (\text{D.4.6})$$

#### First approach

Our goal is now to use the two point function of the trace of the stress energy tensor to extract the one particle form factor  $\mathcal{F}_1^\Theta$ . To this end we can use the Euclidean spectral decomposition

$$\begin{aligned} \langle \Theta(x)\Theta(0) \rangle_c &= \int_0^\infty ds \rho_\Theta(s) \Delta_E(x, s) \\ &= |\mathcal{F}_1^\Theta|^2 \Delta_E(x, m^2) + \mathcal{O}(e^{-2mx}), \end{aligned} \quad (\text{D.4.7})$$

where we used to explicit form of the Euclidean propagator and its asymptotic form

$$\Delta_E(x, m^2) = \frac{1}{2\pi} K_0(mx) \underset{x \rightarrow \infty}{\sim} \frac{1}{2\pi} \sqrt{\frac{\pi}{2mx}} e^{-mx}. \quad (\text{D.4.8})$$

On the other hand the two point function (D.4.7) can be written as a path integral

$$\langle \Theta(x)\Theta(0) \rangle = \frac{1}{Z} \int [\mathcal{D}\phi] e^{-S_0} \left( 1 - h \int d^2y \sigma(y) + \frac{h^2}{2} \int d^2y d^2z \sigma(y)\sigma(z) + \mathcal{O}(h^3) \right) \Theta(x)\Theta(0). \quad (\text{D.4.9})$$

We can therefore get a perturbative expression for this two point function in terms of correla-

<sup>3</sup>When  $h = 0$ , one can check that the normalization for  $\Theta$  is compatible with  $\mathcal{F}_2^\Theta(s=0) = -2m^2$  and the CFT normalization of the operator  $\epsilon$ . On the one hand, we have

$$\langle \Theta(x)\Theta(0) \rangle_0 = \left( \frac{m}{2\pi} \right)^2 \langle \epsilon(x)\epsilon(0) \rangle \xrightarrow{x \rightarrow 0} \left( \frac{m}{2\pi} \right)^2 \frac{1}{|x|^2}. \quad (\text{D.4.3})$$

On the other hand, using that only the  $n = 2$  form factor  $\mathcal{F}_2^\Theta = im\sqrt{s-4m^2}$  is non vanishing when  $h = 0$  we also have

$$\langle \Theta(x)\Theta(0) \rangle_0 = \int_{4m^2}^\infty ds \frac{|\mathcal{F}_2^\Theta(s)|^2}{4\pi\sqrt{s(s-4m^2)}} \Delta_E(x, s) \xrightarrow{x \rightarrow 0} \left( \frac{m}{2\pi} \right)^2 \frac{1}{|x|^2}, \quad (\text{D.4.4})$$

showing that the normalizations are compatible.

## Appendix D. Appendix to Chapter 5

---

tion functions in the theory with  $h = 0$ , which we denote as  $\langle \dots \rangle_0$ . We get

$$\begin{aligned} \langle \Theta(x)\Theta(0) \rangle_c &= \left(\frac{m}{2\pi}\right)^2 \langle \epsilon(x)\epsilon(0) \rangle_0 + \left(\frac{15h}{8}\right)^2 \langle \sigma(x)\sigma(0) \rangle_0 \\ &\quad - \frac{15mh^2}{8\pi} \int d^2y \langle \epsilon(x)\sigma(0)\sigma(y) \rangle_0 \\ &\quad + \left(\frac{m^2h^2}{8\pi^2}\right) \int d^2y d^2z \langle \epsilon(x)\epsilon(0)\sigma(y)\sigma(z) \rangle_0 + \mathcal{O}(h^3). \end{aligned} \quad (\text{D.4.10})$$

Comparing (D.4.7) and (D.4.10), the one particle form factor can be computed as

$$|\mathcal{F}_1^\Theta|^2 = h^2 \left[ \left(\frac{15}{8}\right)^2 G^{(2)} - \frac{15m}{8\pi} G^{(3)} + \frac{m^2}{8\pi^2} G^{(4)} \right] + \mathcal{O}(h^3), \quad (\text{D.4.11})$$

where the coefficients  $G^{(i)}$  are defined as

$$\begin{aligned} G^{(2)} &\equiv \lim_{|x| \rightarrow \infty} \frac{1}{\Delta_E(x, m^2)} \langle \sigma(x)\sigma(0) \rangle_0, \\ G^{(3)} &\equiv \lim_{x \rightarrow \infty} \frac{1}{\Delta_E(x, m^2)} \int d^2y \langle \epsilon(x)\sigma(0)\sigma(y) \rangle_0, \\ G^{(4)} &\equiv \lim_{x \rightarrow \infty} \frac{1}{\Delta_E(x, m^2)} \int d^2y d^2z \langle \epsilon(x)\epsilon(0)\sigma(y)\sigma(z) \rangle_0. \end{aligned} \quad (\text{D.4.12})$$

The two point function contribution is immediately obtained by using again the spectral representation

$$G^{(2)} = \lim_{x \rightarrow \infty} \frac{1}{\Delta_E(x, m^2)} \int_0^\infty \rho_\sigma(s) \Delta_E(x, s) = |\mathcal{F}_1^\sigma|^2. \quad (\text{D.4.13})$$

To evaluate the 3 and 4 point functions in the thermal deformation we can use the known form factors [228, 279]

$$\begin{aligned} \mathcal{F}_2^\epsilon(p_1, p_2) &= -2\pi \sqrt{4m^2 - s_{12}}, \\ \mathcal{F}_3^\sigma(p_1, p_2, p_3) &= 2\mathcal{F}_1^\sigma \sqrt{\frac{4m^2 - s_{12}}{s_{12}}} \sqrt{\frac{4m^2 - s_{13}}{s_{13}}} \sqrt{\frac{4m^2 - s_{23}}{s_{23}}}, \\ \mathcal{F}_1^\sigma &= 2^{1/12} e^{-1/8} m^{1/8} A_G^{3/2} \approx 1.3578\dots, \end{aligned} \quad (\text{D.4.14})$$

where  $A_G$  is the Glaisher's constant and we use the  $s$  Mandelstam variable defined as

$$s_{12} \equiv -(p_1 + p_2)^2 = 2m^2 + 2(E_{p_1}E_{p_2} - \mathbf{p}_1 \cdot \mathbf{p}_2). \quad (\text{D.4.15})$$

We will also need the parity reversed 2-momentum  $\tilde{p}$  and the rest frame 2-momentum  $\bar{k}$  defined as

$$p \equiv \begin{pmatrix} E_p \\ \mathbf{p} \end{pmatrix}, \quad \tilde{p} \equiv \begin{pmatrix} E_p \\ -\mathbf{p} \end{pmatrix}, \quad \bar{k} \equiv \begin{pmatrix} m \\ 0 \end{pmatrix}. \quad (\text{D.4.16})$$

We can evaluate the correlation functions written as a time ordered vacuum correlator. With-

out loss of generality, we choose  $x$  to be pointing in the Euclidean time direction and we parametrize  $y$  as

$$x = \begin{pmatrix} |x| \\ \mathbf{0} \end{pmatrix}, \quad y = \begin{pmatrix} y^1 \\ y^2 \end{pmatrix}. \quad (\text{D.4.17})$$

Then, we can write

$$\begin{aligned} \int d^2 y \langle \epsilon(x) \sigma(0) \sigma(y) \rangle_0 &= \int dy^2 \int_{-\infty}^0 dy^1 \langle 0 | \epsilon(x) \sigma(0) \sigma(y) | 0 \rangle \\ &+ \int dy^2 \int_0^{|x|} dy^1 \langle 0 | \epsilon(x) \sigma(y) \sigma(0) | 0 \rangle \\ &+ \int dy^2 \int_{|x|}^{\infty} dy^1 \langle 0 | \sigma(y) \epsilon(x) \sigma(0) | 0 \rangle. \end{aligned} \quad (\text{D.4.18})$$

Using that the operators can be translated as <sup>4</sup>

$$\mathcal{O}(y) = e^{P_1 y^1 - i P_2 y^2} \mathcal{O}(0) e^{-P_1 y^1 + i P_2 y^2}, \quad (\text{D.4.19})$$

the first term in (D.4.18) reads

$$\begin{aligned} G_1^{(3)} &\equiv \int dy^2 \int_{-\infty}^0 dy^1 \langle 0 | \epsilon(x) \sigma(0) \sigma(y) | 0 \rangle \\ &= \int dy^2 \int_{-\infty}^0 dy^1 \int d\Phi_{12} d\Phi_3 \langle 0 | \epsilon(0) | p_1, p_2 \rangle_{in} \langle p_1, p_2 | \sigma(0) | p_3 \rangle_{out} \langle p_3 | \sigma(0) | 0 \rangle \\ &\quad \times e^{-|x|(E_{p_1} + E_{p_2})} e^{y^1 E_{p_3}} e^{-i y^2 p_3} + \mathcal{O}(e^{-2m|x|}) \\ &= \int d\Phi_{12} \frac{1}{4m^2} e^{-|x|(E_{p_1} + E_{p_2})} \mathcal{F}_2^\epsilon(p_1, p_2) \mathcal{F}_3^{\sigma,*}(\bar{k}, -p_1, -p_2) \mathcal{F}_1^\sigma + \mathcal{O}(e^{-2m|x|}) = \mathcal{O}(e^{-2m|x|}). \end{aligned} \quad (\text{D.4.20})$$

In the first line we inserted a complete set of states between each operator, using (5.1.5) and the notation

$$d\Phi_{12\dots n} = \frac{1}{n!} \frac{d\mathbf{p}_1}{(2\pi)2E_{\mathbf{p}_1}} \dots \frac{d\mathbf{p}_n}{(2\pi)2E_{\mathbf{p}_n}}. \quad (\text{D.4.21})$$

Between  $\epsilon(x)$  and  $\sigma(0)$  only two particle states can contribute because  $\epsilon$  can only create two particles from the vacuum. Between  $\sigma(0)$  and  $\sigma(y)$ , there are many states that contribute to the correlator but only the single particle state can hope to survive the limit (D.4.12). In the second line we integrated over  $y^2$  to get a spatial delta function that we used to integrate over  $\mathbf{p}_3$ , and we also integrated over  $y^1$ . We also used [216]

$$out \langle p_1, \dots, p_n | \mathcal{O}(0) | k_1, \dots, k_m \rangle_{in} = \mathcal{F}_{m+n}^\mathcal{O}(p_1, \dots, p_n, -k_1, \dots, -k_m), \quad (\text{D.4.22})$$

for hermitian operators  $\mathcal{O}$ . This contribution does not survive the limit (D.4.12).

<sup>4</sup>With these conventions,  $P_1$  is the hamiltonian and  $P_2$  is the spatial momentum and both are hermitian operators on the physical Hilbert space.

## Appendix D. Appendix to Chapter 5

We now treat the second term in (D.4.18) that reads

$$\begin{aligned}
G_2^{(3)} &\equiv \int dy^2 \int_0^{|x|} dy^1 \langle 0 | \varepsilon(x) \sigma(y) \sigma(0) | 0 \rangle \\
&= \int dy^2 \int_0^{|x|} dy^1 \int d\Phi_{12} d\Phi_3 \langle 0 | \varepsilon(0) | p_1, p_2 \rangle_{in\ in} \langle p_1, p_2 | \sigma(0) | p_3 \rangle_{out\ out} \langle p_3 | \sigma(0) | 0 \rangle \\
&\quad \times e^{-|x|(E_{p_1}+E_{p_2})} e^{y^1(E_{p_1}+E_{p_2}-E_{p_3})} e^{-iy^2(\mathbf{p}_1+\mathbf{p}_2-\mathbf{p}_3)} + \mathcal{O}(e^{-2m|x|}) \\
&= \int d\Phi_{12} \frac{1}{2E_{\mathbf{p}_1+\mathbf{p}_2}} \frac{1}{E_{\mathbf{p}_1}+E_{\mathbf{p}_2}-E_{\mathbf{p}_1+\mathbf{p}_2}} e^{-|x|E_{\mathbf{p}_1+\mathbf{p}_2}} \mathcal{F}_2^\varepsilon(p_1, p_2) \mathcal{F}_3^{\sigma,*}(p_3, -p_1, -p_2) \mathcal{F}_1^\sigma \\
&\quad + \mathcal{O}(e^{-2m|x|}).
\end{aligned} \tag{D.4.23}$$

where  $p_3 = (E_{\mathbf{p}_1+\mathbf{p}_2}, \mathbf{p}_1 + \mathbf{p}_2)$ . The steps are identical as above and we now get a non-zero contribution to the limit (D.4.12). A similar calculation shows that the third term (D.4.18) is

$$G_3^{(3)} \equiv \int dy^2 \int_{|x|}^\infty dy^1 \langle 0 | \sigma(y) \varepsilon(x) \sigma(0) | 0 \rangle = \int d\Phi_1 \frac{1}{2m^2} e^{-E_{p_1}|x|} (\mathcal{F}_1^\sigma)^2 \mathcal{F}_2^{\varepsilon,*}(p_1, -\bar{k}) \tag{D.4.24}$$

To evaluate the  $x \rightarrow \infty$  limit we can use that the  $x$  dependence in the integrand only comes from the exponential. If the integral is only over  $\mathbf{p}$  we have

$$\begin{aligned}
&\lim_{x \rightarrow \infty} \frac{1}{\Delta_E(x, m^2)} \int d\mathbf{p} f(\mathbf{p}) e^{-|x|E_{\mathbf{p}}} = \\
&= \lim_{x \rightarrow \infty} \frac{1}{\Delta_E(x, m^2)} \int \frac{d\mathbf{p}}{\sqrt{|x|}} f\left(\frac{\mathbf{p}}{\sqrt{|x|}}\right) e^{-|x|(m+\mathbf{p}^2/(2m|x|))+\mathcal{O}(\mathbf{p}^3/\sqrt{|x|})} = 4\pi f(0),
\end{aligned} \tag{D.4.25}$$

where we rescaled the integration variable by  $1/\sqrt{|x|}$  and expanded the energy with its Taylor series. When we have an integral over  $\mathbf{p}_1$  and  $\mathbf{p}_2$  and the exponential damping contains  $E_{\mathbf{p}_1+\mathbf{p}_2}$ , we get

$$\lim_{x \rightarrow \infty} \frac{1}{\Delta_E(x, m^2)} \int d\mathbf{p}_1 d\mathbf{p}_2 f(\mathbf{p}_1, \mathbf{p}_2) e^{-|x|E_{\mathbf{p}_1+\mathbf{p}_2}} = 4\pi \int d\mathbf{p} f(\mathbf{p}, -\mathbf{p}). \tag{D.4.26}$$

This result is obtained by first changing variables to  $\mathbf{p}_1 + \mathbf{p}_2$  and  $\mathbf{p}_1 - \mathbf{p}_2$  and then rescaling as above.

Using these results we can take the limit (D.4.12) and get the contribution of the 3 point function that reads

$$\begin{aligned}
G^{(3)} &= 4\pi \frac{1}{8\pi m^3} \mathcal{F}_2^{\varepsilon,*}(\bar{k}, -\bar{k}) (\mathcal{F}_1^\sigma)^2 \\
&\quad - 4\pi i \int d\mathbf{p} \frac{1}{2(2\pi 2E_{\mathbf{p}})^2} \frac{1}{2m} \frac{1}{2E_{\mathbf{p}} - m} \mathcal{F}_2^\varepsilon(p, \tilde{p}) \mathcal{F}_1^\sigma \mathcal{F}_3^{\sigma,*}(\bar{k}, -p, -\tilde{p})
\end{aligned} \tag{D.4.27}$$

The contributions from the 4 point function are similar. We have

$$\int d^2y d^2z \langle \epsilon(x)\epsilon(0)\sigma(y)\sigma(z) \rangle_0 = 2 \int dy^2 dz^2 \int_{-\infty}^{\infty} dy^1 \int_{-\infty}^{y^1} dz^1 \langle \epsilon(x)\epsilon(0)\sigma(y)\sigma(z) \rangle_0. \quad (\text{D.4.28})$$

Splitting up the integrals in time-ordered correlators, we get four contributing terms

$$\begin{aligned} G_1^{(4)} &\equiv \int dy^2 dz^2 \int_0^{|x|} dy^1 \int_{-\infty}^0 dz^1 \langle 0 | \epsilon(x)\sigma(y)\epsilon(0)\sigma(z) | 0 \rangle \\ &= \int d\Phi_2 \frac{1}{2m^2} \frac{1}{E_{\mathbf{p}_1} + E_{\mathbf{p}_2} - E_{\mathbf{p}_1 + \mathbf{p}_2}} e^{-|x|(E_{\mathbf{p}_1 + \mathbf{p}_2})} \mathcal{F}_2^\epsilon(\mathbf{p}_1, \mathbf{p}_2) \mathcal{F}_3^{\sigma,*}(\mathbf{p}_1, \mathbf{p}_2, -\mathbf{p}_3) \mathcal{F}_1^\sigma \mathcal{F}_2^\epsilon(-\mathbf{p}_3, \bar{\mathbf{k}}), \end{aligned} \quad (\text{D.4.29})$$

where  $p_3 = (E_{\mathbf{p}_1 + \mathbf{p}_2}, \mathbf{p}_1 + \mathbf{p}_2)$ ,

$$\begin{aligned} G_2^{(4)} &\equiv \int dy^2 dz^2 \int_0^{|x|} dy^1 \int_0^{y^1} dz^1 \langle 0 | \epsilon(x)\sigma(y)\sigma(z)\epsilon(0) | 0 \rangle \\ &= \int d\Phi_2 d\Phi'_2 \frac{1}{2E_{\mathbf{p}_1 + \mathbf{p}_2}} \frac{1}{E_{\mathbf{p}_1} + E_{\mathbf{p}_2} - E_{\mathbf{p}_1 + \mathbf{p}_2}} \frac{1}{E_{\mathbf{p}_1} + E_{\mathbf{p}_2} - E_{\mathbf{p}'_1 + \mathbf{p}'_2}} e^{-|x|(E_{\mathbf{p}_1 + \mathbf{p}_2})} \\ &\quad (2\pi)\delta(\mathbf{p}_1 + \mathbf{p}_2 - \mathbf{p}'_1 - \mathbf{p}'_2) \times \mathcal{F}_2^\epsilon(\mathbf{p}_1, \mathbf{p}_2) \mathcal{F}_2^{\epsilon,*}(\mathbf{p}'_1, \mathbf{p}'_2) \mathcal{F}_3^\sigma(\mathbf{p}'_1, \mathbf{p}'_2, -\mathbf{p}'_3) \mathcal{F}_3^{\sigma,*}(\mathbf{p}_1, \mathbf{p}_2, -\mathbf{p}_3), \end{aligned} \quad (\text{D.4.30})$$

where  $p_3 = (E_{\mathbf{p}_1 + \mathbf{p}_2}, \mathbf{p}_1 + \mathbf{p}_2)$  and  $p'_3 = (E_{\mathbf{p}'_1 + \mathbf{p}'_2}, \mathbf{p}'_1 + \mathbf{p}'_2)$ ,

$$\begin{aligned} G_3^{(4)} &\equiv \int dy^2 dz^2 \int_{|x|}^{\infty} dy^1 \int_{-\infty}^0 dz^1 \langle 0 | \sigma(y)\epsilon(x)\epsilon(0)\sigma(z) | 0 \rangle \\ &= \int d\Phi_1 \frac{1}{4m^2} e^{-|x|E_{\mathbf{p}_1}} (\mathcal{F}_1^\sigma)^2 |\mathcal{F}_2^\epsilon(-\mathbf{p}_1, \bar{\mathbf{k}})|^2, \end{aligned} \quad (\text{D.4.31})$$

and finally

$$\begin{aligned} G_4^{(4)} &\equiv \int dy^2 dz^2 \int_{|x|}^{\infty} dy^1 \int_0^{|x|} dz^1 \langle 0 | \sigma(y)\epsilon(x)\sigma(z)\epsilon(0) | 0 \rangle \\ &= \int d\Phi_2 \frac{1}{2m^2} \frac{1}{E_{\mathbf{p}_1} + E_{\mathbf{p}_2} - E_{\mathbf{p}_1 + \mathbf{p}_2}} e^{-|x|(E_{\mathbf{p}_1 + \mathbf{p}_2})} \mathcal{F}_2^\epsilon(\mathbf{p}_1, \mathbf{p}_2) \mathcal{F}_3^{\sigma,*}(\mathbf{p}_1, \mathbf{p}_2, -\mathbf{p}_3) \mathcal{F}_1^\sigma \mathcal{F}_2^\epsilon(-\mathbf{p}_3, \bar{\mathbf{k}}) \\ &= G_1^{(4)}, \end{aligned} \quad (\text{D.4.32})$$

where  $p_3 = (E_{\mathbf{p}_1 + \mathbf{p}_2}, \mathbf{p}_1 + \mathbf{p}_2)$ . We can take the  $|x| \rightarrow \infty$  limit and we get for the total 4 point

## Appendix D. Appendix to Chapter 5

---

function contribution

$$\begin{aligned}
G^{(4)} &= 32\pi \int d\mathbf{p} \frac{1}{2(2\pi 2E_{\mathbf{p}})^2} \frac{1}{4m^3} \frac{1}{2E_{\mathbf{p}} - 2m} \mathcal{F}_2^\epsilon(p, \tilde{p}) \mathcal{F}_3^{\sigma,*}(p, \tilde{p}, -\bar{k}) \mathcal{F}_2^\epsilon(-\bar{k}, \bar{k}) \mathcal{F}_1^\sigma \\
&+ 16\pi \int d\mathbf{p}_1 d\mathbf{p}_2 \frac{1}{2(2\pi 2E_{\mathbf{p}_1})^2} \frac{1}{2(2\pi 2E_{\mathbf{p}_2})^2} \frac{1}{2m} \frac{1}{2E_{\mathbf{p}_1} - m} \frac{1}{2E_{\mathbf{p}_2} - m} (2\pi) \\
&\quad \times \mathcal{F}_2^\epsilon(p_1, \tilde{p}_1) \mathcal{F}_2^{\epsilon,*}(p_2, \tilde{p}_2) \mathcal{F}_3^\sigma(p_2, \tilde{p}_2, -\bar{k}) \mathcal{F}_3^{\sigma,*}(p_1, \tilde{p}_1, -\bar{k}) \\
&+ 16\pi \frac{1}{2\pi 2m} \frac{(\mathcal{F}_1^\sigma)^2}{4m^4} |\mathcal{F}_2^\epsilon(-\bar{k}, \bar{k})|^2.
\end{aligned} \tag{D.4.33}$$

The integrals in (D.4.27) and (D.4.33) can be evaluated and we find

$$\begin{aligned}
G^{(3)} &= |\mathcal{F}_1^\sigma|^2 \left( 2\pi + 2(\sqrt{3} - 1)\pi - 1 \right), \\
G^{(4)} &= 2|\mathcal{F}_1^\sigma|^2 \left[ \left( 2(\sqrt{3} - 1)\pi - 1 \right)^2 + 8\pi \left( (\sqrt{3} - 1)\pi - \frac{1}{2} \right) + 4\pi^2 \right].
\end{aligned} \tag{D.4.34}$$

Plugging those results in (D.4.11) we obtain

$$\begin{aligned}
|\mathcal{F}_1^\Theta| &= h |\mathcal{F}_1^\sigma| \sqrt{\left( \frac{15}{8} - \sqrt{3} + \frac{1}{2\pi} \right)^2} + \mathcal{O}(h^2) \\
&= h |\mathcal{F}_1^\sigma| \times 0.302104\dots + \mathcal{O}(h^2)
\end{aligned} \tag{D.4.35}$$

### Second approach

This computation can be verified by doing an independent derivation. Our strategy is to follow the lines of perturbative quantum mechanics and generalize them to quantum field theory. We split the total hamiltonian as

$$H = H_0 + hV, \quad V = \int d\mathbf{x} \sigma(x), \tag{D.4.36}$$

where  $H_0$  is the hamiltonian of the free Majorana fermion described by the theory at  $h = 0$ . We denote by  $|\psi\rangle$  the eigenstates of the full hamiltonian  $H$  with eigenvalues  $E$  that can be expanded as

$$|\psi\rangle = |\psi\rangle^{(0)} + h|\psi\rangle^{(1)} + \mathcal{O}(h^2), \quad E = E^{(0)} + hE^{(1)} + \mathcal{O}(h^2), \tag{D.4.37}$$

where  $|\psi\rangle^{(0)}$  is an eigenstate of  $H_0$  with eigenvalue  $E^{(0)}$ . In QFT a convenient basis for those states are the multi-particle states  $|p_1 \dots p_n\rangle$ . The form factor  $\mathcal{F}_1^\Theta$  reads

$$\begin{aligned}
\mathcal{F}_1^\Theta &= {}_{out} \langle p | \Theta(0) | 0 \rangle_{in} = \left( {}_{out}^{(0)} \langle p | + {}_{out}^{(1)} \langle p | h \right) \left( \frac{m}{2\pi} \epsilon(0) + \frac{15h}{8} \sigma(0) \right) \left( |0\rangle_{in}^{(0)} + h|0\rangle_{in}^{(1)} \right) + \mathcal{O}(h^2) \\
&= h \left[ \frac{m}{2\pi} \left( {}_{out}^{(0)} \langle p | \epsilon(0) | 0 \rangle_{in}^{(1)} + {}_{out}^{(1)} \langle p | \epsilon(0) | 0 \rangle_{in}^{(0)} \right) + \frac{15}{8} \mathcal{F}_1^\sigma \right] + \mathcal{O}(h^2).
\end{aligned} \tag{D.4.38}$$



## D.4 Form factor perturbation theory

The problem we need to solve is now to compute the first correction to the energy eigenstates  $|\psi\rangle^{(1)}$  and  $|0\rangle^{(1)}$ . For this we expand the Schrödinger equation

$$H|\psi\rangle = E|\psi\rangle \implies (H_0 - E^{(0)})|\psi\rangle^{(1)} = (E^{(1)} - V)|\psi\rangle^{(0)}, \quad (\text{D.4.39})$$

where the implication follows by comparing terms in first order in  $\hbar$ . Multiplying the equation by  ${}^{(0)}\langle\psi|$  and using that the form factors of  $\sigma$  are zero for an even number of particles we get  $E^{(1)} = 0$ . Inserting the identity (5.1.5) we get

$$\sum_{\mathbf{p}_1 \dots \mathbf{p}_n} \langle \mathbf{p}_1 \dots \mathbf{p}_n | (E_n^{(0)} - E^{(0)}) | \psi \rangle^{(1)} = - \sum_{\mathbf{p}_1 \dots \mathbf{p}_n} \langle \mathbf{p}_1 \dots \mathbf{p}_n | V | \psi \rangle^{(0)}, \quad (\text{D.4.40})$$

where  $E_n \equiv E_{\mathbf{p}_1} + \dots + E_{\mathbf{p}_n}$ . Here we are already at order  $\hbar$  so we can consider the states  $|\mathbf{p}_1 \dots \mathbf{p}_n\rangle$  as eigenstates of  $H_0$ . We need to be careful with degeneracies. For our problem  $|\psi\rangle^{(0)}$  will either be a one particle state or the vacuum. Due to Lorentz invariance we can set  $\mathbf{p} = \vec{k} = (m, \mathbf{0})$  so that  $E_{\mathbf{p}}^{(0)} = m$  will never be degenerate. The vacuum is assumed to have zero energy and is also never degenerate. If  $|\mathbf{p}_1 \dots \mathbf{p}_n\rangle \neq |\psi\rangle^{(0)}$ , we can then invert (D.4.40) to get

$$\langle \mathbf{p}_1 \dots \mathbf{p}_n | \psi \rangle^{(1)} = - \frac{\langle \mathbf{p}_1 \dots \mathbf{p}_n | V | \psi \rangle^{(0)}}{E_n^{(0)} - E^{(0)}}. \quad (\text{D.4.41})$$

This gives all the components of  $|\psi\rangle^{(1)}$  except along  $|\psi\rangle^{(0)}$ . Assuming that the norm is conserved, ie  $\langle \psi | \psi \rangle = {}^{(0)}\langle \psi | \psi \rangle^{(0)}$  we get  ${}^{(0)}\langle \psi | \psi \rangle^{(1)} = 0$ . Therefore we found

$$|\psi\rangle^{(1)} = \sum_{\mathbf{n} \neq \psi} |\mathbf{p}_1 \dots \mathbf{p}_n\rangle \frac{\langle \mathbf{p}_1 \dots \mathbf{p}_n | V | \psi \rangle^{(0)}}{E^{(0)} - E_n^{(0)}}, \quad (\text{D.4.42})$$

where we defined

$$\sum_{\mathbf{n} \neq \psi} |\mathbf{p}_1 \dots \mathbf{p}_n\rangle \equiv \sum_{\mathbf{p}_1 \dots \mathbf{p}_n} |\mathbf{p}_1 \dots \mathbf{p}_n\rangle - \frac{|\psi\rangle^{(0)}}{{}^{(0)}\langle \psi | \psi \rangle^{(0)}} \quad \text{such that} \quad {}^{(0)}\langle \psi | \sum_{\mathbf{n} \neq \psi} |\mathbf{p}_1 \dots \mathbf{p}_n\rangle = 0. \quad (\text{D.4.43})$$

The result (D.4.42) is the direct generalization of the familiar quantum mechanical result. We can now proceed to the evaluation of the matrix elements in (D.4.38). First we have

$${}^{(0)}_{out} \langle \vec{k} | \epsilon(0) | 0 \rangle_{in}^{(1)} = - \int \frac{d\mathbf{p}_1}{(2\pi)2E_{\mathbf{p}_1}} {}_{out} \langle \vec{k} | \epsilon(0) | \mathbf{p}_1 \rangle_{int} \frac{{}_{in} \langle \mathbf{p}_1 | V | 0 \rangle_{out}}{E_{\mathbf{p}_1}}, \quad (\text{D.4.44})$$

where we dropped the 0 superscripts in the RHS because everything is in the free theory sector and we used that  $\epsilon$  only interpolates between free particles and  $|0\rangle_{in} = |0\rangle_{out}$  in free theory. To continue we compute

$$\langle \mathbf{p}_1 | V | 0 \rangle_{out} = \int d\mathbf{x} e^{-i\mathbf{x}\mathbf{p}_1} \mathcal{F}_1^\sigma = (2\pi)\delta(\mathbf{p}_1)\mathcal{F}_1^\sigma, \quad (\text{D.4.45})$$

## Appendix D. Appendix to Chapter 5

---

where we used the time independence of the Hamiltonian to set  $t = 0$  in  $\sigma(t, \mathbf{x})$  and  $\mathcal{F}_1^{\sigma,*} = \mathcal{F}_1^\sigma$ . Using this spatial delta function to perform the integral we get

$${}_{out}^{(0)}\langle \bar{k} | \epsilon(0) | 0 \rangle_{in}^{(1)} = -\frac{1}{2m^2} \mathcal{F}_2^\epsilon(\bar{k}, -\bar{k}) \mathcal{F}_1^\sigma = \frac{2\pi}{m} \mathcal{F}_1^\sigma. \quad (\text{D.4.46})$$

The second term in (D.4.38) is computed by similar methods and we get

$$\begin{aligned} {}_{out}^{(1)}\langle \bar{k} | \epsilon(0) | 0 \rangle_{in}^{(0)} &= -\frac{1}{2} \int \frac{d\mathbf{p}_1}{(2\pi)2E_{\mathbf{p}_1}} \frac{1}{2E_{\mathbf{p}_1}} \frac{1}{2E_{\mathbf{p}_1} - m} \mathcal{F}_3^{\sigma,*}(p_1, \tilde{p}_1, -\bar{k}) \mathcal{F}_2^\epsilon(p_1, \tilde{p}_1) \\ &= \left(1 - 2\pi(\sqrt{3} - 1)\right) \mathcal{F}_1^\sigma. \end{aligned} \quad (\text{D.4.47})$$

Plugging those results back in (D.4.38) we get

$$\mathcal{F}_1^\Theta = h\mathcal{F}_1^\sigma \left( \frac{15}{8} - \sqrt{3} + \frac{1}{2\pi} \right), \quad (\text{D.4.48})$$

which is identical to our previous result (D.4.35).

### D.4.2 Perturbation theory for $S(s)$

The first order correction to the scattering amplitude in presence of a small magnetic field was computed in [229]. More precisely they derived the term  $S^{(1)}(s)$  in

$$S(s) = -1 + h^2 S^{(1)}(s) + \mathcal{O}(h^4). \quad (\text{D.4.49})$$

We introduce the change of variables

$$s \mapsto w(s) \equiv \frac{s(s - 4m^2)}{4m^4}, \quad w \mapsto s(w) \equiv 2m^2(1 + \sqrt{1 + w}). \quad (\text{D.4.50})$$

The correction  $S^{(1)}$  can then be written

$$S^{(1)}(s) = -\frac{iA(w(s))}{\sqrt{w(s)}}, \quad (\text{D.4.51})$$

where

$$A(w) = \frac{rw}{w + \frac{3}{4}} + w \int_{45/4}^{\infty} \frac{dv}{2\pi} \frac{\sigma_{2 \rightarrow 3}(s(v))}{(v - w)\sqrt{v}}, \quad (\text{D.4.52})$$

where  $\sigma_{2 \rightarrow 3}$  is the part of the inelastic cross section giving the total probability to scatter 2 particles and end up with 3 particles, and  $s(v)$  is the function defined in (D.4.50). The numerator of the pole term is given by

$$r = 36|\mathcal{F}_1^\sigma|^2, \quad (\text{D.4.53})$$

and the inelastic scattering cross section can be written as

$$\begin{aligned}
 \sigma_{2 \rightarrow 3}(s) &= B(s)I(s) \\
 B(s) &= \frac{4|\mathcal{F}_1^\sigma|^2}{\pi} \frac{(\sqrt{s}+2)^{\frac{5}{2}}(2\sqrt{s}-1)^4(\sqrt{s}-3)^3}{(\sqrt{s}-2)^{\frac{3}{2}}(\sqrt{s}+1)(\sqrt{s}-1)^{\frac{5}{2}}(\sqrt{s}+3)^{\frac{3}{2}}s^{\frac{3}{2}}} \\
 I(s) &= \int_{-1}^1 dt \left( \frac{1-\mu t^2}{1-\nu t^2} \right)^2 \frac{\sqrt{1-t^2}}{(1-\lambda t^2)^{\frac{5}{2}}} \\
 \lambda &= \frac{(\sqrt{s}+1)(\sqrt{s}-3)^3}{(\sqrt{s}-1)(\sqrt{s}+3)^3}, \quad \mu = \frac{(\sqrt{s}-2)(2\sqrt{s}+1)^2}{(\sqrt{s}+2)(2\sqrt{s}-1)^2} \lambda, \quad \nu = \frac{\sqrt{s}+2}{\sqrt{s}-2} \lambda.
 \end{aligned} \tag{D.4.54}$$

From this result we can find out a perturbative expression for the residue  $g^2$  of the scattering amplitude

$$\mathcal{F}(s) = -\frac{g^2}{s-m^2} + \dots \implies S(s) = -\frac{i}{\mathcal{N}_2} \frac{g^2}{s-m^2} + \dots \tag{D.4.55}$$

where the dots denote all terms that are not the pole term. Using (D.4.50) we have  $\mathcal{N}_2 = 4\sqrt{w}$ . Therefore we get

$$\begin{aligned}
 S(s) &= -\frac{ih^2 A(w(s))}{\sqrt{w(s)}} + \dots = -ih^2 r \frac{4}{\mathcal{N}_2} \frac{s(s-4m^2)}{s(s-4m^2)+3m^4} + \dots \\
 \implies \frac{g^2}{s-m^2} + \dots &= 4h^2 r \left( 1 - \frac{3}{s(s-4m^2)+3m^4} \right) + \dots = 12h^2 r \frac{1}{(s-m^2)(s-3m^2)} + \dots \\
 &= \frac{6h^2 r}{s-m^2} + \dots
 \end{aligned} \tag{D.4.56}$$

Therefore we have

$$g^2 = 6rh^2 + \mathcal{O}(h^4). \tag{D.4.57}$$

We can also get a relation between  $h^2$  and the position of the zero in the S-matrix parametrized by  $x$ . Indeed setting  $S(m^2(1-x)) = 0$  we get

$$-1 - 4m^4 ih^2 \frac{A(s=m^2(1-x))}{\sqrt{m^2(1-x)}\sqrt{m^2(1-x)-4m^2}} = 0, \tag{D.4.58}$$

where we abused the notation by setting  $A(s) \equiv A(w(s))$ . Solving for  $h^2$  we have

$$h^2 = -\frac{1}{2} \sqrt{1-x} \sqrt{3+x} \frac{1}{A(s=m^2(1-x))}. \tag{D.4.59}$$

If  $x$  is sufficiently small we can expand around  $x=0$  to get

$$h \approx \frac{3^{-1/4}}{6\mathcal{F}_1^\sigma} \sqrt{x}. \tag{D.4.60}$$

## D.5 Integral representation for $c_{UV}$ : c-sum rule

Here we review the argument from [217] to derive a sum rule relating the two point function of the trace of the stress energy tensor to the central charge of the UV CFT.

In Euclidean space and complex coordinates the conservation of the stress energy tensor becomes

$$\bar{\partial}T + \frac{\pi}{2}\partial\Theta = 0, \quad (\text{D.5.1})$$

where we defined  $T(z, \bar{z}) \equiv 2\pi T_{zz}(z, \bar{z})$  and  $\bar{T}(z, \bar{z}) \equiv 2\pi T_{\bar{z}\bar{z}}(z, \bar{z})$ . This gives the following relations between two point functions

$$\langle \bar{\partial}T(z, \bar{z})T(0, 0) \rangle = -\frac{\pi}{2}\langle \partial\Theta(z, \bar{z})T(0, 0) \rangle, \quad \langle \bar{\partial}T(z, \bar{z})\Theta(0, 0) \rangle = -\frac{\pi}{2}\langle \partial\Theta(z, \bar{z})\Theta(0, 0) \rangle. \quad (\text{D.5.2})$$

On the other hand we know how  $T$  and  $\bar{T}$  transform under rotations, and it constrains the two point functions to take the form

$$\langle T(z, \bar{z})T(0, 0) \rangle = \frac{F(z\bar{z})}{z^4}, \quad \langle T(z, \bar{z})\Theta(0, 0) \rangle = \frac{G(z\bar{z})}{z^3\bar{z}}, \quad \langle \Theta(z, \bar{z})\Theta(0, 0) \rangle = \frac{H(z\bar{z})}{z^2\bar{z}^2}, \quad (\text{D.5.3})$$

where  $F$ ,  $G$  and  $H$  are unknown functions that do not transform under rotations. Furthermore invariance under translations also gives

$$\langle T(z, \bar{z})\Theta(0, 0) \rangle = \langle \Theta(z, \bar{z})T(0, 0) \rangle. \quad (\text{D.5.4})$$

Comparing (D.5.2) and (D.5.3) we get that the functions  $F, G$  and  $H$  must obey

$$z\bar{z}F' + \frac{\pi}{2}(z\bar{z}G' - 3G) = 0, \quad z\bar{z}G' - G + \frac{\pi}{2}(z\bar{z}H' - 2H) = 0. \quad (\text{D.5.5})$$

We now define the C function by

$$C \equiv 2F - 2\pi G - \frac{3\pi^2}{2}H. \quad (\text{D.5.6})$$

Taking a derivative and multiplying by  $z\bar{z}$ , a direct comparison with (D.5.5) gives

$$z\bar{z}C'(z\bar{z}) = -3\pi^2 H. \quad (\text{D.5.7})$$

In the UV CFT the OPE of the stress tensor takes the form

$$T(z)T(w) = \frac{c/2}{(z-w)^4} + 2\frac{T(w)}{(z-w)^2} + \frac{\partial T(w)}{z-w} + \dots, \quad (\text{D.5.8})$$

where the coefficient  $c$  of the most singular term is called the central charge of the 2D CFT.

With this OPE in hands it is a simple task to compute the two point functions in (D.5.3) in the

## D.6 Normalization of the stress energy tensor form factors

UV CFT, or equivalently in the short distance asymptotic regime  $z\bar{z} \rightarrow 0$ . We get

$$F_{UV} = \frac{c}{2}, \quad G_{UV} = H_{UV} = 0, \quad (\text{D.5.9})$$

where we used  $\Theta = 0$  in the CFT, as follows from invariance under global scale transformations. Going back to Euclidean cartesian coordinates we therefore have

$$\int_0^\infty dr^2 C'(r^2) = C(\infty) - C(0) = C_{IR} - C_{UV} = c_{IR} - c_{UV}, \quad (\text{D.5.10})$$

where in the last equality we used the definition of  $C$  (D.5.6) and the expressions of  $F, G$  and  $H$  in the CFT (D.5.9). If we assume a massive theory the IR CFT is trivial and we have  $c_{IR} = 0$ . We can therefore use (D.5.7) and the last expression to get

$$c_{UV} = - \int_0^\infty dr^2 C'(r^2) = \int_0^\infty 2r dr 3\pi^2 \frac{H(r^2)}{r^2} = 3\pi \int d^2 x x^2 \langle \Theta(x) \Theta(0) \rangle. \quad (\text{D.5.11})$$

Then using the Euclidean spectral representation we get

$$\int d^2 x x^2 \langle \Theta(x) \Theta(0) \rangle = \int_0^\infty ds \int d^2 x x^2 \rho(s) \int \frac{d^2 p}{(2\pi)^2} e^{ip \cdot x} \frac{1}{p^2 + s}. \quad (\text{D.5.12})$$

The  $x$  integral can be easily evaluated by using

$$\int d^2 x x^2 e^{ipx} = -(2\pi)^2 \nabla_p^2 \delta^{(2)}(p), \quad (\text{D.5.13})$$

and then we integrate by parts two times to perform the  $p$  integral. We get

$$\int d^2 p p \frac{1}{p^2 + s} \nabla_p^2 \delta^{(2)}(p) = \nabla_p^2 \frac{1}{p^2 + s} \Big|_{p=0} = -\frac{4}{s^2}. \quad (\text{D.5.14})$$

This finally yields the sum-rule for the central charge of the UV CFT in terms of the spectral density of the trace of the stress energy tensor

$$c_{UV} = 12\pi \left( m^{-4} |\mathcal{F}_1^\Theta|^2 + \int_{4m^2}^\infty ds \frac{\rho(s)}{s^2} \right), \quad (\text{D.5.15})$$

where we used (5.1.7) to integrate the delta function contribution to the spectral density.

## D.6 Normalization of the stress energy tensor form factors

Here we derive a normalization condition that needs to be satisfied by  $\mathcal{F}_2^\Theta(s)$ . We follow closely [216]. Because of Lorentz invariance the most general expression for the 2 particle form factor of the full stress tensor is

$$\mathcal{F}_2^{T^{\mu\nu}}(p_1, p_2) = a_1 p^\mu p^\nu + a_2 q^\mu q^\nu + a_3 p^\mu q^\nu + a_4 p^\nu q^\mu + a_5 \eta^{\mu\nu}, \quad (\text{D.6.1})$$

## Appendix D. Appendix to Chapter 5

---

where  $p \equiv p_1 + p_2$  and  $q \equiv p_1 - p_2$ . The symmetry condition  $T^{\mu\nu} = T^{\nu\mu}$  gives  $a_3 = a_4$  and conservation gives

$$\partial_\mu T^{\mu\nu} = 0 \implies (p_1 + p_2)_\mu \mathcal{F}_2^{T^{\mu\nu}}(p_1, p_2) = 0, \quad (\text{D.6.2})$$

which yields  $a_1 p^2 = -a_5$  and  $a_3 = 0$ . Therefore the most general form for the form factor of the stress tensor is

$$\mathcal{F}_2^{T^{\mu\nu}}(p_1, p_2) = A(s)(p^\mu p^\nu - p^2 \eta^{\mu\nu}) + B(s)q^\mu q^\nu, \quad (\text{D.6.3})$$

where  $A$  and  $B$  are Lorentz invariant. However the two terms in (D.6.3) are linearly dependent as it can be seen for example by going to the center of mass frame and writing the two terms explicitly. Therefore there is no loss of generality in setting  $A(s) = 0$ , which leads to

$$\mathcal{F}_2^{T^{\mu\nu}}(s) = B(s)q^\mu q^\nu, \quad \mathcal{F}_2^\Theta(s) = (s - 4m^2)B(s), \quad (\text{D.6.4})$$

where we used  $q^2 = s - 4m^2$ .

On the other hand the stress energy tensor is normalized when acting on one particle states such that

$$P^\mu |p\rangle = \int dx T^{0\mu}(x) |p\rangle = p^\mu |p\rangle. \quad (\text{D.6.5})$$

Hence we get

$$\begin{aligned} \langle p_1 | P^\mu | p_2 \rangle &= p_2^\mu (2\pi) 2E_{p_2} \delta(\mathbf{p}_2 - \mathbf{p}_1) \\ &= \mathcal{F}_2^{T^{0\mu}}(p_1, -p_2) \int dx e^{ix \cdot (p_1 - p_2)} = \mathcal{F}_2^{T^{0\mu}}(p_1, -p_2) (2\pi) \delta(\mathbf{p}_1 - \mathbf{p}_2), \end{aligned} \quad (\text{D.6.6})$$

where in the last equality the exponential with time components simply gives 1 because the particles have the same mass.

Analytic continuing (D.6.4) we have

$$\mathcal{F}_2^{T^{0\mu}}(p_1, -p_2) = B(s - 4m^2)(E_{p_1} + E_{p_2})(p_1^\mu + p_2^\mu). \quad (\text{D.6.7})$$

Subtracting the expressions multiplying the spatial delta function in the first and second line of (D.6.6) we get

$$(B(s - 4m^2)(p_1^\mu + p_2^\mu) - p_2^\mu) \delta(\mathbf{p}_1 - \mathbf{p}_2) = 0, \quad (\text{D.6.8})$$

where we used (D.6.7). Evaluating this for  $\mu = 0$  at  $s = 4m^2$  yields

$$B(s = 0) = \frac{1}{2}. \quad (\text{D.6.9})$$

Combining (D.6.4) and (D.6.9) we therefore derived the implication of the normalization of the stress tensor on the 2 particle form factor of the trace, which reads

$$\mathcal{F}_2^\Theta(s = 0) = -2m^2. \quad (\text{D.6.10})$$

# Bibliography

- [1] M.F. Paulos, J. Penedones, J. Toledo, B.C. van Rees and P. Vieira, *The S-matrix bootstrap. Part III: higher dimensional amplitudes*, *JHEP* **12** (2019) 040 [1708.06765].
- [2] G. Chew, *The Analytic S Matrix: A Basis for Nuclear Democracy*, W. A. Benjamin (1966).
- [3] M. Kruczenski, J. Penedones and B.C. van Rees, *Snowmass White Paper: S-matrix Bootstrap*, 2203.02421.
- [4] C. Cheung, *TASI Lectures on Scattering Amplitudes*, in *Proceedings, Theoretical Advanced Study Institute in Elementary Particle Physics : Anticipating the Next Discoveries in Particle Physics (TASI 2016): Boulder, CO, USA, June 6-July 1, 2016*, R. Essig and I. Low, eds., pp. 571–623 (2018), DOI [1708.03872].
- [5] S. Badger, J. Henn, J. Plefka and S. Zoia, *Scattering Amplitudes in Quantum Field Theory*, 2306.05976.
- [6] S. Weinberg, *The Quantum theory of fields. Vol. 1: Foundations*, Cambridge University Press (6, 2005), 10.1017/CBO9781139644167.
- [7] M. Correia, A. Sever and A. Zhiboedov, *An analytical toolkit for the S-matrix bootstrap*, *JHEP* **03** (2021) 013 [2006.08221].
- [8] R.J. Eden, P.V. Landshoff, D.I. Olive and J.C. Polkinghorne, *The analytic S-matrix*, Cambridge Univ. Press, Cambridge (1966).
- [9] A. Martin and F. Cheung, *Analyticity properties and bounds of the scattering amplitudes*, in *10th Brandeis University Summer Institute in Theoretical Physics, Elementary particle physics and scattering theory*, vol. V2, pp. 303–434, 1970.
- [10] R.J. Eden, *Theorems on high energy collisions of elementary particles*, *Rev. Mod. Phys.* **43** (1971) 15.
- [11] V.N. Gribov, *The theory of complex angular momenta: Gribov lectures on theoretical physics*, Cambridge Monographs on Mathematical Physics, Cambridge University Press (6, 2007), 10.1017/CBO9780511534959.

## Bibliography

---

- [12] R. Rattazzi, V.S. Rychkov, E. Tonni and A. Vichi, *Bounding scalar operator dimensions in 4D CFT*, *JHEP* **12** (2008) 031 [0807.0004].
- [13] D. Poland, S. Rychkov and A. Vichi, *The Conformal Bootstrap: Theory, Numerical Techniques, and Applications*, *Rev. Mod. Phys.* **91** (2019) 015002 [1805.04405].
- [14] S. El-Showk, M.F. Paulos, D. Poland, S. Rychkov, D. Simmons-Duffin and A. Vichi, *Solving the 3D Ising Model with the Conformal Bootstrap*, *Phys. Rev. D* **86** (2012) 025022 [1203.6064].
- [15] F. Kos, D. Poland, D. Simmons-Duffin and A. Vichi, *Bootstrapping the  $O(N)$  Archipelago*, *JHEP* **11** (2015) 106 [1504.07997].
- [16] N.B. Agmon, S.M. Chester and S.S. Pufu, *The  $M$ -theory Archipelago*, *JHEP* **02** (2020) 010 [1907.13222].
- [17] M.F. Paulos, J. Penedones, J. Toledo, B.C. van Rees and P. Vieira, *The  $S$ -matrix bootstrap II: two dimensional amplitudes*, *JHEP* **11** (2017) 143 [1607.06110].
- [18] Y. He, A. Irrgang and M. Kruczenski, *A note on the  $S$ -matrix bootstrap for the 2d  $O(N)$  bosonic model*, *JHEP* **11** (2018) 093 [1805.02812].
- [19] L. Córdova and P. Vieira, *Adding flavour to the  $S$ -matrix bootstrap*, *JHEP* **12** (2018) 063 [1805.11143].
- [20] L. Córdova, Y. He, M. Kruczenski and P. Vieira, *The  $O(N)$   $S$ -matrix Monolith*, *JHEP* **04** (2020) 142 [1909.06495].
- [21] P. Dorey, *Exact  $S$  matrices*, in *Eotvos Summer School in Physics: Conformal Field Theories and Integrable Models*, pp. 85–125, 8, 1996 [hep-th/9810026].
- [22] S.O. Aks, *Proof that Scattering Implies Production in Quantum Field Theory*, *J. Math. Phys.* **6** (1965) 516.
- [23] A.L. Guerrieri, J. Penedones and P. Vieira, *Bootstrapping QCD Using Pion Scattering Amplitudes*, *Phys. Rev. Lett.* **122** (2019) 241604 [1810.12849].
- [24] R. Haag, *Local quantum physics: Fields, particles, algebras* (1992).
- [25] A. Martin, *INABILITY OF FIELD THEORY TO EXPLOIT THE FULL UNITARITY CONDITION*, .
- [26] C. Itzykson and J.B. Zuber, *Quantum Field Theory*, International Series In Pure and Applied Physics, McGraw-Hill, New York (1980).
- [27] G. Sommer, *Present state of rigorous analytic properties of scattering amplitudes*, *Fortsch. Phys.* **18** (1970) 577.



- 
- [28] N.N. Bogolyubov, B.V. Medvedev and M.K. Polivanov, *Theory of dispersion relations* (1958).
- [29] J. Bros, H. Epstein and V. Glaser, *A proof of the crossing property for two-particle amplitudes in general quantum field theory*, *Commun. Math. Phys.* **1** (1965) 240.
- [30] H. Lehmann, *Analytic properties of scattering amplitudes as functions of momentum transfer*, *Nuovo Cim.* **10** (1958) 579.
- [31] J. Bros, H. Epstein and V.J. Glaser, *Some rigorous analyticity properties of the four-point function in momentum space*, *Nuovo Cim.* **31** (1964) 1265.
- [32] H. Lehmann, *Analytic properties of scattering amplitudes in two variables in general quantum field theory*, *Commun. Math. Phys.* **2** (1966) 375.
- [33] S. Mandelstam, *Some rigorous analytic properties of transition amplitudes*, *Il Nuovo Cimento (1955-1965)* **15** (1960) 658.
- [34] A. Martin, *Extension of the axiomatic analyticity domain of scattering amplitudes by unitarity. I.*, *Nuovo Cim. A* **42** (1965) 930.
- [35] R.J. Eden, *Proof of the Mandelstam Representation for Every Order in Perturbation Theory*, *Phys. Rev.* **121** (1961) 1567.
- [36] R.J. Eden, P.V. Landshoff, J.C. Polkinghorne and J.C. Taylor, *Mandelstam representation with anomalous thresholds*, *Phys. Rev.* **122** (1961) 307.
- [37] J. Bros, *DERIVATION OF ASYMPTOTIC CROSSING DOMAINS FOR MULTIPARTICLE PROCESSES IN AXIOMATIC QUANTUM FIELD THEORY: A GENERAL APPROACH AND A COMPLETE PROOF FOR  $2 \rightarrow 3$  PARTICLE PROCESSES*, *Phys. Rept.* **134** (1986) 325.
- [38] D.I. Olive, *Unitarity and the evaluation of discontinuities*, *Il Nuovo Cimento (1955-1965)* **26** (1962) 73.
- [39] A. Martin, *Constraints imposed on mandelstam representation by unitarity*, *Phys. Rev. Lett.* **9** (1962) 410.
- [40] A. Martin and J.-M. Richard, *New result on phase shift analysis*, *Phys. Rev. D* **101** (2020) 094014 [2004.11156].
- [41] E.T. Whittaker and G.N. Watson, *A Course of Modern Analysis*, Cambridge Mathematical Library, Cambridge University Press, 4 ed. (1996), 10.1017/CBO9780511608759.
- [42] J. Kupsch, *Towards the saturation of the Froissart bound*, 0801.4871.
- [43] C. Chandler and H.P. Stapp, *Macroscopic causality conditions and properties of scattering amplitudes*, *J. Math. Phys.* **10** (1969) 826.

## Bibliography

---

- [44] D. Williams, *Macroscopic causality and permanence of smoothness for two-particle scattering*, .
- [45] S. Mandelstam, *Determination of the pion - nucleon scattering amplitude from dispersion relations and unitarity. General theory*, *Phys. Rev.* **112** (1958) 1344.
- [46] K.E. Cahill and H.P. Stapp, *A basic discontinuity equation*, *Phys. Rev. D* **6** (1972) 1007.
- [47] O. Steinmann, *Über den zusammenhang zwischen wightmanfunktionen und retardierten kommutatoren, i, ii*, *Helv. Physica Acta* (1960) .
- [48] K.E. Cahill and H.P. Stapp, *OPTICAL THEOREMS AND STEINMANN RELATIONS*, *Annals Phys.* **90** (1975) 438.
- [49] S. Caron-Huot, L.J. Dixon, A. McLeod and M. von Hippel, *Bootstrapping a Five-Loop Amplitude Using Steinmann Relations*, *Phys. Rev. Lett.* **117** (2016) 241601 [1609.00669].
- [50] V.N. Gribov and I.T. Dyatlov, *Analytic continuation of the three-particle unitarity condition. Simplest diagrams*, *Sov. Phys. JETP* **15** (1962) 140.
- [51] R.W. Lardner, *Unitarity and the mandelstam representation*, *Il Nuovo Cimento (1955-1965)* **19** (1961) 77.
- [52] Y.S. Kim, *Anomalous thresholds and three-particle unitarity integral*, *Phys. Rev.* **132** (1963) 927.
- [53] G. Mahoux and A. Martin, *Some rigorous inequalities satisfied by double-spectral functions*, *Il Nuovo Cimento (1955-1965)* 33.3 (1964) .
- [54] A. Martin, *On Positive spectral functions in the Mandelstam representations*, *Nuovo Cim. A* **61S10** (1969) 56.
- [55] M. Froissart, *Asymptotic behavior and subtractions in the Mandelstam representation*, *Phys. Rev.* **123** (1961) 1053.
- [56] A.W. Martin, *\*impossibility\* of positive double spectral functions*, *Phys. Lett. B* **28** (1969) 679.
- [57] F.F. Cheung, *On the necessity of production amplitudes in s-matrix theory. ii*, *Annals of Physics* **46** (1968) 220.
- [58] F.F.K. Cheung and J.S. Toll, *Necessity of production amplitudes in quantum field theory*, *Phys. Rev.* **160** (1967) 1072.
- [59] F.F.K. Cheung, *Necessity of N-particle production amplitudes*, *Phys. Lett. B* **27** (1968) 302.
- [60] X.O. Camanho, J.D. Edelstein, J. Maldacena and A. Zhiboedov, *Causality Constraints on Corrections to the Graviton Three-Point Coupling*, *JHEP* **02** (2016) 020 [1407.5597].

- 
- [61] H.A. Bethe, *Theory of the Effective Range in Nuclear Scattering*, *Phys. Rev.* **76** (1949) 38.
- [62] R.V. Reid, Jr., *Local phenomenological nucleon-nucleon potentials*, *Annals Phys.* **50** (1968) 411.
- [63] G. Colangelo, J. Gasser and H. Leutwyler,  *$\pi\pi$  scattering*, *Nucl. Phys. B* **603** (2001) 125 [hep-ph/0103088].
- [64] M.M. Nagels, T.A. Rijken, J.J. De Swart, G.C. Oades, J.L. Petersen, A.C. Irving et al., *Compilation of Coupling Constants and Low-Energy Parameters. 1978 Edition*, *Nucl. Phys. B* **147** (1979) 189.
- [65] J. Bros and D. Iagolnitzer, *Universality of low-energy scattering in three-dimensional field theory*, *Phys. Rev. D* **59** (1999) 081701 [hep-th/9812146].
- [66] A.J. Dragt, *Amount of four-particle production required in s-matrix theory*, *Phys. Rev.* **156** (1967) 1588.
- [67] S. L., *Die gewichtsfunktion der mandelstam-darstellung am rande ihres tragers*, *Il Nuovo Cimento (1955-1965)* (1962) 934.
- [68] A.W. Martin, *Unitarity and the mandelstam representation. ii. large-angular-momentum partial-wave amplitudes*, *Phys. Rev.* **173** (1968) 1439.
- [69] A.L. Fitzpatrick, J. Kaplan, D. Poland and D. Simmons-Duffin, *The Analytic Bootstrap and AdS Superhorizon Locality*, *JHEP* **12** (2013) 004 [1212.3616].
- [70] Z. Komargodski and A. Zhiboedov, *Convexity and Liberation at Large Spin*, *JHEP* **11** (2013) 140 [1212.4103].
- [71] S. Caron-Huot, *Analyticity in Spin in Conformal Theories*, *JHEP* **09** (2017) 078 [1703.00278].
- [72] G. Nemes and A.B.O. Daalhuis, *Large-parameter asymptotic expansions for the legendre and allied functions*, *SIAM Journal on Mathematical Analysis* **52** (2020) 437.
- [73] O. Haan and K.H. Mutter, *A Scaling Law for s-Channel Partial Wave Amplitudes from t-Channel Unitarity*, *Phys. Lett. B* **52** (1974) 472.
- [74] E.J. Yndurain, *S Channel Implications of T Channel Unitarity*, *Nucl. Phys. B* **92** (1975) 51.
- [75] M. Kologlu, P. Kravchuk, D. Simmons-Duffin and A. Zhiboedov, *Shocks, Superconvergence, and a Stringy Equivalence Principle*, *JHEP* **11** (2020) 096 [1904.05905].
- [76] A. Martin and S.M. Roy, *Lower bound on inelasticity in pion-pion scattering*, *Phys. Rev. D* **96** (2017) 114014 [1710.07140].

## Bibliography

---

- [77] V. Vladimirov, L. Ehrenpreis and S. Technica, *Methods of the Theory of Functions of Many Complex Variables*, Dover Books on Mathematics Series, Dover Publications (2007).
- [78] P. Kravchuk, J. Qiao and S. Rychkov, *Distributions in CFT. Part I. Cross-ratio space*, *JHEP* **05** (2020) 137 [2001.08778].
- [79] H. Epstein, V. Glaser and A. Martin, *Polynomial behaviour of scattering amplitudes at fixed momentum transfer in theories with local observables*, *Commun. Math. Phys.* **13** (1969) 257.
- [80] P. Tourkine and A. Zhiboedov, *Scattering amplitudes from dispersive iterations of unitarity*, 2303.08839.
- [81] D. Simmons-Duffin, D. Stanford and E. Witten, *A spacetime derivation of the Lorentzian OPE inversion formula*, *JHEP* **07** (2018) 085 [1711.03816].
- [82] D. Carmi and S. Caron-Huot, *A Conformal Dispersion Relation: Correlations from Absorption*, *JHEP* **09** (2020) 009 [1910.12123].
- [83] D. Simmons-Duffin, *The Lightcone Bootstrap and the Spectrum of the 3d Ising CFT*, *JHEP* **03** (2017) 086 [1612.08471].
- [84] D. Meltzer, E. Perlmutter and A. Sivaramakrishnan, *Unitarity Methods in AdS/CFT*, *JHEP* **03** (2020) 061 [1912.09521].
- [85] M.F. Paulos, J. Penedones, J. Toledo, B.C. van Rees and P. Vieira, *The S-matrix bootstrap. Part I: QFT in AdS*, *JHEP* **11** (2017) 133 [1607.06109].
- [86] J. Penedones, J.A. Silva and A. Zhiboedov, *Nonperturbative Mellin Amplitudes: Existence, Properties, Applications*, *JHEP* **08** (2020) 031 [1912.11100].
- [87] J. Qiao, *Classification of Convergent OPE Channels for Lorentzian CFT Four-Point Functions*, *SciPost Phys.* **13** (2022) 093 [2005.09105].
- [88] A.B. Zamolodchikov, *CONFORMAL SYMMETRY IN TWO-DIMENSIONS: AN EXPLICIT RECURRENCE FORMULA FOR THE CONFORMAL PARTIAL WAVE AMPLITUDE*, *Commun. Math. Phys.* **96** (1984) 419.
- [89] J. Maldacena, D. Simmons-Duffin and A. Zhiboedov, *Looking for a bulk point*, *JHEP* **01** (2017) 013 [1509.03612].
- [90] S. Mandelstam, *Cuts in the Angular Momentum Plane. 2*, *Nuovo Cim.* **30** (1963) 1148.
- [91] A. Bissi, P. Dey and T. Hansen, *Dispersion Relation for CFT Four-Point Functions*, *JHEP* **04** (2020) 092 [1910.04661].
- [92] P. Benincasa and F. Cachazo, *Consistency Conditions on the S-Matrix of Massless Particles*, 0705.4305.

- 
- [93] N. Arkani-Hamed, T.-C. Huang and Y.-t. Huang, *Scattering amplitudes for all masses and spins*, *JHEP* **11** (2021) 070 [1709.04891].
- [94] C. de Rham, S. Melville, A.J. Tolley and S.-Y. Zhou, *Positivity Bounds for Massive Spin-1 and Spin-2 Fields*, *JHEP* **03** (2019) 182 [1804.10624].
- [95] S. Mandelstam, *Determination of the pion-nucleon scattering amplitude from dispersion relations and unitarity. general theory*, in *Memorial Volume for Stanley Mandelstam*, pp. 151–167, World Scientific (1958).
- [96] V. Kolkunov, L. Okun, A. Rudik and V. Sudakov, *Location of the nearest singularities of the  $\pi\pi$ -scattering amplitude*, *JETP* **12** (1961) 242.
- [97] V. Kolkunov, L. Okun and A. Rudik, *The singular points of some feynman diagrams*, *JETP* **11** (1960) 634.
- [98] H.P. Stapp, *Finiteness of the number of positive- $\alpha$  landau surfaces in bounded portions of the physical region*, *Journal of Mathematical Physics* **8** (1967) 1606.
- [99] J. Polkinghorne, *Analyticity and unitarity*, *Il Nuovo Cimento (1955-1965)* **23** (1962) 360.
- [100] J. Polkinghorne, *Analyticity and unitarity—ii*, *Il Nuovo Cimento Series 10* **25** (1962) 901.
- [101] R. Diestel, *Graph Theory*, Springer Publishing Company, Incorporated, 5th ed. (2017).
- [102] S. Mizera, *Crossing symmetry in the planar limit*, *Phys. Rev. D* **104** (2021) 045003 [2104.12776].
- [103] R.J. Eden, *Analytic structure of collision amplitudes in perturbation theory*, *Physical Review* **119** (1960) 1763.
- [104] S. Coleman and R.E. Norton, *Singularities in the physical region*, *Nuovo Cim.* **38** (1965) 438.
- [105] B.D. McKay and A. Piperno, *Practical graph isomorphism, ii*, *Journal of Symbolic Computation* **60** (2014) 94.
- [106] G. Csardi and T. Nepusz, *The igraph software package for complex network research*, *InterJournal Complex Systems* (2006) 1695.
- [107] S. Horvát, *Igraph/m*, Oct., 2020. 10.5281/zenodo.4081566.
- [108] J.D. Bjorken and T.T. Wu, *Perturbation Theory of Scattering Amplitudes at High Energies*, *Phys. Rev.* **130** (1963) 2566.
- [109] J. Bros and D. Iagolnitzer, *Structure of scattering functions at  $m$ -particle thresholds in a simplified theory and nonholonomic character of the  $S$ -matrix and Green's functions*, *Phys. Rev. D* **27** (1983) 811.

## Bibliography

---

- [110] R. Karplus, C.M. Sommerfield and E.H. Wichmann, *Spectral Representations in Perturbation Theory. I. Vertex Function*, *Phys. Rev.* **111** (1958) 1187.
- [111] R. Karplus, C.M. Sommerfield and E.H. Wichmann, *Spectral Representations in Perturbation Theory. II. Two-Particle Scattering*, *Phys. Rev.* **114** (1959) 376.
- [112] Y. Nambu, *Dispersion relations for form factors*, *Il Nuovo Cimento (1955-1965)* **9** (1958) 610.
- [113] J. Boyling, *Hermitian analyticity and extended unitarity in S-matrix theory*, *Il Nuovo Cimento (1955-1965)* **33** (1964) 1356.
- [114] R. Cutkosky, *Anomalous thresholds*, *Reviews of Modern Physics* **33** (1961) 448.
- [115] R. Eden, P. Landshoff, J. Polkinghorne and J. Taylor, *Acnodes and cusps on landau curves*, *Journal of Mathematical Physics* **2** (1961) 656.
- [116] S. Mandelstam, *Analytic properties of transition amplitudes in perturbation theory*, *Phys. Rev.* **115** (1959) 1741.
- [117] Y. He and M. Kruczenski, *S-matrix bootstrap in 3+1 dimensions: regularization and dual convex problem*, *JHEP* **08** (2021) 125 [2103.11484].
- [118] V. Gribov and I. Dyatlov, *Contribution of three-particle states to the spectral function equation*, *JETP* **15** (1962) 140.
- [119] J.N. Islam and Y. Kim, *Analytic property of three-body unitarity integral*, *Physical Review* **138** (1965) B1222.
- [120] A. Guerrieri and A. Sever, *Rigorous Bounds on the Analytic S Matrix*, *Phys. Rev. Lett.* **127** (2021) 251601 [2106.10257].
- [121] D. Atkinson, *Introduction to the use of non-linear techniques in s-matrix theory*, *Acta Phys. Austriaca Suppl.* **7** (1970) 32.
- [122] P. Tourkine and A. Zhiboedov, “work in progress.”
- [123] S. Mizera and S. Telen, *Landau Discriminants*, 2109.08036.
- [124] H.S. Hannesdottir, A.J. McLeod, M.D. Schwartz and C. Vergu, *Implications of the Landau Equations for Iterated Integrals*, 2109.09744.
- [125] S. Mizera, *Bounds on Crossing Symmetry*, *Phys. Rev. D* **103** (2021) 081701 [2101.08266].
- [126] D.Y. Petrina, *The mandelstam representation and the continuity theorem*, *JETP* **19** (1964) 370.
- [127] J. Penedones, *Writing CFT correlation functions as AdS scattering amplitudes*, *JHEP* **03** (2011) 025 [1011.1485].

- 
- [128] E. Hijano, *Flat space physics from AdS/CFT*, *JHEP* **07** (2019) 132 [1905 . 02729].
- [129] S. Komatsu, M.F. Paulos, B.C. Van Rees and X. Zhao, *Landau diagrams in AdS and S-matrices from conformal correlators*, *JHEP* **11** (2020) 046 [2007 . 13745].
- [130] Y.-Z. Li, *Notes on flat-space limit of AdS/CFT*, *JHEP* **09** (2021) 027 [2106 . 04606].
- [131] S. Caron-Huot, Z. Komargodski, A. Sever and A. Zhiboedov, *Strings from Massive Higher Spins: The Asymptotic Uniqueness of the Veneziano Amplitude*, *JHEP* **10** (2017) 026 [1607 . 04253].
- [132] S. Mandelstam, *Unitarity Condition Below Physical Thresholds in the Normal and Anomalous Cases*, *Phys. Rev. Lett.* **4** (1960) 84.
- [133] D. Olive, *Unitarity and the evaluation of discontinuities - II*, *Il Nuovo Cimento (1955-1965)* **29** (1963) 326.
- [134] D.I. Olive, *Exploration of S-matrix theory*, *Phys. Rev.* **135** (1964) B745.
- [135] A. Homrich, J. Penedones, J. Toledo, B.C. van Rees and P. Vieira, *The S-matrix Bootstrap IV: Multiple Amplitudes*, *JHEP* **11** (2019) 076 [1905 . 06905].
- [136] D. Karateev, S. Kuhn and J. Penedones, *Bootstrapping Massive Quantum Field Theories*, *JHEP* **07** (2020) 035 [1912 . 08940].
- [137] A.L. Guerrieri, A. Homrich and P. Vieira, *Dual S-matrix bootstrap. Part I. 2D theory*, *JHEP* **11** (2020) 084 [2008 . 02770].
- [138] H.S. Hannesdottir and S. Mizera, *What is the  $i\epsilon$  for the S-matrix?*, 2204 . 02988.
- [139] A. Martin, *Selected topics on analyticity in potential scattering*, *Nuovo Cimento* **21** (1961) 157.
- [140] G. Barton, *Introduction to Dispersion Techniques in Field Theory*, Lecture notes and supplements in physics, W.A. Benjamin (1965).
- [141] A. Zhiboedov, *Notes on the analytic S-matrix*, GGI Lectures on the Theory of Fundamental Interactions (January, 2022).
- [142] F.-K. Guo, C. Hanhart, Q. Wang and Q. Zhao, *Could the near-threshold XYZ states be simply kinematic effects?*, *Phys. Rev. D* **91** (2015) 051504 [1411 . 5584].
- [143] A.P. Szczepaniak, *Triangle Singularities and XYZ Quarkonium Peaks*, *Phys. Lett. B* **747** (2015) 410 [1501 . 01691].
- [144] X.-H. Liu, M. Oka and Q. Zhao, *Searching for observable effects induced by anomalous triangle singularities*, *Phys. Lett. B* **753** (2016) 297 [1507 . 01674].
- [145] M. Mikhasenko, *A triangle singularity and the LHCb pentaquarks*, 1507 . 06552.

## Bibliography

---

- [146] F.-K. Guo, U.G. Meißner, J. Nieves and Z. Yang, *Remarks on the  $P_c$  structures and triangle singularities*, *Eur. Phys. J. A* **52** (2016) 318 [1605 . 05113].
- [147] M. Bayar, F. Aceti, F.-K. Guo and E. Oset, *A Discussion on Triangle Singularities in the  $\Lambda_b \rightarrow J/\psi K^- p$  Reaction*, *Phys. Rev. D* **94** (2016) 074039 [1609 . 04133].
- [148] F.-K. Guo, X.-H. Liu and S. Sakai, *Threshold cusps and triangle singularities in hadronic reactions*, *Prog. Part. Nucl. Phys.* **112** (2020) 103757 [1912 . 07030].
- [149] M. Mikhasenko, B. Ketzner and A. Sarantsev, *Nature of the  $a_1(1420)$* , *Phys. Rev. D* **91** (2015) 094015 [1501 . 07023].
- [150] F. Aceti, L.R. Dai and E. Oset,  *$a_1(1420)$  peak as the  $\pi f_0(980)$  decay mode of the  $a_1(1260)$* , *Phys. Rev. D* **94** (2016) 096015 [1606 . 06893].
- [151] S. Mandelstam, *Analytic properties of transition amplitudes in perturbation theory*, *Phys. Rev.* **115** (1959) 1741.
- [152] R.J. Eden, P.V. Landshoff, J.C. Polkinghorne and J.C. Taylor, *Acnodes and cusps on landau curves*, *Journal of Mathematical Physics* **2** (1961) 656 [<https://doi.org/10.1063/1.1703752>].
- [153] M. Correia, A. Sever and A. Zhiboedov, *Probing multi-particle unitarity with the Landau equations*, *SciPost Phys.* **13** (2022) 062 [2111 . 12100].
- [154] L.D. Landau, *On analytic properties of vertex parts in quantum field theory*, *Nucl. Phys.* **13** (1959) 181.
- [155] A.B. Zamolodchikov, *Exact Two Particle S Matrix of Quantum Sine-Gordon Solitons*, *Pisma Zh. Eksp. Teor. Fiz.* **25** (1977) 499.
- [156] P. Christe and G. Mussardo, *Elastic S Matrices in (1+1)-Dimensions and Toda Field Theories*, *Int. J. Mod. Phys. A* **5** (1990) 4581.
- [157] V.A. Fateev and A.B. Zamolodchikov, *Conformal field theory and purely elastic S matrices*, *Int. J. Mod. Phys. A* **5** (1990) 1025.
- [158] S.R. Coleman and H.J. Thun, *On the Prosaic Origin of the Double Poles in the Sine-Gordon S Matrix*, *Commun. Math. Phys.* **61** (1978) 31.
- [159] A.B. Zamolodchikov, *Integrals of Motion and S Matrix of the (Scaled)  $T=T(c)$  Ising Model with Magnetic Field*, *Int. J. Mod. Phys. A* **4** (1989) 4235.
- [160] T.J. Hollowood and P. Mansfield, *Rational conformal field theories at, and away from, criticality as Toda field theories*, *Physics Letters B* **226** (1989) 73.
- [161] H.W. Braden, E. Corrigan, P.E. Dorey and R. Sasaki, *Affine Toda Field Theory and Exact S Matrices*, *Nucl. Phys. B* **338** (1990) 689.



- 
- [162] G. Delfino, *Integrable field theory and critical phenomena: The Ising model in a magnetic field*, *J. Phys. A* **37** (2004) R45 [hep-th/0312119].
- [163] R. Blankenbecler and Y. Nambu, *Anomalous thresholds in dispersion theory-i*, *Il Nuovo Cimento (1955-1965)* **18** (1960) 595.
- [164] R. Blankenbecler and L.F. Cook, *Bound states and dispersion relations*, *Phys. Rev.* **119** (1960) 1745.
- [165] R. Oehme, *Continuation of scattering amplitudes and form factors through two-particle branch lines*, *Phys. Rev.* **121** (1961) 1840.
- [166] R. Blankenbecler, M.L. Goldberger, S.W. MacDowell and S.B. Treiman, *Singularities of scattering amplitudes on unphysical sheets and their interpretation*, *Phys. Rev.* **123** (1961) 692.
- [167] L.F. Cook and B.W. Lee, *Unitarity and production amplitudes*, *Phys. Rev.* **127** (1962) 283.
- [168] J.S. Ball, W.R. Frazer and M. Nauenberg, *Scattering and production amplitudes with unstable particles*, *Phys. Rev.* **128** (1962) 478.
- [169] J.B. Bronzan and C. Kacser, *Khuri-treiman representation and perturbation theory*, *Phys. Rev.* **132** (1963) 2703.
- [170] I.J.R. Aitchison, *Logarithmic singularities in processes with two final-state interactions*, *Phys. Rev.* **133** (1964) B1257.
- [171] V. Gribov, *Analytic properties of partial wave amplitudes and asymptotic behaviour of scattering amplitude*, *Nuclear Physics* **40** (1963) 107.
- [172] J.M. Greben and L.P. Kok, *Anomalous thresholds in an  $\frac{N}{D}$  approach to nuclear reactions*, *Phys. Rev. C* **13** (1976) 489.
- [173] M. Hoferichter, G. Colangelo, M. Procura and P. Stoffer, *Virtual photon-photon scattering*, *Int. J. Mod. Phys. Conf. Ser.* **35** (2014) 1460400 [1309.6877].
- [174] G. Colangelo, M. Hoferichter, M. Procura and P. Stoffer, *Dispersive approach to hadronic light-by-light scattering*, *JHEP* **09** (2014) 091 [1402.7081].
- [175] G. Colangelo, M. Hoferichter, M. Procura and P. Stoffer, *Dispersion relation for hadronic light-by-light scattering: theoretical foundations*, *JHEP* **09** (2015) 074 [1506.01386].
- [176] M. Hoferichter and P. Stoffer, *Dispersion relations for  $\gamma^* \gamma^* \rightarrow \pi\pi$ : helicity amplitudes, subtractions, and anomalous thresholds*, *Journal of High Energy Physics* **2019** (2019) 1.
- [177] I. Danilkin, O. Deineka and M. Vanderhaeghen, *Dispersive analysis of the  $\gamma^* \gamma^* \rightarrow \pi\pi$  process*, *Phys. Rev. D* **101** (2020) 054008.

## Bibliography

---

- [178] B. Moussallam, *Unified dispersive approach to real and virtual photon-photon scattering at low energy*, *Eur. Phys. J. C* **73** (2013) 2539 [1305 . 3143].
- [179] M. Dimou, J. Lyon and R. Zwicky, *Exclusive chromomagnetism in heavy-to-light fcncs*, *Phys. Rev. D* **87** (2013) 074008.
- [180] M.F.M. Lutz and C.L. Korpa, *On coupled-channel dynamics in the presence of anomalous thresholds*, *Phys. Rev. D* **98** (2018) 076003.
- [181] C.L. Korpa, M.F.M. Lutz, X.-Y. Guo and Y. Heo, *A coupled-channel system with anomalous thresholds and unitarity*, 2211 . 03508.
- [182] F. Jegerlehner and A. Nyffeler, *The Muon  $g-2$* , *Phys. Rept.* **477** (2009) 1 [0902 . 3360].
- [183] J. Prades, E. de Rafael and A. Vainshtein, *The Hadronic Light-by-Light Scattering Contribution to the Muon and Electron Anomalous Magnetic Moments*, *Adv. Ser. Direct. High Energy Phys.* **20** (2009) 303 [0901 . 0306].
- [184] J. Boyling, *Normal threshold behaviour in the presence of anomalous thresholds*, *Il Nuovo Cimento A (1971-1996)* **45** (1966) 706.
- [185] P. Goddard, *Anomalous threshold singularities in S-matrix theory*, *Il Nuovo Cimento A (1965-1970)* **59** (1969) 335.
- [186] B.C. van Rees and X. Zhao, *QFT in AdS instead of LSZ*, 2210 . 15683.
- [187] S. Weinberg, *The Quantum Theory of Fields, Volume 1: Foundations*, Cambridge University Press (2005).
- [188] V.N. Gribov, *Analytic properties of the partial wave amplitudes and the asymptotic behavior of the scattering amplitude*, *Sov. Phys. JETP* **15** (1962) 873.
- [189] J.R. Pelaez, *From controversy to precision on the sigma meson: a review on the status of the non-ordinary  $f_0(500)$  resonance*, *Phys. Rept.* **658** (2016) 1 [1510 . 00653].
- [190] G. Delfino, *Integrable field theory and critical phenomena: the ising model in a magnetic field*, *Journal of Physics A: Mathematical and General* **37** (2004) R45–R78 [<https://arxiv.org/abs/hep-th/0312119v1>].
- [191] A. Homrich, J. Penedones, J. Toledo, B.C. van Rees and P. Vieira, *The s-matrix bootstrap IV: multiple amplitudes*, *Journal of High Energy Physics* **2019** (2019) .
- [192] G. Delfino, P. Simonetti and J. Cardy, *Asymptotic factorisation of form factors in two-dimensional quantum field theory*, *Physics Letters B* **387** (1996) 327.
- [193] B. Henning, H. Murayama, F. Riva, J.O. Thompson and M.T. Walters, *Towards a nonperturbative construction of the S-matrix*, 2209 . 14306.

- 
- [194] L. Córdova, Y. He and M.F. Paulos, *From conformal correlators to analytic S-matrices: CFT<sub>1</sub>/QFT<sub>2</sub>*, *JHEP* **08** (2022) 186 [2203 . 10840].
- [195] N. Doroud and J. Elias Miró, *S-matrix bootstrap for resonances*, *JHEP* **09** (2018) 052 [1804 . 04376].
- [196] J. Elias Miró, A.L. Guerrieri, A. Hebbar, J.a. Penedones and P. Vieira, *Flux Tube S-matrix Bootstrap*, *Phys. Rev. Lett.* **123** (2019) 221602 [1906 . 08098].
- [197] M.F. Paulos and Z. Zheng, *Bounding scattering of charged particles in 1 + 1 dimensions*, *JHEP* **05** (2020) 145 [1805 . 11429].
- [198] C. Bercini, M. Fabri, A. Homrich and P. Vieira, *S-matrix bootstrap: Supersymmetry, Z<sub>2</sub>, and Z<sub>4</sub> symmetry*, *Phys. Rev. D* **101** (2020) 045022 [1909 . 06453].
- [199] A.L. Guerrieri, J. Penedones and P. Vieira, *S-matrix bootstrap for effective field theories: massless pions*, *JHEP* **06** (2021) 088 [2011 . 02802].
- [200] A. Hebbar, D. Karateev and J. Penedones, *Spinning S-matrix bootstrap in 4d*, *JHEP* **01** (2022) 060 [2011 . 11708].
- [201] A. Guerrieri, J. Penedones and P. Vieira, *Where Is String Theory in the Space of Scattering Amplitudes?*, *Phys. Rev. Lett.* **127** (2021) 081601 [2102 . 02847].
- [202] H. Chen, A.L. Fitzpatrick and D. Karateev, *Bootstrapping 2d  $\phi^4$  theory with Hamiltonian truncation data*, *JHEP* **02** (2022) 146 [2107 . 10286].
- [203] D. Karateev, J. Marucha, J. Penedones and B. Sahoo, *Bootstrapping the a-anomaly in 4d QFTs*, 2204 . 01786.
- [204] H. Chen, A.L. Fitzpatrick and D. Karateev, *Nonperturbative Bounds on Scattering of Massive Scalar Particles in  $d \geq 2$* , 2207 . 12448.
- [205] J.E. Miro, A. Guerrieri and M.A. Gumus, *Bridging Positivity and S-matrix Bootstrap Bounds*, 2210 . 01502.
- [206] C. Lopez, *A lower bound to the  $\pi_0\pi_0$  s-wave scattering length*, *Nuclear Physics B* **88** (1975) 358.
- [207] C. Lopez, *Rigorous Lower Bounds for the  $\pi_i \pi_i$  p-Wave Scattering Length*, *Lett. Nuovo Cim.* **13** (1975) 69.
- [208] C. Lopez and G. Mennessier, *A new absolute bound on the  $\pi_0\pi_0$  s-wave scattering length*, *Physics Letters B* **58** (1975) 437.
- [209] B. Bonnier, C. Lopez and G. Mennessier, *Improved absolute bounds on the  $\pi_0\pi_0$  amplitude*, *Physics Letters B* **60** (1975) 63.

## Bibliography

---

- [210] C. Lopez and G. Mennessier, *Bounds on the  $\pi^0 \pi^0$  Amplitude*, *Nucl. Phys. B* **118** (1977) 426.
- [211] A.L. Guerrieri, A. Homrich and P. Vieira, *Dual s-matrix bootstrap. part i. 2d theory*, *Journal of High Energy Physics* **2020** (2020) .
- [212] M. Kruczenski and H. Murali, *The R-matrix bootstrap for the 2d  $O(N)$  bosonic model with a boundary*, *JHEP* **04** (2021) 097 [2012 . 15576].
- [213] J. Elias Miró and A. Guerrieri, *Dual EFT bootstrap: QCD flux tubes*, *JHEP* **10** (2021) 126 [2106 . 07957].
- [214] D. Simmons-Duffin, *A Semidefinite Program Solver for the Conformal Bootstrap*, *JHEP* **06** (2015) 174 [1502 . 02033].
- [215] W. Landry and D. Simmons-Duffin, *Scaling the semidefinite program solver SDPB*, 1909 . 09745.
- [216] D. Karateev, S. Kuhn and J. Penedones, *Bootstrapping massive quantum field theories*, *Journal of High Energy Physics* **2020** (2020) .
- [217] J.L. Cardy, *Central charge and universal combinations of amplitudes in two-dimensional theories away from criticality*, *Phys. Rev. Lett.* **60** (1988) 2709.
- [218] D. Friedan, Z. Qiu and S. Shenker, *Conformal invariance, unitarity, and critical exponents in two dimensions*, *Phys. Rev. Lett.* **52** (1984) 1575.
- [219] H. Chen, A.L. Fitzpatrick and D. Karateev, *Bootstrapping 2d  $\phi^4$  theory with hamiltonian truncation data*, *Journal of High Energy Physics* **2022** (2022) .
- [220] A. Zamolodchikov, *Ising Spectroscopy II: Particles and poles at  $T > T_c$* , 1310 . 4821.
- [221] B. Gabai and X. Yin, *On the S-matrix of Ising field theory in two dimensions*, *JHEP* **10** (2022) 168 [1905 . 00710].
- [222] P. Fonseca and A. Zamolodchikov, *Ising spectroscopy. I. Mesons at  $T < T(c)$* , hep-th/0612304.
- [223] P. Fonseca and A. Zamolodchikov, *Ising field theory in a magnetic field: Analytic properties of the free energy*, hep-th/0112167.
- [224] D. Karateev, *Two-point functions and bootstrap applications in quantum field theories*, *JHEP* **02** (2022) 186 [2012 . 08538].
- [225] D. Olive, *Unitarity and the evaluation of discontinuities*, *Nuovo Cimento* **26** (1962) 73.
- [226] M. Slater, *Lagrange multipliers revisited*, Cowles Foundation Discussion Papers 80, Cowles Foundation for Research in Economics, Yale University (1959).

- [227] H. Chen, A.L. Fitzpatrick and D. Karateev, *Nonperturbative Bounds on Scattering of Massive Scalar Particles in  $d \geq 2$* , 2207 . 12448.
- [228] G. Mussardo, *Statistical field theory: an introduction to exactly solved models in statistical physics; 1st ed.*, Oxford graduate texts, Oxford Univ. Press, New York, NY (2010).
- [229] A. Zamolodchikov and I. Ziyatdinov, *Inelastic scattering and elastic amplitude in ising field theory in a weak magnetic field at . perturbative analysis*, *Nuclear Physics B* **849** (2011) 654–674.
- [230] P. Tourkine and A. Zhiboedov, *Scattering from production in 2d*, *JHEP* **07** (2021) 228 [2101 . 05211].
- [231] M. Creutz, *Rigorous bounds on coupling constants in two-dimensional field theories*, *Phys. Rev. D* **6** (1972) 2763.
- [232] M.F. Paulos, J. Penedones, J. Toledo, B.C. van Rees and P. Vieira, *The s-matrix bootstrap. part i: QFT in AdS*, *Journal of High Energy Physics* **2017** (2017) .
- [233] L. Castillejo, R.H. Dalitz and F.J. Dyson, *Low's scattering equation for the charged and neutral scalar theories*, *Phys. Rev.* **101** (1956) 453.
- [234] J.L. Cardy, O.A. Castro-Alvaredo and B. Doyon, *Form factors of branch-point twist fields in quantum integrable models and entanglement entropy*, *Journal of Statistical Physics* **130** (2007) 129.
- [235] O.A. Castro-Alvaredo, B. Doyon and D. Fioravanti, *Conical twist fields and null polygonal wilson loops*, *Nuclear Physics B* **931** (2018) 146.
- [236] B. Schroer and T. Truong, *The order/disorder quantum field operators associated with the two-dimensional ising model in the continuum limit*, *Nuclear Physics B* **144** (1978) 80.
- [237] P.J.M. Bastiaansen and H.J.F. Knops, *Monte carlo method to calculate the central charge and critical exponents*, *Physical Review E* **57** (1998) 3784.
- [238] L. Giusti and M. Pepe, *Energy-momentum tensor on the lattice: Nonperturbative renormalization in yang-mills theory*, *Physical Review D* **91** (2015) .
- [239] M. Correia, *Nonperturbative Anomalous Thresholds*, 2212 . 06157.
- [240] A. Coser, M. Beria, G.P. Brandino, R.M. Konik and G. Mussardo, *Truncated Conformal Space Approach for 2D Landau-Ginzburg Theories*, *J. Stat. Mech.* **1412** (2014) P12010 [1409 . 1494].
- [241] S. Rychkov and L.G. Vitale, *Hamiltonian truncation study of the  $\phi^4$  theory in two dimensions*, *Phys. Rev. D* **91** (2015) 085011 [1412 . 3460].

## Bibliography

---

- [242] Z. Bajnok and M. Lajer, *Truncated Hilbert space approach to the 2d  $\phi^4$  theory*, *JHEP* **10** (2016) 050 [1512.06901].
- [243] P. Bosetti, B. De Palma and M. Guagnelli, *Monte Carlo determination of the critical coupling in  $\phi_2^4$  theory*, *Phys. Rev. D* **92** (2015) 034509 [1506.08587].
- [244] N. Anand, V.X. Genest, E. Katz, Z.U. Khandker and M.T. Walters, *RG flow from  $\phi^4$  theory to the 2D Ising model*, *JHEP* **08** (2017) 056 [1704.04500].
- [245] M. Serone, G. Spada and G. Villadoro,  *$\lambda\phi^4$  Theory I: The Symmetric Phase Beyond NNNNNNNLO*, *JHEP* **08** (2018) 148 [1805.05882].
- [246] H. Chen, A.L. Fitzpatrick and D. Karateev, *Form factors and spectral densities from Lightcone Conformal Truncation*, *JHEP* **04** (2022) 109 [2107.10285].
- [247] W. Heisenberg, *Die "beobachtbaren Größen" in der Theorie der Elementarteilchen*, *Zeitschrift für Physik* **120** (1943) 513.
- [248] T. Regge, *The Analytic S Matrix: A Basis for Nuclear Democracy and The Analytic S Matrix*, *Physics Today* **20** (1967) 82 [[https://pubs.aip.org/physicstoday/article-pdf/20/9/82/11193262/82\\_2\\_online.pdf](https://pubs.aip.org/physicstoday/article-pdf/20/9/82/11193262/82_2_online.pdf)].
- [249] W.R. Frazer and J.R. Fulco, *Effect of a Pion-Pion Scattering Resonance on Nucleon Structure. II*, *Phys. Rev.* **117** (1960) 1609.
- [250] G.F. Chew and S.C. Frautschi, *Principle of Equivalence for All Strongly Interacting Particles Within the S Matrix Framework*, *Phys. Rev. Lett.* **7** (1961) 394.
- [251] G.F. Chew and S.C. Frautschi, *Regge Trajectories and the Principle of Maximum Strength for Strong Interactions*, *Phys. Rev. Lett.* **8** (1962) 41.
- [252] G. Veneziano, *Construction of a crossing - symmetric, Regge behaved amplitude for linearly rising trajectories*, *Nuovo Cim. A* **57** (1968) 190.
- [253] S. Weinberg, *What is quantum field theory, and what did we think it is?*, in *Conference on Historical Examination and Philosophical Reflections on the Foundations of Quantum Field Theory*, pp. 241–251, 3, 1996 [hep-th/9702027].
- [254] W.R. Frazer, *The analytic s matrix and the ideal mentor*, in *Geoffrey Chew: Architect of the Bootstrap*, pp. 3–11 DOI [[https://www.worldscientific.com/doi/pdf/10.1142/9789811219832\\_0001](https://www.worldscientific.com/doi/pdf/10.1142/9789811219832_0001)].
- [255] S.M. Roy, *Exact integral equation for pion pion scattering involving only physical region partial waves*, *Phys. Lett. B* **36** (1971) 353.
- [256] A.B. Kaidalov, *Regge poles in QCD*, hep-ph/0103011.
- [257] J.H. Schwarz, *String theory: The Early years*, 7, 2000 [hep-th/0007118].

- [258] H.S. Hannesdottir, A.J. McLeod, M.D. Schwartz and C. Vergu, *Constraints on sequential discontinuities from the geometry of on-shell spaces*, *JHEP* **07** (2023) 236 [2211 . 07633].
- [259] A. Adams, N. Arkani-Hamed, S. Dubovsky, A. Nicolis and R. Rattazzi, *Causality, analyticity and an IR obstruction to UV completion*, *JHEP* **10** (2006) 014 [hep-th/0602178].
- [260] A.M. Polyakov, *Conformal symmetry of critical fluctuations*, *JETP Lett.* **12** (1970) 381.
- [261] A.A. Belavin, A.M. Polyakov and A.B. Zamolodchikov, *Infinite Conformal Symmetry in Two-Dimensional Quantum Field Theory*, *Nucl. Phys. B* **241** (1984) 333.
- [262] A. Guerrieri, H. Murali, J. Penedones and P. Vieira, *Where is M-theory in the space of scattering amplitudes?*, 2212 . 00151.
- [263] JPAC collaboration, *Snowmass white paper: Need for amplitude analysis in the discovery of new hadrons*, in *Snowmass 2021*, 3, 2022 [2203 . 08208].
- [264] Y. He and M. Kruczenski, *Bootstrapping gauge theories*, 2309 . 12402.
- [265] S. Caron-Huot, M. Giroux, H.S. Hannesdottir and S. Mizera, *What can be measured asymptotically?*, 2308 . 02125.
- [266] A. Cristofoli, R. Gonzo, D.A. Kosower and D. O’Connell, *Waveforms from amplitudes*, *Phys. Rev. D* **106** (2022) 056007 [2107 . 10193].
- [267] B.L. Ioffe, *On V. N. Gribov*, in *Under the Spell of Landau: When Theoretical Physics was Shaping Destinies. Edited by Shifman Mikhail. Published by World Scientific Publishing Co. Pte. Ltd*, pp. 296–301 (2013), DOI.
- [268] B.M. Project, H. Bateman, A. Erdélyi and U.S.O. of Naval Research, *Higher Transcendental Functions*, no. v. 1 in Bateman manuscript project, McGraw-Hill (1953).
- [269] V.N. Gribov, *Possible Asymptotic Behavior of Elastic Scattering*, *JETP Lett.* **41** (1961) 667.
- [270] V.N. Gribov, *Asymptotic behaviour of the scattering amplitude at high energies*, *Nucl. Phys.* **22** (1961) 249.
- [271] R.C. Brower, J. Polchinski, M.J. Strassler and C.-I. Tan, *The Pomeron and gauge/string duality*, *JHEP* **12** (2007) 005 [hep-th/0603115].
- [272] B.R. Desai and B. Sakita, *Threshold regge poles and the effective-range expansion*, *Phys. Rev.* **136** (1964) B226.
- [273] A.A. Logunov, I.T. Todorov and N.A. Chernikov, *Analytical properties of Feynman graphs*, in *11th International Conference on High-energy Physics*, pp. 695–698, 1962.
- [274] J.S. Provan and D.R. Shier, *A paradigm for listing (s, t)-cuts in graphs*, *Algorithmica* **15** (1996) 351.

## Bibliography

---

- [275] M. Correia, J. Penedones and A. Vuignier, *Injecting the UV into the Bootstrap: Ising Field Theory*, 2212.03917.
- [276] G. Delfino, G. Mussardo and P. Simonetti, *Nonintegrable quantum field theories as perturbations of certain integrable models*, *Nucl. Phys. B* **473** (1996) 469 [hep-th/9603011].
- [277] G. Delfino and G. Mussardo, *The Spin spin correlation function in the two-dimensional Ising model in a magnetic field at  $T = T(c)$* , *Nucl. Phys. B* **455** (1995) 724 [hep-th/9507010].
- [278] G. Delfino, P. Grinza and G. Mussardo, *Decay of particles above threshold in the Ising field theory with magnetic field*, *Nucl. Phys. B* **737** (2006) 291 [hep-th/0507133].
- [279] B. Berg, M. Karowski and P. Weisz, *Construction of green's functions from an exact  $s$  matrix*, *Phys. Rev. D* **19** (1979) 2477.



# MIGUEL CORREIA

2 Rue des Hautains, Saint-Genis-Pouilly, France

(+351)912456144 ◊ miguel.alexandre.ribeiro.correia@cern.ch ◊ miguel.correia@epfl.ch

## EDUCATION

---

**CERN Theory Department**, Geneva, Switzerland *2019 - Present*  
Visiting PhD student

**École Polytechnique Fédérale de Lausanne**, Switzerland *2018 - Present*  
Doctoral Program in Physics  
Supervisor: João Penedones.

**Instituto Superior Técnico**, Lisbon, Portugal *2012-2018*  
Engineering Physics MSc (final grade: 19/20 - top of the class)

## PUBLICATIONS

---

### **Nonperturbative Anomalous Thresholds**

M. Correia  
arXiv:2212.06157 (preprint)

### **Injecting the UV into the Bootstrap: Ising Field Theory**

M. Correia, J. Penedones, and A. Vuignier  
arXiv:2212.03917 (preprint)

### **A covariant formulation of relativistic mechanics**

M. Correia  
Phys. Rev. D **105** (2022).

### **Probing multi-particle unitarity with the Landau equations**

M. Correia, A. Sever, and A. Zhiboedov  
SciPost Phys. **13** (2022).

### **An Analytical Toolkit for the S-matrix Bootstrap**

M. Correia, A. Sever, and A. Zhiboedov  
JHEP **03** (2021).

### **Black holes, gravitational waves and fundamental physics: a roadmap**

L. Barack *et al*  
Class. Quant. Grav. **36** (2019).

### **Characterization of echoes: A Dyson-series representation of individual pulses**

M. Correia and V. Cardoso  
Phys. Rev. D **97** (2018).

## INVITED TALKS

---

*Nonperturbative Anomalous Thresholds* May 2023  
**École Polytechnique**, Paris

*Nonperturbative Anomalous Thresholds* May 2023  
**University of Geneva**

*Nonperturbative Anomalous Thresholds* May 2023  
**University of Edinburgh**

<i>Nonperturbative Anomalous Thresholds</i> <b>Caltech</b> , Los Angeles	Mar 2023
<i>Review of S-matrix analyticity properties</i> <b>Harvard University</b> (remote)	Feb 2023
<i>Nonperturbative Anomalous Thresholds</i> <b>University of Porto</b>	Jan 2023
<i>Old (and some new) results on Non-perturbative Scattering Amplitudes</i> <b>Perimeter Institute</b> , Waterloo	Oct 2022
<i>Old (and some new) results on Non-perturbative Scattering Amplitudes</i> <b>Institute for Advanced Study</b> , Princeton	Oct 2022
<i>A covariant formulation of relativistic mechanics</i> <b>Gravitational wave probes of black hole environments</b> , Rome (conference)	Jun 2022
<i>Probing multi-particle unitarity with the Landau equations</i> <b>S-matrix Bootstrap IV</b> , Crete (conference)	Apr 2022
<i>Probing multi-particle unitarity with the Landau equations</i> <b>CERN</b> , Geneva (remote)	Jan 2022
<i>Probing multi-particle unitarity with the Landau equations</i> <b>University of Porto</b> (remote)	Nov 2021
<i>Does a charge in free-fall radiate?</i> (review talk) <b>École Polytechnique Fédérale de Lausanne</b> (remote)	Jun 2021
<i>An Analytical Toolkit for the S-matrix Bootstrap</i> <b>NORDITA</b> , Stockholm (remote)	Jul 2020
<i>An Analytical Toolkit for the S-matrix Bootstrap</i> <b>CERN</b> , Geneva (remote)	May 2020
<i>An Analytical Toolkit for the S-matrix Bootstrap</i> <b>University of Porto</b> (remote)	May 2020
<i>Bounds on the <math>\pi^0\pi^0</math> amplitude</i> (informal talk) <b>S-matrix Bootstrap III</b> , ICTP-SAIFR, São Paulo (conference)	Sep 2019
<i>Characterization of echoes: A Dyson-series representation of individual pulses</i> <b>CENTRA Meeting 2018</b> , Lisbon (conference)	May 2018

## TEACHING & STUDENT SUPERVISION

---

At École Polytechnique Fédérale de Lausanne:

- Co-supervision of Antoine Vuignier (assisting João Penedones) 2022  
*Dual Bootstrap methods in 2 dimensional Quantum Field Theories* (master thesis)
- Co-supervision of Marko Pesut (assisting João Penedones) 2021  
*Primal and Dual S-matrix Bootstrap* (master thesis)
- *Quantum Field Theory I and II* (assisting Riccardo Rattazzi) 2020-2021
- *General physics: Mechanics* (assisting Philippe Müllhaupt) 2019-2020

At Instituto Superior Técnico:

- *Electromagnetism and Optics* (exercise classes) Fall 2017

- *Thermodynamics* (exercise classes) Spring 2017
- *Mechanics and Waves* (laboratory) Fall 2016

### SCHOLARSHIPS & AWARDS

---

Teaching Excellence Award (École Polytechnique Fédérale de Lausanne) (1,000 CHF)	2021
Fulbright Scholarship for Graduate Studies in the United States (\$25,000 - declined)	2018
Distinction of Academic Excellence (Instituto Superior Técnico)	2018
Best Master Dissertation (Instituto Superior Técnico)	2018
Swiss-European Mobility Scholarship (École Polytechnique Fédérale de Lausanne)	2016
(Three) Undergraduate Teaching Scholarships	2016-2018
Bronze medal in the National Championship of Mathematical Games	2011

## CONFERENCES & SCHOOLS

---

Strings 2023, Perimeter Institute, Waterloo, Canada	July 2023
Bootstrapping Quantum Gravity, KITP Program, California	Feb 2023
Simons Confinement Collaboration Inaugural Workshop, Princeton University, USA	Sep 2022
Amplitudes 2022, Prague, Czech Republic (poster presentation)	Aug 2022
Bootstrap 2022, University of Porto, Portugal	Jun 2022
Gravitational wave probes of black hole environments, La Sapienza, Rome, Italy (invited speaker)	Jun 2022
Nonperturbative Methods in Quantum Field Theory, CERN, Geneva, Switzerland	May 2022
S-matrix Bootstrap IV, Crete, Greece (invited speaker)	Apr 2022
Virtual QCD Meets Gravity 2021, UCLA, Los Angeles, USA (remote)	Dec 2021
Strings 2021, ICTP-SAIFR, São Paulo, Brazil (remote)	Jun 2021
Bootstat 2021, Institut Pascal, Orsay, France (remote)	May 2021
Gravitational scattering, inspiral, and radiation, GGI, Florence, Italy (remote)	Apr 2021
7th SwissMAP General Meeting, Saanenmöser, Switzerland	Sep 2020
Bootstrap 2020, Harvard University, Cambridge, United States (remote)	Jun 2020
CERN Winter School on Supergravity, Strings and Gauge Theory, Geneva, Switzerland	Feb 2020
S-matrix Bootstrap III, ICTP-SAIFR, São Paulo, Brazil	Sep 2019
Bootstrap 2019, Perimeter Institute, Waterloo, Canada	Jul 2019
CERN Winter School on Supergravity, Strings and Gauge Theory, Geneva, Switzerland	Feb 2019
CENTRA Meeting 2018, Instituto Superior Técnico, Lisbon, Portugal	May 2018

## SKILLS

---

Programming: Mathematica, nauty & Traces, igraph, SDPB.

Languages: Portuguese (native), English (fluent), French (intermediate).